HAIR FOLLICLE STEM CELL REGENERATION IN AGING

EDITED BY: Mingxing Lei, Sung-Jan Lin and Cheng Ming Chuong

PUBLISHED IN: Frontiers in Cell and Developmental Biology

frontiers Research Topics

Frontiers eBook Copyright Statement

The copyright in the text of individual articles in this eBook is the property of their respective authors or their respective institutions or funders. The copyright in graphics and images within each article may be subject to copyright of other parties. In both cases this is subject to a license granted to Frontiers.

The compilation of articles constituting this eBook is the property of Frontiers.

Each article within this eBook, and the eBook itself, are published under the most recent version of the Creative Commons CC-BY licence. The version current at the date of publication of this eBook is CC-BY 4.0. If the CC-BY licence is updated, the licence granted by Frontiers is automatically updated to the new version.

When exercising any right under the CC-BY licence, Frontiers must be attributed as the original publisher of the article or eBook, as applicable.

Authors have the responsibility of ensuring that any graphics or other materials which are the property of others may be included in the CC-BY licence, but this should be checked before relying on the CC-BY licence to reproduce those materials. Any copyright notices relating to those materials must be complied with.

Copyright and source acknowledgement notices may not be removed and must be displayed in any copy, derivative work or partial copy which includes the elements in question.

All copyright, and all rights therein, are protected by national and international copyright laws. The above represents a summary only. For further information please read Frontiers' Conditions for Website Use and Copyright Statement, and the applicable CC-BY licence.

ISSN 1664-8714
ISBN 978-2-88974-062-8
DOI 10.3389/978-2-88974-062-8

About Frontiers

Frontiers is more than just an open-access publisher of scholarly articles: it is a pioneering approach to the world of academia, radically improving the way scholarly research is managed. The grand vision of Frontiers is a world where all people have an equal opportunity to seek, share and generate knowledge. Frontiers provides immediate and permanent online open access to all its publications, but this alone is not enough to realize our grand goals.

Frontiers Journal Series

The Frontiers Journal Series is a multi-tier and interdisciplinary set of open-access, online journals, promising a paradigm shift from the current review, selection and dissemination processes in academic publishing. All Frontiers journals are driven by researchers for researchers; therefore, they constitute a service to the scholarly community. At the same time, the Frontiers Journal Series operates on a revolutionary invention, the tiered publishing system, initially addressing specific communities of scholars, and gradually climbing up to broader public understanding, thus serving the interests of the lay society, too.

Dedication to Quality

Each Frontiers article is a landmark of the highest quality, thanks to genuinely collaborative interactions between authors and review editors, who include some of the world's best academicians. Research must be certified by peers before entering a stream of knowledge that may eventually reach the public - and shape society; therefore, Frontiers only applies the most rigorous and unbiased reviews.
Frontiers revolutionizes research publishing by freely delivering the most outstanding research, evaluated with no bias from both the academic and social point of view. By applying the most advanced information technologies, Frontiers is catapulting scholarly publishing into a new generation.

What are Frontiers Research Topics?

Frontiers Research Topics are very popular trademarks of the Frontiers Journals Series: they are collections of at least ten articles, all centered on a particular subject. With their unique mix of varied contributions from Original Research to Review Articles, Frontiers Research Topics unify the most influential researchers, the latest key findings and historical advances in a hot research area! Find out more on how to host your own Frontiers Research Topic or contribute to one as an author by contacting the Frontiers Editorial Office: frontiersin.org/about/contact

HAIR FOLLICLE STEM CELL REGENERATION IN AGING

Topic Editors:
Mingxing Lei, Chongqing University, China
Sung-Jan Lin, National Taiwan University, Taiwan
Cheng Ming Chuong, University of Southern California, United States

Citation: Lei, M., Lin, S.-J., Chuong, C. M., eds. (2022). Hair Follicle Stem Cell Regeneration in Aging. Lausanne: Frontiers Media SA.
doi: 10.3389/ 978-2-88974-062-8

Table of Contents

05 ***Editorial: Hair Follicle Stem Cell Regeneration in Aging***
Mingxing Lei, Sung-Jan Lin and Cheng-Ming Chuong

10 ***Purified Vitexin Compound 1 Inhibits UVA-Induced Cellular Senescence in Human Dermal Fibroblasts by Binding Mitogen-Activated Protein Kinase 1***
Ben Wang, Sha Yan, Yuxin Yi, Yingxue Huang, Zhili Deng, Yiya Zhang, Qingchuan Zheng, Hongfu Xie and Ji Li

21 ***Twist1 Contributes to the Maintenance of Some Biological Properties of Dermal Papilla Cells* in vitro *by Forming a Complex With Tcf4 and β-Catenin***
Nanlan Yu, Tianxing Hu, Haichao Yang, Lian Zhang, Qin Song, Fei Xiang, Xichuan Yang and Yuhong Li

33 ***IL-36α Promoted Wound Induced Hair Follicle Neogenesis via Hair Follicle Stem/Progenitor Cell Proliferation***
Lin Gong, Jian Xiao, Xiaokun Li, Yuanhong Li, Xinghua Gao and Xuegang Xu

44 ***Knockdown of FOXA2 Impairs Hair-Inductive Activity of Cultured Human Follicular Keratinocytes***
Soon-Sun Bak, Jung Min Park, Ji Won Oh, Jung Chul Kim, Moon Kyu Kim and Young Kwan Sung

52 ***Wound Induced Hair Neogenesis – A Novel Paradigm for Studying Regeneration and Aging***
Myan Bhoopalam, Luis A. Garza and Sashank K. Reddy

60 ***Epidermal Stem Cells in Hair Follicle Cycling and Skin Regeneration: A View From the Perspective of Inflammation***
Elena I. Morgun and Ekaterina A. Vorotelyak

78 ***"Two-Cell Assemblage" Assay: A Simple* in vitro *Method for Screening Hair Growth-Promoting Compounds***
Sunhyae Jang, Jungyoon Ohn, Bo Mi Kang, Minji Park, Kyu Han Kim and Ohsang Kwon

86 ***Human Fetal Scalp Dermal Papilla Enriched Genes and the Role of R-Spondin-1 in the Restoration of Hair Neogenesis in Adult Mouse Cells***
Erin L. Weber, Yung-Chih Lai, Mingxing Lei, Ting-Xin Jiang and Cheng-Ming Chuong

97 ***Effects of ALA-PDT on the Healing of Mouse Skin Wounds Infected With* Pseudomonas aeruginosa *and Its Related Mechanisms***
Tao Yang, Yang Tan, Wentao Zhang, Weijiang Yang, Jiefu Luo, Ling Chen, Hong Liu, Guihong Yang and Xia Lei

108 ***An Intrinsic Oscillation of Gene Networks Inside Hair Follicle Stem Cells: An Additional Layer That Can Modulate Hair Stem Cell Activities***
Patrycja Daszczuk, Paula Mazurek, Tomasz D. Pieczonka, Alicja Olczak, Łukasz M. Boryń and Krzysztof Kobielak

129 ***miR-140-5p in Small Extracellular Vesicles From Human Papilla Cells Stimulates Hair Growth by Promoting Proliferation of Outer Root Sheath and Hair Matrix Cells***
Yuxin Chen, Junfei Huang, Zhen Liu, Ruosi Chen, Danlan Fu, Lunan Yang, Jin Wang, Lijuan Du, Lihong Wen, Yong Miao and Zhiqi Hu

149 ***Increased Expression of Zyxin and Its Potential Function in Androgenetic Alopecia***
Qingmei Liu, Xiangguang Shi, Yue Zhang, Yan Huang, Kai Yang, Yulong Tang, Yanyun Ma, Yuting Zhang, Ji'an Wang, Li Zhang, Qi Zhang, Xiao Liu, Jinran Lin, Jiucun Wang and Wenyu Wu

159 ***Skin Cyst: A Pathological Dead-End With a New Twist of Morphogenetic Potentials in Organoid Cultures***
Weiming Qiu, Pei-Rong Gu, Cheng-Ming Chuong and Mingxing Lei

167 ***Rapamycin Protects Skin Fibroblasts From UVA-Induced Photoaging by Inhibition of p53 and Phosphorylated HSP27***
Gen-Long Bai, Ping Wang, Xin Huang, Zi-Yue Wang, Di Cao, Chuan Liu, Yi-Yi Liu, Ruo-Lin Li and Ai-Jun Chen

178 ***Dietary Vitamin A Impacts Refractory Telogen***
Liye Suo, Christine VanBuren, Eylul Damla Hovland, Natalia Y. Kedishvili, John P. Sundberg and Helen B. Everts

189 ***UVA-Triggered Drug Release and Photo-Protection of Skin***
Vega Widya Karisma, Wei Wu, Mingxing Lei, Huawen Liu, Muhammad Farrukh Nisar, Matthew D. Lloyd, Charareh Pourzand and Julia Li Zhong

205 ***Tissue Mechanics in Haired Murine Skin: Potential Implications for Skin Aging***
Hans I-Chen Harn, Chih-Chiang Chen, Sheng-Pei Wang, Mingxing Lei and Cheng-Ming Chuong

214 ***Establishment of an Efficient Primary Culture System for Human Hair Follicle Stem Cells Using the Rho-Associated Protein Kinase Inhibitor Y-27632***
Lihong Wen, Yong Miao, Zhexiang Fan, Jiarui Zhang, Yixuan Guo, Damao Dai, Junfei Huang, Zhen Liu, Ruosi Chen and Zhiqi Hu

230 ***Human iPS Cell-Derived Cell Aggregates Exhibited Dermal Papilla Cell Properties in* in vitro *Three-Dimensional Assemblage Mimicking Hair Follicle Structures***
Masahiro Fukuyama, Aki Tsukashima, Momoko Kimishima, Yoshimi Yamazaki, Hideyuki Okano and Manabu Ohyama

245 ***Transcriptome Analysis Reveals an Inhibitory Effect of Dihydrotestosterone-Treated 2D- and 3D-Cultured Dermal Papilla Cells on Hair Follicle Growth***
Yufan Zhang, Junfei Huang, Danlan Fu, Zhen Liu, Hailin Wang, Jin Wang, Qian Qu, Kaitao Li, Zhexiang Fan, Zhiqi Hu and Yong Miao

frontiers in Cell and Developmental Biology

EDITORIAL
published: 25 November 2021
doi: 10.3389/fcell.2021.799268

Editorial: Hair Follicle Stem Cell Regeneration in Aging

Mingxing Lei[1,2]*, *Sung-Jan Lin*[3,4] *and Cheng-Ming Chuong*[5]

[1]111 Project Laboratory of Biomechanics and Tissue Repair, College of Bioengineering, Chongqing University, Chongqing, China, [2]Key Laboratory of Biorheological Science and Technology of the Ministry of Education, College of Bioengineering, Chongqing University, Chongqing, China, [3]Department of Biomedical Engineering and Department of Dermatology, College of Engineering and College of Medicine, National Taiwan University, Taipei, Taiwan, [4]Department of Dermatology, National Taiwan University Hospital, Taipei, Taiwan, [5]Department of Pathology, Keck School of Medicine, University of Southern California, Los Angeles, CA, United States

Keywords: aging, hair regeneration, niche, skin organoid, wound-induced hair neogenesis

Editorial on the Research Topic

Hair Follicle Stem Cell Regeneration in Aging

With stem cells that can be activated and silenced cyclically, hair follicle experiences multiple rounds of growth phase (anagen), regression phase (catagen), and resting phase (telogen) during lifespan. Hair cycling is initiated by cyclic renewal or physiological cyclic regeneration of stem cells. However, tissues and organs undergo structural and functional declines in the aging process, with physiological and pathological changes regulated by intrinsic and extrinsic factors that dictate the cell fate (Lei and Chuong, 2016) (**Figure 1**). As one of the important appendages of the skin, the hair follicle is a complex mini-organ with visible signs, such as decreased regenerative ability that leads to alopecia, and hair graying due to less melanin production by melanocyte stem cells during aging (Qiu et al., 2019). Hair regenerative ability is gradually decreased because hair follicle stem cells enter a long quiescent state (Chen et al., 2014), or differentiate into other skin epithelial lineages (Matsumura et al., 2016), or escape from the hair follicle niche during aging (Zhang C. et al., 2021). These features promote hair follicle to become a widely used model for studying regeneration. As over 30% of the population all over the world suffer from partial or complete hair loss, particularly most people undergo alopecia during aging, understanding the mechanism by which hair follicle changes during aging is of great interest in regenerative biology and is essential for regenerative medicine.

The field of hair follicle biology has expanded tremendously with broader scales and diverse approaches that aim to elucidate the mechanisms of hair follicle regeneration, as well as to devise potential therapeutic strategies to delay the aging processes or restore the regenerative ability. Here we organize this Research Topic with a collection of original research and review articles that explore aging-related hair follicle stem cell regeneration. Although not fully covering the comprehensive hair follicle stem cell field, this issue provides new insight into hair regeneration from different perspectives, mainly at the physiological, wound healing, and *in vitro* cultivation levels.

Skin which covers the surface of our human body is constantly subjected to environmental insults. Ultraviolet (UV) radiation is the major cause of skin aging that is called photoaging, which provokes oxidative stress, inflammatory responses, and DNA damage. Three papers in this Research Topic focus on studying the role of UVA in skin aging (Wang et al., 2020; Bai et al., 2021; Karisma et al., 2021). Bai et al. investigated rapamycin as a macrolide immunosuppressant that protects skin fibroblasts from UVA-induced photoaging (Bai et al., 2021). They found that rapamycin-treated human dermal fibroblasts have a decreased expression of p53 and phosphorylated HSP27, as well as reduced genotoxic and oxidative stress levels. Wang et al. identified purified vitexin compound 1 as a novel lignanoid that attenuates UVA-induced senescence in human dermal fibroblasts *in vitro* and

OPEN ACCESS

Edited and reviewed by:
Valerie Kouskoff,
The University of Manchester,
United Kingdom

****Correspondence:***
Mingxing Lei
mingxing@cqu.edu.cn

Specialty section:
This article was submitted to Stem Cell Research, a section of the journal Frontiers in Cell and Developmental Biology

Received: *21 October 2021*
Accepted: *05 November 2021*
Published: *25 November 2021*

Citation:
Lei M, Lin S-J and Chuong C-M (2021) Editorial: Hair Follicle Stem Cell Regeneration in Aging. Front. Cell Dev. Biol. 9:799268. doi: 10.3389/fcell.2021.799268

mouse skin *in vivo*, through repressing UVA-induced phosphorylation of MAPK1 (Wang et al., 2020). Although UVA has a harmful effect to cause skin photoaging, it is a double-edged sword that can be used as a stimulus to switch the photo-controlled drug release upon a "switch on-switch off" procedure, which can be developed for clinical use. A review comprehensively summarized how UVA-triggered drug release as a promising potential for skin photoprotection and phototherapy (Karisma et al., 2021). In addition to UVA-induced photoaging, recent advancements suggest that tissue mechanics is largely involved in regulating skin aging. Another review by Harn et al. described the manifestations of the aging skin, and fully summarized how tissue mechanics influences extracellular matrix dysregulation, wrinkling, and wound healing during skin aging (Harn et al., 2021). They also proposed how perturbed tensional homeostasis impacts physiological functioning of the skin, including how skin tension influences hair regeneration and wound healing. Then, they enumerated several potential chemical and mechanical approaches that may be used for developing new drugs against skin aging.

Hair follicle is one of the skin appendages that is mostly influenced by aging. Hairs are gradually lost during the aging process, which is largely controlled by intrinsic epigenetic/genetic status and extrinsic environmental stimuli that regulate the hair follicle stem cell behavior during hair cycling. Decreased expression of activators and increased expression of inhibitors lead to decreased or failed hair regeneration in aged skin, which may cause alopecia eventually. The telogen phase of the hair follicle, particularly the refractory telogen phase becomes longer and longer, compared to the competent telogen phase during aging. In this Research Topic, Suo et al. identified that different levels of Vitamin A have different roles in regulating hair cycling. High-level of dietary retinyl esters results in a greater percentage of hair follicles in refractory telogen, and vice versa (Suo et al., 2021). They showed that Vitamin A regulates hair follicle stem cell activity through BMP and Wnt signaling pathways. This study identified a new intrinsic factor that regulates hair follicle stem cell activity. Two reviews summarized the recent progress on how intrinsic and extrinsic factors modulate hair follicle stem cells activities. Daszczuk et al. discussed the current views on the intrinsic molecular mechanisms that regulate cyclic hair regeneration (Daszczuk et al., 2020). They proposed an intrinsic oscillation of gene networks model in control of hair cycling, which has potential instruction for translational regenerative medicine. Morgun and Vorotelyak reviewed how inflammation as one of the extrinsic factors that regulates hair cycling, re-epithelialization, and wound-induced hair neogenesis (Morgun and Vorotelyak, 2020). They also discussed how inflammation influences hair follicle stem cell activation during wound healing at the cellular and molecular levels. These two reviews developed further the concept that synergistic action of intrinsic and extrinsic factors is essential for proper hair regeneration.

Dermal papilla (DP) is the signaling center for regulating hair growth and regeneration. In this Research Topic, comparative transcriptome analyses by Weber et al. identified a Wnt agonist, R-spondin-1, is significantly decreased in the DP of adult human hair follicles compared to that of the fetal scalp hair follicles (Weber et al., 2020). Adult cells which lose the regenerative ability can be partially restored to regenerate hair follicles with addition of R-spondin-1 recombinant protein. Another research by Yu et al. showed that Twist1 functions on regulating hair follicle induction ability in the DP by forming a ternary complex with Tcf4 and b-catenin, which delays the aging process of the DP cells by Tcf4-mediated Wnt/b-catenin signaling pathway (Yu et al., 2020). Under pathological conditions such as androgenetic alopecia (AGA) which is occurring in more than half of men aged over 50 years old, hair follicles are attacked by dihydrotestosterone and then become miniaturized. Liu et al. identified that Zyxin, an actin-interacting protein, is increased in the DP of AGA-affected frontal hair follicles compared to that of the unaffected occipital hair follicles (Liu et al., 2020). Knockout of Zyxin leads to enhanced hair growth and anagen reentry, indicating that Zyxin is an inhibitor for hair regeneration. This offers a potential therapeutic target for treating AGA.

As skin is located at the outmost of our body, it is vulnerable to be injured by mechanical, chemical, or biological insults. Research conducted by Yang et al. used a promising new method called photodynamic therapy to treat mouse skin wounds infected with *Pseudomonas aeruginosa* (Yang et al., 2020). They showed that 5-aminolevulinic acid photodynamic therapy is beneficial for eliminating *Pseudomonas aeruginosa* and accelerating skin wound healing in mice, by modulating the expression of inflammatory factors (TNF-a and IL-1b) and growth factors (TGF-b1 and VEGF). Since the establishment of the wound-induced hair neogenesis model by Ito et al., in 2007 (Chuong, 2007; Ito et al., 2007), a number of following studies aimed to study the molecular mechanisms by which *de novo* hairs regenerate at the center of the wound bed during healing of large cutaneous wounds. Bhoopalam in this Research Topic reviewed the recent progress in digging the underpinnings of wound-induced hair neogenesis, at the cellular (hair follicle stem cells, fibroblasts, inflammatory cells) and molecular (Wnt/b-catenin, Hedgehog, dsRNA/IL-6/STAT3/Retinoic Acid, Hippo signaling pathways) levels (Bhoopalam et al., 2020). They also proposed several wonderful interesting questions that remain to be further investigated in this field. Besides, this issue also included one research paper which identified IL-36a as a new factor modulating the outcome of wound-induced hair neogenesis (Gong et al., 2020). They show that IL-36a is increased during wound healing, and application of recombinant murine IL-36a protein into large skin wound promotes wound-induced hair neogenesis, probably through regulating the IL-6/STAT3 pathway.

Scientists also have been trying to restore hair regeneration using *in vitro* culture models, with focuses on modulating hair follicle stem cells and DP cells. Bak et al. in this Research Topic transplanted the cultured human outer root sheath (ORS) cells along with freshly isolated neonatal mouse dermal cells to the nude mice, and observed that the long-term (42 days) cultured ORS cells have a decreased trichogenicity compared to the short-term (20 days) cultured ORS cells (Bak et al., 2020). They identified that FOXA2 in ORS cells functions in regulating the

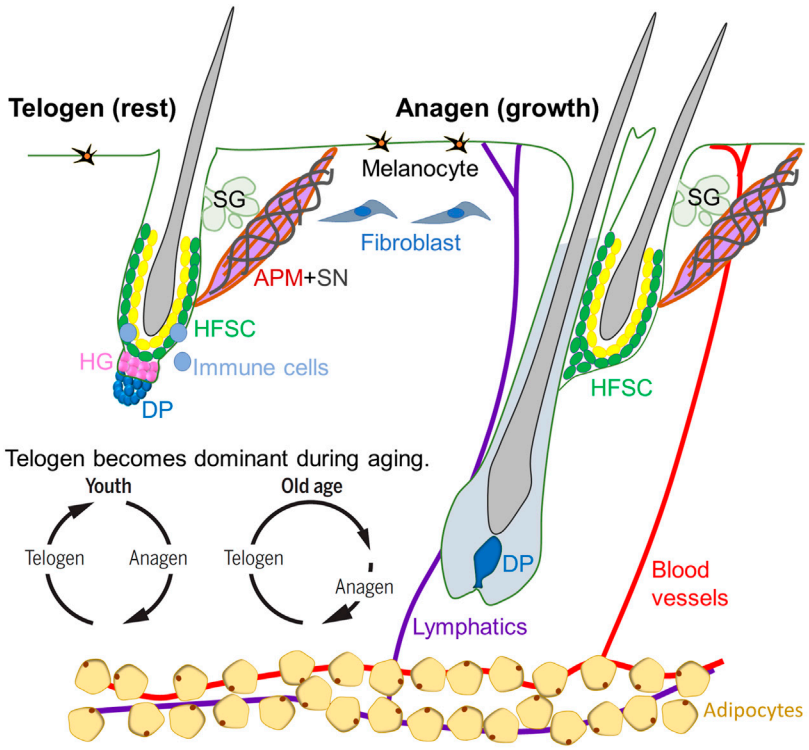

Stem cell	Niche	Environment
(Daszczuk et al., 2020; Suo et al., 2021)	(Liu et al., 2020; Morgun and Vorotelyak, 2020; Weber et al., 2020; Yu et al., 2020)	(Wang et al., 2020; Bai et al., 2021; Harn et al., 2021; Karisma et al., 2021)
WIHN	**Culture model**	
(Bhoopalam et al., 2020; Gong et al., 2020; Yang et al., 2020)	(Bak et al., 2020; Chen et al., 2020; Jang et al., 2020; Qiu et al., 2020; Fukuyama et al., 2021; Wen et al., 2021; Zhang et al., 2021b)	

FIGURE 1 | Hair follicle stem cell regeneration in aging. Hair follicle undergoes cyclic renewal, which is regulated by cyclic activation of quiescent stem cells controlled by a core circuit involving beta-catenin. This core molecular circuit involves interactions between hair follicle stem cell (HFSC) and dermal papilla within the hair follicle. Adjacent to the follicles, blood vessels, nerves, arrector pili muscle, intradermal adipose tissues, etc. form a larger niche that also can affect HFSC activation. Further, outside environment can also modulate the cyclic renewal behavior of hair follicles. The effects of these modulators change during aging. The telogen phase of the hair cycle becomes dominant during aging, leading to decreased hair regeneration. Aged cells can be reactivated to regenerate hair follicles under wound-induced hair neogenesis condition or using several 2D or 3D culture models. APM, arrector pili muscle; DP, dermal papilla; HFSC, hair follicle stem cells; HG, hair germ; SG, sebaceous gland; SN, sympathetic nerve.

trichogenicity of human ORS cells. Wen et al. revealed that inhibition of Rho-Associated Protein Kinase by a specific inhibitor Y-27632 can increase the adhesion, proliferation, and stemness of the primary cultured human hair follicle stem cells through the ERK/MAPK pathway (Wen et al., 2021). As two-dimensional (2D) cultured cells quickly lose their regenerative ability, most researches turned to modulate hair regeneration under 3D culture conditions. Zhang et al. compared the gene expression in 2D and 3D cultured DP cells treated with dihydrotestosterone, which can inhibit proliferation but induce apoptosis in DP cells co-cultured with ORS cells (Zhang Y. et al., 2021). Without dihydrotestosterone treatment, the ORS cells showed significant proliferation when co-cultured with DP cells. They used RNA-sequencing to identify that extracellular matrix synthesis is increased in 3D culture DP cells, and set up a transcription factor–miRNA coregulatory network in this co-culture system, which may be beneficial for future AGA studies at the molecular level. In addition to the extracellular matrix, the same group also identified that miR-140-5p in small extracellular vesicles secreted by DP cells suppresses Bmp2 expression to promote proliferation of ORS and hair matrix cells in a co-culture model (Chen et al., 2020). Tissue engineering models have been established to promote hair follicle neogenesis. One research article by Fukuyama et al. set up a reconstitution assay, in which

human-induced pluripotent stem cell-derived DP cell aggregates were co-cultured with human keratinocytes in a 3D cylindrical structure inserted with a fragment of guide nylon fiber (a mimic hair fiber). They observed morphologically resembled hair follicle structure that expresses hair follicle-related genes in the 2-week culture (Fukuyama et al., 2021). This study adds a new tissue engineering model for hair regeneration, based on the principle of epithelial-mesenchymal interaction.

In vitro culture models have been established for drug screening. Jang et al. set up a 3D co-culture system, in which human DP cells and ORS cells were cultured in an ultra-low attachment plate, and formed a "two-cell assemblage" structure that can be used as a model to test the hair growth-promoting effect of library molecules (Jang et al., 2020). Epithelial-mesenchymal interaction also leads to the formation of a skin cyst when mouse epidermal and dermal cells were mixed and 3-dimensionally cultured on a transwell insert, namely organoid culture (Lei et al., 2017). The dissociated single cells can self-organize and undergo a series of morphological transitions, forming a planar hair-bearing skin through aggregation, polarization, coalescence, and planarization stages. Compared to the clinically diagnosed skin cyst, we proposed that the skin cyst forming during skin organoid culture is not a pathological dead-end, but harbors the potential to regenerate skin appendages such as hair follicle and sebaceous gland (Qiu et al., 2020).

In conclusion, recent understanding of aging includes stem cell exhaustion, cellular senescence, altered intercellular communication, epigenetic alterations, genomic instability, telomere attrition, loss of proteostasis, deregulated nutrient sensing, mitochondrial dysfunction, environmental stresses, etc. These changes lead to obvious features in the skin such as hair loss and graying, skin wrinkling, age spots, loss of elasticity, laxity, sagging, and rough-textured appearance (Harn et al., 2021). The experimental discoveries and perspectives presented in this Research Topic add new layers for understanding hair follicle stem cell regeneration during aging. With cutting-edge experimental methodologies and ever-increasing cross-discipline approaches employed in this Research Topic, we witness the robust progress in this field. We hope this Research Topic will pave new ways for elucidating new mechanisms of aging-related hair follicle stem cell regeneration, and also inspire the development of new therapeutic strategies for treating aging-related hair disorders with this momentum.

AUTHOR CONTRIBUTIONS

All authors listed have made substantial contributions to the Research Topic, and approved it for publication.

FUNDING

ML is supported by National Natural Science Foundation of China (82003384), Fundamental Research Funds for the Central Universities (2020CDJYGSG003), Chongqing Talents: Exceptional Young Talents Project (cstc2021ycjh-bgzxm0197), and Scientific Research Foundation from Chongqing University (02210011044110), China. S-JL is supported by Taiwan National Health Research Institutes (NHRI-EX110-10811EI), Taiwan Ministry of Science and Technology (110-2314-B-002-190-MY3) and National Taiwan University Hospital (111IF0006, 110-S5094). C-MC is supported by NIH R01 AR047364, AR060306, and GM125322.

REFERENCES

Bai, G.-L., Wang, P., Huang, X., Wang, Z.-Y., Cao, D., Liu, C., et al. (2021). Rapamycin Protects Skin Fibroblasts from UVA-Induced Photoaging by Inhibition of P53 and Phosphorylated HSP27. *Front. Cel Dev. Biol.* 9, 633331. doi:10.3389/fcell.2021.633331

Bak, S.-S., Park, J. M., Oh, J. W., Kim, J. C., Kim, M. K., and Sung, Y. K. (2020). Knockdown of FOXA2 Impairs Hair-Inductive Activity of Cultured Human Follicular Keratinocytes. *Front. Cel Dev. Biol.* 8, 575382. doi:10.3389/fcell.2020.575382

Bhoopalam, M., Garza, L. A., and Reddy, S. K. (2020). Wound Induced Hair Neogenesis - A Novel Paradigm for Studying Regeneration and Aging. *Front. Cel Dev. Biol.* 8, 582346. doi:10.3389/fcell.2020.582346

Chen, C.-C., Murray, P. J., Jiang, T. X., Plikus, M. V., Chang, Y.-T., Lee, O. K., et al. (2014). Regenerative Hair Waves in Aging Mice and Extra-follicular Modulators Follistatin, Dkk1, and Sfrp4. *J. Invest. Dermatol.* 134 (8), 2086–2096. doi:10.1038/jid.2014.139

Chen, Y., Huang, J., Liu, Z., Chen, R., Fu, D., Yang, L., et al. (2020). miR-140-5p in Small Extracellular Vesicles from Human Papilla Cells Stimulates Hair Growth by Promoting Proliferation of Outer Root Sheath and Hair Matrix Cells. *Front. Cel Dev. Biol.* 8, 593638. doi:10.3389/fcell.2020.593638

Chuong, C.-M. (2007). New Hair from Healing Wounds. *Nature* 447 (7142), 265–266. doi:10.1038/447265a

Daszczuk, P., Mazurek, P., Pieczonka, T. D., Olczak, A., Boryń, Ł. M., and Kobielak, K. (2020). An Intrinsic Oscillation of Gene Networks inside Hair Follicle Stem Cells: An Additional Layer that Can Modulate Hair Stem Cell Activities. *Front. Cel Dev. Biol.* 8, 595178. doi:10.3389/fcell.2020.595178

Fukuyama, M., Tsukashima, A., Kimishima, M., Yamazaki, Y., Okano, H., and Ohyama, M. (2021). Human iPS Cell-Derived Cell Aggregates Exhibited Dermal Papilla Cell Properties in In Vitro Three-Dimensional Assemblage Mimicking Hair Follicle Structures. *Front. Cel Dev. Biol.* 9, 590333. doi:10.3389/fcell.2021.590333

Gong, L., Xiao, J., Li, X., Li, Y., Gao, X., and Xu, X. (2020). IL-36α Promoted Wound Induced Hair Follicle Neogenesis via Hair Follicle Stem/Progenitor Cell Proliferation. *Front. Cel Dev. Biol.* 8, 627. doi:10.3389/fcell.2020.00627

Harn, H. I.-C., Chen, C.-C., Wang, S.-P., Lei, M., and Chuong, C.-M. (2021). Tissue Mechanics in Haired Murine Skin: Potential Implications for Skin Aging. *Front. Cel Dev. Biol.* 9, 635340. doi:10.3389/fcell.2021.635340

Ito, M., Yang, Z., Andl, T., Cui, C., Kim, N., Millar, S. E., et al. (2007). Wnt-dependent De Novo Hair Follicle Regeneration in Adult Mouse Skin After Wounding. *Nature* 447 (7142), 316–320. doi:10.1038/nature05766

Jang, S., Ohn, J., Kang, B. M., Park, M., Kim, K. H., and Kwon, O. (2020). "Two-Cell Assemblage" Assay: A Simple In Vitro Method for Screening Hair Growth-Promoting Compounds. *Front. Cel Dev. Biol.* 8, 581528. doi:10.3389/fcell.2020.581528

Karisma, V. W., Wu, W., Lei, M., Liu, H., Nisar, M. F., Lloyd, M. D., et al. (2021). UVA-triggered Drug Release and Photo-Protection of Skin. *Front. Cel Dev. Biol.* 9, 598717. doi:10.3389/fcell.2021.598717

Lei, M., and Chuong, C.-M. (2016). Aging, Alopecia, and Stem Cells. *Science* 351 (6273), 559–560. doi:10.1126/science.aaf1635

Lei, M., Schumacher, L. J., Lai, Y.-C., Juan, W.-T., Yeh, C.-Y., Wu, P., et al. (2017). Self-organization Process in Newborn Skin Organoid Formation Inspires Strategy to Restore Hair Regeneration of Adult Cells. *Proc. Natl. Acad. Sci. USA* 114 (34), E7101–E7110. doi:10.1073/pnas.1700475114

Liu, Q., Shi, X., Zhang, Y., Huang, Y., Yang, K., Tang, Y., et al. (2020). Increased Expression of Zyxin and its Potential Function in Androgenetic Alopecia. *Front. Cel Dev. Biol.* 8, 582282. doi:10.3389/fcell.2020.582282

Matsumura, H., Mohri, Y., Binh, N. T., Morinaga, H., Fukuda, M., Ito, M., et al. (2016). Hair Follicle Aging Is Driven by Transepidermal Elimination of Stem Cells via COL17A1 Proteolysis. *Science* 351 (6273), aad4395. doi:10.1126/science.aad4395

Morgun, E. I., and Vorotelyak, E. A. (2020). Epidermal Stem Cells in Hair Follicle Cycling and Skin Regeneration: A View from the Perspective of Inflammation. *Front. Cel Dev. Biol.* 8, 581697. doi:10.3389/fcell.2020.581697

Qiu, W., Chuong, C. M., and Lei, M. (2019). Regulation of Melanocyte Stem Cells in the Pigmentation of Skin and its Appendages: Biological Patterning and Therapeutic Potentials. *Exp. Dermatol.* 28 (4), 395–405. doi:10.1111/exd.13856

Qiu, W., Gu, P.-R., Chuong, C.-M., and Lei, M. (2020). Skin Cyst: A Pathological Dead-End with a New Twist of Morphogenetic Potentials in Organoid Cultures. *Front. Cel Dev. Biol.* 8, 628114. doi:10.3389/fcell.2020.628114

Suo, L., VanBuren, C., Hovland, E. D., Kedishvili, N. Y., Sundberg, J. P., and Everts, H. B. (2021). Dietary Vitamin A Impacts Refractory Telogen. *Front. Cel Dev. Biol.* 9, 571474. doi:10.3389/fcell.2021.571474

Wang, B., Yan, S., Yi, Y., Huang, Y., Deng, Z., Zhang, Y., et al. (2020). Purified Vitexin Compound 1 Inhibits UVA-Induced Cellular Senescence in Human Dermal Fibroblasts by Binding Mitogen-Activated Protein Kinase 1. *Front. Cel Dev. Biol.* 8, 691. doi:10.3389/fcell.2020.00691

Weber, E. L., Lai, Y.-C., Lei, M., Jiang, T.-X., and Chuong, C.-M. (2020). Human Fetal Scalp Dermal Papilla Enriched Genes and the Role of R-Spondin-1 in the Restoration of Hair Neogenesis in Adult Mouse Cells. *Front. Cel Dev. Biol.* 8, 583434. doi:10.3389/fcell.2020.583434

Wen, L., Miao, Y., Fan, Z., Zhang, J., Guo, Y., Dai, D., et al. (2021). Establishment of an Efficient Primary Culture System for Human Hair Follicle Stem Cells Using the Rho-Associated Protein Kinase Inhibitor Y-27632. *Front. Cel Dev. Biol.* 9, 632882. doi:10.3389/fcell.2021.632882

Yang, T., Tan, Y., Zhang, W., Yang, W., Luo, J., Chen, L., et al. (2020). Effects of ALA-PDT on the Healing of Mouse Skin Wounds Infected with *Pseudomonas aeruginosa* and its Related Mechanisms. *Front. Cel Dev. Biol.* 8, 585132. doi:10.3389/fcell.2020.585132

Yu, N., Hu, T., Yang, H., Zhang, L., Song, Q., Xiang, F., et al. (2020). Twist1 Contributes to the Maintenance of Some Biological Properties of Dermal Papilla Cells In Vitro by Forming a Complex with Tcf4 and β-Catenin. *Front. Cel Dev. Biol.* 8, 824. doi:10.3389/fcell.2020.00824

Zhang, C., Wang, D., Wang, J., Wang, L., Qiu, W., Kume, T., et al. (2021). Escape of Hair Follicle Stem Cells Causes Stem Cell Exhaustion During Aging. *Nat. Aging* 1, 889–903. doi:10.1038/s43587-021-00103-w

Zhang, Y., Huang, J., Fu, D., Liu, Z., Wang, H., Wang, J., et al. (2021). Transcriptome Analysis Reveals an Inhibitory Effect of Dihydrotestosterone-Treated 2D- and 3D-Cultured Dermal Papilla Cells on Hair Follicle Growth. *Front. Cel Dev. Biol.* 9, 724310. doi:10.3389/fcell.2021.724310

Conflict of Interest: The authors declare that the research was conducted in the absence of any commercial or financial relationships that could be construed as a potential conflict of interest.

Publisher's Note: All claims expressed in this article are solely those of the authors and do not necessarily represent those of their affiliated organizations, or those of the publisher, the editors and the reviewers. Any product that may be evaluated in this article, or claim that may be made by its manufacturer, is not guaranteed or endorsed by the publisher.

Copyright © 2021 Lei, Lin and Chuong. This is an open-access article distributed under the terms of the Creative Commons Attribution License (CC BY). The use, distribution or reproduction in other forums is permitted, provided the original author(s) and the copyright owner(s) are credited and that the original publication in this journal is cited, in accordance with accepted academic practice. No use, distribution or reproduction is permitted which does not comply with these terms.

frontiers in Cell and Developmental Biology

ORIGINAL RESEARCH
published: 31 July 2020
doi: 10.3389/fcell.2020.00691

Purified Vitexin Compound 1 Inhibits UVA-Induced Cellular Senescence in Human Dermal Fibroblasts by Binding Mitogen-Activated Protein Kinase 1

Ben Wang[1,2†], Sha Yan[1,2†], Yuxin Yi[1], Yingxue Huang[1,2], Zhili Deng[1,2], Yiya Zhang[1,2], Qingchuan Zheng[3], Hongfu Xie[1,2] and Ji Li[1,2,4,5]**

[1] Department of Dermatology, Xiangya Hospital, Central South University, Changsha, China, [2] National Clinical Research Center for Geriatric Disorders, Xiangya Hospital, Central South University, Changsha, China, [3] Laboratory of Theoretical and Computational Chemistry, Institute of Theoretical Chemistry, Jilin University, Changchun, China, [4] Key Laboratory of Organ Injury, Aging and Regenerative Medicine of Hunan Province, Changsha, China, [5] Center for Molecular Medicine, Xiangya Hospital, Central South University, Changsha, China

OPEN ACCESS

Edited by:
Mingxing Lei,
Chongqing University, China

Reviewed by:
Xia Lei,
Army Medical University, China
Chih-Chiang Chen,
National Yang-Ming University, Taiwan

***Correspondence:**
Hongfu Xie
xiehongfu@csu.edu.cn
Ji Li
liji_xy@csu.edu.cn

† These authors have contributed equally to this work

Specialty section:
This article was submitted to Stem Cell Research, a section of the journal Frontiers in Cell and Developmental Biology

Received: 04 May 2020
Accepted: 07 July 2020
Published: 31 July 2020

Citation:
Wang B, Yan S, Yi Y, Huang Y, Deng Z, Zhang Y, Zheng Q, Xie H and Li J (2020) Purified Vitexin Compound 1 Inhibits UVA-Induced Cellular Senescence in Human Dermal Fibroblasts by Binding Mitogen-Activated Protein Kinase 1. Front. Cell Dev. Biol. 8:691. doi: 10.3389/fcell.2020.00691

Purified vitexin compound 1 (VB1), a novel lignanoid isolated from the seeds of the Chinese herb Vitex negundo, has strong antioxidant abilities and broad antitumor activities. However, little is known about its anti-photoaging effect on the skin and the underlying mechanism. Here, we demonstrated that VB1 significantly attenuates ultraviolet A (UVA)-induced senescence in human dermal fibroblasts (HDFs), as evidenced by senescence-associated β-gal staining, MTT assays, and western blot analysis of the expression of p16 and matrix metalloproteinase-1 (MMP-1). Furthermore, mass spectrometry revealed that VB1 could directly bind to Mitogen-Activated Protein Kinase 1 (MAPK1). Molecular docking and molecular dynamics simulation methods confirmed the mass spectroscopy results and predicted six possible binding amino acids of MAPK1 that most likely interacted with VB1. Subsequent immunoprecipitation analysis, including different MAPK1 mutants, revealed that VB1 directly interacted with the residues, glutamic acid 58 (E58) and arginine 65 (R65) of MAPK1, leading to the partial reversal of UVA-induced senescence in HEK293T cells. Finally, we demonstrated that the topical application of VB1 to the skin of mice significantly reduced photoaging phenotypes *in vivo*. Collectively, these data demonstrated that VB1 reduces UVA-induced senescence by targeting MAPK1 and alleviates skin photoaging in mice, suggesting that VB1 may be applicable for the prevention and treatment of skin photoaging.

Keywords: purified vitexin compound 1, VB1, senescence, skin photoaging, MAPK1

Abbreviations: ATRA, all-trans-retinoic acid; ERK1/2, Extracellular signal-regulated protein kinases1/2; FDA, Food and Drug Administration; HDFs, human dermal fibroblasts; JNK, c-Jun NH2-terminal kinase; MAPK1, Mitogen Activated Protein Kinase 1; MMP1, matrix metalloproteinase-1; p-MAPK1, Phosphorylated MAPK1; UVA, ultraviolet A; VB1, Purified vitexin compound 1.

INTRODUCTION

Chronic exposure to ultraviolet (UV) irradiation is the major cause of skin damage leading to premature aging of the skin, a condition called photoaging (Kruglikov and Scherer, 2016). Clinical changes in the course of skin photoaging include the formation of fine and coarse wrinkles, increased skin thickness, dryness, laxity, and pigmentation (Lei et al., 2018). Solar UV radiation is divided into three categories according to their wavelength. UV radiation can penetrate the skin to different extents and interact with skin cells (Bravo et al., 2017). UVA (320–400 nm) is more abundant in sunlight and penetrates the skin deeper than UVB (280–315 nm). Previous studies have revealed that UVA plays an important role in skin photoaging (Kammeyer and Luiten, 2015; Lei et al., 2018).

To date, the mechanisms of skin photoaging is still unknown, however, it is mainly associated with oxidative stress, inflammatory responses, and DNA damage (Shin et al., 2019). Oxidative stress can increase the secretion of proteases and produce a large number of oxidative intermediates due to an imbalance between the production of oxidants and antioxidants. Accumulation of reactive oxygen species (ROS) induced by oxidative stress can affect skin cells in both epidermis and dermis, promoting cellular senescence (Stellavato et al., 2018). Oxidative stress, one of the most important mechanisms underlying skin photoaging, activates the Mitogen Activated Protein Kinase (MAPK) family, including extracellular signal-regulated protein kinases1/2 (ERK 1/2), c-Jun NH2-terminal kinase (JNK or SAPK), and p38 MAPK, and their downstream pathways to promote cellular senescence (Sun et al., 2015). MAPK1, also called ERK2, is one of the key molecules in signal transduction pathways associated with cellular senescence and only functional when phosphorylated. Recent studies revealed that MAPK1 plays a major role in the unbalanced growth of human cells (Kobayashi et al., 2012). Vitamin D protects endothelial cells from irradiation-induced senescence and apoptosis by modulating the MAPK/Sirtuin 1 (SirT1) axis (Marampon et al., 2016). Naringenin exerts potent anti-photoaging effects by suppressing UVB-induced phosphorylated MAPK1 activity in JB6 P + cells, indicating that MAPK1 plays an important role in the cellular senescence (Jung et al., 2016). In addition, some other well-studied genes act as aging markers that are often studied: Meis1 is a putative regulators of neurotransmission and neurogenesis during aging (Chang-Panesso et al., 2018). Rb1, another aging marker, induces senescence in human skin fibroblasts by regulating by DNA methyltransferase 1 (DNMT1) (Wang et al., 2017).

Purified vitexin compound 1 (VB1), a novel lignanoid isolated from the seeds of the Chinese herb, *Vitex negundo*, has strong antioxidant abilities and broad antitumor activities in many cancer cell lines and xenograft models (Liu et al., 2018). VB1 suppresses the growth of melanoma cells and induces apoptosis in breast cancer cells by increasing the ROS level (Liu et al., 2014). However, VB1 failed to induce ROS generation in the immortalized non-cancerous breast cell line, indicating that it has different effects on oxidative stress processes depending on cellular conditions. In addition, VB-1 can exert hair growth-promoting effects by augmenting Wnt/β-catenin signaling in human dermal papilla cells and protect PC12 cells from hypoxia/reoxygenation-induced injury via NADPH oxidase inhibition (Yang et al., 2014; Luo et al., 2018). However, little is known about the role of VB1 in skin photoaging. Considering that oxidative stress is an important mechanism of skin photoaging, and VB1 an antioxidative agent, we speculated that VB1 may play an important role in skin photoaging.

In this study, we found that VB1 significantly inhibited UVA-induced senescence in human dermal fibroblasts (HDFs). Using mass spectrometry, we also revealed that VB1 could directly bind to MAPK1. Computer-aided methods and immunoprecipitation demonstrated that VB1 binds to MAPK1 in 293T cells by interacting with the residues E58 and R65. We further verified that VB1 partially reverses UVA-induced senescence by the above-mentioned binding to MAPK1. Finally, topical VB1 gel remarkably reduced the phenotype of skin photoaging in mice. For the first time, we demonstrate that VB1 reduces UVA-induced senescence in HDFs by targeting the residues E58 and R65 in MAPK1 and alleviates skin photoaging in mice. Our results indicate that VB1 is a potential new drug for the prevention and treatment of skin photoaging in the future.

MATERIALS AND METHODS

Reagents

VB1 [vitexin compound-1, 6-hydroxy-4-(4-hydroxy-3-methoxyphenyl)-3-hydroxymethyl-7-methoxy-3,4-dihydro-2-naphthaldehyde] was a kind gift from the School of Pharmacy at Central South University (Changsha, Hunan, China). The gel containing 2% VB1 or the vehicle gel lacking VB1 were also given from the School of Pharmacy at Central South University. Primary antibodies specific for human against MMP-1, p16, MAPK1, and p-MAPK1 were purchased from Cell Signaling Technology (Boston, MA, United States).

Cell Culture

Primary HDFs were isolated from circumcised foreskins of healthy human donors aged from 5 to 12 years. Primary HDFs were cultured at 37°C and 5% CO_2 in a humidified incubator in Dulbecco's modified Eagle media (DMEM; Gibco, Grand Island, NY, United States), supplemented with penicillin (100 U/mL), streptomycin (100 ng/mL), and 10% fetal bovine serum (FBS; Gibco). Primary HDFs were obtained with written consent from voluntary, informed donors, following a protocol approved by the Clinical Research Ethics Committee at the Xiangya Hospital of Central South University in Changsha, China.

UVA Irradiation

Before UVA irradiation, HDFs cells were rinsed and submerged under a thin layer of PBS to prevent UVA absorption by components of the medium, such as VB1. Cells were then irradiated using a Philips UVA lamp with an emission spectrum between 320 and 400 nm. Mock-irradiated cells were manipulated identically, except that they were not exposed to UVA. The dose of UVA irradiation was 10 J/cm^2 per day, as

verified with a UV light meter (Sigma, Shanghai, China) for 3 days. Following each UVA irradiation, cells were incubated in complete medium, supplemented with indicated compounds.

Western Blotting

Thirty micrograms of protein from each cell lysate was resolved by 10% SDS-PAGE, followed by electrotransfer to PVDF membranes (Millipore, MA, United States). Blots were probed with primary antibodies at 4°C overnight, followed by incubation with an HRP-conjugated secondary antibody for 1 h at room temperature. Bands of interest in western blots were visualized with a western blot HRP substrate (Millipore, Billerica, MA, United States).

SA β-Gal Staining

Senescence-associated β-galactosidase (SA-β-gal) activity was measured with a β-galactosidase staining kit (Cell Signaling Technology Boston, MA, United States) according to the manufacturer's instructions. Briefly, cells were washed in PBS, fixed at room temperature for 15 min in fixing solution, and incubated overnight at 37°C in staining solution. Relative SA-β-gal activities under each studied condition were determined by calculating the percentages of cells with SA-β-gal activity out of all cells counted in four continuous visual fields under a microscope (200x).

MTT Assays

Cell viabilities were determined by performing 3-(4,5-dimethylthiazol-2-yl)-2,5 -diphenyltetrazoliumbromide (MTT) assays. Briefly, cells were seeded into 96-well plates at a density of 2,000 cells/well. After adhesion, cells were exposed to UVA irradiation and grown in complete medium containing VB1 (0.6 μM). At 1, 3, or 5 days post-irradiation, the medium was aspirated, and cells were incubated for 4 h in fresh medium containing 0.5 mg/mL of MTT (Sigma, St. Louis, MO, United States). Subsequently, the medium was removed and purple formazan crystals were dissolved in DMSO (150 μl/well) with a brief vortexing step. Absorbance at 570 nm was measured using a Synergy 2 Multi-Mode Microplate Reader (BioTek, Seattle, United States). All experiments were performed in triplicate, and the data presented represent the means of 3 independent experiments ± SD.

Molecular Docking and Molecular Dynamics Simulation

The crystal structure of the wild type MAPK1 protein was obtained from Protein Data Bank (PDB code: 5BVF) (Bagdanoff et al., 2015). The missing residues and atoms were repaired by software Discovery Studio 2.5 (BIOVIA, CA, United States). The MAPK1-VB1 binding site was predicted by Discovery Studio 2.5 and Autodock Vina (Trott and Olson, 2010). The molecular docking study was performed employing the program Autodock Vina. And the Molecular dynamics (MD) simulations were performed to explore the binding details base the docking results. The partial atomic charge of VB1 was assigned by AM1-BCC method (Wang et al., 2006) and the topology files of VB1 were generated by AMBER force field (GAFF) (Wang et al., 2004). The protonation states of ionizable residues were determined at pH = 7.0 using H++ server (Gordon et al., 2005). The MD simulations were carried out using the AMBER 16 software package (Alma Rosa Agorilla, University of California, San Francisco, United States). First, 10,000 steps minimization (4,000 steps of steepest decent followed by 6,000 steps of conjugate gradient) was carried out with protein and inhibitor constrained (100 kcal mol-1 Å-2). Subsequently, the minimization was repeated with no constrain. Then, the system was gradually heated from 0 to 310 K over a period of 300 ps with 5.0 kcal mol-1 Å-2 restrain on the solute. Thereafter, another 1 ns equilibrium simulation was followed at 310 K with 2.0 kcal mol-1 Å-2 restrain on the solute. Finally, 100 ns MD simulation was performed for each system under NPT condition to produce trajectory. The time step was set to 2 fs.

Synthesis and Modification of Gold Nanoparticles

Gold nanoparticles were synthesized according to following procedures. Briefly, 3 mL sodium citrate (w/v, 2%) was added to 100 mL boiling HAuCl4 (0.01%) solution and kept heated for 10 min. With continuous stirring until cooled to room temperature, the gold nanoparticles were synthesized. To conjugate lignin onto gold nanoparticles, cysteamine was first linked onto gold nanoparticles through the thiol group on the cysteamine to introduce amino group onto gold nanoparticles. Cysteamine was added into gold nanoparticles (final concentration of cysteamine is 10 M) and reacted for 2 h. After centrifuge, the gold nanoparticles were reacted with 1-(3-Dimethylaminopropyl)-3-ethylcarbodiimide hydrochloride (EDC, 100 mM) and N-hydroxysuccinimide (NHS, 100 mM) for 30 min. Then, lignin was added into the solution to reach a concentration of 10 g/mL. After another 2 h of reaction, the gold nanoparticles were centrifuged and re-dispersed into water for further use.

HPLC – Mass Spectrometry Analysis

Each sample of enriched nanogold-VB1 compound was reconstituted in 7 μl of HPLC buffer A (0.1%(v/v) formic acid in water), and 5 μl was injected into a Nano-LC system (EASY-nLC 1000, Thermo Fisher Scientific, Waltham, MA, United States). Each sample was separated by a C18 column (50 μm inner-diameter × 15 cm, 2 μm C18) with a 125 min HPLC-gradient. The mass spectrometric analysis was carried out in a data-dependent mode with an automatic switch between a full MS scan and an MS/MS scan in the orbitrap. The resulting MS/MS data were searched against UniProt P. mirabilis ATCC 29906 database using MaxQuant software (v1.5.2.8).

Generation of MAPK1 Mutants

The plasmid MAPK1-pENTER was purchased from vigenebio (Shandong, China). Mutants of MAPK1 were generated with a QuickChange II XL Site-Directed Mutagenesis Kit (Agilent Technologies, Palo Alto, CA, United States) according to the

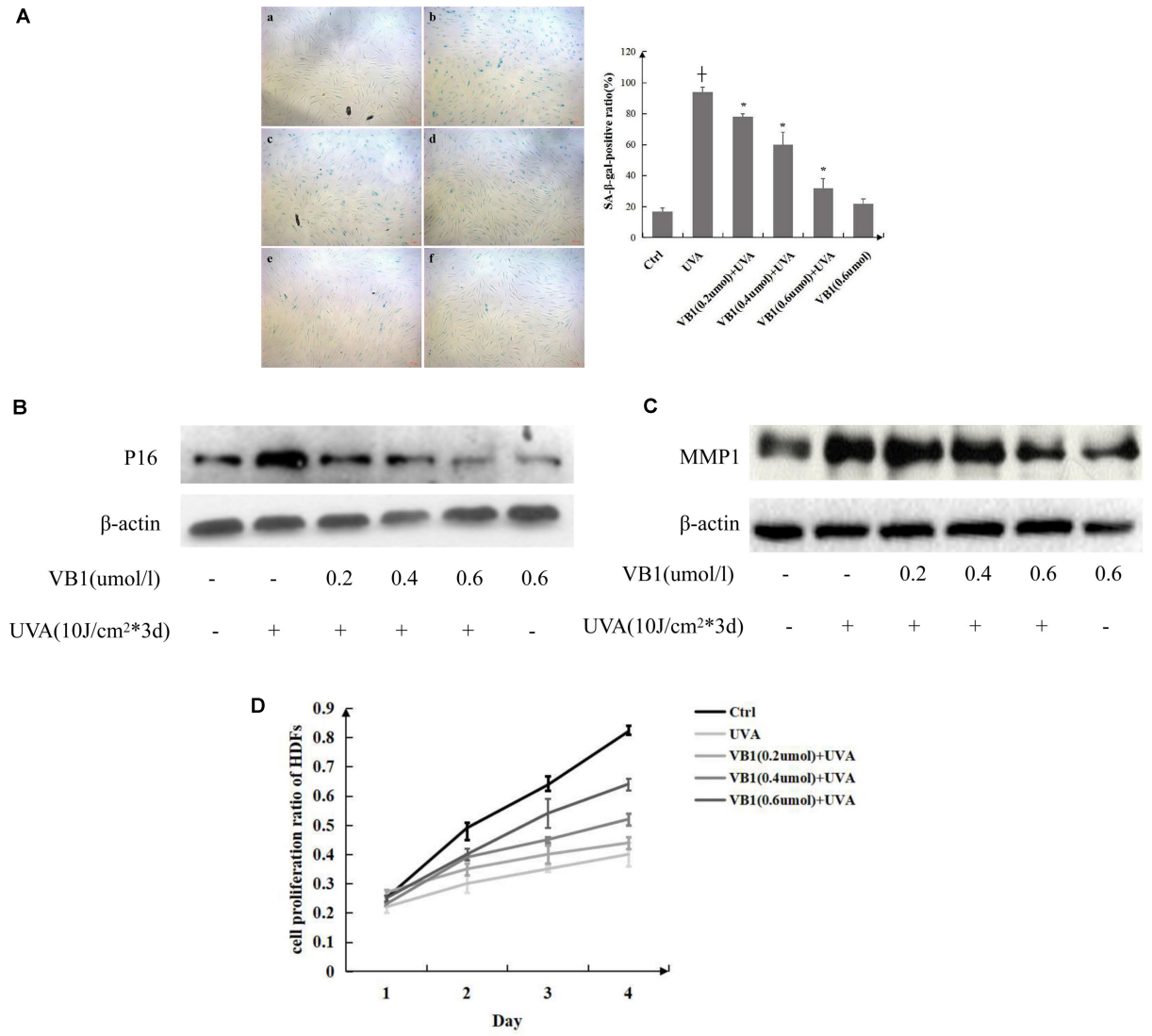

FIGURE 1 | VB1 protects HDFs from UVA-induced senescence. **(A)** HDFs senescence was evaluated by measuring the number of SA-β-gal-positive cells (left panel) [a, Ctrl; b, UVA; c, VB1 (0.2 μmol/l) + UVA; d, VB1 (0.4 μmol/l) + UVA; e, VB1 (0.6 μmol/l) + UVA; f, VB1 (0.6 μmol/l)]. Percentages of SA-β-gal-positive cells were determined by counting stained cells and total cells in four continuous visual fields under a microscope (200x). The SA-β-gal-positive rate was obviously enhanced in UVA-induced HDFs, while VB1 inhibited UVA-induced SA-β-gal activity in a dose-dependent manner. The analysis data was shown in right panel. Data are presented as mean HDFs ± SD ($n = 3$; + vs. ctrl, $p < 0.05$, * vs UVA, $p < 0.05$). **(B)** p16 levels were detected by western blot analysis. Cells were irradiated as described and harvested 24 h after the final UVA exposure. Blots were probed to detect p16, stripped, and then reprobed for β-actin. VB1 inhibited UVA-induced p16 expression in a dose-dependent manner. Images are representative of 3 independent experiments. **(C)** MMP1 levels were detected by western blot analysis. VB1 inhibited UVA-induced MMP1 expression in a dose-dependent manner. Images are representative of 3 independent experiments. **(D)** The HDFs growth rate was determined by performing MTT assays. The growth rate of UVA-exposed HDFs was significantly decreased compared with control HSFs, while VB1 could reverse the decrease ($n = 3$ for each time point).

manufacturer's instructions. The primers used for the Mutants were used were shown in **Supplementary Table 1**.

Immunoprecipitation

HEK293 cells were transfected with MAPK1 or mut-MAPK1. The cells were collected and washed with ice-cold PBS and lysed in buffer, and the VB1 modified by gold nanoparticles was added and incubation continued overnight at 4°C. Precipitates were washed three times with ice-cold lysis buffer at 400 g for 10 min. Bound proteins were separated on an SDS – polyacrylamide gel and analyzed by western blotting using the anti-MAPK1 antibodies.

Animals and UVA Radiation

Eight-week-old female FVB mice were obtained from the National Key Laboratory of Genetics (Changsha, Hunan, China). Animals were housed at 23 ± 1°C and 50 ± 10% relative humidity in a specific pathogen-free environment. Animal experiments

were approved by the Animal Research Committee at the Xiang Ya Hospital of Central South University. The dorsal skin area of mice was shaved before and during experiments. Mice were divided into control, UVA,vehicle gel and VB1 groups, with 10 mice in each group. All Mice except control group were irradiated 3 times/week for 12 weeks with 20 J/cm^2 doses under a Philips UVA lamp placed 20 cm away (emission spectrum: 320–400 nm). The dorsal skin of mice was washed with 75% ethanol before each irradiation exposure to avoid blocking or absorption of UVA rays by previous applications of the VB1 gel. UVA doses were verified with a UV light meter. A Carbomer substrate gel containing 2% VB1 or vehicle gel lacking VB1 was applied dorsally to the mice accordingly every day. No topical application or irradiation was performed in the control group.

Histological Analysis

Mice were sacrificed by cervical dislocation under chloral hydrate anesthesia at the end of experiments. For histological analyses, central dorsum skin specimens were fixed in 4% paraformaldehyde and sectioned after paraffin embedding. Hematoxylin-eosin staining and Masson-trichrome staining was then performed. Photographs of 5 randomly-chosen fields in each section were taken under a microscope (200x). Epidermal thicknesses were measured as the distance from the basement membrane to the bottom of the stratum corneum.

Statistical Analysis

All data presented are representative of at least 3 independent experiments and are expressed as means ± SD. Statistical significances were determined by a one-way analysis of variance, followed by further analysis by the LSD (least significant difference) test. $P < 0.05$ was considered statistically significant.

TABLE 1 | The 26 possible target proteins of VB1.

The abbreviation of proteins	Proteins full names
MPRIP	Myosin phosphatase Rho-interacting protein
FLII	Flightless-1 homolog
ANPEP	Alanyl aminopeptidase
FLOT2	Flotillin 2
SERPINH1	Serpin family H member 1
ARHGAP23	Rho GTPase-activating protein 23
EIF2S1	Eukaryotic translation initiation factor 2 subunit 1
TWF1	Twinfilin actin binding protein 1
NPM1	Nucleophosmin 1
EEF1A	Elongation factor 1-alpha
ATP6V0D1	ATPase H^+ transporting V0 subunit d1
HNRNPA3	Heterogeneous nuclear ribonucleoprotein A3
TPM1	Tropomyosin 1
NEFH	Neurofilament heavy polypeptide
MAPK1	Mitogen-activated protein kinase 1
CAPZB	Capping actin protein of muscle Z-line subunit beta
YWHAQ	Tyrosine 3-monooxygenase/tryptophan 5-monooxygenase activation protein theta
YWHAZ	Tyrosine 3-monooxygenase/tryptophan 5-monooxygenase activation protein zeta
ZNF366	Zinc finger protein 366
SLC25A1	Solute carrier family 25 member 1
DPM1	Dolichol-phosphate mannosyltransferase1
SLC25A5	Solute carrier family 25 member 5
DEDD	Death effector domain-containing protein
DECR1	2,4-dienoyl-CoA reductase 1
ZYG11B	Zyg-11 family member B
THY1	Thy-1 membrane glycoprotein

RESULTS

VB1 Protects HDFs From UVA-Induced Senescence

SA-β-gal activity was measured in HDFs to investigate the effects of VB1 on cellular senescence induced by UVA. Our results showed that the percentage of senescent cells (SA-β-gal-positive cells) was significantly increased in UVA-irradiated HDFs compared with that in non-irradiated control cells. VB1 inhibited UVA-induced SA-β-gal activity in a dose-dependent manner (**Figure 1A**). Additionally, we found that the expression of p16, a hallmark of cellular senescence, was significantly increased after UVA irradiation and that VB1 showed dose-dependent inhibition of p16 expression (**Figure 1B**). Previous studies have shown that UVA irradiation causes photoaging through MMP-1 induction, and MMP1 was also considered as an indicator of senescence-Associated Secretory Phenotype (Gorgoulis et al., 2019). Thus, MMP-1 expression was analyzed by western blotting to examine whether VB1 regulates its expression following UVA exposure. The results confirmed that UVA irradiation increased MMP-1 protein expression in HDFs, however, the UVA-induced induction of MMP-1 expression was inhibited by VB1 in a dose-dependent manner (**Figure 1C**). By MTT assays, we showed that UVA irradiation decreased the cell proliferation of HDFs and that VB1 treatment partially reversed this UVA-induced effect (**Figure 1D**). These data indicated that VB1 partially protected HDFs from UVA-induced senescence.

Potential Target Proteins and Target Sites of VB1 for MAPK1

To screen the potential binding target proteins of VB1, we used mass spectrometry. For this purpose, VB1 was linked to modified gold nanoparticles (**Figure 2**). **Table 1** shows the potential target proteins of VB1 identified by mass spectrometry. Based on previous research on senescence, we chose MAPK1 as the target protein of VB1 for further experiments. To accurately predict the possible target sites of VB1 for MAPK1, we employed computer-aided methods, including molecular docking and molecular dynamics simulation were employed. The *in silico* results showed that VB1 could directly bind MAPK1 (**Figure 3A**), and we finally predicted that five likely interacting amino acid residues (G32, Y34, K46, E58, and R65) of MAPK1 (**Figure 3B**), and K338 was another possible key residue.

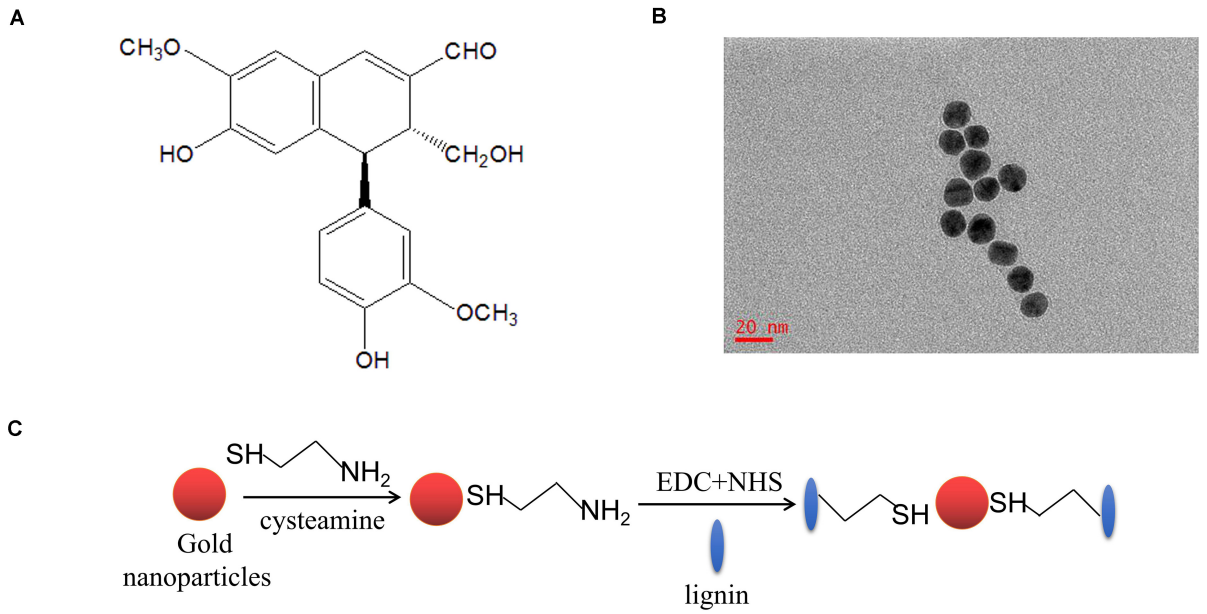

FIGURE 2 | VB1 is linked with modified gold nanoparticles for further HPLC and immunoprecipitation. **(A)** The chemical structure diagram of VB1. **(B)** The gold nanoparticles were synthesized and shown in the transmission electron microscope (TEM) image. **(C)** Gold nanoparticles was modified by lignin via reacting with 1-(3-Dimethylaminopropyl)-3-ethylcarbodiimide hydrochloride (EDC, 100 mM) and N-hydroxysuccinimide (NHS, 100 mM).

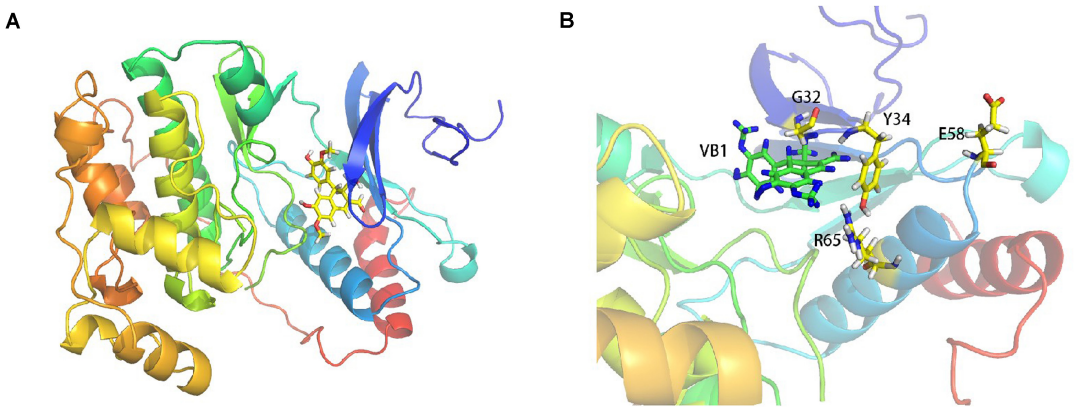

FIGURE 3 | The possible target sites of MAPK1 binding VB1 are predicted by computer-aided methods including molecular docking and molecular dynamics simulation. The MAPK1-VB1 binding site was predicted by Discovery Studio 2.5 and Autodock Vina. The molecular docking study and the Molecular dynamics (MD) simulations were performed to explore the binding details base the docking results. **(A)** The molecular docking and molecular dynamics simulation results showed VB1 could directly bind MAPK1 protein. **(B)** The five amino acid residues (G32, Y34, K46, E58, and R65) of MAPK1 were predicted and K338 residue was another possible key residue through computer-aid calculation (data not shown).

VB1 Binds to MAPK1 by Interacting With the Residues E58 and R65

We performed endogenous immunoprecipitation assays to confirm whether VB1 directly binds to MAPK1. HEK293T cells transfected with unlinked (control) or VB1-linked nanogold particles were used for immunoprecipitation, and MAPK1 was then detected by western blotting. The results showed that MAPK1 was detectable in the nanogold-VB1-immunoprecipitated complexes but not in the control nanogold immunocomplexes (**Figure 4A**), revealing that MAPK1 directly bound to VB1. To precisely identify the interaction sites of VB1 with MAPK1, we established wild-type and mutant MAPK1 vectors and used them to transfect HEK293T cells, together with nanogold-VB1 particles. Then, we determined the interactions between VB1 and wild-type/mutant MAPK1 using immunoprecipitation. MAPK1 was not detected in HEK293T cells transfected with the E58- and R65-mutants of MAPK1, while it was detectable in cells transfected with wild-type MAPK1 and the other four MAPK1 mutants (**Figure 4A**). Then, we modeled the complex between VB1 and MAPK1, considering

the interacting residues E58 and R65, by *in silico* method (**Figure 4B**). These findings indicated that VB1 bound to MAPK1 by interacting with the residues E58 and R65.

VB1 Can Partially Reverses UVA-Induced Phosphorylation of MAPK1

Only phosphorylated MAPK1 (p-MAPK1), which is the active form of MAPK1, can activate the activity of a series of downstream transcription factors, thereby regulating cell function. To clarify the effect of VB1 on the MAPK1 pathway, p-MAPK1 was detected in HDFs by western blotting in HDFs. The results revealed that p-MAPK1 expression was significantly increased after UVA irradiation, however, VB1 could significantly reverse this UVA-mediated effect (**Figure 4C**).

VB1 Protects HEK293T Cells From UVA-Induced Senescence via Binding to MAPK1

To examine whether VB1 reduces UVA-induced senescence through MAPK1 binding, we co-transfected HEK293T cells, with down-regulated endogenous MAPK1, with VB1 and wild-type or mutant MAPK1 (E58- or R65-mutants) and irradiated the cells with UVA rays. We found that the UVA-induced expression of p16 and MMP1 was significantly decreased in HEK293T cells transfected with wild-type MAPK1 and VB1. In contrast, the UVA-induced expression of these proteins was partially reversed in cells co-transfected with both MAPK1 mutants and VB1 (**Figures 4D–F**). These data revealed that VB1 could protect HEK293T cells from UVA-induced senescence by binding the E58 and R65 residues of MAPK1.

Topical VB1 Gel Alleviates the Skin Photoaging Phenotype in Mice

To further evaluate the anti-photoaging ability of VB1, we applied a gel containing 2% VB1 or a vehicle gel lacking VB1 topically on the UVA-irradiated dorsal skin of mice. In the vehicle group, the dorsal skin of the animals was rough and scaly, showing increased thickness and deep wrinkles after 12 weeks of UVA-irradiation compared with the corresponding parameters in the non-irradiated control group. In contrast, the skin conditions of VB1-treated mice were visibly improved, and the formation of skin wrinkles was significantly reduced (**Figure 5A**). Mouse dorsal skin from each group was harvested for hematoxylin and eosin (HE) staining. The epidermal thickness was markedly higher in the vehicle group than in the non-irradiated control group (**Figure 5B**). Daily topical application of VB1 gel significantly reduced the thickening of the epidermal layers. These data demonstrated that VB1 could alleviates UVA-induced skin photoaging *in vivo*.

DISCUSSION

Skin photoaging, an essential aspect of skin aging, is mainly characterized by skin relaxation, wrinkle formation, pigmentation, and telangiectasia, etc. Recent evidence has shown that UVA irradiation produces ROS and induces cell senescence, ultimately leading to skin photoaging (Wlaschek et al., 2001; Yi et al., 2018). Thus, finding the ideal antioxidants that can act as anti-aging drugs is very promising.

Previous studies have demonstrated that VB1 acts as a novel antitumor agent by regulating the cell cycle arrest and apoptosis induction in various cancers. Some studies have shown that VB1 has a strong antioxidant effect and can inhibit multiple protein kinases and signal transduction pathways (Liu et al., 2014, 2018; Yang et al., 2014; Luo et al., 2018). However, the role of VB1 in skin photoaging has never been reported. Here, we showed that VB1 protects HDFs from UVA-induced senescence. Thus, for the first time, the role of VB1 in the skin cellular senescence was explored.

How does VB1 protect HDFs from UVA-induced senescence? To answer this question, we explored potential target proteins of VB1 via mass spectrometry and nanogold-based immunoprecipitation. Nanogold particles, also called gold nanoparticles (AuNPs), have been widely used for the identification of both biological and chemical materials (Lee et al., 2018). When it is combined with recognition proteins, such as antibodies or receptors, this nanomaterial can act as a biosensor molecule (Egea et al., 2019). To date, nanogold particles have been used as a biological tool in many studies, especially in cancer-related studies (Shen et al., 2018). In the present study, nanogold particles were used to pull down VB1 micromolecules for subsequent mass spectrometry and immunoprecipitation analyses. Through mass spectrometry, we identified 26 proteins that potentially bind VB1. Among those 26 proteins, some proteins were tumor-related, such as YWHAQ and eEF1A1, and others were proteins were involved in various biological processes, such as DEDD and MAPK1. The MAPK pathway is one of the most important pathways in aging. It mainly triggers a series of downstream biological effects through MAPK family molecules, including ERK1, ERK2, ERK5, JNK, and p38 MAPK, thereby regulating cell proliferation, differentiation, and development. Some reports suggest that the activation of the MAPK pathway is the central event in UV-induced intracellular signaling, causing nuclear and DNA damage-originated cellular responses (Bode and Dong, 2003). MAPK1, also called ERK2, plays an indispensable role in the MAPK pathway. Only phosphorylated (active) MAPK1 can trigger the activation a series of downstream transcription factors, such as Sata1/3 and FoxO3 to regulate cellular processes, however, it also plays an important regulatory role in aging (Gkotinakou et al., 2019; Zhu et al., 2019). Due to its important role in photoaging, we chose MAPK1 for *in silico* experiments to identify potential VB1-binding sites.

A new computer-aided method, including molecular docking and molecular dynamics simulation, which was widely used to find the "best" matching between two molecules and also can predict their "correct" binding (Akbarabadi et al., 2019; Sakr et al., 2019), was also applied to predict potential binding sites of VB1 in MAPK1. Based on the *in silico* results, we concluded that VB1 could directly target MAPK1 by interacting with several amino acid residues (G32, Y34, K46, E58, R65, and K338). Then, through transfection of HEK293T cells with

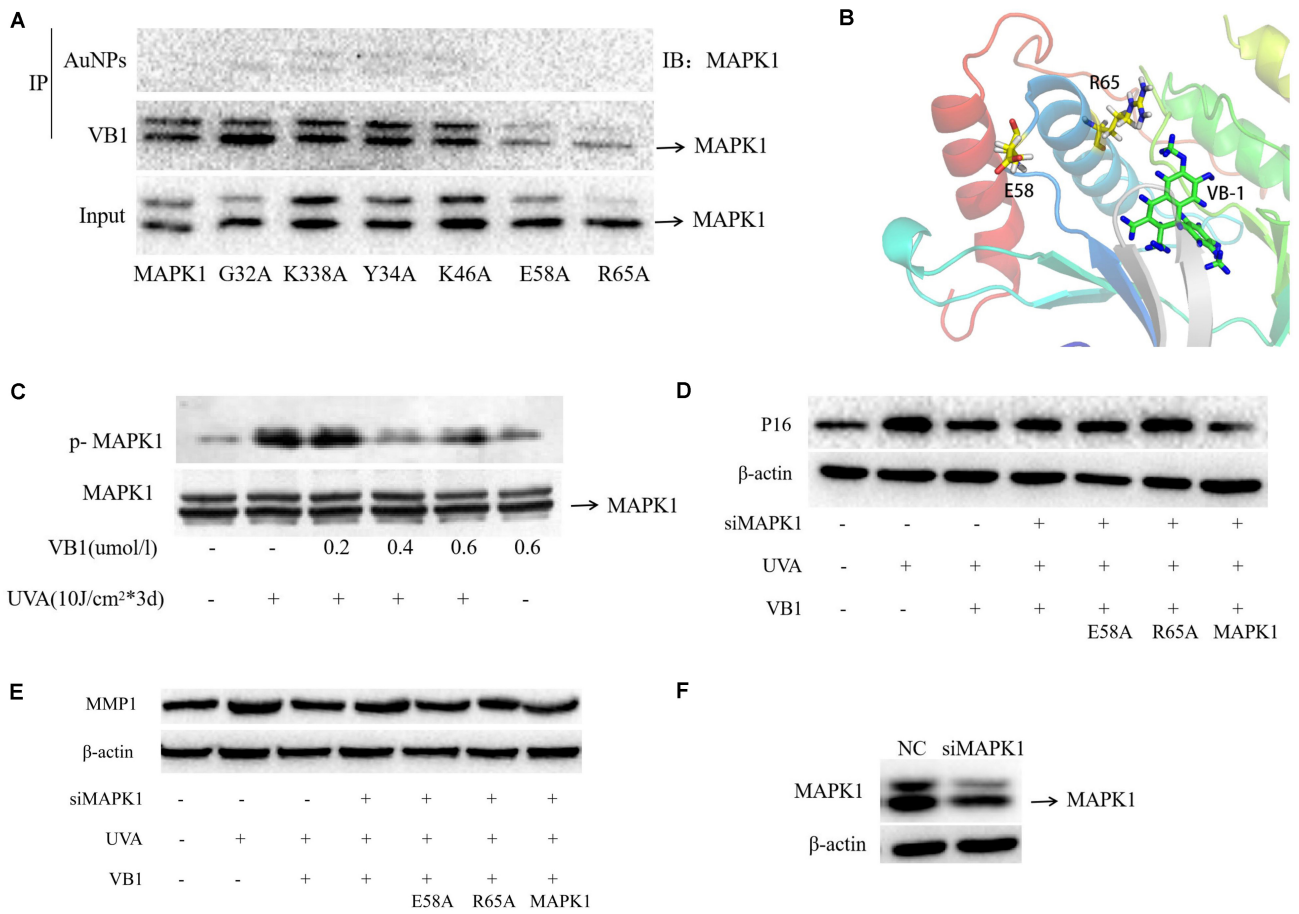

FIGURE 4 | VB1 binds to MAPK1 through E58 and R65 residues of MAPK1 and VB1 protects 293T cells from UVA-induced senescence via binding the two residues. **(A)** VB1 linked with gold nanoparticles was used for the immunoprecipitation in 293T cells. In the gold nanoparticles (AuNPs) immunocomplexes, MAPK1 was not detectable by western blot analysis, while MAPK1 was detectable by western blot analysis in nanogold-VB1-immunoprecipitated complexes. In the 293T cells transfected with E58-mutant MAPK1 and R65-mutant MAPK1, MAPK1 was not detected, while MAPK1 was detectable in cells transfected with other four mutant MAPK1. **(B)** The combination form between VB1 and MAPK1 via E58 and R65 residues using computer-aided methods. **(C)** p-MAPK1 expression was detected by western blot analysis. p-MAPK1 was significantly increased after UVA irradiation and that VB1 could significantly decrease UVA-induced p-MAPK1 expression in a dose-dependent manner. **(D,E)** 293T cells was used in further co-transfected experiments because of difficulty in HDFs. Endogenous MAPK1 in 293T cells was knockdown by MAPK1 siRNA. Then UVA-irradiated 293T cells were co-transfected with VB1 and wild-type or mutant MAPK1 (E58-mutant or R65-mutant), and p16 and MMP1 expression was detected by western blot analysis. UVA-induced p16 and MMP1 were significantly decreased in 293T cells tranfected with wild-type MAPK1 and VB1, while p16 and MMP1 were partially reversed in 293T cells transfected with E58-mutant or R65-mutant MAPK1 and VB1. **(F)** MAPK1 siRNA could significantly knockdown the endogenous MAPK1 expression in 293T cells.

MAPK1 vectors containing mutant residues and subsequent immunoprecipitation, we discovered that VB1 delayed UVA-induced cellular senescence by binding to the residues E58 and R65. Thus, we hypothesized that VB1 reduced cellular senescence by regulating the expression of phosphorylated MAPK1 expression through direct interaction with MAPK1. Previous studies have shown that TGF-β alone induced Ras-Raf-MEK1 and phosphorylated MAPK1 to increase the expression of MMP1, so we speculate that VB1 could decrease MMP1 and p16 by reducing p-MAPK1 (Amatangelo et al., 2012).

The demand for products that diminish wrinkles and maintain a youthful appearance of the skin is increasing. Currently, all-trans-retinoic acid (ATRA) is the only topical drug that is approved by the Food and Drug Administration (FDA) for the treatment of photoaged skin (Behairi et al., 2016). However, the topical use of ATRA might induce local skin side effects, including irritation, erythema, burning, pruritus, and scaling. Therefore, there is a need for safe and efficacious agents for the prevention and treatment of photoaging. To analyze whether VB1-containing preparations can effectively delay skin photoaging, we prepared a VB-1 gel and demonstrated that the gel exhibited a good permeate rate and low lag time (Li et al., 2016). In addition, topical administration of the VB1 gel to mice remarkably reduced skin photoaging phenotypes caused by long-term UVA irradiation.

In summary, we demonstrated that VB1 significantly inhibits UVA-induced senescence in HDFs by targeting the E58 and R65 residues of MAPK1 and effectively reduces skin

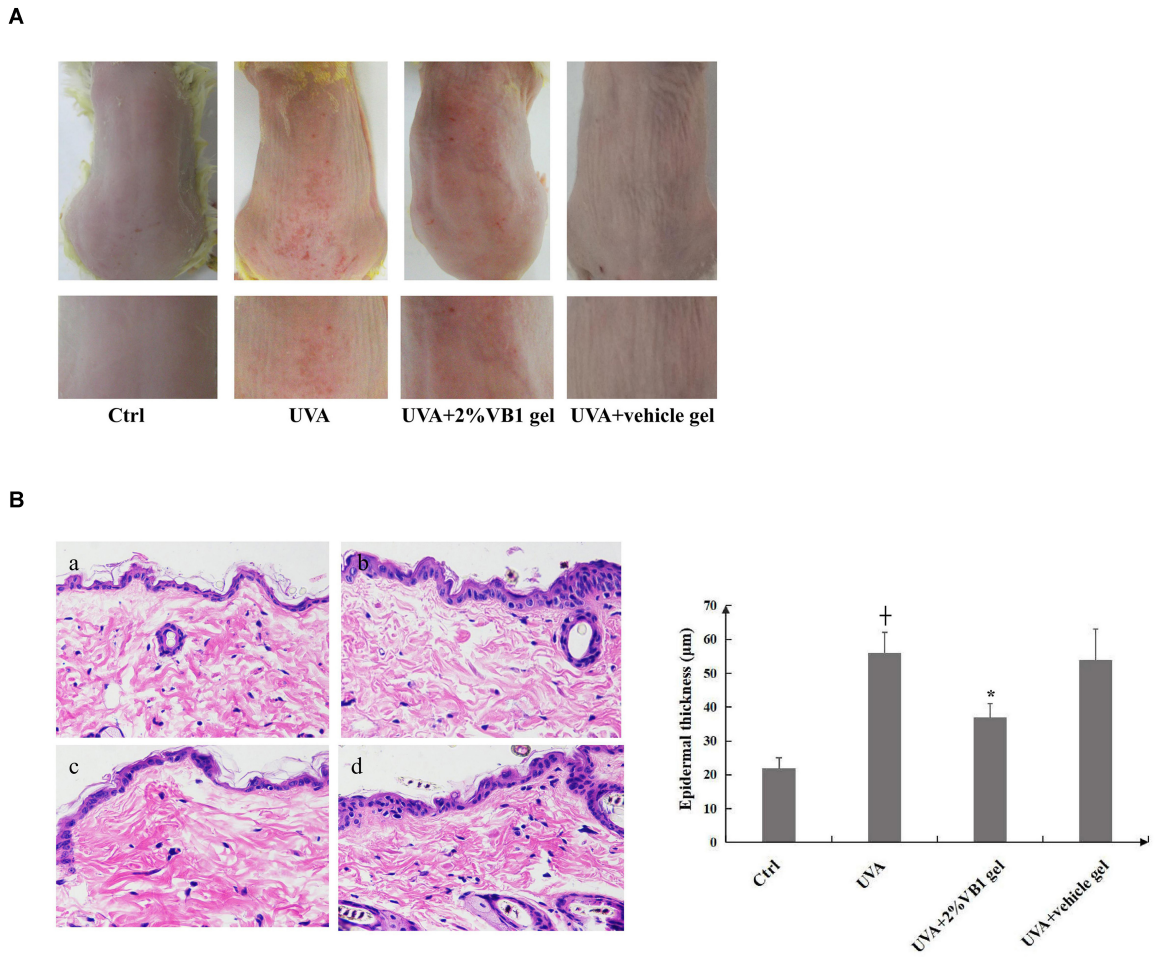

FIGURE 5 | Topical VB1 gel palliates skin photoaging phenotype induced by UVA irradiation in mice. Mice were irradiated with UVA 3 times per week at doses of 20 J/cm^2 for 12 weeks. A gel containing 2% VB1 or a vehicle gel lacking VB1 (negative control) was applied topically to the dorsal skin areas of mice at 1 h after each irradiation. The control group consisted of untreated mice at the same age. **(A)** Representative photographs of mice dorsal skin in mice from control group, UVA-irradiated group, the experimental group receiving VB1 gel and the vehicle only group. **(B)** Representative photographs of hematoxylin-eosin (HE)-stained dorsal skin sections obtained at the end of the experiment from (a) control group, (b) UVA-irradiated group, (c) the experimental group receiving VB1 gel and (d) the vehicle only group (left panel, magnification 200x). Epidermal thicknesses were estimated at 5 different random sites with each mouse from digital images of HE-stained sections and are depicted as means ± SEM (n = 10 per group). The right panel showed the analysis data (+ vs. ctrl, $p < 0.05$, * vs. UVA, $p < 0.05$).

photoaging in UVA-irradiated mice, indicating that VB1 could serve as a novel agent for the prevention and the potential treatment of photoaging.

DATA AVAILABILITY STATEMENT

All datasets generated for this study are included in the article/**Supplementary Material**.

ETHICS STATEMENT

The animal study was reviewed and approved by the Clinical Research Ethics Committee at the Xiangya Hospital of Central South University.

AUTHOR CONTRIBUTIONS

BW and SY performed all the experiments and prepared the figures and tables. SY, QZ, ZD, YZ, and YY provided with the technical and statistical assistance. BW, HX, and YH analyzed and interpreted the data. JL provided all the theoretical direction. BW, SY, HX, and JL wrote and edited the manuscript. All authors read and approved the final manuscript.

FUNDING

This work was primarily supported by the National Natural Science Foundation of China (Grant Nos. 81502750, 81602784, 81773351, 81874251, and 81573314) and the Cultivation Project

of National Natural Science Foundation Major Research Program (Grant No. 91749114).

ACKNOWLEDGMENTS

We thank Minghui Yang and members of the Institute of Chemistry and Chemical Engineering of Central South University for the synthesis and modification of gold nanoparticles. We thank members of the Institute of Theoretical Chemistry in Jilin University for the target amino residues prediction. We also would like to thank Editage (www.editage.cn) for English language editing.

SUPPLEMENTARY MATERIAL

The Supplementary Material for this article can be found online at: https://www.frontiersin.org/articles/10.3389/fcell.2020.00691/full#supplementary-material

REFERENCES

Akbarabadi, A., Ismaili, A., Kahrizi, D., and Nazarian Firouzabadi, F. (2019). Resistance determination of the ACCase-inhibiting herbicide of clodinafop propargyl in *Avena ludoviciana* (Durieu), and study of their interaction using molecular docking and simulation. *Mol. Biol. Rep.* 46, 415–424. doi: 10.1007/s11033-018-4489-9

Amatangelo, M. D., Goodyear, S., Varma, D., and Stearns, M. E. (2012). c-Myc expression and MEK1-induced Erk2 nuclear localization are required for TGF-beta induced epithelial-mesenchymal transition and invasion in prostate cancer. *Carcinogenesis* 33, 1965–1975. doi: 10.1093/carcin/bgs227

Bagdanoff, J. T., Jain, R., Han, W., Zhu, S., Madiera, A. M., Lee, P. S., et al. (2015). Tetrahydropyrrolo- diazepenones as inhibitors of ERK2 kinase. *Bioorg. Med. Chem. Lett.* 25, 3788–3792. doi: 10.1016/j.bmcl.2015.07.091

Behairi, N., Belkhelfa, M., Rafa, H., Labsi, M., Deghbar, N., Bouzid, N., et al. (2016). All-trans retinoic acid (ATRA) prevents lipopolysaccharide-induced neuroinflammation, amyloidogenesis and memory impairment in aged rats. *J. Neuroimmunol.* 300, 21–29. doi: 10.1016/j.jneuroim.2016.10.004

Bode, A. M., and Dong, Z. (2003). Mitogen-activated protein kinase activation in UV-induced signal transduction. *Sci STKE* 167:RE2. doi: 10.1126/stke.2003.167.re2

Bravo, K., Duque, L., Ferreres, F., Moreno, D. A., and Osorio, E. (2017). Passiflora tarminiana fruits reduce UVB-induced photoaging in human skin fibroblasts. *J Photochem Photobiol B Biol.* 168, 78–88. doi: 10.1016/j.jphotobiol.2017.01.023

Chang-Panesso, M., Kadyrov, F. F., Machado, F. G., Kumar, A., and Humphreys, B. D. (2018). Meis1 is specifically upregulated in kidney myofibroblasts during aging and injury but is not required for kidney homeostasis or fibrotic response. *Am. J. Physiol. Renal Physiol.* 315, F275–F290. doi: 10.1152/ajprenal.00030.2018

Egea, E., Mendoza, D., Garavito, G., Saavedra, S., Gómez, H., and Sanjuan, M. (2019). Nanogold – IgY antibodies. An immunoconjugated for the detection of house dust mite (*Dermatophagoides*) allergens. *J. Immunol. Methods* 464, 15–21. doi: 10.1016/j.jim.2018.08.013

Gkotinakou, I. M., Befani, C., Simos, G., and Liakos, P. (2019). ERK1/2 phosphorylates HIF-2α and regulates its activity by controlling its CRM1-dependent nuclear shuttling. *J. Cell Sci.* 132:jcs225698. doi: 10.1242/jcs.225698

Gordon, J. C., Myers, J. B., Folta, T., Shoja, V., Heath, L. S., and Onufriev, A. (2005). H++: server for estimating pKas and adding missing hydrogens to macromolecules. *Nucleic Acids Res.* 33, W368–W371. doi: 10.1093/nar/gki464

Gorgoulis, V., Adams, P. D., Alimonti, A., Bennett, D. C., Bischof, O., Bishop, C., et al. (2019). Cellular senescence: defifining a path forward. *Cell* 179, 813–827. doi: 10.1016/j.cell.2019.10.005

Jung, S. K., Ha, S. J., Jung, C. H., Kim, Y. T., Lee, H. K., Kim, M. O., et al. (2016). Naringenin targets ERK2 and suppresses UVB-induced photoaging. *J Cell Mol Med.* 20, 909–919. doi: 10.1111/jcmm.12780

Kammeyer, A., and Luiten, R. M. (2015). Oxidation events and skin aging. *Ageing Res. Rev.* 21, 16–29. doi: 10.1016/j.arr.2015.01.001

Kobayashi, Y., Lee, S. S., Arai, R., Miki, K., Fujii, M., and Ayusawa, D. (2012). ERK1/2 mediates unbalanced growth leading to senescence induced by excess thymidine in human cells. *Biochem. Biophys. Res. Commun.* 425, 897–901. doi: 10.1016/j.bbrc.2012.08.006

Kruglikov, I. L., and Scherer, P. E. (2016). Skin aging: are adipocytes the next target? *Aging* 8, 1457–1469. doi: 10.18632/aging.100999

Lee, N., Lee, D.-W., and Lee, S.-M. (2018). Gold nanoparticle-stabilized, tyrosine-rich peptide self-assemblies and their catalytic activities in the reduction of 4-nitrophenol. *Biomacromolecules* 19, 4534–4541. doi: 10.1021/acs.biomac.8b01221

Lei, D., Huang, Y., Xie, H., Yi, Y., Long, J., Lin, S., et al. (2018). Fluorofenidone inhibits UV-A induced senescence in human dermal fibroblasts via the mammalian target of rapamycin-dependent SIRT1 pathway. *J. Dermatol.* 45, 791–798. doi: 10.1111/1346-8138.14304

Li, S., Wang, T., and Ding, J. S. (2016). Transdermal behavior of VBE-1 and its interference effect on skin pigmentation of guinea pig induced by Ultraviolet B Irradiation. *Nat. Prod. Res. Dev.* 28, 1024–1028. doi: 10.16333/j.1001-6880.2016.7.007

Liu, L. H., Zhou, Y. J., Ding, L., Zhang, S. Z., Sun, J., and Cao, J. G. (2014). Induction of apoptosis by VB1 in breast cancer cells: the role of reactive oxygen species and Bcl-2 family proteins. *Int. J. Mol. Med.* 33, 423–430. doi: 10.3892/ijmm.2013.1567

Liu, N., Wang, K. S., Qi, M., Zhou, Y. J., Zeng, G. Y., Tao, J., et al. (2018). Vitexin compound 1, a novel extraction from a Chinese herb, suppresses melanoma cell growth through DNA damage by increasing ROS levels. *J. Exp. Clin. Cancer Res.* 37:269. doi: 10.1186/s13046-018-0897-x

Luo, J., Chen, M., Liu, Y., Xie, H., Yuan, J., Zhou, Y., et al. (2018). Nature-derived lignan compound VB-1 exerts hair growth-promoting effects by augmenting Wnt/ β-catenin signaling in human dermal papilla cells. *PeerJ* 6:e4737. doi: 10.7717/peerj.4737

Marampon, F., Gravina, G. L., Festuccia, C., Popov, V. M., Colapietro, E. A., Sanità, P., et al. (2016). Vitamin D protects endothelial cells from irradiation-induced senescence and apoptosis by modulating MAPK/SirT1 axis. *J. Endocrinol. Invest.* 39, 411–422. doi: 10.1007/s40618-015-0381-9

Sakr, A., Kothayer, H., Ibrahim, S. M., Baraka, M. M., and Rezq, S. (2019). 1,4-Dihydroquinazolin-3(2H)-yl benzamide derivatives as anti-inflammatory and analgesic agents with an improved gastric profile: design, synthesis, COX-1/2 inhibitory activity and molecular docking study. *Bioorg. Chem.* 84, 76–86. doi: 10.1016/j.bioorg.2018.11.030

Shen, C., Liu, S., Li, X., Zhao, D., and Yang, M. (2018). Immunoelectrochemical detection of the human epidermal growth factor receptor 2 (HER2) via gold nanoparticle-based rolling circle amplification. *Microchim. Acta* 185:547. doi: 10.1007/s00604-018-3086-x

Shin, J. W., Kwon, S. H., Choi, J. Y., Na, J. I., Huh, C. H., Choi, H. R., et al. (2019). Molecular mechanisms of dermal aging and antiaging approaches. *Int. J. Mol. Sci.* 20:E2126. doi: 10.3390/ijms20092126

Stellavato, A., Pirozzi, A. V. A., Donato, S., Scognamiglio, I., Reale, S., Di Pardo, A., et al. (2018). Positive effects against UV-A induced damage and oxidative stress on an in vitro cell model using a hyaluronic acid based formulation containing amino acids. Vitamins, and Minerals. *Biomed. Res. Int.* 2018:8481243. doi: 10.1155/2018/8481243

Sun, Y., Liu, W. Z., Liu, T., Feng, X., Yang, N., and Zhou, H. F. (2015). Signaling pathway of MAPK/ERK in cell proliferation, differentiation, migration, senescence and apoptosis. *J. Recept. Signal Transduct. Res.* 35, 600–604. doi: 10.3109/10799893.2015.1030412

Trott, O., and Olson, A. J. (2010). AutoDock Vina: improving the speed and accuracy of docking with a new scoring function, efficient optimization, and multithreading. *J. Comput. Chem.* 31, 455–461. doi: 10.1002/jcc.21334

Wang, B., Du, R., Xiao, X., Deng, Z. L., Jian, D., Xie, H. F., et al. (2017). Microrna-217 modulates human skin fibroblast senescence by directly targeting DNA methyltransferase 1. *Oncotarget* 8, 33475–33486. doi: 10.18632/oncotarget.16509

Wang, J., Wang, W., Kollman, P. A., and Case, D. A. (2006). Automatic atom type and bond type perception in molecular mechanical calculations. *J. Mol. Graph. Model.* 25, 247–260. doi: 10.1016/j.jmgm.2005.12.005

Wang, J., Wolf, R. M., Caldwell, J. W., Kollman, P. A., and Case, D. A. (2004). Development and testing of a general amber force field. *J. Comput. Chem.* 25, 1157–1174. doi: 10.1002/jcc.20035

Wlaschek, M., Tantcheva-Poór, I., Naderi, L., Ma, W., Schneider, L. A., Razi-Wolf, Z., et al. (2001). Solar UV irradiation and dermal photoaging. *J. Photochem. Photobiol. B Biol.* 63, 41–51. doi: 10.1016/s1011-1344(01)00201-9

Yang, Z. B., Tan, B., Li, T. B., Lou, Z., Jiang, J. L., Zhou, Y. J., et al. (2014). Protective effect of vitexin compound B-1 against hypoxia/reoxygenation-induced injury in differentiated PC12 cells via NADPH oxidase inhibition. *Naunyn Schmiedebergs Arch. Pharmacol.* 387, 861–871. doi: 10.1007/s00210-014-1006-0

Yi, Y., Xie, H., Xiao, X., Wang, B., Du, R., Liu, Y., et al. (2018). Ultraviolet a irradiation induces senescence in human dermal fibroblasts by down-regulating DNMT1 via ZEB1. *Aging* 10, 212–228. doi: 10.18632/aging.101383

Zhu, Y., Yang, T., Duan, J., Mu, N., and Zhang, T. (2019). MALAT1/miR-15b-5p/MAPK1 mediates endothelial progenitor cells autophagy and affects coronary atherosclerotic heart disease via mTOR signaling pathway. *Aging* 11, 1089–1109. doi: 10.18632/aging.101766

Conflict of Interest: The authors declare that the research was conducted in the absence of any commercial or financial relationships that could be construed as a potential conflict of interest.

Copyright © 2020 Wang, Yan, Yi, Huang, Deng, Zhang, Zheng, Xie and Li. This is an open-access article distributed under the terms of the Creative Commons Attribution License (CC BY). The use, distribution or reproduction in other forums is permitted, provided the original author(s) and the copyright owner(s) are credited and that the original publication in this journal is cited, in accordance with accepted academic practice. No use, distribution or reproduction is permitted which does not comply with these terms.

frontiers in Cell and Developmental Biology

ORIGINAL RESEARCH
published: 19 August 2020
doi: 10.3389/fcell.2020.00824

Twist1 Contributes to the Maintenance of Some Biological Properties of Dermal Papilla Cells *in vitro* by Forming a Complex With Tcf4 and β-Catenin

Nanlan Yu[1†], Tianxing Hu[1,2†], Haichao Yang[1], Lian Zhang[1], Qin Song[1], Fei Xiang[3], Xichuan Yang[1] and Yuhong Li[2*]*

[1] Department of Dermatology, The First Affiliated Hospital of the Army Medical University, Chongqing, China, [2] Department of Cell Biology, Army Medical University, Chongqing, China, [3] State Key Laboratory of Trauma, Burns and Combined Injury, Southwest Hospital, Institute of Burn Research, Army Medical University, Chongqing, China

OPEN ACCESS

Edited by:
Cheng Ming Chuong,
University of Southern California,
United States

Reviewed by:
Michael Rendl,
Icahn School of Medicine at Mount Sinai, United States
Manabu Ohyama,
School of Medicine, Kyorin University, Japan

***Correspondence:**
Xichuan Yang
drxcyang@163.com
Yuhong Li
liyuhongtmmu@hotmail.com

[†] These authors have contributed equally to this work

Specialty section:
This article was submitted to Stem Cell Research, a section of the journal Frontiers in Cell and Developmental Biology

Received: 01 March 2020
Accepted: 03 August 2020
Published: 19 August 2020

Citation:
Yu N, Hu T, Yang H, Zhang L, Song Q, Xiang F, Yang X and Li Y (2020) Twist1 Contributes to the Maintenance of Some Biological Properties of Dermal Papilla Cells in vitro by Forming a Complex With Tcf4 and β-Catenin. Front. Cell Dev. Biol. 8:824. doi: 10.3389/fcell.2020.00824

Objective: During hair follicle regeneration, hair follicle stem cells (HFSCs) are regulated by signals from dermal papilla cells (DPCs). Previously we found that Tcf4 could promote the proliferation of DPCs. In this study, we focused on whether and how the biological properties of Tcf4-induced DPCs were regulated by Twist1.

Methods: Twist1 was overexpressed or knocked down in DPCs following different adenovirus or lentivirus infection. Phase-contrast microscopy was used to observe the agglutinative growth of DPCs. The CCK-8 assay was used to test the proliferation of DPCs. Western blot and qPCR experiments were used to determine the expression of HGF, IGF-1, VEGF, c-myc, survivin, and CyclinD1 in DPCs. ELISAs were used to test the growth factors secreted by DPCs. Conditional medium culture was used to detect the inductive ability of DPCs. Co-immunoprecipitation and immunofluorescence were used to test the binding of Twist1, Tcf4, and β-catenin in DPCs. Immunofluorescence was also used to test the expression of Twist1, Tcf4, and KRT15 in hair follicles.

Results: Twist1 induced DPC agglutinative growth and proliferation. Twist1 upregulated the expression of downstream target genes downstream of Tcf4, c-myc, survivin, in Tcf4-induced DPCs, as well as the expression and secretion of growth factors HGF, IGF-1, VEGF, which had the ability to induce hair follicle growth. The conditional medium from Twist1-treated DPCs increased the expression of KRT40 and MSX2 in HaCaT cells. Twist1 and Tcf4 co-localized in DPCs both *in vitro* and *in vivo.* Anti-Twist1 precipitated Tcf4 and β-catenin.

Conclusion: These results indicate that Tcf4 and Twist1 play a synergistic role in regulating the hair follicle induction ability of DPCs. Twist1 functions by forming a ternary complex with Tcf4 and β-catenin. Thus, we report new data that elucidate whether and how Twist1 regulates some biological properties of DPCs.

Keywords: Twist1, Tcf4, β-catenin, dermal papilla cells, hair follicle stem cells

INTRODUCTION

Hair loss is one of the most common dermatological diseases. Alopecia, represented by androgentic alopecia or alopecia areata, may last for a long time, or easily relapse. It causes great mental strain for patients (Williamson et al., 2001; Hunt and McHale, 2005). At the same time, the hair itself also has physiological functions such as temperature regulation or skin protection, as well as roles in information interaction and beauty. It has been reported that some patients with alopecia problems, such as baldness, can even experience devastating physical and mental disorders such as anxiety and depression (Van Der Donk et al., 1994; Williamson et al., 2001; Fabbrocini et al., 2013; Yu et al., 2016). At present, the treatment methods for hair loss include drug treatments to promote hair growth and hair transplantation, which require hair follicles from the patients themselves (Miao et al., 2014). The hair follicle is an appendage of the skin, the structure of which is composed of epidermis and dermis, further, the follicle experiences the periodic stages of growth, degeneration, and quiescence (Al-Nuaimi et al., 2010). Dermal papilla cells (DPCs) are mesenchymal cells located at the hair follicle bulb. DPCs not only play a regulatory role in the hair follicle cycle but also play a maintenance and induction role, which is characterized by agglutinative growth behavior *in vitro* and the ability to induce the formation of new hair follicles during the embryonic and postnatal periods (Driskell et al., 2011). DPCs promote the formation and development of hair follicles through the interaction of various signaling pathways. For example, the BMP signaling pathway and Wnt/β-catenin signaling pathway are considered to be key signaling pathways in the activation of hair follicle stem cells (HFSCs) and regeneration of hair follicles (Wu et al., 2019). BMP signaling has an inhibitory effect on the activation of HFSCs. TGF-β signaling from DPCs can inhibit the inhibitory effect of BMP signal in HFSCs (Oshimori and Fuchs, 2012; Amberg et al., 2016). When the Wnt signal is activated, the cytoplasmic signal molecule β-catenin cannot be phosphorylated and it becomes enriched in the cytoplasm before being transferred into the nucleus, where it forms a complex with Lef/Tcf. Once there, β-catenin plays a role in transcription activation, thus transcribing the molecules that activate HFSCs and hair follicle regeneration (Li et al., 2013; Bejaoui et al., 2019).

In our previous study, we found that Tcf4, a family member of Lef/Tcf encoded by the *Tcf7L2* gene, was upregulated in DPCs in the anagen (Xiong et al., 2014). Tcf4 and β-catenin form a complex in the nucleus, which leads to the transcriptional activation of genes downstream of the Wnt/β-catenin signaling pathway. In addition, Tcf4 was highly expressed in low passage number DPCs *in vitro*. However, the ability of hair follicle induction and the mode of agglutinative growth are often lost in the course of the passage of DPCs, as well as the expression of Tcf4, which shows that Tcf4 is closely related to the activation of HFSCs and hair follicle regeneration. Moreover, another previous study also found that mitotic arrest defective protein MAD2B, can bind with Tcf4 and reduce Tcf4-mediated Wnt/β-catenin signaling activity, thus inhibiting the proliferation of DPCs. However, it is interesting that the knockdown of MAD2B did not affect the secretion function of DPCs induced by Tcf4. In contrast, it further promoted the proliferation of Tcf4-induced DPCs (Yu et al., 2017). Based on these reports, we propose that the cytokine-mediated effects of MAD2B knockdown may be counteracted by other factors.

Twist1 is a transcription factor with a basic helix loop helix (bHLH). The Twist1 and Wnt/β-catenin signaling pathways play important roles in the development of osteosarcoma, in which Twist1 promotes the expression of specific cell surface receptors in osteosarcoma cells via activating Tcf4-mediated Wnt/β-catenin signaling pathway (Wu et al., 2014). Thus, we hypothesize that Twist1/Tcf4 interaction can promote the proliferation of Tcf4-induced DPCs. Through *in vitro* and *in vivo* experiments, we found that Twist1 may be an important factor that regulates the aging of DPCs, and can delay the disappearance of some biological properties of DPCs during passage. In addition, we found that Twist1 performed these activities by forming a complex with Tcf4 and β-catenin.

MATERIALS AND METHODS

Cell Culture

This study was approved by the Ethics Committee of The First Affiliated Hospital of the Third Military Medical University (ethics approval No. ky201977). All experiments were carried out in accordance with the relevant guidelines and regulations. The patients/participants provided their written informed consent to participate in this study. The scalp samples containing hair follicles were collected in the Department of Dermatology of The First Affiliated Hospital of the Third Military Medical University from patients with a pigmented nevus and sebaceous nevus, whose size was 0.5 × 0.5 cm ∼ 0.5 ×1 cm. After collection, they were immediately stored in 4℃ sterile saline, and primary cells were extracted by a two-step enzyme digestion. Primary DPCs were cultured with DMEM containing 10% FBS and 100 U/L penicillin-streptomycin in a 37℃, 5% CO_2 incubator. The medium was changed every 3 days until the primary cells stopped growing, and then the cells were passaged and cultured at a ratio of 1:2. Primary human fibroblasts were obtained and cultured as previously described Chen et al. (2017), and were kindly provided by Chunmeng Shi in the Third Military Medical University.

Virus Construction and Infection

An adenoviral vector mediating overexpression of Tcf4 was generated previously (Yu et al., 2017). The empty vector pAdeno-MCMV-3Flag-T2A-mCherry was used to construct an adenovirus-mediated Twist1 (NM_000474) overexpression vector. The construction and amplification of the Twist1 overexpression vector was performed by OBIO Technology Corp., Ltd. The empty vector pLKD-CMV-mCherry-2A-Puro-U6-shRNA was used to construct the lentiviral vector mediating siTwist1 knockdown. The construction and amplification of the siTwist1 vector was performed by OBIO Technology Corp., Ltd. The target sequence is: 5′-gcaagattcagaccctcaa-3′.

Before virus infection, DPCs were seeded into 6-well plates at a density of 3×10^5 cells per well. When DPCs grew to ∼70%, virus-mediated GFP, Twist1, siTwist1, Tcf4, Tcf4 and Twist1,

Tcf4, and siTwist1 were added into the culture medium. Cell morphology was monitored under a microscope.

Cell Proliferation Assay

DPCs were seeded into 96-well plates at a density of 1×10^3 cells per well. After overnight culture, cells were divided into 6 groups and were separately infected with viral vectors expressing GFP, Twist1, siTwist1, Tcf4, Tcf4 and Twist1, Tcf4, and siTwist1. Twenty-four hours later, a 10 μL cell counting kit-8 (CCK-8) solution (Beyotime, Shanghai, China) was added to the culture. After incubation in the dark for 1.5 h, the absorbance optical density (OD) value was measured at a wavelength of 450 nm.

Western Blot Analysis

DPCs were seeded into 60 mm dishes at a density of 1×10^6 cells per dish. Forty-eight hours after viral infection, the cells were washed twice with cold PBS and then lysed with RIPA buffer (Beyotime, Shanghai, China). Cell lysates were collected and the protein concentration was measured with a BCA protein assay (Beyotime, Shanghai, China). Subsequently, the protein was separated by SDS-PAGE and transferred to a PVDF membrane. The membrane was then blocked with 5% non-fat milk in TBS, and incubated overnight at 4℃ with diluted primary antibodies. The primary antibodies were as follows: GAPDH, c-myc, survivin, CyclinD1, IGF-1, HGF, VEGF (R&D Systems, Minneapolis, MN, United States), Twist1 (Santa Cruz, CA, United States), KRT40 (Santa Cruz, CA, United States), MSX2 (Santa Cruz, CA, United States), KRT5 (Sangon, Shanghai, China), KRT15 (Sangon, Shanghai, China), and FGF7 (Boster, Wuhan, China). After washing, the membrane was incubated with HRP-labeled secondary antibodies. A Bio-Rad imaging system was used to collect and quantify images.

Quantitative Polymerase Chain Reaction (qPCR)

Total RNA was extracted from DPCs with an RNA extraction kit (Takara, Dalian, China) and cDNA was synthesized by reverse transcription (Toyobo, Osaka, Japan). Quantitative polymerase chain reactions (qPCRs) were carried out with the following primers: 5′-ccgggatgctttacgttg-3′ (forward) and 5′-aattcaaaaagatgcagctta-3′ (reverse) for c-myc, 5′-ctttacgtggac tccagtct-3′ (forward) and 5′-acaagacctcaactgtggctcga-3′ (reverse) for survivin, 5′-agatgcagctttacgtggaagactcga-3′ (forward) and 5′-tacgtggaagactcgagtcttgtaa-3′ (reverse) for cyclin D1, 5′-cag cagtcttccaacccaat-3′ (forward) and 5′-cacgaactgaagagcatcca-3′ (reverse) for IGF-1, 5′-cagagggacaaaggaaaagaag-3′ (forward) and 5′-atgctattgaaggggaaccag-3′ (reverse) for HGF, 5′-gtcca acttctgggctgtct-3′ (forward) and 5′-ccctctcctcttccttctcttc-3′ (reverse) for VEGF.

ELISA

The concentrations of IGF-1, HGF, and VEGF in the medium were determined by ELISA kits (Boster, Wuhan, China) according to the manufacturer's instructions. The optical density (OD) was measured at 450 nm by a Varioskan Flash reader (Thermo Fisher Scientific, MA, United States).

Conditional Medium Culture

DPCs were infected with viruses as mentioned before. At 24, 48, and 72 h after infection, the culture medium was changed. The medium at 48 and 72 h later was collected, mixed, and stored in a 4°C refrigerator. HaCaT cells were cultured in 1,640 culture medium with 10% FBS. At 24 and 48 h after seeding the cells, the culture medium was changed to conditional medium from the DPC culture. At 72 h after seeding, the total protein and total RNA of the HaCaT cells were extracted as mentioned before, and they were analyzed by Western blot or qPCR.

Immunofluorescence

DPCs were cultured overnight in 35 mm glass dishes at a density of 1×10^5 cells per dish. The next day, the DPCs were fixed with 4% paraformaldehyde. For paraffin-embedded scalps, the samples were sectioned into 5 μm sections and gradually hydrated. Then the sections were microwaved in citrate buffer (pH 6) for antigen retrieval and rinsed in PBS. Then, the DPCs or sections were treated with 0.1% Triton X-100, blocked with 5% BSA, and incubated overnight at 4°C with anti-KRT15 (Sangon, Shanghai, China), anti-Tcf4 (Proteintech, Shanghai, China), and anti-Twist (Santa Cruz, CA, United States). After washing, the DPCs or sections were incubated with Alexa Fluor 488-labeled donkey anti-rabbit and cy3-labeled goat anti-mouse secondary antibodies, then, they were counterstained with DAPI and observed under a fluorescence microscope.

Co-immunoprecipitation (Co-IP)

Cultured DPCs were lysed with RIPA buffer (Beyotime, Shanghai, China), the protein concentration was measured with BCA, and a small part of the lysate was prepared as input. The rest of the lysate was incubated with immunoglobulin G (IgG; negative control), anti-Twist1 (Santa Cruz, CA, United States), or anti-Tcf4 (Proteintech, Shanghai, China) overnight. Then protein A/G agarose was added to couple to the antibody. Finally, the immunoprecipitate was eluted and analyzed by Western blot.

RESULTS

Twist1 Promotes the Growth of DPCs

Agglutinative growth is one of the characteristics of intact DPCs. To determine whether Twist1 affects the agglutinative growth of DPCs, an adenovirus mediating overexpression of Twist1 was added to cultured DPCs. At 48 and 72 h after overexpression of Twist1, the agglutinative growth behavior of DPCs increased significantly. In contrast, the DPCs in the control group maintained aggregation behavior but did not have the characteristics of agglutinative growth (**Figures 1A,B**). However, the traditional aggregative behavior of DPCs has been demonstrated by self-aggregation of cultured DPC to form three-dimensional cell aggregates (Kiratipaiboon et al., 2015; Topouzi et al., 2017). We did not observe any three-dimensional cell aggregates in our two-dimensional culture system. The agglutinative growth of DPCs in this manuscript is defined as DPCs gather in clusters when growing. The DPC clusters

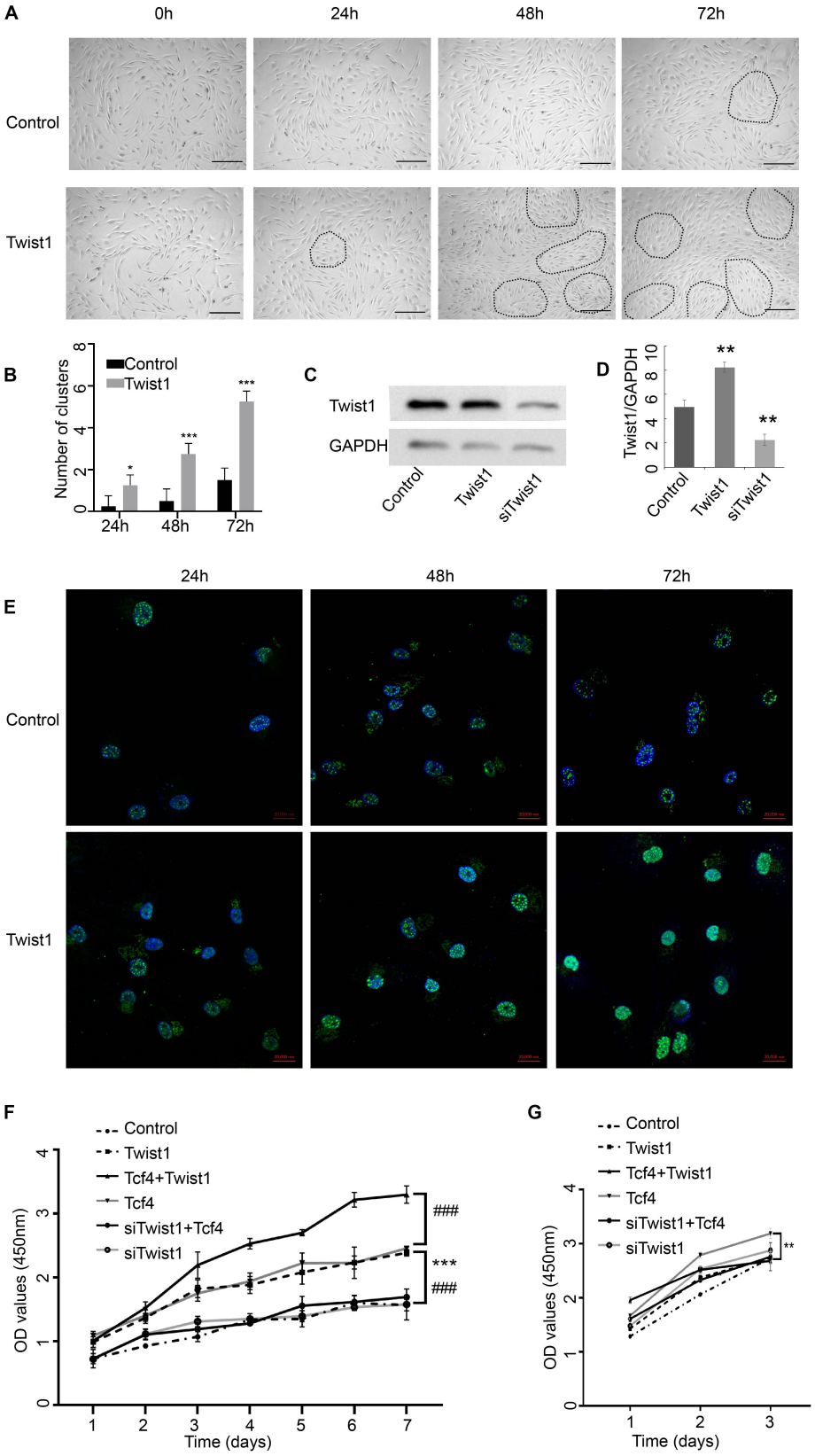

FIGURE 1 | Continued

FIGURE 1 | The impact of Twist1 on the growth of DPCs. **(A,B)** Changes in the morphology of Twist1 overexpressing DPCs. Dashed lines depict the DPC clusters. Scale bar = 50 μm. **(B)** Statistical analysis of **(A)**. **(C,D)** The overexpression and knockdown efficiency of Twist1 vectors. The expression of Twist1 was detected by Western blot. **(D)** Statistical analysis of **(C)**. The expression of Twist1 was normalized to that of GAPDH. **(E)** The expression of Twist1 detected by immunofluorescence in Twist1 overexpressed DPCs. DAPI was used to counterstain the nucleus. Scale bar = 20 μm **(F)** The growth curve of DPCs. **(G)** The growth curve of human fibroblast cells. Equal amounts of DPCs or human fibroblast cells were treated with virus vectors expressing GFP, Twist1, siTwist1, Tcf4, Tcf4, and Twist1, as well as Tcf4 and siTwist1. The proliferation of cells was detected by CCK-8 assay every day from 1 day after treatments. OD, optical density. $N = 3$. $^{\#\#\#}P < 0.001$ when compared with the Tcf4-treated group. $^{*}P < 0.05$ when compared with the control group. $^{**}P < 0.01$ when compared with the control group. $^{***}P < 0.001$ when compared with the control group.

were depicted out with dashed lines in **Figure 1A**. These data indicate that Twist1 plays a specific role in promoting the agglutinative growth of DPCs.

Adenovirus-mediated Twist1 expression or lentivirus-mediated siTwist1 expression effectively overexpressed or knocked down the expression level of Twist1, respectively (**Figures 1C,D**). Immunofluorescence assay demonstrated that the cells in the Twist1-overexpressing conditions maintain high Twist1 expression until 72 h after treatments (**Figure 1E**). Because our previous studies showed that Tcf4 can promote the proliferation of DPCs *in vitro*, we next tried to determine whether Twist1 played a role in the proliferation of DPCs induced by Tcf4. The proliferation rate of DPCs infected with adenovirus-mediated Tcf4 alone increased significantly compared with the control. Interestingly, the proliferation rate of DPCs infected with the virus expressing Tcf4 and siTwist1 was significantly lower than that of DPCs infected with the Tcf4 virus alone, which indicated that the knockdown of Twist1 could inhibit the proliferation of DPCs induced by Tcf4. The proliferation rate of the group co-infected with virus expressing Tcf4 and Twist1 was significantly higher than that of the other groups, which indicated that overexpression of Twist1 could further enhance Tcf4-induced DPC proliferation (**Figure 1F**). The above results imply that Twist1 may interact with Tcf4 in regulating DPC proliferation. We also tested the proliferation of human dermal fibroblast by CCK-8. The dermal fibroblast grew too fast, so we only tested it for 3 days. The effect of Twist1 on dermal fibroblast was different from its effect on DPCs (**Figure 1G**).

Twist1 Promotes the Expression of Tcf4-Induced Target Genes in DPCs

To further research the functional interaction between Twist1 and Tcf4, the effect of Twist1 overexpression on the expression of target genes downstream of Tcf4 (including proto-oncogene c-myc, apoptotic protein survivin, cell cycle protein cyclinD1) was detected in Tcf4 overexpressing DPCs. Both overexpression of Tcf4 and Twist1 promoted the mRNA and protein expression of these downstream target genes in DPCs. Overexpression of Tcf4 and Twist1 together effectively promotes the mRNA and protein expression of c-myc and survivin. The overexpression of Twist1 did not significantly increase the expression of cyclinD1 when compared with Tcf4 overexpressing group. These results indicate that Twist1 is positively correlated with Tcf4-mediated activation of downstream target genes. However, knockdown of Twist1 in DPCs or Tcf4 overexpressing DPCs did not significantly change the expression of these target genes (**Figure 2**).

Twist1 Promotes the Expression and Secretion of Tcf4-Induced Growth Factors in DPCs

DPCs usually regulate hair follicle regeneration by secreting growth factors. To investigate the effect of Twist1 on hair follicle regeneration, the expression and release of hair growth-related growth factors (VEGF, HGF, and IGF-1) were detected after Twist1 was overexpressed in DPCs. Consistent with the role of Tcf4 in DPC proliferation, both overexpression of Tcf4 and Twist1 promoted the mRNA and protein expression of these growth factors in DPCs. Overexpression of Tcf4 and Twist1 together promoted the mRNA and protein expression of these growth factors more effectively than either factor by itself. On the other hand, knockdown of Twist1 in Tcf4-treated DPCs had a lower expression level of these growth factors than that of control cells. However, compared with the control, siTwist1 alone did not significantly change the expression of these growth factors (**Figures 3A–I**). The trends of the expression of these growth factors in the supernatant were the same as they were in DPCs (**Figures 3J–L**). These results indicate that Twist1 is positively related to the production and secretion of growth factors regulated by Tcf4.

Twist1 Maintains Some Biological Properties of DPCs

DPCs were treated with adenoviral vectors expressing Tcf4 and Twist1 or lentiviral vector expressing siTwist1 together or separately. After treatments, the DPCs still maintained expression of intact DPC markers (**Figure 4A**). HaCaT cells are from the basal layer of the skin, and can be induced to differentiate into cells resembling various types of skin cells. The conditioned medium from Twist1-treated DPCs induced HaCaT cells to express higher levels of KRT40, MSX2, KRT5, and KRT15 (**Figures 4B–F**). These results suggest that Twist1 can maintain the ability of DPCs to induce the differentiation of epidermal cells *in vitro*.

Twist1 Physically Interacts With Tcf4 in DPCs

The above data show that there is a functional interaction between Twist1 and Tcf4. Therefore, we next attempted to detect whether there was a physical interaction between Twist1 and Tcf4. Immunofluorescence showed that both Twist1 and Tcf4 were mainly distributed in the nucleus of DPCs. Interestingly, Tcf4 co-localized with a subset of

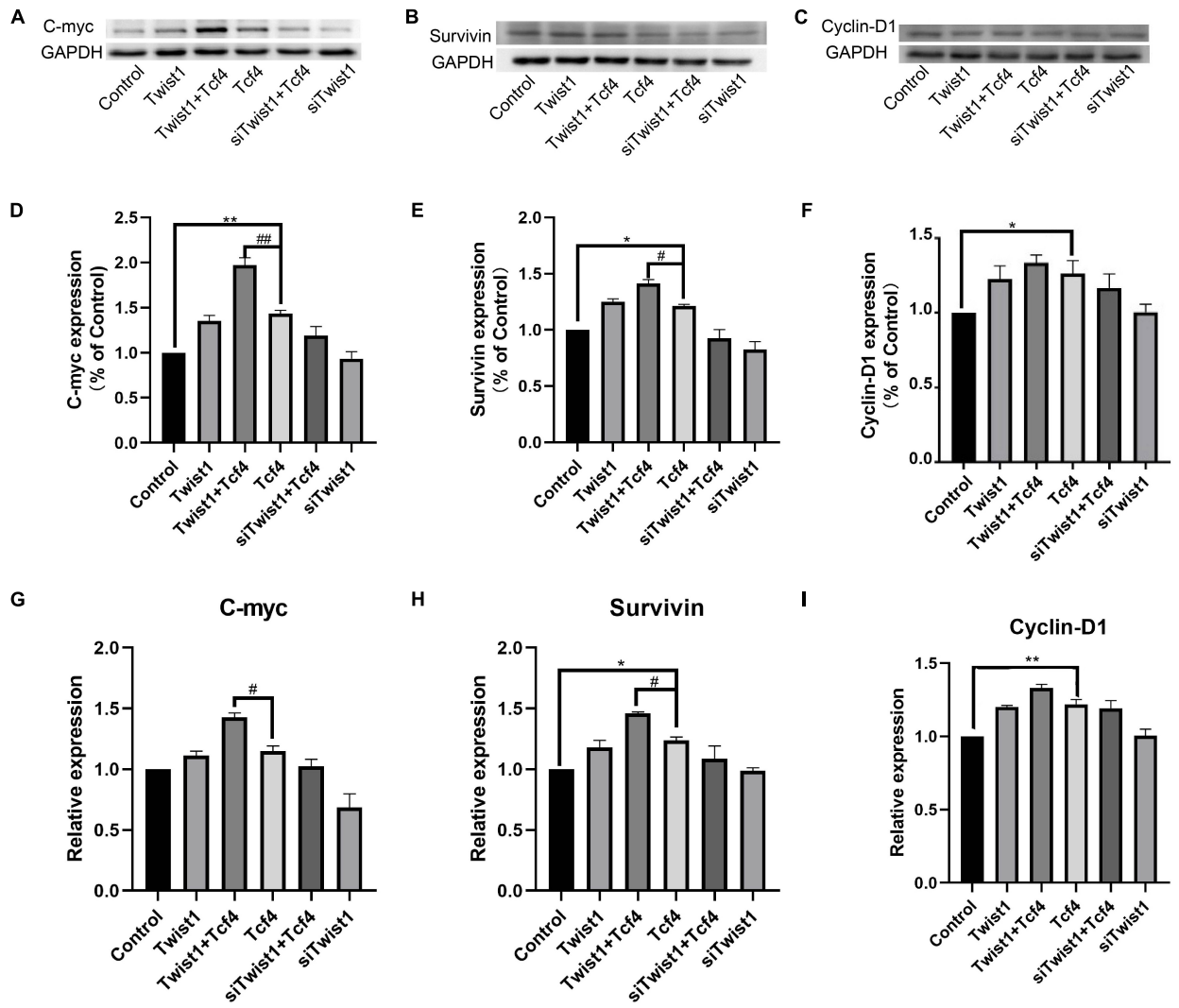

FIGURE 2 | The expression of Tcf4 target genes in DPCs treated with Twist1, Tcf4, and siTwist1. **(A–C)** Western blot results of c-myc, survivin, and cyclinD1. **(D–F)** Quantitative analysis of **(A–C)**. The expression levels of target genes were standardized to that of GAPDH. **(G–I)** qPCR results of c-myc, survivin, and cyclinD1, the expression level of target genes was standardized to that of GAPDH. $N = 3$. $^{\#}P < 0.05$, $^{\#\#}P < 0.01$ when compared with the Tcf4-treated group. $^{*}P < 0.05$, $^{**}P < 0.01$ when compared with the control group.

Twist1 in the nucleus of DPCs (**Figures 5A,B**). Western blot analysis of total protein and nuclear extracts also showed that Twist1 was mainly expressed in the nucleus of DPCs (**Figure 5C**). In co-immunoprecipitation experiments, both Tcf4 and β-catenin were found to be precipitated by anti-Twist1, and both Twist1 and β-catenin were precipitated by anti-Tcf4 (**Figures 5D,E**).

To investigate the role of Twist1 in HFSCs and hair follicle regeneration, the expression of Twist1, Tcf4, and KRT15 was determined by immunofluorescent double labeling. In the hair follicle, KRT15 and Twist1 did not exhibit any kind of co-localization (**Figures 6A,B**). Whereas Tcf4 was colocalized with a subset of Twist1 in the nucleus of some Twist1 expressing DPCs *in vivo* (**Figures 6C,D**). These results demonstrate that Twist1 may physically interact with Tcf4 and β-catenin in DPCs.

DISCUSSION

Tcf4 is encoded by the *Tcf7L2* gene, and it is an important member of the Lef/Tcf protein family. In the process of tissue development and differentiation, Tcf4 responds to the β-catenin signal and initiates the downstream Wnt signaling pathway, thus promoting cell proliferation and differentiation (Cadigan, 2012). Disruption of Tcf4 or β-catenin can block the Wnt signaling pathway and lead to complete loss of cell proliferation (Ma et al., 2020). Our previous studies have shown that Tcf4 was highly expressed in growing hair follicles and in DPCs cultured *in vitro* when its morphological features were still in the agglutinative growth mode (Xiong et al., 2014). The Wnt signaling pathway mediated by the Tcf4/β-catenin complex plays an important role in hair follicle morphogenesis.

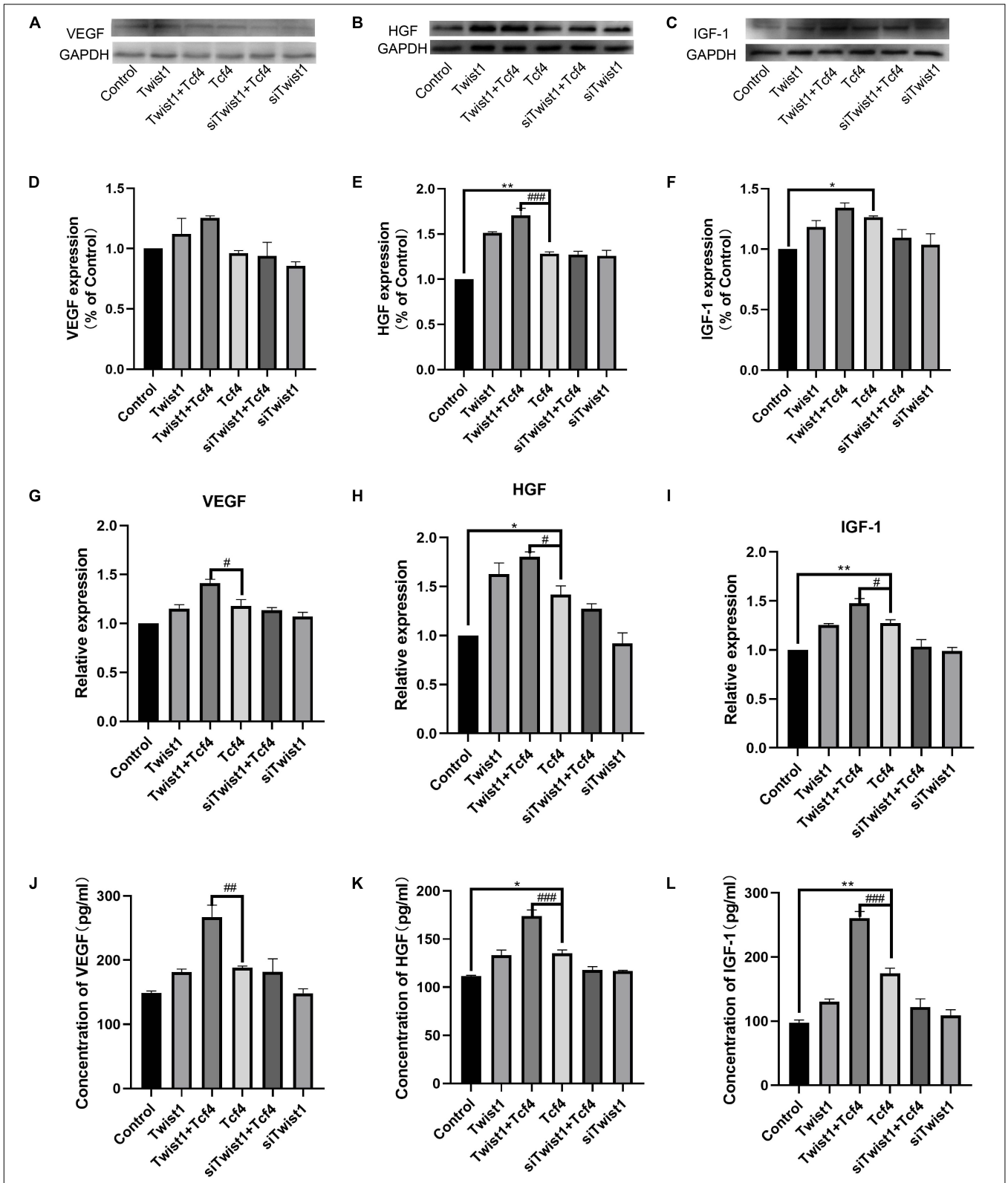

FIGURE 3 | The expression and secretion of hair follicle inductive molecules in DPCs. **(A–C)** Western blot results of VEGF, HGF, and IGF-1. **(D–F)** Quantitative analysis of **(A–C)**. The expression levels of target genes were standardized to that of GAPDH. **(G–I)** qPCR result of VEGF, HGF, and IGF-1. The expression level of target genes was standardized to that of GAPDH. **(J–L)** Expression of VEGF, HGF, and IGF-1 detected by ELISA in the culture supernatant of DPCs. $N = 3$. $^{\#}P < 0.05$, $^{\#\#}P < 0.01$ when compared with the Tcf4-treated group, $^{\#\#\#}P < 0.001$ when compared with the Tcf-treated group. $^{*}P < 0.05$, $^{**}P < 0.01$ when compared with the control group.

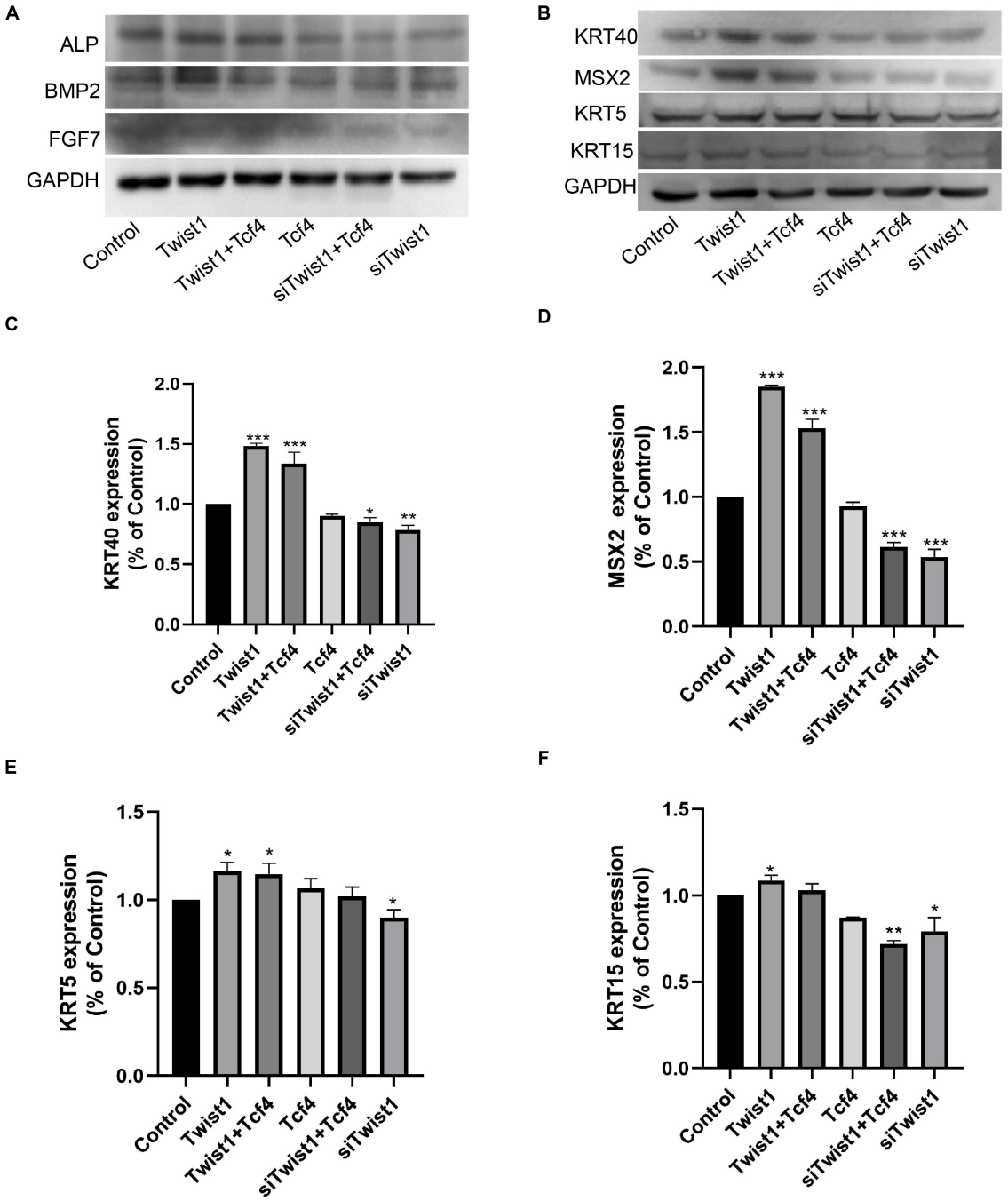

FIGURE 4 | The inductive ability of DPCs. **(A)** The intact DPC markers ALP, BMP2, and FGF7 were detected by Western blot. **(B–F)** HaCaT cells were cultured with conditioned medium from DPCs treated with virus expressing Tcf4, Twist1, and siTwist1. Differentiation markers KRT40, MSX2, KRT5, and KRT15 were detected by Western blot. **(C–F)** Quantitative analysis of **(B)**. The expression levels of target genes were standardized to that of GAPDH. $^{*}P < 0.05$ when compared with the control group. $^{**}P < 0.01$ when compared with the control group. $^{***}P < 0.001$ when compared with the control group.

However, it is not clear how Tcf4/β-catenin participates in the process of hair follicle induction and growth. In this study, we found that Twist1 could promote the proliferation of DPCs (**Figure 1**), and the overexpression of Twist1 could promote the expression of downstream target genes of Tcf4 and the secretion and release of growth factors in DPCs (**Figures 2**, **3**). The function of Twist1 was consistent with that in a previous report (Shen et al., 2019). Therefore, Twist1 may be a positive regulatory partner of Tcf4. However, the knockdown of Twist1 did not affect the target gene expression, growth factors secretion or release of DPCs. One possible explanation for this difference is that the effects of downstream gene activation

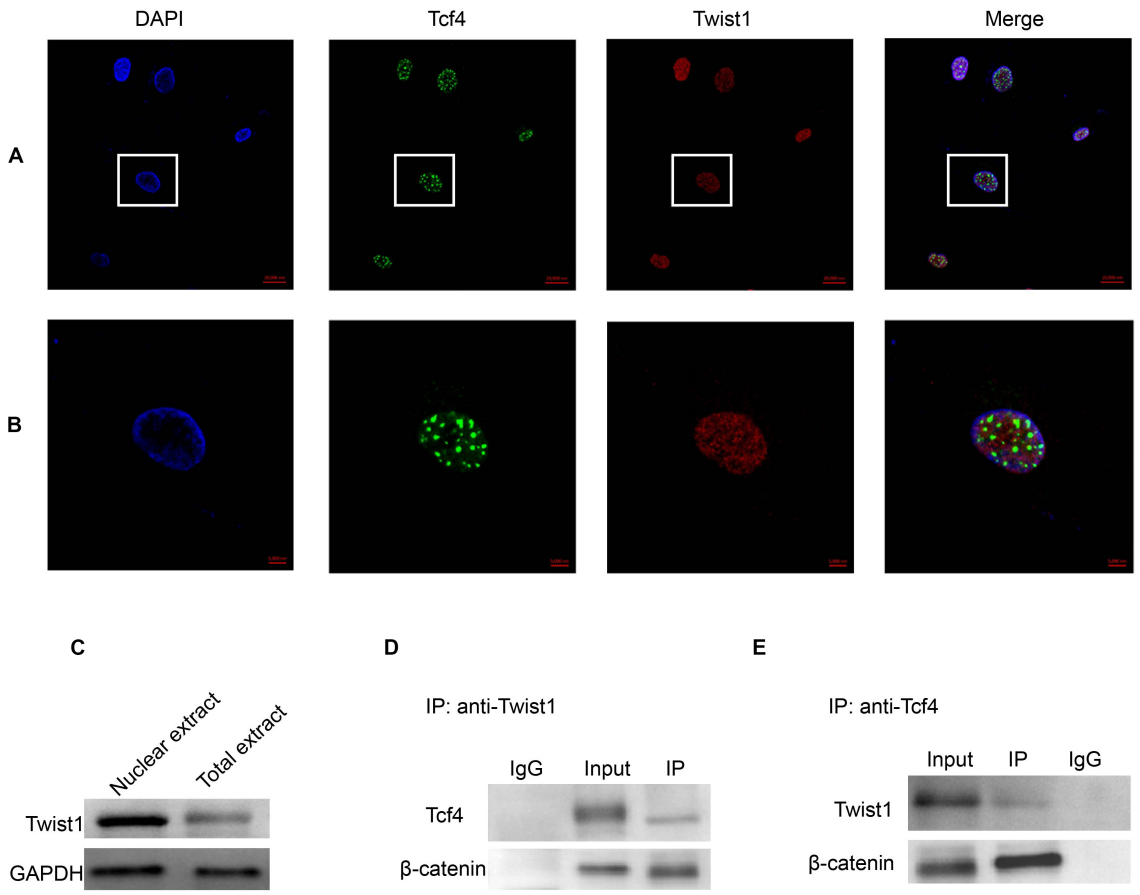

FIGURE 5 | The interaction of Tcf4 and Twist1 in DPCs. **(A,B)** The expression of Tcf4 and Twist1 were detected by immunofluorescence in cultured DPCs. **(A)** Scale bar = 20 μm. **(B)** Scale bar = 5 μm. **(C)** The expression of Twist1 was determined by Western blot in nuclear extract and total extract from cultured DPCs. **(D)** The expression of Tcf4 and β-catenin in the anti-Twist1 precipitated complex in cultured DPCs. **(E)** The expression of Twist1 and β-catenin in the anti-Tcf4 precipitated complex in cultured DPCs.

and transcription may be compensated for or replaced by other molecules.

DPCs located at the bottom of hair follicles can induce hair follicle regeneration and control the periodic growth of hair follicles. These characteristics of DPCs have been used to develop treatments for alopecia, including hair follicle autografts. It has been proven that DPCs cultured *in vitro* have the ability to induce hair growth only when they have the characteristics of agglutinative growth. At the same time, this agglutinative growth mode gradually disappears with an increase in the number of passages (Lei et al., 2017). Higgins et al. found that the transcription profiles of intact dermal papilla can be partially restored by culturing DPCs in 3D spheroid cultures (Higgins et al., 2013). Due to the decreased expression level of Tcf4 in DPCs during passages, there may be a correlation between Tcf4 expression and the agglutinative growth mode of DPCs. In this study, we first proved that Twist1 could promote the agglutinative growth behavior of DPCs *in vitro*, which shows that Tcf4 and Twist1 have a similar effect on the agglutinative growth behavior of DPCs. It is well known that downstream target genes of Tcf4 in Wnt signaling, c-myc, survivin and cyclinD1, are involved in cell growth and cell cycle regulation, and growth factors HGF, VEGF, and IGF-1 promote hair growth. C-myc was required to maintain the stem cell-like phenotypes of DPCs (Muchkaeva et al., 2014), which was a critical biological process that kept the high rate of hair growth (Kiratipaiboon et al., 2015). The expression level of survivin in DPCs is related to hair growth (Zhang et al., 2016). CyclinD1 is one of the main factors that regulates DPCs' entry into the S phase (Kang et al., 2017). Our data demonstrated that Twist1 and Tcf4 co-overexpression increased the expression of c-myc and survivin, but did not increase the expression of cyclin D1 distinguishably, when compared with Tcf4 overexpressing group. Maybe cyclin D1 is very sensitive to Tcf4 and Twist1 in this case, so that the overexpression of Twist1 or Tcf4 alone had already increased the expression of cyclin D1 to the highest level of the cell needed. HGF was first found to be a polypeptide factor that promotes cell mitosis in plasma and platelets and has been reported to activate hair follicle morphogenesis during the growth period (Fujie et al., 2001). IGF-1 is a structural homolog of insulin, which is expressed in mesenchymal cells of the hair bulb and dermis. It has a significant impact on the hair follicle cycle and plays an active role in regulating hair follicle development

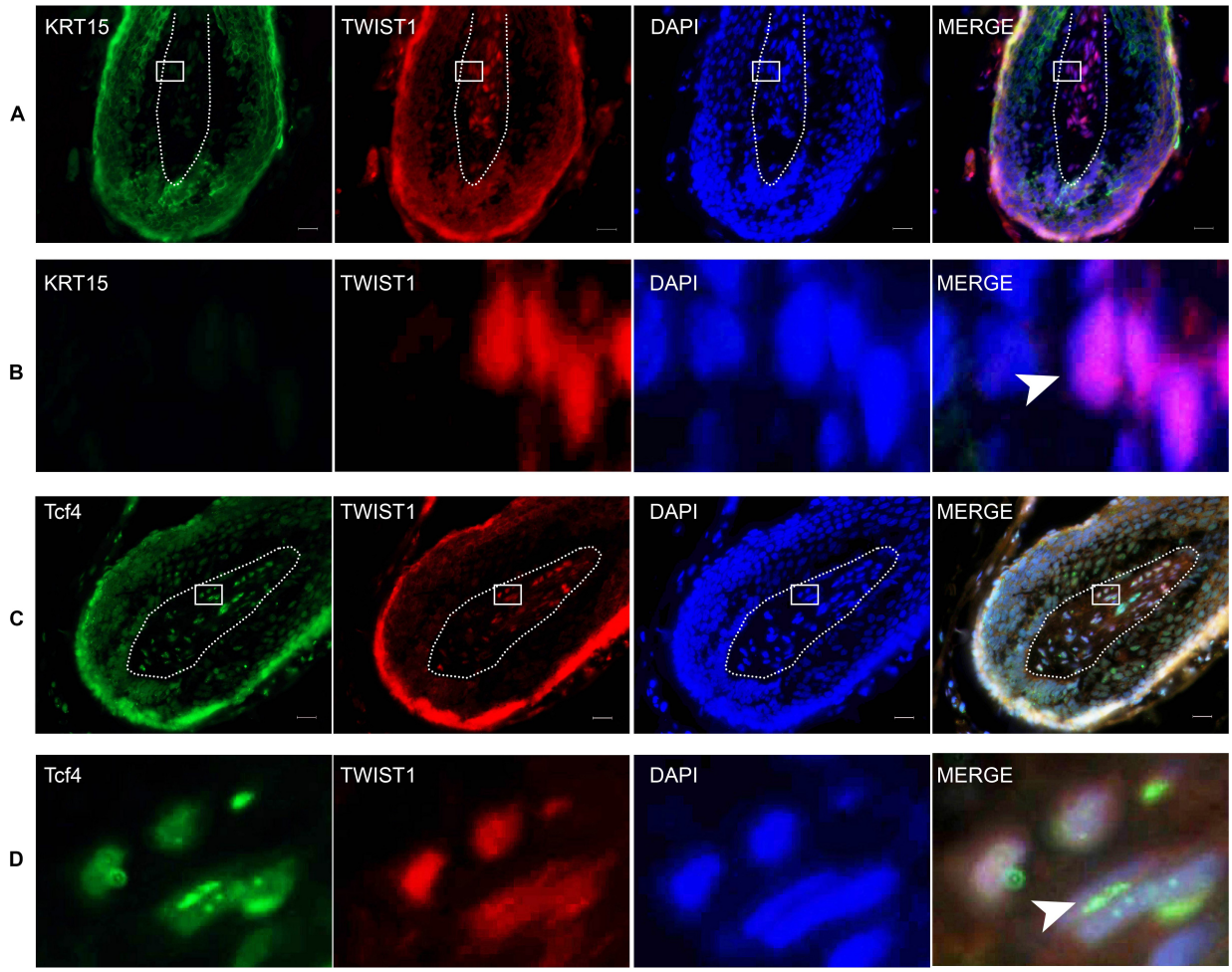

FIGURE 6 | The expression of KRT15, Twist1, and Tcf4 in the scalp. The right panel is a merged image of the left three panels. Dashed lines depict the structure of the dermal papilla. **(B)** The enlarged picture of the framed area in **(A)**. Arrowhead denotes the positive expression of Twist1 in the nucleus. **(D)** Is the enlarged picture of the framed area in **(C)**. Arrowhead denotes the co-expression of Tcf4 and Twist1 in the nucleus. Scale bar = 20 μm.

(Ben Amitai et al., 2006). VEGF is a vascular endothelial factor that can promote hair growth by inducing capillary formation around hair follicles (Zhang et al., 2019). Consistent with these results, Tcf4 and Twist1 increased the mRNA and protein levels of c-myc, survivin, and cyclin-D1 and the secretion of HGF, VEGF, and IGF-1 (**Figures 2**, **3**). In addition, conditioned medium from Twist1-treated DPCs induced HaCaT cells to express differential markers (**Figure 4**). These effects were enhanced when Tcf4 and Twist1 were overexpressed together, indicating that Twist1 had a positive effect on the maintenance of some biological properties of DPCs.

Twist1 is an autosomal bHLH transcription factor. Its structure includes an N-terminal, a C-terminal, and a highly conserved bHLH domain. The domain with DNA binding sites is the main domain required for Twist1 to function as a transcription factor. Epithelial-mesenchymal transition (EMT) is very important for the development of metastatic diseases. Twist1 is considered to be an inducer of EMT and a basic regulator of some metastatic diseases (Shen et al., 2019). It has been reported that skin formed by the interaction of epithelial and mesenchymal components. The hair follicle has become one of the main models to research this special regeneration structure. Hair follicle epithelium and HFSCs respond to signals from DPCs (Lei et al., 2017). Because Twist1 is a positive regulator of TCF4, Twist1 may play a key role in regulating the Wnt signaling pathway as it relates to DPC growth and hair follicle induction. However, from our data, we found that only a subset of Twist1 expressing cells expressed Tcf4, and only a sunset of Twist1 expressing foci also expressed Tcf4 in the cell nucleus. All Tcf4 expressing cells or foci expressed Twist1. These expression patterns suggested that Twist1 might have other functions in the cell.

CONCLUSION

In conclusion, we reported that Twist1 promoted the agglutinative growth of DPCs, promoted the proliferation of DPCs induced by Tcf4 and promoted the expression of target

genes of Tcf4 and the secretion of growth factors that regulate HFSC activation and hair follicle regeneration. We also reported that Twist1 functioned by forming a ternary complex with Tcf4 and β-catenin. Thus, we report new data that elucidate whether and how Twist1 regulates some biological properties of DPCs *in vitro*. Targeting the Twist1/Tcf4 complex is a potential treatment strategy for hair loss.

DATA AVAILABILITY STATEMENT

All datasets generated for this study are included in the article/supplementary material.

ETHICS STATEMENT

This study was approved by the Ethics Committee of The First Affiliated Hospital of the Third Military Medical University (ethics approval no. ky201977). The patients/participants provided their written informed consent to participate in this study.

AUTHOR CONTRIBUTIONS

XY and YL designed the conceptual idea for this study. NY and TH performed most of the experiments. HY and LZ performed some of the experiments. QS and FX analyzed the data. NY and YL wrote the manuscript. All authors approved the submission of this manuscript in its final form.

FUNDING

This work was supported by the National Natural Science Foundation of China (No. 81472895) and the Natural Science Foundation of Chongqing (No. cstc2019jcyj-msxmX0625).

REFERENCES

Al-Nuaimi, Y., Baier, G., Watson, R. E., Chuong, C. M., and Paus, R. (2010). The cycling hair follicle as an ideal systems biology research model. *Exp. Dermatol.* 19, 707–713. doi: 10.1111/j.1600-0625.2010.01114.x

Amberg, N., Holcmann, M., Stulnig, G., and Sibilia, M. (2016). Effects of imiquimod on hair follicle stem cells and hair cycle progression. *J. Invest. Dermatol.* 136, 2140–2149. doi: 10.1016/j.jid.2016.06.613

Bejaoui, M., Villareal, M. O., and Isoda, H. (2019). beta-catenin-mediated hair growth induction effect of 3,4,5-tri-O-caffeoylquinic acid. *Aging* 11, 4216–4237. doi: 10.18632/aging.102048

Ben Amitai, D., Lurie, R., and Laron, Z. (2006). I-GF-1 signalling controls the hair growth cycle and the differentiation of hair shafts. *J. Invest. Dermatol.* 126:2135. doi: 10.1038/sj.jid.5700436

Cadigan, K. M. (2012). TCFs and Wnt/beta-catenin signaling: more than one way to throw the switch. *Curr. Top. Dev. Biol.* 98, 1–34. doi: 10.1016/B978-0-12-386499-4.00001-X

Chen, Z., Wang, X., Jin, T., Wang, Y., Hong, C. S., Tan, L., et al. (2017). Increase in the radioresistance of normal skin fibroblasts but not tumor cells by mechanical injury. *Cell Death Dis.* 8:e2573. doi: 10.1038/cddis.2016.416

Driskell, R. R., Clavel, C., Rendl, M., and Watt, F. M. (2011). Hair follicle dermal papilla cells at a glance. *J. Cell. Sci.* 124(Pt 8), 1179–1182. doi: 10.1242/jcs.082446

Fabbrocini, G., Panariello, L., De Vita, V., Vincenzi, C., Lauro, C., Nappo, D., et al. (2013). Quality of life in alopecia areata: a disease-specific questionnaire. *J. Eur. Acad. Dermatol. Venereol.* 27, e276–e281. doi: 10.1111/j.1468-3083.2012.04629.x

Fujie, T., Katoh, S., Oura, H., Urano, Y., and Arase, S. (2001). The chemotactic effect of a dermal papilla cell-derived factor on outer root sheath cells. *J. Dermatol. Sci.* 25, 206–212.

Higgins, C. A., Chen, J. C., Cerise, J. E., Jahoda, C. A., and Christiano, A. M. (2013). Microenvironmental reprogramming by three-dimensional culture enables dermal papilla cells to induce de novo human hair-follicle growth. *Proc. Natl. Acad. Sci. U.S.A.* 110, 19679–19688. doi: 10.1073/pnas.1309970110

Hunt, N., and McHale, S. (2005). The psychological impact of alopecia. *BMJ* 331, 951–953. doi: 10.1136/bmj.331.7522.951

Kang, J. I., Kim, M. K., Lee, J. H., Jeon, Y. J., Hwang, E. K., Koh, Y. S., et al. (2017). Undariopsis peterseniana Promotes Hair Growth by the Activation of Wnt/beta-Catenin and ERK pathways. *Mar. Drugs* 15:130. doi: 10.3390/md15050130

Kiratipaiboon, C., Tengamnuay, P., and Chanvorachote, P. (2015). Glycyrrhizic acid attenuates stem cell-like phenotypes of human dermal papilla cells. *Phytomedicine* 22, 1269–1278. doi: 10.1016/j.phymed.2015.11.002

Lei, M., Yang, L., and Chuong, C. M. (2017). Getting to the core of the dermal papilla. *J. Invest. Dermatol.* 137, 2250–2253. doi: 10.1016/j.jid.2017.07.824

Li, Y. H., Zhang, K., Yang, K., Ye, J. X., Xing, Y. Z., Guo, H. Y., et al. (2013). Adenovirus-mediated Wnt10b overexpression induces hair follicle regeneration. *J. Invest. Dermatol.* 133, 42–48. doi: 10.1038/jid.2012.235

Ma, X., Xiang, F., Pei, Z., Miao, J., Wu, P., Song, X., et al. (2020). Circ-Smad5 retards the G1/S transition of cell cycle via inhibiting the activity of wnt/lef/cyclind1 signaling in JB6 cells. *Genes Dis.* (in press). doi: 10.1016/j.gendis.2020.01.001

Miao, Y., Sun, Y. B., Liu, B. C., Jiang, J. D., and Hu, Z. Q. (2014). Controllable production of transplantable adult human high-passage dermal papilla spheroids using 3D matrigel culture. *Tissue Eng. Part A* 20, 2329–2338. doi: 10.1089/ten.TEA.2013.0547

Muchkaeva, I. A., Dashinimaev, E. B., Artyuhov, A. S., Myagkova, E. P., Vorotelyak, E. A., Yegorov, Y. Y., et al. (2014). Generation of iPS cells from human hair follice dermal papilla cells. *Acta Nat.* 6, 45–53.

Oshimori, N., and Fuchs, E. (2012). Paracrine TGF-beta signaling counterbalances BMP-mediated repression in hair follicle stem cell activation. *Cell Stem Cell* 10, 63–75. doi: 10.1016/j.stem.2011.11.005

Shen, X., Jiang, H., Chen, Z., Lu, B., Zhu, Y., Mao, J., et al. (2019). MicroRNA-145 Inhibits Cell Migration and Invasion in Colorectal Cancer by Targeting TWIST. *OncoTargets Therapy* 12, 10799–10809. doi: 10.2147/OTT.S216147

Topouzi, H., Logan, N. J., Williams, G., and Higgins, C. A. (2017). Methods for the isolation and 3D culture of dermal papilla cells from human hair follicles. *Exp. Dermatol.* 26, 491–496. doi: 10.1111/exd.13368

Van Der Donk, J., Hunfeld, J. A., Passchier, J., Knegt-Junk, K. J., and Nieboer, C. (1994). Quality of life and maladjustment associated with hair loss in women with alopecia androgenetica. *Soc. Sci. Med.* 38, 159–163. doi: 10.1016/0277-9536(94)90311-5

Williamson, D., Gonzalez, M., and Finlay, A. Y. (2001). The effect of hair loss on quality of life. *J. Eur. Acad. Dermatol. Venereol.* 15, 137–139. doi: 10.1046/j.1468-3083.2001.00229.x

Wu, J., Liao, Q., He, H., Zhong, D., and Yin, K. (2014). TWIST interacts with beta-catenin signaling on osteosarcoma cell survival against cisplatin. *Mol. Carcinogen.* 53, 440–446. doi: 10.1002/mc.21991

Wu, P., Zhang, Y., Xing, Y., Xu, W., Guo, H., Deng, F., et al. (2019). The balance of Bmp6 and Wnt10b regulates the telogen-anagen transition of hair follicles. *Cell Commun. Signal.* 17:16. doi: 10.1186/s12964-019-0330-x

Xiong, Y., Liu, Y., Song, Z., Hao, F., and Yang, X. (2014). Identification of Wnt/beta-catenin signaling pathway in dermal papilla cells of human scalp hair follicles: TCF4 regulates the proliferation and secretory activity of dermal papilla cell. *J. Dermatol.* 41, 84–91. doi: 10.1111/1346-8138.12313

Yu, N., Song, Z., Zhang, K., and Yang, X. (2017). MAD2B acts as a negative regulatory partner of TCF4 on proliferation in human dermal papilla cells. *Sci. Rep.* 7:11687. doi: 10.1038/s41598-017-10350-w

Yu, N. L., Tan, H., Song, Z. Q., and Yang, X. C. (2016). Illness perception in patients with androgenetic alopecia and alopecia areata in China. *J. Psychosom. Res.* 86, 1–6. doi: 10.1016/j.jpsychores.2016.04.005

Zhang, H., Nan, W., Wang, S., Zhang, T., Si, H., Wang, D., et al. (2016). Epidermal growth factor promotes proliferation of dermal papilla cells via Notch signaling pathway. *Biochimie* 127, 10–18. doi: 10.1016/j.biochi.2016.04.015

Zhang, X., Zhou, D., Ma, T., and Liu, Q. (2019). Vascular endothelial growth factor protects CD200-rich and CD34-positive hair follicle stem cells against androgen-induced apoptosis through the phosphoinositide 3-Kinase/Akt pathway in patients with androgenic alopecia. *Dermatol. Surg.* 46, 358–368. doi: 10.1097/DSS.0000000000002091

Conflict of Interest: The authors declare that the research was conducted in the absence of any commercial or financial relationships that could be construed as a potential conflict of interest.

Copyright © 2020 Yu, Hu, Yang, Zhang, Song, Xiang, Yang and Li. This is an open-access article distributed under the terms of the Creative Commons Attribution License (CC BY). The use, distribution or reproduction in other forums is permitted, provided the original author(s) and the copyright owner(s) are credited and that the original publication in this journal is cited, in accordance with accepted academic practice. No use, distribution or reproduction is permitted which does not comply with these terms.

frontiers in Cell and Developmental Biology

ORIGINAL RESEARCH
published: 02 September 2020
doi: 10.3389/fcell.2020.00627

IL-36α Promoted Wound Induced Hair Follicle Neogenesis via Hair Follicle Stem/Progenitor Cell Proliferation

Lin Gong[1,2], Jian Xiao[3], Xiaokun Li[3], Yuanhong Li[1], Xinghua Gao[1] and Xuegang Xu[1]**

[1] Department of Dermatology, The First Hospital of China Medical University, Shenyang, China, [2] Department of Dermatology, The First Affiliated Hospital of Dalian Medical University, Dalian, China, [3] School of Pharmaceutical Sciences, Wenzhou Medical University, Wenzhou, China

Background: Wound-induced hair follicle neogenesis (WIHN) is a phenomenon of hair neogenesis that occurs at the center of a scar when the wound area is sufficiently large. Neogenic hair follicles are separated from the pre-existing follicles at the wound edge by a hairless circular region. This WIHN study provides a unique model for developing treatments for hair loss and deciphering the mechanisms underlying organogenesis in adult mammals.

Methods: The skin of a mouse was wounded by excising a 1.5 × 1.5 cm^2 square of full-thickness dorsal skin. iTRAQ technology was used to screen proteins differentially expressed between the inner and outer scar areas in a mouse model of WIHN, on post-wounding day 15, to identify the regulators of WIHN. Owing to the overexpression of interleukin-36α (IL-36α) in the *de novo* hair follicle growth area, the regulating effect of IL-36α overexpression in WIHN was investigated. Hair follicle stem/progenitor cells were counted by flow cytometry while the expression of hair follicle stem/progenitor cell markers (*Lgr5, Lgr6, Lrig1, K15,* and *CD34*) and that of Wnt/β-catenin and IL-6/STAT3 pathway intermediaries was detected by qPCR and western blotting.

Results: We found that wounding induced IL-36α expression. Incorporation of recombinant murine IL-36α (mrIL-36α) into murine skin wounds resulted in a greater number of regenerated hair follicles ($p < 0.005$) and a faster healing rate. The expression of hair follicle stem/progenitor cell markers was upregulated in the mrIL-36α-injected site ($p < 0.05$). Additionally, mrIL-36α upregulated the IL-6/STAT3 pathway intermediaries.

Conclusion: IL-36α is upregulated in *de novo* hair follicle growth areas and can promote wound epithelialization and WIHN.

Keywords: hair follicle, wound epithelialization, IL-36α, stem cell, IL-6/STAT3 pathway

OPEN ACCESS

Edited by:
Mingxing Lei,
Chongqing University, China

Reviewed by:
Ji Li,
Xiangya Hospital, Central South University, China
Weiming Qiu,
General Hospital of Central Theater Command, China

****Correspondence:***
Xuegang Xu
xuxuegang2749290@163.com
Xinghua Gao
gaobarry@hotmail.com

Specialty section:
This article was submitted to Stem Cell Research, a section of the journal Frontiers in Cell and Developmental Biology

Received: *25 February 2020*
Accepted: *23 June 2020*
Published: *02 September 2020*

Citation:
Gong L, Xiao J, Li X, Li Y, Gao X and Xu X (2020) IL-36α Promoted Wound Induced Hair Follicle Neogenesis via Hair Follicle Stem/Progenitor Cell Proliferation. Front. Cell Dev. Biol. 8:627. doi: 10.3389/fcell.2020.00627

INTRODUCTION

Wound-induced hair follicle neogenesis (WIHN) is a phenomenon in which the skin, sebaceous glands, and hair follicles regenerate following the occurrence of large, full-thickness wound in adult mice. WIHN has also been observed in rabbits, sheep, and spiny mice (Billingham and Russell, 1956; Brook et al., 1960; Seifert et al., 2012), while there are conflicting reports about

WIHN in rats (Guerrero-Juarez et al., 2018). Studying WIHN in different species is helpful for deciphering mechanisms underlying the regeneration in mammals and may provide insights into novel approaches for hair loss treatments.

In addition to the canonical Wnt/β-catenin pathway (Ito et al., 2007), inflammation-related factors are also believed to play important roles in WIHN. Macrophages regulate WIHN through the AKT/β-catenin pathway by secreting a cytokine known as tumor necrosis factor (TNF) (Wang et al., 2017). Activated γδT cells secrete FGF9 (fibroblast growth factor 9), which promotes WIHN (Gay et al., 2013). Further, interleukin 1 (IL-1), along with IL-7 can activate the T cells to promote the proliferation of hair follicle stem cells (Lee et al., 2017). The IL-6/STAT3 (signal transducers and activators of transcription 3) axis, which is induced in response to tissue damage and double-stranded RNA production, also promotes WIHN (Nelson et al., 2015).

Interleukin-36α is a pro-inflammatory cytokine of the IL-1 family. It acts on both epithelial cells and specific immune cells, by inducing cellular activation and secretion of cytokines and chemokines, leading to the recruitment and activation of a variety of immune cells (Bassoy et al., 2018). Using iTRAQ (isobaric tags for relative and absolute quantitation) technology, we analyzed the differential protein expression in the inner and outer scar regions in a WIHN mouse model. We found that IL-36α was upregulated in the center of the scar, which is the main area for *de novo* hair follicle growth. Previous studies demonstrated that inflammation-related factors, such as IL-1, IL-6, and TNF, could promote WIHN. IL-36α has been proven to induce the secretion of these inflammation-related factors (Dietrich et al., 2016). Accordingly, we evaluated the effects of IL-36α with respect to promoting WIHN and investigated the underlying pathways responsible for regulating the hair growth.

MATERIALS AND METHODS

Animal Model

Mice with a C57BL/6 background were purchased from Liaoning Changsheng Biotechnology Co., Ltd. (Benxi, China). Female mice (7–10 weeks old) were used in all *in vivo* experiments. All animal procedures were performed ethically in accordance with the institutional guidelines for animal experiments and was approved by the Institutional Animal Care and Use Committee at China Medical University, China.

WIHN Surgical Procedure

Mice were anesthetized *via* isoflurane inhalation (RWD Life Science Co., Shenzhen, China) and had their dorsal hair shaved off. Skin wounds were introduced by excising a 1.5 × 1.5 cm^2 square of full-thickness dorsal skin (used for investigating wound healing and related hair neogenesis as indicated). Subsequently, either 1 ng/μL recombinant murine IL-36α (mrIL-36α; R&D systems, Minneapolis, MN, United States) – dissolved in 50 μL phosphate-buffered-saline (PBS) – or PBS alone (Solarbio, Beijing, China) was injected into the healing wound (beneath the scab into the granulation tissue) once a day for post-wound day (PWD) 7–14. Full-thickness healed skin was harvested at PWD 15 and divided into two groups – the *de novo* hair follicle area (inner area) and no hair follicle area (outer area) – and used for proteomic analysis, real time quantitative PCR (qPCR), and western blotting for IL-36α expression detection. Full-thickness healed skin from wounded mice was harvested at PWD 7, 10, 12, 15, and 20, and normal skin from non-wounded mice was used for immunohistochemistry, qPCR, and western blotting to detect the spatiotemporal expression of IL-36α .

In addition, 50 μL of 1 ng/μL mrIL-36α – dissolved in PBS – or PBS only was injected intradermally into two separate dorsal skin regions of 7-week-old mice once a day. Full-thickness injected skin was harvested for qPCR and western blotting at day 3- and flow cytometry at day 4-post injection.

Hair Follicle Quantification

Healed skin was collected at PWD 28 and incubated in 5% dispase (Gibco, Carlsbad, CA, United States) overnight at 25 ± 1°C. The epidermis was removed under a stereoscopic microscope (ZSA302,COIC, Chongqing, China) and the remaining dermis was fixed in 10% buffered formalin for 10 min, rinsed thrice with PBS and incubated with BCIP/NBT (BCIP/NBT Alkaline Phosphatase Color Development Kit, Jiangsu, China) for 30 min. Lastly, the dermal preparation was rinsed twice with distilled water to stop the reaction. Hair follicle quantification was performed under a dissecting microscope.

Proteomic Analysis

In order to meet the minimum sample size and to minimize potential confounding factors in iTRAQ experiments, we pooled 15 mice for our proteomic analyses. Experiments were performed in triplicate, and only proteins with confirmed identification in all three experiments have been reported here. The proteins were extracted, resolved by sodium dodecyl-sulfate polyacrylamide gel electrophoresis (SDS-PAGE) on a 10% gel, and visualized using Coomassie Blue staining to check for protein quality. The protein samples (200 μg) were mixed with dl-dithiothreitol (DTT) and alkylated with iodoacetamide (IAA). Subsequently, samples were subjected to repeated ultrafiltration by UA (urea, Tris–HCl, pH 8) twice, tetraethyl-ammonium bromide (TEAB) thrice, and treated with trypsin overnight at a trypsin-to-protein ratio of 1:50 at 37°C.

Peptides (100 μg) from each group were labeled using an iTRAQ reagent-8 plex multiplex kit (AB SCIEX, Framingham, MA, United States). One microliter sample was tested from each group to analyze labeling and extraction efficiency. All samples were pooled and vacuum-dried. Next, the mixed lyophilized peptides were resuspended in solution A (20 mM ammonium formate, pH 10) and supernatants were collected after centrifugation at 12,000 × *g* for 20 min. Subsequently, the samples were loaded onto C18 reversed-phase columns (Michrom Bioresources, Inc., Auburn, CA, United States) and eluted with a non-linear gradient ramped from 0 to 90% mobile phase B (phase A: 20 mM ammonium formate, pH 10, phase B: 20 mM ammonium formate in ACN, pH 10) at a 0.7 μL/min flow rate for 53 min. After 5 min, the eluates were collected

at 1.5 min intervals. A total of 60 fractions were collected and subsequently combined into six fractions according to peak intensities. Supernatants were collected after centrifuging the collected fractions at 14,000 × *g* for 10 min for analysis.

Peptides were analyzed using an ultra-performance liquid chromatography–mass spectrometry/mass spectrometry (LC-MS/MS) platform. The LC separation was performed on an Easy nLC 1000 (Thermo Fisher Scientific, Waltham, MA, United States) with an in-house packed capillary column (150 μm I.D. × 12 cm) with 1.9 μm C18 reverse-phase fused-silica (Michrom Bioresources). The sample was eluted with a non-linear gradient ramped from 8 to 95% mobile phase B (phase A: 0.1% formic acid in water, phase B: 0.1% FA in ACN) at a 0.6 μL/min flow rate for 78 min.

The raw mass data for the peptide data analysis were processed using the Proteome Discoverer Software with a false discovery rate (FDR) $\leq$ 0.01 whilst searching the Uniprot-mouse_170221.fasta database. Protein with at least two unique peptides were identified. The upregulated or downregulated proteins in both replicates with relative quantification $p < 0.05$ and 1.5-fold changes (FC) were selected to be the differentially expressed proteins (DEPs).

Real Time Quantitative PCR (qPCR)

Total RNA from the full-thickness murine skin was extracted using a miRNeasy mini kit (Qiagen, Hilden, Germany) following the manufacturer's instructions. cDNA was synthesized from RNA using a GoScript Reverse Transcription System (Promega, Madison, WI, United States). qPCR was performed in 96-well plates using a 7900HT Fast qPCR system (Applied Biosystems, Foster City, CA, United States); *GAPDH* expression was used as the internal control to normalize the expression of the target genes; fold change in expression was calculated using the ΔΔCt method. Primer sequences used to amplify the murine genes are listed in **Supplementary Table S1**.

Total Skin Epithelial Cell Isolation and Flow Cytometry Analysis

Subcutaneous fat was mechanically removed, and the dorsal skins were incubated in dispase (2 mg/mL) for 40 min at 37°C. Epidermis was harvested by mechanical scraping with a scalpel and incubated in digestive fluid [0.05% Trypsin (Gibco), 100 μg/mL DNase (Lablead, Beijing, China)] for 40 min at 37°C. An equivalent volume of complete medium was then added to stop the digestion. Cells were strained through a 70 μm cell filter (Solarbio), and the resulting solution was centrifuged at 1000 × *g* for 8 min. The supernatant was discarded and the remaining adult mouse-derived primary skin epithelial cells (MPSECs) were washed twice with PBS (containing 1% fetal calf serum).

Single cell suspensions of MPSECs in PBS were incubated with anti-mCD49f-FITC (BioLegend, United States), anti-mCD34-PE (BD Pharmingen, Franklin Lakes, NJ, United States), and anti-mP-cadherin-APC (R&D systems) for 25 min at 4°C. After washing twice, the cells were resuspended in PBS. FACS analyses were performed using a Flow Cytometer (BD LSRFortessa, BD Biosciences, Franklin Lakes, NJ, United States).

Western Blotting

Total protein was extracted in RIPA lysis buffer (Beyotime Biotechnology, Haimen, China) supplemented with protease inhibitors and phosphatase inhibitors (Beyotime Biotechnology). Protein concentration was determined using the BCA assay (Thermo Fisher Scientific). Protein samples of 30 μg were separated by SDS-PAGE (Thermo Fisher Scientific) and transferred to polyvinylidene difluoride (PVDF) membranes (Beyotime Biotechnology). The membranes were incubated with anti-mIL-36α (1:1000, R&D systems), anti-mpSTAT3 (1:2000, Cell Signaling Technology, Danvers, MA, United States) and anti-mSTAT3 (1:2000, Cell Signaling Technology) overnight at 4°C, then incubated with horseradish peroxidase-conjugated secondary antibodies for 2 h at 25 ± 1°C. The protein bands were visualized using BeyoECL Plus (Beyotime Biotechnology).

Immunohistochemistry

Full-thickness skin tissue was fixed using 10% formaldehyde, embedded in paraffin, and cut into 4-μm-thick sections. The sections were deparaffinized in xylene and then rehydrated using an alcohol series. Following which, the sections were incubated with the anti-IL-36α antibody (1:500; Abcam, Cambridge, United Kingdom) overnight at 4°C. The sections were then incubated with a secondary antibody at 25 ± 1°C for 30 min, followed by incubation with a diaminobenzidine tetrachloride solution at 25 ± 1°C for 1 min and counterstained with Mayer's hematoxylin. Images were captured using an optical microscope (Olympus, Tokyo, Japan).

Statistical Analysis

All statistical analyses were performed using SPSS 18.0 (IBM, Armonk, NY, United States). Differential RNA expression levels were compared using a Wilcoxon matched pair test and the Student's *t*-test was used to analyze the differences between groups. A two-sided $p < 0.05$ was considered statistically significant in all analyses.

RESULTS

Proteins Differentially Expressed Between *de novo* Hair Follicles Areas and No Hair Follicle Areas Within the Scar Region

We replicated the WIHN model as described by Ito et al., 2007, and observed that all *de novo* hair follicles grew in the center of the scar. In the WIHN mouse model, neogenic hair follicles appeared within a fairly narrow time window of between PWD 14–21 (Ito et al., 2007; Fan et al., 2011). In order to identify the factors that promote hair follicle growth at the scar center, we analyzed DEPs between the inner and outer areas of the scar at PWD 15 using iTRAQ technology (**Supplementary Figure S1**). A total of 4,378 proteins were identified and 129 DEPs were detected among the inner and outer scar areas with 46 upregulated and 83 downregulated proteins in outer area vs. inner area (**Supplementary Table S2**). Data are available via

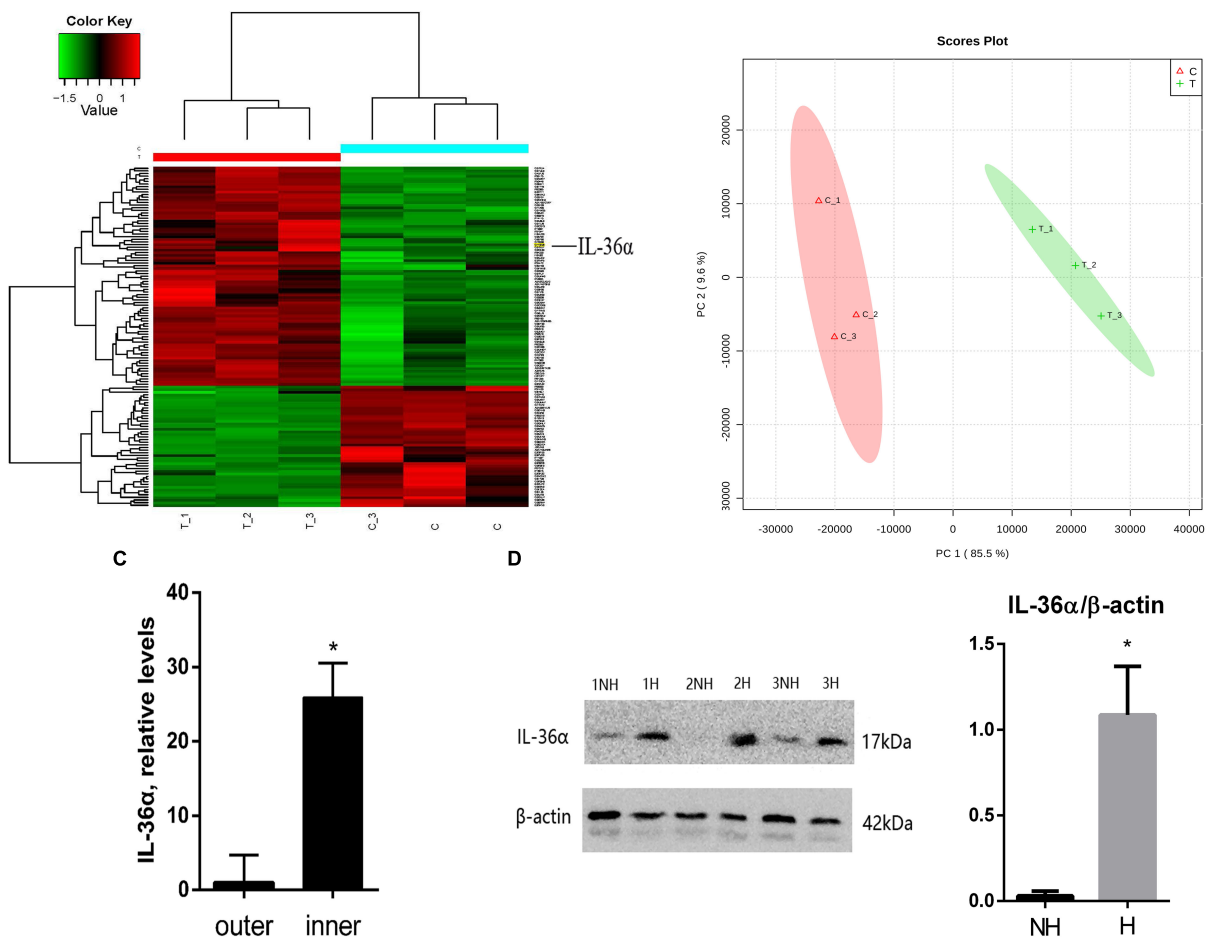

FIGURE 1 | Proteins differentially expressed between *de novo* hair follicle areas and no hair follicle areas within the scar region with upregulation of IL-36α in the inner area of the wound. **(A)** Heat map representing 129 differentially expressed proteins between *de novo* hair follicle areas (inner) and no hair follicle areas (outer) within the scar region. **(B)** Principal Component Analysis (PCA) reveals distinct separation between tissue types (inner and outer scar areas). Real-time quantitative PCR (qPCR) **(C)** and western blot **(D)** analyzed the difference of IL-36α expression between inner (H = *de novo* hair follicle area) and outer (NH = no hair follicle area) scar areas at post-wound day (PWD) 15 ($n = 3$; $^*p < 0.05$).

ProteomeXchange with identifier PXD012868 (**Figures 1A,B**). We performed a gene ontology (GO[1]) bioinformatics analysis on the DEPs and observed that 28 proteins upregulated in the inner area were involved in biological regulation. Among these, 10 proteins were involved in signaling, eight in developmental processes, and three in inflammatory responses (**Table 1**).

IL-36α Is Upregulated in Inner Area of Wound

Considering that inflammatory factors play an important role in WIHN (Gay et al., 2013; Nelson et al., 2015; Wang et al., 2017), we focused on the activity of IL-36α (also called IL-1F6). The results of the proteomic analysis showed that IL-36α was upregulated in the inner scar area with FC = 1.799. As predicted, our data showed that IL-36α expression at the mRNA and protein levels was significantly increased in the inner scar area at PWD 15 (**Figures 1C,D**). Furthermore, the spatiotemporal expression pattern of IL-36α was analyzed. qPCR (**Figure 2A**) and western blotting (**Figures 2B,C**) revealed an increase in the IL-36α expression in the wound area during wound healing until PWD 12, before it gradually declined. Immunohistochemistry showed that the expression of IL-36α followed a specific spatiotemporal pattern during epithelialization. Low expression of IL-36α was observed in the normal epidermis, but higher levels of IL-36α were noted at edge of the wound at PWD 7. In addition, the expression of IL-36α was increased in the *de novo* epidermis along with wound healing. Following re-epithelialization, IL-36α was predominantly localized in the inner wounded area (compared to the outer wounded area) at PWD 15. At PWD 20, the expression of IL-36α was decreased to a normal level in the center of the wounded area where *de novo* hair follicles were present (**Figures 2D–I**).

[1]http://www.geneontology.org

TABLE 1 | Proteomic analysis showing 28 upregulated proteins in the inner area (*de novo* hair follicle growth area) that are involved in biological regulation.

Genes	Fold change (inner vs. outer)	*P* -value	Biological process		
			Signaling	Developmental process	Inflammatory response
Tnn	2.262	0.000		✓	
Grb10	2.147	0.004	✓		
Krt19	2.035	0.007	✓	✓	
Pawr	1.880	0.028	✓	✓	
Txndc9	1.821	0.026			
IL-36α	1.800	0.009			✓
Gsto1	1.795	0.001			
Krt6a	1.789	0.000	✓	✓	
Yod1	1.783	0.003	✓		
Rhoc	1.740	0.043	✓	✓	
Sptlc1	1.708	0.037			
Prkd3	1.675	0.015	✓		
Eps8l2	1.669	0.033			
Klk7	1.648	0.004			
Tab1	1.642	0.028	✓	✓	
Hist1h3b	1.633	0.007			
Aif1	1.624	0.012	✓		✓
Dek	1.599	0.001			
Hnrnpa0	1.598	0.002			✓
Stfa1	1.596	0.001			
Arg1	1.589	0.006		✓	
Edf1	1.589	0.008		✓	
Crabp1	1.578	0.003			
Taf5l	1.571	0.001			
Glrx	1.571	0.025			
Igf2bp2	1.530	0.018			
Ferritin	1.513	0.038			
Eif1	1.502	0.012			

IL-36α Promotes Wound Epithelialization and Wound Induced Hair Follicle Neogenesis

To explore the function of IL-36α in WIHN, we injected 50 ng mrIL-36α (dissolved in PBS) or PBS into the wound area (beneath the scab) from PWD 7–14. In the mrIL-36α-treated group, the scab sloughed off at around PWD 10, which remained present in the control group until around PWD 12–14 (**Figure 3A** and **Supplementary Figure S2**). Moreover, the addition of mrIL-36α into murine skin wounds led to a greater number of regenerated hair follicles (average 29 hair follicles) compared to the control group (average seven hair follicles) (**Figures 3B,C**).

IL-36α Causes an Increase in the Expression of Hair Follicle Stem/Progenitor Cell Markers

Quantitative PCR analyses showed increased expression of *Lgr5, Lgr6, Lrig1, K15,* and *CD34* in the mrIL-36α-injected group. Among these, the increase in *Lgr6, Lrig1*, and *CD34* were statistically significant, when compared to the controls (**Figure 4A**). Flow cytometry results showed an increased number of $CD49f^{+}CD34^{+}$ cells were observed in the mrIL-36α-injected region compared to the vehicle-injected region (**Figures 4B,C**). Although the difference in hair germ cells between the two groups was not statistically significant, a higher number of $CD34^{-}CD49f^{+}Pcad^{hi}$ cells was observed in the IL-36α-treated group (**Figures 4D,E**).

IL-36α Upregulates β-Catenin and IL-6/STAT3 Pathway Intermediaries

Wnt/β-catenin pathway was thought to play a vital role in hair growth and development. Although our qPCR analysis showed that IL-36α failed to regulate the expression of the key factors in Wnt pathway, β-*catenin* was highly expressed in the IL-36α-injected regions (**Figure 5A**). A previous work has demonstrated that the IL-6/STAT3 signaling pathway promotes WIHN (Nelson et al., 2015). Our qPCR analysis showed increased mRNA levels of *IL-6* in the mrIL-36α-injected regions compared to the controls (**Figure 5B**). Western blot analysis showed increased phosphorylated levels of STAT3 in IL-36α-treated regions when compared to the control regions (**Figure 5C**).

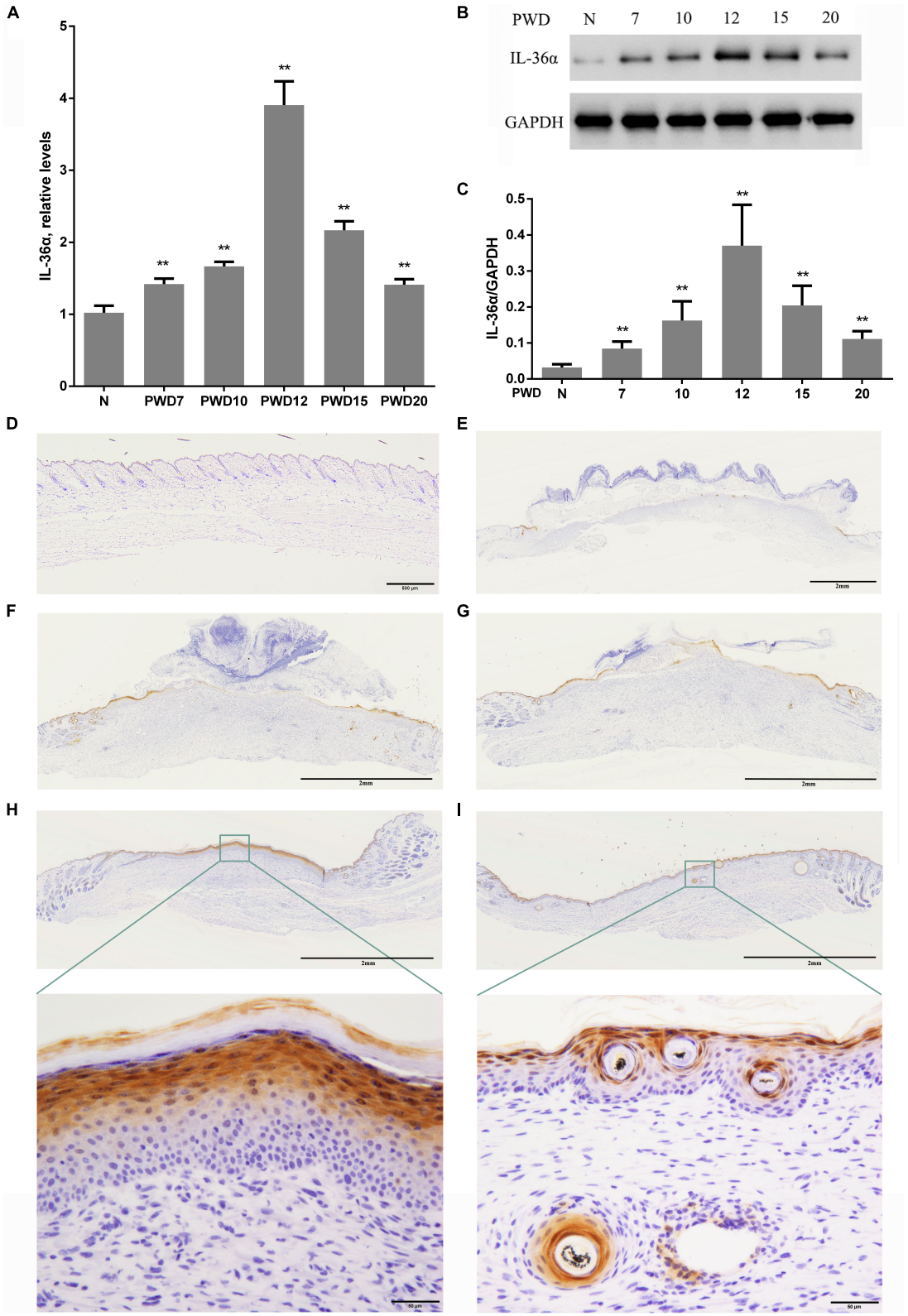

FIGURE 2 | Wound-induced spatiotemporal expression of IL-36α. qPCR **(A)** and western blotting **(B,C)** for IL-36α expression at the wound area from PWD 7–20 and normal mouse skin (control). **(D–I)** Immunohistochemistry of wounded and unwounded mouse skin paraffin sections to detect IL-36α in the wound area and wound edge at PWD 0 **(D)**, 7 **(E)**, 10 **(F)**, 12 **(G)**, 15 **(H)**, and 20 **(I)** ($n = 5$, $^{**}p < 0.005$, N, normal skin; PWD, post-wound day).

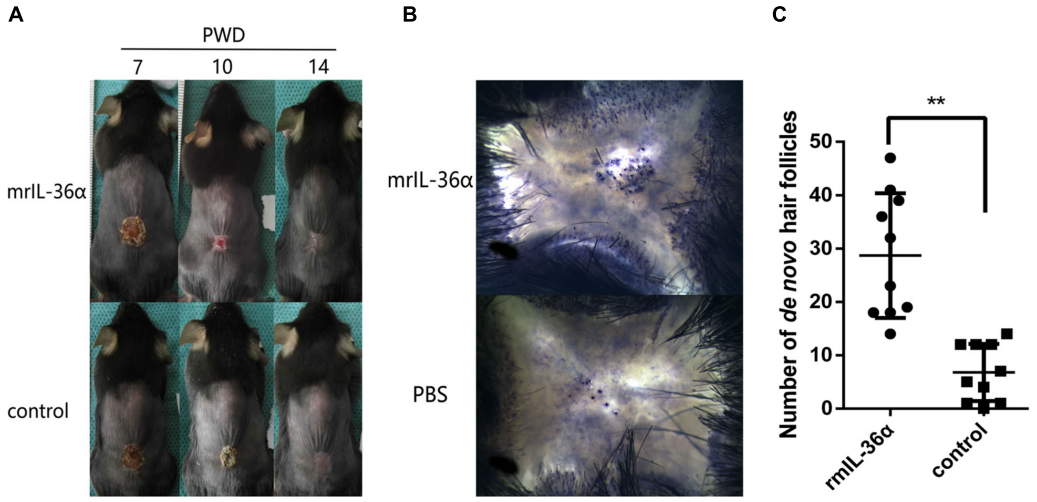

FIGURE 3 | IL-36α promotes wound epithelialization and wound induced hair follicle neogenesis. A full-thickness wound of 1.5 × 1.5 cm^2 square was made. A total of 50 μL of 1 ng/μL mrIL-36α dissolved in PBS or PBS only was injected into the healing wound (beneath the scab into the granulation tissue) from post-wound day (PWD) 7–14. **(A)** Wound model photographs of murine recombinant IL-36α (mrIL-36α)-injected group (n = 10) and control group (n = 10). **(B)** *De novo* hair follicles in skin stained for alkaline phosphatase activity at PWD 28. **(C)** *De novo* hair follicle counting in wild type mice after single dose of mrIL-36α (50 ng) compared to PBS control (**$p < 0.005$, n = 20).

DISCUSSION

Although inflammation plays an important role in hair growth and regeneration, its exact effect on hair growth and regeneration remains unclear. Inhibiting inflammation facilitates the treatment of alopecia areata (Strazzulla et al., 2018). Many studies have shown that inflammatory immune cells, such as $CD4^+$ and $CD8^+$ T cells, lead to dystrophic hair follicle cycling with premature entry into the telogen phase in alopecia areata-affected mice or human models (Strazzulla et al., 2018). There is no existing evidence to show that inhibiting inflammation can treat androgenic alopecia, although more inflammatory molecules were found in skin regions affected by androgenic alopecia areas than the unaffected areas (Bao et al., 2017). However, previous WIHN studies have shown that inflammation-related factors are capable of promoting *de novo* hair follicle growth (Gay et al., 2013; Nelson et al., 2015; Wang et al., 2017). In the present study, we identified many inflammation-related factors upregulated in new hair growth scar areas, including *IL-36α* (*Il1f6*), *Aif1* (Wang et al., 2013), *Pawr*, *Yod1* (Sehrawat et al., 2013), *Stk11ip*, and *Nlrp10* (Damm et al., 2016), with the fold change in IL-36α being the highest. According to Wang et al. (2015) full re-epithelialization coincides with the onset of HF neogenesis and on PWD 13–14 (Wang et al., 2015). IL-36α upregulation was initiated at the edge of the wound and gradually progressed to the inner wounded area. Following re-epithelialization, upregulation of IL-36α in the inner wounded area was higher than that in the outer wounded area. Our study demonstrated that wound induced IL-36α expression, which in turn gradually increased the expression of IL-36α with reepithelization. Further experiments demonstrated that IL-36α enhanced the IL-6/STAT3 pathway and the expression of hair follicle stem/progenitor cell markers, and significantly impacted WIHN and wound healing. Therefore, we predicted that inflammation was crucial for organ neogenesis, and different inflammation-related factors may have different effects on hair growth, development and regeneration.

Interleukin-36α is highly expressed in psoriatic lesions (Boutet et al., 2016), and it plays a significant role in driving the imiquimod-associated psoriatic skin pathology (Milora et al., 2015). Although population studies have revealed that patients with psoriasis have an odds ratio (OR) of 2.5 for developing alopecia areata (Wu et al., 2012), there is no evidence showing that psoriasis directly causes alopecia as the hair of patients with scalp psoriasis may be normal. Imiquimod can induce psoriasis-like skin lesions and is therefore commonly used to establish mouse psoriasis models. Amberg et al. (2016) found that imiquimod treatment during late telogen can induce hair follicle stem cell activation and premature hair cycle entry. STAT3 is also highly phosphorylated in the psoriasis lesions (Calautti et al., 2018). Activation of STAT3 can promote wound healing, keratinocytes migration, hair follicle growth and participate in tumor occurrence (Sano et al., 2008). STAT3 phosphorylation has been shown to promote the proliferation of hair follicle stem/progenitor cells (Rao et al., 2015) and WIHN (Nelson et al., 2015). Our results show that IL-36α can upregulate the IL-6/STAT3 pathway, further induce hair follicle stem/progenitor cell activation and WIHN. Together with previous studies, these data suggest that increased IL-36α in patients with psoriasis does not directly induce alopecia. Although IL-36α upregulated β-catenin it failed to regulate the expression of the key genes in the Wnt pathway. A previous study had demonstrated that AKT/β-catenin signaling but not Wnt/β-catenin pathway was crucial for TNF-induced hair

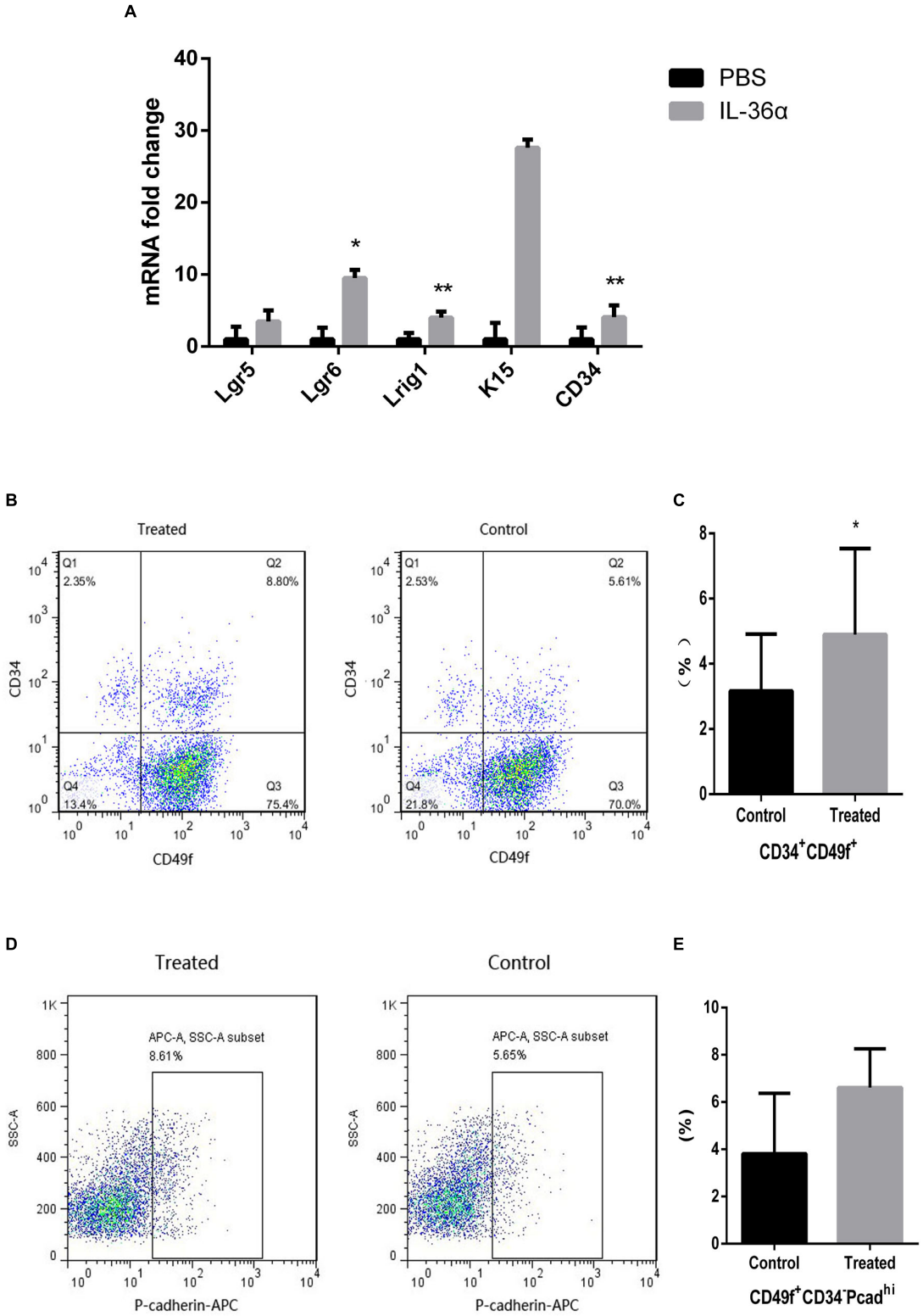

FIGURE 4 | IL-36α causes an increase in the expression of hair follicle stem/progenitor cell markers in mice skin. A total of 50 μL of 1 ng/μL mrIL-36α dissolved in PBS or PBS only was injected intradermally into two separate dorsal regions of skin of 7-week-old mice for 3 days. **(A)** The relative mRNA expression levels of hair follicle stem/progenitor cell markers (*Lgr5, Lgr6, Lrig1, K15,* and *CD34*) in mrIL-36α-injected region and control region were evaluated using real time quantitative PCR ($n = 4$). Total epithelial cells were subjected to flow cytometry analysis after staining for CD34, CD49f and Pcad. Flow cytometry analysis of hair follicle stem/progenitor cells marked by $CD34^{+}CD49f^{+}$ **(B,C)** and $CD34^{-}CD49f^{+}Pcad^{hi}$ **(D,E)** (*$p < 0.05$, **$p < 0.005$, $n = 4$).

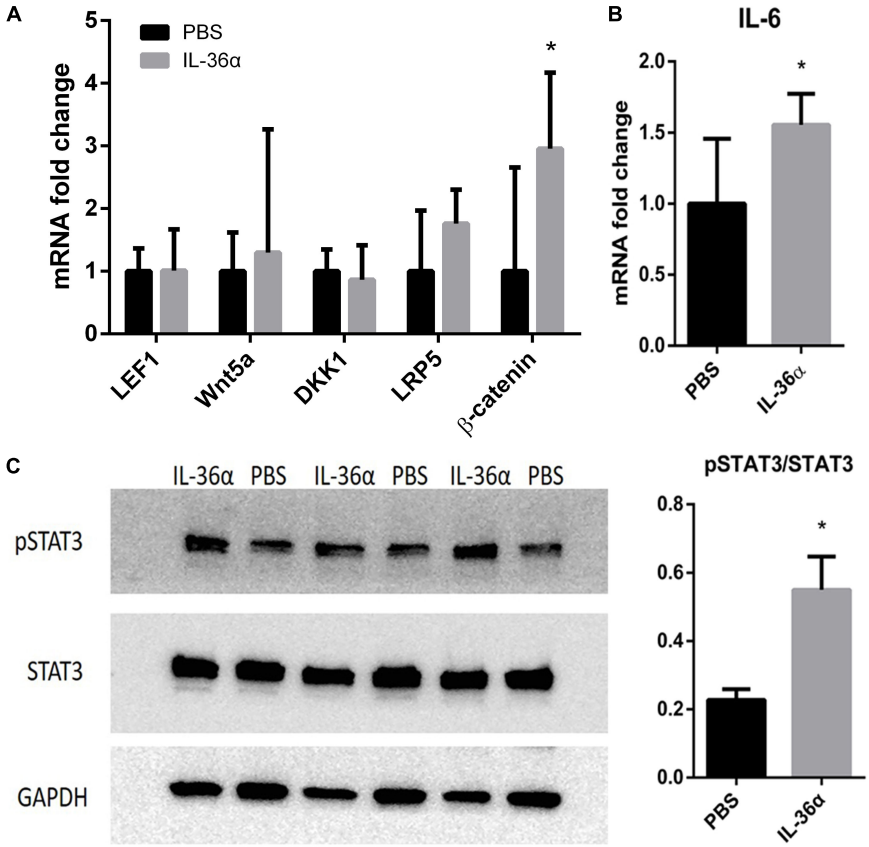

FIGURE 5 | mrIL-36α causes increased expression level of β-*catenin* and *IL-6* and activates STAT3. A total of 50 μL of 1 ng/μL mrIL-36α dissolved in PBS or PBS only was injected intradermally into two separate dorsal regions of skin of 7-week-old mice for 3 days. **(A,B)** Total mRNA was isolated from mrIL-36α-injected region and control region, and mRNA levels of *LEF1, Wnt5a, DKK1, LRP5*, β-*catenin* (key genes in Wnt/β-catenin pathway) and *IL-6* were analyzed by qPCR ($n = 4$). **(C)** The phosphorylation level of STAT3 in the IL-36α-treated region and the control region analyzed by western blot (*$p < 0.05$, $n = 3$).

follicle neogenesis. Although our study does not address the mechanism of IL-36α-driven β-catenin regulation, it will be interesting to obtain further insight into how IL-36α induces β-catenin and IL-6/STAT3 signaling and how the negative feedback is regulated.

Stem cell activation is essential for wound epithelialization and hair follicle growth. Ito et al. (2007) pointed out that stem cells in the epidermis and upper portion of the follicle (infundibulum) are mainly involved in *de novo* hair follicles formation after wounding (Ito et al., 2007). However, a recent study by Wang et al. (2017) reported the crucial role of $Lgr5^+$ hair follicle stem cells in WIHN (Wang et al., 2017). Hair follicle stem cells in the bulge region can be identified by many proteins, such as K15, Lgr5, and CD34 (Cotsarelis et al., 1990; Ito et al., 2005; Plikus et al., 2012). Lgr6 is one of the earliest placode markers and its stem cells located in the hair follicle isthmus are thought to give rise to hair follicle, sebaceous gland, and inter-follicular epidermal lineage, and have been verified to promote WIHN (Snippert et al., 2010; Lough et al., 2016). $Lrig1^+$ stem cells tend to contribute predominantly to infundibulum and sebaceous gland lineages and only occasionally to the inter-follicular epidermis (Jensen et al., 2009). $CD34^+CD49f^+$ stem cells are the most studied as hair follicle stem/progenitor cells in mice (Ouji et al., 2010). In addition, hair germ cells can be identified as $CD34^-CD49f^+Pcad^{hi}$ (Greco et al., 2009), which is the principal source of the rapidly proliferating cells that contribute to the initial stages of hair follicle regeneration. From our data, we learnt that IL-36α promotes hair follicle stem/progenitor cell proliferation.

Hair follicles are the smallest, complete anatomical organs that have the ability to regenerate. Following a full-thickness wound, the hair follicle in the wound area was thought to be lost entirely. However, hair follicle neogenesis occurred after reepithelization at around PWD 14–15. Therefore, we chose the time point of PWD 15 to assay DEPs between the hair-growth area and non-hair-growth area, in order to identify the regulators of hair follicle neogenesis. We collected the skin to count the number of *de novo* hair follicles at PWD 28, as mature anagen *de novo* hair follicles were present and entered the first telogen phase at around PWD 35 (Wang et al., 2015). In our study, the WIHN model presents a phenomenon of *de novo* hair follicle growth without pigmentation at the center of scar, irrespective of whether it is treated with mrIL-36α or PBS. Similar to previous studies, wound

can induce an embryonic-like hair follicle regeneration (Gong et al., 2018). As we know, the survival rate of hair transplantation in scars are lower than that of the normal skin. Future studies can focus on the microenvironment and growth situation of the *de novo* hair follicles induced by wound, which could provide aid to improving the survival rate of hair transplantation.

In conclusion, inflammation appears to play an important role in hair follicle neogenesis. In particular, IL-36α is upregulated in scar areas with *de novo* hair follicular growth, and can promote WIHN, which may induce hair follicle stem/progenitor cell proliferation and secretion of inflammation-related factors. Further research on WIHN will contribute to a better understanding of hair neogenesis and new insights into the treatment of hair-related disorders.

DATA AVAILABILITY STATEMENT

The datasets generated for this study can be found in the ProteomeXchange with identifier PXD012868.

ETHICS STATEMENT

The animal study was reviewed and approved by the Institutional Animal Care and Use Committee at China Medical University.

AUTHOR CONTRIBUTIONS

XG and XX designed this study. LG and XX performed the experiments and analyzed the data. LG drafted the manuscript. JX and XL revised the manuscript for important intellectual content. All authors have read and approved the final manuscript.

FUNDING

This study was supported by the National Natural Science Foundation of China (Grant Nos. 81602740 and 81972956) and the 111 project by the Ministry of Science and Technology, China (D18011).

ACKNOWLEDGMENTS

We are grateful to our colleagues at the Dermatology Department of The First Hospital of China Medical University for their cooperation and support.

SUPPLEMENTARY MATERIAL

The Supplementary Material for this article can be found online at: https://www.frontiersin.org/articles/10.3389/fcell.2020.00627/full#supplementary-material

REFERENCES

Amberg, N., Holcmann, M., Stulnig, G., and Sibilia, M. (2016). Effects of imiquimod on hair follicle stem cells and hair cycle progression. *J. Invest. Dermatol.* 136, 2140–2149. doi: 10.1016/j.jid.2016.06.613

Bao, L., Yu, A., Luo, Y., Tian, T., Dong, Y., Zong, H., et al. (2017). Genomewide differential expression profiling of long non-coding RNAs in androgenetic alopecia in a Chinese male population. *J. Eur. Acad. Dermatol. Venereol.* 31, 1360–1371. doi: 10.1111/jdv.14278

Bassoy, E. Y., Towne, J. E., and Gabay, C. (2018). Regulation and function of interleukin-36 cytokines. *Immunol. Rev.* 281, 169–178. doi: 10.1111/imr.12610

Billingham, R. E., and Russell, P. S. (1956). Incomplete wound contracture and the phenomenon of hair neogenesis in rabbits' skin. *Nature* 177, 791–792.

Boutet, M. A., Bart, G., Penhoat, M., Amiaud, J., Brulin, B., Charrier, C., et al. (2016). Distinct expression of interleukin (IL)-36alpha, beta and gamma, their antagonist IL-36Ra and IL-38 in psoriasis, rheumatoid arthritis and Crohn's disease. *Clin. Exp. Immunol.* 184, 159–173. doi: 10.1111/cei.12761

Brook, A. H., Short, B. F., and Lyne, A. G. (1960). Formation of new wool follicles in the adult sheep. *Nature* 185:51.

Calautti, E., Avalle, L., and Poli, V. (2018). Psoriasis: a STAT3-centric view. *Int. J. Mol. Sci.* 19:171. doi: 10.3390/ijms19010171

Cotsarelis, G., Sun, T. T., and Lavker, R. M. (1990). Label-retaining cells reside in the bulge area of pilosebaceous unit: implications for follicular stem cells, hair cycle, and skin carcinogenesis. *Cell* 61, 1329–1337.

Damm, A., Giebeler, N., Zamek, J., Zigrino, P., and Kufer, T. A. (2016). Epidermal NLRP10 contributes to contact hypersensitivity responses in mice. *Eur. J. Immunol.* 46, 1959–1969. doi: 10.1002/eji.201646401

Dietrich, D., Martin, P., Flacher, V., Sun, Y., Jarrossay, D., Brembilla, N., et al. (2016). Interleukin-36 potently stimulates human M2 macrophages, Langerhans cells and keratinocytes to produce pro-inflammatory cytokines. *Cytokine* 84, 88–98. doi: 10.1016/j.cyto.2016.05.012

Fan, C., Luedtke, M. A., Prouty, S. M., Burrows, M., Kollias, N., and Cotsarelis, G. (2011). Characterization and quantification of wound-induced hair follicle neogenesis using in vivo confocal scanning laser microscopy. *Skin Res. Technol.* 17, 387–397. doi: 10.1111/j.1600-0846.2011.00508.x

Gay, D., Kwon, O., Zhang, Z., Spata, M., Plikus, M. V., Holler, P. D., et al. (2013). Fgf9 from dermal gammadelta T cells induces hair follicle neogenesis after wounding. *Nat. Med.* 19, 916–923. doi: 10.1038/nm.3181

Gong, L., Xu, X. G., and Li, Y. H. (2018). Embryonic-like regenerative phenomenon: wound-induced hair follicle neogenesis. *Regen. Med.* 13, 729–739. doi: 10.2217/rme-2018-0028

Greco, V., Chen, T., Rendl, M., Schober, M., Pasolli, H. A., Stokes, N., et al. (2009). A two-step mechanism for stem cell activation during hair regeneration. *Cell Stem Cell* 4, 155–169. doi: 10.1016/j.stem.2008.12.009

Guerrero-Juarez, C. F., Astrowski, A. A., Murad, R., Dang, C. T., Shatrova, V. O., Astrowskaja, A., et al. (2018). Wound regeneration deficit in rats correlates with low morphogenetic potential and distinct transcriptome profile of epidermis. *J. Invest. Dermatol.* 138:1409. doi: 10.1016/j.jid.2017.12.030

Ito, M., Liu, Y., Yang, Z., Nguyen, J., Liang, F., Morris, R. J., et al. (2005). Stem cells in the hair follicle bulge contribute to wound repair but not to homeostasis of the epidermis. *Nat. Med.* 11, 1351–1354. doi: 10.1038/nm1328

Ito, M., Yang, Z., Andl, T., Cui, C., Kim, N., Millar, S. E., et al. (2007). Wnt-dependent de novo hair follicle regeneration in adult mouse skin after wounding. *Nature* 447, 316–320. doi: 10.1038/nature05766

Jensen, K. B., Collins, C. A., Nascimento, E., Tan, D. W., Frye, M., Itami, S., et al. (2009). Lrig1 expression defines a distinct multipotent stem cell population in mammalian epidermis. *Cell Stem Cell* 4, 427–439. doi: 10.1016/j.stem.2009.04.014

Lee, P., Gund, R., Dutta, A., Pincha, N., Rana, I., Ghosh, S., et al. (2017). Stimulation of hair follicle stem cell proliferation through an IL-1 dependent activation of gammadeltaT-cells. *eLife* 6:e28875. doi: 10.7554/eLife.28875

Lough, D. M., Wetter, N., Madsen, C., Reichensperger, J., Cosenza, N., Cox, L., et al. (2016). Transplantation of an LGR6+ epithelial stem cell-enriched scaffold for repair of full-thickness soft-tissue defects: the in vitro development of polarized hair-bearing skin. *Plast. Reconstr. Surg.* 137, 495–507. doi: 10.1097/01.prs.0000475761.09451.00

Milora, K. A., Fu, H., Dubaz, O., and Jensen, L. E. (2015). Unprocessed Interleukin-36alpha Regulates Psoriasis-Like Skin Inflammation in Cooperation With Interleukin-1. *J. Invest. Dermatol.* 135, 2992–3000. doi: 10.1038/jid.2015.289

Nelson, A. M., Reddy, S. K., Ratliff, T. S., Hossain, M. Z., Katseff, A. S., Zhu, A. S., et al. (2015). dsRNA released by tissue damage activates TLR3 to drive skin regeneration. *Cell Stem Cell* 17, 139–151. doi: 10.1016/j.stem.2015.07.008

Ouji, Y., Yoshikawa, M., Nishiofuku, M., Ouji-Sageshima, N., Kubo, A., and Ishizaka, S. (2010). Effects of Wnt-10b on proliferation and differentiation of adult murine skin-derived CD34 and CD49f double-positive cells. *J. Biosci. Bioeng.* 110, 217–222. doi: 10.1016/j.jbiosc.2010.01.020

Plikus, M. V., Gay, D. L., Treffeisen, E., Wang, A., Supapannachart, R. J., and Cotsarelis, G. (2012). Epithelial stem cells and implications for wound repair. *Semin. Cell Dev. Biol.* 23, 946–953. doi: 10.1016/j.semcdb.2012.10.001

Rao, D., Macias, E., Carbajal, S., Kiguchi, K., and DiGiovanni, J. (2015). Constitutive Stat3 activation alters behavior of hair follicle stem and progenitor cell populations. *Mol. Carcinog.* 54, 121–133. doi: 10.1002/mc.22080

Sano, S., Chan, K. S., and DiGiovanni, J. (2008). Impact of Stat3 activation upon skin biology: a dichotomy of its role between homeostasis and diseases. *J. Dermatol. Sci.* 50, 1–14. doi: 10.1016/j.jdermsci.2007.05.016

Sehrawat, S., Koenig, P. A., Kirak, O., Schlieker, C., Fankhauser, M., and Ploegh, H. L. (2013). A catalytically inactive mutant of the deubiquitylase YOD-1 enhances antigen cross-presentation. *Blood* 121, 1145–1156. doi: 10.1182/blood-2012-08-447409

Seifert, A. W., Kiama, S. G., Seifert, M. G., Goheen, J. R., Palmer, T. M., and Maden, M. (2012). Skin shedding and tissue regeneration in African spiny mice (Acomys). *Nature* 489, 561–565. doi: 10.1038/nature11499

Snippert, H. J., Haegebarth, A., Kasper, M., Jaks, V., van Es, J. H., Barker, N., et al. (2010). Lgr6 marks stem cells in the hair follicle that generate all cell lineages of the skin. *Science* 327, 1385–1389. doi: 10.1126/science.1184733

Strazzulla, L. C., Wang, E. H. C., Avila, L., Lo Sicco, K., Brinster, N., Christiano, A. M., et al. (2018). Alopecia areata: an appraisal of new treatment approaches and overview of current therapies. *J. Am. Acad. Dermatol.* 78, 15–24. doi: 10.1016/j.jaad.2017.04.1142

Wang, J., Zhao, Y., Wang, W., Du, Z., Yan, D., Li, C., et al. (2013). Daintain/AIF-1 plays roles in coronary heart disease via affecting the blood composition and promoting macrophage uptake and foam cell formation. *Cell Physiol. Biochem.* 32, 121–126. doi: 10.1159/000350130

Wang, X., Chen, H., Tian, R., Zhang, Y., Drutskaya, M. S., Wang, C., et al. (2017). Macrophages induce AKT/beta-catenin-dependent Lgr5+ stem cell activation and hair follicle regeneration through TNF. *Nat. Commun.* 8:14091. doi: 10.1038/ncomms14091

Wang, X., Hsi, T. C., Guerrero-Juarez, C. F., Pham, K., Cho, K., McCusker, C. D., et al. (2015). Principles and mechanisms of regeneration in the mouse model for wound-induced hair follicle neogenesis. *Regeneration* 2, 169–181. doi: 10.1002/reg2.38

Wu, J. J., Nguyen, T. U., Poon, K. Y., and Herrinton, L. J. (2012). The association of psoriasis with autoimmune diseases. *J. Am. Acad. Dermatol.* 67, 924–930. doi: 10.1016/j.jaad.2012.04.039

Conflict of Interest: The authors declare that the research was conducted in the absence of any commercial or financial relationships that could be construed as a potential conflict of interest.

Copyright © 2020 Gong, Xiao, Li, Li, Gao and Xu. This is an open-access article distributed under the terms of the Creative Commons Attribution License (CC BY). The use, distribution or reproduction in other forums is permitted, provided the original author(s) and the copyright owner(s) are credited and that the original publication in this journal is cited, in accordance with accepted academic practice. No use, distribution or reproduction is permitted which does not comply with these terms.

frontiers in Cell and Developmental Biology

BRIEF RESEARCH REPORT
published: 08 October 2020
doi: 10.3389/fcell.2020.575382

Knockdown of FOXA2 Impairs Hair-Inductive Activity of Cultured Human Follicular Keratinocytes

*Soon-Sun Bak[1], Jung Min Park[2,3], Ji Won Oh[2,3,4], Jung Chul Kim[1,4], Moon Kyu Kim[1,4] and Young Kwan Sung[1]**

[1] Department of Immunology, School of Medicine, Kyungpook National University, Daegu, South Korea, [2] Department of Anatomy, School of Medicine, Kyungpook National University, Daegu, South Korea, [3] Clinical Omics Institute, Kyungpook National University, Daegu, South Korea, [4] Hair Transplantation Center, Kyungpook National University Hospital, Daegu, South Korea

Reciprocal interactions between hair-inductive dermal cells and epidermal cells are essential for *de novo* genesis of hair follicles. Recent studies have shown that outer root sheath (ORS) follicular keratinocytes can be expanded *in vitro,* but the cultured cells often lose receptivity to hair-inducing dermal signals. In this study, we first investigated whether the hair-inductive activity (trichogenicity) of cultured human ORS follicular keratinocytes was correlated with the cultivation period. ORS follicular keratinocytes from the scalp were cultured for 3, 4, 5, or 6 weeks and were then implanted into nude mice along with freshly isolated neonatal mouse dermal cells. We observed that the trichogenicity of the implanted ORS cells was inversely correlated with their cultivation period. These initial findings prompted us to investigate the differentially expressed genes between the short-term (20 days) and long-term (42 days) cultured ORS cells, trichogenic and non-trichogenic, respectively, by microarray analysis. We found that forkhead box protein A2 (FOXA2) was the most up-regulated transcription factor in the trichogenic ORS cells. Thus, we investigated whether the trichogenicity of the cells was affected by FOXA2 expression. We found a significant decrease in the number of induced hair follicles when the ORS cells were transfected with a FOXA2 small interfering RNA versus control small interfering RNA. Taken together, our data strongly suggest that FOXA2 significantly influences the trichogenicity of human ORS cells.

Keywords: forkhead box protein A2, hair induction, outer root sheath, transcription factor, trichogenicity

OPEN ACCESS

Edited by:
Mingxing Lei,
Chongqing University, China

Reviewed by:
Yuhong Li,
Army Medical University, China
Charareh Pourzand,
University of Bath, United Kingdom

Correspondence:
Young Kwan Sung
ysung@knu.ac.kr

Specialty section:
This article was submitted to Stem Cell Research, a section of the journal Frontiers in Cell and Developmental Biology

Received: *23 June 2020*
Accepted: *17 September 2020*
Published: *08 October 2020*

Citation:
Bak S-S, Park JM, Oh JW, Kim JC, Kim MK and Sung YK (2020) Knockdown of FOXA2 Impairs Hair-Inductive Activity of Cultured Human Follicular Keratinocytes. Front. Cell Dev. Biol. 8:575382. doi: 10.3389/fcell.2020.575382

INTRODUCTION

Reciprocal interactive events between the dermal mesenchyme and the overlying epithelium are essential for hair follicle (HF) morphogenesis (Paus and Cotsarelis, 1999; Millar, 2002). Likewise, reciprocal interactions between hair-inductive dermal cells and epithelial cells are needed for *de novo* genesis or neogenesis of HFs (Yang and Cotsarelis, 2010). However, these cells often lose hair-inductive potency (trichogenicity) after conventional *in vitro* culture (Ohyama et al., 2010; Yang and Cotsarelis, 2010). Therefore, to generate HFs by implantation of cells in recipient skin,

Abbreviations: DP, dermal papilla; FOXA2, forkhead box protein A2; HF, hair follicle; ORS, outer root sheath; PBS, phosphate-buffered saline; PCR, polymerase chain reaction; siRNA, small interfering RNA.

restoration or maintenance of the trichogenicity of those cells together with expansion of cell numbers is required.

Several strategies have been attempted to restore the trichogenicity of cultured follicular dermal cells, especially dermal papilla (DP) cells, and at least partial restoration was achieved, particularly by spheroid formation and complementation of activators of DP signature pathways (Kang et al., 2012; Ohyama et al., 2012; Higgins et al., 2013; Ohyama and Veraitch, 2013). Regarding epithelial cells for neogenesis of HFs, follicular outer root sheath (ORS) keratinocytes containing hair follicle stem cells (HFSCs) are considered the optimal cells. However, thus far, reports on the restoration of trichogenicity of cultured ORS cells are rare. Chan et al. from Lin's laboratory have shown that coculture of high-passage rat ORS cells with rat vibrissae DP cells restores trichogenicity (Chan et al., 2015). More recently, we have also shown that the trichogenicity of human ORS cells from occipital scalp can be restored by coculturing with human DP cells (Bak et al., 2018).

In this study, we observed that forkhead box protein A2 (FOXA2), a member of the forkhead/winged-helix family of transcription factors, is the most differentially expressed transcription factor between the short-term and long-term cultured ORS cells by microarray analysis. This, along with inverse correlation of hair-inducing capacity of ORS cells with their cultivation period, led us to investigate whether the trichogenicity of the cells was affected by FOXA2 expression. Using a hair reconstitution assay in combination with a FOXA2 small interfering RNA (siRNA)-mediated knockdown of ORS cells, we show that FOXA2 augments the trichogenicity of cultured human follicular keratinocytes.

MATERIALS AND METHODS

Isolation of Hair Follicles

Biopsy specimens were obtained from non-balding (occipital) scalp of male patients undergoing hair transplantation surgery for androgenetic alopecia. The medical ethical committee of the Kyungpook National University Hospital (Daegu, South Korea) approved all described studies. Written informed consent was obtained from study participants. HFs were isolated using a previously described method with minor modifications (Philpott et al., 1994; Magerl et al., 2002). Briefly, the subcutaneous fat portion of the scalp skin, including the lower HFs, was dissected from the epidermis and dermis. HFs were then isolated under a binocular microscope by forceps.

Cultivation of Outer Root Sheath Cells

The hair shaft and hair bulb regions of the HFs were cut off to prevent contamination with other cells. The ORS cells were cultured as described before (Kwack et al., 2008). Trimmed hair follicles were immersed in Dulbecco's modified eagle medium supplemented with 20% fetal bovine serum in Biocoat collagen type I-coated tissue culture dishes (Corning, Kennebunk, ME, United States). On the third day of culture, the medium was changed to EpiLife (Gibco-BRL, Gaithersburg, MD, United States) containing 1% antibiotic-antimycotic solution and 1% EpiLife defined growth supplement. Once subconfluent, the cells were harvested with 0.25% trypsin/10 mM EDTA in phosphate-buffered saline (PBS), split at a 1:5 ratio, and maintained in EpiLife medium. ORS cells in passages 1–4 were used in this study.

Knockdown of FOXA2 in ORS Cells

The siRNAs used in this study were purchased from Bioneer (Daejeon, South Korea). Cultured human ORS cells were transfected with a control siRNA or a FOXA2 siRNA (Bioneer) at a final concentration of 10 nM in the presence of RNAiMAX reagent (Invitrogen, Carlsbad, CA, United States) for 24 h. Transfected cells (10^4) were harvested 48 h after transfection and were used for a hair reconstitution assay after the confirmation of a significant knockdown of the genes by real-time polymerase chain reaction (PCR) analysis.

In vivo Patch Hair Reconstitution Assay

Patch hair reconstitution assays were used in this study (Zheng et al., 2005). Dorsal skin from C57BL/6 neonates was collected and incubated overnight with 1 mg/ml collagenase/dispase (Roche, Mannheim, Germany). The dermis and epidermis were separated by incubating the skin with 0.25% trypsin/10 mM EDTA in PBS at 37°C for 15 min. Dermal cells were filtered through 100 μm cell strainers (Becton Dickinson, Franklin, NJ, United States), and then centrifuged at 1,500 rpm for 5 min. Cultured human ORS cells (1×10^6 cells) were combined with freshly isolated neonatal mouse dermal cells (1×10^6 cells) and then subcutaneously implanted into the skin on the backs of 7-week-old female nude mice. After 2 weeks, photos were taken of excised skin samples under a stereoscope, and the reconstituted HFs were quantified. All animal procedures were approved by the Animal Care and Use Committee at Kyungpook National University (Daegu, South Korea).

Microarrays and Data Analysis

Five micrograms of total RNA from short-term (20 days) and long-term (42 days) ORS cell cultures was used for labeling. Probe synthesis, hybridization, detection, and scanning were performed as described previously (Bak et al., 2018) according to standard protocols from Affymetrix, Inc (Santa Clara, CA, United States). Microarray data were analyzed as we conducted in previous studies (Choi et al., 2017; Wang et al., 2017). Briefly, a bubble chart was used to present biological processes revealed by gene ontology (GO) analysis. The size of circle is dependent on total number of the associated differentially expressed genes (DEGs), while the rank of the circle is set according to *P*-value of analysis. Genes that were significantly associated with these processes were used to compare DEGs with gene set enrichment analysis (GSEA) information related to the skin-associated gene sets as well. Kyoto Encyclopedia of Genes and Genomes (KEGG) 2019 was used for pathway analysis.

Real-Time PCR

Total RNA was isolated using RNeasy Mini Kit (Qiagen, Austin, TX, United States) according to the manufacturer's

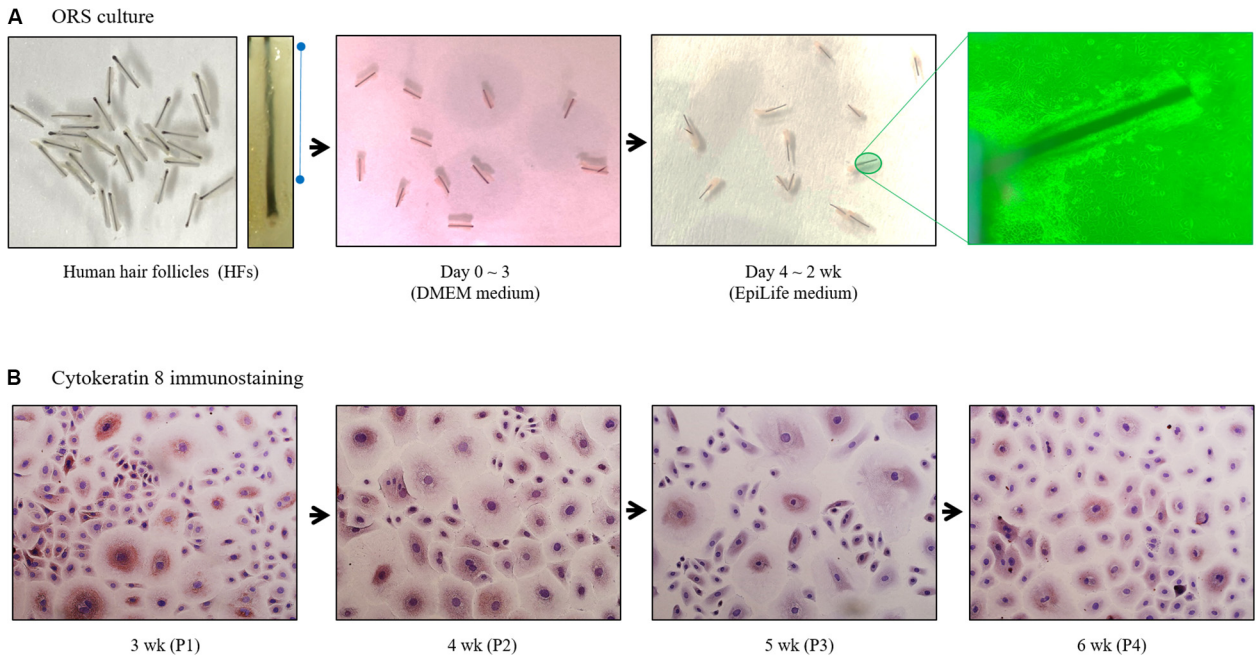

FIGURE 1 | Diagram of human outer root sheath (ORS) follicular keratinocytes cultivation. **(A)** Human ORS cells were cultured as described in the Materials and Methods section. Representative images from a patient (male, age 37 years) are shown. **(B)** Cells in various culture periods (3, 4, 5, and 6 weeks) from a patient (male, age 28 years) were immunostained with cytokeratin 8 antibody.

protocol. The purity and integrity of the RNA was measured using a NanoDrop (NanoDrop Technologies, Wilmington, DE, United States). Complementary DNA (cDNA) was synthesized from 3 μg total RNA using a cDNA synthesis kit containing Improm-II reverse transcriptase and oligo-dT primers according to the manufacturer's instructions (Promega, Madison, WI, United States). Real-time PCR was performed using a StepOnePlus Real-time PCR System (Applied Biosystems, Foster City, CA, United States). All reactions were performed using Power SYBR Green premix (Applied Biosystems), 10 ng cDNA, and 10 μM primers. Amplification was performed under the following cycling conditions: 95°C for 10 min, followed by 40 cycles of 95°C for 15 s and 60°C for 60 s. Primer sequences used were as follows: FOXA2, forward primer 5′-CCCCACAAAATGGACCTCAAG-3′ and reverse primer 5′-GAGTACACCCCCTGGTAGTAG-3′; and GAPDH, forward primer 5′-TGGAAATCCCATCACCATCTTC-3′ and reverse primer 5′-CGCCCCACTTGATTTTGG-3′. Differences between samples and controls were calculated using StepOnePlus Real-Time PCR analysis software (Applied Biosystems).

Immunocytochemistry

Cultured human ORS cells were plated in each eight-chamber slide (Nunc, Rosklide, Denmark) at a density of 100,000 cells per well. After cultivation in EpiLife medium for 24 h, the chamber slides were fixed with methanol for 20 min at −20°C and equilibrated in PBS for 10 min at 25°C. After blocking with 4% bovine serum albumin (Jackson) for 1 h at 25°C, the slides were incubated with a rabbit polyclonal antibody to SOX9 (1:100 dilution; Abcam) at 4°C overnight, washed four times with PBS, and incubated with donkey anti-rabbit horseradish peroxidase-conjugated antibody (1:100 dilution; Jackson ImmunoResearch, West Grove, PA, United States) for 1 h at 25°C. AEC substrate chromogen (DAKO, Glostrup, Denmark) was used as a color formation reagent for horseradish peroxidase. Finally, slides were counterstained with hematoxylin for 2 min. We used normal rabbit IgG (R&D Systems, Minneapolis, CA, United States) for immunostaining negative controls.

Statistical Analysis

Data are expressed as mean ± standard deviation (SD). Differences between pairs of groups were analyzed by Student's *t*-test. A *P*-value of less than 0.05 was considered statistically significant.

RESULTS AND DISCUSSION

Trimmed HFs (25–30 HFs/10 cm^2 dish) were immersed in Dulbecco's modified eagle medium supplemented with fetal bovine serum in collagen type I-coated tissue culture dishes. Culture medium was then changed to EpiLife medium on the third day of culture (**Figure 1A**). Once subconfluent, ORS cells were harvested and split at a 1:5 ratio, and maintained in EpiLife medium. Cells were cultured up to 6 weeks and immunostained with cytokeratin 8 antibodies (**Figure 1B**).

To investigate whether the hair-inductive activity (trichogenicity) of ORS cells was correlated with the cultivation period, cells in various cultivation periods (3, 4, 5, and

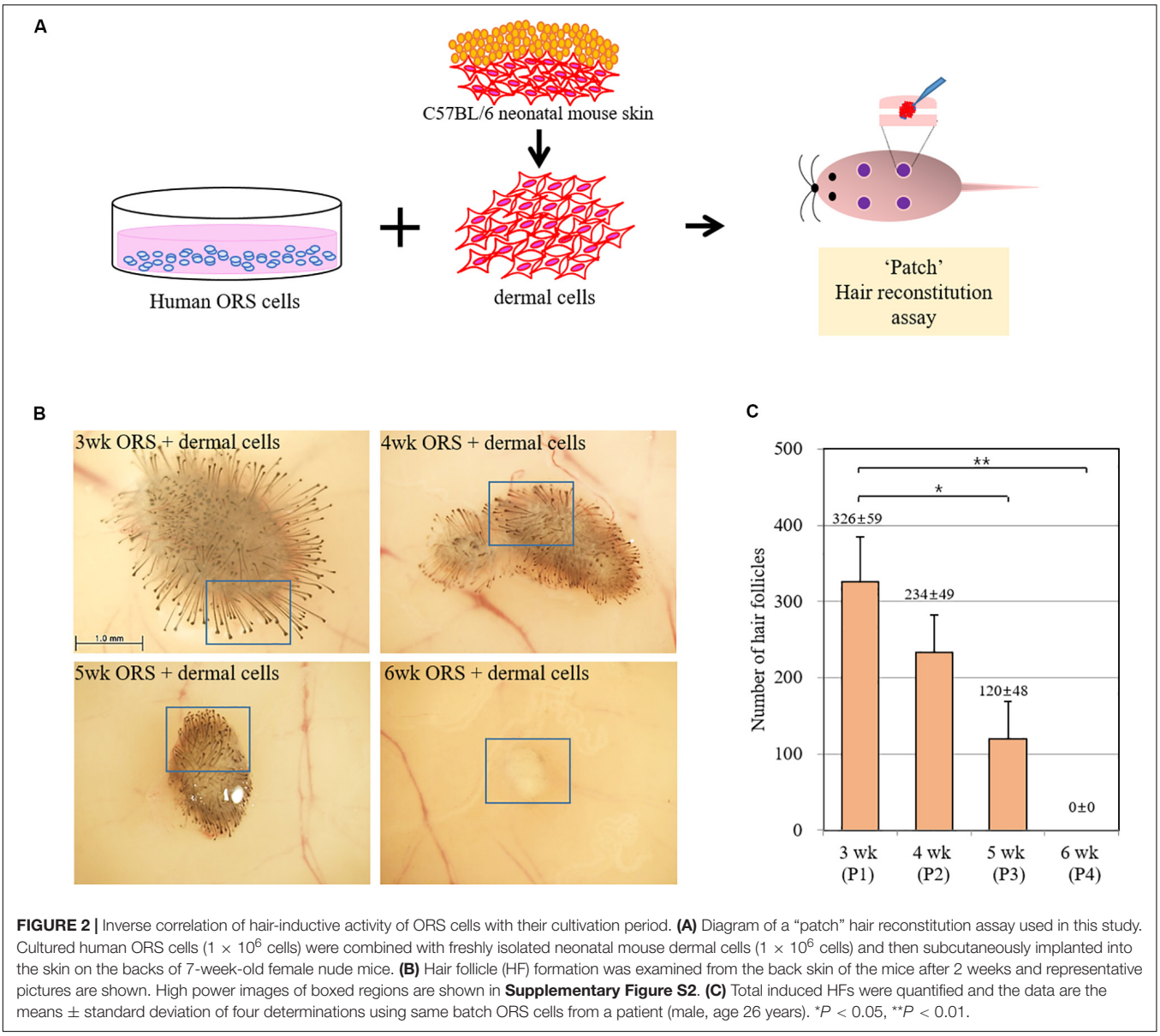

FIGURE 2 | Inverse correlation of hair-inductive activity of ORS cells with their cultivation period. **(A)** Diagram of a "patch" hair reconstitution assay used in this study. Cultured human ORS cells (1×10^6 cells) were combined with freshly isolated neonatal mouse dermal cells (1×10^6 cells) and then subcutaneously implanted into the skin on the backs of 7-week-old female nude mice. **(B)** Hair follicle (HF) formation was examined from the back skin of the mice after 2 weeks and representative pictures are shown. High power images of boxed regions are shown in **Supplementary Figure S2**. **(C)** Total induced HFs were quantified and the data are the means ± standard deviation of four determinations using same batch ORS cells from a patient (male, age 26 years). $^*P < 0.05$, $^{**}P < 0.01$.

6 weeks) were implanted into nude mice along with freshly isolated neonatal mouse dermal cells (**Figure 2A**). When quantified, induced hairs were inversely correlated with the cultivation period, and no HF induction was observed in co-implants containing 6-week-old ORS cells and mouse dermal cells (**Figures 2B,C** and **Supplementary Figure S1**). The human origin of epithelial cells of reconstituted hair follicles and the mouse origin of mesenchymal part of follicles remains to be proved.

Next, we compared the gene expression profiles between the short-term (20 days) and long-term (42 days) cultured ORS cells from two individuals (#1 and #2) by microarray analysis. A number of genes were found to be differentially expressed (**Figure 3**). Among the 144 genes with a more than twofold increase in short-term cultured ORS cells (**Supplementary Table S1**), we found 6 transcription factors, including FOXA2, BARX2, and BHLHA15. Also, among the 278 genes with a more than twofold decrease in short-term cultured ORS cells (**Supplementary Table S2**), we found four transcription factors, including ZNF257and TBX3. Next, we visualized the expression value of DEGs to compare the up-regulated genes and down-regulated genes using Heatmap (**Figure 3B**) to show the global patterns of the DEGs dynamics between short-term and long-term culture. Then, we used GSEA information to look for the genes that are related to the potential skin associated pathway. Among our findings, FOXA2 is associated with the Hedgehog (HH) signaling pathway, while the other specific genes are related to each pathway (FGF, VEFG, Notch, BMP, TGF-b) (**Figure 3C**). Intriguingly, FGF5 is highly down-regulated in the short-term culture. At the same time, several genes related to the TGF-b signaling pathway are significantly down-regulated in the short-term

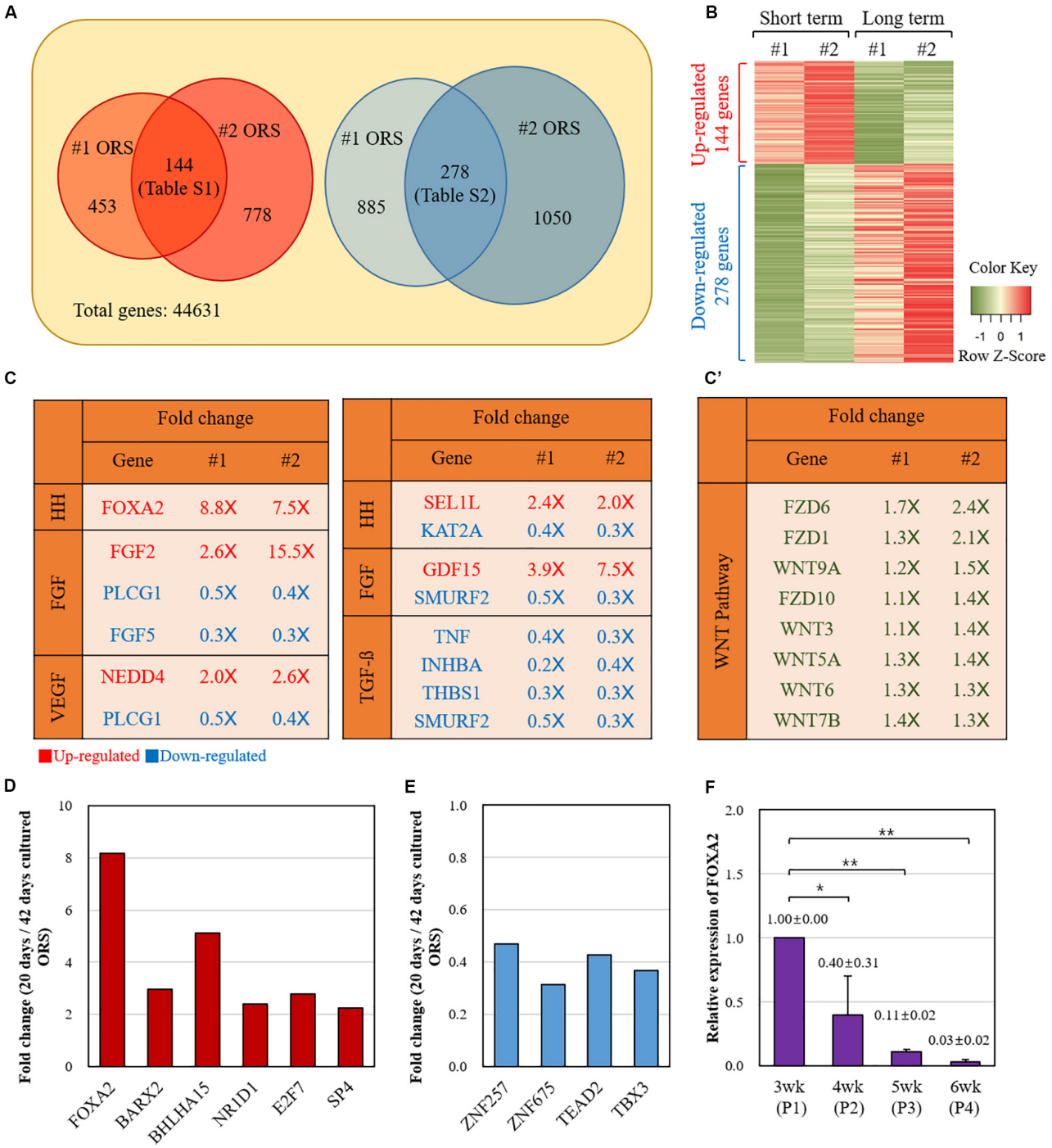

	Gene	Fold change #1	Fold change #2
HH	FOXA2	8.8X	7.5X
FGF	FGF2	2.6X	15.5X
	PLCG1	0.5X	0.4X
	FGF5	0.3X	0.3X
VEGF	NEDD4	2.0X	2.6X
	PLCG1	0.5X	0.4X

	Gene	Fold change #1	Fold change #2
HH	SEL1L	2.4X	2.0X
	KAT2A	0.4X	0.3X
FGF	GDF15	3.9X	7.5X
	SMURF2	0.5X	0.3X
TGF-ß	TNF	0.4X	0.3X
	INHBA	0.2X	0.4X
	THBS1	0.3X	0.3X
	SMURF2	0.5X	0.3X

	Gene	Fold change #1	Fold change #2
WNT Pathway	FZD6	1.7X	2.4X
	FZD1	1.3X	2.1X
	WNT9A	1.2X	1.5X
	FZD10	1.1X	1.4X
	WNT3	1.1X	1.4X
	WNT5A	1.3X	1.4X
	WNT6	1.3X	1.3X
	WNT7B	1.4X	1.3X

FIGURE 3 | Comparison of the gene expression profiles between the short-term and long-term cultured ORS cells. **(A)** Diagram of twofold up- and down-regulated genes in short-term cultured ORS cells. Two independent cell lines (#1 and #2) from two male patients (ages 50 and 64 years) were cultured for 20 days and 42 days, and microarray analysis was performed with transcripts derived from those cells. The number of genes with a more than twofold increase and decrease in the short-term cultured ORS cells are shown on the left and right, respectively. A total of 144 genes had a more than twofold increase in both short-term cultured ORS cells (listed in **Supplementary Table S1**), and 278 genes had a more than twofold decrease in both short-term cultured ORS cells (listed in **Supplementary Table S2**). **(B)** Heat map of differentially expressed genes (DEGs). The up-regulated genes were shown in red color and down-regulated genes in green color. **(C)** List of genes related to the skin signaling pathways from twofold up-regulated (2.0×) and down-regulated (0.5×) genes. Genes were selected based on gene-set enrichment analysis (GSEA) information in each pathway (HH, FGF, VEGF, Notch, BMP, and TGF-b). **(C')** List of up-regulated Wnts and their receptor (FZD) among WNT signaling pathway. **(D)** Relative fold changes of six up-regulated transcription factors. **(E)** Relative fold changes of four down-regulated transcription factors. **(F)** Relative levels of FOXA2 expression of ORS cells in various cultivation periods (3, 4, 5, and 6 weeks). Data are expressed as means ± standard deviation of three different ORS cell lines from three male patients (ages 33, 38, and 67 years).

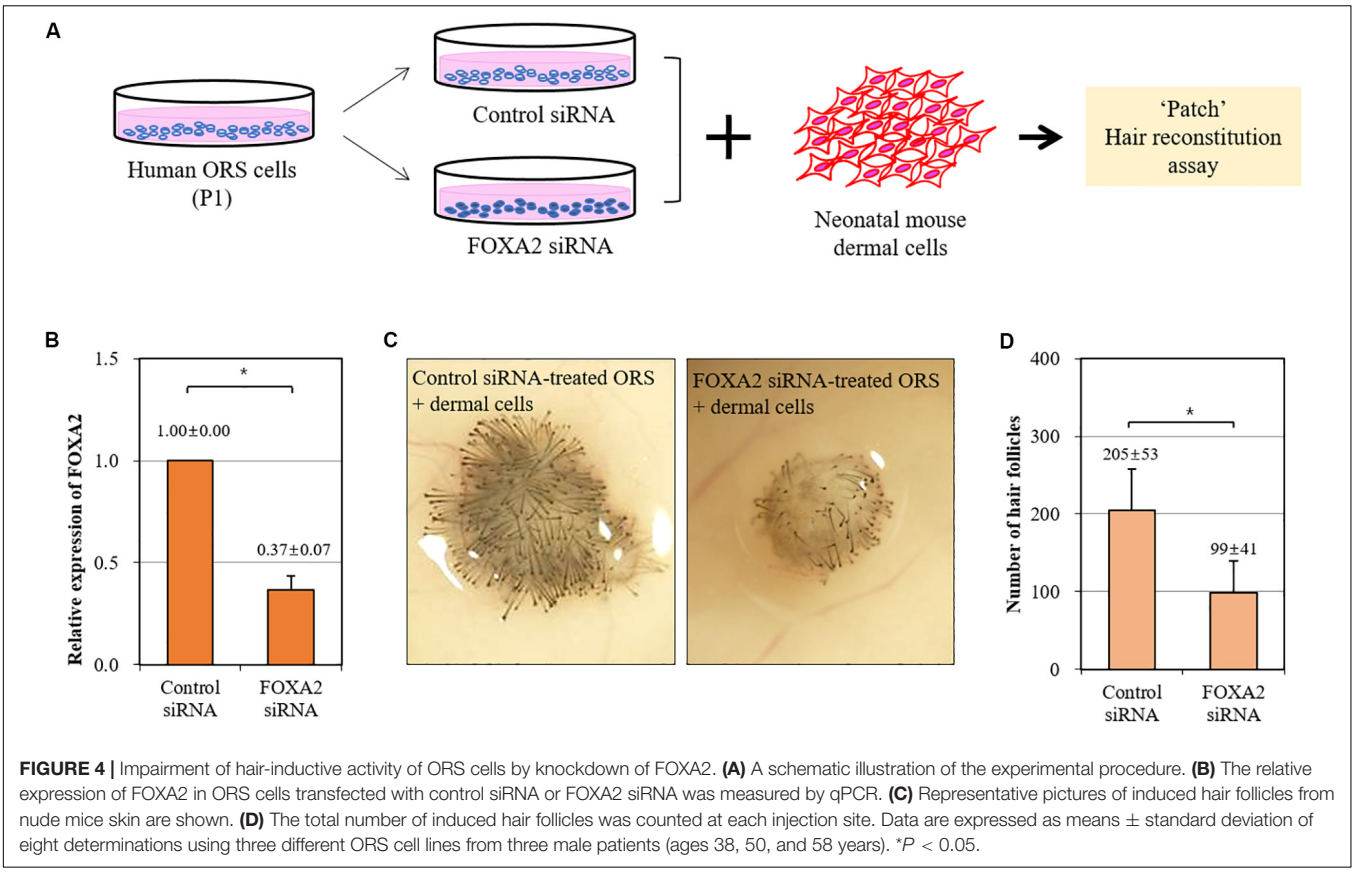

FIGURE 4 | Impairment of hair-inductive activity of ORS cells by knockdown of FOXA2. **(A)** A schematic illustration of the experimental procedure. **(B)** The relative expression of FOXA2 in ORS cells transfected with control siRNA or FOXA2 siRNA was measured by qPCR. **(C)** Representative pictures of induced hair follicles from nude mice skin are shown. **(D)** The total number of induced hair follicles was counted at each injection site. Data are expressed as means ± standard deviation of eight determinations using three different ORS cell lines from three male patients (ages 38, 50, and 58 years). $^*P < 0.05$.

culture as well. We also speculated the WNT-related genes between two groups. Total eight genes including WNT7b, WNT9a, WNT3, WNT5a, WNT6, FZD6, FZD1, and FZD10 were identified to be up-regulated, although they are not statistically significant, in WNT signaling pathway (**Figure 3C**'). To further analysis to find the potential mechanism, the DEGs were used to investigate GO biological process and KEGG pathway (**Supplementary Figure S3** and **Supplementary Tables S3–S6**). The up-regulated genes were enriched in regulation of stem cell proliferation, positive regulation of endothelial cell proliferation, regulation of embryonic development, and negative regulation of cell death. The down-regulated genes were enriched in epidermal cell differentiation, keratinocyte differentiation, and epidermis development (**Supplementary Figure S3** and **Supplementary Tables S3–S6**). The statistically enriched list is summarized in **Supplementary Tables S3–S6**.

Relative fold changes of the transcription factors, averaged between two individual samples, are shown in **Figures 3D,E**. We next focused on FOXA2, the most up-regulated transcription factor in the short-term cultured ORS cells compared with long-term cultured ORS cells. In line with microarray data, quantitative reverse transcription-PCR showed that the FOXA2 expression levels gradually decreased as the cultivation period increased (**Figure 3F**).

We then investigated whether the trichogenicity of ORS cells was affected by the expression level of FOXA2. We adopted a siRNA-mediated knockdown of FOXA2 in ORS cells in combination with a patch hair reconstitution assay (**Figure 4A**). Short-term cultured ORS cells were plated for transfection with a FOXA2 siRNA. After transfection for 2 days, the decreased expression of a FOXA2 was confirmed by real-time PCR (**Figure 4B**). As expected, freshly isolated newborn mouse dermal cells (10^6 cells) induced HFs when co-transplanted with negative control siRNA-transfected ORS cells (10^6 cells) (**Figure 4C**). However, we found a significantly decreased number of induced HFs using FOXA2 siRNA-transfected ORS cells (**Figure 4D**).

Our data in this study suggest that FOXA2, a transcription factor, may regulate downstream target genes which, in turn, enhance the trichogenicity of ORS cells. Considering that FOXA2 binds to the promoter of WNT7b (Weidenfeld et al., 2002), we propose that FOXA2 might function through WNT7b. Consistent with this hypothesis, we found that the relative fold changes of WNT7b were 1.393 and 1.257 in two individual samples exhibiting 8.840- and 7.506-fold increases of FOXA2, respectively. We speculate that secreted WNT7b from follicular keratinocytes activates inductive dermal cells or makes follicular keratinocytes more susceptible to dermal signals. In this regard, it is interesting to note that loss of WNT7b results in perturbed HF development and differentiation with aberrant hair shaft production (Kandyba and Kobielak, 2014). Overexpression of FOXA2 in cultured ORS cells may help to determine whether

this factor can enhance or restore trichogenicity of the cells; these experiments might yield intriguing results and are worthy of further consideration.

CONCLUSION

Our data strongly suggest that FOXA2 significantly influences the trichogenicity of human ORS cells. Our findings will provide a rationale for a new strategy for preparing competent human epidermal cells.

DATA AVAILABILITY STATEMENT

The raw data supporting the conclusions of this article will be made available by the authors, without undue reservation.

ETHICS STATEMENT

The studies involving human participants were reviewed and approved by The Medical Ethical Committee of the Kyungpook National University Hospital (Daegu, South Korea). The patients/participants provided their written informed consent to participate in this study. The animal study was reviewed and approved by the Animal Care and Use Committee at Kyungpook National University (Daegu, South Korea).

AUTHOR CONTRIBUTIONS

S-SB and YS designed the research and wrote the manuscript. S-SB performed the experiments. S-SB, JP, and JO analyzed the data. JK and MK contributed the materials that are essential to perform the project. All authors contributed to the article and approved the submitted version.

FUNDING

This research was supported by the Basic Science Research Program through the National Research Foundation of Korea (NRF-2018R1A2A2A05018574).

ACKNOWLEDGMENTS

We acknowledge other members of our laboratory (Hyun Woo Joo, Min Kyu Kim, Mee Sook Jun, Mi Hee Kwack, Eun Kyung Kim) for their technical help and valuable discussions.

SUPPLEMENTARY MATERIAL

The Supplementary Material for this article can be found online at: https://www.frontiersin.org/articles/10.3389/fcell.2020.575382/full#supplementary-material

Supplementary Figure 1 | Hair follicles quantified in **Figure 2** from the nude mice skin.

Supplementary Figure 2 | High power images of boxed regions in **Figure 2B**.

Supplementary Figure 3 | GO analysis and KEGG pathway analysis of microarray data.

Supplementary Table 1 | List of genes with a more than twofold increase in short-term cultured ORS cells.

Supplementary Table 2 | List of genes with a more than twofold decrease in short-term cultured ORS cells.

Supplementary Table 3 | Detail list of up-regulated genes related to GO biological process.

Supplementary Table 4 | Detail list of down-regulated genes related to GO biological process.

Supplementary Table 5 | Detail list of up-regulated genes related to KEGG pathway.

Supplementary Table 6 | Detail list of down-regulated genes related to KEGG pathway.

REFERENCES

Bak, S. S., Kwack, M. H., Shin, H. S., Kim, J. C., Kim, M. K., and Sung, Y. K. (2018). Restoration of hair-inductive activity of cultured human follicular keratinocytes by co-culturing with dermal papilla cells. *Biochem. Biophys. Res. Commun.* 505, 360–364. doi: 10.1016/j.bbrc.2018.09.125

Chan, C. C., Fan, S. M., Wang, W. H., Mu, Y. F., and Lin, S. J. (2015). A two-stepped culture method for efficient production of trichogenic keratinocytes. *Tissue Eng. Part C Methods.* 21, 1070–1079. doi: 10.1089/ten.TEC.2015.0033

Choi, J. W., Kim, Y. H., and Oh, J. W. (2017). Comparative analyses of signature genes in acute rejection and operational tolerance. *Immune Network.* 17, 237–249. doi: 10.4110/in.2017.17.4.237

Higgins, C. A., Chen, J. C., Cerise, J. E., Jahoda, C. A., and Christiano, A. M. (2013). Microenvironmental reprogramming by three-dimensional culture enables dermal papilla cells to induce de novo human hair-follicle growth. *Proc. Natl. Acad. Sci. U.S.A.* 110, 19679–19688. doi: 10.1073/pnas.1309970110

Kandyba, E., and Kobielak, K. (2014). Wnt7b is an important intrinsic regulator of hair follicle stem cell homeostasis and hair follicle cycling. *Stem Cells* 32, 886–901. doi: 10.1002/stem.1599

Kang, B. M., Kwack, M. H., Kim, M. K., Kim, J. C., and Sung, Y. K. (2012). Sphere formation increases the ability of cultured human dermal papilla cells to induce hair follicles from mouse epidermal cells in a reconstitution assay. *J. Invest. Dermatol.* 132, 237–239. doi: 10.1038/jid.2011.250

Kwack, M. H., Sung, Y. K., Chung, E. J., Im, S. U., Ahn, J. S., Kim, M. K., et al. (2008). Dihydrotestosterone-inducible dickkopf 1 from balding dermal papilla cells causes apoptosis in follicular keratinocytes. *J. Invest. Dermatol.* 128, 262–269. doi: 10.1038/sj.jid.5700999

Magerl, M., Kauser, S., Paus, R., and Tobin, D. J. (2002). Simple and rapid method to isolate and culture follicular papillae from human scalp hair follicles. *Exp. Dermatol.* 11, 381–385. doi: 10.1034/j.1600-0625.2002.110414.x

Millar, S. E. (2002). Molecular mechanisms regulating hair follicle development. *J. Invest. Dermatol.* 118, 216–225. doi: 10.1046/j.0022-202x.2001.01670.x

Ohyama, M., Kobayashi, T., Sasaki, T., Shimizu, A., and Amagai, M. (2012). Restoration of the intrinsic properties of human dermal papilla in vitro. *J. Cell Sci.* 125, 4114–4125. doi: 10.1242/jcs.105700

Ohyama, M., and Veraitch, O. (2013). Strategies to enhance epithelial-mesenchymal interactions for human hair follicle bioengineering. *J. Dermatol. Sci.* 70, 78–87. doi: 10.1016/j.jdermsci.2013.02.004

Ohyama, M., Zheng, Y., Paus, R., and Stenn, K. S. (2010). The mesenchymal component of hair follicle neogenesis: background, methods and molecular characterization. *Exp. Dermatol.* 19, 89–99. doi: 10.1111/j.1600-0625.2009.00935.x

Paus, R., and Cotsarelis, G. (1999). The biology of hair follicles. *N. Engl. J. Med.* 341, 491–497. doi: 10.1056/NEJM199908123410706

Philpott, M. P., Sanders, D., Westgate, G. E., and Kealey, T. (1994). Human hair growth in vitro: a model for the study of hair follicle biology. *J. Dermatol. Sci.* 7(Suppl.), S55–S72. doi: 10.1016/0923-1811(94)90036-1

Wang, Q., Oh, J. W., Lee, H. L., Dhar, A., Peng, T., Ramos, R., et al. (2017). A multi-scale model for hair follicles reveals heterogeneous domains driving rapid spatiotemporal hair growth patterning. *eLife* 6:e22772. doi: 10.7554/eLife.22772

Weidenfeld, J., Shu, W., Zhang, L., Millar, S. E., and Morrisey, E. E. (2002). The WNT7b promoter is regulated by TTF-1. GATA6, and Foxa2 in lung epithelium. *J. Biol. Chem.* 277, 21061–21070. doi: 10.1074/jbc.M111702200

Yang, C. C., and Cotsarelis, G. (2010). Review of hair follicle dermal cells. *J. Dermatol. Sci.* 57, 2–11. doi: 10.1016/j.jdermsci.2009.11.005

Zheng, Y., Du, X., Wang, W., Boucher, M., Parimoo, S., and Stenn, K. (2005). Organogenesis from dissociated cells: generation of mature cycling hair follicles from skin-derived cells. *J. Invest. Dermatol.* 124, 867–876. doi: 10.1111/j.0022-202X.2005.23716.x

Conflict of Interest: The authors declare that the research was conducted in the absence of any commercial or financial relationships that could be construed as a potential conflict of interest.

Copyright © 2020 Bak, Park, Oh, Kim, Kim and Sung. This is an open-access article distributed under the terms of the Creative Commons Attribution License (CC BY). The use, distribution or reproduction in other forums is permitted, provided the original author(s) and the copyright owner(s) are credited and that the original publication in this journal is cited, in accordance with accepted academic practice. No use, distribution or reproduction is permitted which does not comply with these terms.

frontiers in Cell and Developmental Biology

REVIEW
published: 15 October 2020
doi: 10.3389/fcell.2020.582346

Wound Induced Hair Neogenesis – A Novel Paradigm for Studying Regeneration and Aging

*Myan Bhoopalam[1], Luis A. Garza[2] and Sashank K. Reddy[1]**

[1] Department of Plastic and Reconstructive Surgery, Johns Hopkins University School of Medicine, Baltimore, MD, United States, [2] Department of Dermatology, Johns Hopkins University School of Medicine, Baltimore, MD, United States

Hair follicles are the signature dermal appendage of mammals. They can be thought of as mini-organs with defined polarity, distinct constituent cell types, dedicated neurovascular supply, and specific stem cell compartments. Strikingly, some mammals show a capacity for adult hair follicle regeneration in a phenomenon known as wound-induced hair neogenesis (WIHN). In WIHN functional hair follicles reemerge during healing of large cutaneous wounds, and they can be counted to provide an index of regeneration. While age-related decline in hair follicle number and cycling are widely appreciated in normal physiology, it is less clear whether hair follicle regeneration also diminishes with age. WIHN provides an extraordinary quantitative system to address questions of mammalian regeneration and aging. Here we review cellular and molecular underpinnings of WIHN, explore known age-related changes to these elements, and present unanswered questions for future exploration.

Keywords: wound-induced hair follicle neogenesis, aging, hair follicle stem cells, hair follicle neogenesis, Wnt, STAT3, regeneration

OPEN ACCESS

Edited by:
Cheng Ming Chuong, University of Southern California, Los Angeles, United States

Reviewed by:
Maria Fernanda Forni, Yale University, United States
Katerina Strati, University of Cyprus, Cyprus

***Correspondence:**
Sashank K. Reddy
sreddy6@jhmi.edu

Specialty section:
This article was submitted to Stem Cell Research, a section of the journal Frontiers in Cell and Developmental Biology

Received: *11 July 2020*
Accepted: *04 September 2020*
Published: *15 October 2020*

Citation:
Bhoopalam M, Garza LA and Reddy SK (2020) Wound Induced Hair Neogenesis – A Novel Paradigm for Studying Regeneration and Aging. Front. Cell Dev. Biol. 8:582346. doi: 10.3389/fcell.2020.582346

INTRODUCTION

Regeneration in mammalian systems is limited when compared to those of other phyla. In making this comparison, we distinguish between renewal and regeneration. Many mammalian tissues are capable of renewal in response to physiological need or limited damage. Epithelia of skin, lung, and gastrointestinal tract for example, turn over regularly to replace cells at the surface. However, regeneration of complex tissue or organ architectures in mammals is rare. Urodele salamanders can famously regenerate missing limbs, zebrafish can replace cardiac muscle, and planarians can reconstitute most of the body plan from small vestiges. Notwithstanding exceptions like significant skin regeneration in African spiny mouse and limited liver regeneration, such complex organ regeneration is not evident in mammals (Seifert et al., 2012).

A recently characterized process of hair follicle regeneration – wound induced hair neogenesis (WIHN) – offers an additional window into mammalian regeneration. WIHN is characterized by the emergence of hair follicles in the center of large full-thickness cutaneous wounds in mice, rats, and rabbits (Wier and Garza, 2020). While cutaneous wounds in many mammals including humans heal by fibrotic contracture and scarring, WIHN can produce healthy bilaminar skin, hair follicles, and subdermal supports including adipocytes (Plikus et al., 2017). The regeneration of hair follicles during WIHN is particularly striking, as these key dermal appendages were thought to arise only in embryonic development. In their seminal cellular and molecular characterization of

WIHN, Ito et al. (2007) showed that these hair follicles truly arise *de novo* in adults in a process that recapitulates key steps in embryonic hair follicle development.

Hair follicles can be thought of as organs in miniature with their defined polarity, distinct cell types, dedicated neurovascular supply, and stem cell compartments that support continued renewal. True regeneration of such complex structures is rare in mammals, establishing the WIHN system as an important tool to uncover principles of mammalian regeneration. A further advantage of studying WIHN is the ability to easily count novel hair follicles. This provides a quantitative index of regeneration by which to test perturbations that may inhibit or stimulate the process. The WIHN system may be particularly good at addressing an enduring mystery in mammalian regeneration – the extent to which regenerative capacity declines with age. Below we review critical cellular and molecular processes underlying WIHN and explore age-dependent changes in those processes.

OVERVIEW OF WIHN AND AGING

The healing of wounds with hair follicle regeneration in rodents and rabbits was first uncovered in the 1950s (Lacassagne and Latarjet, 1946; Breedis, 1954; Billingham and Russell, 1956; Chuong, 2007). The process was rediscovered and characterized in cellular and molecular terms in 2007 in a publication by Ito et al. that termed it wound induced hair neogenesis (WIHN). This group discovered that hair follicles emerge 2–3 weeks after full-thickness cutaneous wounds are created on common laboratory mouse strains (*Mus musculus*). Intriguingly, only large wounds (>1 cm^2) exhibited WIHN, whereas smaller wounds contracted in a fashion similar to larger ones but with the absence of hair follicle generation. Furthermore, hair follicles were only found in the center of these large wounds, not in the periphery. Morphologically, *de novo* hair follicles exhibited nearly all features of neighboring follicles in unwounded skin. The WIHN follicles were similarly polarized, associated with blood vessels, nerves, and sebaceous glands, and were embedded in dermis with subdermal adipocytes. The bulge region of the *de novo* follicles was populated by stem cells capable of supporting subsequent cycling. Differences from follicles generated during embryonic development were few, including an absence of melanocytes and erector pili muscles (Ito et al., 2007). Interestingly, African spiny mice (*Acomys cahirinus*) show even more robust WIHN and can regenerate erector pili muscles as well.

In Ito's original description of WIHN no significant differences were found in *de novo* hair forming capacity of young (3 week or 7–8 week) or middle-aged (10 month) mice when initial wound size was adjusted to achieve a similarly sized final healed area. It was noted in these original studies that efficient WIHN did not occur in wounds smaller than 1 cm^2. By contrast, in examining smaller initial wounds much earlier in life, Rognoni et al. (2016) uncovered a major difference in the ability of neonatal mice to undergo WIHN compared to even slightly older counterparts. Specifically, P2 mice exhibited significant hair follicle neogenesis in response to small (2 mm) wounds, whereas this decreased in age-dependent manner plateauing at P21 (Rognoni et al., 2016). Thus, in the immediate post-natal period, WIHN appears more robust than it does in even young animals. This enhanced perinatal wound healing in mice comports with our understanding of fetal wound healing in other systems, which occurs in a scarless fashion with more robust regeneration (Gurtner et al., 2008). Combining the results of these two studies, it appears that very young mice have an enhanced capacity for regeneration that is attenuated shortly thereafter. Yet, the capacity for regeneration in extremely aged animals remains unaddressed by these experiments.

There are reasons to believe WIHN may be less robust in animals at the end of their lifespan. First, wound healing responses in very old mice (∼2 years) differ markedly from their young counterparts, recapitulating the dermal fragility and poor wound healing observed in elderly humans (Keyes et al., 2016). When compared to young mice (2–4 month), elderly mice (22–24 months) showed decreased kinetics of wound closure and decreased capacity for keratinocyte proliferation. Skin thickness in these older mice was also attenuated. As discussed below, major cytokine pathways driving this decline in cutaneous wound healing are also implicated in WIHN. Further, this same group examined the response of young (2 month) and old (2 year) mice to partial thickness cutaneous wounds (Ge et al., 2020). Skin was removed to the depth of epidermis and partial dermis but with hair follicle bulges left intact. Interestingly, while hair follicle stem cells (HFSCs) were found to be present in near normal numbers in the old mice and had retained their identity, they engaged in aberrant cycles of hair follicle renewal in response to wounding. As discussed below, since some of these same HFSCs are involved in hair follicle neogenesis, it will be interesting to examine whether similar abortive regeneration occurs in response to full thickness wounds that normally produce WIHN.

CELLULAR PROCESSES IN WIHN

Disparate cellular elements coordinate the regeneration of epidermis, dermis, and hair follicles during WIHN. These include keratinocytes and hair follicle stem cells (HFSCs) concentrated in different areas of the interfollicular epidermis and hair follicle (HF). Here we consider what is known about the age-related dynamics of these cells in homeostasis and wound repair. Distinct lineages of HFSCs have a particular niche both during the normal HF cycle and upon wounding. The ability of HFSCs to effectively maintain this niche can be affected by age-related factors such as changing gene expression programs, stem cell location, DNA and oxidative damage, and extrinsic factors in the tissue microenvironment.

Hair Follicle Stem Cells

Hair follicle stem cells are clustered in specific regions of the hair follicle and surrounding skin including the bulge (Krt15$^+$, CD34$^+$, Lgr5$^+$, Sox9, Tcf3), isthmus (Lgr6$^+$, Plet1$^+$), infundibulum (Lrig1$^+$) interfollicular epidermis (Lgr6$^+$), and sebaceous gland (Lgr6$^+$, Blimp1$^+$, Gata6 lineage) (Dekoninck and Blanpain, 2019; Wier and Garza, 2020). The bulge is the area of the hair follicle that contains long-lived HFSCs responsible

for hair renewal throughout life – cycles of anagen (growth), catagen (degeneration), and telogen (resting stage) (Cotsarelis et al., 1990; Blanpain and Fuchs, 2006). Given their key early role in healing of the intrafollicular epidermis, it was surprising that Krt15$^+$ bulge stem cells from adjacent HFs were shown to be insignificant contributors to hair follicle regeneration in WIHN (Ito et al., 2005, 2007). As these cells are critical for normal hair follicle cycling, their lack of contribution to WIHN reveals an important difference between physiologic renewal and damage-induced regeneration. It was later shown that certain bulge stem cells were not essential for WIHN as long as there remained a functional interaction between the epithelium and mesenchymal dermal papilla (Ito et al., 2007; Rompolas et al., 2013). The latter study showed that following laser ablation of the bulge, distant epithelial cells above the bulge (infundibulum) contributed to creating the missing bulge compartment and subsequent hair growth (Rompolas et al., 2013), consistent with a role for stem cells of the isthmus in contributing to neogenic follicles (Snippert et al., 2010). This suggests that non-bulge stem cells have greater lineage plasticity following wounding and are primary contributors to WIHN.

Stem cells characterized by other marks in the bulge and isthmus have been shown to be important contributors to WIHN. Leucine-rich-repeat-containing-G-protein-coupled-receptor (Lgr) cells are critical for physiologic renewal of stratified epithelia and for regeneration in WIHN. Lgr6$^+$ cells are the most primitive epidermal stem cell lineage, capable of generating many if not all epidermal structures during development and contributing to maintenance of the IFE in homeostatic conditions. Lineage tracing experiments showed that descendants of these cells contribute to newly generated hair follicles and IFE during WIHN (Snippert et al., 2010). Lgr5$^+$ SCs are derived from the Lgr6$^+$ pool early in the life and become independent soon thereafter. Lgr5$^+$ cells contribute to all hair lineages but not to sweat glands or interfollicular epidermis (Snippert et al., 2010). Wang et al. (2017) showed through lineage tracing during WIHN that descendants of Lgr5$^+$ epithelial stem cells were present in 40% of the regenerated HFs and that Lgr5$^+$ cell depletion reduced WIHN by over 50%.

Recent studies using high throughput lineage tracing of Lgr5$^+$ and Lgr6$^+$ SCs and transcriptomic analysis capture the molecular adaptation of SC progeny from different niches during wound healing. The results demonstrate remarkable plasticity in HFSCs whereby wounds productive of WIHN displayed downregulation of bulge stem cell gene expression and induction of an IFE-like signature in Lgr5$^+$ HF progeny (Joost et al., 2018). This IFE-like signature and improved regenerative ability largely resulted from an increase in surface receptors that could interact with the wound environment. Lgr6$^+$ progeny possessed that ability even before wounding (Joost et al., 2018). This increase in regenerative capacity with improved crosstalk between HFSCs and the wound environment underscores the importance of the microenvironment on the plasticity of HFSCs. Interestingly, similar lineage infidelity is also evident in HFSCs mobilized in both young and old animals during the healing response to partial thickness wounds (Ge et al., 2020). In aged animals, these HFSCs migrate from the bulge and express both IFE and HF markers. However, these cells fail to complete hair follicle renewal resulting in smaller, morphologically variant follicles. It is important to note that the partial thickness wounding utilized in these experiments does not completely destroy hair follicles so the failure here is one of hair follicle renewal rather than a failure of *de novo* hair follicle regeneration. Therefore, it will be interesting to see whether the same blurring of IFE and HFSC transcriptional programs is maintained in aging animals during WIHN and whether there are functional consequences for number and morphology of neogenic follicles.

Insights gleaned from non-hair follicle systems are also shedding light on changes in the function of Lgr5$^+$ and Lgr6$^+$ stem cells with aging. In the hyponychium – the portion of the nail bed responsible for nail renewal – absolute numbers of Lgr6$^+$ cells do not seem to vary in young and aged human samples (Shi et al., 2018). However, the younger Lgr6$^+$ cells demonstrated a greater proliferative capacity than older cells, and the younger nails had higher growth rates. It is in the intestinal system that Lgr + epithelial stem cells first came to prominence due to their roles in mucosal turnover and intestinal organoid formation. In studies comparing Lgr5$^+$ intestinal stem cells in young mice (2 month) and old mice (22–24 month) there was no significant change in the number of intestinal crypts with Lgr5$^+$ cells nor in their relative percentage compared to other cell types (Nalapareddy et al., 2017). However, there was a decline in Lgr5$^+$ SC function – migratory capacity and ability to contribute to crypt morphology and viability – and turnover in the old mice. Similarly, in both mouse and human samples, the numbers of Lgr5$^+$ intestinal stem cells and their proliferative capacity were undiminished with age (Pentinmikko et al., 2019). Yet the regenerative capacity of these cells as judged by organoid formation was markedly decreased. Strikingly, this change was due to the production of a soluble Wnt inhibitor – notum – by adjacent Paneth cells in the crypt. The observations of Lgr5$^+$ and Lgr6$^+$ SCs in these systems suggest that we can expect greater age-related changes in the response of these cells to regenerative stimuli during WIHN rather than changes in their absolute number.

Changes in HFSC microenvironment can result in significant attenuation of hair follicle cycling with aging. Ge et al. (2020) used scRNAseq to compare the transcriptomic identities of bulge, hair germ, isthmus, infundibular, sebaceous gland, basal epidermal, and supra-basal epidermal stem cells of 2-mo-old (young) and 2-y-old (aged) mice during telogen. There was little noticeable difference between the cellular pattern of young and aged epithelia, suggesting no age-related blurring of cellular states. Specifically, aged bulge HFSCs did not show signs of lineage infidelity marked by induction of epidermal genes or loss of key HF identity transcripts. However, and in agreement with their earlier studies, transcriptomic analysis of young and aged cells showed that aged HFSCs had significant changes in expression profiles of ECM, ECM-remodeling genes, basement membrane, and secreted signaling factors (Keyes et al., 2013; Ge et al., 2020). Strikingly, modulating the stem cell environment by commingling these cells with cells from neonatal dermis allowed even aged HFSCs to regenerate hair follicles

when transplanted onto nude mice. This suggests that certain secreted factors or ECM components in the neonatal dermis can rejuvenate aged HFSCs.

Fibroblasts

The importance of fibroblasts to regeneration of follicles and subdermal tissues has been demonstrated in several studies. Emerging evidence points to a role for fibroblasts in the age-related attenuation of WIHN (Gay et al., 2013; Rognoni et al., 2016). Two primary lineages of fibroblasts include upper dermal (papillary) fibroblasts marked by Lrig1$^+$ and responsible for regulation of hair growth and the arrector pili muscle, and lower dermal (reticular) fibroblasts that secrete fibrillar ECM (Driskell et al., 2013). Upon wounding, lower dermal fibroblasts proliferate first, and start producing collagen. After this and only following re-epithelialization, the upper dermal fibroblasts migrate to regenerate the papillary dermis that is important for HF formation and growth (Driskell et al., 2013). Rognoni et al. (2016) found that following 2 mm circular full-thickness wounds on the back of P2 and P21 mice, P21 mice formed far fewer HFs than did P2 mice. Interestingly between P2 and P50, fibroblast density was lower in the dermis, but the rate of proliferation was the same. This was observed even in wound beds that have a lower ability to support HF neogenesis such as in the tail. Interestingly, the post-natal decline in WIHN correlated with a dramatic reduction in Lrig1$^+$ papillary fibroblasts around P10 suggesting that the balance between the two lineages of fibroblast is more critical for regeneration than absolute numbers. This increase in recruitment of lower lineage fibroblasts at the expense of papillary fibroblasts occurs in a Wnt-dependent fashion (Rognoni et al., 2016).

While the data from Rognoni et al. (2016) compare regeneration in neonatal and young adult mice, their observations of fibroblast dynamics comport with those seen in older mice. In a study comparing the relative thickness of papillary dermis and reticular dermis of young (2 month), middle-aged (9 month), and old (18 month) mice, the old mice had a decrease in the thickness and density of the papillary dermis, but a significant increase in thickness of the reticular layer (Salzer et al., 2018). These changes were already visible albeit not as pronounced in the middle-aged mice. Transcriptomic analysis of fibroblasts from these animals revealed that CD26 + old papillary fibroblasts differentially expressed genes involved in promoting cytoskeletal extensions, cell contacts, and cell-cell repulsion signals (Salzer et al., 2018). These data support a mechanism in which aged dermal fibroblasts prefer to fill the empty dermal space created by surrounding dying fibroblasts with membrane protrusion rather than through proliferation (Salzer et al., 2018), a conclusion supported by tracking fibroblasts over time with intravital imaging (Marsh et al., 2018). Interestingly, membrane extension rather than proliferation is also utilized by these aged fibroblasts in response to wounding. Taken together, these data suggest that the decreased density of papillary fibroblasts that occurs post-natally continues into old age with likely attendant consequences for diminished WIHN. Augmenting this fibroblast population could lead to more robust regeneration in aging animals.

Inflammatory Cells

Inflammatory cells including dermal γ-δ T-cells, dendritic epidermal T-cells (DETCs), and macrophages have emerged as important regulators of WIHN. In mice, γ-δ T-cells (named for the two chains that make up their T-cell receptor) are present in substantial numbers in epidermis and play a key role in triggering WIHN (Gay et al., 2013). Specifically, dermal γ-δ T-cells secrete fibroblast growth factor 9 (Fgf9) which induces hair follicle neogenesis after wounding in a Wnt-dependent fashion (Gay et al., 2013). Reducing Fgf9 expression by using mice lacking γ-δ T-cells or mice with Fgf9-deleted T cells led to a dramatic reduction in WIHN with 60% fewer regenerated hair follicles (Gay et al., 2013). By contrast, overexpression of FGF9 resulted in a two- to threefold increase in the number of neogenic hair follicles. In a different study, after making full-thickness dorsal skin wounds in mice, the absolute copy numbers of mRNAs encoding various fibroblast growth factors were quantified in young adult mice (2 month) and old mice (9 month) (Komi-Kuramochi et al., 2005). In young mice, Fgf9 mRNA copy numbers were fivefold higher than in the aged animals. It is interesting to note that the proportion of γ-δ T-cells amongst CD45$^+$ T-cells in the wound site did not change after full-thickness wounding in young (2–4 month) versus aged (22–24 month) mice (Keyes et al., 2016). These data raise the intriguing possibility that downregulation of Fgf9 secretion by aging γ-δ T-cells rather than a reduction in cell numbers may attenuate WIHN in aging animals.

SIGNALING PATHWAYS

Wnt/β-Catenin Signaling

Since its characterization by Ito et al. (2007), WIHN has been shown to be driven by a number of signaling pathways including Wnt/β-catenin, Fgf9, Shh, IL-6/STAT3, and retinoic acid pathways. The canonical Wnt/β-catenin pathway was the first and most extensively characterized pathway to be implicated in WIHN (Ito et al., 2007). Given the key role of Wnt signaling in establishing hair follicles during embryonic development, it is not surprising that this pathway is reactivated during neogenic follicle development in adults. Ito originally found that expression of Wnt inhibitors in healing epidermis abrogated WIHN, while upregulation of Wnt/β-catenin signaling in the same system led to an increase in neogenic follicle numbers (Ito et al., 2007). In subsequent work, Wnt/β-catenin activation has emerged as a key node integrating roles of disparate cellular and signaling events to promote follicle neogenesis in response to wounding. Gay et al. (2013) found that dermal γ-δ T-cells secrete Fgf9 which triggers Wnt2a secretion and subsequent activation of myofibroblasts. This results in a positive feedback loop by which activated fibroblasts express more Fgf9 and further upregulate dermal Wnts (Gay et al., 2013). Since the γ-δ T-cells of aged mice secrete considerably less Fgf9 than their young counterparts, the decrease in subsequent dermal Wnt activation may account for a decline in WIHN with aging (Komi-Kuramochi et al., 2005). Surprisingly, given the pro-regenerative role of Wnt/β-catenin signaling in the epidermis, increasing

Wnt/β-catenin signaling in dermal fibroblasts of young adult mice led to attenuation of WIHN as compared with neonates (Rognoni et al., 2016). The increased activation of β-catenin in the adult mice resulted in increased recruitment of lower dermal fibroblasts, which are unable to induce HF formation, at the expense of papillary dermal fibroblast as discussed above (Rognoni et al., 2016). Given the complex interplay between epithelia and fibroblasts in formation of the dermal papilla and subsequent events in hair follicle morphogenesis, restriction of Wnt morphogens to particular geographies may be needed to promote regeneration. In addition to these spatial dynamics, temporal dynamics in Wnt/β-catenin signaling within the epidermal compartment also come into play. Castilho et al. (2009) found that prolonged Wnt1 expression induced rapid growth of HFs but subsequently led to the exhaustion of HFSCs as seen through the diminution of $CD34^+$ cells in the HFSC niche and activation of cell senescence pathways. Indeed, the silencing of this stem cell population upon prolonged Wnt exposure in older animals that have seen numerous hair cycles seems to serve a protective role by preventing these cells from nucleating follicular cancers. Therefore, far from being an on/off switch for promoting regeneration, Wnt/β-catenin signaling must be carefully governed in time and space to generate optimal WIHN.

Hedgehog Signaling

Sonic hedgehog (Shh) is a critical signaling molecule in the hair cycle and in WIHN. Knocking out Musashi 2 (Msi2), an evolutionarily conserved RNA binding protein that represses Shh signaling, in tissue-specific stem cells resulted in a dramatic reduction of *de novo* hair follicle regeneration (Sugiyama-Nakagiri et al., 2006; Ma et al., 2017). Lim et al. (2018) showed that Shh signaling is essential for WIHN and that Shh activation shifts dermal fibroblast fate toward the dermal papilla. This suggests that reticular dermal fibroblasts that promote scarring can be redirected to a regenerative phenotype, similar to the fate switch that embryonic fibroblasts must undergo when encountering epidermal hair follicle placodes to generate hair follicles in development. Further underscoring the importance of hedgehog (Hh) signaling in adult hair follicle regeneration, Sun et al. (2020) demonstrated that exogenous activation of the pathway in cutaneous epithelia and stroma can lead to *de novo* hair follicle formation. This was observed even in normally non-hair-bearing areas of the mouse such as the paw and occurred in the absence of wounding. While the Hh pathway is critical for follicular morphogenesis in embryonic development and adult regeneration, there have been no studies comparing Shh expression in young and old mice during WIHN. However, age-related decrease Shh expression has been observed in other systems including endometrium where decreased Shh levels lead to impaired endometrial stem cell activity and poor endometrial renewal (Cho et al., 2019). Interestingly, in HFSCs isolated from hair follicle bulges in young and old human scalp biopsies, Hh pathway genes were expressed at similar levels (Rittie et al., 2009). Whether this similarity in gene expression occurs during normal homeostasis only or whether it also obtains in the context of wounding remains to be seen. Further, given the interplay between Shh and other signaling systems in skin that demonstrate age-related changes such as Wnts, deconvoluting the role of Shh in regeneration and aging will be an important area for future investigation (Ouspenskaia et al., 2016).

dsRNA/IL-6/STAT3/RA

The innate immune receptor Toll-Like Receptor 3 (TLR3) is an important driver of WIHN (Nelson et al., 2015). Activation of TLR3 signaling in keratinocytes promotes expression of stem cell markers and leads to induction of key hair follicle morphogenic programs. TLR3 responds to dsRNA species which are released by damaged or dying cells, thereby serving as a direct link between damage sensing and regeneration. Downstream effectors of TLR3 in WIHN include interleukin 6 (IL-6) and signal transducer and activator 3 (STAT3) (Nelson et al., 2015). Nelson et al. found that HF generation after full-thickness wounding in TLR3 null mice was dramatically reduced compared to controls. Comparing gene expression signatures from healed wound beds of mice with robust HF regeneration to those of mice with poor regeneration, they found that IL-6 was significantly upregulated in the prolific regenerators. They further showed that this IL-6 induction was TLR3 dependent with TLR3-null mice having far less IL-6 mRNA post-wounding than strain-matched controls. Activation of the IL-6 receptor results in the phosphorylation of STAT3 (pSTAT3), which leads to its nuclear translocation and transcriptional activation (Heinrich et al., 2003). When mice were treated with cucurbitacin I, a highly selective pharmacological inhibitor of STAT3, they had a more than threefold decrease in the number of regenerated HFs following wounding showing that STAT3 is functionally required for WIHN (Nelson et al., 2015). In summary, TLR activation in response to wounding leads to IL-6 production and STAT3 phosphorylation, activating a STAT3-dependent gene expression program to promote WIHN. This conclusion agrees with recent studies that have characterized other IL-6 type molecules such as IL-36α that activate STAT3 and induce WIHN (Gong et al., 2020).

Strikingly, the same IL-6/STAT3 pathway that governs WIHN is implicated in impaired cutaneous wound healing in aged mice. In comparison to young mice (2–4 month), aged mice (22–24 month) had significantly slowed wound healing and diminished capacity for keratinocyte proliferation and migration. This correlated with a 4.5-fold reduction in IL-6 transcription in keratinocytes of aged mice (Keyes et al., 2016). Exogenous application of IL-6 rescued the poor wound healing kinetics in aged mice, reminiscent of its ability to augment WIHN (Nelson et al. and **Figure 1**). Additionally, the age-related attenuation in wound healing observed by Keyes et al. (2016) is mediated largely through STAT3 signaling in dendritic epithelial T cells (DETCs), a major resident subtype of cutaneous γ-δ T-cells. Keyes et al. (2016) found that in the unwounded state, DETC numbers were unaffected by STAT3 loss. However, after wounding, DETC number declined dramatically in the skin of STAT3 cKO mice. Thus, the epithelial-DTEC crosstalk examined here is critical for normal wound healing, converges on IL-6/STAT3 signaling, and is attenuated in aged animals with impaired wound healing. While this study did not directly assess hair follicle regeneration in young and old mice, it is interesting to speculate that this

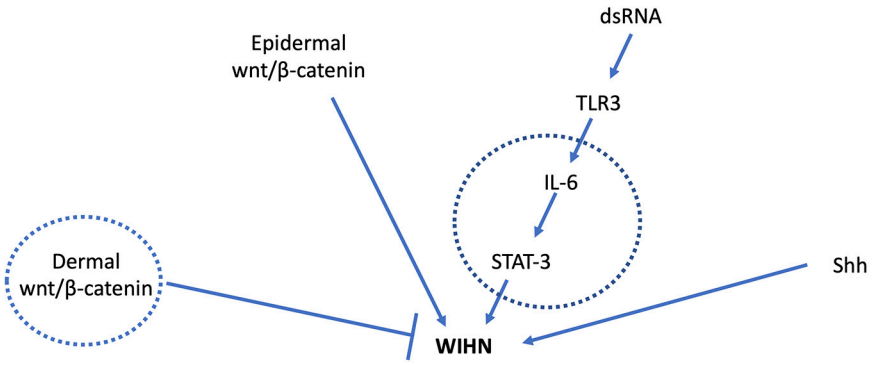

FIGURE 1 | Major signal transduction pathways involved in WIHN. Circles indicate mediators known to have age-related changes. Young adult mice with high wnt/β-catenin levels in the dermis had fewer pro-regenerative fibroblasts and impaired WIHN (Rognoni et al., 2016). IL-6 levels are lower in aged mouse skin with impaired wound healing (Keyes et al., 2016), and low IL-6/STAT-3 is also observed in mice with low WIHN (Nelson et al., 2015). Shh signaling is a major driver of developmental and regenerative hair follicle morphogenesis. Age-related changes in Shh during WIHN have not been demonstrated.

too will be reduced given its common dependence on IL-6 and STAT3.

Retinoic acid (RA), was recently discovered to induce WIHN following TLR3 activation by dsRNA (Kim et al., 2019). Kim et al. (2019) found that TLR3 signaling induces RA accumulation, and that exogenous RA can rescue deficient hair follicle regeneration in TLR3 deleted mice. It is interesting to note that the TLR3/RA pathway is connected to the STAT3 pathway. STAT3 stimulates aldehyde dehydrogenase1a3 which converts retinaldehyde to RA (Canino et al., 2015). Furthermore, laser treatment of skin, which can be done for facial rejuvenation, results in elevation of RA synthesis (Kim et al., 2019). This suggests that the rejuvenation of aged human skin likely works by a similar mechanism involving dsRNA/damage-induced RA synthesis. RA-based compounds known as retinoids have also been used clinically for decades to rejuvenate aging skin and function by both increasing collagen production by stimulating fibroblasts and inhibiting ECM degradation by matrix metallopeptidases (MMPs) (Lateef et al., 2004; Mukherjee et al., 2006). Aged skin has been shown to have an upregulation of MMPs as well as decreased collagen production due to the age-dependent alteration of fibroblast function (Varani et al., 2006). Thus, an interesting avenue of investigation would be to see if the TLR3/RA pathway is downregulated or compromised during WIHN in aged mice.

Hippo Signaling

The ECM may modulate WIHN via mechanotransduction activation of the transcriptional cofactor Yes-associate protein (YAP). YAP is a key effector of the Hippo signaling pathway that is involved in organ size control (Pan, 2010). Physico-mechanical stresses applied to ECM can result in changes in substrate stiffness. These forces can in turn alter cytoskeletal dynamics on attached cells leading to activation and nuclear translocation of YAP (Dupont et al., 2011). In uninjured skin, YAP is activated in HFs and epidermal cells but not in surrounding dermal cells (Lee et al., 2014). Upon wounding, YAP localized to the nucleus in dermal skin cells in 2 days with expression throughout the wound area by 7 days (Lee et al., 2014). This is likely due not only to the inhibition of the Hippo pathway due to decreased cell-crowding but also to mechanical cues that act independently from the Hippo pathway (Dupont et al., 2011). Wound closure has been shown to be delayed following downregulation of YAP by siRNA treatment and is likely a result of decreased activity and production of TGF-ß1, a downstream factor activated by YAP (Lee et al., 2014). During HF development, transgenic activation of YAP leads to increased proliferation of basal epidermal SCs at the expense of terminal differentiation (Zhang et al., 2011). Furthermore, the study also found that nuclear YAP progressively declines with age and correlates with the proliferative potential of epidermal SCs. Given the known role of these cells in regeneration of HFs and IFE in WIHN, it will be interesting to see if this age-related dysregulation of YAP activation leads to impaired WIHN in older animals.

REMAINING QUESTIONS AND CONCLUSION

Impaired capacity for renewal and regeneration – seen notably in cutaneous wound healing (Keyes et al., 2016) – is an important source of age-related morbidity. As one of the few truly regenerative phenomena in adult mammals, WIHN represents a powerful lens with which to investigate this decline and offer solutions for its reversal. We have described a number of cellular – HFSC and epidermal stem cell, fibroblast, T cell – and molecular – Wnt, IL-6/STAT3, Hippo pathway – players in WIHN that show alterations with age (**Figure 1**). The production of neogenic follicles itself declines from the neonatal period through youth in mice, paralleling a later decline in the capacity for wound-induced hair follicle renewal (Ge et al., 2020) and for cutaneous wound healing (Keyes et al., 2016). This raises the tantalizing possibility that WIHN may continue to decline throughout age, though no rigorous studies have been performed to test this. Quantitative investigation of WIHN in middle aged

and extremely aged animals may better elucidate regenerative decline and define its mechanisms.

Such mechanisms fall into three broad categories. First, older animals may be less sensitive to damage-induced molecular cues that initiate the regeneration cascade. Second, such animals may fail to mobilize precursor cells to rebuild missing structures. Given the number of cells that seem to contribute to regenerated hair follicles – keratinocytes, epidermal stem cells, and HFSCs that constitute the new follicles, and immune cells that coordinate their response – there are many places where regeneration could break down. Finally, precursors even when appropriately mobilized may fail to reconstitute *de novo* follicles resulting in frustrated, incomplete morphogenesis. Indeed, the failure of otherwise present and genetically stable HFSCs to create new hair follicles is evident in aged mice subjected to partial thickness wounding, suggesting that a similar situation may obtain in WIHN (Ge et al., 2020). Discriminating between these three possibilities or combinations of them will provide a rich ground for future studies and may afford insights into improving regenerative capacity with age.

AUTHOR CONTRIBUTIONS

SR defined the structure of the manuscript. MB and SR wrote the manuscript. SR and LG edited the manuscript. All authors contributed to the article and approved the submitted version.

FUNDING

This work was supported by the American Association of Plastic Surgeons – Hoopes Academic Scholar Award (SR) and National Institute of Arthritis, Musculoskeletal, and Skin Diseases, part of the National Institutes of Health, R01AR064297/AR068280 (LG).

SUPPLEMENTARY MATERIAL

The Supplementary Material for this article can be found online at: https://www.frontiersin.org/articles/10.3389/fcell.2020.582346/full#supplementary-material

REFERENCES

Billingham, R. E., and Russell, P. S. (1956). Incomplete wound contracture and the phenomenon of hair neogenesis in rabbits' skin. *Nature* 177, 791–792. doi: 10.1038/177791b0

Blanpain, C., and Fuchs, E. (2006). Epidermal stem cells of the skin. *Annu. Rev. Cell Dev. Biol.* 22, 339–373. doi: 10.1146/annurev.cellbio.22.010305.104357

Breedis, C. (1954). Regeneration of hair follicles and sebaceous glands from the epithelium of scars in the rabbit. *Cancer Res.* 14, 575–579.

Canino, C., Luo, Y., Marcato, P., Blandino, G., Pass, H. I., and Cioce, M. (2015). A STAT3-NFkB/DDIT3/CEBPβ axis modulates ALDH1A3 expression in chemoresistant cell subpopulations. *Oncotarget* 6, 12637–12653. doi: 10.18632/oncotarget.3703

Castilho, R. M., Squarize, C. H., Chodosh, L. A., Williams, B. O., and Gutkind, J. S. (2009). mTOR mediates wnt-induced epidermal stem cell exhaustion and aging. *Cell Stem Cell* 5, 279–289. doi: 10.1016/j.stem.2009.06.017

Cho, A., Park, S., Kim, S., Nam, S., Lim, S., Park, C. H., et al. (2019). An endogenous anti-aging factor, sonic hedgehog, suppresses endometrial stem cell aging through SERPINB2. *Mol. Ther.* 27, 1286–1298. doi: 10.1016/j.ymthe.2019.04.019

Chuong, C. (2007). New hair from healing wounds. *Nature* 447, 265–266. doi: 10.1038/447265a

Cotsarelis, G., Sun, T., and Lavker, R. M. (1990). Label-retaining cells reside in the bulge area of pilosebaceous unit: implications for follicular stem cells, hair cycle, and skin carcinogenesis. *Cell* 61, 1329–1337. doi: 10.1016/0092-8674(90)90696-c

Dekoninck, S., and Blanpain, C. (2019). Stem cell dynamics, migration and plasticity during wound healing. *Nat. Cell Biol.* 21, 18–24. doi: 10.1038/s41556-018-0237-6

Driskell, R. R., Lichtenberger, B. M., Hoste, E., Kretzschmar, K., Simons, B. D., Charalambous, M., et al. (2013). Distinct fibroblast lineages determine dermal architecture in skin development and repair. *Nature* 504, 277–281. doi: 10.1038/nature12783

Dupont, S., Morsut, L., Aragona, M., Enzo, E., Giulitti, S., Cordenonsi, M., et al. (2011). Role of YAP/TAZ in mechanotransduction.(yes-associated protein). *Nature* 474, 179–183. doi: 10.1038/naturel0137

Gay, D., Kwon, O., Zhang, Z., Spata, M., Plikus, M. V., Holler, P. D., et al. (2013). Fgf9 from dermal γδ T cells induces hair follicle neogenesis after wounding. *Nat. Med.* 19, 916–923. doi: 10.1038/nm.3181

Ge, Y., Miao, Y., Gur-Cohen, S., Gomez, N., Yang, H., Nikolova, M., et al. (2020). The aging skin microenvironment dictates stem cell behavior. *Proc. Natl. Acad. Sci. U.S.A.* 117, 5339–5350. doi: 10.1073/pnas.1901720117

Gong, L., Xiao, J., Li, X., Li, Y., Gao, X., and Xu, X. (2020). IL-36α promoted wound induced hair follicle neogenesis via hair follicle stem/progenitor cell proliferation. *Front. Cell Dev. Biol.* 8:627. doi: 10.3389/fcell.2020.00627

Gurtner, G. C., Werner, S., Barrandon, Y., and Longaker, M. T. (2008). Wound repair and regeneration. *Nature* 45, 585–703. doi: 10.1038/nature07039

Heinrich, P. C., Behrmann, I., Haan, S., Hermanns, H. M., Müller-Newen, G., and Schaper, F. (2003). Principles of interleukin (IL)-6-type cytokine signalling and its regulation. *Biochem. J.* 374(Pt 1), 1–20. doi: 10.1042/bj20030407

Ito, M., Liu, Y., Yang, Z., Nguyen, J., Liang, F., Morris, R. J., et al. (2005). Stem cells in the hair follicle bulge contribute to wound repair but not to homeostasis of the epidermis. *Nat. Med.* 11, 1351–1354. doi: 10.1038/nm1328

Ito, M., Yang, Z., Andl, T., Cui, C., Kim, N., Millar, S. E., et al. (2007). Wnt-dependent de novo hair follicle regeneration in adult mouse skin after wounding. *Nature* 447, 316–320. doi: 10.1038/nature05766

Joost, S., Jacob, T., Sun, X., Annusver, K., La Manno, G., Sur, I., et al. (2018). Single-cell transcriptomics of traced epidermal and hair follicle stem cells reveals rapid adaptations during wound healing. *Cell Rep.* 25, 585.e7–597.e7. doi: 10.1016/j.celrep.2018.09.059

Keyes, B. E., Liu, S., Asare, A., Naik, S., Levorse, J., Polak, L., et al. (2016). Impaired epidermal to dendritic T cell signaling slows wound repair in aged skin. *Cell* 167, 1323.e14–1338.e14. doi: 10.1016/j.cell.2016.10.052

Keyes, B. E., Segal, J. P., Heller, E., Lien W. H., Chang C. Y., Guo X., et al. (2013). Nfatc1 orchestrates aging in hair follicle stem cells. *Proc. Natl. Acad. Sci.* 110, E4950–9. doi: 10.1073/pnas.1320301110

Kim, D., Chen, R., Sheu, M., Kim, N., Kim, S., Islam, N., et al. (2019). Noncoding dsRNA induces retinoic acid synthesis to stimulate hair follicle regeneration via TLR3. *Nat. Commun.* 10:2811. doi: 10.1038/s41467-019-10811-y

Komi-Kuramochi, A., Kawano, M., Oda, Y., Asada, M., Suzuki, M., Oki, J., et al. (2005). Expression of fibroblast growth factors and their receptors during full-thickness skin wound healing in young and aged mice. *J. Endocrinol.* 186, 273–289. doi: 10.1677/joe.1.06055

Lacassagne, A., and Latarjet, R. (1946). Action of methylcholanthrene on certain scars of the skin in mice. *Cancer Res.* 6, 183–188.

Lateef, H., Stevens, M. J., and Varani, J. (2004). All- trans-retinoic acid suppresses matrix metalloproteinase activity and increases collagen synthesis in diabetic human skin in organ culture. *Am. J. Pathol.* 165, 167–174. doi: 10.1016/S0002-9440(10)63285-3

Lee, M., Byun, M. R., Furutani-Seiki, M., Hong, J., and Jung, H. (2014). YAP and TAZ regulate skin wound healing. *J. Investig. Dermatol.* 134, 518–525. doi: 10.1038/jid.2013.339

Lim, C. H., Sun, Q., Ratti, K., Lee, S., Zheng, Y., Takeo, M., et al. (2018). Hedgehog stimulates hair follicle neogenesis by creating inductive dermis during murine skin wound healing. *Nat. Commun.* 9:4903. doi: 10.1038/s41467-018-07142-9

Ma, X., Tian, Y., Song, Y., Shi, J., Xu, J., Xiong, K., et al. (2017). Msi2 maintains quiescent state of hair follicle stem cells by directly repressing the hh signaling pathway. *J. Investig. Dermatol.* 137, 1015–1024. doi: 10.1016/j.jid.2017.01.012

Marsh, E., Gonzalez, D. G., Lathrop, E. A., Boucher, J., and Greco, V. (2018). Positional stability and membrane occupancy define skin fibroblast homeostasis in vivo. *Cell* 175, 1620.e13–1633.e13. doi: 10.1016/j.cell.2018.10.013

Mukherjee, S., Date, A., Patravale, V., Korting, H. C., Roeder, A., and Weindl, G. (2006). Retinoids in the treatment of skin aging: an overview of clinical efficacy and safety. *Clin. Intervent. Aging* 1, 327–348. doi: 10.2147/ciia.2006.1.4.327

Nalapareddy, K., Nattamai, K. J., Kumar, R. S., Karns, R., Wikenheiser-Brokamp, K. A., Sampson, L. L., et al. (2017). Canonical Wnt signaling ameliorates aging of intestinal stem cells. *Cell Rep.* 18, 2608–2621. doi: 10.1016/j.celrep.2017.02.056

Nelson, A., Reddy, S., Ratliff, T., Hossain, M., Katseff, A., Zhu, A., et al. (2015). dsRNA released by tissue damage activates TLR3 to drive skin regeneration. *Cell Stem Cell* 17, 139–151. doi: 10.1016/j.stem.2015.07.008

Ouspenskaia, T., Matos, I., Mertz, A., Fiore, V., and Fuchs, E. (2016). WNT-SHH antagonism specifies and expands stem cells prior to niche formation. *Cell* 164, 156–169. doi: 10.1016/j.cell.2015.11.058

Pan, D. (2010). The hippo signaling pathway in development and cancer. *Dev. Cell* 19, 491–505. doi: 10.1016/j.devcel.2010.09.011

Pentinmikko, N., Iqbal, S., Mana, M., Andersson, S., Cognetta, A. B., Suciu, R. M., et al. (2019). Notum produced by Paneth cells attenuates regeneration of aged intestinal epithelium. *Nature* 571, 398–402. doi: 10.1038/s41586-019-1383-0

Plikus, M. V., Guerrero-Juarez, C. F., Ito, M., Li, Y. R., Dedhia, P. H., Zheng, Y., et al. (2017). Regeneration of fat cells from myofibroblasts during wound healing. *Science* 355, 748–752. doi: 10.1126/science.aai8792

Rittie, L., Stoll, S. W., Kang, S., Voorhees, J. J., and Fisher, G. J. (2009). Hedgehog signaling maintains hair follicle stem cell phenotype in young and aged human skin. *Aging Cell* 8, 738–751. doi: 10.1111/j.1474-9726.2009.00526.x

Rognoni, E., Gomez, C., Pisco, A. O., Rawlins, E. L., Simons, B. D., Watt, F. M., et al. (2016). Inhibition of β-catenin signalling in dermal fibroblasts enhances hair follicle regeneration during wound healing. *Development* 143, 2522–2535. doi: 10.1242/dev.131797

Rompolas, P., Mesa, K. R., and Greco, V. (2013). Spatial organization within a niche as a determinant of stem-cell fate. *Nature* 502, 513–518. doi: 10.1038/nature12602

Salzer, M. C., Lafzi, A., Berenguer-Llergo, A., Youssif, C., Castellanos, A., Solanas, G., et al. (2018). Identity noise and adipogenic traits characterize dermal fibroblast aging. *Cell* 175, 1575.e22–1590.e22. doi: 10.1016/j.cell.2018.10.012

Seifert, A. W., Kiama, S. G., Seifert, M. G., Goheen, J. R., Palmer, T. M., and Maden, M. (2012). Skin shedding and tissue regeneration in African spiny mice (Acomys). *Nature* 489, 561–565. doi: 10.1038/nature11499

Shi, J., Lv, Z., Nie, M., Lu, W., Liu, C., Tian, Y., et al. (2018). Human nail stem cells are retained but hypofunctional during aging. *J. Mol. Hist.* 49, 303–316. doi: 10.1007/s10735-018-9769-0

Snippert, H. J., Haegebarth, A., Kasper, M., Jaks, V., van Es, J. H., Barker, N., et al. (2010). Lgr6 marks stem cells in the hair follicle that generate all cell lineages of the skin. *Science* 327, 1385–1389. doi: 10.1126/science.1184733

Sugiyama-Nakagiri, Y., Akiyama, M., Shibata, S., Okano, H., and Shimizu, H. (2006). Expression of RNA-binding protein musashi in hair follicle development and hair cycle progression. *Am. J. Pathol.* 168, 80–92. doi: 10.2353/ajpath.2006.050469

Sun, X., Are, A., Annusver, K., Sivan, U., Jacob, T., Dalessandri, T., et al. (2020). Coordinated hedgehog signaling induces new hair follicles in adult skin. *eLife* 9:e46756. doi: 10.7554/eLife.46756

Varani, J., Dame, M. K., Rittie, L., Fligiel, S. E. G., Kang, S., Fisher, G. J., et al. (2006). Decreased collagen production in chronologically aged skin: roles of age-dependent alteration in fibroblast function and defective mechanical stimulation. *Am. J. Pathol.* 168, 1861–1868. doi: 10.2353/ajpath.2006.051302

Wang, X., Chen, H., Tian, R., Zhang, Y., Drutskaya, M. S., Wang, C., et al. (2017). Macrophages induce AKT/β-catenin-dependent Lgr5+ stem cell activation and hair follicle regeneration through TNF. *Nat. Commun.* 8:14091. doi: 10.1038/ncomms14091

Wier, E. M., and Garza, L. A. (2020). Through the lens of hair follicle neogenesis, a new focus on mechanisms of skin regeneration after wounding. *Semin. Cell Dev. Biol.* 100, 122–129. doi: 10.1016/j.semcdb.2019.10.002

Zhang, H., Pasolli, H. A., and Fuchs, E. (2011). Yes-associated protein (YAP) transcriptional coactivator functions in balancing growth and differentiation in skin. *Proc. Natl. Acad. Sci. U.S.A.* 1086, 2270–2275. doi: 10.1073/pnas.1019603108

Conflict of Interest: The authors declare that the research was conducted in the absence of any commercial or financial relationships that could be construed as a potential conflict of interest.

Copyright © 2020 Bhoopalam, Garza and Reddy. This is an open-access article distributed under the terms of the Creative Commons Attribution License (CC BY). The use, distribution or reproduction in other forums is permitted, provided the original author(s) and the copyright owner(s) are credited and that the original publication in this journal is cited, in accordance with accepted academic practice. No use, distribution or reproduction is permitted which does not comply with these terms.

frontiers in Cell and Developmental Biology

REVIEW
published: 09 November 2020
doi: 10.3389/fcell.2020.581697

Epidermal Stem Cells in Hair Follicle Cycling and Skin Regeneration: A View From the Perspective of Inflammation

Elena I. Morgun and Ekaterina A. Vorotelyak*

Laboratory of Cell Biology, Koltzov Institute of Developmental Biology of Russian Academy of Sciences, Moscow, Russia

There are many studies devoted to the role of hair follicle stem cells in wound healing as well as in follicle self-restoration. At the same time, the influence of the inflammatory cells on the hair follicle cycling in both injured and intact skin is well established. Immune cells of all wound healing stages, including macrophages, γδT cells, and T_{regs}, may activate epidermal stem cells to provide re-epithelization and wound-induced hair follicle neogenesis. In addition to the ability of epidermal cells to maintain epidermal morphogenesis through differentiation program, they can undergo de-differentiation and acquire stem features under the influence of inflammatory milieu. Simultaneously, a stem cell compartment may undergo re-programming to adopt another fate. The proportion of skin resident immune cells and wound-attracted inflammatory cells (e.g., neutrophils and macrophages) in wound-induced hair follicle anagen and plucking-induced anagen is still under discussion to date. Experimental data suggesting the role of reactive oxygen species and prostaglandins, which are uncharacteristic of the intact skin, in the hair follicle cycling indicates the role of neutrophils in injury-induced conditions. In this review, we discuss some of the hair follicles stem cell activities, such as wound-induced hair follicle neogenesis, hair follicle cycling, and re-epithelization, through the prism of inflammation. The plasticity of epidermal stem cells under the influence of inflammatory microenvironment is considered. The relationship between inflammation, scarring, and follicle neogenesis as an indicator of complete wound healing is also highlighted. Taking into consideration the available data, we also conclude that there may exist a presumptive interlink between the stem cell activation, inflammation and the components of programmed cell death pathways.

Keywords: hair follicle, stem cells, regeneration, wound, skin, inflammation

OPEN ACCESS

Edited by:
Mingxing Lei,
Chongqing University, China

Reviewed by:
Zhili Deng,
Central South University, China
Stéphanie Claudinot,
Centre Hospitalier Universitaire Vaudois (CHUV), Switzerland

****Correspondence:***
Elena I. Morgun
lady.morgun2016@yandex.ru

Specialty section:
This article was submitted to Stem Cell Research, a section of the journal Frontiers in Cell and Developmental Biology

Received: *09 July 2020*
Accepted: *20 October 2020*
Published: *09 November 2020*

Citation:
Morgun EI and Vorotelyak EA (2020) Epidermal Stem Cells in Hair Follicle Cycling and Skin Regeneration: A View From the Perspective of Inflammation. Front. Cell Dev. Biol. 8:581697. doi: 10.3389/fcell.2020.581697

INTRODUCTION

As an outmost barrier of the organism, the skin has multiple functions, including a vitally important protective mission. Being exposed to an aggressive environment, it has developed a complex system of mutually dependent stem cell populations as well as immune response. Stem cells replenish regular tissue losses and are ready to upregulate their activity in case of injury. Immune system supports regenerative processes via direct interactions with invaders and clearance of wound debris.

Also, it has the ability to intensify stem cell activity for production of differentiated progeny and restoration of lesions (Rahmani et al., 2020).

Epidermal homeostasis is maintained by stem cells that either self-renew or undergo differentiation forming the spinous, granular and cornified layers of the interfollicular epidermis (IFE) or multiple types of keratinocytes in the hair follicle (HF) generating the hair shaft (Gonzales and Fuchs, 2017).

The concept of epidermal stem cells (EpiSC) evolved from the assumption of equipotent basal cells of IFE toward the scheme of complicated hierarchy, kinetics, and behavior. Several approaches were proposed to determine stem cells in IFE and epithelial part of appendages. Among the most prominent characteristics is their ability to retain DNA label (for review see: Terskikh et al., 2012). Another widely accepted property of EpiSC is to form large clones (holoclones) *in vitro* in contrast to small abortive clones produced by their progeny as it was shown by pioneering experiments performed by Barrandon and Green (Barrandon and Green, 1987). Potten proposed the concept of proliferating epidermal unit containing slow-cycling stem cell in the center (Potten, 1974) for murine IFE where columnar structures could be observed at certain sites (Mackenzie, 1970). Labeling of EpiSC progeny in mouse epidermis confirmed the clonal organization of IFE (Ghazizadeh and Taichman, 2001). At the same time, the hypothesis of a single population of progenitor cells in homeostatic IFE of mouse tail with no role for stem cells was proposed (Clayton et al., 2007). The authors pointed out that the stem cell population undetectable in steady-state conditions might be recruited in wound healing. To identify interfollicular EpiSC, β1- and α6-integrins as well as keratin 15 (Krt15), LRIG1, and MCSP were utilized as markers (Solanas and Benitah, 2013).

The most potent EpiSC reside in a specialized niche of HF named the bulge, where label-retaining cells were found by landmark paper of Cotsarelis with colleagues (Cotsarelis et al., 1990). They provide continuous cycling of HF and its regeneration (Jahoda et al., 1996) as well as the source of epithelial cells in the course of skin regeneration. The bulge zone of HF contains several subsets of EpiSC with diverse functions and regenerative potential. Pioneering experiments by Cotsarelis and his group revealed Krt15 as a putative marker of bulge cells (Lyle et al., 1998; Liu et al., 2003). *In vitro* lineage tracing showed that the progeny of Krt15 + cells contribute to all HF epithelial cell lines (Morris et al., 2004). Later on, the list of bulge markers was supplemented with CD34, Keratin 19, Lgr5, Gli1, Hopx, Lhx2, Nfatc1, Sox9, Tcf3/4, integrin α6, and Lhx2 (Rompolas and Greco, 2014; Gonzales and Fuchs, 2017). Another region of HF, the isthmus, contains cells with stem-like properties. They are expressing Lrig1, Gli1, MTS24, and Lgr6. Lrig1 + cells of the isthmus are involved in the infundibulum regeneration, at the top of which there is a population of cells expressing Sca-1 (Rompolas and Greco, 2014). The secondary germ is believed to be another source of HF renewal (Panteleyev et al., 2001).

Healthy human and mouse skin is populated by several types of immune cells such as dendritic cells, innate lymphoid cells (ILCs), T lymphocytes and macrophages (Mansfield and Naik, 2020), as well as mast cells and neutrophils (Nakamizo et al., 2020). Immune cells that are located above the basement membrane include CD8 + resident memory T cells (T_{RM}), Langerhans cells, ILCs, and dendritic epidermal DT cells (DETCs). The dermal immune cells are represented by macrophages located near blood vessels, and T cells, which include near-follicular effector and regulatory CD4 + T cells (T_{regs}), and γδT cells. Thus, each type of immune cell is situated in a specific compartment of the skin, and this is achieved by the homing to the corresponding microenvironment – different fractions of the HF and IFE keratinocytes have diverse chemokine signatures (Mansfield and Naik, 2020). It was shown *in vivo* and *in vitro* experiments that T_{regs}, which express CCR6 on their surface, migrate to CCL20 ligand, derived from infundibulum cells (Scharschmidt et al., 2017). A similar mechanism of homing is implemented in the case of ILCs migration toward the upper part of HF. However, in addition to the CCR6-CCL20 interaction, ILCs are attracted to the epidermis by cytokines IL-7 and TSLP (Kobayashi et al., 2019). CD10-expressing DETCs, as well as T_{RM} are recruited to IFE cells due to the expression of CCL27 (Morales et al., 1999; Jin et al., 2010). Thus, the steady skin state is immunologically active, and there is an interplay between keratinocytes and inflammatory cells. Subsequently, EpiSC is in close interaction with cells of the immune system and are able to recruit them when the tissue is damaged (Naik et al., 2018).

Wound healing begins with an inflammatory phase involving cells of the immune system. Macrophages and neutrophils are the first and foremost, which secrete inflammatory mediators and phagocytize debris disinfecting the wound bed and enabling its further successful closure (Eming et al., 2007). Wound regeneration is incomplete without wound resurfacing, i.e., re-epithelization (Santoro and Gaudino, 2005). Dermal part of the skin is subjected to active regeneration and reorganization during wound healing and affects its outcome (Rippa et al., 2019). Blood and lymphatic vessels which supply the skin with nutrients and replenish immune cell pool in steady-state are extensively reorganized during wound healing providing proper regulation and structural reconstruction of damaged tissue. The effectiveness of wound healing correlates with the phase of HF cycle. It was found that skin containing anagen HF regenerates more effectively than that with HF in telogen. Wounds of mice anagen skin showed improved angiogenesis, increased proliferation of keratinocytes, accelerated transition to terminal differentiation, and ameliorated matrix synthesis, while telogen skin demonstrated an increase in the number of neutrophils and macrophages in the granulation tissue, as well as a high expression of macrophage migration inhibitory factor (Ansell et al., 2011).

During wound healing, epithelial HF stem cells (HFSCs) provide both HF neogenesis and wound re-epithelialization (Rompolas and Greco, 2014). HF regeneration in the middle of a full-thickness wound in mice is similar to embryonic hair morphogenesis. It is called wound-induced hair neogenesis (WIHN) (Wang et al., 2017; Gong et al., 2018). Formation of new HFs in adult skin may also be induced in experimental conditions by ectopic activation of specific signaling pathways (Sun et al., 2020). However, WIHN is appropriate only for mouse wound healing, while most mammals, including humans, do not regenerate skin appendages (Lim et al., 2018).

Activation of EpiSC is important condition for restoration of the structure and functions of the skin after injury. We will overview the characteristics of EpiSC, immune cells and inflammatory-related agents in the context of their interactions and functioning during wound healing and HF morphogenesis. As wound healing and inflammation are tightly connected with cell death, we tried to make brief references to possible interlinks with stem cell activation, where data are available.

EPISC PLASTICITY DURING WOUND HEALING UNDER THE INFLUENCE OF IMMUNE REACTION

Since the skin delimits the body with the environment, it often undergoes damage and healing, and keratinocytes meet a first thrust (Proksch et al., 2008). The inflammatory milieu in the wound gets cells ready for re-epithelialization affecting their migratory and proliferation activities. Inflammation-induced cell dedifferentiation and can modulate cell stemness. However, the details of cellular behavior in the course of re-epithelization are not known at the moment. There is experimental evidence in favor of at least two models. According to the first, the cells of the basal layer migrate to the wound bed and then differentiate into suprabasal, and according to the second, suprabasal cells move from wound edges to the wound bed due to "leapfrog" mechanism and become basal (Rognoni and Watt, 2018). Thereby, epidermal cells possess certain plasticity: they can undergo de-differentiation as well as differentiation under the influence of accompanying wound healing inflammatory agents (Haensel et al., 2020). Noteworthy, similar transitions are known in inflammatory diseases. For example, exposure to IL-17 and IL-22, interleukins, which are elevated in psoriasis (Kim and Krueger, 2015), caused the expression of stem markers p63, CD44, CD29, and CD49f in keratinocytes *in vitro* due to activation of the RAC1/MEC/ERK/NF-κB pathway (Ekman et al., 2019). Nelson and colleagues found that activation of TLR3 by polyriboinosinic-polyribocytidylic acid (polyI: C), simulating the viral dsRNA in keratinocyte cell culture (Takada et al., 2017), causes a loss of Keratin1 and filaggrin (markers of differentiated keratinocytes) and an increase in the expression of Lgr5 and Lgr6 HF progenitor markers as well as Krt15 (Nelson et al., 2015). Besides, the participation of IL-6/STAT3 pathway in the acquisition of stem status is indirectly confirmed by the fact that STAT3 phosphorylation under the influence of IL-6 family members IL-11 and Oncostatin M (OSM) contributes to WIHN (Nelson et al., 2016b_B). There is experimental evidence that TA isoforms of stem/progenitor marker p63, which expression is affected by IL-6/STAT3, are involved both in the inhibition of keratinocytes ability to differentiate and in the stimulation of WIHN (Nelson et al., 2016a_A).

In addition to the acquisition of a stem marker profile by mature keratinocytes, other data are confirming the ability of epidermal cells to de-differentiate under the influence of the wound environment. Haensel and colleagues using RNA velocity analysis showed a significant proportion of *col17a1*^{Hi} basal cells and spinous cells of the SP1 population of wounded mice to demonstrate faster RNA dynamics than those from non-wounded skin. This indicated increased plasticity of cell fate in the skin sample of wounded mice with bidirectional transitions in several cell states between basal and spinous cells, which was not observed in the non-wounded animals. Thus, the wound inflammatory milieu stimulates epidermal cell plasticity and enfeebles restrictions on cell differentiation compared to their non-wounded counterparts (Haensel et al., 2020).

The implication of bulge HFSCs in re-epithelization has been established for a long time. However, different strategies for HFSCs labeling and a variety of markers employed led to a conclusion about different inputs of HFSCs subpopulations into the process (Garcin and Ansell, 2017). Some HF cells have been shown to play a dual role. In mice, Lgr6 + cells of the isthmus area provide ongoing skin restoration, including WIHN (Snippert et al., 2010). However, it seems now that both Lgr6 + and Lgr5 + stem cells are involved in IFE regeneration. Infundibulum Sca-1 + cells and Gli + stem cells are also involved (Brownell et al., 2011; Rompolas and Greco, 2014). HFSCs move downward for the regeneration and neogenesis of HF, while their upward migration contributes to re-epithelization. In spite of intuitive imagination of EpiSC as attached tightly to the niche, they probably may be highly motile making input into morphogenesis far from their original location. Nanba and co-authors showed *in vitro* that human EpiSC could be identified by their motility: the faster the cells move, the higher "stemness" they possess (Nanba et al., 2015). Another activity of HFSCs is linked to the barrier maintenance directly in the bulge niche where they are interacting with recruited immune cells to overcome telogen cell cycle inhibitory signals (Lay et al., 2018).

To accomplish regeneration, EpiSC can undergo reprogramming. Experimental data of Joost et al. suggest that inflammatory environment affects the expression of "follicular" (*Lgr5, Cd34, Cxcl14, and Sparc*) and "interfollicular" (*Krt14, Ifitm3, Eef1b2, Ly6e*) markers. Wound healing experiment with subsequent single-cell analysis showed that after wounding, the Lgr5 + progeny, while still in the bulge, begin to express both interfollicular and HF markers. However, interfollicular markers are upregulated; meanwhile, bulge markers are downregulated. Besides, Lgr6 + progeny in the intact skin expresses numerous receptors for interaction with wound ligands, and when the skin is damaged, their number slightly changes. Lgr5 + progeny expresses a few such receptors; however, when wounded, their number increases. This suggests that Lgr5 + progeny may become competent to interact with the wound environment at the level of Lgr6 + descendants. Moreover, this early upregulation of genes makes Lgr5 + progeny motile, as the number of genes (*Cd44, Cd9, Itgb1, Itga3,* and *Itga6*) that begin to be expressed are associated with cell migration (Joost et al., 2018), which indicates acquisition of the ability to re-epithelization. Thus, epidermal cells, beyond classical differentiation of basal cells to suprabasal ones, may change their status by loss of their maturity or reprogramming. from follicular to interfollicular state. Whether interfollicular cells can be reprogrammed into follicular cells under the influence of inflammation and what conditions determine the direction of differentiation/dedifferentiation/reprogramming, remains unknown and requires further research. Intriguingly,

cells stemness was induced by inflammatory pathways, which intersected with programmed cell death pathways to some extent. It was mentioned above that de-differentiation of mature keratinocytes, and their acquisition of stem features may be associated with the influence of such an inflammatory agent as dsRNA, as well as upregulation of cytokines IL-17 and IL-22, which occurs during wound healing (Sasaki et al., 2011; Zhu et al., 2017). At the same time, the effect of dsRNA on TLR3 is a proven trigger of apoptosis and necroptosis (Seya et al., 2012) and upregulation of IL-17 and IL-22 in the psoriasis model is associated with a decrease in the expression of a RIPK-1, traditionally considered as a necroptosis component (Saito et al., 2018). Therefore, the stem status of epidermal cells may be affected not only by inflammation but also by the components of programmed cell death occurring during wound healing.

However, the relationship of epidermal cells with the immune system is two-component. On the one hand, inflammatory agents can affect epidermal cell activity; on the other hand, keratinocytes possess their own intrinsic immune activity. The basis of this phenomenon is the necessity to respond adequately to the inflammatory milieu that occurs as a result of injury or infection and to transmit a signal to surrounding cells. Epidermal cells are able to release IL-1, IL-6, IL -7, IL -8, IL -10, IL -12, IL -15, IL -18, IL -20, and tumor necrosis factor-alpha (TNF-α), which causes proliferation and differentiation of keratinocytes, production of cytokines by them, and migration of immune cells into the wound (Gröne, 2002). Innate immunity is a well-known characteristic of epidermal keratinocytes, presumably including those located in the basal layer. It was shown that interfolicular EpiSC could "remember" episodes of acute inflammation. Wound healing in mice previously exposed to imiquimod, which induced skin inflammation via TLR7-NALP3 axis, was more effective than in the control group. Moreover, this process was experimentally proven not to depend on macrophages or T cells. "Inflammatory memory" was based both on a transcription of the inflammasome pathway component *Aim2* in interfollicular EpiSC and the expression of its downstream effector *caspase-1* in post-inflamed skin. Caspase-1, in turn, is involved in the maturation and secretion of IL-18 and IL-1β, which were also increased in skin of the experimental animals (Naik et al., 2017). Therefore, previous "inflammation experience" could augment cutaneous wound healing due to EpiSC activity. Interestingly, all of the above agents are participants of the pyroptosis, the type of programmed cell death with morphological signs of necrosis (Vande Walle and Lamkanfi, 2016). However, Naik with colleagues did not show cell death in the experiment (Naik et al., 2017).

To summarize, immunocompetence of stem cells and changes in their stem status under the influence of inflammation are the two facets of the interaction of immunity and stem cells providing re-epithelialization after skin damage. As we can see, these processes involve various members of the TLR family. Activation of TLR7 is responsible for the "inflammatory memory" of interfollicular EpiSC, the influence of dsRNA on TLR3 causes the loss of differentiation markers by mature keratinocytes and the expression of stem cell markers Lgr5 and Lgr6 and Krt15. Therefore, immunoreactivity and the mechanism of dedifferentiation can also be interlinked. Furthermore, activation of pyroptosis and necroptosis also occurs through the TLR receptors. Consequently, various members of TLR family may be the "hubs" through which the pathways of immunity activation, stemness, and cell death can intersect.

Facets of EpiSC plastsicity under the influence of inflammatory agents is summarized in **Figure 1**.

THE HF CYCLE AND IMMUNITY IN PHYSIOLOGICAL AND INJURY-INDUCED CONDITIONS

Cyclic changes in HF, namely, a continuity of successive phases of telogen, anagen, and catagen, partly occur owing to HFSC activity. Immune cell dynamics is associated with the transition of HF through the cycle and, in some degree, provides regulatory keys for it. We will discuss some striking features of this interconnection (for review see: Wang and Higgins, 2020) along with specific stage characteristics.

After the regression, HF passes into telogen, the phase of relative rest in terms of proliferation and biochemical activity (Paus and Cotsarelis, 1999; Krause and Foitzik, 2006). HF stays dormant until it is reactivated by intrafollicular and extrafollicular signals (Paus and Cotsarelis, 1999). Inactivity of HFSCs at this stage is provided mainly by bulge expression of BMP6 and FGF18 (Hsu et al., 2014). At the same time, telogen is supposed to be a stage of "progressive molecular activity". In late telogen, the activity aimed at inhibiting quiescence predominates, whereas, in early and middle telogen, inhibition of cellular activity prevails. Also, there is a proliferative activity of several cell types: while bulge and secondary hair germ HFSCs are quiescent, keratinocytes from upper HF proliferate (Geyfman et al., 2015).

Anagen begins with the proliferation of Lgr5 + HFSCs, which are activated in late telogen. Hair germ HFSCs give rise to transit-amplifying cells that populate the germinative layer of the matrix. Outer root sheath (ORS) is formed by cells of the lower bulge (Welle and Wiener, 2016). It is well known that the key factors that induce anagen are the Wnt proteins, while the level of BMP signaling is downregulated by expression of its antagonist noggin (Botchkarev and Sharov, 2004). Sonic hedgehog, HGF, and FGF7, among others, support this process and stimulate the subsequent HF entry into anagen (Krause and Foitzik, 2006). In mice, anagen induction in response to exogenous stimuli and entry into the second anagen differ by underlying mechanisms, at least in terms of STAT3 signaling (Sano et al., 2000).

Upon completion of anagen, a controlled involution of HF occurs denoting onset of catagen, when most follicular keratinocytes undergo apoptosis (Paus and Cotsarelis, 1999; Krause and Foitzik, 2006; Welle and Wiener, 2016). At this stage, poorly dividing ORS cells create a new bulge, while slightly faster dividing cells form the secondary hair germ (Welle and Wiener, 2016). Unlike ORS and the hair matrix, the cells of DP do not die, though they express the suppressor of apoptosis bcl-2 (Krause and Foitzik, 2006). Toward the end of catagen, DP condenses and moves upward transiting into a resting stage to reside under the bulge (Paus and Cotsarelis, 1999).

Spontaneous HF cycle is mediated by different types of skin resident immune cells, which were listed above. Among multiple signals and niche components, stay of HF in telogen is regulated by FoxP3-expressing CD4 + T cells (also known as regulatory T cells, T_{regs}) (Ali et al., 2017) and macrophages (Castellana et al., 2014). T_{regs} are associated with telogen. The abundance of these cells in telogen is threefold higher as compared to anagen. Moreover, their proliferative index correlates with the phase of the HF cycle: they are more active in telogen. Ali and colleagues found the bulge-associated subpopulation of T_{regs} (Ali et al., 2017). Disruption of adherence of the cell-cell junctions in bulge HFSC niche by E-cadherin removal activated proliferation program in telogen bulge HFSC repurposing new daughters to restore the breached integrity of the niche. In addition to cell cycle genes activation necessary during normal anagen, this proliferation activity needed elevation of the immune-signaling transcriptome. Notably, no transition to anagen was observed. Thus, proliferating stem cells were activated to restore the niche rather than to launch a new hair cycle. Proliferating HFSCs attracted immune cells, including

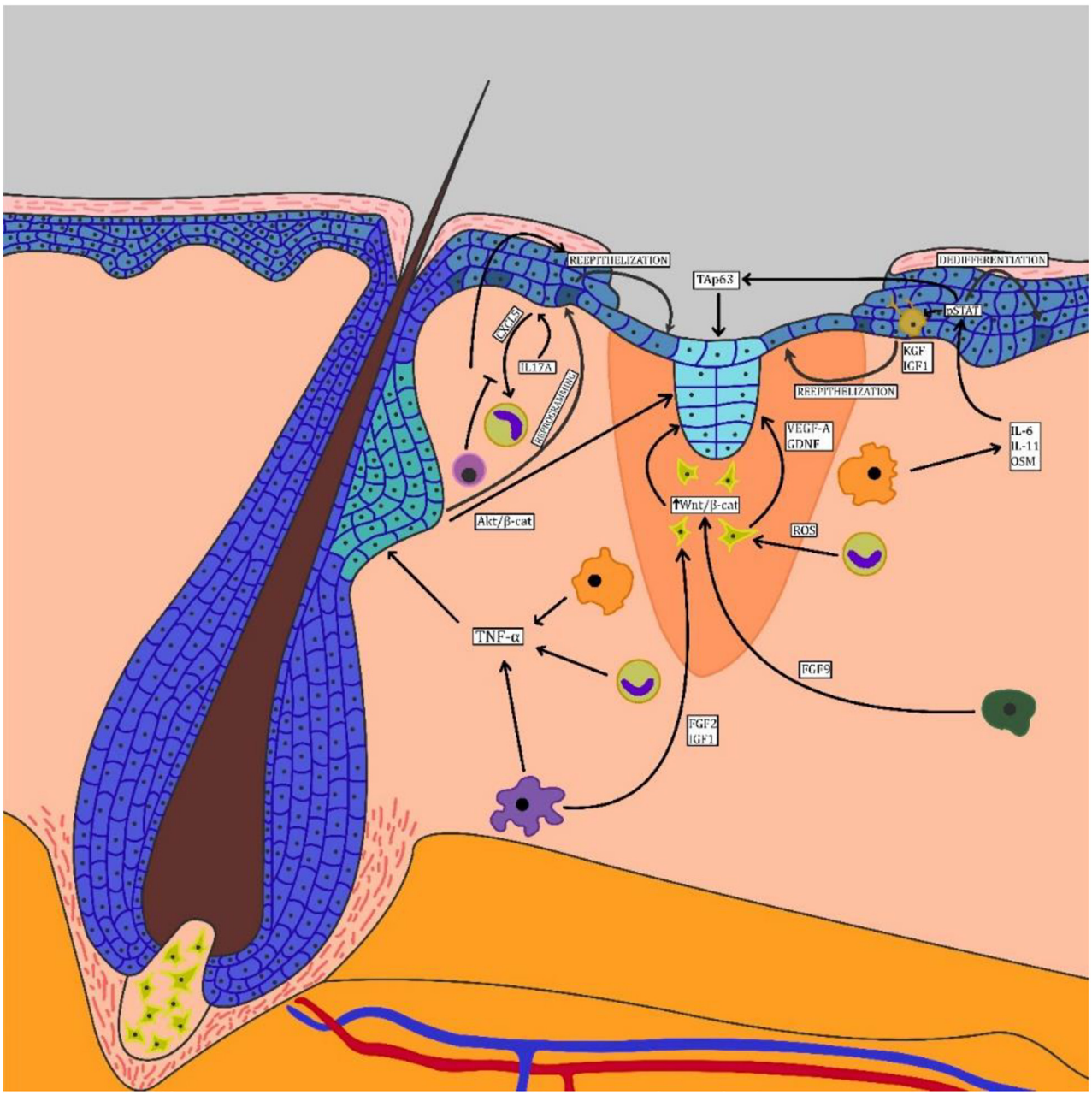

FIGURE 1 | Continued

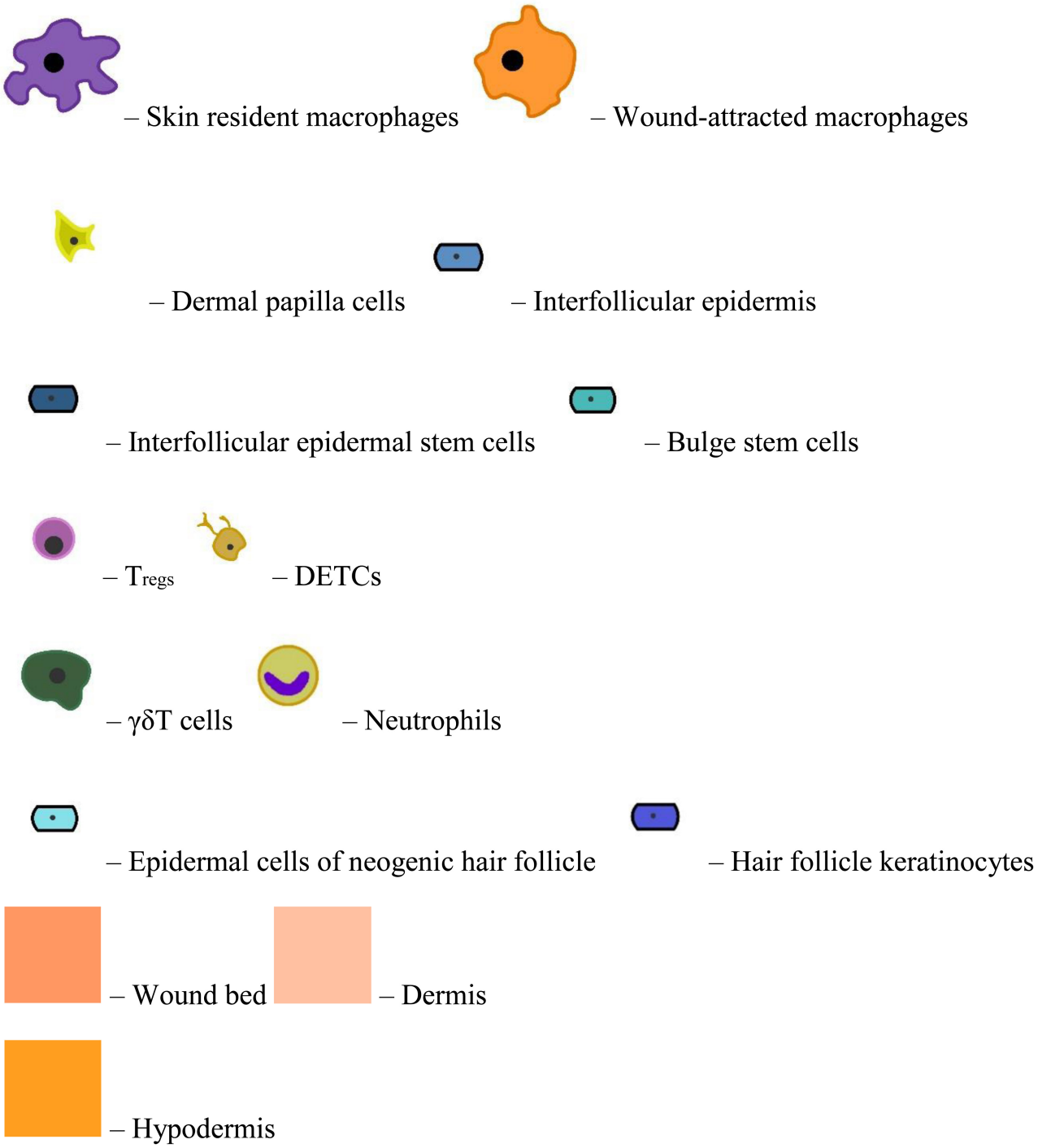

FIGURE 1 | Facets of EpiSC plasticity under the influence of inflammatory agents.

T_{regs}, increasing their numbers as compared to the resident skin population in a steady state.

Interestingly, this effect was independent of microbial presence. Moreover, immune cells, in turn, were necessary for activation of HFSC proliferation as the regular telogen proliferation-inhibitory cues were still active in the disrupted niche (Lay et al., 2018). Thus, telogen bulge cells are capable of proliferation independent of HF activation, and immune cells regulate this activity. The role of macrophages in telogen regulation is controversial. Not only they activate anagen but also prolong telogen: TREM2 + macrophages maintain the dormancy of HFSCs through OSM (Wang et al., 2019). Castellana and

the colleagues showed that macrophage apoptosis promoted the entry of HFSCs into the anagen phase. As soon as the number of macrophages decreased due to liposome-induced apoptosis, HF of the experimental mice entered anagen, while the control group remained in telogen (Castellana et al., 2014).

As mentioned above, the telogen-to-anagen transition (TAT) is associated with macrophage apoptosis. Expression of *Wnt7b* and *Wnt10a* responsible for HFSC activation was elevated in skin resident macrophages during TAT. Moreover, experiments in the culture of mouse macrophages showed that their apoptosis occurs in parallel with the release of Wnts and that apoptotic macrophages stimulate the expression of Wnts by neighboring macrophages (Castellana et al., 2014). Interestingly, macrophages seem to produce extracellular vesicles containing Wnt3a and Wnt7b (Rajendran et al., 2020). Thus, the apoptotic reduction of macrophages during TAT is associated with the activation of the Wnt/β-catenin cascade (Castellana et al., 2014). Therefore, TAT and the Wnt/β-catenin cascade are related both to the activity of inflammatory cells and their apoptosis. Consequently, the activation mechanisms of HFSCs can be coupled with the pathways of programmed cell death.

Tissue-resident T_{regs} localized in close contact with HF sustain the bulge stem cells functions. Ali and colleagues demonstrated the role of T_{regs} in the activation of bulge HFSCs (Ali et al., 2017). In mice with T_{regs} depletion, a proliferative defect of the HFSC bulge zone during depilation-induced TAT was observed. In addition, lineage tracing showed a decrease in genes associated with the proliferation and differentiation of HFSCs (e.g., *Bgn, Bnc1, Cks2, Hmgn3, Gdf10,* and *Sox4*) in CD34 + integrin α6 $(ITGA6)^{high}$ basal bulge HFSCs from depilated mice lacking T_{regs}. When comparing the transcriptome of skin T_{regs} with those of skin draining lymph nodes (SDLN), it was shown that skin T_{regs} express Notch signaling ligand Jagged 1 (Jag1) 150 times higher than SDLN T_{regs} do (Ali et al., 2017). During anagen, the switching on Notch cascade activates Kit signaling and suppresses TGF-β establishing an optimal environment for the proliferation of matrix cells (Rishikaysh et al., 2014). Exogenous administration of Jag1 restores the proliferative function of stem cells in mice lacking T_{regs}. Deletion of *Jag1* in T_{regs} reduces the expression of epidermal differentiation genes *Bgn*, *Ccnd1*, *Gdf10*, *Sox4*, *Sox7*, and *Timp3* as well as provokes anagen deterioration (Ali et al., 2017).

At the end of anagen, some significant changes occur in HF, in particular, downregulation of IGF1 (Krause and Foitzik, 2006). This growth factor is well known for its anagen-stimulating effect, as it decreases the expression of the negative regulator of anagen TGF-β1 and also promotes the proliferation of HF keratinocytes (Li et al., 2014). One of the sources of IGF1 is DETCs, the subpopulation of γδT cells that prevented epidermal apoptosis in a model *in vitro* (Sharp et al., 2005). Presumably, DETCs support anagen through secretion of IGF1 in three ways: through inhibition of TGF-β1, stimulation of keratinocytes proliferation, and downregulation of apoptosis, which is a key catagen pathway. Anagen ends with downregulation not only of IGF1 but also of other factors (including HGF, and FGF5) supporting anagen phase and with upregulation of hair growth inhibitors, such as TGF-β1, TGF-β2, FGF5 (Krause and Foitzik, 2006).

Catagen is induced by growth factors and cytokines, including FGF5 secreted by perifollicular macrophages and IFN-γ (Wang and Higgins, 2020). *Fgf5* mutations cause catagen retention in humans (Higgins et al., 2014). In certain pathological conditions, for example, in case of stress, mast cells were also shown to stimulate the onset of catagen in mice. In this situation, mast cell-deficient mice demonstrated catagen delay, as did knockout mice, which were not able to respond to the substance P produced by nerve fibers in stress conditions (Arck et al., 2005). Mature mast cells release a lot of significant inflammatory mediators and are involved in wound healing (Komi et al., 2020).

Interestingly, mouse vibrissal HF contains precursors capable of differentiation into competent mast cells *in vitro* and probably provide a niche for their differentiation *in vivo* (Kumamoto et al., 2003). Inflammation and HF cells in catagen are interconnected through cell death processes: apoptotic keratinocytes are cleared by macrophages in the mouse, whereas in humans, the macrophages themselves undergo apoptosis. In the experiment by Hardman with colleagues, a cyclic change in the number of perifollicular macrophages in a freshly isolated HF was shown with a minimal rate in late catagen (Hardman et al., 2019). The close interdependence between inflammatory cytokine TNF-α, Keratin 17 and apoptosis in keratinocytes was shown in the next study (Tong and Coulombe, 2006). In *Krt17* $^{-/-}$ mice, alopecia developed in the first week after birth due to increased apoptosis. *Tnf* ablation led to catagen delay. It is thought that apoptosis in *Krt17* $^{-/-}$ keratinocytes occurs due to accelerated sensitivity to TNF-α. In turn, apoptosis in *Krt17*-null keratinocytes led to premature onset of catagen. Consequently, cytoskeletal protein Keratin 17 is responsible for HF detention in anagen, meanwhile TNF-α leads to anagen-catagen transition. Tong and Coulombe suggest that Keratin 17 interacts with the TRADD adapter necessary to transmit a signal from TNFR1 (Tong and Coulombe, 2006).

Thus, HF stays in a specific phase is regulated by various types of skin resident inflammatory cells. Macrophages and T_{regs} play a significant role in telogen and anagen and by mast cells and macrophages in catagen. It is believed that during TAT, the induction of Wnt/β-catenin is associated with the apoptosis of macrophages, and activation of bulge HFSCs is associated with their induction by the T_{reg} cluster. However, it is possible that in certain conditions, inflammatory cells that are absent in normal skin contribute to the HF cycling.

In addition to the physiological conditions, TAT may be induced by injury. In the case of hair plucking, CCL2 is released, which leads to the recruitment of inflammatory macrophages and, as a result, the stimulation of anagen by TNF-α (Chen et al., 2015). Macrophages are also involved in another type of injury-induced TAT, which is called wound-induced hair anagen re-entry/growth (WIH-A), when, under the influence of a wound milieu, HF located at the edges of the wound switch to anagen (Abbasi and Biernaskie, 2019). It was shown that macrophage production of TNF-α invoked an activation of HF Lgr5 + stem cells being important for WIH-A. Suppression of these inflammatory cell infiltration resulted in the loss of WIH-A ability in HFs. To assess the role of macrophages in WIH-A, Wang, and co-authors eliminated these cells with

clodronate liposomes (Wang et al., 2017). It led to an inability of the HF to proceed to WIH-A. Furthermore, an *in vivo* experiment performed to assess the role of TNF-α in these processes showed that $Tnf^{-/-}$ mice did not develop HF anagen on post wound day (PWD) 15. In this study, $Lysm^{cre}/:Tnf^{flox/flox}$ mice with macrophages and neutrophils unable to express *Tnfa* were used. Skin regeneration in these mice occurred with a significantly reduced number of anagen HF, but an injection of lipopolysaccharide stimulated macrophages induced anagen. There is experimental evidence that activation of RAC-alpha serine/threonine-protein kinase (AKT) in Lgr5 + cells plays an essential role in the induction of TAT of HF. Knockdown of *Tnfr1* in Lgr5 + cells caused a decrease in TNF-induced p-AKT activity in cell culture. It is assumed that TNF-α activates β-catenin through the PI3K/AKT/mTOR cascade, and phosphorylation of β-catenin, in turn, is induced by AKT in Lgr5 + HFSC (Wang et al., 2017). There is also another way in which macrophages could cause anagen during skin damage. These cells secrete growth factors (Werner and Grose, 2003) that lead to activation of the PI3K-Akt-mTOR pathway involved in cell growth and survival (Fang et al., 2013) in epithelial cells during wound healing (Squarize et al., 2010). Activation of the mammalian target of rapamycin complex 1 (mTORC1) was observed in the bulge and hair germ cells in a growth phase-dependent manner suggesting its role in anagen activation (Kellenberger and Tauchi, 2013). Thus, macrophages are involved in both physiological TAT, plucking-induced anagen, and WIH-A in the described experiment; therefore, the contribution ratio of skin resident macrophages and those arrived at the wound bed is unknown (Rahmani et al., 2020).

However, there are indirect signs that, in addition to skin resident immune cells, wound cells that are completely unusual for intact skin can be involved in WIH-A. It can be supposed that the persistence of HFSC in anagen is regulated by polymorphonuclear leukocytes, as they can secrete reactive oxygen species (ROS) (Dunnill et al., 2017), and prostaglandins (PG) (Higgs et al., 1975), which are also involved in HF cycling (Valente Duarte de Sousa and Tosti, 2013; Zhao et al., 2015). PGE_2, acting synergistically with PGF_2, prolongs anagen and induces hair growth (Valente Duarte de Sousa and Tosti, 2013). PGE_2 does not induce TAT but has a stimulating effect on early anagen HF manifested by increased hair length. PGF_{2a} promotes protein kinase C (PKC) activation via phosphorylase C-associated receptors. Furthermore, PKC is upregulated in anagen, which indicates its significance for HF activity (Sasaki et al., 2005). ROS is an important mediator of inflammation being secreted during wound healing and contributing to wound disinfection (Dunnill et al., 2017). It was shown that adipose-derived stem cells are also able to secrete ROS this way promoting DP-induced hair growth and thus, may cause TAT (Choi et al., 2019). However, in an *in vivo* study during the transition from anagen to catagen, Zhao and colleagues showed elevation of ROS level by the Foxp1 protein via suppression of ROS scavenger Thioredoxin-1. This is also supported by the fact that administration of NAC antioxidant to *Foxp1* cKO mice led to the arrest of the HF cycle in anagen and increased HFSCs proliferation (Zhao et al., 2015). Thus, it is possible that in certain conditions, not only skin resident but wound-specific immune cells are also involved in the regulation of the HF cycle and morphogenesis. The relationship of the activation mechanisms of EpiSC with molecular cascades of wound healing will be considered in the next section.

HF NEOGENESIS AND RE-EPITHELIALIZATION IN THE COURSE OF WOUND HEALING

Widely recognized course of wound regeneration includes phases of inflammation, proliferation, and remodeling (Gurtner et al., 2008). Below we will consider these phases with critical elements of inflammatory reactions affecting epidermal cell activity, regeneration, and morphogenesis. Surprisingly, some of these elements demonstrate delayed effects in this respect. For example, macrophages acting in the inflammation phase (Eming et al., 2007) contribute to WIHN, which occurs during the time of the scar remodeling phase (Gay et al., 2020), and re-epithelialization begins in the proliferation phase under the influence of T_{regs}.

Inflammation Phase

TNF alpha. Platelets, leukocytes, macrophages, and mast cells are involved in the inflammation phase replacing each other. First of all, after a wound, platelets and polymorphonuclear leukocytes create a blood clot, and thus the tissue reaches hemostasis (Eming et al., 2007). Platelets form a clot interacting by GpIIb-IIIa receptors and adhering to the collagen of the disrupted subendothelium. Fibrin polymerization promotes the formation of a mature clot, which serves as a scaffold for infiltrating leukocytes and fibroblasts playing a sequential role in healing. Platelets also contribute to the subsequent stages of healing, for example, secreting catecholamines and serotonin, which act through receptors on the endothelium and cause vasoconstriction surrounding the wound (Gantwerker and Hom, 2011). In addition, platelets and polymorphonuclear leukocytes secrete TNF-α and IL-1 (Werner and Grose, 2003; Mussano et al., 2016) activating capillary endothelial cells and contributing to leukocyte transmigration (Bevilacqua et al., 1987). Neutrophils disinfect the wound eliminating debris and bacteria and provide antimicrobial protection by releasing H_2O_2, which produce ROS into the surrounding space.

Meanwhile, ROS not only protect the wound from infection, but they are also engaged in normal wound healing. ROS are involved in the proliferation of fibroblasts and vascular endothelial cells, promote proliferation and migration of keratinocytes, stimulate angiogenesis, and act as a chemoattractant for neutrophils, mononuclear phagocytes, eosinophils, basophils, and lymphocytes by stimulating the production of macrophage inflammatory protein (MIP)-1α (Dunnill et al., 2017). The importance of ROS for wound healing was confirmed in a study by Carrasco and colleagues, who showed the beneficial effects of ROS on wound healing and on HFSCs. The researchers induced transient ROS generation via the photodynamic effect as a result of the application of a photosensitizer (5-aminolevulinic acid (ALA) or its methyl derivative (mALA) cream) to mice in combination with red rays.

This effect is used in clinical practice for induction of cell death in tumors. Generation of transient ROS in such a way led to the proliferation of bulge HFSC, as well as epidermal and dermal skin layers (Carrasco et al., 2015). ROS can also affect HF neogenesis through DP. Zheng et al. showed proliferation of DP cells and increased mRNA expression levels of vascular endothelial growth factor (VEGF)-A and glial cell line-derived neurotrophic factor (GDNF), leading to WIHN under ROS-induced hypoxia (Zheng et al., 2019). Also, one of the most critical cellular events mediated by ROS is mitochondrial apoptosis. When the mitochondrial membrane is permeabilized with ROS, apoptosis agents (cytochrome c, AIF, or Smac/Diablo) enter the cytosol (Circu and Aw, 2010), implementing relationship between HFSCs activity and wound healing through ROS as an inflammatory mediator and an apoptotic agent.

However, the role of neutrophils, ROS, and other inflammatory mediators produced by them is controversial. Dysregulation of neutrophils can lead to skin lesions. Abundant neutrophil infiltration into the wound bed is a key factor in the development of chronic inflammation, which underlies non-healing wounds. Excess of neutrophils causes overproduction of ROS, which provokes cell membrane and extracellular matrix (ECM) damage with subsequent premature cell aging (Zhao et al., 2016).

Neutrophils are also capable of recruiting macrophages leading to a transition from the neutrophilic stage of wound healing to the stage of macrophage infiltration (Eming et al., 2007).

Macrophages appear in the wounded skin after neutrophils and phagocytize them (Gurtner et al., 2008; Greenlee-Wacker, 2016). Macrophage infiltration is regulated by fibrin clot platelets, fibroblasts, leukocytes, a gradient of growth factors, pro-inflammatory cytokines and chemokines released by hyperproliferative keratinocytes along the margins of the wound (Werner and Grose, 2003). Macrophages express many receptors on their surface, for example, the TLRs of different types (Karin et al., 2006). In addition to phagocytic and antigen-presenting functions, they produce various growth factors, such as TGF-β, TGF-α, and VEGF, which regulate fibroplasia and angiogenesis (Werner and Grose, 2003). Macrophage ablation during the inflammatory phase in an experimental model of wound regeneration in mice was shown to delay wound healing.

In addition, macrophages are known to play an essential role in angiogenesis. There is a hypothesis, that they form "tunnels" in the ECM which are colonized by capillary sprouts, circulating progenitor endothelial cells or transdifferentiated endothelial cells during later stages of wound healing (Moldovan, 2002). Also, there are experimental data in favor of the fact that macrophages can also participate in lymphangiogenesis during wound healing: the number of macrophages reaches a peak during the period of migration and organization of lymphatic endothelial cells (Rutkowski et al., 2006).

It is well known that macrophages are polarized into two subtypes, M1 and M2, with different phenotypes (Xu et al., 2013) though continuum of intermediate states exists. M1 macrophages are CCR2 + cells (Fadini et al., 2013). They secrete pro-inflammatory cytokines and phagocyte dead cells and pathogens. They can acquire this phenotype under the influence of bacterial metabolites, IFN-γ, and a granulocyte-macrophage colony-stimulating factor (GM-CSF) (Xu et al., 2013). Anti-inflammatory M2 macrophages, which activation is regulated by IL-13 and/or IL-4 (Qing, 2017), secrete angiogenic factors and anti-inflammatory cytokines and stimulate wound closure (Xu et al., 2013). They express CX3CR1 (Fadini et al., 2013). In M2-deficient mice, a delay in healing is observed, which is most prominent in the late stages of regeneration (Minutti et al., 2017).

Macrophage ablation using diphtheria toxin (DT) leads to WIHN inhibition in mouse experiments. M2 macrophages produce follicle-stimulating growth factors, such as FGF2 and IGF1. These factors are thought to take part in WIHN, since they participate in the Wnt pathway (Kasuya et al., 2018). The study of Wang and colleagues, which was mentioned in the previous section, in contrast, showed the valuable role of M1 macrophages in WIHN. It was found that in Lgr5 + HFSCs, TNF-α released by M1 macrophages induced not only TAT and WIH-A but also WIHN through activation of AKT/β-catenin (Wang et al., 2017).

TNF-α is a critical player in the inflammatory response (Efimov et al., 2009). It is upregulated during the inflammatory phase of wound healing (Barrientos et al., 2008). In response to skin damage, TNF-α is secreted by polymorphonuclear leukocytes, then by macrophages over a period from 12 to 24 hours after skin injury (Xu et al., 2013). In keratinocyte culture, TNF-α and IFN-γ stimulate the secretion of growth factors (e.g., TGF- α), HLA-DR, interleukins (IL-1, IL-6 and IL-8), ICAM-1, and monocyte chemotactic and activating factor (MCAF) (Barker et al., 1991). During regeneration, TNF-α is expressed in proliferating keratinocytes along the wound margins (Xu et al., 2013). Exposure of a culture of keratinocytes to TNF-α led to the expression of chemokines, cytokines, growth factors, and cell surface receptors, which can *in vivo* attract hematopoietic cells, monocytes, macrophages, and neutrophils, as well as memory T-cells that provide an innate immune response (Banno et al., 2004).

Íîwever, the upregulation of TNF-α is a noticeable factor in the transition of the acute wound to non-healing status, including diabetic wound development (Siqueira et al., 2010; Xu et al., 2013; Zhang et al., 2017). In *in vivo* and *in vitro* experiments, TNF-α exhibits a pro-inflammatory and pro-apoptotic effect, as well as prevents scar formation, fibroblast migration, re-epithelialization and, as a result, prolongs the period of wound closure.

Overexpression of TNF-α leads to an increase in the number of neutrophils and macrophages in the wound bed through NF-κB signaling. Anti-TNF-α therapy helps to reduce the activity of NF-κB, to normalize the number of inflammatory cells, and to decrease the size of the wound bed. Experiments with mice knockout for the gene of TNF-α inhibitor, a secretory leukocyte protease inhibitor (SLPI), showed that upregulation of TNF-α induces matrix metalloprotease 9 (MMP9), which leads to collagen destruction and, as a result, abnormal healing (Ashcroft et al., 2012). In an *in vivo* experiment, application of recombinant TNF-α to a wound reduced the expression of genes associated with collagen synthesis (Salomon et al., 1991), while TNF-α induced the expression of collagenase in dermal fibroblast culture

in several studies (Dayer et al., 1985; Brenner et al., 1989). In human keratinocyte culture, TNF-α induces the expression of gelatinase capable of degrading type IV collagen (Banno et al., 2004). Secretion of TNF-α in high doses for a long period harms healing because it suppresses the expression of TIMPs and ECM proteins and induces the expression of MMP-1, -2, -3, -9, -13 and MT1-MMP, thus leading to the degradation of ECM, the decline of cell migration, and collagen deposition. TNF-α contributes to non-healing wounds by increasing gelatinases, collagenases, and stromelysins levels (Barrientos et al., 2008). The result of therapy aimed at inhibiting TNF- α is not only a decrease in the inflammatory response but also the normalization of ECM synthesis (Ashcroft et al., 2012).

There is some evidence that TNF-α inhibits normal scar formation not only due to enzyme activity. It was shown in an *in vitro* contacting wound model that TNF-α suppresses TGF-β-induced expression of myofibroblast genes, such as α-*SMA, fibronectin type 1A*, and *collagen*. The authors confirmed that the effect of TNF-α is in the inhibition of TGF-β1-induced differentiation of myofibroblasts, which leads to the formation of a more fragile matrix with reduced contractile properties. It is thought that the high level of TNF-α in a non-healing wound prevents the differentiation of myofibroblasts and changes in the cytoskeleton configuration, which leads to the impairment in normal matrix contraction during wound healing (Goldberg et al., 2007). TNF-α also suppresses re-epithelialization during wound healing (Barrientos et al., 2008). The *in vitro* study showed that administration of TNF-α led to an elevation of the mRNA expression of IL-8, ICAM-1, and MCP-1 in HaCaT through PKCζ; however, TNF-α-induced decline in the proliferative and migratory activity of HaCaT cells did not depend on PKCζ (Zhang et al., 2017). In another study, exposure of human keratinocyte culture to TNF-α stimulated the expression of pro-apoptotic genes *BIK*, *BID*, and *TNFSF10* (Banno et al., 2004).

As one can see, TNF-α is not just an activator of the pro-survival and inflammatory pathways as well as the trigger of apoptosis and necroptosis, itis also involved in wound healing, stem cell activation, and in the HF cycling. Multiple complementary data are indicating that delicate balance of TNF-α expression and related signaling is required for proper skin restoration, including WIHN.

In addition to TNF-α, important mediators of inflammation during wound healing are PG secreted by damaged tissues under the influence of leukocytes and other immune cells (Higgs et al., 1975). The role of PG in wound healing is controversial. They activate apoptotic cascades and thus prevent excessive scarring because impaired apoptosis does not give fibroblasts and myofibroblasts disappear during the later stages of skin regeneration (Su et al., 2010). Dysregulation of PG levels causes both WIHN and wound healing abnormalities. Thus, in a model of a non-healing diabetic wound in *ob/ob* mice, a decrease in PGE_2/PGD_2 levels was shown, and leptin injections retained normal wound healing and proper levels of PGE_2/PGD_2 (Kampfer et al., 2005). However, not only their abnormal decrease but also increase can lead to aberrations in wound healing and HFSCs activation. It was shown that the expression levels of the prostaglandin D_2 synthase enzyme (PTGDS) and its product PGD_2 correlated with WIHN: high levels of PTGDS and PGD_2 were interlinked with impaired neogenesis of HFs (Nelson et al., 2013). Despite the harmful effect of PGD_2 on WIHN, there is a suggestion that another type of prostaglandin, PGE_2, may induce WIHN through Wnt activation, as it was demonstrated in hematopoietic stem cells (Goessling et al., 2009; Gong et al., 2018).

Besides neutrophils and macrophages mast cells also take part in an inflammatory phase. They are a source of pro-inflammatory mediators and cytokines and modulate the number of neutrophils in the wound bed. The number of mast cells in the wound bed returns to its standard value within the first 48 hours after injury and then increases in the course of regeneration (Eming et al., 2007; Gurtner et al., 2008). As mentioned above, mast cells contribute to the regulation of the HF activity, namely, its entry into catagen (Arck et al., 2005).

To summarize, the inflammatory cells, which take part in wound healing, are mainly polymorphonuclear leukocytes (namely, neutrophil compartment) and macrophages. They and their mediators (TNF-α, ROS and PG) are involved not only in the regulation of the HF cycling but also in other activities of EpiSC including WIHN. Excessive inflammation alters HF homeostasis and wound healing process. It is expected that WIHN failure in this respect makes an additional indirect contribution to wound chronicity because of the importance of HF neogenesis in skin regeneration.

Proliferation Phase

***T_{regs}*.** This stage of wound healing is characterized by proliferation and migration of cells, mainly keratinocytes and fibroblasts (Gurtner et al., 2008). The transition from the phase of inflammation to the stages of proliferation and remodeling is controlled by immunomegulatory mechanisms. In particular, T_{regs} are accumulated at inflammatory sites and are involved in modulating the immune response. These cells secrete Amphiregulin, an epidermal growth factor-like growth factor that is associated with maintaining tissue homeostasis, inflammation, and immunity. Amphiregulin via PCLγ induces "inside-out" activation of the integrin-α*v*-containing complex, which causes the transition of TGF-β from an inactive form to an active one. Active TGF-β has a dual role: it suppresses excessive inflammation and makes mesenchymal vascular progenitor cells, pericytes, differentiate into myofibroblasts, thus contributing to angiogenesis (Zaiss et al., 2019). Also, during angiogenesis, endothelial progenitor cells arrive from the bone marrow to the healing tissue to form new vessels (Gurtner et al., 2008). Xu et al. (2013) and Qing (2017).

T_{regs} contribute to re-epithelialization, which occurs due to differentiation of HFSCs into IFE keratinocytes, their proliferation, migration to the center of the wound, and synthesis of a new basement membrane (Gurtner et al., 2008; Gantwerker and Hom, 2011; Mathur et al., 2019). Re-epithelialization is activated by growth factors of the HGF, FGF, and EGF families (Martin and Nunan, 2015).

Mathur and co-authors showed in *in vivo* experiments that T_{regs} stimulated differentiation of HFSCs into IFE through

the control of the IL-17-CXCL5-neutrophil inflammatory cascade. In a model of subacute skin injury inflicted by tape stripping, T_{reg} depleted mice demonstrated thinner epidermis upon regeneration and downregulation of genes related to keratinocyte differentiation and stratum corneum formation. T_{regs} suppress the keratinocyte expression of *Cxcl5*, which is induced by the neutrophil regulator IL-17A. In the T_{reg}-cell-lacking mice, neutralization of CXCL5 by antibodies restored differentiation, while IL-17A neutralization or co-depletion of neutrophils saved the migratory defect of Lgr5-derived cells in IFE during healing (Mathur et al., 2019). Thus, T_{regs} contribute to wound healing affecting a wide range of cells. In addition to initiating re-epithelialization, the fibrin matrix is replaced by granulation tissue consisting of fibroblasts, germinating vessels, and immature type III collagen in the proliferation phase (Gantwerker and Hom, 2011). Either T_{regs} can stimulate bulge cells and cause HF cycle changes in normal conditions or promote re-epithelization during wound healing due to immunomodulating properties.

Fibroblasts are the key players in this phase of wound healing. It is well-known that fibroblasts and myofibroblasts secrete procollagen molecules, as well as fibronectin, thus providing ECM development. Fibroblasts migrating from the edges of the wound under the influence of TGF-β, cell fibronectin, and endothelin-1 differentiate into myofibroblasts contributing to wound contraction (Xu et al., 2013). Nevertheless, there is another surprising way, in which fibroblasts contribute to wound healing: they can produce nitric oxide (NO), an inflammatory mediator, which is also involved in skin regeneration. Several facts are indicating that NO is associated with collagen production. First, *in vitro* wound fibroblasts produce NO, and inhibition of NO synthases (NOS) leads to a decrease in collagen production (Schaffer et al., 1997). Second, transfection of tissues of wounded rats with a plasmid containing murine inducible NOS (iNOS) increased collagen deposition (Thornton et al., 1998). Third, ablation of endothelial NOS (eNOS) in mice leads to prolonged wound healing (Lee et al., 1999). Besides, there is some evidence that NO can affect EpiSC activation. Zhu and colleagues treated burn wounds in rats with NO-gel with sodium nitrite and showed that this treatment improved both wound healing and follicular neogenesis. Application of the gel contributed to re-epithelialization of the wound, caused an increase in the number of procollagen-expressing fibroblasts by 40%. Also, blood vessels number augmentation and neutrophils and monocytes infiltration was observed in the wound bed. In the wound bed of the treated group, more HFs and CD34 + stem cells were observed (Zhu et al., 2008). Wolf et al. in an *in vitro* experiment showed basal production of NO by human DP cells. The authors suggest that NO secretion promotes hair growth by mediating the proliferation and differentiation of matrix keratinocytes surrounding the DP (Wolf et al., 2003).

However, we should note that excessive exposure of the wound to NO can have the opposite outcome. There are some data on the harmful effect of NO on wound healing, for example, the delay in wound healing under its influence in an aged rat model (Bauer et al., 1998).

Scar Remodeling and Re-epithelialization Phase

During this stage, most endothelial cells, macrophages, and myofibroblasts undergo apoptosis or migrate from the wound bed, which consists of collagen and other ECM proteins. Type III collagen is replaced by type I collagen with the assistance of MMPs secreted by fibroblasts, macrophages, and endothelial cells (Gurtner et al., 2008). In this phase, HF neogenesis begins (Gay et al., 2020).

The mechanism of apoptosis that inflammatory cells undergo during healing remains under discussion. There is some evidence that the death receptor pathway mediates it due to TNFR activation, but some data indicate that the mitochondrial pathway via the anti-proliferative protein p53 is also possible. Fibroblasts die after they have synthesized a sufficient amount of fibers. And then, excessive endothelial cells are discarded (Greenhalgh, 1998). Thus, an involution of granulation tissue and retraction of blood vessels are observed (Gantwerker and Hom, 2011).

At the stage of remodeling, T cells are acting (Eming et al., 2007). Lee et al. showed that γδT cells are activated by IL-1α and IL-7, which are secreted by keratinocytes after injury (Lee P. et al., 2017_A). DETCs play diverse roles in wound healing. They contribute to the proliferation of keratinocytes by secretion of IGF1. In the mouse wound healing model, IGF1 secreted by DETCs caused a proliferation of keratin 14 + mouse epidermal cells and inhibited their terminal differentiation. IL-17A secreted by another subtype of γδT cells, Vγ4 T cells, can promote proliferation and terminal differentiation of mouse keratin 14 + epidermal cells (Zhu et al., 2019). There is also evidence of a stimulatory effect of KGF secreted by activated DETCs on keratinocyte proliferation. In addition to participating in the survival and proliferation of keratinocytes, activated DETCs affect inflammatory cells. They produce CCL3 and CCL4, which regulate the recruitment of inflammatory cells. DETC-derived KGF stimulates hyaluronan deposition by keratinocytes attracting macrophages (Ramirez et al., 2015).

γδT cells are the source of FGF9, which is involved in neofolliculogenesis in wounds (Gay et al., 2013). Gay with colleagues showed that *Fgf9* was upregulated in the dermis, just before the development of the hair placode during wound healing begins. The administration of antibodies against FGF9 into wound dermis decreased the number of newly formed HF. The number of γδT cells in the wound increased just before the raise of FGF9. The researchers showed that on PWD 12 Vγ4 + γδT population was the predominant source of FGF9, while DETCs was inactive in this respect. The study on $Tcrd^{-/-}$ mice lacking γδT cells showed a significant decrease in the number of newly formed HF in the wound bed compared with control. An analysis of the timeline of *Fgf9* expression and *in situ* hybridization of wound skin at different time points allowed the authors to conclude that γδT cells are the primary source of FGF9 at PWD 10–12, which caused the expression of Wnt2a

in dermal fibroblasts and thus led to the activation of Wnt pathway as well as to the expression of FGF9 in fibroblasts later on, and, consequently, increased Wnt activation in the dermis. Researchers found a small number of resident γδT cells in the human dermis with low density per area compared with the mouse dermis. Also, there were differences in the localization of γδT cells. In mice, cells were scattered throughout the dermis, usually at a distance from αβT cells and blood vessels. Human cells formed clusters with αβ T cells in vascularized dermal "pockets," indicating that they rarely migrate between skin and blood. A small number of γδT cells in the human skin, as compared to mice, may explain the lower regeneration ability of human skin when injured (Gay et al., 2013).

The Wnt pathway makes an important contribution to *de novo* HF formation (Gong et al., 2018). Myung and co-authors used K14-CreER;*Wls*$^{fl/fl}$ (WlsK14cKO) mice with knockout of *Wintless*, the gene, corresponding to Wnt secretion in the basal cells of IFE and HF. In the mouse model of wound healing, the absence of DP formation in the dermis of mutant animals was shown using alkaline phosphatase (AP) whole-mount staining (Myung et al., 2013). Transfection of human HFDP cells by negative Wnt regulator *CXXC5* led to downregulation of β-catenin, AP and PCNA, and knockdown of CXXC5 had the opposite effect. Lee and colleagues assume that Wnt3a activates CXXC5. Exposure of human DP cells to Wnt3a increased CXXC5 via a negative feedback mechanism. It is suggested that interruption of Wnt inhibitory signaling may stimulate WIHN, especially in humans (Lee S.H. et al., 2017_B). As it was mentioned above, in addition to γδT cells, the Wnt pathway can be activated by macrophages.

Lee and colleagues showed that γδT cells affect HFSCs not only indirectly through Wnt-mediated contributions to WIHN. These cells are an excellent example of the direct relationship between wound healing and HFSCs activation, as they stimulate the proliferation of bulge CD34 + HFSCs. The authors used the conditional knockout model for the *caspase-8* gene in epidermal cells for simulating wound healing to investigate the role of IL-1 in EpiSC activation during this process (Lee P. et al., 2017_A). Previously it was shown that *caspase-8* loss led to upregulation of IL-1α secretion because of an influence on caspase-1, which take part in the conversion of IL-1 precursor into an active form (Lee et al., 2009). Caspase-8 is widely known for its participation in the process of death receptor apoptosis, but besides, it has other functions. For example, it is involved in the processing of IL-1β, which contributes to inflammation (Gurung and Kanneganti, 2015).

Furthermore, IL-1β can indirectly influence HF: transplantation of IL-1β-stimulated bone marrow-derived macrophages into mice induced hair growth (Osaka et al., 2007). Lee and colleagues proposed the following HFSCs activation scheme: after wounding, the expression of caspase-8 decreases and, as a result, IL-1α is released from keratinocytes, which, together with IL-7, increases the population of γδT-cells (Lee P. et al., 2017_A). The latter stimulates the proliferation of bulge stem cells and mobilize them for wound healing. In inflammatory conditions keratinocytes also secrete CCL2 (Behfar et al., 2018), which attracts macrophages secreting IL-1β inducing hair growth. This mechanism potentiates the effect of IL-1 and IL-7/γδT cells on HFSCs proliferation (Lee P. et al., 2017_A). The above data once again proves the complicated interconnections between HFSCs activation pathways, inflammation participants, and cell death.

The scarring, which accomplishes the regeneration, much depends on the inflammatory process features, as well as on the expression of the cytokine profile (Liechty et al., 2000). However, scar development precludes restoration of the structure and functions of the wounded skin amply, not to mention severe complications such as keloids (Lim et al., 2018). Therefore, studies focusing on the possibility of regulating scar development via modulating the inflammation are of great practical importance. For example, in mice lacking T-lymphocytes, wounds heal without scars; however, in mice that do not develop both T- and B-lymphocytes, skin regeneration ends with scarring (Gawronska-Kozak et al., 2006). In the fetus, the skin regenerates without scars, since fetal wound healing occurs with a reduced inflammatory reaction, in part because macrophages, neutrophils, and mast cells of the fetus differ in size and maturity from those in adult tissues (Takeo et al., 2015). Martin et al. (2003) argue that inflammation is not prerequisite for effective wound healing if antibiotics stop the development of a bacterial infection. In the *pu.1* $^{-/-}$ mouse model, which does not develop functioning neutrophils and macrophages, skin regeneration is similar to fetal healing without the development of an inflammatory response and, as a result, under conditions of lower levels of TGF-β and IL-6. Thus, at the moment, information about the possibility of a direct influence on the scar through inflammation modulation is contradictory.

Nevertheless, studies are pointing out the possibility of indirect eliminating the effects of excess inflammation manifested by fibrotic scarring via agents produced by dermal cells. Lim and colleagues showed in their work that activation of Sonic hedgehog pathway leads to the formation of DP, which is a necessary condition for follicular neogenesis, which, in turn, leads to the restoration of skin functions at the site of injury and prevents the formation of scars (Lim et al., 2018).

Consequently, inflammation, scarring, and WIHN are interlinked. This is confirmed by fibrotic healing in WIHN^{-} mice wounds. In this type of wounds, unlike WIHN^{+} ones, late macrophages phagocytized a Wnt inhibitor SFRP4. In the late stages of wound healing, Wnt ligands paradoxically induced fibrotic healing, and these ligands are decreased in WIHN^{+} wounds. A similar process occurs in humans (Gay et al., 2020), where wounds lack WIHN and commonly heal with a cosmetic defect. Thereby, the role of Wnt ligands in wound healing is controversial: on the one hand, they can promote WIHN, which prevents scar formation and causes skin restoration; on the other hand, chronic expression of such ligands can cause wound fibrosis. Since macrophages phagocytize Wnt-inhibitor, it can be assumed that the chronic presence of Wnt ligands in the wound may be a consequence of prolonged inflammation, causing impaired regeneration and abnormal scarring.

At the moment, the involvement of different types of stem cells in HF neogenesis is under discussion (Plikus et al., 2015).

There is evidence that first telogen Lgr6 + stem cells transplanted onto the backs of nude mice are capable of reconstructing HF (Snippert et al., 2010). Another study gives a key role in follicular neogenesis to bulge Lgr5 + stem cells. Depletion of Lgr5 + cells in Lgr5-Cre:R26^{DTR}/ + mice resulted in WIH-A arrest on PWD 15 as well as a decrease in the number of neogenic HF by PWD 21-23 (Wang et al., 2017). However, another type of bulge stem cells, Krt15-expressing cells, are not involved in WIHN (Plikus et al., 2015).

Proper WIHN requires dermal papilla (DP) formation likely occurring by condensation of dermal fibroblasts or pre-existing progenitors. Experiments on *Blimp-1* knock-out mice demonstrated a violation of WIHN, suggesting an essential function of fibroblasts expressing Blimp-1 in DP neogenesis (Telerman et al., 2017). On the other hand, DP cells themselves take part in wound healing. Being one of the main components of the wound environment, TGF-β1 upregulates the expression of fibroblast-specific protein 1 (FSP1) and vimentin in DP cells and downregulated α-SMA expression suggesting that DP cells can differentiate into fibroblasts during wound healing (Bin et al., 2013). DP can also contribute to wound healing by secreting the anagen-inducing hormone leptin (Jimenez et al., 2015), which was shown to improve the migration and proliferation of keratinocytes as well as to accelerate angiogenesis (Tadokoro et al., 2015).

Thus, to sum up, inflammation during wound healing is like a double-edged sword. On the one hand, excessive inflammation leads to the establishment of long-term non-healing wounds. The optionality of inflammation for wound healing was shown by a series of experiments, for example, with the ablation of functioning neutrophils and macrophages. On the other hand, the release of the inflammatory cytokine TNF-α is a significant factor in WIHN, which is a prerequisite for scar formation without a cosmetic defect. Also, we can make one more conclusion about the potential intersection of wound healing and activation of HFSCs not only through wound healing cascades but also in other ways, for example, through programmed cell death. These considerations are prompted by data on the role of the upstream activator of apoptosis and necroptosis TNF-α and the downstream participant of apoptosis Caspase-8 (Varfolomeev and Vucic, 2018) in the activation of HFSCs as well as in normal and pathological wound healing.

DISCUSSION

Undoubtedly, there is a close interplay between the activation of EpiSC, specifically, HFSCs, as a whole and WIHN as its particular manifestation with the participation of wound healing via inflammatory cells, mediators, and dsRNA. Inflammation is involved in the regulation of HF cycling in intact skin and into the activation of HFSCs during wound healing. However, there is a reason to believe that the relationship between HFSCs functioning and wound healing has a much more complex regulation. We want to take a chance here and suppose that this regulation may comprise not only inflammatory agents but also components of the signaling pathways of cell death, including apoptosis and necroptosis. As it was discussed above, ROS, activators of pro-apoptotic and inflammatory cascades, together with the "external" apoptosis and necroptosis activators TNF-α and dsRNA, and the downstream mediator of apoptosis caspase-8 influence wound healing and HFSC activation. These findings are particularly interesting since apoptosis is classically considered to be a non-inflammatory way of cell death (Nagata, 2018). There are also new data suggesting that apoptotic cells are not inert: they may trigger genes associated with wound healing, proliferation, and a decrease in inflammation in adjacent cells (Medina et al., 2020). It is known that the signaling pathways of inflammation and cell death are interconnected through RIPK-1 and RIPK-3, including the situation of wound healing, as shown in several studies (Takahashi et al., 2014; Godwin et al., 2015; Moriwaki et al., 2015; Gupta et al., 2018). Such intersections can also occur in the HF. Moreover, it can be speculated that RIPK-1 and RIPK-3 play an unexpected role in HF dynamics. We found the cycle-related expression of RIPK-1 and RIPK-3 in mouse and human HF cells: It was found in the anagen HFs and absent in telogen ones (Morgun et al., 2020). As it was described above, hair growth may be promoted via dsRNA/TLR3/IL-6/STAT3 pathway (Nelson et al., 2015, 2016a_A; Nelson et al., 2016b_B). Based on Moriwaki data obtained in a mouse model of colitis, as well as in an experiment on bone-marrow-derived dendritic cells, it can be concluded that after LPS-induced stimulation of TLR4, RIPK-3 participates in the activation of the NF-κβ pathway, which leads to interleukin expression and STAT3 phosphorylation (Moriwaki et al., 2014). It may be speculated that RIPK-3-induced activation of NF-κβ is an additional intermediate link between the stimulation of the TLR3 and IL-6/STAT3-induced hair growth.

The regulation of inflammation and other processes that occur during wound healing is very complex and multidirectional. Excessive scarring can cause a cosmetic defect, while a delay in the formation of a scar (like in a non-healing wound) can cause severe complications during the wound healing process. The functions of HF in wound healing are also a two-way street: it is a source of stem cells both for re-epithelialization and for self-regeneration, while its neogenesis in the wound bed is essential for the functional recovery of the skin after injury. However, humans are unable to accomplish WIHN. Likewise, there is no adequate model for studying the damaged human HF. There are several *in vivo* and *in vitro* models admitting studies of human HF life activities. For example, researchers offer a humanized scalp model (Yamao et al., 2015), a SCID mouse xenotransplantation model (Oh et al., 2016), and *in vitro* culture model of a single human HF (Ma et al., 2016), and DP organoid model (Gupta et al., 2018). It is believed that the use of HF or their cellular components can significantly affect the course of wound healing, while *in situ* induction of hair growth during wound healing can stimulate epimorphic regeneration instead of scarring (Rippa et al., 2019). Attempts to transplant or "grow" HF in the wound bed have a long history. There is a classic work of the Jahoda with co-authors, where the induction of hair growth by

transplantation of cultured DP cells in the lower part-amputated HF, was shown (Jahoda et al., 1984). Kageyama and colleagues showed HF development after the transplantation of bead-based HF germs, which were prepared with mouse embryonic mesenchymal cells or human DP cells and epithelial cells, into the back of nude mice (Kageyama et al., 2019). Lei and co-workers accomplish *in vivo* hair growth after transplantation of organoids, which were developed from mice neonatal epidermal and dermal cells (Lei et al., 2017). Lee and co-authors generated the artificial HF using mouse pluripotent stem cells in an *in vitro* study (Lee et al., 2018). Using skin epidermal keratinocytes and human DP cells we fabricated an artificial hair germ-like structures expressing a number markers, such as Lef1, EpCAM, and P cadherin attributed to folliculogenesis (Kalabusheva et al., 2017). Abaci and colleagues managed to compose a factitious human HF inside bioengineered skin constructs (HSCs) using 3D-printed molds. Transfection of DP cells with *Lef-1* restored the intact transcription signature of the DP and significantly increased expression of markers of the inner and outer root sheath, as well as the medulla, which indicated the efficiency of cell differentiation within the HSCs toward the HF. Moreover, human umbilical vein endothelial cells (HUVECs) were encapsulated into HSCs, and this resulted in HF vascularization and in the hair growth stimulation in immunodeficient mice (Abaci et al., 2018). Returning to the subject of our review, we suggest that engagement of inflammatory cells during HF-like structure fabrication may improve the outcome of transplantation. Notably, there could be used not only distinctive for skin in steady state immune cells, such as T_{regs} or γδT cells but also polymorphonuclear leukocytes (in particular, neutrophils) and macrophages. Thus, partial simulation of wound milieu may be helpful to reproduce WIH-A and WIHN microenvironment during hair transplantation into the scar, which is a promising method of its amelioration (Jung et al., 2013), or into the balding scalp. It may be proposed, that macrophages within the hair-bearing graft could improve hair growth by three ways: trough AKT/β-catenin activation (Wang et al., 2017); via induction of Wnt-signaling by dint of growth factors release (Kasuya et al., 2018), or production of Wnt-ligands upon their apoptosis activation (Castellana et al., 2014). Neutrophils, releasing ROS, could stimulate secretion of growth factors by DP cells and, thus, cause hair growth, maintain DP identity and support correct epithelial-mesenchymal interactions through the restoration of native DP signature (Zheng et al., 2019).

Thereby, the study of the components of inflammatory cascades as general targets for the treatment of wound healing and pathologies assumes a new significance. According to EpiSC plasticity, it may be proposed, that inflammation milieu can promote HF development from cultured cells transplanted into the wound. However, inflammation- induced effect on stemness can not only ameliorate wound healing but also cause diseases associated with pathological cell proliferation and differentiation failure, for example, psoriasis. Likewise, several germinative epidermal cells have an "inflammatory memory", which in the experiment leads to better healing, though the long-term outcome of this approach in humans is unknown. In addition, it is known, that skin pathologies characterized by excessive inflammation such as epidermolysis bullosa (Mallipeddi, 2002) and burns (Koh et al., 2014) improve the risk of squamous cell carcinoma. It can be assumed that inflammation so radically affects the homeostasis of the epidermis that differentiated epidermal cells acquire stem features, and epidermal SC overreact, resulting in malignant skin degeneration. This is another indirect evidence of the ambiguity of the effect of inflammation on the differentiation status of epidermal cells. Consequently, using TNF-α, ROS, and NO, as well as cells, which release these inflammatory agents, can be problematic, as they can cause quite severe skin pathologies. Thus, it is necessary to find a delicate regulation of inflammatory cascades.

AUTHOR CONTRIBUTIONS

EM analyzed the literature and wrote the manuscript. EV edited the text and proposed ideas. Both authors contributed to the article and approved the submitted version.

FUNDING

The work was funded by the Russian Science Foundation (Project No. 16-14-00204).

ACKNOWLEDGMENTS

The authors would like to thank Ekaterina P. Kalabusheva, Elina S. Chermnykh, and Alexandra A. Rippa for valuable consultations, Evgeny I. Kiselev for assisting with the figure.

REFERENCES

Abaci, H. E., Coffman, A., Doucet, Y., Chen, J., Jacków, J., Wang, E., et al. (2018). Tissue engineering of human hair follicles using a biomimetic developmental approach. *Nat. Commun.* 9:5301. doi: 10.1038/s41467-018-07579-y

Abbasi, S., and Biernaskie, J. (2019). Injury modifies the fate of hair follicle dermal stem cell progeny in a hair cycle-dependent manner. *Exp. Dermatol.* 28, 419–424. doi: 10.1111/exd.13924

Ali, N., Zirak, B., Rodriguez, R. S., Pauli, M. L., Truong, M. A., Lai, K., et al. (2017). Regulatory T cells in skin facilitate epithelial stem cell differentiation. *Cell* 169, 1119–1129.e11. doi: 10.1016/j.cell.2017.05.002

Ansell, D. M., Kloepper, J. E., Thomason, H. A., Paus, R., and Hardman, M. J. (2011). Exploring the "hair growth–wound healing connection": anagen phase promotes wound re-epithelialization. *J. Invest. Dermatol.* 131, 518–528. doi: 10.1038/jid.2010.291

Arck, P. C., Handjiski, B., Kuhlmei, A., Peters, E. M. J., Knackstedt, M., Peter, A., et al. (2005). Mast cell deficient and neurokinin-1 receptor knockout mice are protected from stress-induced hair growth inhibition. *J. Mol. Med.* 83, 386–396. doi: 10.1007/s00109-004-0627-z

Ashcroft, G. S., Jeong, M. J., Ashworth, J. J., Hardman, M., Jin, W., Moutsopoulos, N., et al. (2012). Tumor necrosis factor-alpha (TNF-α) is a therapeutic target for impaired cutaneous wound healing. *Wound Repair Regen.* 20, 38–49. doi: 10.1111/j.1524-475x.2011.00748.x

Banno, T., Gazel, A., and Blumenberg, M. (2004). Effects of tumor necrosis factor-α (TNFα) in epidermal keratinocytes revealed using global transcriptional profiling. *J. Biol. Chem.* 279, 32633–32642. doi: 10.1074/jbc.m400642200

Barker, J. N. W. N., Mitra, R. S., Griffiths, C. E. M., Dixit, V. M., and Nickoloff, B. J. (1991). Keratinocytes as initiators of inflammation. *Lancet* 337, 211–214. doi: 10.1016/0140-6736(91)92168-2

Barrandon, Y., and Green, H. (1987). Three clonal types of keratinocyte with different capacities for multiplication. *Proc. Natl. Acad. Sci. U.S.A.* 84, 2302–2306. doi: 10.1073/pnas.84.8.2302

Barrientos, S., Stojadinovic, O., Golinko, M. S., Brem, H., and Tomic-Canic, M. (2008). Perspective article: growth factors and cytokines in wound healing. *Wound Repair Regen.* 16, 585–601. doi: 10.1111/j.1524-475x.2008.00410.x

Bauer, J. A., Rao, W., and Smith, D. (1998). Evaluation of linear polyethyleneimine/nitric oxide adduct on wound repair: therapy versus toxicity. *Wound Repair Regen.* 6, 569–577. doi: 10.1046/j.1524-475x.1998.60609.x

Behfar, S., Hassanshahi, G., Nazari, A., and Khorramdelazad, H. (2018). A brief look at the role of monocyte chemoattractant protein-1 (CCL2) in the pathophysiology of psoriasis. *Cytokine* 110, 226–231. doi: 10.1016/j.cyto.2017.12.010

Bevilacqua, M. P., Pober, J. S., Mendrick, D. L., Cotran, R. S., and Gimbrone, M. A. (1987). Identification of an inducible endothelial-leukocyte adhesion molecule. *Proc. Natl. Acad. Sci. U.S.A.* 84, 9238–9242. doi: 10.1073/pnas.84.24.9238

Bin, S., Li, H. D., Xu, Y. B., Qi, S. H., Li, T. Z., Liu, X. S., et al. (2013). BMP-7 attenuates TGF-β1-induced fibroblast-like differentiation of rat dermal papilla cells. *Wound Repair Regen.* 21, 275–281. doi: 10.1111/wrr.12015

Botchkarev, V. A., and Sharov, A. A. (2004). BMP signaling in the control of skin development and hair follicle growth. *Differentiation* 72, 512–526. doi: 10.1111/j.1432-0436.2004.07209005.x

Brenner, D. A., O'Hara, M., Angel, P., Chojkier, M., and Karin, M. (1989). Prolonged activation of jun and collagenase genes by tumour necrosis factor-α. *Nature* 337, 661–663. doi: 10.1038/337661a0

Brownell, I., Guevara, E., Bai, C. B., Loomis, C. A., and Joyner, A. L. (2011). Nerve-derived sonic hedgehog defines a niche for hair follicle stem cells capable of becoming epidermal stem cells. *Cell Stem Cell* 8, 552–565. doi: 10.1016/j.stem.2011.02.021

Carrasco, E., Calvo, M., Blázquez-Castro, A., Vecchio, D., Zamarrón, A., Dias de Almeida, I. J., et al. (2015). Photoactivation of ROS production *in situ* transiently activates cell proliferation in mouse skin and in the hair follicle stem cell niche promoting hair growth and wound healing. *J. Invest. Dermatol.* 135, 2611–2622. doi: 10.1038/jid.2015.248

Castellana, D., Paus, R., and Perez-Moreno, M. (2014). Macrophages contribute to the cyclic activation of adult hair follicle stem cells. *PLoS Biol.* 12:e1002002. doi: 10.1371/journal.pbio.1002002

Chen, C. C., Wang, L., Plikus, M. V., Jiang, T. X., Murray, P. J., Ramos, R., et al. (2015). Organ-level quorum sensing directs regeneration in hair stem cell populations. *Cell* 161, 277–290. doi: 10.1016/j.cell.2015.02.016

Choi, N., Kim, W. S., Oh, S. H., and Sung, J. H. (2019). HB-EGF improves the hair regenerative potential of adipose-derived stem cells via ros generation and Hck phosphorylation. *Int. J. Mol. Sci.* 21:122. doi: 10.3390/ijms21010122

Circu, M. L., and Aw, T. Y. (2010). Reactive oxygen species, cellular redox systems, and apoptosis. *Free Radic. Biol. Med.* 48, 749–762. doi: 10.1016/j.freeradbiomed.2009.12.022

Clayton, E., Doupé, D. P., Klein, A. M., Winton, D. J., Simons, B. D., and Jones, P. H. (2007). A single type of progenitor cell maintains normal epidermis. *Nature* 446, 185–189. doi: 10.1038/nature05574

Cotsarelis, G., Sun, T. T., and Lavker, R. M. (1990). Label-retaining cells reside in the bulge area of pilosebaceous unit: implications for follicular stem cells, hair cycle, and skin carcinogenesis. *Cell* 61, 1329–1337. doi: 10.1016/0092-8674(90)90696-c

Dayer, J. M., Beutler, B., and Cerami, A. (1985). Cachectin/tumor necrosis factor stimulates collagenase and prostaglandin E2 production by human synovial cells and dermal fibroblasts. *J. Exp. Med.* 162, 2163–2168. doi: 10.1084/jem.162.6.2163

Dunnill, C., Patton, T., Brennan, J., Barrett, J., Dryden, M., Cooke, J., et al. (2017). Reactive oxygen species (ROS) and wound healing: the functional role of ROS and emerging ROS-modulating technologies for augmentation of the healing process. *Int. Wound J.* 14, 89–96. doi: 10.1111/iwj.12557

Efimov, G. A., Kruglov, A. A., Tillib, S. V., Kuprash, D. V., and Nedospasov, S. A. (2009). Tumor necrosis factor and the consequences of its ablation *in vivo*. *Mol. Immunol.* 47, 19–27. doi: 10.1016/j.molimm.2009.01.007

Ekman, A.-K., Bivik Eding, C., Rundquist, I., and Enerback, C. (2019). IL-17 and IL-22 promote keratinocyte stemness in the germinative compartment in psoriasis. *J. Invest. Dermatol.* 139, 1564–1573.e8. doi: 10.1016/j.jid.2019.03.368

Eming, S. A., Krieg, T., and Davidson, J. M. (2007). Inflammation in wound repair: molecular and cellular mechanisms. *J. Invest. Dermatol.* 127, 514–525. doi: 10.1038/sj.jid.5700701

Fadini, G. P., Cappellari, R., Mazzucato, M., Agostini, C., Vigili de Kreutzenberg, S., and Avogaro, A. (2013). Monocyte–macrophage polarization balance in pre-diabetic individuals. *Acta Diabetol.* 50, 977–982. doi: 10.1007/s00592-013-0517-3

Fang, X., Zhou, X., and Wang, X. (2013). Clinical development of phosphatidylinositol 3-kinase inhibitors for non-Hodgkin lymphoma. *Biomark. Res.* 1:30. doi: 10.1186/2050-7771-1-30

Gantwerker, E. A., and Hom, D. B. (2011). Skin: histology and physiology of wound healing. facial plast surg clin. *North Am.* 19, 441–453. doi: 10.1016/j.fsc.2011.06.009

Garcin, C. L., and Ansell, D. M. (2017). The battle of the bulge: re-evaluating hair follicle stem cells in wound repair. *Exp. Dermatol.* 26, 101–104. doi: 10.1111/exd.13184

Gawronska-Kozak, B., Bogacki, M., Rim, J. S., Monroe, W. T., and Manuel, J. A. (2006). Scarless skin repair in immunode cient mice. *Wound Repair Regen.* 14, 265–276. doi: 10.1111/j.1743-6109.2006.00121.x

Gay, D., Ghinatti, G., Guerrero-Juarez, C. F., Ferrer, R. A., Ferri, F., Lim, C. H., et al. (2020). Phagocytosis of Wnt inhibitor SFRP4 by late wound macrophages drives chronic Wnt activity for fibrotic skin healing. *Sci. Adv.* 6:eaay3704. doi: 10.1126/sciadv.aay3704

Gay, D., Kwon, O., Zhang, Z., Spata, M., Plikus, M. V., Holler, P. D., et al. (2013). Fgf9 from dermal γδ T cells induces hair follicle neogenesis after wounding. *Nat. Med.* 19, 916–923. doi: 10.1038/nm.3181

Geyfman, M., Plikus, M., Treffeisen, E., Andersen, B., and Paus, R. (2015). Resting no more: re-defining telogen, the maintenance stage of the hair growth cycle. *Biol. Rev.* 90, 1179–1196. doi: 10.1111/brv.12151

Ghazizadeh, S., and Taichman, L. B. (2001). Multiple classes of stem cells in cutaneous epithelium: a lineage analysis of adult mouse skin. *EMBO J.* 20, 1215–1222. doi: 10.1093/emboj/20.6.1215

Godwin, A., Sharma, A., Yang, W.-L., Wang, Z., Nicastro, J., Coppa, G. F., et al. (2015). Receptor-interacting protein kinase 3 deficiency delays cutaneous wound healing. *PLoS One* 10:e0140514. doi: 10.1371/journal.pone.0140514

Goessling, W., North, T. E., Loewer, S., Lord, A. M., Lee, S., Stoick-Cooper, C. L., et al. (2009). Genetic interaction of PGE2 and Wnt signaling regulates developmental specification of stem cells and regeneration. *Cell* 136, 1136–1147. doi: 10.1016/j.cell.2009.01.015

Goldberg, M. T., Han, Y. P., Yan, C., Shaw, M. C., and Garner, W. L. (2007). TNF-α suppresses α-Smooth Muscle Actin expression in human dermal fibroblasts: an implication for abnormal wound healing. *J. Invest. Dermatol.* 127, 2645–2655. doi: 10.1038/sj.jid.5700890

Gong, L., Xu, X. G., and Li, Y. H. (2018). Embryonic-like regenerative phenomenon: wound-induced hair follicle neogenesis. *Regen. Med.* 13, 729–739. doi: 10.2217/rme-2018-0028

Gonzales, K. A. U., and Fuchs, E. (2017). Skin and its regenerative powers: an alliance between stem cells and their niche. *Dev. Cell* 43, 387–401. doi: 10.1016/j.devcel.2017.10.001

Greenhalgh, D. G. (1998). The role of apoptosis in wound healing. *Int. J. Biochem. Cell Biol.* 30, 1019–1030. doi: 10.1016/s1357-2725(98)00058-2

Greenlee-Wacker, M. C. (2016). Clearance of apoptotic neutrophils and resolution of inflammation. *Immunol. Rev.* 273, 357–370. doi: 10.1111/imr.12453

Gröne, A. (2002). Keratinocytes and cytokines. *Vet. Immunol. Immunopathol.* 88, 1–12. doi: 10.1016/s0165-2427(02)00136-8

Gupta, A. C., Chawla, S., Hegde, A., Singh, D., Bandyopadhyay, B., Lakshmanan, C. C., et al. (2018). Establishment of an *in vitro* organoid model of dermal papilla of human hair follicle. *J. Cell. Physiol.* 233, 9015–9030. doi: 10.1002/jcp.26853

Gurtner, G. C., Werner, S., Barrandon, Y., and Longaker, M. T. (2008). Wound repair and regeneration. *Nature* 453, 314–321. doi: 10.1038/nature07039

Gurung, P., and Kanneganti, T. D. (2015). Novel roles for caspase- 8 in IL-1beta and inflammasome regulation. *Am. J. Pathol.* 185, 17–25.

Haensel, D., Jin, S., Sun, P., Cinco, R., Dragan, M., Nguyen, Q., et al. (2020). Defining epidermal basal cell states during skin homeostasis and wound healing using single-cell transcriptomics. *Cell Rep.* 30, 3932–3947.e6. doi: 10.1016/j.celrep.2020.02.091

Hardman, J. A., Muneeb, F., Pople, J., Bhogal, R., Shahmalak, A., and Paus, R. (2019). Human perifollicular macrophages undergo apoptosis, express wnt ligands, and switch their polarization during catagen. *J. Invest. Dermatol.* 139, 2543–2546.e9. doi: 10.1016/j.jid.2019.04.026

Higgins, C. A., Petukhova, L., Harel, S., Ho, Y. Y., Drill, E., Shapiro, L., et al. (2014). FGF5 is a crucial regulator of hair length in humans. *Proc. Natl. Acad. Sci. U.S.A.* 111, 10648–10653. doi: 10.1073/pnas.1402862111

Higgs, G. A., McCall, E., and Youlten, L. G. F. (1975). A chemotactic role for prostaglandins released from polymorphonuclear leucocytes during phagocytosis. *Br. J. Pharmacol.* 53, 539–546. doi: 10.1111/j.1476-5381.1975.tb07392.x

Hsu, Y., Li, L., and Fuchs, E. (2014). Emerging interactions between skin stem cells and their niches. *Nat. Med.* 20, 847–856. doi: 10.1038/nm.3643

Jahoda, C. A., Horne, K. A., and Oliver, R. F. (1984). Induction of hair growth by implantation of cultured dermal papilla cells. *Nature* 311, 560–562. doi: 10.1038/311560a0

Jahoda, C. A., Oliver, R. F., Reynolds, A., Forrester, J., and Horne, K. (1996). Human hair follicle regeneration following amputation and grafting into the nude mouse. *J. Invest. Dermatol.* 107, 804–807. doi: 10.1111/1523-1747.ep12330565

Jimenez, F., Poblet, E., and Izeta, A. (2015). Reflections on how wound healing-promoting effects of the hair follicle can be translated into clinical practice. *Exp. Dermatol.* 24, 91–94. doi: 10.1111/exd.12521

Jin, Y., Xia, M., Sun, A., Saylor, C. M., and Xiong, N. (2010). CCR10 is important for the development of skin-specific γδT cells by regulating their migration and location. *J. Immunol.* 185, 5723–5731. doi: 10.4049/jimmunol.1001612

Joost, S., Jacob, T., Sun, X., Annusver, K., La Manno, G., Sur, I., et al. (2018). Single-cell transcriptomics of traced epidermal and hair follicle stem cells reveals rapid adaptations during wound healing. *Cell Rep.* 25, 585–597.e7. doi: 10.1016/j.celrep.2018.09.059

Jung, S., Oh, S. J., and Hoon Koh, S. (2013). Hair follicle transplantation on scar tissue. *J. Craniofac. Surg.* 24, 1239–1241. doi: 10.1097/scs.0b013e31828a78ad

Kageyama, T., Yan, L., Shimizu, A., Maruo, S., and Fukuda, J. (2019). Preparation of hair beads and hair follicle germs for regenerative medicine. *Biomaterials* 212, 55–63. doi: 10.1016/j.biomaterials.2019.05.003

Kalabusheva, E. P., Terskikh, V. V., and Vorotelyak, E. A. (2017). Hair germ model in vitro via human postnatal keratinocyte-dermal papilla interactions: impact of hyaluronic acid. *Stem Cells Int.* 2017:9271869. doi: 10.1155/2017/9271869

Kampfer, H., Schmidt, R., Geisslinger, G., Pfeilschifter, J., and Frank, S. (2005). Wound inflammation in diabetic *ob/ob* mice: functional coupling of prostaglandin biosynthesis to cyclooxygenase-1 activity in diabetes-impaired wound healing. *Diabetes Metab. Res. Rev.* 54, 1543–1551. doi: 10.2337/diabetes.54.5.1543

Karin, M., Lawrence, T., and Nizet, V. (2006). Innate immunity gone awry: linking microbial infections to chronic inflammation and cancer. *Cell* 124, 823–835. doi: 10.1016/j.cell.2006.02.016

Kasuya, A., Ito, T., and Tokura, Y. (2018). M2 macrophages promote wound-induced hair neogenesis. *J. Dermatol. Sci.* 91, 250–255. doi: 10.1016/j.jdermsci.2018.05.004

Kellenberger, A., and Tauchi, M. (2013). Mammalian target of rapamycin complex 1 (mTORC1) may modulate the timing of anagen entry in mouse hair follicles. *Exp. Dermatol.* 22, 77–80. doi: 10.1111/exd.12062

Kim, J., and Krueger, J. (2015). The immunopathogenesis of psoriasis. *Dermatol. Clin.* 33, 13–23. doi: 10.1016/j.det.2014.09.002

Kobayashi, T., Voisin, B., Kim, D. Y., Kennedy, E. A., Jo, J., Shih, H. Y., et al. (2019). Homeostatic control of sebaceous glands by innate lymphoid cells regulates commensal bacteria equilibrium. *Cell* 176, 982–997.e16. doi: 10.1016/j.cell.2018.12.031

Koh, S. H., Oh, S. J., Chun, H., and Kim, S. J. (2014). Pseudoangiosarcomatous squamous cell carcinoma developing on a burn scar: a case report and review of the literature. *Burns* 40, e47–e52. doi: 10.1016/j.burns.2014.02.019

Komi, D. E. A., Khomtchouk, K., and Santa Maria, P. L. (2020). A review of the contribution of mast cells in wound healing: involved molecular and cellular mechanisms. *Clin. Rev. Allergy Immunol.* 58, 298–312. doi: 10.1007/s12016-019-08729-w

Krause, K., and Foitzik, K. (2006). Biology of the hair follicle: the basics. *Semin. Cutan. Med. Surg.* 25, 2–10. doi: 10.1016/j.sder.2006.01.002

Kumamoto, T., Shalhevet, D., Matsue, H., Mummert, M. E., Ward, B. R., Jester, J. V., et al. (2003). Hair follicles serve as local reservoirs of skin mast cell precursors. *Blood* 102, 1654–1660. doi: 10.1182/blood-2003-02-0449

Lay, K., Yuan, S., Gur-Cohen, S., Miao, Y., Han, T., Naik, S., et al. (2018). Stem cells repurpose proliferation to contain a breach in their niche barrier. *eLife* 7:e41661. doi: 10.7554/elife.41661

Lee, J., Böscke, R., Tang, P. C., Hartman, B. H., Heller, S., and Koehler, K. R. (2018). Hair follicle development in mouse pluripotent stem cell-derived skin organoids. *Cell Rep.* 22, 242–254. doi: 10.1016/j.celrep.2017.12.007

Lee, P., Gund, R., Dutta, A., Pincha, N., Rana, I., Ghosh, S., et al. (2017). Stimulation of hair follicle stem cell proliferation through an IL-1α dependent activation of γδT-cells. *J. Invest. Dermatol.* 138:S229. doi: 10.1016/j.jid.2018.03.1366_A

Lee, P., Lee, D. J., Chan, C., Chen, S. W., Ch'en, I., and Jamora, C. (2009). Dynamic expression of epidermal caspase 8 simulates a wound healing response. *Nature* 458, 519–523. doi: 10.1038/nature07687

Lee, P. C., Salypongse, N., Bragdon, G. A., Shears, L. L., Watkins, S. C., Endington, H. D., et al. (1999). Impaired wound healing and angiogenesis in eNOS deficient mice. *Am. J. Physiol.* 46, 1600–1608. doi: 10.1152/ajpheart.1999.277.4.H1600

Lee, S. H., Seo, S. H., Lee, D. H., Pi, L. Q., Lee, W. S., and Choi, K. Y. (2017). Targeting of CXXC5 by a competing peptide stimulates hair regrowth and wound-induced hair neogenesis. *J. Invest. Dermat.* 137, 2260–2269. doi: 10.1016/j.jid.2017.04.038_B

Lei, M., Schumacher, L. J., Lai, Y. C., Juan, W. T., Yeh, C. Y., Wu, P., et al. (2017). Self-organization process in newborn skin organoid formation inspires strategy to restore hair regeneration of adult cells. *Proc. Natl. Acad. Sci. U.S.A.* 114, E7101–E7110. doi: 10.1073/pnas.1700475114

Li, J., Yang, Z., Li, Z., Gu, L., Wang, Y., and Sung, C. (2014). Exogenous IGF-1 promotes hair growth by stimulating cell proliferation and down regulating TGF-β1 in C57BL/6 mice in vivo. *Growth Horm. IGF Res.* 24, 89–94. doi: 10.1016/j.ghir.2014.03.004

Liechty, K. W., Kim, H. B., Adzick, N. S., and Crombleholme, T. M. (2000). Fetal wound repair results in scar formation in interleukin-10–deficient mice in a syngeneic murine model of scarless fetal wound repair. *J. Pediatr. Surg.* 35, 866–873. doi: 10.1053/jpsu.2000.6868

Lim, C. H., Sun, Q., Ratti, K., Lee, S.-H., Zheng, Y. I., Takeo, M., et al. (2018). Hedgehog stimulates hair follicle neogenesis by creating inductive dermis during murine skin wound healing. *Nat. Commun.* 9:4903. doi: 10.1038/s41467-018-07142-9

Liu, Y., Lyle, S., Yang, Z., and Cotsarelis, G. (2003). Keratin 15 promoter targets putative epithelial stem cells in the hair follicle bulge. *J. Invest. Dermat.* 121, 963–968. doi: 10.1046/j.1523-1747.2003.12600.x

Lyle, S., Christofidou-Solomidou, M., Liu, Y., Elder, D. E., Albelda, S., and Cotsarelis, G. (1998). The C8/144b monoclonal antibody recognizes cytokeratin 15 and defines the location of human hair follicle stem cells. *J. Cell Sci.* 111, 3179–3188.

Ma, L., Wang, J., Feng, S., Li, Y., Zhao, K., and Lei, M. (2016). Establishment of an *in vitro* culture model of single human hair follicle. *Zhonghua Zheng Xing Wai Ke Za Zhi* 32, 55–59.

Mackenzie, I. C. (1970). Relationship between mitosis and the ordered structure of the stratum corneum in mouse epidermis. *Nature* 226, 653–655. doi: 10.1038/226653a0

Mallipeddi, R. (2002). Epidermolysis bullosa and cancer. *Clin. Exp. Dermatol.* 27, 616–623. doi: 10.1046/j.1365-2230.2002.01130.x

Mansfield, K., and Naik, S. (2020). Unraveling immune-epithelial interactions in skin homeostasis and injury. *Yale J. Biol. Med.* 93, 133–143.

Martin, P., D'Souza, D., Martin, J., Grose, R., Cooper, L., Maki, R., et al. (2003). Wound healing in the PU.1 null mouse—tissue repair is not dependent on inflammatory cells. *Curr. Biol.* 13, 1122–1128. doi: 10.1016/s0960-9822(03)00396-8

Martin, P., and Nunan, R. (2015). Cellular and molecular mechanisms of repair in acute and chronic wound healing. *Br. J. Dermatol.* 173, 370–378. doi: 10.1111/bjd.13954

Mathur, A. N., Zirak, B., Boothby, I. C., Tan, M., Cohen, J. N., Mauro, T. N., et al. (2019). Treg-cell control of a CXCL5-IL-17 inflammatory axis promotes hair-follicle-stem-cell differentiation During Skin-Barrier Repair. *Immunity* 50, 655–667.e4. doi: 10.1016/j.immuni.2019.02.013

Medina, C. B., Mehrotra, P., Arandjelovic, S., Perry, J. S. A., Guo, Y., Morioka, S., et al. (2020). Metabolites released from apoptotic cells act as tissue messengers. *Nature* 580, 130–135. doi: 10.1038/s41586-020-2121-3

Minutti, C. M., Knipper, J. A., Allen, J. E., and Zaiss, D. M. W. (2017). Tissue-specific contribution of macrophages to wound healing. *Semin. Cell Dev. Biol.* 61, 3–11. doi: 10.1016/j.semcdb.2016.08.006

Moldovan, N. I. (2002). Role of monocytes and macrophages in adult angiogenesis: a light at the Tunnel's End. *J. Hematother. Stem Cell Res.* 11, 179–194. doi: 10.1089/152581602753658394

Morales, J., Homey, B., Vicari, A. P., Hudak, S., Oldham, E., Hedrick, J., et al. (1999). CTACK, a skin-associated chemokine that preferentially attracts skin-homing memory T cells. *Proc. Natl. Acad. Sci. U.S.A.* 96, 14470–14475. doi: 10.1073/pnas.96.25.14470

Morgun, E. I., Pozdniakova, E. D., and Vorotelyak, E. A. (2020). Expression of protein kinases RIPK-1 and RIPK-3 in mousee and human hair follicle. Doklady Rossiiskoi Akademii Nauk. *Nauki o Zhizni* 494, 500–503. doi: 10.1134/S1607672920050105 [in English - Doklady Biochemistry and Biophysics (in press)].

Moriwaki, K., Balaji, S., McQuade, T., Malhotra, N., Kang, J., and Chan, F. (2014). The necroptosis adaptor RIPK3 promotes injury-induced cytokine expression and tissue repair. *Immunity* 41, 567–578. doi: 10.1016/j.immuni.2014.09.016

Moriwaki, K., Bertin, J., Gough, P., and Chan, F. K.-M. (2015). A RIPK3–Caspase 8 complex mediates atypical Pro–IL-1β Processing. *J. Immunol.* 194, 1938–1944. doi: 10.4049/jimmunol.1402167

Morris, R. J., Liu, Y., Marles, L., Yang, Z., Tremous, C., Li, S., et al. (2004). Capturing and profiling adult hair follicle stem cells. *Nat. Biotechnol.* 22, 411–417. doi: 10.1038/nbt950

Mussano, F., Genova, T., Munaron, L., Petrillo, S., Erovigni, F., and Carossa, S. (2016). Cytokine, chemokine, and growth factor profile of platelet-rich plasma. *Platelets* 27, 467–471. doi: 10.3109/09537104.2016.1143922

Myung, P. S., Takeo, M., Ito, M., and Atit, R. P. (2013). Epithelial Wnt ligand secretion is required for adult hair follicle growth and regeneration. *J. Invest. Dermatol.* 133, 31–41. doi: 10.1038/jid.2012.230

Nagata, S. (2018). Apoptosis and clearance of apoptotic cells. *Annu. Rev. Immunol.* 36, 489–517. doi: 10.1146/annurev-immunol-042617-053010

Naik, S., Larsen, S. B., Cowley, C. J., and Fuchs, E. (2018). Two to tango: dialog between immunity and stem cells in health and dsease. *Cell* 175, 908–920. doi: 10.1016/j.cell.2018.08.071

Naik, S., Larsen, S. B., Gomez, N. C., Alaverdyan, K., Sendoel, A., Yuan, S., et al. (2017). Inflammatory memory sensitizes skin epithelial stem cells to tissue damage. *Nature* 550, 475–480. doi: 10.1038/nature24271

Nakamizo, S., Egawa, G., Tan, J. T. K., and Kabashima, K. (2020). Intravital imaging of cutaneous immune responses. *Cell. Immunol.* 350:103813. doi: 10.1016/j.cellimm.2018.05.006

Nanba, D., Toki, F., Tate, S., Imai, M., Matsushita, N., Shiraishi, K., et al. (2015). Cell motion predicts human epidermal stemness. *J. Exp. Med.* 212:2125OIA31. doi: 10.1084/jem.2125oia31

Nelson, A. M., Katseff, A. S., Ratliff, T. S., and Garza, L. A. (2016a). Interleukin 6 and STAT3 regulate p63 isoform expression in keratinocytes during regeneration. *Exp. Dermatol.* 25, 155–157. doi: 10.1111/exd.12896_A

Nelson, A. M., Katseff, A. S., Resnik, S. R., Ratliff, T. S., Zhu, A. S., and Garza, L. A. (2016b). Interleukin-6 null mice paradoxically display increased STAT3 activity and wound-induced hair neogenesis. *J. Invest. Dermatol.* 136, 1051–1053. doi: 10.1016/j.jid.2015.12.043_B

Nelson, A. M., Loy, D. E., Lawson, J. A., Katseff, A. S., FitzGerald, G. A., and Garza, L. A. (2013). Prostaglandin D2 inhibits wound-induced hair follicle neogenesis through the receptor, Gpr44. *J. Invest. Dermatol.* 133, 881–889. doi: 10.1038/jid.2012.398

Nelson, A. M., Reddy, S. K., Ratliff, T. S., Hossain, M. Z., Katseff, A. S., Zhu, A. S., et al. (2015). dsRNA released by tissue damage activates TLR3 to drive skin regeneration. *Cell Stem Cell* 17, 139–151. doi: 10.1016/j.stem.2015.07.008

Oh, J. W., Kloepper, J., Langan, E. A., Kim, Y., Yeo, J., Kim, M. J., et al. (2016). A guide to studying human hair follicle cycling *in vivo*. *J. Invest. Dermat.* 136, 34–44. doi: 10.1038/JID.2015.354

Osaka, N., Takahashi, T., Murakami, S., Matsuzawa, A., Noguchi, T., Fujiwara, T., et al. (2007). ASK1-dependent recruitment and activation of macrophages induce hair growth in skin wounds. *J. Exp. Med.* 204:i9. doi: 10.1084/jem2044oia9

Panteleyev, A. A., Jahoda, C. A. B., and Christiano, A. M. (2001). Hair follicle predetermination. *J. Cell Sci.* 114, 3419–3431.

Paus, R., and Cotsarelis, G. (1999). The biology of hair follicles. *N. Engl. J. Med.* 341, 491–497.

Plikus, M. V., Guerrero-Juarez, C. F., Treffeisen, E., and Gay, D. V. (2015). Epigenetic control of skin and hair regeneration after wounding. *Exp. Dermatol.* 24, 167–170. doi: 10.1111/exd.12488

Potten, C. S. (1974). The epidermal proliferative unit: the possible role of the central basal cell. *Cell Prolif.* 7, 77–88. doi: 10.1111/j.1365-2184.1974.tb00401.x

Proksch, E., Brandner, J. M., and Jensen, J.-M. (2008). The skin: an indispensable barrier. *Exp. Dermatol.* 17, 1063–1072. doi: 10.1111/j.1600-0625.2008.00786.x

Qing, C. (2017). The molecular biology in wound healing & non-healing wound. *Chin. J. Traumatol.* 20, 189–193. doi: 10.1016/j.cjtee.2017.06.001

Rahmani, W., Sinha, S., and Biernaskie, J. (2020). Immune modulation of hair follicle regeneration. *NPJ Regen. Med.* 5:9. doi: 10.1038/s41536-020-0095-2

Rajendran, R. L., Gangadaran, P., Seo, C. H., Kwack, M. H., Oh, J. M., Lee, H. W., et al. (2020). Macrophage-derived extracellular vesicle promotes hair growth. *Cells* 9:856. doi: 10.3390/cells9040856

Ramirez, K., Witherden, D. A., and Havran, W. L. (2015). All hands on DE(T)C: epithelial-resident γδ T cells respond to tissue injury. *Cell. Immunol.* 296, 57–61. doi: 10.1016/j.cellimm.2015.04.003

Rippa, A. L., Kalabusheva, E. P., and Vorotelyak, E. A. (2019). Regeneration of dermis: scarring and cells involved. *Cells* 8:607. doi: 10.3390/cells8060607

Rishikaysh, P., Dev, K., Diaz, D., Qureshi, W. M. S., Filip, S., and Mokry, J. (2014). Signaling involved in hair follicle morphogenesis and development. *Int. J. Mol. Sci.* 15, 1647–1670. doi: 10.3390/ijms15011647

Rognoni, E., and Watt, F. M. (2018). Skin cell heterogeneity in development, wound healing, and cancer. *Trends Cell Biol.* 28, 709–722. doi: 10.1016/j.tcb.2018.05.002

Rompolas, P., and Greco, V. (2014). Stem cell dynamics in the hair follicle niche. *Semin. Cell Dev. Biol.* 2, 34–42. doi: 10.1016/j.semcdb.2013.12.005

Rutkowski, J. M., Boardman, K. C., and Swartz, M. A. (2006). Characterization of lymphangiogenesis in a model of adult skin regeneration. *Am. J. Physiol. Heart Circ. Physiol.* 291, H1402–H1410. doi: 10.1152/ajpheart.00038.2006

Saito, N., Honma, M., Shibuya, T., Iinuma, S., Igawa, S., Kishibe, M., et al. (2018). RIPK1 downregulation in keratinocyte enhances TRAIL signaling in psoriasis. *J. Dermatol. Sci.* 91, 79–86. doi: 10.1016/j.jdermsci.2018.04.007

Salomon, G. D., Kasid, A., Cromack, D. T., Director, E., Talbot, T. L., Sank, A., et al. (1991). The local effects of cachectin/tumor necrosis factor on wound healing. *Ann. Surg.* 214, 175–180. doi: 10.1097/00000658-199108000-00012

Sano, S., Kira, M., Takagi, S., Yoshikawa, K., Takeda, J., and Itami, S. (2000). Two distinct signaling pathways in hair cycle induction: Stat3-dependent and -independent pathways. *Proc. Natl. Acad. Sci. U.S.A.* 97, 13824–13829. doi: 10.1073/pnas.240303097

Santoro, M. M., and Gaudino, G. (2005). Cellular and molecular facets of keratinocyte reepithelization during wound healing. *Exp. Cell Res.* 304, 274–286. doi: 10.1016/j.yexcr.2004.10.033

Sasaki, J. R., Zhang, Q., and Schwacha, M. G. (2011). Burn induces a Th-17 inflammatory response at the injury site. *Burns* 37, 646–651. doi: 10.1016/j.burns.2011.01.028

Sasaki, S., Hozumi, Y., and Kondo, S. (2005). Influence of prostaglandin F2alpha and its analogues on hair regrowth and follicular melanogenesis in a murine model. *Exp. Dermatol.* 14, 323–328. doi: 10.1111/j.0906-6705.2005.00270.x

Schaffer, M. R., Efron, P. A., Thorton, F. J., Klingel, K., Gross, S., and Barbul, A. (1997). Nitric oxide, an autocrine regulator of wound fibroblast synthetic function. *J. Immunol.* 158, 2275–2381.

Scharschmidt, T. C., Vasquez, K. S., Pauli, M., Leitner, E., Chu, K., Truong, H., et al. (2017). Commensal microbes and hair follicle morphogenesis coordinately

drive treg migration into neonatal skin. *Cell Host Microbe* 21, 467–477.e5. doi: 10.1016/j.chom.2017.03.001

Seya, T., Shime, H., Takaki, H., Azuma, M., Oshiumi, H., and Matsumoto, M. (2012). TLR3/TICAM-1 signaling in tumor cell RIP3-dependent necroptosis. *Oncoimmunology* 1, 917–923. doi: 10.4161/onci.21244

Sharp, L. L., Jameson, J. M., Cauvi, G., and Havran, W. L. (2005). Dendritic epidermal T cells regulate skin homeostasis through local production of insulin-like growth factor 1. *Nat. Immunol.* 6, 73–79. doi: 10.1038/ni1152

Siqueira, M. F., Li, J., Chehab, L., Desta, T., Chino, T., Krothpali, N., et al. (2010). Impaired wound healing in mouse models of diabetes is mediated by TNF-α dysregulation and associated with enhanced activation of forkhead box O1 (FOXO1). *Diabetologia* 53, 378–388. doi: 10.1007/s00125-009-1529-y

Snippert, H. J., Haegebarth, A., Kasper, M., Jaks, V., van Es, J. H., Barker, N., et al. (2010). Lgr6 marks stem cells in the hair follicle that generate all cell lineages of the skin. *Science* 327, 1385–1389. doi: 10.1126/science.1184733

Solanas, G., and Benitah, S. A. (2013). Regenerating the skin: a task for the heterogeneous stem cell pool and surrounding niche. *Nat. Rev. Mol. Cell Biol.* 14, 737–748. doi: 10.1038/nrm3675

Squarize, C. H., Castilho, R. M., Bugge, T. H., and Gutkind, J. S. (2010). Accelerated wound healing by mTOR activation in genetically defined mouse models. *PLoS One* 5:e10643. doi: 10.1371/journal.pone.0010643

Su, W. H., Cheng, M. H., Lee, W. L., Tsou, T. S., Chang, W. H., Chen, C. S., et al. (2010). Nonsteroidal anti-inflammatory drugs for wounds: pain relief or excessive scar formation? *Mediators Inflamm.* 2010:413238. doi: 10.1155/2010/413238

Sun, X., Are, A., Annusver, K., Sivan, U., Jacob, T., Dalessandri, T., et al. (2020). Coordinated hedgehog signaling induces new hair follicles in adult skin. *eLife* 9:e46756. doi: 10.7554/elife.46756

Tadokoro, S., Ide, S., Tokuyama, R., Umeki, H., Tatehara, S., Kataoka, S., et al. (2015). Leptin promotes wound healing in the skin. *PLoS One* 10:e0121242. doi: 10.1371/journal.pone.0121242

Takada, K., Komine-Aizawa, S., Hirohata, N., Trinh, Q. D., Nishina, A., Kimura, H., et al. (2017). Poly I:C induces collective migration of HaCaT keratinocytes via IL-8. *BMC Immunol.* 18:19. doi: 10.1186/s12865-017-0202-3

Takahashi, N., Vereecke, L., Bertrand, M. J. M., Duprez, L., Berger, S. B., Divert, T., et al. (2014). RIPK1 ensures intestinal homeostasis by protecting the epithelium against apoptosis. *Nature* 513, 95–99. doi: 10.1038/nature13706

Takeo, M., Lee, W., and Ito, M. (2015). Wound healing and skin regeneration. *Cold Spring Harb. Perspect. Med.* 5, a023267. doi: 10.1101/cshperspect.a023267

Telerman, S. B., Rognoni, E., Sequeira, I., Pisco, A. O., Lichtenberger, B. M., Culley, O. J., et al. (2017). Dermal Blimp1 acts downstream of epidermal TGFβ and Wnt/β-catenin to regulate hair follicle formation and growth. *J. Invest. Dermatol.* 137, 2270–2281. doi: 10.1016/j.jid.2017.06.015

Terskikh, V. V., Vasiliev, A. V., and Vorotelyak, E. A. (2012). Label retaining cells and cutaneous stem cells. *Stem Cell Rev. Rep.* 8, 414–425. doi: 10.1007/s12015-011-9299-6

Thornton, F. J., Schaffer, M. R., Witte, M. B., Moldawer, L. L., MacKay, S. L., Abouhamze, A., et al. (1998). Enhanced collagen accumulation following direct transfection of the inducible nitric oxide synthase gene in cutaneous wounds. *Biochem. Biophys. Res. Commun.* 246, 654–659. doi: 10.1006/bbrc.1998.8681

Tong, X., and Coulombe, P. A. (2006). Keratin 17 modulates hair follicle cycling in a TNF-dependent fashion. *Genes Dev.* 20, 1353–1364. doi: 10.1101/gad.1387406

Valente Duarte de Sousa, I. C., and Tosti, A. (2013). New investigational drugs for androgenetic alopecia. *Expert Opin. Investig. Drugs* 22, 573–589. doi: 10.1517/13543784.2013.784743

Vande Walle, L., and Lamkanfi, M. (2016). Pyroptosis. *Curr. Biol.* 26, R568–R572. doi: 10.1016/j.cub.2016.02.019

Varfolomeev, E., and Vucic, D. (2018). Intracellular regulation of TNF activity in health and disease. *Cytokine* 101, 26–32. doi: 10.1016/j.cyto.2016.08.035

Wang, E. C. E., Dai, Z., Ferrante, A. W., Drake, C. G., and Christiano, A. M. (2019). A subset of TREM2+ dermal macrophages secretes oncostatin M to maintain hair follicle stem cell quiescence and Inhibit Hair Growth. *Cell Stem Cell* 24, 654–669.e6. doi: 10.1016/j.stem.2019.01.011

Wang, E. C. E., and Higgins, C. A. (2020). Immune cell regulation of the hair cycle. *Exp. Dermatol.* 29, 322–333. doi: 10.1111/exd.14070

Wang, X., Chen, H., Tian, R., Zhang, Y., Drutskaya, M. S., Wang, C., et al. (2017). Macrophages induce AKT/β-catenin-dependent Lgr5+ stem cell activation and hair follicle regeneration through TNF. *Nat. Commun.* 8:14091. doi: 10.1038/ncomms14091

Welle, M. M., and Wiener, D. J. (2016). The hair follicle. *Toxicol. Pathol.* 44, 564–574. doi: 10.1177/0192623316631843

Werner, S., and Grose, R. (2003). Regulation of wound healing by growth factors and cytokines. *Physiol. Rev.* 83, 835–870. doi: 10.1152/physrev.2003.83.3.835

Wolf, R., Schönfelder, G., Paul, M., and Blume-Peytavi, U. (2003). Nitric oxide in the human hair follicle: constitutive and dihydrotestosterone-induced nitric oxide synthase expression and NO production in dermal papilla cells. *J. Mol. Med.* 81, 110–117. doi: 10.1007/s00109-002-0402-y

Xu, F., Zhang, C., and Graves, D. T. (2013). Abnormal cell responses and role of TNF-α in impaired diabetic wound healing. *Biomed Res. Int.* 2013:754802. doi: 10.1155/2013/754802

Yamao, M., Inamatsu, M., Okada, T., Ogawa, Y., Ishida, Y., Tateno, C., et al. (2015). Restorative effect of hair follicular dermal cells on injured human hair follicles in a mouse model. *Exp. Dermatol.* 24, 225–227. doi: 10.1111/exd.12625

Zaiss, D. M., Minutti, C. M., and Knipper, J. A. (2019). Immune- and non-immune-mediated roles of regulatory T-cells during wound healing. *Immunology* 157, 190–197. doi: 10.1111/imm.13057

Zhang, J., Yang, X., Wang, H., Zhao, B., Wu, X., Su, L., et al. (2017). PKCζ as a promising therapeutic target for TNFα-induced inflammatory disorders in chronic cutaneous wounds. *Int. J. Mol. Med.* 40, 1335–1346. doi: 10.3892/ijmm.2017.3144

Zhao, J., Li, H., Zhou, R., Ma, G., Dekker, J. D., Tucker, H. O., et al. (2015). Foxp1 regulates the proliferation of hair follicle stem cells in response to oxidative stress during hair cycling. *PLoS One* 10:e0131674. doi: 10.1371/journal.pone.0131674

Zhao, R., Liang, H., Clarke, E., Jackson, C., and Xue, M. (2016). Inflammation in chronic wounds. *Int. J. Mol. Sci.* 17:2085. doi: 10.3390/ijms17122085

Zheng, M., Jang, Y., Choi, N., Kim, D. Y., Han, T. W., Yeo, J. H., et al. (2019). Hypoxia improves hair inductivity of dermal papilla cells via nuclear NADPH oxidase 4-mediated reactive oxygen species generation'. *Br. J. Dermatol.* 181, 523–534. doi: 10.1111/bjd.17706

Zhu, A. S., Li, A., Ratliff, T. S., Melsom, M., and Garza, L. A. (2017). After skin wounding, Noncoding dsRNA coordinates prostaglandins and wnts to promote regeneration. *J. Invest. Dermatol.* 137, 1562–1568. doi: 10.1016/j.jid.2017.03.023

Zhu, H., Wei, X., Bian, K., and Murad, F. (2008). Effects of nitric oxide on skin burn wound healing. *J. Burn Care Res.* 29, 804–814. doi: 10.1097/bcr.0b013e3181848119

Zhu, H. J., Li, Y. S., Wang, Y. P., Hu, X. H., Zhang, X. R., Qiu, L., et al. (2019). Effects of skin γδ T lymphocytes on wound healing of mice through regulating proliferation and differentiation of mice epidermal cells. *Zhonghua Shao Shang Za Zhi* 35, 298–307. doi: 10.3760/cma.j.issn.1009-2587.2019.04.010

Conflict of Interest: The authors declare that the research was conducted in the absence of any commercial or financial relationships that could be construed as a potential conflict of interest.

Copyright © 2020 Morgun and Vorotelyak. This is an open-access article distributed under the terms of the Creative Commons Attribution License (CC BY). The use, distribution or reproduction in other forums is permitted, provided the original author(s) and the copyright owner(s) are credited and that the original publication in this journal is cited, in accordance with accepted academic practice. No use, distribution or reproduction is permitted which does not comply with these terms.

frontiers in Cell and Developmental Biology

ORIGINAL RESEARCH
published: 24 November 2020
doi: 10.3389/fcell.2020.581528

"Two-Cell Assemblage" Assay: A Simple *in vitro* Method for Screening Hair Growth-Promoting Compounds

Sunhyae Jang[1,2,3†], Jungyoon Ohn[1,2,3†], Bo Mi Kang[1,2,3], Minji Park[1,2,3], Kyu Han Kim[1,2,3] and Ohsang Kwon[1,2,3*]

[1] Laboratory of Cutaneous Aging and Hair Research, Clinical Research Institute, Seoul National University Hospital, Seoul, South Korea, [2] Institute of Human Environment Interface Biology, Seoul National University, Seoul, South Korea, [3] Department of Dermatology, Seoul National University College of Medicine, Seoul, South Korea

Alopecia arises due to inadequate hair follicle (HF) stem cell activation or proliferation, resulting in prolongation of the telogen phase of the hair cycle. Increasing therapeutic and cosmetic demand for alleviating alopecia has driven research toward the discovery or synthesis of novel compounds that can promote hair growth by inducing HF stem cell activation or proliferation and initiating the anagen phase. Although several methods for evaluating the hair growth-promoting effects of candidate compounds are being used, most of these methods are difficult to use for large scale simultaneous screening of various compounds. Herein, we introduce a simple and reliable *in vitro* assay for the simultaneous screening of the hair growth-promoting effects of candidate compounds on a large scale. In this study, we first established a 3D co-culture system of human dermal papilla (hDP) cells and human outer root sheath (hORS) cells in an ultra-low attachment 96-well plate, where the two cell types constituted a polar elongated structure, named "two-cell assemblage (TCA)." We observed that the long axis length of the TCA gradually increased for 5 days, maintaining biological functional integrity as reflected by the increased expression levels of hair growth-associated genes after treatment with hair growth-promoting molecules. Interestingly, the elongation of the TCA was more prominent following treatment with the hair growth-promoting molecules (which occurred in a dose-dependent manner), compared to the control group ($p < 0.05$). Accordingly, we set the long axis length of the TCA as an endpoint of this assay, using a micro confocal high-content imaging system to measure the length, which can provide reproducible and reliable results in an adequate timescale. The advantages of this assay are: (i) it is physiologically and practically advantageous as it uses 3D cultured two-type human cells which are easily available; (ii) it is simple as it uses length as the only endpoint; and (iii) it is a high throughput system, which screens various compounds simultaneously. In conclusion, the "TCA" assay could serve as an easy and reliable method to validate the hair growth-promoting effect of a large volume of library molecules.

Keywords: alopecia, hair follicle, *in vitro* assay, outer root sheath cell, screening assay, dermal papilla cell

OPEN ACCESS

Edited by:
Sung-Jan Lin,
National Taiwan University, Taiwan

Reviewed by:
Zi-Bing Jin,
Capital Medical University, China
João Tadeu Ribeiro-Paes,
University of São Paulo, Brazil

****Correspondence:***
Ohsang Kwon
oskwon@snu.ac.kr

† These authors have contributed equally to this work

Specialty section:
This article was submitted to Stem Cell Research, a section of the journal Frontiers in Cell and Developmental Biology

Received: *09 July 2020*
Accepted: *30 October 2020*
Published: *24 November 2020*

Citation:
Jang S, Ohn J, Kang BM, Park M, Kim KH and Kwon O (2020) "Two-Cell Assemblage" Assay: A Simple in vitro Method for Screening Hair Growth-Promoting Compounds. Front. Cell Dev. Biol. 8:581528. doi: 10.3389/fcell.2020.581528

INTRODUCTION

Each mammalian hair follicle (HF) is a mini organ that undergoes regenerative cycling, consisting of the following phases: telogen (quiescence), anagen (regeneration), and catagen (degeneration) (Lei and Chuong, 2016). Inadequate HF stem cell activation or proliferation with telogen phase prolongation causes alopecia (Lei and Chuong, 2016). This condition can present in numerous pathologies, such as premature aging, overt hormonal effects, or drug side effects (Price, 1999). In terms of quality of life, alopecia is a distressing event affecting millions of people worldwide (Hunt and Mchale, 2005), potentially causing severe negative psychological effects (Cash, 1992).

To date, two FDA approved drugs, finasteride and minoxidil (MNX), are used to treat patients with certain types of alopecia in respect of modulating the HF regeneration cycle and promoting hair growth (Rittmaster, 1994; Messenger and Rundegren, 2004). However, new molecules that can effectively treat alopecia are needed, considering the limited usage range and/or ineffectiveness of finasteride and MNX in a proportion of patients. The increasing therapeutic and cosmetic demand for the alleviation of alopecia has driven research toward the discovery or synthesis of novel compounds that can promote hair growth by mirroring HF stem cell activation or proliferation and initiating the anagen phase.

To date, several methods for evaluating the hair growth-promoting effects of candidate compounds have been used: *in vitro* human dermal papilla (hDP) and human outer root sheath (hORS) cell assays, *ex vivo* human HF (hHF) organ culture, and animal models (Ohn et al., 2019). However, most of these methods are difficult to use for large scale simultaneous screening of various compounds, because of the limited availability of hHFs (Havlickova et al., 2009). In order to screen the hair growth-promoting efficacy of candidate substances in a large molecular library scale, an easily obtainable and accessible platform is essential. Herein, we introduce a simple and reliable *in vitro* assay, named the "two-cell assemblage (TCA)" assay, using two types of hHF-constituting cells, hDP and hORS, for the simultaneous screening of the hair growth-promoting effects of candidate compounds on a large scale.

MATERIALS AND METHODS

Ethics Statement

This study protocol was approved by the Institutional Review Board of Seoul National University (2005-067-1124), adhering to Helsinki guidelines. All subjects provided written informed consent before scalp skin tissues were taken.

hDP and hORS Cells Preparation

Healthy young Koreans, with no obvious scalp diseases, provided occipital scalp skin tissue for this study. From the tissue, hHFs were isolated and dissected into single follicular units with a No. 20 blade under a stereomicroscope (Olympus). The micro-dissected hHFs were used for primary hDP and hORS cell cultures. The hDP cells were cultured as described previously (Magerl et al., 2002). In short, candlelight-shaped dermal papilla (DP) of HFs were dissociated in Dulbecco's Modified Eagle's Medium (Welgene) supplemented with 10% fetal bovine serum (Welgene) and antibiotic/antimycotic solution (penicillin and streptomycin; Gibco). For hORS cells, the hair shaft and bulb region of the dissected hHF were cut off and immersed in DMEM supplemented with 20% FBS, as described by Choi et al. (2019). On the third day, the medium was changed to Epilife medium (Gibco) supplemented with human keratinocyte growth supplement (Gibco) and antibiotics/antimycotics. We used a fluorochrome (Cell Tracker CM-DiI Dye or Qtracker 525 Cell Labeling Kit, Invitrogen), in accordance with the manufacturer's instruction, to label the cultured hORS or hDP cells, respectively. All cells were kept in a humidified 5% CO_2 atmosphere at 37°C.

TCA Structure Preparation and Treatment With Hair Growth-Promoting Molecules

The TCA assay employed herein is a simple *in vitro* method for screening hair growth-promoting compounds. Each TCA structure was prepared in an ultra-low attachment 96-well plate (**Figure 1A**), in which the two kinds of human cells (3D co-cultured hDP and hORS) constituted a unipolar elongated structure (**Figure 1B**). In detail, the cultured hDP cells (passage 2 or 3; 5×10^3 cells/well) were combined in a single cell suspension and seeded in each well of the 96-well plate in Dulbecco's Modified Eagle's Medium supplemented with 10% fetal bovine serum and an antibiotic/antimycotic solution. The seeded hDP cells amassed and aggregated into a spherical structure in each well on day 0. On day 1, we added cultured hORS cells (passage 2 or 3; 5×10^3 cells/well) into each well, replacing the media with William's E medium (Gibco) supplemented with 2 mM L-glutamine, 10 ng/mL hydrocortisone, and 10 μg/mL insulin. From days 1 to 5, culture media supplemented with each hair growth-promoting molecule at the designated concentration was used for the TCA culture and changed every other day (**Figure 1B**). All procedures were undertaken at 37°C in a 5% CO_2 atmosphere.

Hematoxylin/Eosin (H&E) and Immunofluorescence Staining

Two-cell assemblage structures were mounted in Tissue-Tek cryo-OCT compound (Thermo Fisher) and frozen on dry ice. The frozen blocks were sectioned at a thickness of 8 μm at −25°C and were stained with hematoxylin/eosin (H&E). For immunofluorescence staining, the cryosections were incubated at 4°C overnight in a primary mouse antibody against human alkaline phosphatase (ALP) or Keratin 14 (K14), diluted in diluent reagent (Invitrogen). The nuclei were counterstained with 4′,6-diamidino-2-phenylindole (DAPI; Invitrogen). The stained slides were observed and photographed under a Nikon Eclipse Ci-L microscope or a Nikon Eclipse Ni-E fluorescence microscope (Nikon).

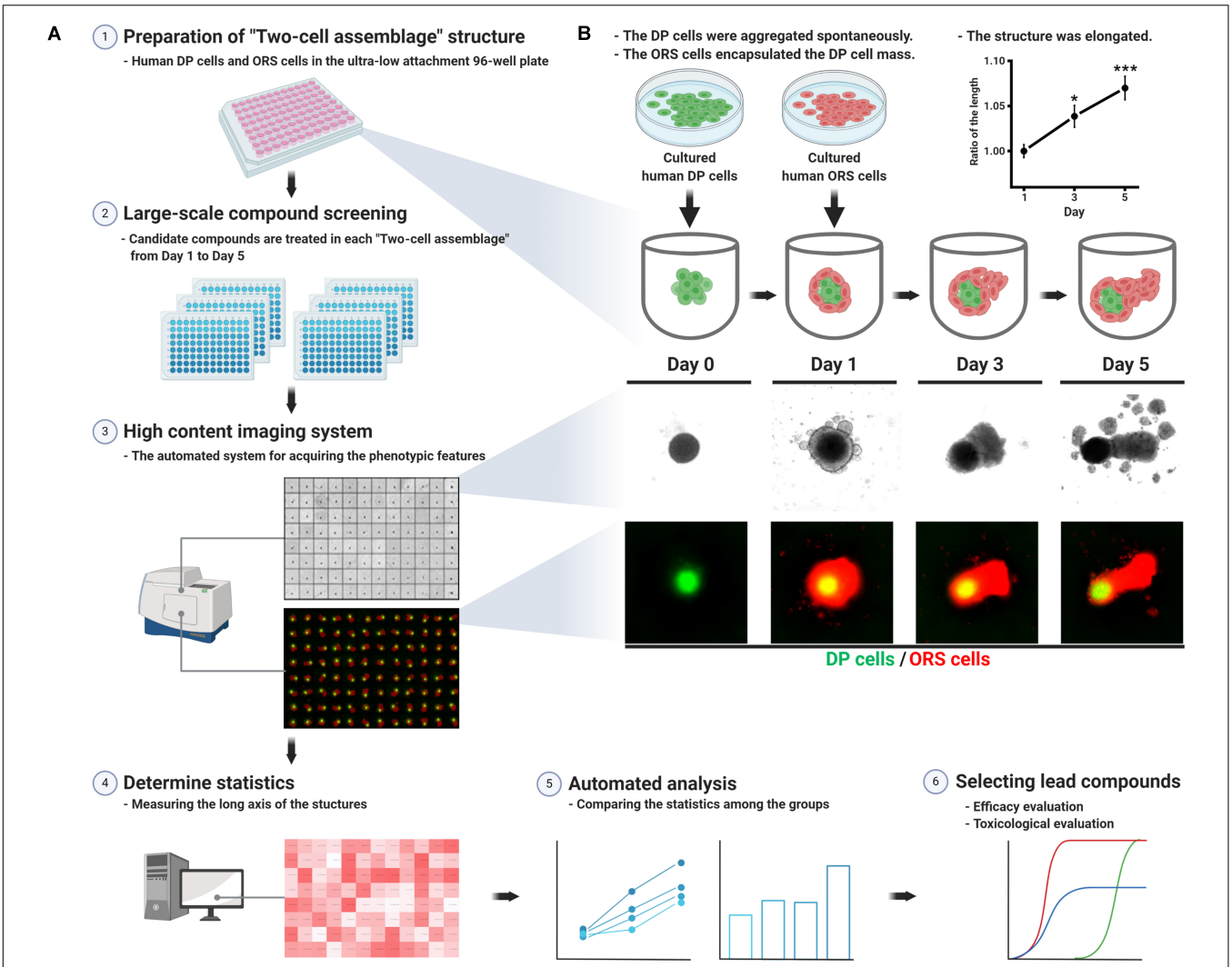

FIGURE 1 | Schematic work flow for preparing the "two-cell assemblage (TCA)" structure and screening hair growth-promoting compounds. **(A)** Each TCA was loaded into each well of the ultra-low attachment 96-well plate, in which candidate compounds were treated for 5 days. The long axis length of the TCAs was acquired using a high content imaging system. The data for each candidate compound-treated group were compared to reveal the most effective compound, which would then require further evaluation. **(B)** Preparation of the TCA consisting of human dermal papilla (hDP) and human outer root sheath (hORS) cells, which was elongated for 5 days. The long axis length was measured without any treatment and compared with the culture day time points (right upper panel, data are presented as mean ± SEM and were evaluated using one-way analysis of variance with Tukey's multiple comparisons test. $^{*}p < 0.05$ or $^{***}p < 0.001$, compared to day 1).

Quantitative Real-Time Polymerase Chain Reaction (qPCR)

Experiments were performed by pooling 48 TCA structures for each quantitative real-time polymerase chain reaction (qPCR) experiment. Total RNA was isolated from the collected TCA structures 24 h after each hair growth-promoting molecule was used, using RNA iso Plus (TaKaRa Bio) and DNase I (Roche Pharmaceuticals). We used 1 μg of total RNA for the cDNA synthesis using a First Strand cDNA Synthesis Kit (Fermentas), according to the manufacturer's instructions. The qPCR was performed in a 7500 Real-Time PCR System (Applied Biosystems) using SYBR Premix Ex Taq (TaKaRa Bio), according to the manufacturer's instructions. The primer sequences are shown in **Table 1**. All experiments were performed in triplicate and were independently repeated three or four times. Data are presented as fold change relative to a control group, which was normalized to GAPDH expression.

Image Acquisition for TCA and Statistical Analysis

A high content screening system (ImageXpress Micro Confocal High-Content Imaging System, Molecular Devices) was used for TCA image acquisition from day 1 to 5, every other day (**Figure 1**). Quantification of the long axis length of the TCA structures was performed automatically, based on the statistical analysis being employed. All statistical analyses were performed in the Prism 8 software package (GraphPad Software), using the Kruskal–Wallis test with a *post hoc* test, one-way analysis of

TABLE 1 | Primer sequence for real-time polymerase chain reaction.

Human VEGFA	
Sense	ACT TCT GGG CTG TTC TCG
Antisense	TCC TCT TCC TTC TCT TCT TC
Human HGF	
Sense	CGC AGC TAC AAG GGA ACA GT
Antisense	TCC TGT AGG TCT TTA CCC CGA
Human IGF-1	
Sense	TTC AAC AAG CCC ACA GGG
Antisense	GGT GCG CAA TAC ATC TCC
Human FGF-7	
Sense	TTG TGG CAA TCA AAG GGG TG
Antisense	CCT CCG TTG TGT GTC CAT TT
Human FGF-10	
Sense	TTC AAG GAG ATG TCC GCT
Antisense	GAT GCT GTA CGG GCA GTT
Human PDGFA	
Sense	GCC CAT TCG GAG GAA GAG
Antisense	TTG GCC ACC TTG ACG CTG CG
Human PDGFB	
Sense	GAA GGA GCC TGG GTT CCC
Antisense	TTT CTC ACC TGG ACA GGT

variance with a *post hoc* test, or two-way analysis of variance with a *post hoc* test. All tests were two-tailed, and $p < 0.05$ was considered statistically significant.

RESULTS

TCA Structures Configured Spontaneously and Elongated in a Unipolar Manner Over 5 Days

The hDP cells seeded in the ultra-low attachment 96-well plate spontaneously aggregated into a 3D spherical structure within 24 h. The spheroidal hDP cellular mass was surrounded by hORS cells, which were subsequently seeded, resulting in a TCA structure (**Figure 1B**). The TCA became elongated in a unipolar manner over the 5 days of the study, with a statistically significant difference in the long axis length on day 5 compared to day 1 (**Figure 1B**, upper right panel). The hORS cells in the TCA constituted the elongated portion of the structure (**Figure 1B**).

The Microstructure of the TCA *in vitro*

Microscopic observation of the H&E stained TCA revealed spatial segregation in the inner cell mass and the outer shell cell layer (**Figure 2**). To check whether the inner cell mass was composed of hDP cells, we performed immunohistochemical staining for ALP, a signature marker of DP cells (Yang and Cotsarelis, 2010). Indeed, ALP was detected in the inner cellular mass, indicating that the amassed cells were hDP cells, as they mimicked the DP structure of an intact hHF organ (**Figure 2**). Immunofluorescent staining for K14 confirmed that the cells in the outer shell cell layer and the elongated portion of the TCA were hORS cells (Stark et al., 1987) (**Figure 2**). Furthermore, we used a cell tracking method to check the origin of the inner cell mass and outer shell cell layer. Green and red fluorescent colors were detected in the inner mass and the outer layer, respectively, confirming that our cultured hDP and hORS cells constituted the TCA structure (**Figures 1B**, **2**).

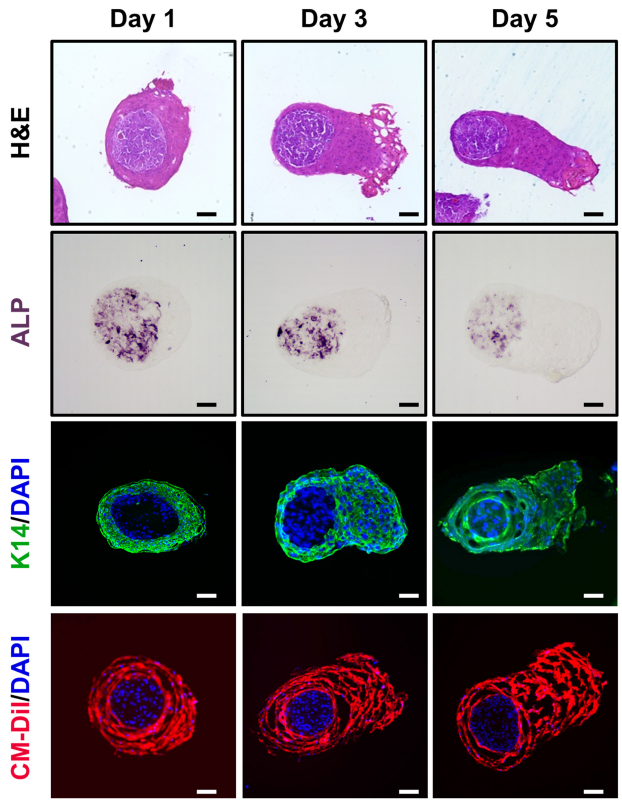

FIGURE 2 | Histological characterizations of the "two-cell assemblage (TCA)" structure. Microscopic images of the TCA were visualized at days 1, 3, and 5 of culture, using hematoxylin and eosin stain, immunohistochemical stain (alkaline phosphatase, ALP), or immunofluorescence stain (keratin 14, K14; cell-labeling dye, CM-Dil). Bar: 100 μm.

Hair Growth-Associated Gene Expression in the TCA Increased After Treatment With Hair Growth-Promoting Molecules

To evaluate the biological integrity of the TCA structure consisting of hDP and hORS cells, we measured the expression of hair growth-associated genes using real-time PCR, after treatment with well-established hair growth-promoting molecules, namely, MNX (Messenger and Rundegren, 2004), valproic acid (Jo et al., 2014), purmophamine (Paladini et al., 2005), and tofacitinib (Harel et al., 2015). If treatment of the established HF growth promotors on the TCA induced notable changes in the expression of genes associated with regulating HF growth or cycling, it could be inferred that the TCA would function as a suitable model for a HF mimetic. Among the hair growth-associated genes, we checked the mRNA expression levels

of vascular endothelial growth factor (VEGF) (Yano et al., 2001), hepatocyte growth factor (HGF) (Shimaoka et al., 1995), insulin-like growth factor 1 (IGF1) (Philpott et al., 1994), fibroblast growth factor (FGF) 7 (Iino et al., 2007), FGF10 (Jang, 2005), and platelet-derived growth factor (alpha and beta; PDGFA and PDGFB) (Tomita et al., 2006) in the TCA (**Figure 3**). Indeed, most of the investigated genes showed increased expression levels with statistical significance after treatment with the hair growth-promoting molecules (**Figure 3**). Thus, we confirmed that the TCA maintained biological functional integrity when reacting to hair growth-promoting molecules.

The Phenotypic Feature of the TCA as an Indicator of Hair Growth-Promoting Potential

Based on the findings that the TCA was elongated in the *in vitro* culture environment and had intact biological functionality, we observed its phenotypic features every other day during treatment with the hair growth-promoting molecules, paying particular attention to the long axis length. We used a micro confocal high-content imaging system, which could provide reproducible and reliable results in a timely manner when carrying out statistical analyses. Interestingly, we observed that the degree of TCA elongation increased with increasing treatment of the hair growth-promoting molecules (**Figure 4A**). On the fifth day of culture, for all molecules, we observed a statistically significant difference in the length of the TCA compared to each control group, revealing that the TCAs in groups treated with hair growth-promoting molecules were elongated prominently in a dose-dependent manner, compared to those in the control group (**Figure 4A**). The long axis length of the TCA on day 5 (**Figure 4B**) serves as an indication of the hair growth-promoting potential of the candidate molecule.

DISCUSSION

To date, several methods for evaluating the hair growth-promoting effects of candidate compounds have been used,

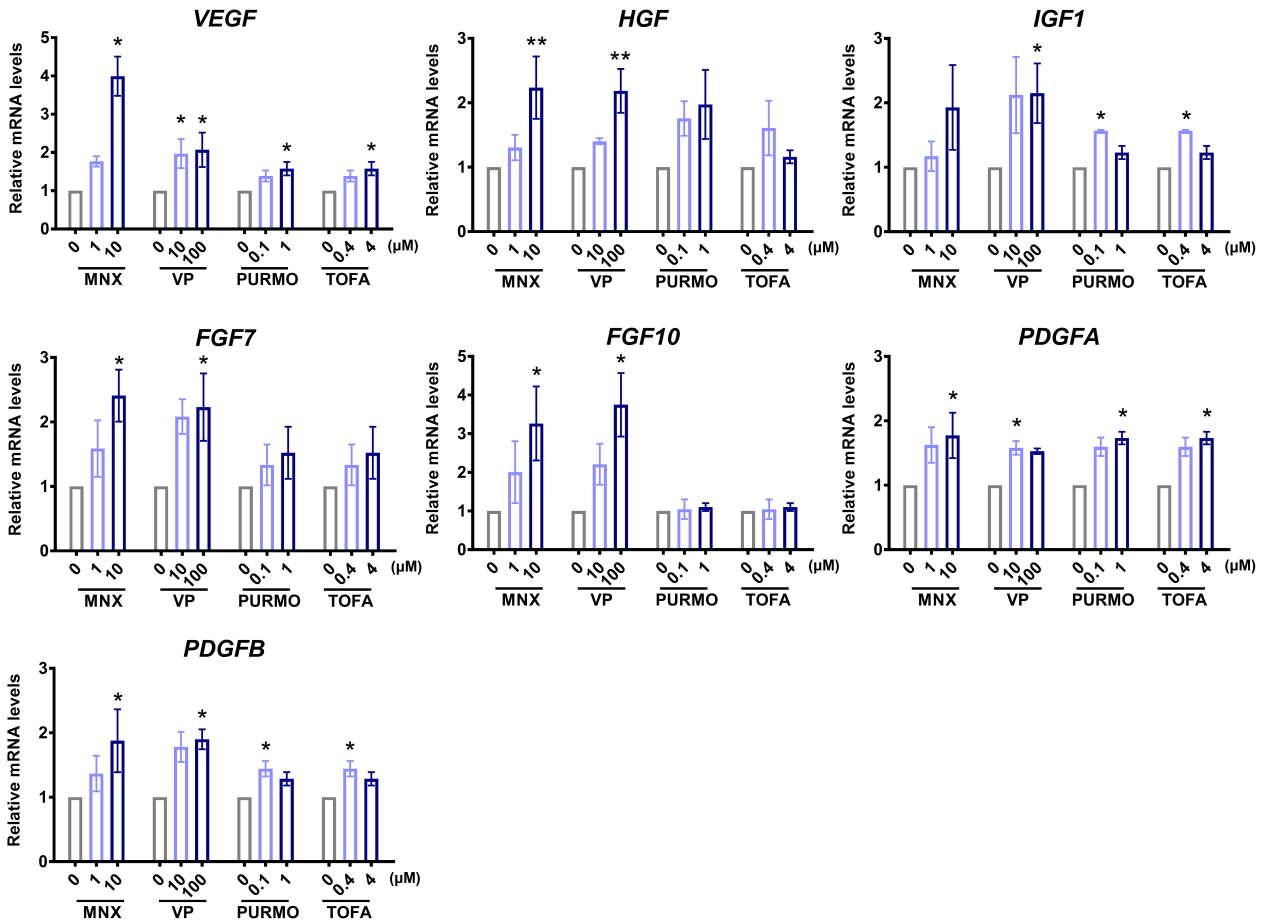

FIGURE 3 | Characterizations of biological functionality in the "two-cell assemblage (TCA)" structure. Quantitative analysis of changes in the expression of hair growth-associated genes of the TCA after treatment with minoxidil (MNX), valproic acid (VP), purmophamine (PURMO), or tofacitinib (TOFA). The expression levels of genes were normalized to levels of the reference gene, GAPDH. Data are presented as mean ± SEM and were evaluated using the Kruskal–Wallis test with Dunn's multiple comparison test.*$p < 0.05$ or **$p < 0.01$, compared to each control group (0 μM). Three or four independent experiments were carried out for each condition.

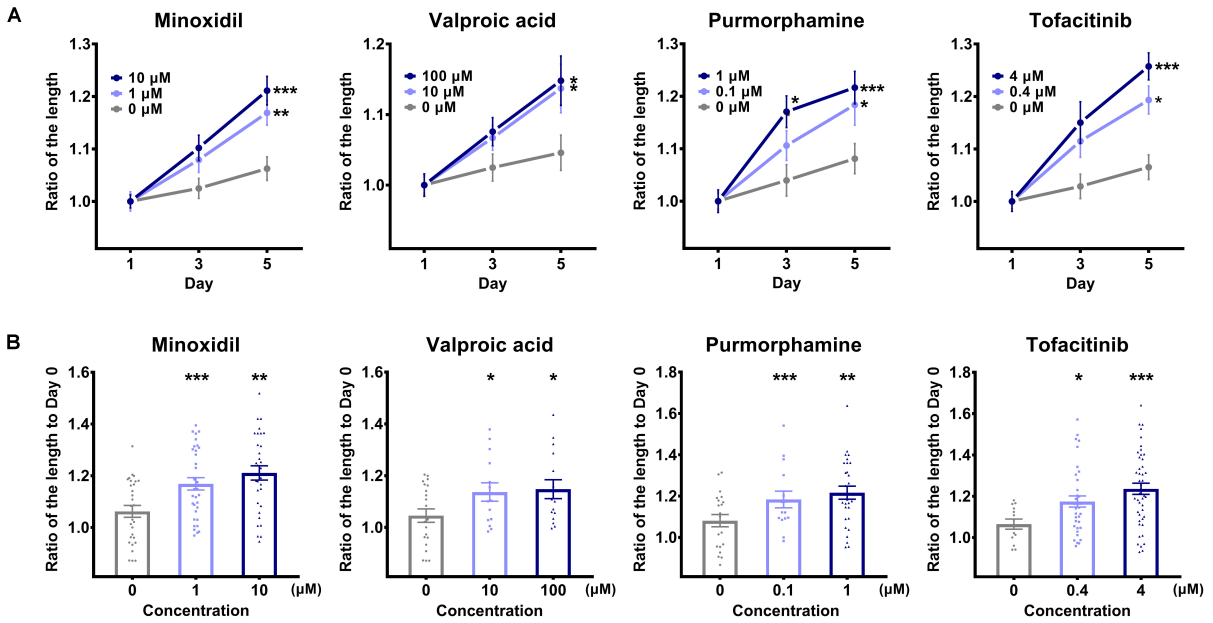

FIGURE 4 | Comparison of the long axis length of the "two-cell assemblage (TCA)" structure. **(A)** The long axis length of the TCA was compared after treatment with each molecule, with designated concentrations on the TCA structures, across three time points. Data are presented as mean ± SEM and were evaluated using one-way analysis of variance with Tukey's multiple comparisons test. $^{*}p < 0.05$, $^{**}p < 0.01$, or $^{***}p < 0.001$, compared to each control group on day 1. **(B)** The long axis length of the TCA was compared on day 5 among the different concentrations of each molecule. Data are presented as mean ± SEM and were evaluated using one-way analysis of variance with Tukey's multiple comparisons test. $^{*}p < 0.05$, $^{**}p < 0.01$, or $^{***}p < 0.001$, compared to each control group (0 μM).

mainly based on hHF cells or the hHF organ (Yoo et al., 2010). Additionally, a human epidermal keratinocytes-based system measuring TGF-β1 promoter activity has been proposed (Huh et al., 2009). Although the hHF organ culture method has the advantage of being reliable (Philpott et al., 1996), its limited availability makes it difficult to screen many compounds. In order to evaluate and compare the hair growth-promoting efficacy of candidate substances in a large molecular library at once, an easily obtainable and accessible platform is necessary.

We established, herein, an hDP cellular mass structure as a backbone of the TCA assay. hDP cells are commercially available and can be easily cultured and mass produced. Indeed, *in vitro* assays using hDP cells have been widely used as validating models for hair growth-promoting molecules (Madaan et al., 2018), based on the fact that DP play crucial roles in hair growth and HF regeneration by regulating HF cells (Yang and Cotsarelis, 2010; Lei et al., 2017b). In this assay, hDP cells were observed to have spontaneously aggregated into a spherical structure within 24 h, which is consistent with previous studies (Higgins et al., 2010; Huang et al., 2013; Topouzi et al., 2017). The cellular properties of 3D spheroid cultured hDP cells were different from those observed for cultured cells in a 2D culture environment (Higgins et al., 2010). These differences include enhanced expression profiles of key DP signature genes (Gupta et al., 2018; Tan et al., 2019), and HF inductive ability (Kang et al., 2012; Higgins et al., 2013), suggesting that 3D cultured hDP cells are more similar, having exhibited physiologic intact DP status *in vivo*. Consequently, 3D cultured hDP spheroid-based drug assay systems that employ direct quantitation of DP cell proliferation or enhanced gene expression of growth factors and extracellular matrix proteins as efficacy indicators after treatment with hair growth-modulating molecules have been suggested (Lim et al., 2013; Gupta et al., 2018).

However, hDP cells alone cannot fully reflect the HF growth-promoting effect of candidate molecules, as HF is a mini-organ consisting of epithelial and mesenchymal components that interact reciprocally (Rendl et al., 2005; Chan et al., 2015; Huang et al., 2017). Accordingly, we grafted hORS cells into the 3D spheroid hDP cell mass structures to mimic the epithelial part of the HF, maintaining the spatial separation of two kinds of cells, thus resembling HF *in vivo*. We observed that the dissociated hORS cells encapsulated the hDP cell mass without any manipulation. Indeed, it has previously been found that dissociated skin cells have the potential to undergo a self-organization process (Lei et al., 2017a; Weber et al., 2019). The inner core–outer shell micro structures with unipolar orientation were not limited to our hORS and DP cell co-culture model. A recent study found that a keratinocyte and hDP cell co-culture system formed a similar structure with migratory polarization conserving central hDP cell aggregation (Tan et al., 2019). In another study attempting to establish an *in vitro* 3D organoid model, DP spheroids with a silk-gelatin were encapsulated by HF epithelial cells in a co-culture system (Gupta et al., 2018). Furthermore, hDP cell aggregates cultured with epithelial cells more prominently expressed DP-specific signature genes than those without epithelial cells (Gupta et al., 2018; Kageyama et al., 2019). Collectively, using a 3D aggregation of hDP cells co-cultured with hORS cells would be a reasonable

methodology mimicking a physiologic HF organ *in vivo*, as inaugurated in our TCA assay for screening the hair growth-promoting effects of candidate compounds.

Previously, Havlickova et al. (2009) proposed a simplified HF-like 3D *in vitro* system for discovering hair growth-promoting drugs, consisting of hDP and hORS cells within an extracellular matrix. Their system used immunofluorescent staining-based findings for Ki67+ or TUNEL+ cells in the folliculoid microsphere structure as endpoints for determining the HF growth potential of candidate compounds. While this is a reasonably well implemented system, an additional step for staining each microsphere structure is needed to quantify the immunofluorescent signals. Herein, we obtained screening results based only on the length of the polar elongated TCA structures, without any further evaluation. Using length as an indicator for screening the hair growth-promoting effects can be optimized by complementing it with a high-throughput automated confocal microscopy platform, which is widely used for rapid large scale drug discovery (Dorval et al., 2018). In this way, we further cut down the labor and time demands required to measure the statistics, relative to the manual quantifying process (**Figure 1A**). Our phenotypic screening system would provide researchers with a high-throughput system with automated analytic processing of raw datasets, enabling the identification of the most promising molecule among a group of candidate molecules.

In this TCA assay, we used two types of hHF-constituting cells: hDP and hORS. However, the hair growth cycle is affected by the *in vivo* microenvironment around the hHFs, considering that each *in vivo* hHF organ interacts with neighboring cells, such as fibroblasts, endothelia, immunocytes, melanocytes, nerve cells, and adipocyte, as well as the extracellular matrix (Chen et al., 2016; Fan et al., 2018; Chen et al., 2020). Hence, using two kinds of hHF constituent cells, as done in this method, would not be enough to fully reflect the *in vivo* microenvironment (Abaci et al., 2017). Indeed, a combination of an outer adipose-derived stem cell shell and an inner DP core has been shown to exhibit superior DP signatures compared to DP cells alone (Huang et al., 2016). It is therefore necessary to develop an *in vitro* assay system integrating other types of cells and extracellular structures to simulate the *in vivo* hHF in the future.

Nevertheless, the advantages of this assay are: (i) it is physiologically and practically advantageous as it uses 3D cultured two-type human cells, which are easily available; (ii) it is simple as it uses length as the only endpoint; (iii) the presence of a high throughput system, which screens various compounds simultaneously. In conclusion, the "TCA" assay could serve as a method to validate the hair growth-promoting effect of a large volume of library molecules, although this assay needs to be validated further.

DATA AVAILABILITY STATEMENT

The raw data supporting the conclusions of this article will be made available by the authors, without undue reservation.

ETHICS STATEMENT

The studies involving human participants were reviewed and approved by the Institutional Review Board of Seoul National University. The patients/participants provided their written informed consent to participate in this study.

AUTHOR CONTRIBUTIONS

SJ, JO, and OK conceived and planned the experiments. SJ, BMK, and MP carried out the experiments. SJ, JO, KHK, and OK contributed to the interpretation of the results. SJ and JO took the lead in writing the manuscript. All authors provided critical feedback and helped shape the research, analysis, and manuscript. OK supervised the project.

FUNDING

This research was supported by a grant of the Korea Health Technology R&D Project through the Korea Health Industry Development Institute (KHIDI), funded by the Ministry of Health and Welfare, Republic of Korea (Grant No. HP20C0146).

REFERENCES

Abaci, H. E., Guo, Z., Doucet, Y., Jackow, J., and Christiano, A. (2017). Next generation human skin constructs as advanced tools for drug development. *Exp. Biol. Med.* 242, 1657–1668. doi: 10.1177/1535370217712690

Cash, T. F. (1992). The psychological effects of androgenetic alopecia in men. *J. Am. Acad. Dermatol.* 26, 926–931. doi: 10.1016/0190-9622(92)70134-2

Chan, C. C., Fan, S. M., Wang, W. H., Mu, Y. F., and Lin, S. J. (2015). A two-stepped culture method for efficient production of trichogenic keratinocytes. *Tissue Eng. Part. C Methods* 21, 1070–1079. doi: 10.1089/ten.tec.2015.0033

Chen, C. C., Plikus, M. V., Tang, P. C., Widelitz, R. B., and Chuong, C. M. (2016). The modulatable stem cell niche: tissue interactions during hair and feather follicle regeneration. *J. Mol. Biol.* 428, 1423–1440. doi: 10.1016/j.jmb.2015.07.009

Chen, C. L., Huang, W. Y., Wang, E. H. C., Tai, K. Y., and Lin, S. J. (2020). Functional complexity of hair follicle stem cell niche and therapeutic targeting of niche dysfunction for hair regeneration. *J. Biomed. Sci.* 27:43.

Choi, M., Choi, S. J., Jang, S., Choi, H. I., Kang, B. M., Hwang, S. T., et al. (2019). Shikimic acid, a mannose bioisostere, promotes hair growth with the induction of anagen hair cycle. *Sci. Rep.* 9:17008.

Dorval, T., Chanrion, B., Cattin, M. E., and Stephan, J. P. (2018). Filling the drug discovery gap: is high-content screening the missing link? *Curr. Opin. Pharmacol.* 42, 40–45. doi: 10.1016/j.coph.2018.07.002

Fan, S. M., Chang, Y. T., Chen, C. L., Wang, W. H., Pan, M. K., Chen, W. P., et al. (2018). External light activates hair follicle stem cells through eyes via an ipRGC-SCN-sympathetic neural pathway. *Proc. Natl. Acad. Sci. U S A.* 115, E6880–E6889.

Gupta, A. C., Chawla, S., Hegde, A., Singh, D., Bandyopadhyay, B., Lakshmanan, C. C., et al. (2018). Establishment of an in vitro organoid model of dermal papilla of human hair follicle. *J. Cell. Physiol.* 233, 9015–9030. doi: 10.1002/jcp.26853

Harel, S., Higgins, C. A., Cerise, J. E., Dai, Z., Chen, J. C., Clynes, R., et al. (2015). Pharmacologic inhibition of JAK-STAT signaling promotes hair growth. *Sci. Adv.* 1:e1500973. doi: 10.1126/sciadv.1500973

Havlickova, B., Bíró, T., Mescalchin, A., Tschirschmann, M., Mollenkopf, H., Bettermann, A., et al. (2009). A human folliculoid microsphere assay for exploring epithelial- mesenchymal interactions in the human hair follicle. *J. Invest. Dermatol.* 129, 972–983. doi: 10.1038/jid.2008.315

Higgins, C. A., Chen, J. C., Cerise, J. E., Jahoda, C. A., and Christiano, A. M. (2013). Microenvironmental reprogramming by three-dimensional culture enables dermal papilla cells to induce de novo human hair-follicle growth. *Proc. Natl. Acad. Sci. U S A.* 110, 19679–19688. doi: 10.1073/pnas.1309970110

Higgins, C. A., Richardson, G. D., Ferdinando, D., Westgate, G. E., and Jahoda, C. A. (2010). Modelling the hair follicle dermal papilla using spheroid cell cultures. *Exp. Dermatol.* 19, 546–548. doi: 10.1111/j.1600-0625.2009.01007.x

Huang, C.-F., Chang, Y.-J., Hsueh, Y.-Y., Huang, C.-W., Wang, D.-H., Huang, T.-C., et al. (2016). Assembling composite dermal papilla spheres with adipose-derived stem cells to enhance hair follicle induction. *Sci. Rep.* 6:26436.

Huang, W. Y., Huang, Y. C., Huang, K. S., Chan, C. C., Chiu, H. Y., Tsai, R. Y., et al. (2017). Stress-induced premature senescence of dermal papilla cells compromises hair follicle epithelial-mesenchymal interaction. *J. Dermatol. Sci.* 86, 114–122. doi: 10.1016/j.jdermsci.2017.01.003

Huang, Y. C., Chan, C. C., Lin, W. T., Chiu, H. Y., Tsai, R. Y., Tsai, T. H., et al. (2013). Scalable production of controllable dermal papilla spheroids on PVA surfaces and the effects of spheroid size on hair follicle regeneration. *Biomaterials* 34, 442–451. doi: 10.1016/j.biomaterials.2012.09.083

Huh, S., Lee, J., Jung, E., Kim, S. C., Kang, J. I., Lee, J., et al. (2009). A cell-based system for screening hair growth-promoting agents. *Arch. Dermatol. Res.* 301, 381–385. doi: 10.1007/s00403-009-0931-0

Hunt, N., and Mchale, S. (2005). The psychological impact of alopecia. *BMJ* 331, 951–953. doi: 10.1136/bmj.331.7522.951

Iino, M., Ehama, R., Nakazawa, Y., Iwabuchi, T., Ogo, M., Tajima, M., et al. (2007). Adenosine stimulates fibroblast growth factor-7 gene expression via adenosine A2b receptor signaling in dermal papilla cells. *J. Invest. Dermatol.* 127, 1318–1325. doi: 10.1038/sj.jid.5700728

Jang, J. H. (2005). Stimulation of human hair growth by the recombinant human keratinocyte growth factor-2 (KGF-2). *Biotechnol. Lett.* 27, 749–752. doi: 10.1007/s10529-005-5624-y

Jo, S. J., Shin, H., Park, Y. W., Paik, S. H., Park, W. S., Jeong, Y. S., et al. (2014). Topical valproic acid increases the hair count in male patients with androgenetic alopecia: a randomized, comparative, clinical feasibility study using phototrichogram analysis. *J. Dermatol.* 41, 285–291. doi: 10.1111/1346-8138.12422

Kageyama, T., Yan, L., Shimizu, A., Maruo, S., and Fukuda, J. (2019). Preparation of hair beads and hair follicle germs for regenerative medicine. *Biomaterials* 212, 55–63. doi: 10.1016/j.biomaterials.2019.05.003

Kang, B. M., Kwack, M. H., Kim, M. K., Kim, J. C., and Sung, Y. K. (2012). Sphere formation increases the ability of cultured human dermal papilla cells to induce hair follicles from mouse epidermal cells in a reconstitution assay. *J. Invest. Dermatol.* 132, 237–239. doi: 10.1038/jid.2011.250

Lei, M., and Chuong, C.-M. (2016). Aging, alopecia, and stem cells. *Science* 351, 559–560. doi: 10.1126/science.aaf1635

Lei, M., Schumacher, L. J., Lai, Y.-C., Juan, W.-T., Yeh, C.-Y., Wu, P., et al. (2017a). Self-organization process in newborn skin organoid formation inspires strategy to restore hair regeneration of adult cells. *Proc. Natl. Acad. Sci. U S A.* 114, E7101–E7110.

Lei, M., Yang, L., and Chuong, C.-M. (2017b). Getting to the core of the dermal papilla. *J. Invest. Dermatol.* 137, 2250–2253. doi: 10.1016/j.jid.2017.07.824

Lim, T. C., Leong, M. F., Lu, H., Du, C., Gao, S., Wan, A. C., et al. (2013). Follicular dermal papilla structures by organization of epithelial and mesenchymal cells in interfacial polyelectrolyte complex fibers. *Biomaterials* 34, 7064–7072. doi: 10.1016/j.biomaterials.2013.05.068

Madaan, A., Verma, R., Singh, A. T., and Jaggi, M. (2018). Review of hair follicle dermal papilla cells as in vitro screening model for hair growth. *Int. J. Cosmet. Sci.* 40, 429–450. doi: 10.1111/ics.12489

Magerl, M., Kauser, S., Paus, R., and Tobin, D. J. (2002). Simple and rapid method to isolate and culture follicular papillae from human scalp hair follicles. *Exp. Dermatol.* 11, 381–385. doi: 10.1034/j.1600-0625.2002.110414.x

Messenger, A. G., and Rundegren, J. (2004). Minoxidil: mechanisms of action on hair growth. *Br. J. Dermatol.* 150, 186–194. doi: 10.1111/j.1365-2133.2004.05785.x

Ohn, J., Kim, K. H., and Kwon, O. (2019). Evaluating hair growth promoting effects of candidate substance: a review of research methods. *J. Dermatol. Sci.* 93, 144–149. doi: 10.1016/j.jdermsci.2019.02.004

Paladini, R. D., Saleh, J., Qian, C., Xu, G. X., and Rubin, L. L. (2005). Modulation of hair growth with small molecule agonists of the hedgehog signaling pathway. *J. Invest. Dermatol.* 125, 638–646. doi: 10.1111/j.0022-202x.2005.23867.x

Philpott, M. P., Sanders, D. A., and Kealey, T. (1994). Effects of insulin and insulin-like growth factors on cultured human hair follicles: IGF-I at physiologic concentrations is an important regulator of hair follicle growth in vitro. *J. Invest. Dermatol.* 102, 857–861. doi: 10.1111/1523-1747.ep12382494

Philpott, M. P., Sanders, D. A., and Kealey, T. (1996). Whole hair follicle culture. *Dermatol. Clin.* 14, 595–607. doi: 10.1016/s0733-8635(05)70387-9

Price, V. H. (1999). Treatment of hair loss. *N. Engl. J. Med.* 341, 964–973.

Rendl, M., Lewis, L., and Fuchs, E. (2005). Molecular dissection of mesenchymal–epithelial interactions in the hair follicle. *PLoS Biol.* 3:e331. doi: 10.1371/journal.pbio.0030331

Rittmaster, R. S. (1994). Finasteride. *N. Engl. J. Med.* 330, 120–125.

Shimaoka, S., Tsuboi, R., Jindo, T., Imai, R., Takamori, K., Rubin, J. S., et al. (1995). Hepatocyte growth factor/scatter factor expressed in follicular papilla cells stimulates human hair growth in vitro. *J. Cell. Physiol.* 165, 333–338. doi: 10.1002/jcp.1041650214

Stark, H. J., Breitkreutz, D., Limat, A., Bowden, P., and Fusenig, N. E. (1987). Keratins of the human hair follicle: "hyperproliferative" keratins consistently expressed in outer root sheath cells in vivo and in vitro. *Differentiation* 35, 236–248. doi: 10.1111/j.1432-0436.1987.tb00174.x

Tan, J. J. Y., Common, J. E., Wu, C., Ho, P. C. L., and Kang, L. (2019). Keratinocytes maintain compartmentalization between dermal papilla and fibroblasts in 3D heterotypic tri-cultures. *Cell Prolif* 52:e12668.

Tomita, Y., Akiyama, M., and Shimizu, H. (2006). PDGF isoforms induce and maintain anagen phase of murine hair follicles. *J. Dermatol. Sci.* 43, 105–115. doi: 10.1016/j.jdermsci.2006.03.012

Topouzi, H., Logan, N. J., Williams, G., and Higgins, C. A. (2017). Methods for the isolation and 3D culture of dermal papilla cells from human hair follicles. *Exp. Dermatol.* 26, 491–496. doi: 10.1111/exd.13368

Weber, E. L., Woolley, T. E., Yeh, C. Y., Ou, K. L., Maini, P. K., and Chuong, C. M. (2019). Self-organizing hair peg-like structures from dissociated skin progenitor cells: new insights for human hair follicle organoid engineering and turing patterning in an asymmetric morphogenetic field. *Exp. Dermatol.* 28, 355–366. doi: 10.1111/exd.13891

Yang, C.-C., and Cotsarelis, G. (2010). Review of hair follicle dermal cells. *J. Dermatol. Sci.* 57, 2–11. doi: 10.1016/j.jdermsci.2009.11.005

Yano, K., Brown, L. F., and Detmar, M. (2001). Control of hair growth and follicle size by VEGF-mediated angiogenesis. *J. Clin. Invest.* 107, 409–417. doi: 10.1172/jci11317

Yoo, B.-Y., Shin, Y.-H., Yoon, H.-H., Seo, Y.-K., and Park, J.-K. (2010). Hair follicular cell/organ culture in tissue engineering and regenerative medicine. *Biochem. Eng. J.* 48, 323–331. doi: 10.1016/j.bej.2009.09.008

Conflict of Interest: The authors declare that the research was conducted in the absence of any commercial or financial relationships that could be construed as a potential conflict of interest.

Copyright © 2020 Jang, Ohn, Kang, Park, Kim and Kwon. This is an open-access article distributed under the terms of the Creative Commons Attribution License (CC BY). The use, distribution or reproduction in other forums is permitted, provided the original author(s) and the copyright owner(s) are credited and that the original publication in this journal is cited, in accordance with accepted academic practice. No use, distribution or reproduction is permitted which does not comply with these terms.

frontiers in Cell and Developmental Biology

BRIEF RESEARCH REPORT
published: 26 November 2020
doi: 10.3389/fcell.2020.583434

Human Fetal Scalp Dermal Papilla Enriched Genes and the Role of R-Spondin-1 in the Restoration of Hair Neogenesis in Adult Mouse Cells

*Erin L. Weber[1,2†], Yung-Chih Lai[3†], Mingxing Lei[3,4], Ting-Xin Jiang[1] and Cheng-Ming Chuong[1]**

[1] Department of Pathology, University of Southern California, Los Angeles, CA, United States, [2] Division of Plastic Surgery, Indiana University School of Medicine, Indianapolis, IN, United States, [3] Integrative Stem Cell Center, China Medical University Hospital, China Medical University, Taichung, Taiwan, [4] 111 Project Laboratory of Biomechanics and Tissue Repair, College of Bioengineering, Chongqing University, Chongqing, China

OPEN ACCESS

Edited by:
Masatake Osawa,
Gifu University, Japan

Reviewed by:
Takashi Matsuzaki,
Shimane University, Japan
Carlos Clavel,
Skin Research Institute of Singapore,
Agency for Science, Technology
and Research (A*STAR), Singapore

***Correspondence:**
Cheng-Ming Chuong
cmchuong@usc.edu

† These authors have contributed equally to this work

Specialty section:
This article was submitted to Stem Cell Research, a section of the journal Frontiers in Cell and Developmental Biology

Received: 14 July 2020
Accepted: 09 November 2020
Published: 26 November 2020

Citation:
Weber EL, Lai Y-C, Lei M, Jiang T-X and Chuong C-M (2020) Human Fetal Scalp Dermal Papilla Enriched Genes and the Role of R-Spondin-1 in the Restoration of Hair Neogenesis in Adult Mouse Cells. Front. Cell Dev. Biol. 8:583434. doi: 10.3389/fcell.2020.583434

Much remains unknown about the regulatory networks which govern the dermal papilla's (DP) ability to induce hair follicle neogenesis, a capacity which decreases greatly with age. To further define the core genes which characterize the DP cell and to identify pathways prominent in DP cells with greater hair inductive capacity, comparative transcriptome analyses of human fetal and adult dermal follicular cells were performed. 121 genes were significantly upregulated in fetal DP cells in comparison to both fetal dermal sheath cup (DSC) cells and interfollicular dermal (IFD) populations. Comparison of the set of enriched human fetal DP genes with human adult DP, newborn mouse DP, and embryonic mouse dermal condensation (DC) cells revealed differences in the expression of Wnt/β-catenin, Shh, FGF, BMP, and Notch signaling pathways. We chose R-spondin-1, a Wnt agonist, for functional verification and show that exogenous administration restores hair follicle neogenesis from adult mouse cells in skin reconstitution assays. To explore upstream regulators of fetal DP gene expression, we identified twenty-nine transcription factors which are upregulated in human fetal DP cells compared to adult DP cells. Of these, seven transcription factor binding motifs were significantly enriched in the candidate promoter regions of genes differentially expressed between fetal and adult DP cells, suggesting a potential role in the regulatory network which confers the fetal DP phenotype and a possible relationship to the induction of follicle neogenesis.

Keywords: hair induction, follicle neogenesis, skin reconstitution, dermal papilla, human

Abbreviations: DC, dermal condensate; DP, dermal papilla; DS, dermal sheath; DSC, dermal sheath cup; IFD, interfollicular dermis.

INTRODUCTION

The DP, though distinctly different from the DC and primarily responsible for cyclical regeneration of the mature follicle, retains the follicle-inducing property of its DC progenitor. Many studies have demonstrated the capacity of the whole DP or cultured DP cells to induce new hair follicle formation in hairless epidermis (Jahoda, 1992; Jahoda et al., 1993). However, the efficiency of follicle neogenesis varies greatly by organism, follicle type, and age, with rat vibrissae and newborn mouse pelage DPs exhibiting much higher rates of follicle neogenesis than adult mouse or human DPs (Jahoda et al., 2001; Higgins et al., 2013; Thangapazham et al., 2013). Clinically, the efficiency of human adult DP inductivity is ineffectively low to be useful for the treatment of alopecia and requires the harvest of functional follicles, making it no less invasive or limiting than the current gold standard of follicular transplantation. If existing adult DP cells could be expanded in culture and reprogrammed to possess higher inductive capacity akin to the fetal DC or DP, transplantation of such cells may offer a new treatment for androgenetic alopecia or skin injury (Chueh et al., 2013; Higgins and Christiano, 2014).

With this in mind, we investigated the gene expression profile of the human fetal DP, a structure which is more anatomically distinct than the DC, and, through comparative transcriptomics, determined differences in gene expression between fetal and adult DP cells. We identified 121 enriched human fetal DP genes and a subset of transcription factors upregulated in fetal DP cells compared to adult DP cells which may regulate the developmentally active fetal DP. Our previous work on the differences between murine neonatal and adult hair follicle neogenesis identified important signaling pathways and described robust *in vitro* and *in vivo* hair reconstitution assays for the examination of key factors in follicle development (Lei et al., 2017a). In this analysis of human fetal DP cells, the R-spondins, a family of *Wnt* agonists, were differentially upregulated and the exogenous administration of R-spondin-1 rescued hair follicle neogenesis in adult mouse reconstitution assays.

MATERIALS AND METHODS

Human Tissue

Two adult, non-balding scalp specimens were obtained through the National Disease Research Interchange (Philadelphia) from deceased 36- and 54-year old males. Two fetal scalp specimens were obtained through Novogenix, Inc. (Los Angeles) from second trimester fetuses electively aborted at developmental ages 16 and 17 weeks. Procurement protocols for both organizations involved appropriate informed consent for donated tissues.

Isolation of Cell Populations

Frozen sections were stained with the Arcturus Histogene Kit. IFD regions and DP and DSC cells from anagen-phase follicles were dissected using pulled glass capillary tubes under magnification (**Figure 1A**). RNA was extracted with the Arcturus PicoPure RNA Isolation Kit. cDNA was amplified from 500 pg of RNA per sample using the Nugen Ovation RNA-Seq System V2 and fragmented into 300bp segments using a Covaris sonicator. RNA-Seq libraries were constructed from 80 to 100 ng of cDNA with the Nugen Ovation Ultralow System V2. Sample concentration and quality was assessed with the Agilent Bioanalyzer.

RNA-Seq Analysis

More than 100 million 75-bp single-end reads were generated for each RNA-Seq sample using an Illumina NextSeq 500 sequencer. QualiMap2 was used to measure RNA degradation and genomic DNA contamination (Okonechnikov et al., 2015). For secondary RNA-Seq analysis, the human hg19 assembly, including unplaced and unlocalized scaffolds and RefGene annotation, was downloaded from the UCSC Genome Browser on 2016.2.6 (Speir et al., 2016). Low quality bases were trimmed based on the Phred quality score (>20) from both the 5′- and 3′-ends. After trimming, reads <50bp or with ambiguous bases were discarded. Alignment, quantification, normalization, and differential expression analysis were performed by STAR 2.4.1d (Dobin et al., 2013) through Partek Flow (Partek Inc.), htseq-count 0.6.0 (Anders et al., 2014), TMM (Robinson and Oshlack, 2010), and edgeR 3.10.5 (Robinson and Smyth, 2008), respectively. Genes with count-per-million values >1 in at least two samples were retained. The false discovery rate (FDR) was set at <0.05. Principal component analysis, Ward's hierarchical method (Ward, 1963), and Venn diagrams were performed with Partek Genomics Suite 6.16 (Partek Inc.). Pathway enrichment analysis using Fisher's exact test and Upstream Regulator Analysis were performed with QIAGEN's Ingenuity® Pathway Analysis. IPA was also used to build a regulatory network for hair follicle regenerative potential between fetal and adult DP cells. Transcription factor binding sites (TFBSs) within candidate promoter regions were predicted by FMatch (Kel et al., 2003) based on the TRANSFAC database (Matys et al., 2006). Candidate promoter sequences were defined as 1,000bp upstream and 100bp downstream of transcription start sites. The 882 non-differentially expressed genes with the largest FDR values were used as the background set. The specified cut-offs were selected as the minimum of the sum of both error rates (minSUM) for the matrix similarity score and p-value <0.01 for TFBSs enrichment.

Murine Hair Reconstitution Assay

Dorsal skin from 2 month old K14-H2B-GFP transgenic mice was incubated in 0.25% trypsin solution at 4°C overnight. The epidermis was dissociated into a single-cell suspension by repeated pipette titration and passage through a 70 μm filter. A single-cell dermal suspension was achieved by incubation in 0.35% collagenase I solution (Worthington) for 30 min at 37°C, followed by the addition of DNAse I (Qiagen) and 5 min incubation at room temperature. Medium containing 10% fetal bovine serum (FBS) was added and the dermal cells were dissociated by repeated pipette titration and filtration through a 40 μm filter. Epidermal and dermal cells were recombined in a 1:9 ratio in DMEM/F12 culture medium (1:1, Gibco) with 10% FBS (Gibco) and plated drop-wise on a 6-well culture insert submerged in culture medium. Cultures were incubated at 37°C

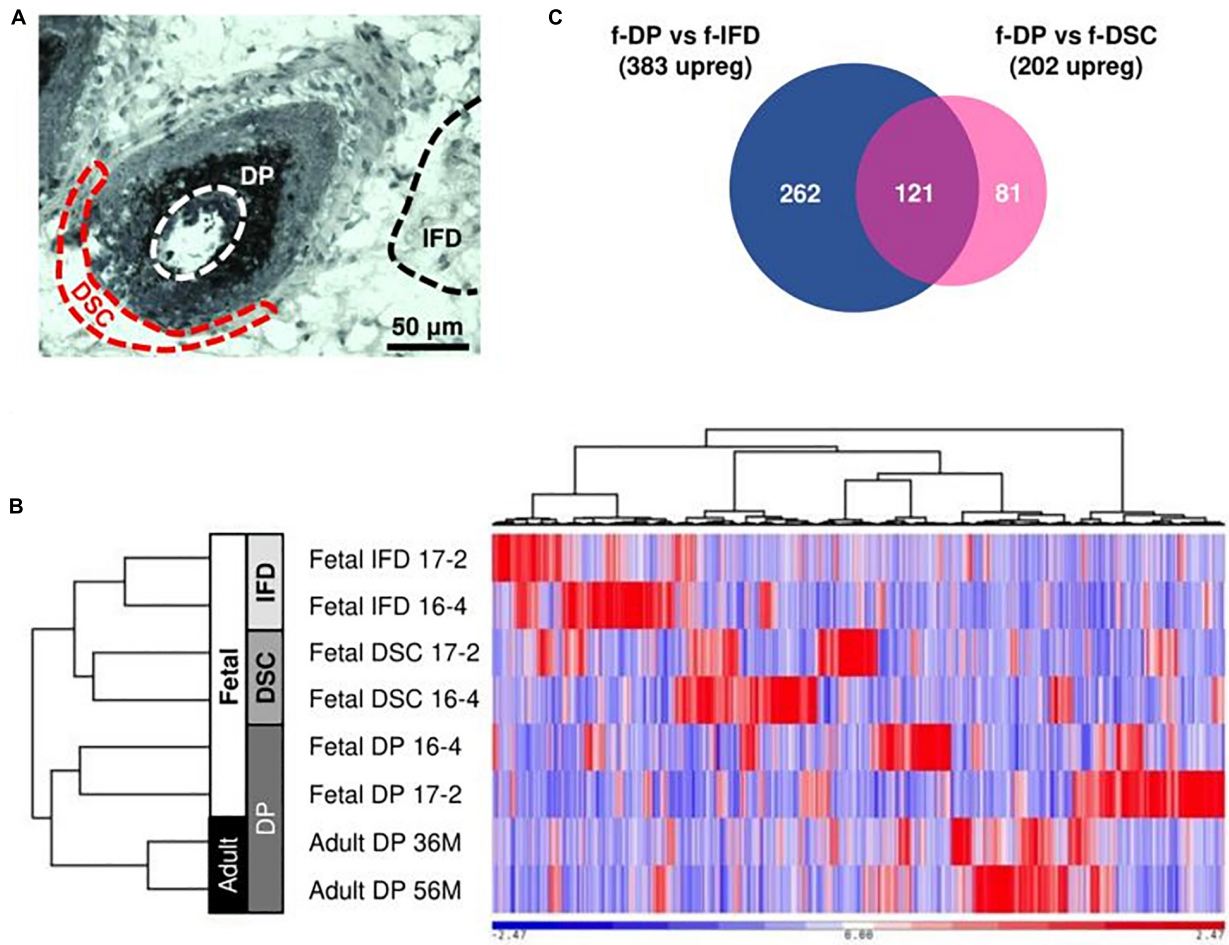

FIGURE 1 | Low-input RNA-Seq analysis of human scalp. **(A)** DP, DSC, and IFD cells were manually harvested from frozen sections of human scalp tissue. **(B)** Hierarchical clustering of RNA-Seq samples demonstrated clustering of similar cell types despite intersample variation. **(C)** 121 enriched fetal DP genes were identified from comparison of the fetal DP transcriptome with fetal DSC and IFD transcriptomes.

and 5% CO_2. The following factors were added to the culture medium: 5 µM protein kinase C inhibitor (Bisindolyl maleimide I, Cayman Chemical, day 0–6), 25 ng/ml R-spondin-1 (R&D Systems, day 0–2), 10 ng/ml Wnt3a (R&D Systems, day 1–4), and 10 ng/ml MMP14 (R&D Systems, day 3–6). On day 6, cell culture inserts were sutured droplet-side down to full-thickness dermal wounds on nude mice. Hair growth was observed over 6 weeks. Culture droplets and skin biopsies were stained with propidium iodide and imaged with a confocal microscope. Epidermal cells from transgenic mice were detected by GFP fluorescence.

RESULTS

Hair follicle DP cells from different body regions or developmental ages display varying patterns of gene expression (Chen et al., 2015). We employed the following strategy to identify important human fetal scalp DP genes. To identify genes unique to the fetal DP, we dissected DP cells from mature, anagen-phase, fetal follicles and compared them with adjacent DSC cells, known to be transcriptionally distinct but developmentally related to DP cells, and IFD cells, comprised of a heterogeneous mixture of non-follicular fibroblasts. To identify core genes shared by DP cells across different organisms, ages, and follicle types, we compared the fetal scalp DP transcriptome with human adult DP, newborn mouse DP, and embryonic mouse DC datasets. To elucidate signaling pathways which may confer fetal DP cells with a greater ability to induce follicle neogenesis, we compared transcriptomes from human fetal and adult anagen-phase DP cells. We identified key transcription factor binding motifs in promoter regions upstream of genes differentially expressed in fetal compared to adult DP cells to determine potential upstream regulators and a foundation for multiple downstream signaling networks. Finally, we employed skin reconstitution assays using adult murine skin cells, which inefficiently induce follicle neogenesis, to demonstrate that R-spondin-1, a member of one of the gene families upregulated in human fetal DP cells, can restore the ability to form new follicles.

Identification of Human Fetal Dermal Papilla Enriched Genes

Cluster analysis of 16,623 expressed genes demonstrated appropriate grouping of biological replicates, with adult and fetal DP cells clustering distinctly from DSC and IFD cells (**Figure 1B**). We must note that, due to the necessary protocols surrounding ethical acquisition of human tissue, all libraries were derived from moderately degraded, low quantity samples amplified by random primers. Consequently, biological variation within replicates was apparent (**Figure 1B**). The 3′ enrichment of sequencing reads reflected RNA degradation (**Supplementary Figure 1** and **Supplementary Table 1**) and an increased proportion of intergenic and intronic reads indicated genomic DNA contamination detected by random primers (**Supplementary Figure 1** and **Supplementary Table 1**). Nonetheless, due to the lack of better human tissue acquisition methods, the RNA-Seq libraries were acceptable for further comparative analysis.

1,035 differentially expressed genes (383 upregulated, 652 downregulated) were identified between fetal DP and IFD cells and 564 differentially expressed genes (202 upregulated, 362 downregulated) were identified between fetal DP and DSC cells. The DP expression profile differed more markedly from IFD cells than DSC (DP vs. IFD: $r = 0.42 \pm 0.02$, DP vs. DSC: $r = 0.66 \pm 0.04$, $p < 0.001$). 121 genes were upregulated in fetal DP cells compared to DSC and IFD cells and were designated enriched human fetal DP genes (**Figures 1C**, **2A** and **Supplementary Table 2**). Compared with published datasets, the enriched human fetal DP genes identified in this study significantly overlapped with human adult DP signature genes identified by Ohyama et al. (2012) (11/108, $p = 5.3 \times 10^{-11}$), neonatal mouse DP signature genes identified by Rendl et al. (2005) (16/228, $p = 6.0 \times 10^{-13}$) and Rezza et al. (2016) (12/202, $p = 3.6 \times 10^{-9}$), and embryonic mouse DC genes identified by Sennett et al., 2015 (17/395, $p = 2.6 \times 10^{-10}$) and Mok et al., 2019 (15/315, $p = 7.8 \times 10^{-10}$) (**Figure 2B**). *Edn3* was present in all six datasets; *Bmp4, Fgf10, and Trps1* were present in five; and *Col23a1, Igfbp3, Inhba, Rspo3, Spon1, and Sox2* were present in four, suggesting that expression may play an important role in the DP during hair follicle neogenesis, development, or cycling. Gene ontology analysis of the enriched human fetal DP genes confirmed multiple pathways known to be important for hair follicle development, including BMP, Wnt, and epithelial-mesenchymal signaling (**Figure 2C**).

Differential Gene Expression Between Human Fetal and Adult Dermal Papillae

822 differentially expressed genes (356 upregulated, 466 downregulated) were identified between fetal and adult DP cells (**Supplementary Table 3**). Validation of fetal RNAseq data was performed through immunofluorescent staining of fetal and adult scalp with genes present in the enriched fetal DP dataset, upregulated in fetal versus adult DP, and minimally expressed in DSC and IFD cells (**Supplementary Figure 2**). Hair follicle-associated pathways were significantly enriched, including Wnt/β-catenin ($p = 0.004$), sonic hedgehog ($p = 0.0006$), FGF ($p = 0.01$), Notch ($p = 0.002$), and BMP signaling ($p = 0.02$) (**Figure 3A**). Twenty-nine transcription factors were upregulated in fetal compared to adult DP cells (**Figure 3B**). Enrichment analysis of TFBSs within candidate promoter regions of genes differentially expressed between fetal and adult DP identified seven significantly enriched transcription factors, suggesting a role as important upstream regulators for the fetal DP phenotype (**Figure 3C**). Using the IPA database, we constructed a working hypothesis of a regulatory network with 110 genes differentially expressed between fetal and adult DP cells (**Figure 3D**). Within this model, SOX2 and GLI1, two of the seven enriched TFBSs, interact with a high proportion of the enriched fetal DP genes and are promising hubs for regulation of downstream differential gene expression. SOX2 was predicted as the top transcriptional regulator ($p = 2.88 \times 10^{-15}$).

R-Spondin-1 Is Important for the Restoration of Hair Follicle Neogenesis From Adult Mouse Skin Cells

Wnt signaling is critical for both developmental hair follicle neogenesis and temporal hair cycling. The nuances of such signaling, which distinguish the two types of hair regeneration, are less clear. R-spondins are Wnt agonists which are important for the development of numerous organs, as well as the maintenance of stem cells and epithelial regeneration in the intestine (De Lau et al., 2012; Neufeld et al., 2012; Cambler et al., 2014; Harnack et al., 2019). R-spondin-3 (*Rspo3*) and R-spondin-4 (*Rspo4*) were present in the human fetal DP enriched gene set while R-spondin-1 (*Rspo1*) and *Rspo3* were upregulated in fetal, compared to adult, DP cells. *Rspo2* and *Rspo4* were more highly expressed in adult DP cells. *Rspo3* has been identified as a signature gene in some transcriptional analyses of embryonic and newborn mouse DP (Sennett et al., 2015; Rezza et al., 2016) but there are no reports of defects in follicular development or hair cycling associated with *Rspo3* mutation. *Rspo1* is upregulated in mice in late telogen and early anagen and intradermal injection into telogen skin induces early transition into the anagen phase through activation of epidermal follicle stem cells (Li et al., 2016).

Rspo1 is expressed in both epithelial and DP cells of the murine hair follicle (Harshuk-Shabso et al., 2020). By immunofluorescent staining, we also observed that *Rspo1* is expressed in the epithelial and DP cells of both mouse and human hair follicles. *Rspo1* expression is decreased in the DP of adult mouse and human hair follicles, compared to newborn mouse and fetal scalp hair follicles (**Figure 4A**). *Rspo1* is also expressed in the newborn mouse epidermal and dermal cells subjected to skin organoid culture. In particular, *Rspo1* is more highly expressed in dermal cells adjacent to epidermal aggregates in day 6 cultures.

Without a robust human hair induction or hair cycling assay at hand, we used a murine skin organoid culture system to test the function of R-spondins during human follicle neogenesis, as it permits the study of dissociated epidermal and dermal cells as they undergo morphological transitions through early skin and appendage development (**Figures 4B,D**; Lei et al., 2017a). After six days in three-dimensional (3D) culture, newborn mouse epidermal and dermal cells form mature, hair-producing follicles upon grafting to a nude mouse (**Figures 4B,E**). Adult mouse skin

A

Signature fetal DP genes

Signaling			Transcription	ECM/Adhesion		Enzyme		
ADRB2	FST	NRG1	HAND1	CDH8	PCDHB15	CARNS1	MAPK12	SPINT1
APCDD1	FZD10	PRLR	MSX1	CDH24	PKP4	CRYM	MMP1	TNK2
APCDD1L	GFRA1	RGS2	NCOA3	CENPW	PPFIA2	DIO3	MPPED1	TRIM2
AVPR1A	GNAL	RSPO3	PKNOX2	CNTNAP4	SCUBE1	DPY19L2	NOTUM	TYR
BAMBI	GNAZ	RSPO4	SALL4	COL23A1	SNED1	HIPK2	PAPPA2	
BMP4	GRID1	SFRP1	SIM1	FRAS1	SPON1	HS3ST3A1	PCSK2	
BMP7	IFITM1	SHH	SOX2	ITGA8		HS3ST3B1	PDE3A	
CYTL1	IGFBP3	TGFB2	TAF11	LAMA3		KDM7A	PGM2L1	
EDN3	INHBA	TMEM51	TBX3	LAMBP21		LPL	RGCC	
FGF10	NET1	TNFRSF19	TRPS1	MEGF11		MAOA	RNF144B	
FGFR3	NKD2	WNT5A	ZMYND8	NRXN3		MAPK4	RPS6KA5	

B

Human adult DP genes

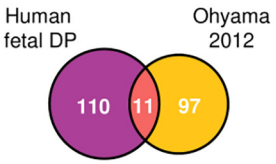

Ohyama et al., 2012
108 genes
10.2%, p = 5.3 x 10^{-11}
BAMBI, **BMP4**, **EDN3**, LPL, NET1, RGS2, **SPON1**, TRIM2, **TRPS1**, **WNT5A**, ZMYND8

Newborn mouse DP genes

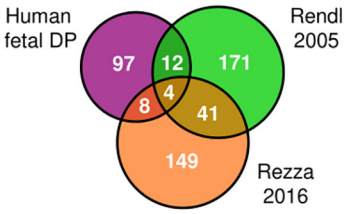

Rendl et al., 2005
228 genes
7.0%, p = 6.0 x 10^{-13}
BMP4, **EDN3**, **FGF10**, FST, GFRA1, **IGFBP3**, **INHBA**, NKD2, NOTUM, **PCDHB15**, **PRLR**, **SCUBE1**, **SOX2**, **SPON1**, **TRPS1**, **WNT5A**

Rezza et al., 2016
202 genes
5.9%, p = 3.6 X 10^{-9}
COL23A1, **EDN3**, **FGF10**, MPPED1, NCOA3, PAPPA2, RSPO3, RSPO4, **SCUBE1**, SFRP1, SNED1, **SPON1**

Embryonic mouse DC genes

Sennett et al., 2015
395 genes
4.3%, p = 2.6 x 10^{-10}
ANO2, **AVPR1A**, **BMP4**, **BMP7**, **COL23A1**, **EDN3**, **FGF10**, **HS3ST3B1**, **IGFBP3**, **INHBA**, **PCDHB15**, **PDE3A**, **PRLR**, **RSPO3**, SEZ6L, **SOX2**, **TRPS1**

Mok et al., 2019
315 genes
4.8%, p = 7.8 x 10^{-10}
AVPR1A, **BMP4**, **BMP7**, **COL23A1**, **EDN3**, **FGF10**, HS3ST3A1, **HS3ST3B1**, **IGFBP3**, **INHBA**, KDM7A, **PDE3A**, **RSPO3**, **SOX2**, **TRPS1**

C

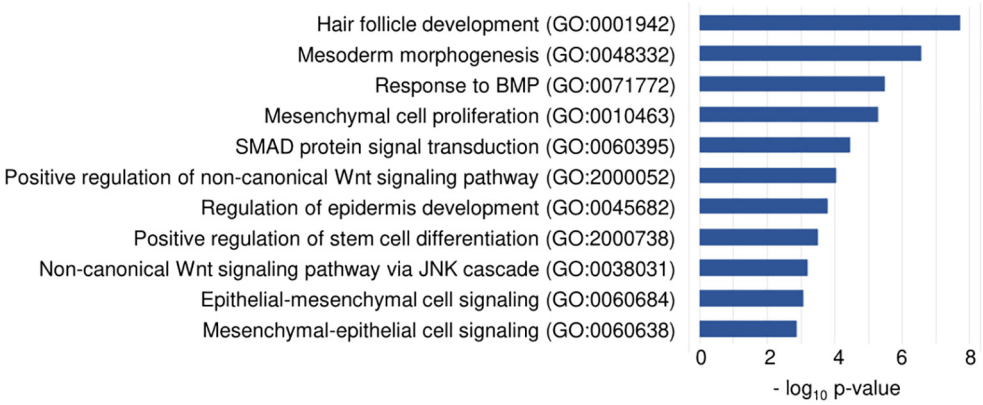

FIGURE 2 | Molecular enrichment for the human fetal DP. **(A)** Enriched human fetal DP genes. **(B)** Comparison of the human fetal DP enriched gene profile with previously published human adult DP, newborn mouse DP, and embryonic mouse DC signature gene sets demonstrated significant overlap. Genes listed in red were present in 6 datasets, genes in blue in 5, genes in bold black in 4, and genes in green in 3. **(C)** Gene ontology analysis of the human fetal DP enriched genes confirmed the prevalence of pathways known to be important for hair follicle development.

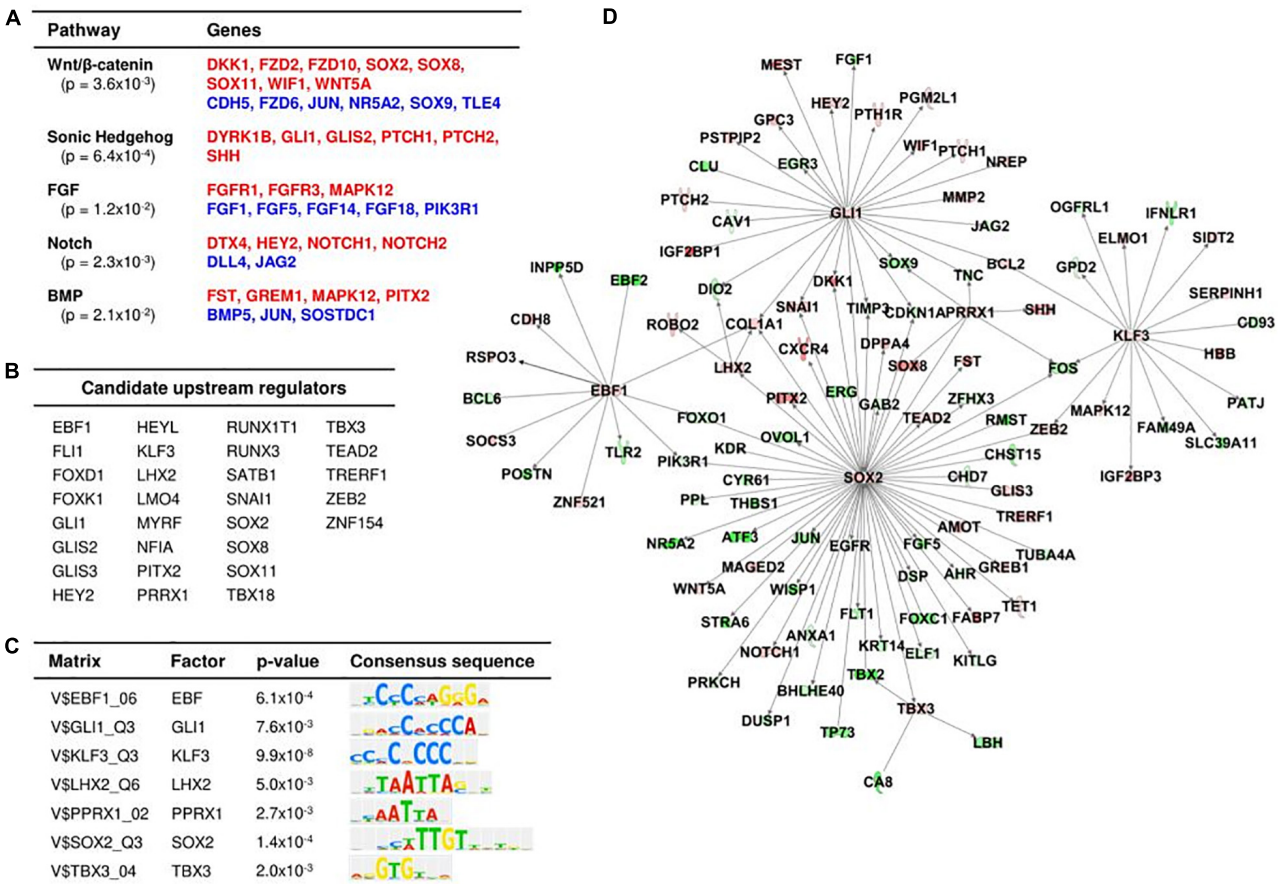

FIGURE 3 | Differential gene expression in human fetal DP compared to adult DP cells. **(A)** Significantly enriched pathways of differentially expressed genes between fetal DP and adult DP. The red and blue highlighted genes indicate upregulation and downregulation, respectively, in fetal DP cells compared to adult DP cells. **(B)** Candidate upstream transcriptional regulators upregulated in fetal versus adult DP. **(C)** Significantly enriched transcription factor binding motifs in the promoter sequences of differentially expressed genes between fetal and adult DP. **(D)** Predicated regulatory network of fetal DP gene expression. Red and green highlighting denotes upregulation and downregulation, respectively, in fetal DP compared to adult DP cells.

cells, however, have lost the ability to self-organize during skin organoid culture and do not generate hair follicles after grafting (**Figures 4D,E**). Our previous work defined a combination of exogenous growth factors which, when added to the 3D culture medium, stimulated adult cells to progress through aggregation steps similar to newborn mouse cells (**Figure 4C**; Lei et al., 2017a).

To avoid bias introduced by species-specific variation, we chose to investigate the role of *Rspo1* in murine hair follicle neogenesis, as a role in the hair cycling is known (Neufeld et al., 2012; Li et al., 2016). The addition of RSPO1 from day 0–2 resulted in larger cell aggregates at day 2. The aggregates progressed to form larger cysts at day 4 and, consistent with our previous findings, the cysts further coalesced to form planar skin at day 6, after the addition of WNT3A and MMP14 (**Figures 4C,D**). Significantly more hair-bearing follicles were generated after the RSPO1/WNT3A/MMP14/iPKC treated cells were grafted onto the backs of nude mice, compared to adult controls in the absence of growth factors (**Figures 4E,F**). GFP fluorescence confirmed that the newly regenerated hair follicles were derived from donor cells (**Figure 4G**).

DISCUSSION

The human fetal DP, like the newborn mouse, can induce new hair follicle formation. Much effort has focused on identification of the transcriptional profile of the newborn mouse DP and embryonic mouse DC. As the human hair follicle differs anatomically and functionally from the mouse follicle, an assessment of the transcriptional profile of the human fetal DP has the potential to reveal new genes or pathways important for human follicle neogenesis (Cotsarelis, 2006; Panteleyev, 2016). Here, we identified a set of 121 genes significantly upregulated in human fetal DP cells, compared to fetal DSC and IFD cells. Fourteen genes (*Apcdd1, Bmp4, Bmp7, Fgf10, Fst, Gfra1, Inhba, Prlr, Shh, Sox2, Spint1, Tgfβ2, Tnfrsf19, and Trps1*) are known to be important for hair follicle morphology and development (St-Jacques et al., 1998; Foitzik et al., 1999; Botchkareva et al., 2000; Brown et al., 2000; Ohuchi et al., 2000; Botchkarev et al., 2001; Craven et al., 2001; Malik et al., 2002; Nakamura et al., 2003; Szabo et al., 2007; Pispa et al., 2008; Driskell et al., 2009; Zouvelou et al., 2009; Shimomura et al., 2010). Comparison with published

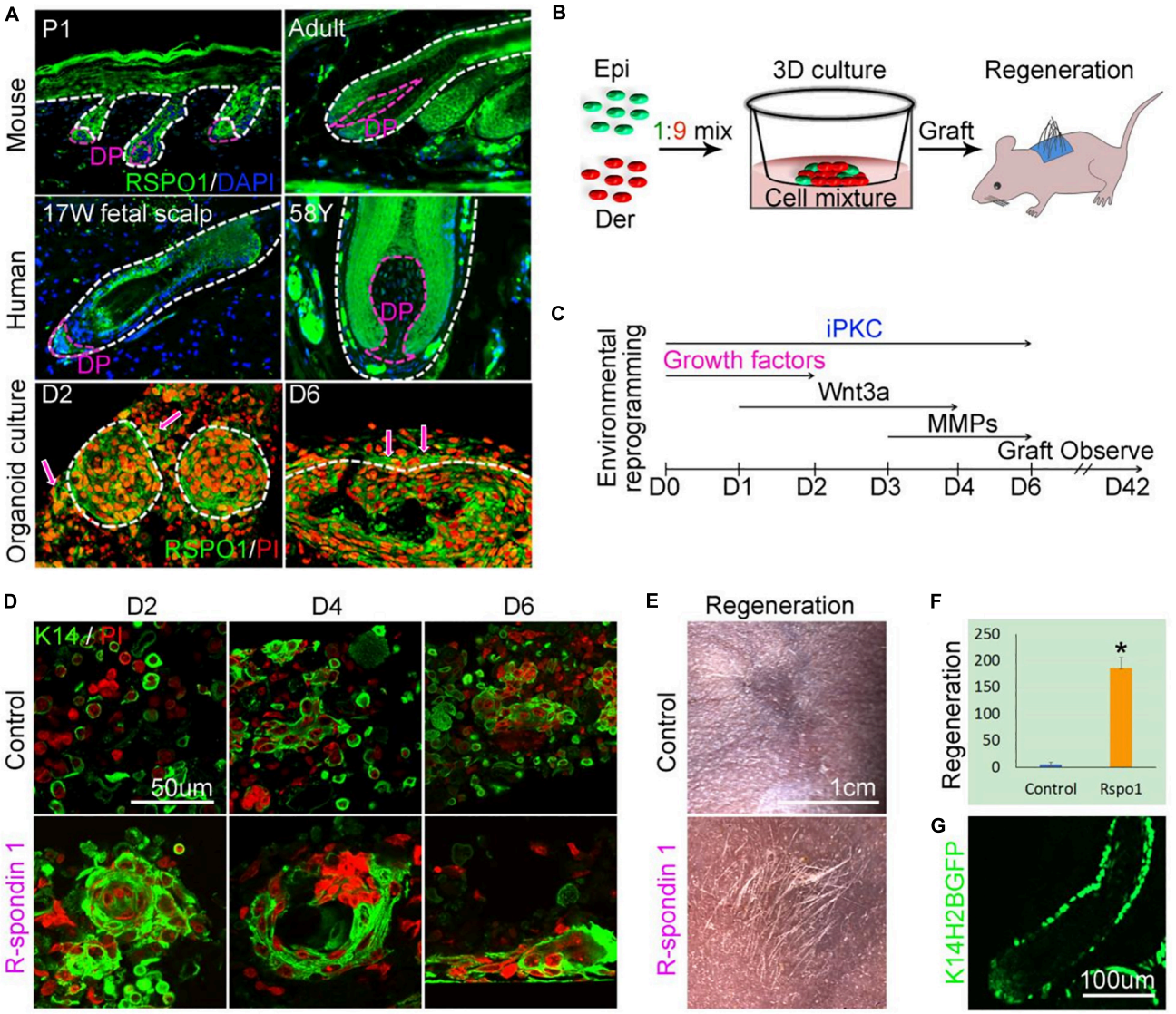

FIGURE 4 | Recovery of follicle neogenesis from adult mouse epidermal and dermal cells through environmental reprogramming. **(A)** Characterization of RSPO1 expression in mouse and human samples. **(B)** Experimental design of the murine skin organoid culture, followed by grafting of cells to dermal wounds on nude mice. **(C)** Environmental reprogramming through the sequential administration of exogenous factors to culture medium from days 0 – 6 (D0 – D6). **(D,E)** Adult epidermal and dermal cells treated with *RSPO1, iPKC, WNT3A,* and *MMP14* demonstrate keratinocyte aggregation (day 2), cyst formation (day 4), planar epidermis formation (day 6), and mature hair follicle formation with hair shafts (D42) compared to untreated (control) adult cells which are unable to organize. Green immunofluorescence reflects K14 positive cells, nuclei are labeled with propidium iodide in red. Clusters of nuclei appear as larger red areas. **(F)** Quantification of hair regeneration, $p < 0.05$. **(G)** K14-H2BGFP immunofluorescence demonstrates derivation of hair follicle epidermal cells from donor adult cells.

signature gene datasets for human adult DP, newborn mouse DP, and embryonic mouse DC demonstrated 5–10% shared genes (Rendl et al., 2005; Sennett et al., 2015; Rezza et al., 2016; Mok et al., 2019). While low, this degree of overlap is statistically significant. Transcriptomic differences may arise from differences in species, age, or body region. Only deeply shared genes will be selected in common. Genes which are present in the majority of signature gene datasets are likely to be of fundamental importance for specification of the DP cell.

Edn3 was present in our human fetal DP enriched dataset as well as the human adult DP, newborn mouse DP, and embryonic mouse DC transcriptomes. EDN3 is upregulated in the DP following epilation but has no known role in follicle neogenesis (Rahmani et al., 2014; Li et al., 2017). Endothelins are most well-known for producing vasoconstriction of smooth muscle cells but also cause contraction of other cell types (Davenport et al., 2016). Recently, Heitman et al. (2020) demonstrated that dermal sheath (DS) cells express many genes characteristic of smooth muscle and DS contraction is responsible for movement of the DP into the superficial dermis during telogen. It is possible that the DP signals DS contraction through Edn3 expression, facilitating DP relocation

during hair germ to peg transitions during development. Given the widespread presence in DP transcriptomes, despite variation in species, age, and developmental stage, the role of *Edn3* deserves further investigation.

Bmp4 and *Trps1* were present in our human fetal DP transcriptome as well as adult human DP, newborn mouse DP, and embryonic mouse DC datasets. *Bmp4* is expressed in the DC and DP of the developing murine follicle and supports DP gene expression in culture (Jang et al., 2010; Chen et al., 2012). BMP expression is downstream of the Wnt/β-catenin pathway and the transcription of many DP genes is predicated upon the expression of BMPs (Rendl et al., 2008; Chen et al., 2012). Redundancy of BMP ligands is likely, as loss of individual BMPs, including BMP4, does not affect follicle neogenesis (Rendl et al., 2008; Nakamura et al., 2013). BMP signaling is believed to play a role in follicular patterning by inhibiting follicle fate in adjacent cells and is required for hair follicle induction by DP cells, through unclear mechanisms (Botchkarev et al., 2001; Rendl et al., 2008; Li et al., 2015). *Trps1* is expressed in the DC and DP of developing mouse follicles and is believed to function as both a transcriptional repressor and activator, increasing the expression of *Wnt* inhibitors (Fantauzzo et al., 2008, 2012). Though the absence of DP *Trps1* expression does not ablate hair follicle development, mutant mice lack vibrissae and exhibit a 50% reduction in pelage follicles (Nakamura et al., 2013).

Comparison of the human fetal DP transcriptome with other published transcriptomes demonstrated a subset of genes, including *Col23a1*, *Fgf10*, *Igfbp3*, *Inhba*, *Rspo3*, and *Sox2,* which were present in neonatal and embryonic, but not adult, DP cells, proposing importance for a stem cell-like state capable of inducing follicle formation. The Wnt/β-catenin pathway plays a critical role in hair follicle neogenesis from the earliest stages and may mediate the first dermal signal for placode formation (Saxena et al., 2019). Thus, a signaling molecule expressed by the DP which stimulates the *Wnt* pathway could be a critical signal for hair follicle induction. R-spondins are *Wnt* activators which function through both the canonical and non-canonical *Wnt*/β-catenin pathways. All four R-spondins are expressed in the mouse anagen DP and injection of *Rspo1*, *Rspo2*, and *Rspo3* into adult mouse dermis induces rapid telogen to anagen transition and activation of epidermal follicular stem cells (Li et al., 2016; Smith et al., 2016; Hagner et al., 2020; Harshuk-Shabso et al., 2020). Much less is known about the role of R-spondins in hair follicle development. *Rspo3* can activate the *Wnt*/planar cell polarity (PCP) pathway, known to play a role in hair follicle cell differentiation during development (Ohkawara et al., 2011; Chen and Chuong, 2012). In mice lacking expression of *Fuz*, a PCP gene, hair follicles failed to develop into mature structures (Dai et al., 2011). The absence of *Rspo3* is lethal and conditional knockout yields shorter limbs but no discernible effect on follicle neogenesis (Neufeld et al., 2012). *Rspo1* was also upregulated in human fetal, compared to adult, DP cells but a clear role of *Rspo1* in hair cycling or neogenesis has not been identified to date. For lack of a robust assay using human cells and the inability to conduct cycling or neogenesis assays in humans, we employed murine skin morphogenesis assays to study the effect of R-spondins on follicle development. The addition of *Rspo1* to dissociated adult mouse epidermal and dermal cells, in combination with inhibitors of the PKC pathway, induced epidermal aggregation in culture. With the further addition of WNT and MMP following keratinocyte aggregation, adult mouse epidermal and dermal cells formed functional, mature hair follicles (Lei et al., 2017a). In the absence of these four factors, adult mouse cells are unable to self-organize into any structure resembling a hair follicle. As there is known redundancy in the function of R-spondin genes (Neufeld et al., 2012; Hagner et al., 2020) and *Rspo1* rescues adult hair follicle neogenesis, *Rspo3* is also a promising candidate for the recovery of inductivity in human adult DP cells. In *in vitro* colony-forming assays with human dermal progenitor cells, addition of RSPO2/3 increased proliferation and the number and size of progenitor cell colonies (Hagner et al., 2020).

The functional capacity of hair follicle stem cells depends on the sum of activating and inhibitory signals (Li et al., 2015). While there are core activators and inhibitors shared by all DP cells, DPs of different species, ages, or follicle types may be subjected to alterations in the balance of signals and, thus, possess differing functional capacities, such as the specification of hair filament diameter, temporal and region-specific hair types, or anagen/telogen duration, which affects hair length (Lei et al., 2017b). Here, we sought to identify genes differentially upregulated in fetal DP, compared to adult DP, with the hope of finding transcriptional regulators responsible for fetal DP phenotype and function. Seven transcription factors were enriched in the promoter regions of genes upregulated in the fetal DP. Of these, SOX2 and GLI1 were predicted to be principal regulators of the fetal DP transcriptome. Similarly, *Shh and Wnt* pathways are known to be necessary for hair follicle development and both SOX2 and GLI1 are predicted upstream regulators of numerous *Wnt*-related genes. *Sox2* expression correlates with the trajectory of differentiation from dermal fibroblast to dermal condensate cell fate and is a well-known pluripotency marker (Gupta et al., 2019; Mok et al., 2019). Mutation of *Sox2*, however, does not abolish hair follicle formation but alters the ratio of hair follicle type in mice, suggesting that SOX2 is not the single predominant factor which specifies the fetal DP (Driskell et al., 2009; Nakamura et al., 2013). The downregulation of GLI1, a downstream effector of Shh signaling, in dermal condensates of *Shh* knockout mice is associated with a block in hair follicle development at the DC to DP transition (Chiang et al., 1999). Further evaluation is needed to determine the role of these upstream regulators in the initiation or maintenance of *Shh* and *Wnt* pathways during follicle development.

Limitations of this study include the use of non-clonal human tissue, leading to intersample variation. The acquisition of human tissue is appropriately protected through regulatory procedures, delaying the time from harvest to study and resulting in more sample degradation than murine samples. We extracted RNA from uncultured samples to avoid bias introduced by culturing, which can rapidly affect transcription (Higgins et al., 2013). The trade-off is low quantity RNA samples of lesser quality. However, the transcriptomes of similar tissues clustered together and reflected a hierarchy of similarities consistent with the trajectory of differentiation from fibroblast to DP (Gupta et al., 2019;

Mok et al., 2019). The transcriptome of the fetal DP was more similar to the DSC than IFD, contained signaling factors and transcriptional regulators known to play important roles in hair follicle development, and was similar to published murine DP and DC transcriptomes. This work creates a platform for the further study of candidate factors in human hair follicle development. The ability to understand the human signaling and regulatory milieu offers direct avenues for the treatment of alopecia and severe skin injury (Chueh et al., 2013).

DATA AVAILABILITY STATEMENT

The datasets presented in this study can be found in online repositories. The names of the repository/repositories and accession number(s) can be found below: https://www.ncbi.nlm.nih.gov/geo/, GSE149189.

ETHICS STATEMENT

The animal study was reviewed and approved by the Institutional Animal Care and Use Committee of the University of Southern California.

AUTHOR CONTRIBUTIONS

EW, Y-CL, ML, and C-MC designed the study. EW, ML, and T-XJ performed the experiments. EW and Y-CL performed the bioinformatics analysis. EW, Y-CL, and ML wrote the manuscript. All authors were involved in revision of the manuscript and approved the submitted version.

FUNDING

This work was supported by grants from the California Institute for Regenerative Medicine (TG2-01161), the American College of Surgeons, the A.P. Giannini Foundation, the L.K. Whittier Foundation, and NIH NIAMS AR60306 and GM125322. Y-CL and ML were supported by the Integrative Stem Cell Center, China Medical University and Hospital in Taiwan (CMU). ML was also supported by the National Natural Science Foundation of China (82003384), Fundamental Research Funds for the Central Universities (2020CDJYGSG003), and Scientific Research Foundation from Chongqing University (02210011044110), China. C-MC is a paid science advisor of CMU. Bioinformatics software and computing resources were funded by the USC Office of Research and the Norris Medical Library.

ACKNOWLEDGMENTS

We thank the University of Southern California's Next Generation Sequencing and Molecular Genomics Core for assistance with sample preparation and the Norris Medical Library Bioinformatics Service for assistance with data analysis.

SUPPLEMENTARY MATERIAL

The Supplementary Material for this article can be found online at: https://www.frontiersin.org/articles/10.3389/fcell.2020.583434/full#supplementary-material

REFERENCES

Anders, S., Pyl, P. T., and Huber, W. (2014). HTSeq – a Python framework to work with high-throughput sequencing data. *Bioinformatics* 31, 166–169. doi: 10.1093/bioinformatics/btu638

Botchkarev, V. A., Botchkareva, N. V., Nakamura, M., Huber, O., Funa, K., Lauster, R., et al. (2001). Noggin is required for induction of the hair follicle growth phase in postnatal skin. *FASEB J.* 15, 2205–2214. doi: 10.1096/fj.01-0207com

Botchkareva, N. V., Botchkarev, V. A., Welker, P., Airaksinen, M., Roth, W., Suvanto, P., et al. (2000). New roles for glial cell line-derived neurotrophic factor and neurturin: involvement in hair cycle control. *Am. J. Pathol.* 156, 1041–1053. doi: 10.1016/S0002-9440(10)64972-3

Brown, C. W., Houston-Hawkins, D. E., Woodruff, T. K., and Matzuk, M. M. (2000). Insertion of Inhbb into the Inhba locus rescues the Inhba-null phenotype and reveals new activin functions. *Nat. Genet.* 25, 453–457. doi: 10.1038/78161

Cambler, L., Plate, M., Sucov, H. M., and Pashmforoush, M. (2014). Nkx2-5 regulates cardiac growth through modulation of Wnt signaling by R-spondin3. *Development* 141, 2959–2971. doi: 10.1242/dev.103416

Chen, C. C., Plikus, M. V., Tang, P. C., Widelitz, R. B., and Chuong, C. M. (2015). The modulatable stem cell niche: tissue interactions during hair and feather follicle regeneration. *J. Mol. Biol.* 428, 1423–1440. doi: 10.1016/j.jmb.2015.07.009

Chen, D., Jarrell, A., Guo, C., Lang, R., and Atit, R. (2012). Dermal β-catenin activity in response to epidermal Wnt ligands is required for fibroblast proliferation and hair follicle initiation. *Development* 139, 1522–1533. doi: 10.1242/dev.076463

Chen, J., and Chuong, C. M. (2012). Patterning skin by planar cell polarity: the multi-talented hair designer. *Exp. Dermatol.* 21, 81–85. doi: 10.1111/j.1600-0625.2011.01425.x

Chiang, C., Swan, R. Z., Grachtchouk, M., Bolinger, M., Litingtung, Y., Robertson, E. K., et al. (1999). Essential role for sonic hedgehog during hair follicle morphogenesis. *Dev. Biol.* 205, 1–9. doi: 10.1006/dbio.1998.9103

Chueh, S. C., Lin, S. J., Chen, C. C., Lei, M., Wang, L. M., Widelitz, R. B., et al. (2013). Therapeutic strategy for hair regeneration: hair cycle activation, niche environment modulation, wound-induced follicle neogenesis, and stem cell engineering. *Expert Opin. Biol. Ther.* 13, 377–391. doi: 10.1517/14712598.2013.739601

Cotsarelis, G. (2006). Gene expression profiling gets to the root of human hair follicle stem cells. *J. Clin. Invest.* 116, 19–22. doi: 10.1172/JCI27490

Craven, A. J., Ormandy, C. J., Robertson, F. G., Wilkins, R. J., Kelly, P. A., Nixon, A. J., et al. (2001). Prolactin signaling influences the timing mechanism of the hair follicle: analysis of hair growth cycles in prolactin receptor knockout mice. *Endocrinology* 142, 2533–2539. doi: 10.1210/endo.142.6.8179

Dai, D., Zhu, H., Wlodarczyk, B., Zhang, L., Li, L., Allen, G., et al. (2011). Fuz controls the morphogenesis and differentiation of hair follicles through the formation of primary cilia. *J. Invest. Dermatol.* 131, 302–310. doi: 10.1038/jid.2010.306

Davenport, A. P., Hyndman, K. A., Dhaun, N., Southan, C., Kohan, D. E., Pollock, J. S., et al. (2016). Endothelin. *Pharmacol. Rev.* 68, 357–418. doi: 10.1124/pr.115.011833

De Lau, W. B., Snel, B., and Clevers, H. C. (2012). The R-spondin protein family. *Genome Biol.* 13:242. doi: 10.1186/gb-2012-13-3-242

Dobin, A., Davis, C. A., Schlesinger, F., Drenkow, J., Zaleski, C., Jha, S., et al. (2013). STAR: ultrafast universal RNA-seq aligner. *Bioinformatics* 29, 15–21. doi: 10.1093/bioinformatics/bts635

Driskell, R. R., Giangreco, A., Jensen, K. B., Mulder, K. W., and Watt, F. M. (2009). Sox2-positive dermal papilla cells specify hair follicle type in mammalian epidermis. *Development* 136, 2815–2823. doi: 10.1242/dev.038620

Fantauzzo, K. A., Bazzi, H., Jahoda, C. A. B., and Christiano, A. M. (2008). Dynamic expression of the zinc-finger transcription factor Trps1 during hair follicle morphogenesis and cycling. *Gene Expr. Patterns* 8, 51–57. doi: 10.1016/j.modgep.2007.10.006

Fantauzzo, K. A., Kurban, M., Levy, B., and Christiano, A. M. (2012). Trps1 and its target gene Sox9 regulate epithelial proliferation in the developing hair follicle and are associated with hypertrichosis. *PLoS Genet.* 8:e1003002. doi: 10.1371/journal.pgen.1003002

Foitzik, K., Paus, R., Doetschman, T., and Dotto, G. P. (1999). The TGF-beta 2 isoform is both a required and sufficient inducer of murine hair follicle morphogenesis. *Dev. Biol.* 212, 278–289. doi: 10.1006/dbio.1999.9325

Gupta, K., Levinsohn, J., Linderman, G., Chen, D., Sun, T. Y., Dong, D., et al. (2019). Single-cell analysis reveals a hair follicle dermal niche molecular differentiation trajectory that begins prior to morphogenesis. *Dev. Cell* 48, 17–31.e6. doi: 10.1016/j.devcel.2018.11.032

Hagner, A., Shin, W., Sinha, S., Alpaugh, W., Workentine, M., Abbasi, S., et al. (2020). Transcriptional profiling of the adult hair follicle mesenchyme reveals R-spondin as a novel regulator of dermal progenitor function. *iScience* 23:101019. doi: 10.1016/j.isci.2020.101019

Harnack, C., Berger, H., Antanaviciute, A., Vidal, R., Sauer, S., Simmons, A., et al. (2019). R-spondin 3 promotes stem cell recovery and epithelial regeneration in the colon. *Nat. Commun.* 10:4368. doi: 10.1038/s41467-019-12349-5

Harshuk-Shabso, S., Dressler, H., Niehrs, C., Aamar, E., and Enshell-Seijffers, D. (2020). Fgf and Wnt signaling interaction in the mesenchymal niche regulates the murine hair cycle clock. *Nat. Commun.* 11, 5114–5127. doi: 10.1038/s41467-020-18643-x

Heitman, N., Sennett, R., Mok, K. W., Saxena, N., Srivastava, D., Martino, P., et al. (2020). Dermal sheath contraction powers stem cell niche relocation during hair cycle regression. *Science* 367, 161–166. doi: 10.1126/science.aax9131

Higgins, C. A., Chen, J. C., Cerise, J. E., Jahoda, C. A., and Christiano, A. M. (2013). Microenvironmental reprogramming by three-dimensional culture enables dermal papilla cells to induce de novo human hair-follicle growth. *Proc. Natl. Acad. Sci. U.S.A.* 110, 19679–19688. doi: 10.1073/pnas.1309970110

Higgins, C. A., and Christiano, A. M. (2014). Regenerative medicine and hair loss: how hair follicle culture has advanced our understanding of treatment options for androgenetic alopecia. *Regen. Med.* 9, 101–111. doi: 10.2217/rme.13.87

Jahoda, C. A. (1992). Induction of follicle formation and hair growth by vibrissa dermal papillae implanted into rat ear wounds: vibrissa-type fibres are specified. *Development* 115, 1103–1109.

Jahoda, C. A., Oliver, R. F., Reynolds, A. J., Forrester, J. C., Gillespie, J. W., Cserhalmi-Friedman, P. B., et al. (2001). Trans-species hair growth induction by human hair follicle dermal papillae. *Exp. Dermatol.* 10, 229–237. doi: 10.1034/j.1600-0625.2001.100402.x

Jahoda, C. A., Reynolds, A. J., and Oliver, R. F. (1993). Induction of hair growth in ear wounds by cultured dermal papilla cells. *J. Invest. Dermatol.* 101, 584–590. doi: 10.1111/1523-1747.ep12366039

Jang, C. W., Gao, L., Dickinson, M. E., and Behringer, R. R. (2010). Bmp4-directed nuclear cyan fluorescent protein provides a tool for live imaging and reveals cellular resolution of Bmp4 expression patterns during embryogenesis. *Int. J. Dev. Biol.* 54, 931–938. doi: 10.1387/ijdb.092911cj

Kel, A. E., Gossling, E., Reuter, I., Cheremushkin, E., Kel-Margoulis, O. V., and Wingender, E. (2003). MATCH: a tool for searching transcription factor binding sites in DNA sequences. *Nucleic Acids Res.* 31, 3576–3579. doi: 10.1093/nar/gkg585

Lei, M., Schumacher, L. J., Lai, Y. C., Juan, W. T., Yeh, C. Y., Wu, P., et al. (2017a). Self-organization process in newborn skin organoid formation inspires strategy to restore hair regeneration of adult cells. *Proc. Natl. Acad. Sci. U.S.A.* 114, E7101–E7110. doi: 10.1073/pnas.1700475114

Lei, M., Yang, L., and Chuong, C. M. (2017b). Getting to the core of the dermal papilla. *J. Invest. Dermatol.* 137, 2250–2253. doi: 10.1016/j.jid.2017.07.824

Li, A., Lai, Y. C., Figueroa, S., Yang, T., Widelitz, R. B., Kobeliak, K., et al. (2015). Deciphering principles of morphogenesis from temporal and spatial patterns on the integument. *Dev. Dyn.* 244, 905–920. doi: 10.1002/dvdy.24281

Li, H., Fan, L., Zhu, S., Shin, M. K., Lu, F., Qu, J., et al. (2017). Epilation induces hair and skin pigmentation through an EDN3/EDNRB-dependent regenerative response of melanocyte stem cells. *Sci. Rep.* 7:7272. doi: 10.1038/s41598-017-07683-x

Li, N., Liu, S., Zhang, H. S., Deng, Z. L., Zhao, H. S., Zhao, Q., et al. (2016). Exogenous R-spondin1 induces precocious telogen-to-anagen transition in mouse hair follicles. *Int. J. Mol. Sci.* 17:582. doi: 10.3390/ijms17040582

Malik, T. H., von Stechow, D., Bronson, R. T., and Shivdasani, R. A. (2002). Deletion of the GATA domain of TRPS1 causes an absence of facial hair and provides new insights into the bone disorder in inherited tricho-rhino-phalangeal syndromes. *Mol. Cell. Biol.* 22, 8592–8600. doi: 10.1128/mcb.22.24.8592-8600.2002

Matys, V., Kel-Margoulis, O. V., Fricke, E., Liebich, I., Land, S., Barre-Dirrie, A., et al. (2006). TRANSFAC and its module TRANSCompel: transcriptional gene regulation in eukaryotes. *Nucleic Acids Res.* 34, D108–D110. doi: 10.1093/nar/gkj143

Mok, K. W., Saxena, N., Heitman, N., Grisanti, L., Srivastava, D., Muraro, M. J., et al. (2019). Dermal condensate niche fate specification occurs prior to formation and is placode progenitor dependent. *Dev. Cell* 48, 32–48.e5. doi: 10.1016/j.devcel.2018.11.034

Nakamura, M., Matzuk, M. M., Gerstmayer, B., Bosio, A., Lauster, R., Miyachi, Y., et al. (2003). Control of pelage hair follicle development and cycling by complex interactions between follistatin and activin. *FASEB J.* 17, 497–499. doi: 10.1096/fj.02-0247fje

Nakamura, M., Schneider, M. R., Schmidt-Ulrich, R., and Paus, R. (2013). Mutant laboratory mice with abnormalities in hair follicles morphogenesis, cycling, and/or structure: an update. *J. Dermatol. Sci.* 69, 6–29. doi: 10.1016/j.jdermsci.2012.10.001

Neufeld, S., Rosin, J. M., Ambasta, A., Hui, K., Shaneman, V., Crowder, R., et al. (2012). A conditional allele of Rspo3 reveals redundant function of R-spondins during mouse limb development. *Genesis* 50, 741–749. doi: 10.1002/dvg.22040

Ohkawara, B., Glinka, A., and Niehrs, C. (2011). Rspo3 binds syndecan 4 and induces Wnt/PCP signaling via clathrin-mediated endocytosis to promote morphogenesis. *Dev. Cell* 20, 303–314. doi: 10.1016/j.devcel.2011.01.006

Ohuchi, H., Hori, Y., Yamasaki, M., Harada, H., Sekine, K., Kato, S., et al. (2000). FGF10 acts as a major ligand for FGF receptor 2 IIIb in mouse multi-organ development. *Biochem. Biophys. Res. Commun.* 277, 643–649. doi: 10.1006/bbrc.2000.3721

Ohyama, M., Kobayashi, T., Sasaki, T., Shimizu, A., and Amagai, M. (2012). Restoration of the intrinsic properties of human dermal papilla in vitro. *J. Cell Sci.* 125, 4114–4125. doi: 10.1242/jcs.105700

Okonechnikov, K., Conesa, A., and Garcia-Alcalde, F. (2015). Qualimap 2: advanced multi-sample quality control for high-throughput sequencing data. *Bioinformatics* 32, 292–294. doi: 10.1093/bioinformatics/btv566

Panteleyev, A. A. (2016). Putting the human hair follicle cycle on the map. *J. Invest. Dermatol.* 136, 4–6. doi: 10.1016/j.jid.2015.10.052

Pispa, J., Pummila, M., Barker, P. A., Thesleff, I., and Mikkola, M. L. (2008). Edar and Troy signaling pathways act redundantly to regulate initiation of hair follicle development. *Hum. Mol. Genet.* 17, 3380–3391. doi: 10.1093/hmg/ddn232

Rahmani, W., Abbasi, S., Hagner, A., Raharjo, E., Kumar, R., Hotta, A., et al. (2014). Hair follicle dermal stem cells regenerate the dermal sheath, repopulate the dermal papilla, and modulate hair type. *Dev. Cell* 31, 543–558. doi: 10.1016/j.devcel.2014.10.022

Rendl, M., Lewis, L., and Fuchs, E. (2005). Molecular dissection of mesenchymal-epithelial interactions in the hair follicle. *PLoS Biol.* 3:e331. doi: 10.1371/journal.pbio.0030331

Rendl, M., Polak, L., and Fuchs, E. (2008). BMP signaling in dermal papilla cells is required for their hair follicle-inductive properties. *Genes Dev.* 22, 543–557. doi: 10.1101/gad.1614408

Rezza, A., Wang, Z. C., Sennett, R., Qiao, W. L., Wang, D. M., Heitman, N., et al. (2016). Signaling networks among stem cell precursors, transit-amplifying progenitors, and their niche in developing hair follicles. *Cell Rep.* 14, 3001–3018. doi: 10.1016/j.celrep.2016.02.078

Robinson, M. D., and Oshlack, A. (2010). A scaling normalization method for differential expression analysis of RNA-seq data. *Genome Biol.* 11:R25. doi: 10.1186/gb-2010-11-3-r25

Robinson, M. D., and Smyth, G. K. (2008). Small-sample estimation of negative binomial dispersion, with applications to SAGE data. *Biostatistics* 9, 321–332. doi: 10.1093/biostatistics/kxm030

Saxena, N., Mok, K. W., and Rendl, M. (2019). An updated classification of hair follicle morphogenesis. *Exp. Dermatol.* 28, 332–344. doi: 10.1111/exd.13913

Sennett, R., Wang, Z., Rezza, A., Grisanti, L., Roitershtein, N., Sicchio, C., et al. (2015). An integrated transcriptome atlas of embryonic hair follicle progenitors, their niche, and the developing skin. *Dev. Cell* 34, 577–591. doi: 10.1016/j.devcel.2015.06.023

Shimomura, Y., Agalliu, D., Vonica, A., Luria, V., Wajid, M., Baumer, A., et al. (2010). APCDD1 is a novel Wnt inhibitor mutated in hereditary hypotrichosis simplex. *Nature* 464, 1043–1047. doi: 10.1038/nature08875

Smith, A. A., Li, J., Liu, B., Hunter, D., Pyles, M., Gillette, M., et al. (2016). Activating hair follicle stem cells via R-spondin2 to stimulate hair growth. *J. Invest. Dermatol.* 136, 1549–1558. doi: 10.1016/j.jid.2016.01.041

Speir, M. L., Zweig, A. S., Rosenbloom, K. R., Raney, B. J., Paten, B., Nejad, P., et al. (2016). The UCSC genome browser database: 2016 update. *Nucleic Acids Res.* 44, D717–D725. doi: 10.1093/nar/gkv1275

St-Jacques, B., Dassule, H. R., Karavanova, I., Botchkarev, V. A., Li, J., Danielian, P. S., et al. (1998). Sonic hedgehog signaling is essential for hair development. *Curr. Biol.* 8, 1058–1068. doi: 10.1016/s0960-9822(98)70443-9

Szabo, R., Molinolo, A., List, K., and Bugge, T. H. (2007). Matriptase inhibition by hepatocyte growth factor activator inhibitor-1 is essential for placental development. *Oncogene* 26, 1546–1556. doi: 10.1038/sj.onc.1209966

Thangapazham, R. L., Klover, P., Wang, J. A., Zheng, Y., Devine, A., Li, S., et al. (2013). Dissociated human dermal papilla cells induce hair follicle neogenesis in grafted dermal-epidermal composites. *J. Invest. Dermatol.* 134, 538–540. doi: 10.1038/jid.2013.337

Ward, J. H. Jr. (1963). Hierarchical grouping to optimize an objective function. *J. Am. Stat. Assoc.* 58, 236–244. doi: 10.1080/01621459.1963.10500845

Zouvelou, V., Luder, H. U., Mitsiadis, T. A., and Graf, D. (2009). Deletion of BMP7 affects the development of bones, teeth, and other ectodermal appendages of the orofacial complex. *J. Exp. Zool. B Mol. Dev. Evol.* 312B, 361–374. doi: 10.1002/jez.b.21262

Conflict of Interest: The authors declare that the research was conducted in the absence of any commercial or financial relationships that could be construed as a potential conflict of interest.

Copyright © 2020 Weber, Lai, Lei, Jiang and Chuong. This is an open-access article distributed under the terms of the Creative Commons Attribution License (CC BY). The use, distribution or reproduction in other forums is permitted, provided the original author(s) and the copyright owner(s) are credited and that the original publication in this journal is cited, in accordance with accepted academic practice. No use, distribution or reproduction is permitted which does not comply with these terms.

frontiers in Cell and Developmental Biology

ORIGINAL RESEARCH
published: 04 December 2020
doi: 10.3389/fcell.2020.585132

Effects of ALA-PDT on the Healing of Mouse Skin Wounds Infected With *Pseudomonas aeruginosa* and Its Related Mechanisms

*Tao Yang†, Yang Tan†, Wentao Zhang, Weijiang Yang, Jiefu Luo, Ling Chen, Hong Liu, Guihong Yang and Xia Lei**

Department of Dermatology, Daping Hospital, The Army Medical University, Chongqing, China

OPEN ACCESS

Edited by:
Mingxing Lei,
Chongqing University, China

Reviewed by:
Xiuli Wang,
Tongji University, China
Eunice Lee,
Columbia University, United States
Ji Li,
Central South University, China

***Correspondence:**
Xia Lei
leixia1979@sina.com

† These authors have contributed equally to this work

Specialty section:
This article was submitted to Stem Cell Research, a section of the journal Frontiers in Cell and Developmental Biology

Received: *19 July 2020*
Accepted: *11 November 2020*
Published: *04 December 2020*

Citation:
Yang T, Tan Y, Zhang W, Yang W, Luo J, Chen L, Liu H, Yang G and Lei X (2020) Effects of ALA-PDT on the Healing of Mouse Skin Wounds Infected With Pseudomonas aeruginosa and Its Related Mechanisms. Front. Cell Dev. Biol. 8:585132. doi: 10.3389/fcell.2020.585132

Photodynamic therapy (PDT) is a promising new method to eliminate microbial infection and promote wound healing. Its effectiveness has been confirmed by some studies; however, the mechanisms of PDT in wound healing remain obscure. We used mouse skin wounds infected with *Pseudomonas aeruginosa* as a research object to explore the therapeutic effects and mechanisms of 5-aminolevulinic acid photodynamic therapy (ALA-PDT). ALA-PDT treatment significantly reduced the load of *P. aeruginosa* in the wound and surrounding tissues and promoted the healing of skin wounds in mice. Hematoxylin-eosin (HE) and Sirius red staining showed that ALA-PDT promoted granulation tissue formation, angiogenesis, and collagen regeneration and remodeling. After ALA-PDT treatment, the expression of inflammatory factors (TNF-α and IL-1β) first increased and then decreased, while the secretion of growth factors (TGF-β-1 and VEGF) increased gradually after treatment. Furthermore, ALA-PDT affected the polarization state of macrophages, activating and promoting macrophages from an M1 to an M2 phenotype. In conclusion, ALA-PDT can not only kill bacteria but also promote wound healing by regulating inflammatory factors, collagen remodeling and macrophages. This study further clarifies the mechanism of PDT in the healing of infectious skin wounds and provides further experimental evidence for its clinical treatment of skin wounds infected by *P. aeruginosa*.

Keywords: photodynamic therapy, wound healing, *Pseudomonas aeruginosa*, macrophagocyte, inflammatory factor

INTRODUCTION

Skin wounds are a common refractory disease in dermatology and occur in conjunction with microbial infection. The treatment of skin wounds usually includes systemic antibiotics, localized treatment with conventional clinical dressings, irrigation, negative pressure drainage, and surgical operation. However, these treatments used to address skin wounds are always time-consuming and expensive. Currently, there have been increasing reports of *Pseudomonas aeruginosa* infections resulting from skin wounds. *P. aeruginosa* is both highly resistant and naturally unsusceptible to many antibiotics and tends to form biofilms on infected surfaces.

Photodynamic therapy (PDT) has been shown to be a very successful therapy in clinical practice and is widely used in the treatment of certain skin diseases, such as acne, viral warts, and skin

cancers (St. Denis et al., 2014). Currently, PDT is a promising new method used to eliminate microbial infections because it can produce photochemical reactions using photosensitizers and light, producing singlet oxygen, which is toxic and inactivates target microorganisms. Some studies have confirmed that PDT is very effective against bacterial and fungal infections (Jori et al., 2006; Wardlaw et al., 2012; Sobotta et al., 2019). Additionally, PDT is considered an important innovative alternative treatment for the healing of skin wounds (Nesi-Reis et al., 2018) that can reduce treatment time and promote healing. However, the mechanisms of PDT in wound healing remain obscure.

In this study, we used mouse skin wounds infected with *P. aeruginosa* as a research model of infected skin wounds. The results showed that aminolevulinic acid photodynamic therapy (ALA-PDT) can not only kill bacteria but also promote wound healing by regulating inflammatory factors, collagen remodeling and macrophages.

MATERIALS AND METHODS

Establishment of Infected Skin Wounds on Model Animals

Sixty healthy Kunming mice weighing 30–40 g and aged 4–5 weeks were provided by the Animal Center of Daping Hospital (Army Military Medical University). One week before the experiment, the mice were house in the experimental environment at a room temperature of 20–25°C.

Pseudomonas aeruginosa (ATCC 27853) was stored at −80°C, and the cultures were maintained on Luria Bertani (LB) plates at 37°C with agitation (200 rpm). The bacterial suspensions were diluted to an optical density of 0.5 (approximately 2×10^8 CFU/mL bacteria) in normal saline, as shown by measurement with a turbidimetric instrument.

A model of acute bacterial infection was established after full-thickness skin excision. The mice were anesthetized by intraperitoneal injection of 10% chloral hydrate at a dose of 300 mg/kg. An area of the back (3 cm × 4 cm) was shaved. After disinfection with iodophor, two round symmetrical marks with a diameter of 10 mm were made in the skin along both sides of the spine, and each circle had an area of 0.79 cm^2. Full-thickness skin defects were made along the indentation with aseptic curved surgical scissors without damaging the fascial layer or muscle. A 100-μL suspension of *P. aeruginosa* (1×10^8 strains) was dripped into each wound. The wound was fixed with gauze, and the mice were divided into four groups housed in individual cages. The duration from inoculation to successful modeling is 24 h. After successful modeling, a green purulent secretion was found on the surface of the wounds on the mice, the temperature of the skin around the wound was increased, the behavior of the mice was depressed, the mice showed a poor appetite, and some mice had loose stools. After 7 days of treatment, these symptoms of mice in each group were significantly recovered, and there was no significant difference between the groups.

All the animal care and experimental protocols were reviewed and approved by the Laboratory Animal Welfare and Ethics Committee of Third Military Medical University. All the experiments were performed in accordance with the relevant guidelines for the care and use of laboratory animals.

ALA-PDT Treatment

5-Aminolevulinic acid (ALA) (Fudan Zhangjiang Company, Shanghai, China) was used as the photosensitizer with an incubation of 30 min. A stock solution was prepared by dissolving ALA powder in normal saline to a final concentration of 1.408 mol/L. A 630-nm LED (Omnibus, United Kingdom) light source was used to activate the ALA, and the output power density was 54 J/cm^2 (the laser power used was 90 MW/cm^2, and the treatment time was 10 min.). There were four experimental groups: the control group (without ALA or light irradiation), the red light group (light dose of 54 J/cm^2 without ALA), the ALA group (1.408 mol/L ALA with no light irradiation), and the ALA-PDT group (1.408 mol/L ALA with a light dose of 54 J/cm^2).

The mice were anesthetized and fixed for 24 h after infection. The mice in each group were bandaged, fed regularly and observed until the end of the corresponding time point of the experiment.

Counting of Bacteria on Wounds

The number of bacteria on the wound surface before treatment (day 0) and on the 1st, 3rd, 7th, and 14th days after treatment was measured. At each time point, the tissue at the wound edge for each group was cut, weighed, added to normal saline at a concentration of 0.01 g/ml and homogenized in a sterile homogenizer. For detection, the sample was diluted sixfold in normal saline, and 10 μl of homogenate from each dilution was evenly spread on two ordinary broth agar plates. The colony morphology was observed, and the colonies were counted.

Wound Healing Assay

A digital camera was used to take pictures before treatment (day 0) and on the 1st, 3rd, 7th, and 14th days after treatment, and the wound area and wound healing rate were calculated with standard grid paper as follows: wound healing rate (%) = (wound area before treatment−wound area after treatment)/wound area before treatment.

HE Staining

Before treatment (day 0) and on the 1st, 3rd, 7th, and 14th days after treatment, granulation tissue under the new epithelium was taken from the infected wounds of the mice under sterile conditions, immediately cut into 0.5 cm × 0.5 cm tissue blocks, and fixed in a 4% polycarboxylic acid solution. After conventional dehydration and clearing, the blocks were embedded in paraffin. The slices were 3–5-μm thick. A general optical microscope was used to observe inflammation, fibroblasts, the number of capillaries, and the degree of wound contraction and re-epithelialization after hematoxylin-eosin (HE) staining.

Sirius Red Polarized Light Assay

Before treatment (day 0) and on the 1st, 3rd, 7th, and 14th days after treatment, granulation tissue under the new epithelium

was taken from the infected wounds of the mice under sterile conditions, immediately cut into 0.5 cm × 0.5 cm tissue blocks, and fixed in a 4% polycarboxylic acid solution. After conventional dehydration and clearing, the blocks were embedded in paraffin. The slices were 3–5-μm thick. Then, polarized light microscopy was used to observe collagen remodeling after picric acid/Sirius red staining. Under a polarized light microscope, type I collagen fibers showed strong birefringence and were red or orange-yellow. Type III collagen fibers showed weak birefringence and were green and thin.

Western Blot Analysis

On the 3rd, 7th, and 14th days after treatment, granulation tissue under the new epithelium was taken from the infected wounds of the mice under sterile conditions. Nuclear and cytoplasmic protein lysates were prepared. The protein concentrations were measured with a BCA Protein Assay Kit (Beyotime, Nanjing, China). Equal amounts of protein (30 μg) were loaded into each lane of a 10% sodium dodecyl sulfate polyacrylamide gel electrophoresis (SDS-PAGE) gel and separated. After the proteins had been transferred onto polyvinylidene difluoride membranes, the membranes were blocked and incubated with primary antibodies at 4°C overnight. The following primary antibodies were used: anti-TNF-α, anti-IL-1β, anti-TGFβ-1, and anti-VEGF antibodies from Abcam (United States) and anti-β-actin antibody from Bioworld (United States). After incubation with secondary antibody (goat anti-rabbit), the membranes were treated with an enhanced chemiluminescence reagent mixture (Thermo Fisher Scientific, United States) for 5 min and imaged on a Vilber Lourmat Fusion FX5 system (China).

Immunofluorescence Staining

M1 and M2 macrophage polarization was observed by immunofluorescence staining. The marker of M1 and M2 macrophages are iNOS and CD163, respectively. The primary antibodies anti-iNOS (rabbit polyclonal antibody, 1:100) and anti-CD163 (goat polyclonal antibody, 1:100) from Servicebio (China) and the fluorescent second antibodies goat anti-rabbit (1:300) and rabbit anti-goat (1:300) from Servicebio (China) and DAPI from Abcam (United States) were used. After immunofluorescence staining, the paraffin sections were observed under a fluorescence microscope, and images were collected (DAPI emits blue light at 330–380 and 420 nm; FITC emits green light at 465–495 and 515–555 nm; Cy3 emits red light at 510–560 and 590 nm.). Eight visual fields were randomly selected from each slide, and three separate repeated experiments were conducted. All cells in the visual field were included in the statistical analysis.

Statistical Analyses

All experiments were independently performed with three replicates. The results are presented as the mean ± SD. Statistical differences were analyzed by one-way ANOVA with SPSS Statistics 20.0 (IBM, United States). *P*-values less than 0.05 were considered to indicate statistically significant differences.

RESULTS

Effects of ALA-PDT on *P. aeruginosa* Growth on the Wounds

To investigate the antibacterial effect of ALA-PDT, we detected the amount of *P. aeruginosa* on the wounds before treatment and on the 1st, 3rd, 7th, and 14th days after different treatments. The results are shown in **Table 1**. No significant differences in bacterial growth were observed in the control, light and ALA groups. The ALA-PDT group showed a significant antibacterial effect and significantly less bacteria relative to that in the control group ($P < 0.05$), indicating that ALA-PDT inhibited *P. aeruginosa* growth (**Figure 1**).

Effects of ALA-PDT on the Wounds Healing Rate

To investigate the effect of ALA-PDT on wound healing, we observed the wound healing rates on the 1st, 3rd, 7th, and 14th days after different treatments. The results are shown in **Table 1**. No significant differences in wound healing rate were observed in the control, light and ALA groups. Furthermore, there were no significant differences in wound healing among the groups on 1st day after treatment. The ALA-PDT group showed significantly increased wound healing relative to that in the control group ($P < 0.05$) on the 3rd, 7th, and 14th days (**Figure 2**).

TABLE 1 | Results of *P. aeruginosa* growth on the wounds (units: 10^6CFU/g).

	Control	ALA	Red light	ALA-PDT
Day 0	21.5 ± 2.5	22.0 ± 2.4	19.7 ± 2.8	21.0 ± 2.5
Day 1	18.3 ± 2.0	17.5 ± 2.2	15.9 ± 1.3	2.1 ± 0.1*
Day 3	15.7 ± 1.6	14.6 ± 1.2	12.5 ± 1.6	1.0 ± 0.1*
Day 7	12.0 ± 1.5	10.5 ± 0.6	11.2 ± 1.2	0.3 ± 0.1*
Day 14	7.2 ± 1.3	5.3 ± 0.4	6.2 ± 1.7	0.0 ± 0.0*

$P < 0.05$ versus the other groups.

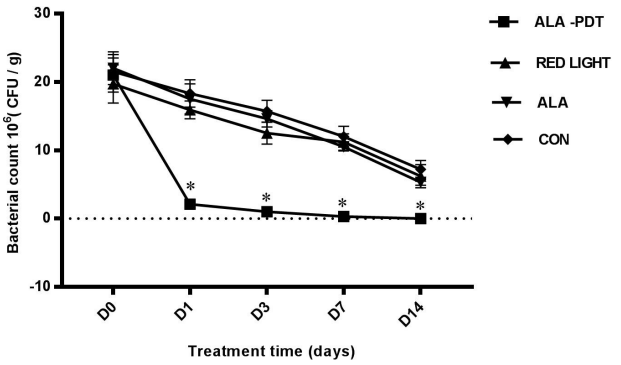

FIGURE 1 | Bacterial counting on wounds. The amounts of *P. aeruginosa* were counted on wounds before treatment (D0) and on the 1st (D1), 3rd (D3), 7th (D7), 14th (D14) day after different treatments. *$P < 0.05$ versus the other groups.

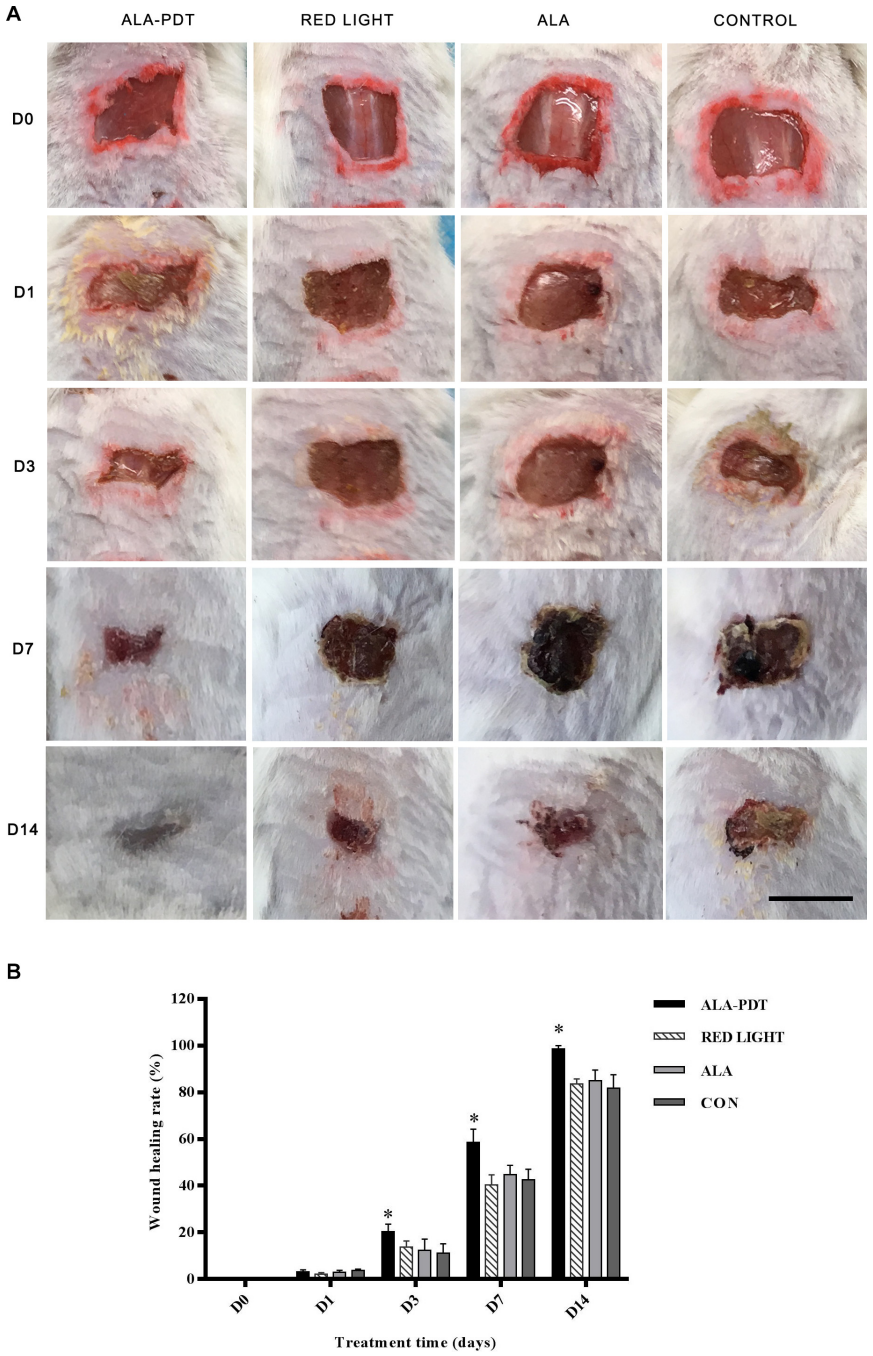

FIGURE 2 | Effects of ALA-PDT for the healing rate on wounds. **(A)** The wound pictures of healing process. Scale bar indicate 1 cm. **(B)** The healing rate was counted before treatment (D0) and on the 1st (D1), 3rd (D3), 7th (D7), 14th (D14) day after different treatments. $^*P < 0.05$ versus the other groups.

Observation of the Effects of ALA-PDT on Wounds by HE Staining

The HE staining results on the 1st and 3rd days after treatment did not significantly differ among the groups. On the 7th day after treatment, obvious ulcer formation was found in the control group, light group and ALA group, there was no epithelioid hyperplasia, and a large number of inflammatory cells had accumulated in the periwound tissues. In the ALA-PDT group, more granulation tissue and neovascularization were observed, and only the superficial dermis contained inflammatory cells; on the 14th day after treatment, some skin defects remained in the control group, light group and ALA group, which contained blisters, blood, scabs, remaining inflammatory cells and granulation tissue formation. In the ALA-PDT group,

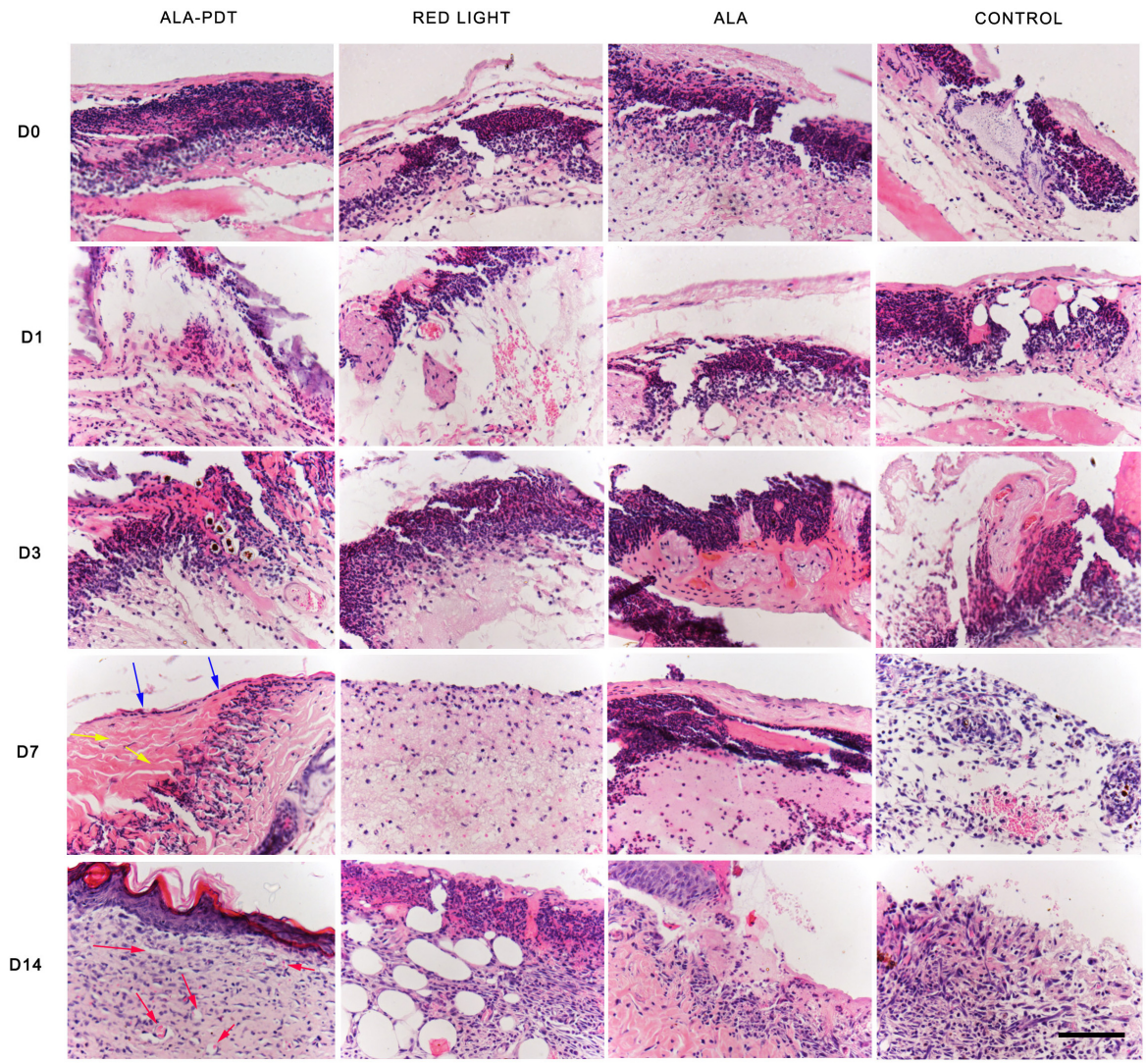

FIGURE 3 | HE staining assay. The HE staining results of each group before treatment (D0) and on the 1st (D1), 3rd (D3), 7th (D7), 14th (D14) day after different treatments. The blue arrows indicate the structure of the new epithelium. The yellow arrows indicate relatively thickened and increased collagen fibers. The red arrows indicate new capillaries. Scale bar indicate 100 μm.

epithelial cells, and fibrous tissue proliferation were clearly observed, and only some inflammatory cells had infiltrated the tissue around blood vessels (**Figure 3**).

Sirius Red Polarized Light Observation of the Effects of ALA-PDT on Wounds

Before treatment (day 0) and on the 1st day after treatment, collagen in each group was short and orderly arranged. On the 3rd day after treatment, the collagen fibers distributed in groups were thickened and increased in varying degrees in each group. Compared with control group, ALA group and red light group, the collagen distribution in ALA-PDT group was more dense. On the 7th day after treatment, compared with that in the control group, ALA group and light group, the collagen in the ALA-PDT group was thicker and denser, and unlike the other groups, the ALA-PDT exhibited collagen distributed in bundles. On the 14th day after treatment, compared with that in the control group, ALA group, and light group, the morphology of the collagen in the ALA-PDT group was coarser, and the collagen was more uniform (**Figure 4**).

Western Blot Analysis of TNF-α, IL-1β, TGFβ-1, and VEGF Levels in Wounds

To determine the mechanism by which ALA-PDT promotes wound healing, we further investigated the levels of TNF-α, IL-1β, TGFβ-1, and VEGF in wounds. Compared to the control group, red light group, and ALA group, the levels of TNF-α and IL-1β in the ALA-PDT group were higher on the 3rd day after treatment ($P < 0.05$) and lower on the 7th and 14th days after treatment ($P < 0.05$). Compared to the control group, red light

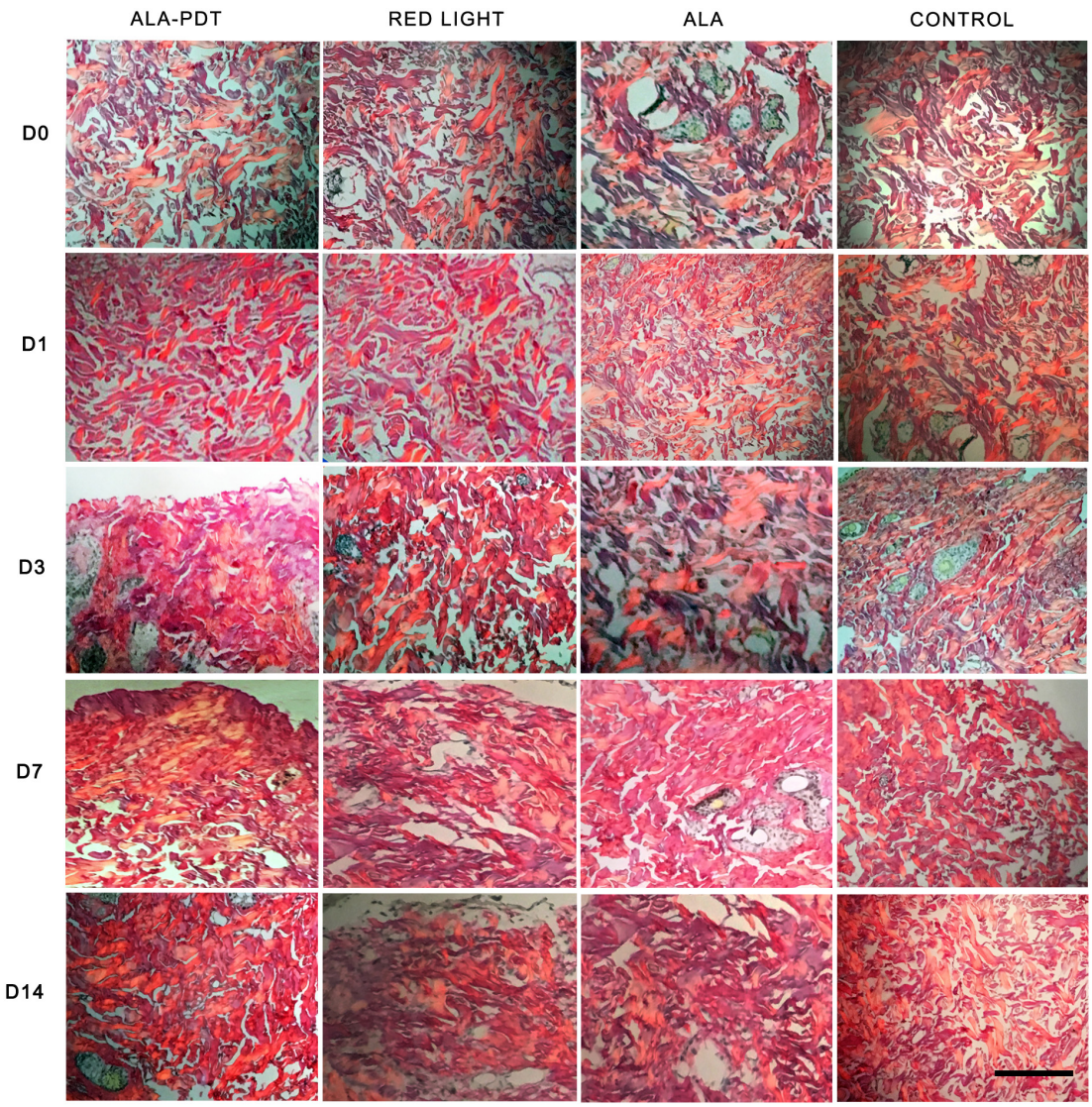

FIGURE 4 | Sirius red polarized light method assay. The picric acid Sirius red staining results of each group before treatment (D0) and on the 1st (D1), 3rd (D3), 7th (D7), 14th (D14) day after different treatments. Scale bar indicate 50 μm.

group, and ALA group, the levels of TGFβ-1 and VEGF in the ALA-PDT group were higher than those in the control group on the 3rd, 7th, and 14th days after treatment ($P < 0.05$) (**Figure 5**).

Effects of ALA-PDT on M1 and M2 Macrophages in Wounds

To gain further insight into the pro-healing effect of ALA-PDT on wounds, we determined the numbers of M1 and M2 macrophages in wounds. Cells stained red were considered M1 macrophages, and cells stained green were considered M2 macrophages.

Immunofluorescence staining showed that the number of M1 macrophages in ALA-PDT group was significantly increased compared with the control group on the 1st day, while on the 7th and 14th day, the number of M1 macrophages in ALA-PDT group was significantly lower than that in control group. On 1st, 3rd, 7th, and 14th day, the number of M2 macrophages in ALA-PDT group was significantly higher than that in control group (**Figure 6**).

DISCUSSION

Photodynamic therapy is a promising new method used to eliminate microbial infection and an important innovative alternative treatment for healing skin wounds. The treatment of infected skin wounds, including skin ulcers, skin abscesses, and skin sinus tracts, has advanced, but the mechanism by which PDT induces healing remains unclear.

Skin-infected wounds are a common refractory disease in dermatology that seriously affects patient quality of life and is

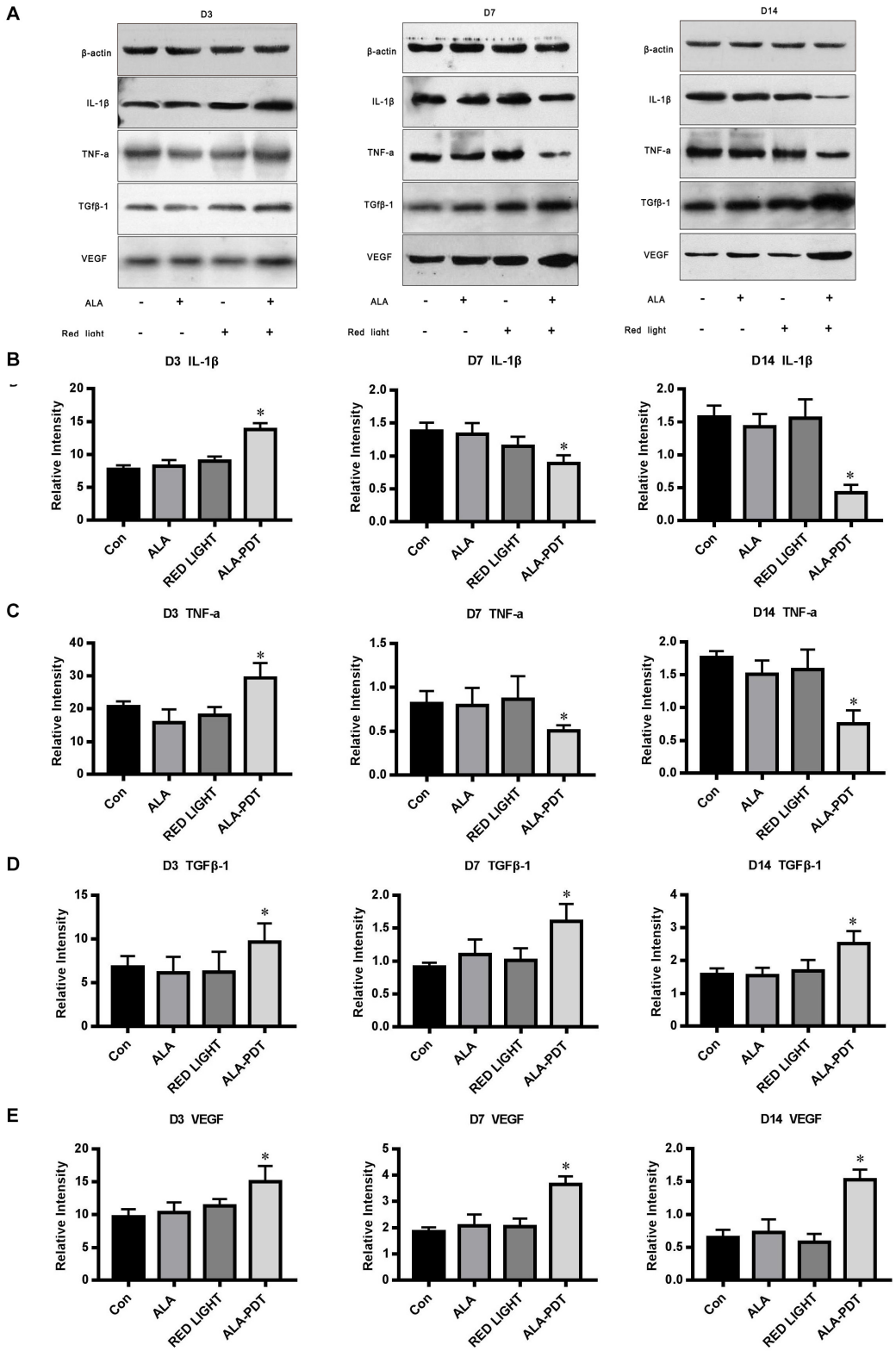

FIGURE 5 | Effects of ALA-PDT on TNF-α, IL-1β, TGFβ-1, and VEGF. **(A)** Western blot assay of TNF-α, IL-1β, TGFβ-1, and VEGF proteins on the 3rd (D3), 7th (D7), 14th (D14) day after different treatments in wounds. **(B)** Western blot analysis of IL-1β. $^*P < 0.05$ versus the other groups. **(C)** Western blot analysis of TNF-α. $^*P < 0.05$ versus the other groups. **(D)** Western blot analysis of TGFβ-1. $^*P < 0.05$ versus the other groups. **(E)** Western blot analysis of VEGF. $^*P < 0.05$ versus the other groups.

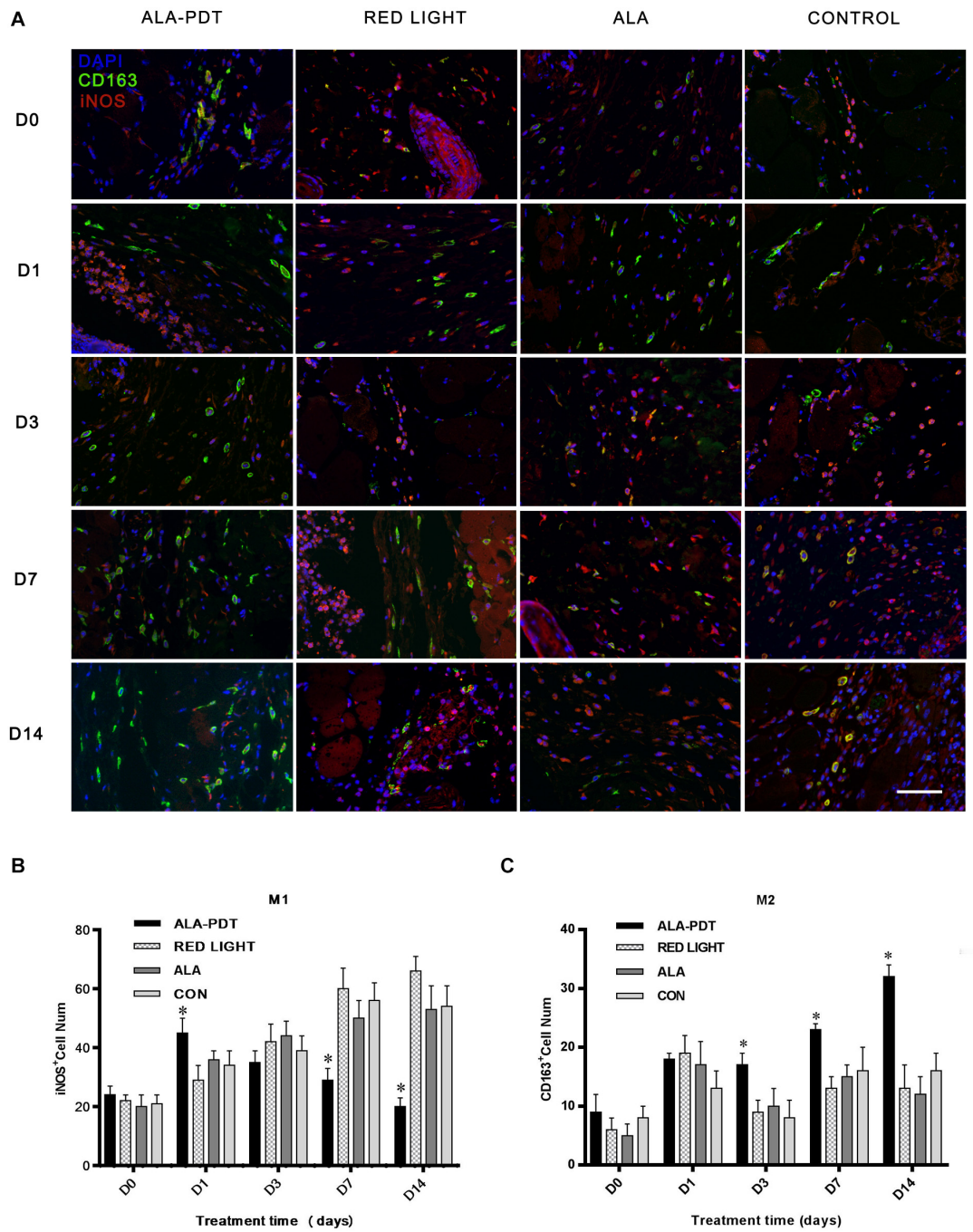

FIGURE 6 | Effects of ALA-PDT on M1 and M2 macrophages in wounds. **(A)** Immunofluorescence staining of M1 and M2 macrophages before treatment (D0) and on the 1st (D1), 3rd (D3), 7th (D7), 14th (D14) day after treatment in wounds. The primary antibodies anti-iNOS (rabbit polyclonal antibody, 1:100) and anti-CD163 (goat polyclonal antibody, 1:100) from Servicebio (China) and the fluorescent second antibodies goat anti-rabbit (1:300) and rabbit anti-goat (1:300) from Servicebio (China) and DAPI from Abcam (United States) were used. The marker of M1 and M2 macrophages are iNOS and CD163, respectively. Cells stained red were considered M1 macrophages, and cells stained green were considered M2 macrophages. **(B,C)** Immunofluorescence staining analysis of M1 and M2 macrophages. $^*P < 0.05$ versus the control groups. Scale bar indicate 20 μm.

costly. Infections with *P. aeruginosa*, a Gram-negative bacterium, are difficult to treat. *P. aeruginosa* is a common pathogen in serious skin wounds and infections of the urinary and respiratory systems. Tan et al. (2018) reported that ALA-PDT can kill planktonic and viable biofilm-associated *P. aeruginosa* cells, destroy biofilm structures, reduce virulence factor secretion, and affect QS system gene expression. Additionally, the incidence of *P. aeruginosa* infection resulting from skin wounds is increasing.

Therefore, in this study, we used skin wounds in mice infected with *P. aeruginosa* as a research model of infected skin wounds.

The principle of PDT is in the administration of a photosensitiser (PS), followed by irradiation of the lesion with visible light in the presence of molecular oxygen, which generates a variety of ROS. The mechanisms by which ROS induce direct cell death through different pathways, including apoptosis, necrosis and/or autophagy, depend on the type of cell treated, dose of light supplied, concentration of PS used and intracellular location of the PS (Agostinis et al., 2011). PDT has been widely used in dermatology to treat certain skin cancers, viral warts, vascular diseases, and acne. With further in-depth research, an increasing number of studies have found that PDT is very effective against microbial infection and can promote the healing of infected skin wounds, especially skin wounds or skin ulcers infected by resistant or rare bacteria. Lei et al. (2015) reported that when half of 26 lower limb ulcers infected with *P. aeruginosa* were treated by PDT, PDT had significant antibacterial and pro-healing effects on the infected ulcers. Brown (2012) reported the potential of PDT to accelerate wound healing and prevent clinical infection. Morley et al. (2013) reported a randomized controlled trial of PDT for the treatment of chronic ulcers, the results of which suggested that PDT significantly reduced the wound bacterial load and clearly tended to promote healing in the PDT group.

The basic physiological process of cutaneous healing is dynamic and complex, involving a diverse set of molecular, cellular, and biochemical events that culminate in the reconstruction of damaged tissue. Wound healing involves a variety of cells, including inflammatory cells, fibroblasts, keratinocytes, and endothelial cells, which produce numerous inflammatory cytokines such as IL-1β and TNF-α (Werner and Grose, 2003). The ability of PDT to effectively eradicate microorganisms contributes significantly to the wound healing process. In this study, the load of *P. aeruginosa* was rapidly reduced after PDT treatment. PDT can also directly affect the process of wound healing. Inflammation is one of the steps involved in the mechanism of PDT in wound healing. Inflammation is divided into acute inflammation and chronic inflammation. Acute inflammation plays a beneficial role against infection and lesions (Kundu and Surh, 2012), contributing to wound healing, while chronic inflammation inhibits the healing process. The inflammatory process is a crucial part of healing since some inflammatory mediators at low-concentrations are related to cell proliferation and migration and also to the host defense against pathogens (Li et al., 2007; Liu et al., 2013). It has been reported that high TNF-α level inhibit angiogenesis (Fajardo et al., 1992) and wound repair is promoted due to inhibition of TNF-α (Mori et al., 2002). PDT can intervene by stimulating acute inflammation, contributing to changes in the physiological processes in chronic wounds, regardless of whether they are infected, promoting healing (Devirgiliis et al., 2011; Cappugi et al., 2014; Lei et al., 2015). Recent studies indicate that PDT induces a localized acute inflammatory response, leading to activation of the immune system (Anzengruber et al., 2015). Neutrophils are the first immune cells to arrive at a lesion, which is facilitated by the generation of TNF-α (Gollnick and Brackett, 2010; Cappugi et al., 2014). Other studies have also shown that PDT has a significant impact on neutrophil activation (Brackett and Gollnick, 2011; Gollnick, 2012), which can contribute to the increase in pro-inflammatory cytokines after PDT (Domínguez et al., 2010; Mroz and Hamblin, 2011). Chronic and persistent inflammation is a hallmark of most chronic wounds, but the relationships between chronic inflammation and PDT have scarcely been reported in the literature. The results of this study indicated increased acute inflammation in the early stage of wound healing and decreased chronic inflammation in the middle and later stages of wound healing in the PDT treatment group compared with the other groups. Through a comparative study of HE staining in the wound tissues in each group at different time points after treatment, it was found that the acute inflammatory reaction was more pronounced in the PDT treatment group than the other groups, accompanied by tissue edema in the early stage of treatment (1–3 days), while the chronic inflammatory reaction was significantly decreased in the PDT treatment group compared with the other groups in the middle and later stages of the healing process (7–14 days). The number of new capillaries increased sharply, and the collagen fibers were also bulkier and more obvious in the PDT treatment group compared to the other groups in the middle and later stages of the healing process. In this study, the expression of TNF-α and IL-1β in first increased and then decreased in the PDT treatment group; that is, the expression of TNF-α and IL-1β was higher in the acute inflammatory stage, while their expression was lower in the chronic stage in the PDT treatment group compared to the other groups. Therefore, PDT can promote wound healing in both the acute and chronic inflammatory stages.

Lesions release mediators (leukocytes and platelet migration) that start the repair process by first stimulating the inflammatory process. In sequence, the proliferative stage, in which re-epithelization, angiogenesis and an increase in fibroblast numbers occur, is first observed. The early onset of wound re-epithelialization after PDT, with the presence of young fibroblasts, fibrin, and granulation tissue, has been described by studies in animal models (Garcia et al., 2010; Sperandio et al., 2010). Garcia et al. (2010) described the positive effects of PDT on collagen deposition, proliferation, and angiogenesis in 3rd degree burns. In this study, the number of new capillaries increased rapidly, and the collagen fibers were thicker, denser, and distributed in bundles after PDT treatment. These results suggested that ALA-PDT can stimulate collagen proliferation and angiogenesis, promoting wound healing.

In the process of proper wound remodeling, balance between the synthesis and degradation of extracellular matrix is required, and it is evident that PDT modulates the production of TGF-β (Faffar et al., 2011). Studies of excisional wounds in human skin revealed an increase in TGF-β1 and β3, promoting the ordered deposition in collagen fibers (Mills et al., 2014). In this study, the expression levels of TGF β-1 and VEGF in the PDT treatment group and other groups tended to be increased in the healing process, while their expression levels were significantly higher in the PDT treatment groups than in the other groups at the same time. Compared with VEGF expression, TGF β-1 expression was

most obviously increased in the 20% ALA-PDT group, suggesting that PDT regulates and activates cell growth factors, which would more deeply affect the wound tissue repair process.

The roles of inflammatory cytokines and the inflammatory response in the mechanism of bacterial infection after wound formation cannot be ignored. These inflammatory factors are partly produced by macrophages, which can be activated by monocytes. Macrophage activation is a continuous process. At the early stage of injury, macrophages can be activated by cytokines to adopt a pro-inflammatory M1 phenotype, while in the middle and later stages of injury, they can be activated to adopt an anti-inflammatory M2 phenotype. M1 macrophages have strong phagocytic and killing abilities, allowing them to phagocytize, ingest and kill pathogenic microorganisms, and other antigens through receptors on the membrane surface and participate in the innate immune response of the body. M1 macrophages are also important antigen-presenting cells that can ingest and process pathogens, present antigens, and stimulate the adaptive immune response. Activated M2 macrophages can secrete a variety of bioactive substances, including cytokines and other complement components, to regulate the immune response and participate in the processes of inflammation, tissue repair and tissue regeneration. When normal tissues are stimulated or damaged by pathogens, growth factors such as TGF-β1 and chemokines can decompose the tissues, promote the translocation of monocytes in the peripheral circulatory system to damaged sites, and stimulate monocytes to further their differentiate into new macrophages. Then, macrophages mediate the immune response, kill pathogens, stimulate angiogenesis, and influence tissue repair (Lingen, 2001). In this study, by double immunofluorescence staining, we observed more M1 macrophages in wound tissues in the PDT treatment groups in the acute inflammatory stage, which indicated that ALA-PDT could promote the activation of macrophages in the early stage of treatment and increase their phagocytic ability. Seven to fourteen days after PDT, the number of M2 macrophages increased significantly, and the M1 macrophages decreased significantly, which was consistent with the proportion of inflammatory factor (IL-1β, TNF-α)/growth factor (TGFβ-1, VEGF) expression. These results suggest that PDT can promote the release of anti-inflammatory factors to weaken the damaging effect of the immune inflammatory response on tissue cells, thus promoting cell proliferation and tissue regeneration.

CONCLUSION

In summary, PDT acts in several stages of the healing process and tends to accelerate tissue repair. Our results demonstrate that ALA-PDT can not only kill bacteria but also promote wound healing by regulating inflammatory factors, collagen remodeling and macrophages. This study further clarifies the mechanism of PDT on infectious skin wound healing and provides further experimental evidence for its clinical treatment of skin wounds infected by *P. aeruginosa*. In addition, these results will be of great benefit to expand research on the mechanism by which PDT affects wound healing.

DATA AVAILABILITY STATEMENT

The original contributions presented in the study are included in the article/supplementary material, further inquiries can be directed to the corresponding author/s.

ETHICS STATEMENT

The animal study was reviewed and approved by the Laboratory Animal Welfare and Ethics Committee of Third Military Medical University.

AUTHOR CONTRIBUTIONS

TY, YT, WZ, WY, and XL conceived and designed the study. TY, JL, LC, and HL performed acquisition and analysis of data. JL and GY performed the statistical analysis. YT wrote the first draft of the manuscript. XL provided the administrative, technical, or material support. All authors contributed to the article and approved the submitted version.

FUNDING

This study was funded by the National Natural Foundation of China (81773348) and the Clinical Research Talent Training Program of Army Medical University of China (2018XLC2030 and 2018XLC3065).

REFERENCES

Agostinis, P., Berg, K., Cengel, K. A., Foster, T. H., Girotti, A. W., Gollnick, S. O., et al. (2011). Photodynamic therapy of cancer: An update. *CA: A Cancer J. Clinic.* 61, 250–281. doi: 10.3322/caac.20114

Anzengruber, F., Avci, P., Freitas, L. F., and Hamblin, M. R. (2015). T-cell mediated anti-tumor immunity after photodynamic therapy: why does it not always work and how can we improve it? *Photochem. Photobiol. Sci.* 14, 1492–1509. doi: 10.1039/c4pp00455h

Brackett, C. M., and Gollnick, S. O. (2011). Photodynamic therapy enhancement of anti-tumor immunity. *Photochem. Photobiol Sci.* 10:649. doi: 10.1039/c0pp00354a

Brown, S. (2012). Clinical Antimicrobial Photodynamic Therapy: Phase II Studies in Chronic Wounds. *J. Natl. Compr. Cancer Net.* 10, 80–83. doi: 10.6004/jnccn.2012.0182

Cappugi, P., Comacchi, C., and Torchia, D. (2014). Photodynamic therapy for chronic venous ulcers. *Acta Dermatovenerol Croat* 22, 129–131.

Devirgiliis, V., Panasiti, V., Fioriti, D., Anzivino, E., Bellizzi, A., Cimillo, M., et al. (2011). Antibacterial Activity of Methyl Aminolevulinate Photodynamic Therapy in the Treatment of a Cutaneous Ulcer. *Int. J. Immunopathol. Pharmacol.* 24, 793–795. doi: 10.1177/039463201102400326

Domínguez, A., Gómez, C., García-Kass, A. I, and García-Nuñez, J. A. (2010). IL-1β, TNF-α, total antioxidative status and microbiological findings in chronic periodontitis treated with fluorescence-controlled Er:YAG laser radiation. *Lasers Surg. Med.* 42, 24–31. doi: 10.1002/lsm.20873

Faffar, M. D., Mills, S. J., Griffiths, C. E. M., Ashcroft, G. S., and Rhodes, L. E. (2011). Photodynamic therapy modulates production of TGF-b1 in association with improved healing in excisional wounds of human skin. *Br. J. Dermatol.* 164:911. doi: 10.1111/j.1365-2133.2011.10279.x

Fajardo, L. F., Kwan, H. H., Kowalski, J., Prionas, S. D., and Allison, A. C. (1992). Dual role of tumor necrosis factor-alpha in angiogenesis. *Am. J. Pathol.* 140, 539–544.

Garcia, V. G., de Lima, M. A., Okamoto, T., Milanezi, L. A., Junior, E. C., Fernandes, L. A., et al. (2010). Effect of photodynamic therapy on the healing of cutaneous third-degree-burn: histological study in rats. *Lasers Med. Sci.* 25, 221–228. doi: 10.1007/s10103-009-0694-z

Gollnick, S. O. (2012). Photodynamic Therapy and Antitumor Immunity. *J. Natl. Compr. Cancer Net.* 10, 40–43. doi: 10.6004/jnccn.2012.0173

Gollnick, S. O., and Brackett, C. M. (2010). Enhancement of anti-tumor immunity by photodynamic therapy. *Immunol. Res.* 46, 216–226. doi: 10.1007/s12026-009-8119-4

Jori, G., Fabris, C., Soncin, M., Ferro, S., Coppellotti, O., Dei, D., et al. (2006). Photodynamic therapy in the treatment of microbial infections: Basic principles and perspective applications. *Lasers Surg. Med.* 38, 468–481. doi: 10.1002/lsm.20361

Kundu, J. K., and Surh, Y. (2012). Emerging avenues linking inflammation and cancer. *Free Rad. Biol. Med.* 52, 2013–2037. doi: 10.1016/j.freeradbiomed.2012.02.035

Lei, X., Liu, B., Huang, Z., and Wu, J. (2015). A clinical study of photodynamic therapy for chronic skin ulcers in lower limbs infected with *Pseudomonas aeruginosa*. *Archiv. Dermatol. Res.* 307, 49–55. doi: 10.1007/s00403-014-1520-4

Li, J., Chen, J., and Kirsner, R. (2007). Pathophysiology of acute wound healing. *Clin. Dermatol.* 25, 9–18. doi: 10.1016/j.clindermatol.2006.09.007

Lingen, M. W. (2001). Role of leukocytes and endothelial cells in the development of angiogenesis in inflammation and wound healing. *Arch. Pathol. Lab. Med.* 125, 67–71.

Liu, J., Du, X., Chen, J., Hu, L., and Chen, L. (2013). The induction expression of human beta-defensins in gingival epithelial cells and fibroblasts. *Arch. Oral. Biol.* 58, 1415–1421. doi: 10.1016/j.archoralbio.2013.04.013

Mills, S. J., Farrar, M. D., Ashcroft, G. S., Griffiths, C. E. M., Hardman, M. J., and Rhodes, L. E. (2014). Topical photodynamic therapy following excisional wounding of human skin increases production of transforming growth factor-β3 and matrix metalloproteinases 1 and 9, with associated improvement in dermal matrix organization. *Br. J. Dermatol.* 171, 55–62. doi: 10.1111/bjd.12843

Mori, R., Kondo, T., Ohshima, T., Ishida, Y., and Mukaida, N. (2002). Accelerated wound healing in tumor necrosis factor receptor p55-deficient mice with reduced leukocyte infiltration. *FASEB J.* 16, 963–974. doi: 10.1096/fj.01-0776com

Morley, S., Griffiths, J., Philips, G., Moseley, H., Grady, C., Mellish, K., et al. (2013). Phase IIa randomized, placebo-controlled study of antimicrobial photodynamic therapy in bacterially colonized, chronic leg ulcers and diabetic foot ulcers: a new approach to antimicrobial therapy. *Br. J. Dermatol.* 168, 617–624. doi: 10.1111/bjd.12098

Mroz, P., and Hamblin, M. R. (2011). The immunosuppressive side of PDT. *Photochem. Photobiol. Sci.* 10:751. doi: 10.1039/c0pp00345j

Nesi-Reis, V., Lera-Nonose, D. S. S. L., Oyama, J., Silva-Lalucci, M. P. P., Demarchi, I. G., Aristides, S. M. A., et al. (2018). Contribution of photodynamic therapy in wound healing: A systematic review. *Photodiagnosis Photodyn. Ther.* 21, 294–305. doi: 10.1016/j.pdpdt.2017.12.015

Sobotta, L., Skupin-Mrugalska, P., Piskorz, J., and Mielcarek, J. (2019). Porphyrinoid photosensitizers mediated photodynamic inactivation against bacteria. *Eur. J. Med. Chem.* 175, 72–106. doi: 10.1016/j.ejmech.2019.04.057

Sperandio, F. F., Simoes, A., Aranha, A. C., Correa, L., and Orsini, M. D. S. S. (2010). Photodynamic therapy mediated by methylene blue dye in wound healing. *Photomed. Laser Surg.* 28, 581–587. doi: 10.1089/pho.2009.2601

St. Denis, T. G., Dai, T., Izikson, L., Astrakas, C., Anderson, R. R., Hamblin, M. R., et al. (2014). All you need is light. *Virulence* 2, 509–520. doi: 10.4161/viru.2.6.17889

Tan, Y., Cheng, Q., Yang, H., Li, H., Gong, N., Liu, D., et al. (2018). Effects of ALA-PDT on biofilm structure, virulence factor secretion, and QS in *Pseudomonas aeruginosa*. *Photodiagnosis and Photodyn. Ther.* 24, 88–94. doi: 10.1016/j.pdpdt.2018.07.005

Wardlaw, J. L., Sullivan, T. J., Lux, C. N., and Austin, F. W. (2012). Photodynamic therapy against common bacteria causing wound and skin infections. *Vet. J.* 192, 374–377. doi: 10.1016/j.tvjl.2011.09.007

Werner, S., and Grose, R. (2003). Regulation of Wound Healing by Growth Factors and Cytokines. *Physiolog. Rev.* 83, 835–870. doi: 10.1152/physrev.2003.83.3.835

Conflict of Interest: The authors declare that the research was conducted in the absence of any commercial or financial relationships that could be construed as a potential conflict of interest.

Copyright © 2020 Yang, Tan, Zhang, Yang, Luo, Chen, Liu, Yang and Lei. This is an open-access article distributed under the terms of the Creative Commons Attribution License (CC BY). The use, distribution or reproduction in other forums is permitted, provided the original author(s) and the copyright owner(s) are credited and that the original publication in this journal is cited, in accordance with accepted academic practice. No use, distribution or reproduction is permitted which does not comply with these terms.

frontiers in Cell and Developmental Biology

REVIEW
published: 10 December 2020
doi: 10.3389/fcell.2020.595178

An Intrinsic Oscillation of Gene Networks Inside Hair Follicle Stem Cells: An Additional Layer That Can Modulate Hair Stem Cell Activities

*Patrycja Daszczuk†, Paula Mazurek†, Tomasz D. Pieczonka, Alicja Olczak, Łukasz M. Boryń and Krzysztof Kobielak**

Laboratory of Stem Cells, Development and Tissue Regeneration, Centre of New Technologies (CeNT), University of Warsaw (UW), Warsaw, Poland

OPEN ACCESS

Edited by:
Cheng Ming Chuong, University of Southern California, Los Angeles, United States

Reviewed by:
Mingxing Lei, Chongqing University, China
Randall Widelitz, University of Southern California, Los Angeles, United States

***Correspondence:**
Krzysztof Kobielak
k.kobielak@cent.uw.edu.pl

†These authors share first authorship

Specialty section:
This article was submitted to Stem Cell Research, a section of the journal Frontiers in Cell and Developmental Biology

Received: *15 August 2020*
Accepted: *16 November 2020*
Published: *10 December 2020*

Citation:
Daszczuk P, Mazurek P, Pieczonka TD, Olczak A, Boryń ŁM and Kobielak K (2020) An Intrinsic Oscillation of Gene Networks Inside Hair Follicle Stem Cells: An Additional Layer That Can Modulate Hair Stem Cell Activities. Front. Cell Dev. Biol. 8:595178. doi: 10.3389/fcell.2020.595178

This article explores and summarizes recent progress in and the characterization of main players in the regulation and cyclic regeneration of hair follicles. The review discusses current views and discoveries on the molecular mechanisms that allow hair follicle stem cells (hfSCs) to synergistically integrate homeostasis during quiescence and activation. Discussion elaborates on a model that shows how different populations of skin stem cells coalesce intrinsic and extrinsic mechanisms, resulting in the maintenance of stemness and hair regenerative potential during an organism's lifespan. Primarily, we focus on the question of how the intrinsic oscillation of gene networks in hfSCs sense and respond to the surrounding niche environment. The review also investigates the existence of a cell-autonomous mechanism and the reciprocal interactions between molecular signaling axes in hfSCs and niche components, which demonstrates its critical driving force in either the activation of whole mini-organ regeneration or quiescent homeostasis maintenance. These exciting novel discoveries in skin stem cells and the surrounding niche components propose a model of the intrinsic stem cell oscillator which is potentially instructive for translational regenerative medicine. Further studies, deciphering of the distribution of molecular signals coupled with the nature of their oscillation within the stem cells and niche environments, may impact the speed and efficiency of various approaches that could stimulate the development of self-renewal and cell-based therapies for hair follicle stem cell regeneration.

Keywords: hair follicle stem cells (hfSCs), dermal papilla, niche, BMP signaling, WNT signaling

INTRODUCTION

Skin is the largest organ, covering the entire human body and extending up to an area of approximately two square meters. Skin is built up of two main layers, the epidermis and the underlying dermis which are formed during embryonic development from the ectoderm and mesoderm, respectively (**Figure 1A**). The top part of the ectodermal skin creates the epidermis which, during morphogenesis, delves into the dermis and develops skin appendages to produce visible skin hair fibers (from hair follicles) with sebum (from sebaceous glands) and sweat glands (**Figures 1A,B**). Keratinocytes are the main building blocks of the epidermis and skin appendages.

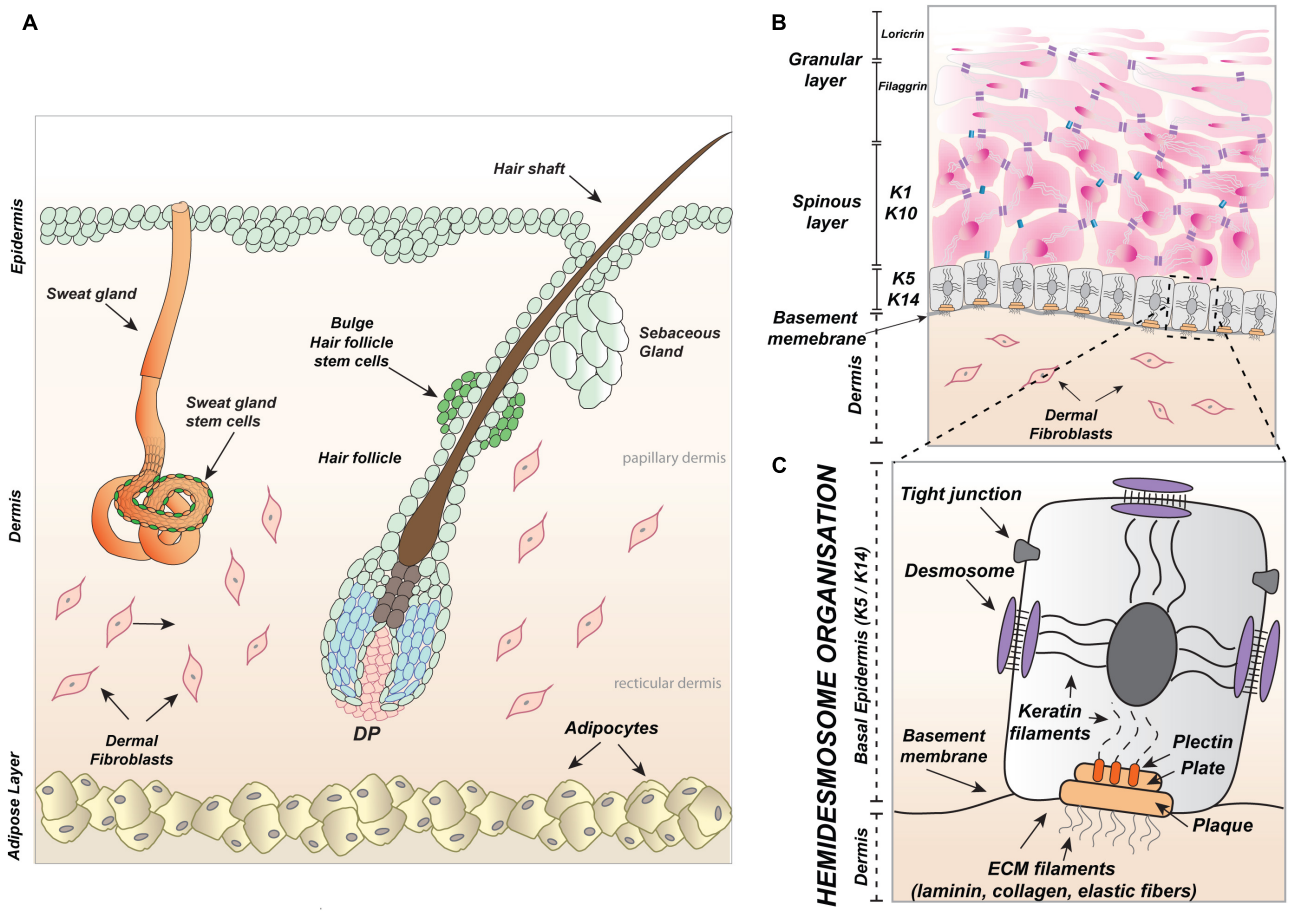

FIGURE 1 | Skin and appendages. **(A)** Schematic, illustrating a section through the skin including hair follicle along with the sebaceous gland as well as the sweat gland protruding into the dermis with fibroblasts and adipocytes and underlying hypodermis. **(B)** Graphic representation of skin epidermis: basal layer with the expression of Keratin 5 (K5) and Keratin 14 (K14) above, spinous layer positive for Keratin 1 (K1) and Keratin 10 (K10) and on the top granular and cornified layers marked accordingly with Filaggrin and Loricrin. **(C)** Illustration of the junctional connection between keratinocytes of basal layer and fibroblasts of the papillary dermis, firmed by hemidesmosomes, which are composed of integrin subunits α and β attached to the basement membrane and bridged by plectin to keratin cytoskeleton filaments. The docking filaments of the basement membrane: laminin, collagen, and elastic fibers form part of the extracellular matrix (ECM) produced by keratinocytes and dermal fibroblasts. Tight adhesion of keratinocytes in the epidermis is created by tight junctions and the formation of desmosomes. The papillary dermis is primarily composed of fibroblasts, arranged in loose networks and elastic fibers of the ECM. DP, dermal papillae.

They create an outside barrier with several epidermal layers (**Figure 1B**) and possess keratin intermediate filaments inside their cytoplasm (**Figure 1C**). Apart from keratinocytes, the epidermis is immersed with other cell types derived from the neural crest (melanocytes), bone marrow (Langerhans cells or dendritic cells), and epithelium (Merkel cells) (Merad et al., 2002; Mende et al., 2006; Van Keymeulen et al., 2009; Ernfors, 2010). The dermis is created by fibroblasts which form an upper and lower layer called the papillary dermis and the reticular dermis, respectively (**Figure 1A**). The epidermis and papillary dermis produce collagen, laminin, and elastic fibers of the extracellular matrix (ECM) which provide an anchoring interface for the basement membrane (**Figures 1B,C**). The part of the anchoring interface outside of the basement membrane is produced by integrin complexes (subunits α and β) present in keratinocytes in the basal or outer root sheath (ORS), known as hemidesmosomes, which connect through plectin to the cytoskeleton composed of keratin filaments (**Figure 1C**). Apart from fibroblasts, the additional cells localized in the skin reticular dermis are adipocytes (fat cells) (**Figure 1A**), immune cells like macrophages, lymphocytes, and mast cells.

During early mouse embryonic development, between embryonic day 9.5 (E9.5) to 12.5 (E12.5), a single layer of the epidermis begins stratifying into the several layers of cells which create a protective wall completely impermeable before birth (Blanpain and Fuchs, 2009). Then, at E13.5, mutual interaction between secreted clues from mouse epidermis and dermis initiates the first hair follicle (HF) placode formation, which begins to delve into the dermis (**Figure 2A**) (Dhouailly, 1973; Li et al., 2015). Currently discovered epithelial signals released from placode, such as fibroblast growth factor 20 (FGF20) guide the initial condensation of fibroblasts to create the dermal papilla (DP), a signaling center, which is essential to complete the

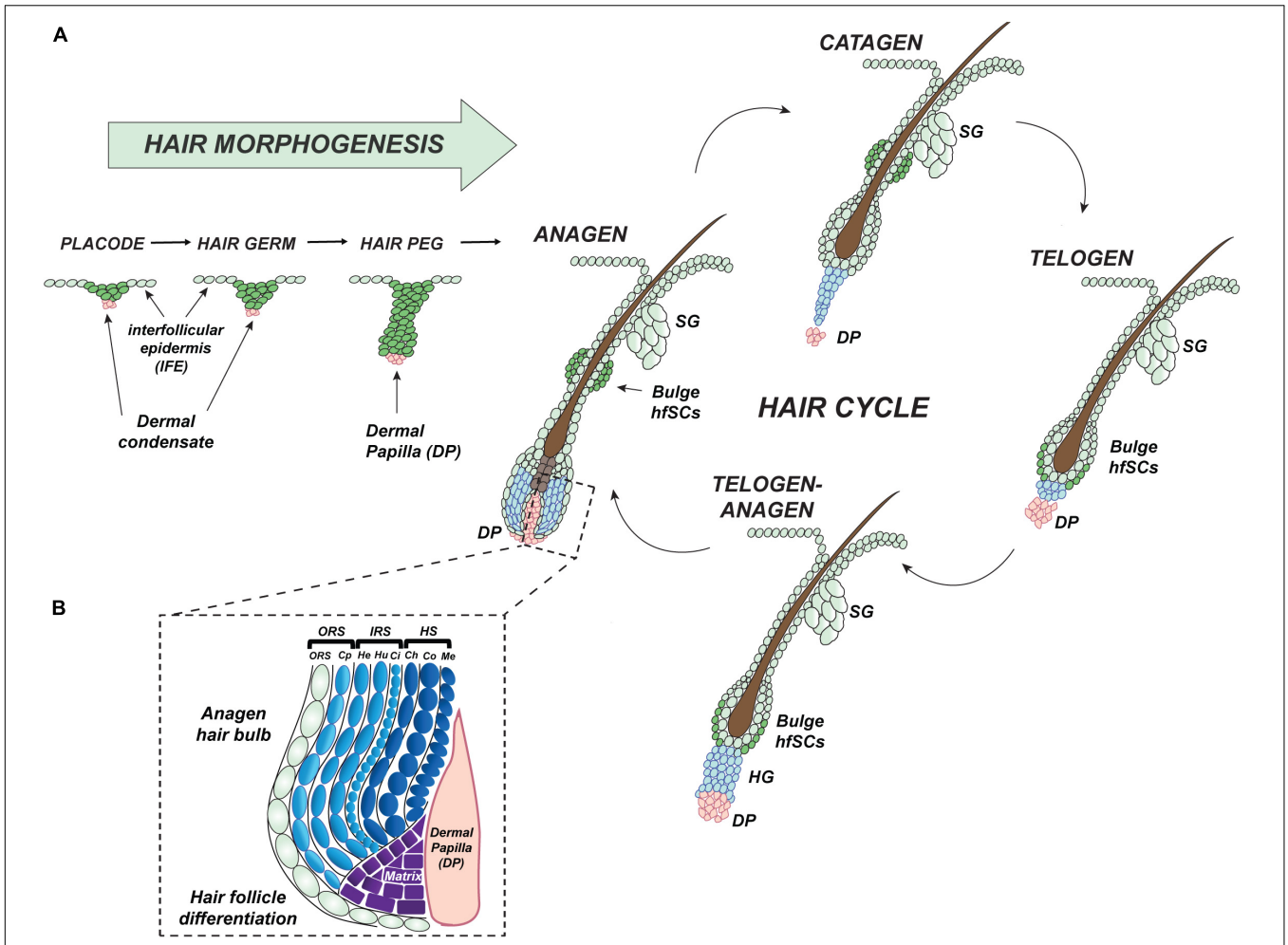

FIGURE 2 | Development and cyclic regeneration of hair follicle. **(A)** Graphic stages of hair follicle (HF) morphogenesis: hair placode (initiation of HFs pattern formation), immature hair germ, hair peg, and fully developed and differentiated anagen hair by the end of first postnatal resting phase of telogen. Mature HF is built of a reservoir of hair follicle Stem Cells (hfSCs) which is connected above to an associated sebaceous gland (SG), located below the responsive hair germ (HG) with underlying dermal papilla (DP). During the cyclic hair growth, each HF undergoes phases of telogen (quiescence, resting), anagen (activation, regrowth), and catagen (degeneration). **(B)** During the growth phase, the hair bulb cells comprise actively proliferative matrix cells which undergo final differentiation creating an inner root sheath (IRS) and hair shaft (HS, protruding out of the skin surface, visible part of HF) layers of the HF mini-organ. HS, hair shaft is composed of Ch, the cuticle of the hair shaft; Co, cortex of hair shaft; Me, medulla; DP, dermal papilla; IRS, inner root sheath contains; He, Henle's layer; Hu, Huxley's layer; Ci, cuticle; Cp, companion layer; ORS, outer root sheath.

development of the hair follicle (**Figure 2A**) (Oliver and Jahoda, 1988; Millar, 2002; Huh et al., 2013).

HFs are very well organized mini-organs with extraordinary potential to undergo coordinated and spontaneous cycles of self-activated regeneration. These synchronized cycles of hair regrowth are characterized by phases of anagen (growth), catagen (degeneration), and telogen (quiescence) that are controlled by reciprocal signal interaction between hair follicle Stem Cell (hfSCs) and predominantly DP (**Figure 2A**) (Muller-Rover et al., 2001; Millar, 2002; Schmidt-Ullrich and Paus, 2005; Alonso and Fuchs, 2006; Rendl et al., 2008). In the growth phase of an HF's cycle, there is sequential activation of cell proliferation: first in the highly responsive region located directly above the DP known as the hair germ (HG); second, in the hfSCs in the bulge of ORS (**Figure 2A**). Subsequently, cells from both structures generate a hair bulb matrix of transit-amplifying (TA) cells which differentiate into several layers of the visible hair shaft (HS) formed by the medulla, cortical layers, and the cuticle, together with the internal tunnel of the inner root sheath (IRS) (**Figures 2A,B**) (Greco et al., 2009). Postnatally, after morphogenesis of HFs and the epidermis is complete, two physiological independent pools of keratinocytes, one in the interfollicular epidermis (IFE) and another in the hair bulge, are responsible for different cell fates (**Figure 2A**) (Ito et al., 2005; Levy et al., 2005; Jaks et al., 2008; Nowak et al., 2008; Lu et al., 2012; Leung et al., 2013). During emergencies like skin injury, SCs (Stem Cells) from skin appendages, such as hair follicles, sweat glands, or nails which under normal conditions are restricted to that specific regeneration fate are capable of actively contributing to the regeneration of the epidermis

(Tumbar et al., 2004; Ito et al., 2005; Levy et al., 2007; Snippert et al., 2010; Lu et al., 2012; Leung et al., 2013, 2014).

The sebaceous gland is located above the bulge with hfSCs and produces sebum, which forms together with HF and the pilosebaceous unit, but is independently preserved by Blimp1+ unipotent progenitor cells (**Figure 3A**) (Horsley et al., 2006). However, hfSCs are also capable of participating in sebaceous gland physiological restoration (Petersson et al., 2011). Similarly, Lgr6+ positive cells, localized in the ORS above the bulge in the HFs isthmus, can renew sebaceous glands as well as IFE (**Figure 3A**) (Snippert et al., 2010; Joost et al., 2018).

In this review, we present current views on the discoveries of molecular mechanisms that allow hfSCs to synergistically integrate homeostasis during quiescence and activation. The review also explores a model of how different populations of skin stem cells consolidate their intrinsic and extrinsic mechanisms, resulting in the maintenance of their stemness and hair regenerative potential. Primarily, we focus on the cyclic nature of HF regeneration and on the question of how the intrinsic oscillation of gene networks in hfSCs sense and influence the surrounding niche environment. We also investigate the existence of a cell-autonomous mechanism and the reciprocal interaction between key niche components and key molecular axes in hfSCs and the environment, demonstrating its critical driving force in either activation of whole mini-organ regeneration or quiescence homeostasis maintenance.

STEMNESS OF HAIR FOLLICLE STEM CELLS AND REGENERATIVE POTENTIAL

Hair follicle stem cells are a small population of SCs residing in the outermost layer of the skin, which is referred to as the HF bulge, below the sebaceous gland (**Figure 3A**), at the arrector pili muscle attachment site (Cotsarelis et al., 1990; Wei et al., 1995; Fujiwara et al., 2011). The putative location of hfSCs was confirmed by pulse-chase experiments employing labeled nucleotides (Cotsarelis et al., 1990; Morris and Potten, 1999; Taylor et al., 2000) and a transgenic mouse model with doxycycline-inducible expression of a histone H2B-GFP labeling system (Tumbar et al., 2004) that proved the existence of quiescent, slow-cycling label-retaining cells (LRCs), specifically in the bulge region (**Figure 3A**) (Panteleyev et al., 2001). Label-retaining slow-cycling cells are already present in the early stage of HF morphogenesis and are marked by Sox9 expression (Nowak et al., 2008). This early Sox9 positive population of SCs is forming in the placode in a Sonic hedgehog (Shh) dependent way by adopting a low WNT (Wingless-type MMTV integration site family) signaling gradient as suprabasal placode cells after the asymmetric division of basal placode cells with high WNT signaling (Ouspenskaia et al., 2016). This early population of SCs is responsible for the formation of quiescence bulge SCs and delivers progeny to all skin lineages, apart from HFs sebaceous glands and IFE (Nowak et al., 2008).

Hair follicles undergo highly coordinated regenerative cycles under normal physiological conditions, with repeating phases of anagen, catagen, and telogen during a lifetime. Most of the time hfSCs are quiescent but periodically become activated to start HF regeneration (**Figure 2A**). In mice, the bulge as an anatomical structure becomes morphologically established during the first postnatal telogen (at P18) at the end of HF morphogenesis, then hfSCs also start to express the mature hfSC cell surface marker CD34 (Trempus et al., 2003). Together with α6-integrin, the CD34 marker can be employed to faithfully isolate basal hfSCs by fluorescence-activated cell sorting (*FACS*) (Trempus et al., 2003; Blanpain et al., 2004; Morris et al., 2004) (**Figure 3A**). Moreover, LRCs-hfSCs reveal the highest level of keratin K15 (K15) expression (**Figure 3A**) (Liu et al., 2003; Morris et al., 2004).

In the past, K15-GFP or intermittently dividing LRCs reporter mice and the application of immunofluorescence staining with α6-integrin+/CD34+ enabled isolation by *FACS* living hfSCs in the first microarray-based experiments (Blanpain et al., 2004; Morris et al., 2004; Tumbar et al., 2004). In addition to CD34, which labels more than 90% of K15-GFP+ hfSCs (Morris et al., 2004), there are high levels of other key SCs stemness markers, such as Lhx2 (LIM homeobox2), Sox9, Tcf3 (T-cell factor3), Tcf4, Lgr5 (Leu-rich repeat-containing G protein-coupled receptor5), NFATc1 (the nuclear factor of activated T-cell cytoplasmic1), and Foxc1 (forkhead box c1) (**Figure 3A**) (Merrill et al., 2001; Vidal et al., 2005; Nguyen et al., 2006; Rhee et al., 2006; Horsley et al., 2008; Nowak et al., 2008; Nguyen et al., 2009; Kadaja et al., 2014; Adam et al., 2015; Lay et al., 2016; Wang et al., 2016). Sox9 is crucial to maintain hfSCs stemness by Activin B/TGFβ/pSmad2 signaling that inhibits the IFE fate (Kadaja et al., 2014). Importantly, Sox9 directly regulates another stemness marker Lhx2 (Kadaja et al., 2014). The special role of Sox9 in orchestrating the formation of hfSCs has been demonstrated by its ablation with subsequent inhibition of Lhx2, Tcf3, and Tcf4 expression (Adam et al., 2015). Thus, Sox9 has been recognized as a pioneer factor coupling stemness transcription factors Lhh2, Tcf3, Tcf4, NFATc1, Tle, and Nfib along with Mediator subunit (Med1) and histone H3 acetylation on lysine 27 (H3K27ac, activation mark), which localize super-enhancers with their epicenters to maintain hfSCs (Adam et al., 2015).

In another recent study, the loss of nuclear factor IB (Nfib) and IX (Nfix) revealed the abolition of the epigenetic landscape of super-enhancers with the inability to maintain hfSCs stemness (Adam et al., 2020). In addition, expression of NFATc1 is directly controlled by canonical BMP/Smad1/5/8 signaling in the hfSCs quiescence, since the NFATc1 promoter possesses Smad's binding sites (Horsley et al., 2008; Kandyba et al., 2013; Genander et al., 2014). BMP (Bone Morphogenetic Protein) signaling, together with Calcium/calcineurin (CN) are required to activate NFATc1, which then suppresses the cyclin dependent kinase 4 gene (Cdk4) expression, keeping the bulge in a quiescent state (Horsley et al., 2008). Another recent study discovered an additional molecular mechanism was discovered where Foxc1 activates NFATc1 and BMP signaling, as major quiescence organizers, while Foxc1 in activated bulge SCs are required to restore and preserve quiescence (Lay et al., 2016; Wang et al., 2016). Foxc1 binding sites were found in promoter or enhancer regions of genes

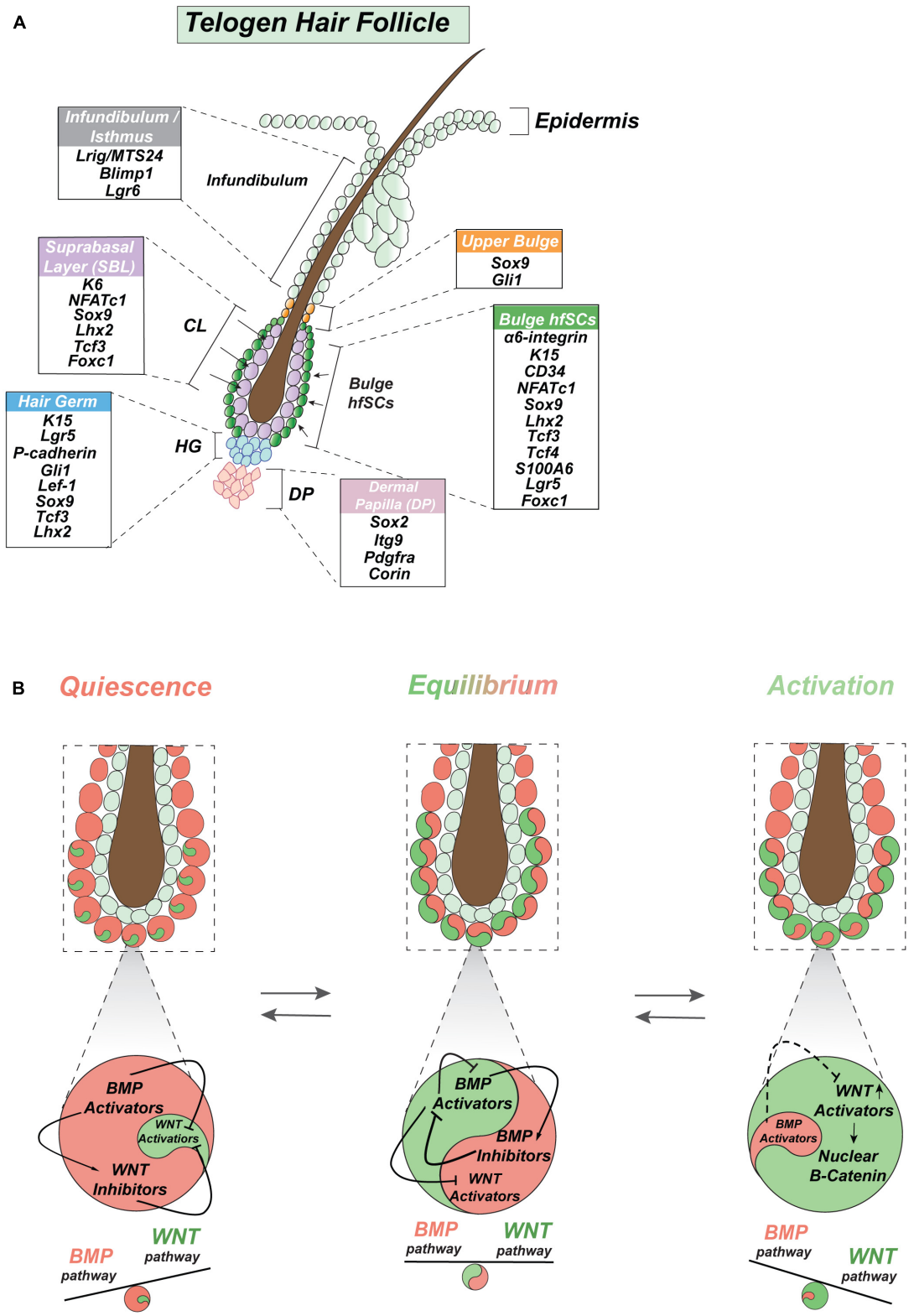

FIGURE 3 | Intrinsic signaling oscillation in hair follicle stem cells. **(A)** Graphic depiction of stemness genes expressed in quiescent telogen including bulge with hfSCs along with upper bulge and infundibulum of HF, hair germ, suprabasal bulge layer (SBL) layer, and DP. **(B)** Model of proposed intrinsic oscillation in hfSCs represents intrinsic dynamic competitive oscillation along BMP signaling axis of activators and inhibitors and its reciprocal interaction between BMP and WNT pathways in SCs (stem cells) homeostasis regulation.

involved in hfSCs quiescence, including Bmp2, Foxp1 (forkhead box p1), NFATc1, and Prlr. Finally, a comparison between gene expression and correlation with specific motifs for Foxc1, NFATc1, and Smad indicates cooperation of gene networks in the regulation of the quiescence state (Wang et al., 2016).

Genome-wide studies depict histone H3 tri-methylation on lysine 4 (H3K4me3) and lysine 79 (H3K79m2) as an indicator of promoters of actively transcribed genes of hfSCs, including all previously reported stemness genes, whereas differentiation genes in hfSCs are repressed by repressive H3 tri-methylation on lysine 27 (H3K27me3) (Lien et al., 2011).

One of the most important characteristics of genuine SCs is the capability to sustain their stem proliferative feature *in vitro* with a long-term self-renewing property in culture (Barrandon and Green, 1987). Indeed, hfSCs demonstrate the highest efficiency in the colony-forming assay when compared to all tested populations of keratinocytes isolated from different parts of the skin *in vitro* (Rochat et al., 1994; Oshima et al., 2001; Trempus et al., 2003; Blanpain et al., 2004; Morris et al., 2004). However, an even more significant test of SCs is their ability to maintain regenerative characteristics *in vivo* by performing a well-established assay of the chamber graft reconstitution (Lichti et al., 1993; Weinberg et al., 1993; Lichti et al., 2008). In this assay, different populations of keratinocytes are tested for SC potential by combining them with DP-enriched fraction of fibroblasts from neonate mice and then the resulting cell suspension is grafted onto the backs of immunocompromised mice to regenerate a full-thickness epidermis with appendages. As expected, hfSCs are capable of regenerating HFs, the epidermis, and the sebaceous glands when grafted into the chamber on athymic (NUDE) mice thereby demonstrating their multipotency (Blanpain et al., 2004; Morris et al., 2004; Claudinot et al., 2005). Similarly, human bulge hfSCs have been also labeled by K15 expression (Lyle et al., 1998, 1999). Using a genetic approach with the reporter mice with K15 – promoter-driven specific bulge hfSCs labeling confirmed that their descendent cells are able to build up all layers of the HF (Liu et al., 2003; Morris et al., 2004). While hfSCs are crucial to regenerate HF, bulge hfSCs can also contribute to wound repair but only temporarily and are not involved in long-term homeostasis of the epidermis (Ito et al., 2005; Levy et al., 2007).

Recently, it has been shown that the isthmus (a region of the HF directly above the bulge) is marked by Lgr6 (leucine-rich repeat-containing G protein-coupled receptor 6) (**Figure 3A**) and that these Lgr6+ cells assist in the homeostasis of the skin epidermis, sebaceous and HFs, they participate in skin epidermis regeneration after injury, and are long lasting (Joost et al., 2018; Snippert et al., 2010).

Above the isthmus in the HF, is a junctional zone containing the upper isthmus and lower infundibulum where the sebaceous gland opens into a hair follicle to secrete sebum. This structure also contains the SC populations which can reconstitute the epidermis, HF, and sebaceous gland in a reconstitution assay, and is labeled by MTS24 and Lrig1 (Leucine-rich repeats and immunoglobulin-like domain protein 1) expression (**Figure 3A**) (Nijhof et al., 2006; Jensen et al., 2008, 2009). Other research has shown that the junctional zone also hosts a different population of unipotent sebaceous gland progenitor cells labeled by Blimp1 (**Figure 3A**) (Horsley et al., 2006).

HAIR GERM INITIATES CYCLIC HAIR REGENERATION

It was originally believed that hfSCs occupied the secondary hair germ, at the bottom of the HF, during the quiescent phase of the HF cycle (Chase et al., 1951). Later research indicated that hfSCs in the bulge and HG cells are equivalently based on keratin15 expression as a specific marker to these cells (Lyle et al., 1998). Although hfSCs constitute the main source of cells in the growing phase of anagen, the HG is responsible for initiating a new hair cycle in direct reaction to molecular signals from the dermal signaling center (DP) at the beginning of anagen (Panteleyev et al., 2001; Greco et al., 2009). The HG is a transient region of the HF, that originated repeatedly from the hfSCs population at the resting phase of the hair cycle. In telogen phase HFs, the HG is located between the DP and bulge hfSCs (**Figure 3A**) (Ito et al., 2004; Greco et al., 2009; Zhang et al., 2009). The precise time point at which the HG starts to specify is still a topic of discussion. One hypothesis claims that the HG is formed directly from the hfSC population during the telogen phase, ignoring the fact that cells located below the bulge region can survive catagen (Greco et al., 2009; Zhang et al., 2009; Mesler et al., 2017; Panteleyev, 2018; Xin et al., 2018). A model reconciling both these hypotheses is proposed, in which such reconcilement is possible due to HG heterogeneity, visible through differential gene and protein expression in the telogen HG cells (Panteleyev, 2018). A different concept suggests that the HG originates from the hfSCs population present in the upper ORS (ORS-SCs). This characteristically located stem cell population is formed during the preceding anagen phase and after catagen survival and gives rise to the "new" unsymmetrical bulge with adjacent HG (Hsu et al., 2011). The HG is defined as being molecularly distinct from hfSCs by lacking hfSC markers such as NFATc1, S100A6, and CD34, yet it displays Lef-1 with specific expression of P-cadherin (**Figure 3A**) (Greco et al., 2009). Moreover, when comparing these two populations of cells at the transcriptional level, HG cells very closely resemble activated bulge hfSCs and function as a closely related, an extended, population of the bulge hfSCs (Ito et al., 2004; Greco et al., 2009). The hfSC and HG populations also express the same markers, such as SCs, K15, Lgr5, Sox9, Tcf3, and Lhx2 (**Figure 3A**) (Trempus et al., 2003; Greco et al., 2009). However, in contrast to hfSCs, isolated and cultured HG keratinocytes generate faster larger colonies but because of limited proliferative potential, they only grow effectively *in vitro* up to 3 passages (Greco et al., 2009). Interestingly, HG keratinocytes cannot maintain SC-like features *in vitro*. Current findings demonstrate that they possess the ability to functionally restore the bulge hfSCs population after injury, depilation, or laser ablation *in vivo*, indicating the reciprocal balance between both populations (Ito et al., 2004; Rompolas et al., 2012, 2013).

During telogen to anagen transition, HG cells exhibit faster activation than hfSC and HGs are a more dynamic population.

They prepare for the onset of anagen by gradually increasing the expression level of genes involved in cell-cycle activation and signal transduction pathways (Greco et al., 2009). The first sign of HG proliferation is β-catenin stabilization along with other consequences of canonical WNT signaling activation. The network of genes involved in cell cycle progression is highly upregulated including a group of cyclins (Ccnb1, Ccna2, Ccnd2, and Ccnd1) and cyclin-dependent kinases (Cks2 and Cdc2a) (Greco et al., 2009). This highly correlates with the activation of WNT signaling in the ΔN-β-catenin mouse model with increased expression of the genes involved in cell cycle progression (Lowry et al., 2005). In addition, recent data demonstrates that at the onset of anagen, HG exchanging Tcf3/Tcf4 for Lef1 at the super-enhancers, and then Lef1 forms the nuclear complex with β-catenin after activation of WNT signaling (as a consequence of BMP inhibition) which drives HG committed progenitors (Merrill et al., 2001; Kobielak et al., 2007; Adam et al., 2018). The decreased BMP signaling observed in HG proliferation has also been promoted by activation of pSmad2 by transforming growth factor-β2 (TGFβ2) at the anagen onset (Oshimori and Fuchs, 2012). Recently, a two-step mechanism of early hair activation has been dissected further by showing the important role of DP in this process by restraining the bulge dependent inhibitors of WNT (such as Wif1, Frzb, Sost, Mest, Shisa3, and Igfbp4), which indirectly activate canonical WNT and Shh expression in HG progenitor cells to maintain a short period of proliferation in the lower part of hfSCs (Avigad Laron et al., 2018).

INTRINSIC SIGNALING OSCILLATION IN hfSCs

The HF oscillation is the repetitive fluctuation between activation and quiescence phases of this mini-organ, leading to visible changes during regenerative hair cycles. Here, we explore how this biological fluctuation is orchestrated on a molecular level, leading to a periodic pattern of hair regeneration.

The recent discovery that BMP signaling maintains hfSCs in a dormant telogen, predominantly by inhibition of the canonical WNT signaling pathway, suggests a new model of intrinsic homeostasis regulation of these stem cells (**Figure 3B**) (Kandyba et al., 2013). Thus, any circumstances that reduce BMP signaling activity result in the upregulation of WNT canonical signaling with subsequent temporal hfSCs activation. Consequently, temporal stochastic activation of hfSCs tips the balance in favor of the dormant phase with high inner bulge BMP activity, thereby creating a cyclical molecular network (Kandyba et al., 2013; Li et al., 2015). Indeed, upon BMP inhibition, which leads to intrinsic hfSCs activation, Bmp6, and Gremlin1 (Grem1) are up- and down- regulated, respectively (Kandyba et al., 2013; Li et al., 2015). Endogenous Grem1 expression in feather buds is controlled by BMP signaling (Bardot et al., 2004), suggesting that activating and inhibiting components of this signaling axis are already reciprocally dependent and drive internal oscillation of gene networks in hfSCs (**Figure 3B**). In addition, a similar inverse relation was described between BMP signaling and the function of another inhibitor, Bambi, in hfSCs regulation (Kandyba et al., 2013). It was also reported that Bambi is antagonized by microRNA-31, which promotes a new hair regeneration cycle (Mardaryev et al., 2010), demonstrating the complexity of the main BMP signaling axis oscillation.

This intrinsic oscillation along the activator and inhibitor axis is consistent with the previous Turing model (Turing, 1990) which was expanded by Gierer and Meinhardt (1972). This concept describes a constant periodic pattern formation of opposing signals where one of the morphogens acts as an activator and the second one as an inhibitor, antagonizing the generation of the former to restrict the range of its activation spikes (Gierer and Meinhardt, 1972; Meinhardt and Gierer, 2000). The activator-inhibitor model proposes that the production of the agonist might promote the induction of its neutralizer – antagonist (Gierer and Meinhardt, 1972), which was also observed in hfSCs oscillation that stimulated opposed, yet synchronized, effects on the whole gene network (Kandyba et al., 2013).

This canonical BMP pathway suppression demonstrated that the intrinsic oscillation of the BMP signaling axis rearranges the WNT signaling pathway in a ligand-dependent fashion. As the result, the hfSCs molecular profile switched to mimic an HG destiny with canonical WNT activation (Kandyba et al., 2013). Consequently, BMP inhibition overcomes self-autonomous regulation with nuclear β-catenin stabilization in hfSCs, preceded by the upregulation of ligands: Wnt7a, Wnt7b, and Wnt16, followed by WNT inhibitor, Dkk3 downregulation (**Figure 3B**) (Kandyba et al., 2013). At the same time, hfSCs sense and respond to inhibition of BMP signaling resulting in a rearrangement of WNT receptors, called Frizzled (Fzd). In this arrangement, Fzd2 and Fzd3 must first be downregulated, simultaneously activating Fzd10, to prepare for canonical WNT activation (**Figures 3B**, **4B**) (Kandyba et al., 2013). Recently, it has been confirmed that the regulatory element of the Fzd10 gene was closed during the quiescence of hfSCs and becomes more open and accessible, as demonstrated by the overlapping of ATAC-seq and Chip-seq data at the early stages of hfSCs activation (Adam et al., 2018).

Furthermore, a functional analysis confirmed that the subcutaneous introduction of the Wnt7a recombinant protein was capable of initiating a new cycle of HF regeneration with hfSCs activation (Ito et al., 2007; Kandyba et al., 2013; Kobielak et al., 2015). Conversely, when the Wnt7b gene was removed from hfSCs it postponed hfSC activation with a shorter anagen (Kandyba and Kobielak, 2014). The direct interaction of canonical BMP pathway effectors, phospho-Smads (pSmad1/5/8) has also been confirmed in the regulatory regions of Wnt7b and Wnt7a genes from *in vivo* isolated hfSCs (Kandyba et al., 2013; Genander et al., 2014; Kandyba and Kobielak, 2014). When the canonical Wnt pathway was inhibited by β-catenin ablation in hfSCs, it led to the upregulation of several BMP inhibitors including Grem1, Bambi, and Noggin, suggesting that WNT signaling suppresses BMP antagonist expression, permitting an increase in BMP signaling (Lim et al., 2016). This is consistent with the intrinsic oscillation model, which demonstrates that regulatory feedback loops are present between canonical BMP-WNT signaling axes and that a network of gene dependency

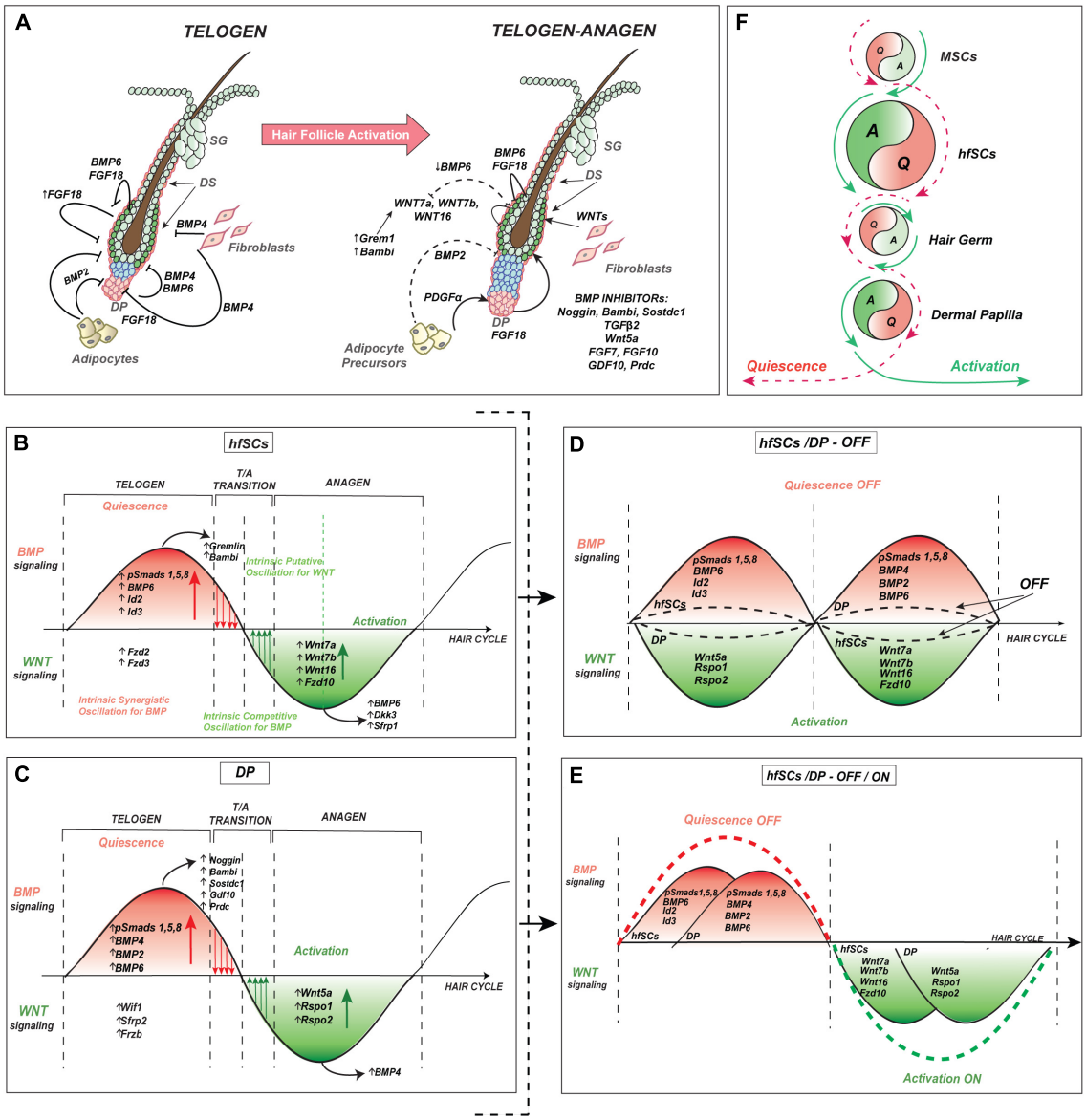

FIGURE 4 | Intrinsic oscillator in hfSCs consolidates with extrinsic signaling in niche environment during hair cycle regeneration. **(A)** Proposed model of the molecular oscillation in hfSCs and its cross-talk during the quiescent-telogen and onset of HF activation during early anagen. The model also depicts intrinsic dynamic oscillation in hfSCs through observed rearrangements in ligand-receptor dependency and cross-talk between the main players of BMP and WNT signaling in SCs, and niche synchronized regulation. **(B)** Model of intrinsic oscillation in hfSCs between BMP and WNT signaling pathways, which sense and respond in an autocrine way to intra bulge hfSCs and in a paracrine way to the surrounding niche environment, including signaling center DP (intrinsic synergistic oscillation vs. intrinsic competitive oscillation with an accumulation of activators and/or inhibitors). **(C)** Model of internal feedback regulatory loop in DP between BMP and WNT signaling pathways, which sense and reciprocally respond to the hfSCs and the surrounding niche environment, especially bulge hfSCs in a paracrine way (synergistic vs. competitive accumulation of activators and/or inhibitors). **(D)** Model of wave interference in opposed phases between either hfSCs with repressive BMP and DP with stimulating WNT or in the reverse situation of hfSCs with activation of WNT and DP with inhibitory BMP signaling. The model of wave interference in opposed phases proposes attenuation with the inhibitory (OFF) effect of signals coming from either the intrinsic hfSCs oscillator or from the internal feedback regulatory loop of DP regardless of whether they are predominantly in BMP or WNT signaling. It results in reducing and flattening the wave amplitude, of BMP or WNT signaling either in hfSCs or DP (a dotted black sinusoid lines), creating a weaker resultant wave than individual waves before, and the mutual influence of these waves causes destructive interference. **(E)** Model of constructive interference with wave interference in the same stages (or in the same phases) of the repeating pattern waves between hfSCs and DP, with either repressive BMP resulting in quiescence (OFF) effect or stimulatory WNT leading to activation (ON) effect. The model of waves interference in the same phases proposes either inhibitory (OFF, a dotted red sinusoid line) effect or activatory (ON, a dotted green sinusoid line) effect of signals coming from either intrinsic hfSCs oscillator or internal feedback regulatory loop of DP and the phases depend on whether synchronization happens in BMP or WNT signaling for both hfSCs and DP. It creates a stronger resultant wave with a higher amplitude of either BMP (stronger inhibition) or WNT (stronger activation) signaling in both hfSCs and DP. **(F)** Model of the intrinsic oscillator in hfSCs which consolidates with extrinsic signaling in surrounding niche environment during hair cycle regeneration. MSCs, melanocyte stem cells.

maintains constant intrinsic oscillation in hfSCs (**Figure 3B**) (Kandyba et al., 2013; Lim et al., 2016).

Another interesting issue is the family of *Id* genes, which are highly sensitive to BMP stimulation. In hfSCs *Id1*, *Id2* and *Id3* are direct targets of pSmads in the canonical BMP signaling pathway, and are also significantly suppressed after *Bmpr1a* ablation (Kandyba et al., 2013; Genander et al., 2014). In other types of SCs *Id* genes are also involved in the preservation of cell identity and prevent premature differentiation (Niola et al., 2012).

This indicates that the regulatory feedback loops between BMP and WNT pathways sense either activation or inhibition of hfSCs during anagen or telogen. Moreover, they respond in opposite ways, either inhibiting hfSCs upon excessive SCs activation or activating hfSCs upon disproportionate SCs inhibition. This keeps the intrinsic oscillator constantly operating in stem cells, which introduces a check and balance mechanism for stem cell homeostasis (**Figures 3B**, **4B,C**) (Kandyba et al., 2013).

THE OSCILLATION OF hfSCs IS UNDER ANTAGONISTIC INFLUENCE OF INNER BULGE LAYER DURING QUIESCENCE

The hypothesis in which multipotent and undifferentiated adult stem cells are seen in direct association with other cells within specific localization was first mentioned by Schofield (1978). This location represents a specialized microenvironment called a niche, which is maintained by the secretion of specific components of ECM to anchor in place and support the SCs. It is well established that niche cells arise from a different cell lineage than the SCs they regulate. Nonetheless, this concept is questioned as more recent niche studies in vertebrate and invertebrate systems consequently identify mechanisms where SCs progeny play a crucial niche element, providing and relaying signals that regulate SCs activity itself. This mode of action might be a substantial program controlling SCs behavior in homeostasis and wound repair. The HF inner bulge layer, positive for Keratin 6 (K6+), known as K6+ suprabasal bulge layer (SBL) is the inmost one, located between the telogen bulge hfSCs and the old HF called club hair (**Figure 3A**). It is widely believed that K6+ SBL cells arise from the hfSCs, exiting the bulge upon anagen onset, and then migrating and proliferating downward along with the exterior ORS. In the HF cycle progression, in late anagen, the ORS cells that survive the destructive phase of catagen atypically differentiate to form the inner bulge layer, SBL, in the newly established bulge region (Hsu et al., 2011). Although K6+ SBL maintains some of the hfSCs markers such as Lhx2, NFATc1, Sox9, Tcf3, and Foxc1 (**Figure 3A**) (Hsu et al., 2011; Lay et al., 2016; Wang et al., 2016), they are neither CD34 nor integrin positive. Regardless of SBL similarities to hfSCs, the former cannot replace SCs function in homeostasis or after an injury during wound repair. It seems that SBL's predominant role is to maintain an attachment to the old hair shaft, therefore, preventing the animal's hair loss when each hair cycle concludes. Interestingly, SBL extends to the K6 positive companion layer (Cp) separating ORS and IRS and both structures express anchoring proteins responsible for old hair club and old hair shaft hooking to the old bulge (Winter et al., 1998; Hanakawa et al., 2004; Lay et al., 2016; Wang et al., 2016). The high expression of Bmp6 and Fgf18 by SBL is sufficient to maintain hfSCs quiescence (**Figure 4A**) (Hsu et al., 2011) indicating the inner bulge layer's crucial role in regulating hfSCs behavior. The removal of K6+ SBLs by hair plucking or genetic ablation leads to premature hfSCs activation and anagen initiation. Additionally, this precocious HF anagen can be blocked with subcutaneous injection of either Bmp6 or Fgf18, which is a primary example of how hfSCs progeny acts as a niche component maintaining hfSCS homeostasis *in vivo* – simply by restricting hfSCs activity through these signaling mechanisms (Blanpain et al., 2004; Greco et al., 2009). Although bulge cells express secreted WNT inhibitors such as Dickkopf 3 (Dkk3) and secreted frizzled-related protein 1 (Sfrp1) (Kandyba et al., 2013; Lim et al., 2016), usually associated with quiescent HF, the former one was found in the WNT-inactive internal bulge in the growth phase of the hair cycle (Lim et al., 2016).

hfSCs SENSE SURROUNDING NICHE COMPONENTS FORMING MULTIFACETED ENVIRONMENTS

In the case of hfSCs, the signals obtained from the niche determine their undifferentiated, multipotent state, and cycling status. The niche contains components of SCs progeny as well as heterologous cell types. In a niche centric view, the microenvironment provides signals necessary to maintain their stemness capacity. Recently, a mechanism indicating that SCs are born during embryogenesis at a stage that occurs long before the establishment of the HF bulge niche has been discovered (Ouspenskaia et al., 2016). The niche acts as an instructive signaling hub(s) that plays a critical role in maintaining SCs homeostasis and determines their behavior. Recent studies of hair follicle niche components have identified a number of additional layers in hfSCs regulation. For a better understanding of the reciprocal interactions during HF regeneration between hfSCs and a niche environment, this review will now discuss the key mechanisms that regulate the surrounding HF niche.

DERMAL PAPILLA AND DERMAL SHEATH INTEGRATE WITH THE INTRINSIC OSCILLATION IN hfSCs AND HAIR REGENERATION

At the end of the hair cycle, during telogen, HFs re-enter the quiescent phase and hfSCs remain dormant till the next anagen. It is generally assumed that during the telogen period, the activatory DP, attached to HG and indirectly to hfSCs, needs hefty inhibitory signals like Bmp4 from dermal fibroblasts and Bmp2 from adipocytes forming the neighboring macroenvironment to sustain hfSCs in the resting phase (**Figure 4A**). Toward the end of the telogen phase, the levels of repressive dermal

BMP cues decline, resulting in increased expression of WNT proteins (Plikus et al., 2008; Plikus et al., 2011). In principle, crosstalk between the hfSCs and the neighboring niche at the local molecular level governs the switch from BMP-high/WNT-low inhibitory state to the BMP-low/WNT-high condition, which promotes the transition from telogen to anagen and a new hair regenerative cycle (**Figure 4A**). An essential structure that releases stimulatory factors to activate HFs is DP, a critical instructive signaling center that is part of the hfSCs niche attached to HG (**Figure 4A**). Recently reported lineage tracing studies have identified the existence of micro-niches alongside the DP axis. These newly discovered niches corresponded to the spatially arranged progenitors within the DP compartment, and are capable of differentiating into different epithelial layers within the hair follicle. These findings raised the possibility that by compartmentalization of progeny into distinct micro-niches where WNT-BMP crosstalk occurs, niches/tissues gain precise control over morphogenesis and regeneration (Yang et al., 2017). Several studies have shown, that during the postnatal HF cycle, DP regulates hfSC activity and promotes hair growth when grafted into HF, and coordinates with the epidermis in generating new HFs *in vivo* (Jahoda et al., 1984, 2001). However, DP cells without BMP receptor 1a (Bmpr1A) are not able to generate HFs in hair reconstitution assays (Rendl et al., 2008). A specific genetic approach with the development of transgenic mice, along with FACS technology, allowed for the isolation of a pure population of DP cells (Rendl et al., 2005). Still, the biggest challenge yet to be resolved, are problems related to the long-term maintenance of DP culture *in vitro*, because, after a few passages, DP cells lose their ability to induce HFs and usually become senescent (Horne et al., 1986). DP cells express several characteristic markers from which DP signature genes are selected. For example, secreted WNT inhibitors contain Wif1, Sfrp2, Frzb, and several BMP agonists like Bmp4 and Bmp6 along with BMP antagonists such as Noggin, Sostdc1/Ectodin/Wise, Gdf10, Prdc (protein related to Dan/Cerberus), and Bambi (Rendl et al., 2005) (**Figure 4C**). Importantly, changes in a gene expression pattern were dramatic only one passage after DP isolation (Rendl et al., 2005). These characteristic core genes indicate the complex signaling that controls DP properties, as well as HF inductive activity. One possible way of improving the culture method is to co-culture isolated DP cells with epidermal keratinocytes (Inamatsu et al., 1998) on extracellular matrix substrates (Havlickova et al., 2009) or with embryonic fibroblasts expressing Wnt3a or Wnt7a (Kishimoto et al., 2000). Other strategies to preserve the loss of trichogenicity assume the activation of the BMP signaling pathway (Rendl et al., 2008). Furthermore, the 3D spheroid culture of human DP cells preserved their *de novo* hair-inducing power for an extended time after combining with hfSCs in chamber graft regeneration (Higgins et al., 2013). In another, using 3D-printing technology, Abaci et al. (2018) generated a three-dimensional growth environment of human dermal papilla cells and successfully regenerated human HFs within human skin constructs. Apart from that, DP can repopulate the dermal sheath (DS) and the HFs surrounding dermal fibroblasts at the time of the reconstruction test and after injury (Rendl et al., 2008). Recent studies have characterized particular DP markers in the skin. Specifically, DP Sox2 expression was necessary for the formation of guard, awl, and auchene, but not zigzag hair (Driskell et al., 2009). Indeed, the genetic ablation of dermal Sox2 decreases the number of awl/auchene follicles with an increasing amount of zigzag hair, however, the overall number of HFs have not been affected during morphogenesis (all remained HFs stayed positive for another DP marker, CD133) (Driskell et al., 2009; Lesko et al., 2013). Moreover, Sox2 marks dermal cells sufficient to develop skin-derived precursors (SKPs) and these cell types are functionally similar and show similar gene expression profiles (Fernandes et al., 2004; Biernaskie et al., 2009). Endogenous and clonal, Sox2 positive, dermal cells functionally contribute to skin homeostasis by inducing hair morphogenesis, maintaining dermis, participating in wound-healing, and HF formation during transplantation, by functioning as dermal stem cells (Biernaskie et al., 2009). When HF is activated during the telogen-anagen transition, the change in DP gene expression causes the release of a plethora of stimulatory factors, such as Noggin and FGF pathway members, FGF7 and FGF10, collectively inducing hfSCs activation at the onset of anagen (**Figure 4A**) (Botchkarev et al., 1999; Kishimoto et al., 2000; Rendl et al., 2005, 2008; Driskell et al., 2009; Greco et al., 2009). A lack of β-catenin expression in DP in anagen HFs induced premature catagen and impaired hair regeneration, by downregulating FGF and IGF signaling pathways, unveiling coordinated reciprocal interaction between DP and epithelial progenitors (Enshell-Seijffers et al., 2010). Recently, the important role of DP in early anagen activation has been demonstrated by repressing the bulge-dependent inhibitors of WNT signaling, which induce canonical WNT and Shh expression in HG progenitor cells and indirectly promotes proliferation in the lower part of hfSCs (Avigad Laron et al., 2018). Furthermore, Rompolas et al. (2013) employed intravital imaging, combined with physical DP ablation to show that DP absence is sufficient to prevent anagen onset, therefore demonstrating DP significance during HF activation.

Recent studies that employed single-cell RNA sequencing (scRNA-seq) have defined a complete skin cell atlas comprising several different subpopulations, including HFs with the surrounding environment during the active and resting phases of the hair cycle (Joost et al., 2020). In the skin, seven fibroblast-like subpopulations have been recognized and classified as DP, DS, and skin fibroblasts. Four of those subpopulations experience prominent remodeling with expansion between the rest and growth phase of HFs (Joost et al., 2020). Furthermore, fibroblasts could be separated into four skin fibroblast subpopulations (FIB1–FIB4), DP into the anagen DP (aDP) and telogen DP (tDP), and DS appear to possess mature dermal sheath cells (DS2, predominantly observed in anagen), and one subtype with a transitional signature between dermal sheath cells (DS1) and skin fibroblasts (Joost et al., 2020). The results of single-molecule RNA-FISH demonstrated the existence of two DP subpopulations by staining for Notum, a deacetylase that inhibits WNT ligands specific for telogen DP cells, and Corin, specific for anagen DP cells (Enshell-Seijffers et al., 2008; Kakugawa et al., 2015; Joost et al., 2020). In terms of different expression markers, skin fibroblast subpopulations could be divided into fibroblasts representing the dermis (FIB1

and FIB2) and the hypodermis (FIB3 and FIB4) (Joost et al., 2020). This corresponds to previous studies in which lineage tracing experiments discovered two distinct lineages of skin fibroblast, representing the upper papillary dermis (CD26+, Blimp1+, Sca1− in mouse and CD26+, SFRP2+, FAP+, CD90− in human) and the lower reticular dermis (Dlk1+, in mouse and SFRP2+, FAP−, CD90+ in human), along with two pro-adipogenic types of fibroblasts (Sca1+, Dlk1−, and Sca1+, Dlk1+) (Driskell et al., 2013; Rinkevich et al., 2015; Salzer et al., 2018; Tabib et al., 2018; Korosec et al., 2019). In a transplantation assay, the papillary dermis forms DP and the arrector pili muscle, and reticular fibroblasts create ECM, preadipocytes, and adipocytes of the hypodermis (Driskell et al., 2013; Korosec et al., 2019). Evolutionary conservation in the papillary dermis between mouse and humans have been observed with the upregulation of components of the WNT signaling pathway such as Wif, Apcdd1, Rspo1, Axin2, Lef1, Wnt5a (Philippeos et al., 2018). During wound healing, the reticular and hypodermis fibroblasts respond first, then re-epithelialization must occur before papillary dermis regeneration (Driskell et al., 2013). Indeed, the upregulation of the canonical WNT signaling in the epidermis stimulates the expansion of the papillary dermis with HFs formation, as well as remodeling the lower dermis (Driskell et al., 2013). The upper dermis fibroblasts, labeled specifically by expression of CD26+, are responsible for scar formation during wound healing, and therefore, inhibition of CD26 significantly diminishes scaring in the skin (Rinkevich et al., 2015). However, as described by the lineage-tracing experiments during adulthood and then aging, the fibroblasts from the papillary layer contribute to the whole dermis, including mature adipocytes, and old fibroblasts increase WNT signaling (Salzer et al., 2018).

Regarding DS, recent discoveries have demonstrated that follicle-encapsulating DS cells are necessary for DP relocation to hfSCs/HG during catagen (Heitman et al., 2020). To facilitate this, DS cells must contract similarly to smooth muscle by activation of voltage-gated Ca^{2+} channels through calmodulin (CaM) → myosin light chain kinase (MLCK) → myosin heavy chain (MYH) and myosin light chain (MYL) with alpha-smooth muscle actin (αSMA) pathway allowing HFs regression movements (Heitman et al., 2020). Thus it seems that this machinery is crucial to maintaining a close proximity between hfSCs and DP cells (Heitman et al., 2020). Apart from the role to sustain mechanical proximity between hfSCs and DP during the catagen phase, DS cells also expressed genes like Fgf18 and Socs2 (Heitman et al., 2020). Thus, Fgf18 expression from outside of the bulge by DS adjacent cells adds an extra layer of regulation to previously described SBL to further integrate signaling and maintaining hfSCs quiescence (Hsu et al., 2011; Heitman et al., 2020). On the other hand, Socs2 is expressed in DS and DP and is known as a suppressor of cytokine signaling which negatively regulates the STAT5 signaling in DP for which inhibition has already been shown to delay the anagen phase, demonstrating yet another layer of signaling integration between different niche components influencing hfSCs quiescence (Udy et al., 1997; Legrand et al., 2016; Heitman et al., 2020).

All these discoveries about molecular DP characteristics suggest that DP might be under the reciprocal influence of hfSCs and other surrounding niche components (as discussed in the next part on subcutaneous adipocytes) to adequately sense and synchronously respond to either inhibiting or promoting HFs cyclic regeneration (**Figures 4A–C**). Since the main part of these molecular pathways mirror the changes observed in bulge hfSCs, regarding the intrinsic competitive cycling between BMP inhibitors and WNT activators and BMP activities in DP, it may suggest that this process is also intrinsic (**Figures 4B,C**). If this is a case, our working model considers the presence of at least one intrinsic oscillator localized in hfSCs and might predict the existence of a second putative one in DPs during hair regeneration (**Figures 4B,C,F**).

SUBCUTANEOUS FAT AND ITS PRECURSORS INTERPLAY WITH THE INTRINSIC hfSCs OSCILLATOR

The behavior of hfSCs is controlled by the regulatory factors provided by DS fibroblasts adjacent to the HG and the hfSCs (**Figure 4A**). Additionally, it was shown that dermal white adipose tissue (DWAT), an important regulator of hfSC activity, is also in close contact with hfSCs (Zwick et al., 2018). Waves of inhibitory and activating signals, produced by the subcutaneous fat cells, facilitate the synchronization of hfSCs, primarily affecting DS and DP activity (**Figure 4A**). It has been revealed that during the hair cycle, the thickness of DWAT shows parallel and synchronized oscillation to HFs, as they are thicker in anagen and thinner in telogen (Chase et al., 1953; Hansen et al., 1984; Festa et al., 2011; Nicu et al., 2019). The enlargement of DWAT during the early anagen is caused by the proliferation and differentiation of preadipocytes, as well as the hypertrophy of adipocytes (Rodeheffer et al., 2008; Festa et al., 2011). Adipogenesis is regulated by WNT/β-catenin and Shh signaling from the growing HFs (Donati et al., 2014; Zhang et al., 2016). In contrast, during the anagen-to-catagen transition, DWAT shrinks, which is caused by lipolytic change and the dedifferentiation of mature adipocytes (Nicu et al., 2019; Zhang et al., 2019). Notably, during the telogen-to-anagen transition, the amount of DWAT increases (Chase et al., 1953; Plikus et al., 2008; Festa et al., 2011). Subcutaneous adipocytes periodically express Bmp2 and Bmp4 to inhibit hfSCs activity and maintain the quiescence and the refractory telogen state (Plikus et al., 2008). The activity of hfSCs can also be suppressed by other dermal inhibitors, such as secreted frizzled-related protein 4 (SFRP-4) and DKK1 (Plikus et al., 2011). DWAT also produces activators including follistatin, which leads to stimulation of hair wave propagation during anagen (Chen et al., 2014). Intradermal immature adipocytes were shown to play a crucial role in controlling the hfSCs through platelet-derived growth factor (PGDF) signaling which stimulates DP cells to activate hair cyclic regeneration (**Figure 4A**) (Festa et al., 2011).

There are some examples of genetically modified mouse models, including mice with human fatty acid transport protein (FATP4) and apolipoprotein C-I overexpression, or mice deficient for Dgat1 and Dgat2, all developing changes in the adipocyte layer, HFs, and skin structure (Jong et al., 1998;

Chen et al., 2002; Herrmann et al., 2003). Other research demonstrated a surprising discovery that fat cells can be regenerated from myofibroblasts during wound healing. For cell lineage reprogramming, neogenic HFs around a wound are necessary to trigger BMP signaling to activate adipocyte-specific transcription factors (Plikus et al., 2017).

Reciprocal signaling and interaction between HFs and DWAT demonstrate the importance of the relationship between hfSCs and their niche to sustain proper skin homeostasis. Although a great deal remains unclear about the comprehensive crosstalk between the HF niche cells, during the various stages of the HF cycle the behavior of hfSCs are largely controlled by the different niche components (Plikus et al., 2008, 2011; Festa et al., 2011).

EXTRA PLAYERS INFLUENCING INTRINSIC hfSCs OSCILLATION AND HAIR REGENERATION

Although still a lot of things remain undiscovered about the comprehensive crosstalk between the HF niche cells, more compound perspectives are appearing in research, showing that during the various stages of the HF cycle the behavior of hfSCs is controlled by the different niche components (Jahoda et al., 1984; Botchkarev et al., 1999; Rendl et al., 2005; Plikus et al., 2008; Festa et al., 2011; Hsu et al., 2011; Kobielak et al., 2015; Joost et al., 2020).

Four types of sensory neurons are concentrated on the top bulge region of the HF to ensure that the sensory responses coordinate the behavior of SCs within the skin (Abraira and Ginty, 2013; Li and Ginty, 2014). Recently it has been found that sensory nerves release Shh to a pool of perineurally located Shh-sensitive upper bulge SCs (Gli1 positive) that permanently participate in wound healing. Hence, their lineage can change into the epidermal SCs, demonstrating the crucial role of the Shh signal to transform and sustain the upper bulge keratinocytes into an epidermal fate (**Figure 3A**) (Brownell et al., 2011). During development, Shh signaling also plays a critical role in the arrector pili muscle-sympathetic nerve niche formation, which in light of recent studies, regulates hair follicle stem cell activity. In this dual-component niche system, norepinephrine, a neurotransmitter, is secreted by sympathetic nerves which activate hfSCs and promote anagen entry. Additionally, the loss of norepinephrine signaling causes stem cell quiescence by down-regulation of cell-cycle and metabolic machinery, as well as up-regulation of two quiescence regulators Fgf18 and Foxp1 (Shwartz et al., 2020).

The HF bulge area is surrounded by blood vessels (part of dermal vasculature – superficial vascular plexus) that provide the nutritional and hormonal input into the hfSCs population, which was confirmed by recent research illustrating the connection between the bulge SCs and the perivascular niche (Amoh et al., 2004; Xiao et al., 2013). Additional research has confirmed that the hair cycle depends on cutaneous angiogenesis and identified Bmp4 regulation as one of the main inhibitory factors of hfSCs anagen progression (Mecklenburg et al., 2000; Li et al., 2019). Furthermore, the K15 negative upper bulge cells located adjacent to the vascular annulus express a signaling factor EGF-like domain- multiple 6 (Egfl6), which is involved in angiogenesis and the recruitment of vascular endothelial cells (Xiao et al., 2013).

A recent study also highlighted that lymphatic remodeling, driven by hfSCs, coordinates HFs regeneration by controlling the composition of fluids and cells in the surrounding environment. HfSCs control the behavior of lymphatic capillaries through the secretion of molecules Angptl7 and Angptl4, which act as an on/off switch for drainage. The niche connection between lymphatic and hfSCs revealed its importance in maintaining the balance between hfSCs self-renewal and quiescence. This novel concept represents a potential source of new therapeutic targets for lymph-related conditions, including hair loss and wound-healing (Gur-Cohen et al., 2019; Pena-Jimenez et al., 2019).

Hair pigmentation depends on the production of melanocytes and their melanin-product deposition inside keratinocytes. Melanocytes come from melanocyte stem cells (MSCs) during each hair cycle activation. During development, MSCs derive from the neural crest and are located in the bulge area, interspersed between hfSCs (Nishimura et al., 2002). The coordinated mutual interaction between MSCs and hfSCs allows for sMSCs activation and differentiation into melanocytes which produce and transfer melanin to the bulb matrix progenitors during each hair regeneration to produce hair color (Tanimura et al., 2011). The coordinated activation of canonical WNT signaling and collaboration between hfSCs and MSCs especially through Wnt7a and Wnt10b ligand, the first, previously described in the intrinsic oscillation model, initiates pigmented hair regeneration. Thus, it suggests that this crosstalk between SCs in the bulge is necessary to couple their behavior and coordinate the outcome of hair regeneration and pigmentation (**Figure 4F**) (Rabbani et al., 2011; Chang et al., 2013). The skin pigmentation pattern named "anagen-coupled melanogenesis" can also serve as a sign of the hfSCs activation, which is manifested by visible pigment production during each new hair cycle (Chase and Eaton, 1959).

Immune cells are crucial for proper hair development, not only during embryogenesis but also to regulate the regeneration of HFs during physiological hair cycling and after skin injury by stimulating the proliferation and differentiation of hfSCs (Paus et al., 1998; Gay et al., 2013; Ali et al., 2017; Lee et al., 2017; Wang et al., 2017; Rahmani et al., 2018). Although it has been shown that T cells are associated with the hair follicle throughout the entire hair growth cycle, they are most abundant during the rest phase, as they participate in telogen to anagen transition. Under normal physiological conditions, regulatory T cells (Tregs), which express skin-resident Foxp3 (forkhead box p3), are located in the follicular epithelium close to hfSCs. They evoke differentiation and proliferation of hfSCs through the Jag1-Notch pathway (Zhang et al., 2019). Research showed that activation of γδ T cells promotes hair growth and helps the wound healing process by stimulation of interfollicular epidermal basal cells (Jameson and Havran, 2007; Lee et al., 2017). The γδ T cells are necessary for HFs neogenesis by secretion Fgf9 that subsequently activate WNT in fibroblasts in the wounded area (Gay et al., 2013). However, immune privilege collapsing may lead to an immune attack on HFs, resulting in diseases such as

Alopecia areata, immunity-mediated hair loss (Paus et al., 2003; Gilhar et al., 2007; Strazzulla et al., 2018). Although the exact cause of this disease remains unknown, most probably it occurs due to increased presentation of autoantigens in surveying T cells which can recognize HF antigen resulting in autoimmune responses against HFs (Gilhar et al., 2007; Strazzulla et al., 2018). The described inflammatory response mainly attacks the lower transient segment of anagen HFs, inhibiting hair growth, and promoting premature anagen-to-telogen transition (Strazzulla et al., 2018). In summary, the influx of autoreacting T cells into the HFSC niche is one of the elements that prevent normal hair growth.

The other immune cells that are located in the HF niche and that have been shown to regulate the hair cycle are macrophages (Paus et al., 1998; Castellana et al., 2014). Macrophages in the skin exist as a heterogeneous population, therefore they can have different effects on hfSCs (Castellana et al., 2014). They occur most abundantly during the telogen state (Castellana et al., 2014). Reduction in the number of macrophages initiates premature anagen onset, while apoptotic macrophages can activate hfSCs via WNT signaling, releasing Wnt7b and Wnt10a ligands (Castellana et al., 2014). In contrast, other studies on murine macrophages during telogen, which utilized scRNA-seq, led to the discovery of TREM2+ dermal macrophages, which can secrete oncostatin M (OSM), a possible antagonist of hfSCs cyclic regeneration (Yu et al., 2008; Wang et al., 2019). OSM activates the JAK-STAT5 signaling pathway, maintaining the hfSCs in the quiescence state during the telogen state (Wang et al., 2019). Therefore, the ablation of these particular macrophages leads to an anagen state (Wang et al., 2019). Additionally, macrophages also play a role in the hfSCs response to injury. Hitherto, several ways of activating macrophages that are caused by wounds to the skin have been already described (Ito et al., 2002; Osaka et al., 2007; Chen et al., 2015). In particular, CX3CR1 high CCR2+ macrophages expressing TGF-β1 and TNF-α play a crucial role in hair growth promoted by injury (Rahmani et al., 2018). Macrophages secreting TNF-α lead to hfSCs activation through the TNF-α/p-AKT/p-β-catenin-Ser552 signaling axis, resulting in anagen onset in the skin of surrounding wounds (Osaka et al., 2007; Wu et al., 2015; Rahmani et al., 2018). Taking it all together, macrophages are potential candidates in promoting hair growth. The activation of WNT/β-catenin signaling can promote their proliferation and accumulation, therefore participating in hair and skin regeneration.

THE INTERPLAY BETWEEN THE EXTRINSIC NICHE ENVIRONMENT AND THE INTRINSIC hfSCs OSCILLATOR DURING HOMEOSTASIS AND HAIR CYCLE REGENERATION

Stem cell reservoirs are localized in dedicated niches that serve as *de facto* macro- and micro- environments that control SCs homeostasis regulation (Spradling et al., 2001; Lin, 2002; Fuchs et al., 2004). HfSCs also release self-stimulating agonists in a self-autonomous way at the initiation of growth while maintaining dormancy throughout the majority of the adult HFs cycle, however, the underlying mechanisms of this process are not well understood (Blanpain et al., 2004; Greco et al., 2009; Zhang et al., 2009; Oshimori and Fuchs, 2012).

Bone morphogenetic protein signaling is one of the most important pathways necessary for correct HFs cyclic regeneration (Botchkarev et al., 2001; Kobielak et al., 2003, 2007; Andl et al., 2004; Plikus et al., 2004; Zhang et al., 2006). HFs ORS, along with bulge hfSCs, exclusively express transmembrane Bmpr1a which is essential to transduce canonical BMP signal after binding with secreted BMP ligands (Bmp2/4/6) by the phosphorylation of Smad transcription factors (pSmad1/5/8) (Andl et al., 2004; Kobielak et al., 2007). After activation of BMP signaling, pSmad1/5/8 forms a heterodimer with Smad4 to *trans*-activate specific target genes in the nucleus during quiescent telogen (Andl et al., 2004; Massague et al., 2005; Kobielak et al., 2007). The genetic removal of the *Bmpr1a* in the HFs contributes to premature and prolonged stimulation of dormant hfSCs with perturbed homeostasis (Kobielak et al., 2007), which results in specific hair tumor formation (Kobielak et al., 2003, 2007; Andl et al., 2004; Zhang et al., 2006). BMP agonists or antagonists are secreted by either intrinsic hfSCs oscillator or by external niche during HFs cyclic regeneration. During the onset of a new anagen, opposing changes in expression occur with down-regulated Bmp4 and up-regulated Noggin, which is simultaneously observed in an extrinsic niche (DP) and intrinsic HG (**Figures 4A–D**) (Botchkarev et al., 2001). Bmpr1a is also expressed in the DP transducing canonical BMP pathway to form HFs (Rendl et al., 2008) and BMP activity fluctuation in the DP results in the generation of distinctive HFs set (Driskell et al., 2009).

Despite the prevailing and crucial function of DP in niche stimulation or suppression of hfSCs, the subcutaneous fat adjacent to hfSCs and HG was shown to release Bmp2 and Bmp4, thus demonstrating that it is an important player in the hfSCs environment (Plikus et al., 2008; Festa et al., 2011). In addition, intrinsic up-regulation of Bmp6 has been proposed to suppress hfSCs, keeping them in a dormant state (**Figure 4A**) (Blanpain et al., 2004; Kandyba et al., 2013).

Bone morphogenetic protein signaling play a fundamental role in SCs homeostasis in several organs in the body (Zhang et al., 2003; Haramis et al., 2004; He et al., 2004; Kobielak et al., 2007). Interestingly, the crucial role of BmpR1A has also been confirmed in hematopoietic stem cells (HSCs), in the intestinal stem cells (ISCs), and more recently in neural stem cells (NSCs) to maintain quiescence of adult SCs by activation of canonical BMP signaling (Zhang et al., 2003; Haramis et al., 2004; He et al., 2004; Mira et al., 2010). In contrast, in embryonic SCs (ESCs) BMP ligands work together with LIF to preserve stemness and promote proliferative conditions in cell culture (Sato et al., 2003; Ying et al., 2003). Similarly, an invertebrate homolog of BMP ligand, *dpp* is needed to set a niche to preserve anterior germline SCs in the fly embryo (Xie and Spradling, 1998).

On the other hand, the WNT signaling with β-catenin nuclear accumulation had been shown as the first pathway crucial

to stimulating HFs anagen by promoting dormant hfSCs to proliferate (Gat et al., 1998; Van Mater et al., 2003; Lo Celso et al., 2004; Lowry et al., 2005). Indeed, the overexpression of the stabilized nuclear form of β-catenin in the HFs of genetically modified mouse models resulted in early hfSCs stimulation, which later led to the development of HFs derived tumors, pilomatricomas, and trichofolliculomas (Gat et al., 1998; DasGupta and Fuchs, 1999). A similar genetic mutation that stabilized β-catenin was found in approximately three-quarters of human pilomatricomas (Chan et al., 1999). In contrast, when β-catenin was genetically removed from hfSCs it caused hfSCs to lose their ability to stimulate new HFs growth, and to maintain the fate of HF progenies, preferentially adapting IFE characteristics (Huelsken et al., 2001; Lowry et al., 2005). After the inside interaction between BMP signaling and the WNT pathway was described in ISCs, where suppression of BMP leads to PTEN inhibition with subsequent β-catenin stabilization (He et al., 2004), a similar probable link between both pathways was suggested in hfSCs (Kobielak et al., 2007). HFs tumors resembling trichofolliculomas were formed after Noggin overexpression that neutralized the BMP pathway, thus linking it directly to WNT signaling (Sharov et al., 2009).

One of the well-defined processes of hfSCs stimulation is the upregulation of WNT pathway after the suppression of the BMP signaling pathway, with nuclear β-catenin stabilization at first in HG, then in hfSCs to push HFs cyclic regeneration (Gat et al., 1998; Botchkarev et al., 1999; Kobielak et al., 2003, 2007; Van Mater et al., 2003; Andl et al., 2004; Lo Celso et al., 2004; Zhang et al., 2006; Ito et al., 2007; Plikus et al., 2008; Greco et al., 2009; Plikus et al., 2011). Until recently, there was a missing link in understanding of how the BMP pathway controls canonical WNT signaling on the molecular level to influence a complex gene network that promotes hfSCs stimulation. A novel machinery that internally integrates a gene network between BMP and WNT signaling was recently uncovered precisely in hfSCs, where the suppression of the BMP pathway boosted the intra-bulge WNT ligands (**Figures 3B**, **4A**) (Kandyba et al., 2013). HGs and hfSCs cells reach early anagen activation after the DP release BMP antagonists, such as Noggin (**Figures 4A,C**) (Botchkarev et al., 1999; Botchkarev et al., 2001; Greco et al., 2009). The study assumed that the hfSCs were randomly activated in the next hair cycle and that they must be in the right oscillation phase to respond to DP secreted Noggin by the preceding intrinsic secretion of Grem1 and Bambi by the hfSCs oscillator during the high BMP refractory phase of telogen (**Figure 4B**) (Kandyba et al., 2013). Thus, BMP inhibition from external and internal sources must further prepare stochastically selected hfSCs to respond to anagen activation by upregulation of the canonical WNT receptor, Fzd10 with simultaneous downregulation Fzd2 and Fzd3 (non-canonical ones) (**Figure 4B**) (Kandyba et al., 2013; Adam et al., 2018). At the same time, there is observed overexpression of the intra-bulge WNT ligands like Wnt7a, Wnt7b, and Wnt16 after inhibition of BMP/pSmads1/5/8 signaling (**Figures 3B**, **4A**) (Kandyba et al., 2013; Genander et al., 2014; Kandyba and Kobielak, 2014). Functionally, the biological consequences of WNT canonical ligand upregulation were confirmed by the subcutaneous introduction of the recombinant protein of Wnt7a, which resulted in hfSCs stimulation, initiating a new regeneration cycle (Kandyba et al., 2013). Collectively, these findings on internal antagonistic competition underline the existence of a previously unknown intrinsic oscillation between the signaling of BMP and WNT gene networks within hfSCs. This fluctuation counterbalances SCs action indicating that halted BMP releases the inhibition of WNT, which forces individual hfSC to the anagen phase, proportionally to the signal strength changes between BMP/WNT (**Figures 3B**, **4A**). These findings propose an additional chain of command to control hfSCs besides the reciprocal interaction between bulge and DP, as well as HFs and subcutaneous fat (Kandyba et al., 2013). Thus, canonical BMP and WNT pathways might serve as one of the common signaling platforms for the reciprocal communication between some extrinsic niche components and hfSCs, allowing SCs to appropriately analyze the surrounding signals to adequately respond during new hair cycles (Kandyba et al., 2013).

Dermal papilla and Noggin secrete transforming growth factor-β2 (TGFβ2) simultaneously during anagen onset (**Figure 4A**) (Oshimori and Fuchs, 2012). TGFβ2 works synergistically with Noggin and causes HG to respond with the upregulation of TMEFF1 (transmembrane protein with EGF-like and two follistatin-like domains 1), which further suppresses BMP signaling (**Figure 4A**) (Oshimori and Fuchs, 2012). Additionally, PDGFα (platelet-derived growth factor-α) is produced by precursors of intradermal fat and activates the dermal cells adjacent to hfSCs, promoting anagen (**Figure 4A**) (Festa et al., 2011). Thus, hfSCs sense the number of surrounding niche cues and respond accordingly to them with activation of HFs anagen, if the niche cues for activation are more prevalent than inhibitory ones (**Figure 4A**) (Oshimori and Fuchs, 2012).

The exact molecular mechanism of the WNT pathway in the activation and proliferation of hfSCs is still unveiling, but recent studies shed light on these intricate interactions. Based on microarray and ChIP analyses, Cyclin D1 was identified as one of the up-regulated cell cycle-promoting factors, upon nuclear β-catenin stabilization, during the beginning of telogen, when SCs become activated and start to proliferate (Lowry et al., 2005). This finding is consistent with previously established chromatin immunoprecipitation (ChIP) assays, where Cyclin D1 was identified as one of the WNT target genes (Chamorro et al., 2005). Moreover, chromatin remodeling factors: Timp3, and Hmgn3, containing Lef1/Tcf-binding sites, were identified as direct genes activated by the β-catenin chromatin complex during telogen- anagen transition (Lowry et al., 2005). Indeed, it seems that switching Tcf3/Tcf4 for Lef1 and nuclear complex Lef1/β-catenin formation after activation of WNT signaling is crucial for anagen onset (Adam et al., 2018).

The length of HF cycle phases is appropriately regulated by DP and the subcutaneous fat adjacent to hfSCs and the SBL of HFs, which cooperatively generate signal modulating hubs by balancing the molecular gene network in SCs (**Figure 4A**) (Plikus et al., 2008, 2011; Greco et al., 2009; Festa et al., 2011; Hsu et al., 2011). Furthermore, the performance of an individual hfSC is adjusted randomly by periodic and recurring interplays. These may have various consequences that depend on changes in

the stimulatory or dormant landscape, influenced by the general macro- or more regional local micro- environment (**Figure 4F**) (Chuong and Widelitz, 2009). There are also two phases of telogen that are marked by the differential expression of dermal BMP, known as refractory and competent telogen according to high or low levels of BMP, which are in opposite phases to canonical WNT signaling (Plikus et al., 2008).

These discoveries have established a novel reciprocal dependency where canonical BMP signaling trumps the canonical WNT pathway in terms of the molecular control of the intrinsic oscillation of hfSCs homeostasis during dormancy and activation (**Figures 3B**, **4A,B**), further integrating the signaling of the surrounding extrinsic niche environment. This model of the intrinsic oscillator within hfSCs might explain how different levels of internal and external signals merge, in either compatible or incompatible phases. This results in either hastened or deferred hfSCs receptiveness to activation by shortening or lengthening the refractory and competent telogen (Kandyba et al., 2013, 2014; Kandyba and Kobielak, 2014; Kobielak et al., 2015). The presence of the hfSCs oscillator, which is responsive to either their own repressive BMP signals or to those of the extrinsic niche environment, resembles the oscillating states described in pattern formation during morphogenesis (Maini et al., 2006). Thus, the permanent intra-bulge and mutually exclusive oscillation between agonists and antagonists are essential for the preservation of hfSCs homeostasis.

Since the activation with WNT or inhibition with BMP and the fact that signaling could be represented as respective waves (**Figures 4B,C**), we propose that the intrinsic oscillator in hfSCs (or the second putative independent one in DP) has two phases, where each of them follows after the other in a constantly alternating rhythm, with the canonical BMP pathway upstream of WNT signaling (**Figure 4B**, intrinsic oscillation for BMP either in synergistic or competitive phase) (Kandyba et al., 2013). It is important to note that hfSCs react to the phase of this rhythm by sensing the level of active pSmads that represent inhibitory canonical BMP signaling, causing either repression of the WNT pathway (BMP/pSmads high) or activation of WNT (BMP/pSmads low) (**Figures 4B,C**). Despite the BMP axis, the WNT pathway itself is a second axis that maintains this constant rhythm, where the canonical nuclear stabilization of β-catenin forces the activation of Bmp6 as well as their inhibitor Dkk3 and Sfrp1, thus allowing WNT to reactivate Bmp with inhibition of activated hfSCs (**Figure 4B**, putative intrinsic oscillation for WNT) (Kandyba et al., 2013; Lim et al., 2016). By these means, stem cells possess an intrinsic regulatory network mechanism that works contrary to the phase of either activation or inhibition, thus maintaining balance and preventing either overactivation (with tumor formation) or over inhibition (with suppression of stem cell homeostasis or stemness).

Taking these findings into account, we, therefore, propose that the intrinsic oscillator in hfSCs may interact with the extrinsic surrounding niche environment. To simplify our model, we performed a comparison with the DP niche, where cells from these different compartments may meet with either opposite waves of WNT and BMP signaling, or in the same waves of these pathways (just for extreme wave interference situations). In the first model, if the opposing waves of WNT and BMP signaling interfere in reverse phases, the prediction will be to observe the attenuation of emerging signals coming from the intrinsic hfSCs oscillator and DP with inhibitory effects (**Figure 4D**, OFF). Consequently, it will reduce the wave amplitude of BMP or WNT signaling either in hfSCs or DP and creating a weaker (than each of waves that merged before) and more flat wave, leading to destructive interference (**Figure 4D**, a dotted black sinusoid lines, OFF). On the contrary, the model of wave interference in concordant phases between hfSCs and DP proposes either an inhibitory effect when waves synchronize in the same stage of BMP signaling (**Figure 4E**, OFF, a dotted red sinusoid line) or an activating effect if waves merge in the same stage of WNT signaling (**Figure 4E**, ON, a dotted green sinusoid line). This results in a stronger wave with a higher amplitude of either BMP (stronger inhibition) or WNT (stronger activation) signaling for both hfSCs and DP, causing a situation of constructive interference (**Figure 4E**, OFF and ON).

In the future, these models might be useful in building a computational design that predicts HFs behavior in terms of mutual interaction with the external niche environment during the hair cycle.

DISCUSSION

This model proposes that the intrinsic oscillation of signals in hfSCs is critical in forming and maintaining a periodic pattern in the cycle of hair regeneration. If stem cells and the surrounding environment niche had a predisposition to reach a constant balance, there would be no spontaneous provoking cues that initiate another hair regeneration cycle. Therefore, the presented model assumes a need for a dynamic oscillating gene network in the stem cell population instead of a static one, which rhythmically fluctuates. It reaches amplitude in any of the two divergent hfSCs states by sensing and responding to surrounding signals (**Figures 4B,C**). As a result, the oscillation of the intrinsic signals is crucial for the stochastic initiation of spontaneous hair cycle activation or its quiescence (**Figure 3B**). Therefore, the regenerative system of HFs has at least one stem cell population intrinsically oscillating and constantly tipping the balance in the favor of either quiescence or activation. Simultaneously, this mini-organ maintains a dynamic self-responding gene network that is primed to be stimulated in an active state or silenced in a quiescent one (**Figure 3B**).

Furthermore, the BMP axis might be one of the key components of the signaling pathway, orchestrating intrinsic stem cell oscillation in HF in an *in vivo* model (Kandyba et al., 2013; Genander et al., 2014). Therefore, this model hypothesizes that the BMP pathway is upstream of the others and defines a center axis of the intrinsic hfSCs oscillation. To date, other well-documented studies have confirmed the existence of canonical BMP-WNT signaling axes that behave like an intrinsic oscillator, resulting in an antagonistic competition between BMP and WNT gene networks in hfSCs (**Figures 3B**, **4A**) (Kandyba et al., 2013; Genander et al., 2014; Adam et al., 2018). These studies were recently supported by the discovery of antagonistic competition

between WNT and BMP gene networks when the canonical WNT pathway was inhibited by β-catenin ablation in hfSCs, adding a new gene network dependency to maintain constant intrinsic oscillation in hfSCs (**Figure 3B**) (Kandyba et al., 2013; Lim et al., 2016). Furthermore, this indicates that the regulatory feedback loops between canonical BMP and WNT pathways not only sense the change of hfSCs activity but that they can respond accordingly to regulate hfSCs. This pathway interaction keeps the intrinsic oscillator of the stem cells constantly active, introducing a check and balance mechanism to maintain stem cells homeostasis (**Figures 3B**, **4B,D**) (Kandyba et al., 2013; Genander et al., 2014; Lim et al., 2016; Adam et al., 2018).

As presented in this review, data suggest that the cyclic regeneration of hair might depend at least on one intrinsic oscillator located in hfSCs that maintains the regeneration rhythm of HF. It would, therefore, be intriguing for future studies to explore whether other components of the hair mini-organ discussed here, such as DP (the second putative independent intrinsic oscillator), also possess such essential oscillation, or whether they just respond to intrinsic clues from the oscillation in hfSCs. It could be presumed that some other stem cell-based regenerative systems might possess a similar system of regulation. Therefore, it would be interesting to investigate if they could maintain their rhythm, by either initiating a subsequent cycle of regeneration or maintaining quiescence.

In conclusion, the model of hfSCs is very instructive for research on how adult SCs, their descendants, and the extrinsic niche environment equalize or cooperate to sustain SCs responsiveness and reactivity during homeostasis. Within the skin, a highly compartmentalized niche forms the macroenvironment in which elements are tightly connected with each other and depend on adipocytes or their precursors, the immune system with macrophages and cells composed directly HF, for example, DP or the $K6^+$ Inner Layer.

Although hfSCs release controlling factors in a self-autonomous way, they stochastically respond to external niche signals and manage mini-organ regenerative urgency, which might be a universal SCs controlling mechanism. Ultimately, the discovery of the mutual interaction and gene networks among different extrinsic niche elements and hfSCs will contribute very useful information that might be applicable in stem cell-based medical therapies. Further understanding of the composition and the signals within the oscillator and environment of the hair mini-organ might speed up the development of potent small-molecule based therapy to safely initiate the regenerative cycle of the hair follicle.

AUTHOR CONTRIBUTIONS

KK contributed to the conception and design of the manuscript. PD, PM, TDP, AO, ŁMB, and KK wrote the article and approved the final version. All authors read and approved the final manuscript.

FUNDING

This work was funded by Foundation for Polish Science (FNP) co-financed by the European Union under the European Regional Development Fund, Team Grant #POIR.04.04.00-00-4222/17-00 (to KK) and National Science Centre, Poland (NCN) Opus Grant 2015/19/B/NZ3/02948 (to KK), Opus Grant 2019/33/B/NZ3/02966 (to KK), PRELUDIUM Grant #2017/25/N/NZ3/02622 (to PD), and PRELUDIUM Grant #2019/33/N/NZ3/03077 (to PM).

ACKNOWLEDGMENTS

We would like to thank Dr. Jeff Palatini (CeNT, University of Warsaw) and other members of the Laboratory of Stem Cells, Development and Tissue Regeneration for critical feedback on this manuscript and helpful discussions.

REFERENCES

Abaci, H. E., Coffman, A., Doucet, Y., Chen, J., Jackow, J., Wang, E., et al. (2018). Tissue engineering of human hair follicles using a biomimetic developmental approach. *Nat. Commun.* 9:5301.

Abraira, V. E., and Ginty, D. D. (2013). The sensory neurons of touch. *Neuron* 79, 618–639. doi: 10.1016/j.neuron.2013.07.051

Adam, R. C., Yang, H., Ge, Y., Infarinato, N. R., Gur-Cohen, S., Miao, Y., et al. (2020). NFI transcription factors provide chromatin access to maintain stem cell identity while preventing unintended lineage fate choices. *Nat. Cell Biol.* 22, 640–650. doi: 10.1038/s41556-020-0513-0

Adam, R. C., Yang, H., Ge, Y., Lien, W. H., Wang, P., Zhao, Y., et al. (2018). Temporal layering of signaling effectors drives chromatin remodeling during hair follicle stem cell lineage progression. *Cell Stem Cell* 22, 398.e7–413.e7.

Adam, R. C., Yang, H., Rockowitz, S., Larsen, S. B., Nikolova, M., Oristian, D. S., et al. (2015). Pioneer factors govern super-enhancer dynamics in stem cell plasticity and lineage choice. *Nature* 521, 366–370. doi: 10.1038/nature 14289

Ali, N., Zirak, B., Rodriguez, R. S., Pauli, M. L., Truong, H. A., Lai, K., et al. (2017). Regulatory T cells in skin facilitate epithelial stem cell differentiation. *Cell* 169, 1119.e11–1129.e11.

Alonso, L., and Fuchs, E. (2006). The hair cycle. *J. Cell Sci.* 119, 391–393.

Amoh, Y., Li, L., Yang, M., Moossa, A. R., Katsuoka, K., Penman, S., et al. (2004). Nascent blood vessels in the skin arise from nestin-expressing hair-follicle cells. *Proc. Natl. Acad. Sci. U.S.A.* 101, 13291–13295. doi: 10.1073/pnas.0405250101

Andl, T., Ahn, K., Kairo, A., Chu, E. Y., Wine-Lee, L., Reddy, S. T., et al. (2004). Epithelial Bmpr1a regulates differentiation and proliferation in postnatal hair follicles and is essential for tooth development. *Development* 131, 2257–2268. doi: 10.1242/dev.01125

Avigad Laron, E., Aamar, E., and Enshell-Seijffers, D. (2018). The mesenchymal niche of the hair follicle induces regeneration by releasing primed progenitors from inhibitory effects of quiescent stem cells. *Cell Rep.* 24, 909.e3–921.e3.

Bardot, B., Lecoin, L., Fliniaux, I., Huillard, E., Marx, M., and Viallet, J. P. (2004). Drm/Gremlin, a BMP antagonist, defines the interbud region during feather development. *Int. J. Dev. Biol.* 48, 149–156. doi: 10.1387/ijdb.15272379

Barrandon, Y., and Green, H. (1987). Three clonal types of keratinocyte with different capacities for multiplication. *Proc. Natl. Acad. Sci. U.S.A.* 84, 2302–2306. doi: 10.1073/pnas.84.8.2302

Biernaskie, J., Paris, M., Morozova, O., Fagan, B. M., Marra, M., Pevny, L., et al. (2009). SKPs derive from hair follicle precursors and exhibit properties of adult dermal stem cells. *Cell Stem Cell* 5, 610–623. doi: 10.1016/j.stem.2009.10.019

Blanpain, C., and Fuchs, E. (2009). Epidermal homeostasis: a balancing act of stem cells in the skin. *Nat. Rev. Mol. Cell Biol.* 10, 207–217. doi: 10.1038/nrm2636

Blanpain, C., Lowry, W. E., Geoghegan, A., Polak, L., and Fuchs, E. (2004). Self-renewal, multipotency, and the existence of two cell populations within an epithelial stem cell niche. *Cell* 118, 635–648. doi: 10.1016/j.cell.2004.08.012

Botchkarev, V. A., Botchkareva, N. V., Nakamura, M., Huber, O., Funa, K., Lauster, R., et al. (2001). Noggin is required for induction of the hair follicle growth phase in postnatal skin. *FASEB J.* 15, 2205–2214. doi: 10.1096/fj.01-0207com

Botchkarev, V. A., Botchkareva, N. V., Roth, W., Nakamura, M., Chen, L. H., Herzog, W., et al. (1999). Noggin is a mesenchymally derived stimulator of hair-follicle induction. *Nat. Cell Biol.* 1, 158–164. doi: 10.1038/11078

Brownell, I., Guevara, E., Bai, C. B., Loomis, C. A., and Joyner, A. L. (2011). Nerve-derived sonic hedgehog defines a niche for hair follicle stem cells capable of becoming epidermal stem cells. *Cell Stem Cell* 8, 552–565. doi: 10.1016/j.stem.2011.02.021

Castellana, D., Paus, R., and Perez-Moreno, M. (2014). Macrophages contribute to the cyclic activation of adult hair follicle stem cells. *PLoS Biol.* 12:e1002002. doi: 10.1371/journal.pbio.1002002

Chamorro, M. N., Schwartz, D. R., Vonica, A., Brivanlou, A. H., Cho, K. R., and Varmus, H. E. (2005). FGF-20 and DKK1 are transcriptional targets of beta-catenin and FGF-20 is implicated in cancer and development. *EMBO J.* 24, 73–84. doi: 10.1038/sj.emboj.7600460

Chan, E. F., Gat, U., McNiff, J. M., and Fuchs, E. (1999). A common human skin tumour is caused by activating mutations in beta-catenin. *Nat. Genet.* 21, 410–413. doi: 10.1038/7747

Chang, C. Y., Pasolli, H. A., Giannopoulou, E. G., Guasch, G., Gronostajski, R. M., Elemento, O., et al. (2013). NFIB is a governor of epithelial-melanocyte stem cell behaviour in a shared niche. *Nature* 495, 98–102. doi: 10.1038/nature11847

Chase, H. B., and Eaton, G. J. (1959). The growth of hair follicles in waves. *Ann. N. Y. Acad. Sci.* 83, 365–368. doi: 10.1111/j.1749-6632.1960.tb40912.x

Chase, H. B., Montagna, W., and Malone, J. D. (1953). Changes in the skin in relation to the hair growth cycle. *Anat. Rec.* 116, 75–81. doi: 10.1002/ar.1091160107

Chase, H. B., Rauch, R., and Smith, V. W. (1951). Critical stages of hair development and pigmentation in the mouse. *Physiol. Zool.* 24, 1–8. doi: 10.1086/physzool.24.1.30152098

Chen, C. C., Murray, P. J., Jiang, T. X., Plikus, M. V., Chang, Y. T., Lee, O. K., et al. (2014). Regenerative hair waves in aging mice and extra-follicular modulators follistatin, dkk1, and sfrp4. *J. Invest. Dermatol.* 134, 2086–2096. doi: 10.1038/jid.2014.139

Chen, C. C., Wang, L., Plikus, M. V., Jiang, T. X., Murray, P. J., Ramos, R., et al. (2015). Organ-level quorum sensing directs regeneration in hair stem cell populations. *Cell* 161, 277–290. doi: 10.1016/j.cell.2015.02.016

Chen, H. C., Smith, S. J., Tow, B., Elias, P. M., and Farese, R. V. (2002). Leptin modulates the effects of acyl CoA : diacylglycerol acyltransferase deficiency on murine fur and sebaceous glands. *J. Clin. Investig.* 109, 175–181. doi: 10.1172/jci0213880

Chuong, C. M., and Widelitz, R. B. (2009). The river of stem cells. *Cell Stem Cell* 4, 100–102. doi: 10.1016/j.stem.2009.01.003

Claudinot, S., Nicolas, M., Oshima, H., Rochat, A., and Barrandon, Y. (2005). Long-term renewal of hair follicles from clonogenic multipotent stem cells. *Proc. Natl. Acad. Sci. U.S.A.* 102, 14677–14682. doi: 10.1073/pnas.0507250102

Cotsarelis, G., Sun, T. T., and Lavker, R. M. (1990). Label-retaining cells reside in the bulge area of pilosebaceous unit: implications for follicular stem cells, hair cycle, and skin carcinogenesis. *Cell* 61, 1329–1337. doi: 10.1016/0092-8674(90)90696-c

DasGupta, R., and Fuchs, E. (1999). Multiple roles for activated LEF/TCF transcription complexes during hair follicle development and differentiation. *Development* 126, 4557–4568.

Dhouailly, D. (1973). Dermo-epidermal interactions between birds and mammals: differentiation of cutaneous appendages. *J. Embryol. Exp. Morphol.* 30, 587–603.

Donati, G., Proserpio, V., Lichtenberger, B. M., Natsuga, K., Sinclair, R., Fujiwara, H., et al. (2014). Epidermal Wnt/beta-catenin signaling regulates adipocyte differentiation via secretion of adipogenic factors. *Proc. Natl. Acad. Sci. U.S.A.* 111, E1501–E1509.

Driskell, R. R., Giangreco, A., Jensen, K. B., Mulder, K. W., and Watt, F. M. (2009). Sox2-positive dermal papilla cells specify hair follicle type in mammalian epidermis. *Development* 136, 2815–2823. doi: 10.1242/dev.038620

Driskell, R. R., Lichtenberger, B. M., Hoste, E., Kretzschmar, K., Simons, B. D., Charalambous, M., et al. (2013). Distinct fibroblast lineages determine dermal architecture in skin development and repair. *Nature* 504, 277–281. doi: 10.1038/nature12783

Enshell-Seijffers, D., Lindon, C., and Morgan, B. A. (2008). The serine protease Corin is a novel modifier of the Agouti pathway. *Development* 135, 217–225. doi: 10.1242/dev.011031

Enshell-Seijffers, D., Lindon, C., Wu, E., Taketo, M. M., and Morgan, B. A. (2010). Beta-catenin activity in the dermal papilla of the hair follicle regulates pigment-type switching. *Proc. Natl. Acad. Sci. U.S.A.* 107, 21564–21569. doi: 10.1073/pnas.1007326107

Ernfors, P. (2010). Cellular origin and developmental mechanisms during the formation of skin melanocytes. *Exp. Cell Res.* 316, 1397–1407. doi: 10.1016/j.yexcr.2010.02.042

Fernandes, K. J., McKenzie, I. A., Mill, P., Smith, K. M., Akhavan, M., Barnabe-Heider, F., et al. (2004). A dermal niche for multipotent adult skin-derived precursor cells. *Nat. Cell Biol.* 6, 1082–1093. doi: 10.1038/ncb1181

Festa, E., Fretz, J., Berry, R., Schmidt, B., Rodeheffer, M., Horowitz, M., et al. (2011). Adipocyte lineage cells contribute to the skin stem cell niche to drive hair cycling. *Cell* 146, 761–771. doi: 10.1016/j.cell.2011.07.019

Fuchs, E., Tumbar, T., and Guasch, G. (2004). Socializing with the neighbors: stem cells and their niche. *Cell* 116, 769–778.

Fujiwara, H., Ferreira, M., Donati, G., Marciano, D. K., Linton, J. M., Sato, Y., et al. (2011). The basement membrane of hair follicle stem cells is a muscle cell niche. *Cell* 144, 577–589. doi: 10.1016/j.cell.2011.01.014

Gat, U., DasGupta, R., Degenstein, L., and Fuchs, E. (1998). De Novo hair follicle morphogenesis and hair tumors in mice expressing a truncated beta-catenin in skin. *Cell* 95, 605–614. doi: 10.1016/s0092-8674(00)81631-1

Gay, D., Kwon, O., Zhang, Z., Spata, M., Plikus, M. V., Holler, P. D., et al. (2013). Fgf9 from dermal gammadelta T cells induces hair follicle neogenesis after wounding. *Nat. Med.* 19, 916–923. doi: 10.1038/nm.3181

Genander, M., Cook, P. J., Ramskold, D., Keyes, B. E., Mertz, A. F., Sandberg, R., et al. (2014). BMP signaling and its pSMAD1/5 target genes differentially regulate hair follicle stem cell lineages. *Cell Stem Cell* 15, 619–633. doi: 10.1016/j.stem.2014.09.009

Gierer, A., and Meinhardt, H. (1972). A theory of biological pattern formation. *Kybernetik* 12, 30–39. doi: 10.1007/bf00289234

Gilhar, A., Paus, R., and Kalish, R. S. (2007). Lymphocytes, neuropeptides, and genes involved in alopecia areata. *J. Clin. Invest.* 117, 2019–2027. doi: 10.1172/jci31942

Greco, V., Chen, T., Rendl, M., Schober, M., Pasolli, H. A., Stokes, N., et al. (2009). A two-step mechanism for stem cell activation during hair regeneration. *Cell Stem Cell* 4, 155–169. doi: 10.1016/j.stem.2008.12.009

Gur-Cohen, S., Yang, H., Baksh, S. C., Miao, Y., Levorse, J., Kataru, R. P., et al. (2019). Stem cell-driven lymphatic remodeling coordinates tissue regeneration. *Science* 366, 1218–1225. doi: 10.1126/science.aay4509

Hanakawa, Y., Li, H., Lin, C., Stanley, J. R., and Cotsarelis, G. (2004). Desmogleins 1 and 3 in the companion layer anchor mouse anagen hair to the follicle. *J. Invest. Dermatol.* 123, 817–822. doi: 10.1111/j.0022-202x.2004.23479.x

Hansen, L. S., Coggle, J. E., Wells, J., and Charles, M. W. (1984). The influence of the hair cycle on the thickness of mouse skin. *Anat. Rec.* 210, 569–573. doi: 10.1002/ar.1092100404

Haramis, A. P., Begthel, H., van den Born, M., van Es, J., Jonkheer, S., Offerhaus, G. J., et al. (2004). De novo crypt formation and juvenile polyposis on BMP inhibition in mouse intestine. *Science* 303, 1684–1686. doi: 10.1126/science.1093587

Havlickova, B., Biro, T., Mescalchin, A., Tschirschmann, M., Mollenkopf, H., Bettermann, A., et al. (2009). A human folliculoid microsphere assay for exploring epithelial- mesenchymal interactions in the human hair follicle. *J. Investig. Dermatol.* 129, 972–983. doi: 10.1038/jid.2008.315

He, X. C., Zhang, J., Tong, W. G., Tawfik, O., Ross, J., Scoville, D. H., et al. (2004). BMP signaling inhibits intestinal stem cell self-renewal through suppression of Wnt-beta-catenin signaling. *Nat. Genet.* 36, 1117–1121. doi: 10.1038/ng1430

Heitman, N., Sennett, R., Mok, K. W., Saxena, N., Srivastava, D., Martino, P., et al. (2020). Dermal sheath contraction powers stem cell niche relocation during hair cycle regression. *Science* 367, 161–166.

Herrmann, T., van der Hoeven, F., Grone, H. J., Stewart, A. F., Langbein, L., Kaiser, I., et al. (2003). Mice with targeted disruption of the fatty acid transport protein 4 (Fatp 4, SlC27a4) gene show features of lethal restrictive dermopathy. *J. Cell Biol.* 161, 1105–1115. doi: 10.1083/jcb.200207080

Higgins, C. A., Chen, J. C., Cerise, J. E., Jahoda, C. A., and Christiano, A. M. (2013). Microenvironmental reprogramming by three-dimensional culture enables dermal papilla cells to induce de novo human hair-follicle growth. *Proc. Natl. Acad. Sci. U.S.A.* 110, 19679–19688. doi: 10.1073/pnas.1309970110

Horne, K. A. C., Jahoda, A. B., and Oliver, R. F. (1986). Whisker growth induced by implantation of cultured vibrissa dermal papilla cells in the adult-rat. *J. Embryol. Exp. Morphol.* 97, 111–124.

Horsley, V., Aliprantis, A. O., Polak, L., Glimcher, L. H., and Fuchs, E. (2008). NFATc1 balances quiescence and proliferation of skin stem cells. *Cell* 132, 299–310. doi: 10.1016/j.cell.2007.11.047

Horsley, V., O'Carroll, D., Tooze, R., Ohinata, Y., Saitou, M., Obukhanych, T., et al. (2006). Blimp1 defines a progenitor population that governs cellular input to the sebaceous gland. *Cell* 126, 597–609. doi: 10.1016/j.cell.2006.06.048

Hsu, Y. C., Pasolli, H. A., and Fuchs, E. (2011). Dynamics between stem cells, niche, and progeny in the hair follicle. *Cell* 144, 92–105.

Huelsken, J., Vogel, R., Erdmann, B., Cotsarelis, G., and Birchmeier, W. (2001). beta-Catenin controls hair follicle morphogenesis and stem cell differentiation in the skin. *Cell* 105, 533–545. doi: 10.1016/s0092-8674(01)00336-1

Huh, S. H., Narhi, K., Lindfors, P. H., Haara, O., Yang, L., Ornitz, D. M., et al. (2013). Fgf20 governs formation of primary and secondary dermal condensations in developing hair follicles. *Genes Dev.* 27, 450–458. doi: 10.1101/gad.198945.112

Inamatsu, M., Matsuzaki, T., Iwanari, H., and Yoshizato, K. (1998). Establishment of rat dermal papilla cell lines that sustain the potency to induce hair follicles from afollicular skin. *J. Investig. Dermatol.* 111, 767–775. doi: 10.1046/j.1523-1747.1998.00382.x

Ito, M., Kizawa, K., Hamada, K., and Cotsarelis, G. (2004). Hair follicle stem cells in the lower bulge form the secondary germ, a biochemically distinct but functionally equivalent progenitor cell population, at the termination of catagen. *Differentiation* 72, 548–557. doi: 10.1111/j.1432-0436.2004.07209008.x

Ito, M., Kizawa, K., Toyoda, M., and Morohashi, M. (2002). Label-retaining cells in the bulge region are directed to cell death after plucking, followed by healing from the surviving hair germ. *J. Invest. Dermatol.* 119, 1310–1316. doi: 10.1046/j.1523-1747.2002.19644.x

Ito, M., Liu, Y., Yang, Z., Nguyen, J., Liang, F., Morris, R. J., et al. (2005). Stem cells in the hair follicle bulge contribute to wound repair but not to homeostasis of the epidermis. *Nat. Med.* 11, 1351–1354. doi: 10.1038/nm1328

Ito, M., Yang, Z., Andl, T., Cui, C., Kim, N., Millar, S. E., et al. (2007). Wnt-dependent de novo hair follicle regeneration in adult mouse skin after wounding. *Nature* 447, 316–320. doi: 10.1038/nature05766

Jahoda, C. A., Horne, K. A., and Oliver, R. F. (1984). Induction of hair growth by implantation of cultured dermal papilla cells. *Nature* 311, 560–562. doi: 10.1038/311560a0

Jahoda, C. A., Oliver, R. F., Reynolds, A. J., Forrester, J. C., Gillespie, J. W., Cserhalmi-Friedman, P. B., et al. (2001). Trans-species hair growth induction by human hair follicle dermal papillae. *Exp. Dermatol.* 10, 229–237. doi: 10.1034/j.1600-0625.2001.100402.x

Jaks, V., Barker, N., Kasper, M., van Es, J. H., Snippert, H. J., Clevers, H., et al. (2008). Lgr5 marks cycling, yet long-lived, hair follicle stem cells. *Nat. Genet.* 40, 1291–1299. doi: 10.1038/ng.239

Jameson, J., and Havran, W. L. (2007). Skin gammadelta T-cell functions in homeostasis and wound healing. *Immunol. Rev.* 215, 114–122. doi: 10.1111/j.1600-065x.2006.00483.x

Jensen, K. B., Collins, C. A., Nascimento, E., Tan, D. W., Frye, M., Itami, S., et al. (2009). Lrig1 expression defines a distinct multipotent stem cell population in mammalian epidermis. *Cell Stem Cell* 4, 427–439. doi: 10.1016/j.stem.2009.04.014

Jensen, K. B., Jones, J., and Watt, F. M. (2008). A stem cell gene expression profile of human squamous cell carcinomas. *Cancer Lett.* 272, 23–31. doi: 10.1016/j.canlet.2008.06.014

Jong, M. C., Gijbels, M. J. J., Dahlmans, V. E. H., van Gorp, P. J. J., Koopman, S. J., Ponec, M., et al. (1998). Hyperlipidemia and cutaneous abnormalities in transgenic mice overexpressing human apolipoprotein C1. *J. Clin. Investig.* 101, 145–152. doi: 10.1172/jci791

Joost, S., Annusver, K., Jacob, T., Sun, X., Dalessandri, T., Sivan, U., et al. (2020). The molecular anatomy of mouse skin during hair growth and rest. *Cell Stem Cell* 26, 441.e7–457.e7.

Joost, S., Jacob, T., Sun, X., Annusver, K., La Manno, G., Sur, I., et al. (2018). Single-cell transcriptomics of traced epidermal and hair follicle stem cells reveals rapid adaptations during wound healing. *Cell Rep.* 25, 585.e7–597.e7.

Kadaja, M., Keyes, B. E., Lin, M., Pasolli, H. A., Genander, M., Polak, L., et al. (2014). SOX9: a stem cell transcriptional regulator of secreted niche signaling factors. *Genes Dev.* 28, 328–341. doi: 10.1101/gad.233247.113

Kakugawa, S., Langton, P. F., Zebisch, M., Howell, S., Chang, T. H., Liu, Y., et al. (2015). Notum deacylates Wnt proteins to suppress signalling activity. *Nature* 519, 187–192. doi: 10.1038/nature14259

Kandyba, E., Hazen, V. M., Kobielak, A., Butler, S. J., and Kobielak, K. (2014). Smad1 and 5 but not Smad8 establish stem cell quiescence which is critical to transform the premature hair follicle during morphogenesis toward the postnatal state. *Stem Cells* 32, 534–547. doi: 10.1002/stem.1548

Kandyba, E., and Kobielak, K. (2014). Wnt7b is an important intrinsic regulator of hair follicle stem cell homeostasis and hair follicle cycling. *Stem Cells* 32, 886–901. doi: 10.1002/stem.1599

Kandyba, E., Leung, Y., Chen, Y. B., Widelitz, R., Chuong, C. M., and Kobielak, K. (2013). Competitive balance of intrabulge BMP/Wnt signaling reveals a robust gene network ruling stem cell homeostasis and cyclic activation. *Proc. Natl. Acad. Sci. U.S.A.* 110, 1351–1356. doi: 10.1073/pnas.1121312110

Kishimoto, J., Burgeson, R. E., and Morgan, B. A. (2000). Wnt signaling maintains the hair-inducing activity of the dermal papilla. *Genes Dev.* 14, 1181–1185.

Kobielak, K., Kandyba, E., and Leung, Y. (2015). Skin and skin appendages regeneration. *Transl. Regenerative Med.* 22, 269–292.

Kobielak, K., Pasolli, H. A., Alonso, L., Polak, L., and Fuchs, E. (2003). Defining BMP functions in the hair follicle by conditional ablation of BMP receptor IA. *J. Cell Biol.* 163, 609–623. doi: 10.1083/jcb.200309042

Kobielak, K., Stokes, N., de la Cruz, J., Polak, L., and Fuchs, E. (2007). Loss of a quiescent niche but not follicle stem cells in the absence of bone morphogenetic protein signaling. *Proc. Natl. Acad. Sci. U.S.A.* 104, 10063–10068. doi: 10.1073/pnas.0703004104

Korosec, A., Frech, S., Gesslbauer, B., Vierhapper, M., Radtke, C., Petzelbauer, P., et al. (2019). Lineage identity and location within the dermis determine the function of papillary and reticular fibroblasts in human skin. *J. Invest. Dermatol.* 139, 342–351. doi: 10.1016/j.jid.2018.07.033

Lay, K., Kume, T., and Fuchs, E. (2016). FOXC1 maintains the hair follicle stem cell niche and governs stem cell quiescence to preserve long-term tissue-regenerating potential. *Proc. Natl. Acad. Sci. U.S.A.* 113, E1506–E1515.

Lee, P., Gund, R., Dutta, A., Pincha, N., Rana, I., Ghosh, S., et al. (2017). Stimulation of hair follicle stem cell proliferation through an IL-1 dependent activation of gamma delta T-cells. *eLife* 6:e28875.

Legrand, J. M. D., Roy, E., Ellis, J. J., Francois, M., Brooks, A. J., and Khosrotehrani, K. (2016). STAT5 activation in the dermal papilla is important for hair follicle growth phase induction. *J. Invest. Dermatol.* 136, 1781–1791. doi: 10.1016/j.jid.2016.04.014

Lesko, M. H., Driskell, R. R., Kretzschmar, K., Goldie, S. J., and Watt, F. M. (2013). Sox2 modulates the function of two distinct cell lineages in mouse skin. *Dev. Biol.* 382, 15–26. doi: 10.1016/j.ydbio.2013.08.004

Leung, Y., Kandyba, E., Chen, Y. B., Ruffins, S., Chuong, C. M., and Kobielak, K. (2014). Bifunctional ectodermal stem cells around the nail display dual fate homeostasis and adaptive wounding response toward nail regeneration. *Proc. Natl. Acad. Sci. U.S.A.* 111, 15114–15119. doi: 10.1073/pnas.1318848111

Leung, Y., Kandyba, E., Chen, Y. B., Ruffins, S., and Kobielak, K. (2013). Label retaining cells (LRCs) with myoepithelial characteristic from the proximal acinar region define stem cells in the Sweat Gland. *PLoS One* 8:e74174. doi: 10.1371/journal.pone.0074174

Levy, V., Lindon, C., Harfe, B. D., and Morgan, B. A. (2005). Distinct stem cell populations regenerate the follicle and interfollicular epidermis. *Dev. Cell* 9, 855–861. doi: 10.1016/j.devcel.2005.11.003

Levy, V., Lindon, C., Zheng, Y., Harfe, B. D., and Morgan, B. A. (2007). Epidermal stem cells arise from the hair follicle after wounding. *FASEB J.* 21, 1358–1366. doi: 10.1096/fj.06-6926com

Li, A., Lai, Y. C., Figueroa, S., Yang, T., Widelitz, R. B., Kobielak, K., et al. (2015). Deciphering principles of morphogenesis from temporal and spatial patterns on the integument. *Dev. Dyn.* 244, 905–920. doi: 10.1002/dvdy.24281

Li, K. N., Jain, P., He, C. H., Eun, F. C., Kang, S., and Tumbar, T. (2019). Skin vasculature and hair follicle cross-talking associated with stem cell activation and tissue homeostasis. *eLife* 8:e45977.

Li, L., and Ginty, D. D. (2014). The structure and organization of lanceolate mechanosensory complexes at mouse hair follicles. *eLife* 3:e01901.

Lichti, U., Anders, J., and Yuspa, S. H. (2008). Isolation and short-term culture of primary keratinocytes, hair follicle populations and dermal cells from newborn mice and keratinocytes from adult mice for in vitro analysis and for grafting to immunodeficient mice. *Nat. Protoc.* 3, 799–810. doi: 10.1038/nprot.2008.50

Lichti, U., Weinberg, W. C., Goodman, L., Ledbetter, S., Dooley, T., Morgan, D., et al. (1993). In vivo regulation of murine hair growth: insights from grafting defined cell populations onto nude mice. *J. Invest. Dermatol.* 101, 124S–129S.

Lien, W. H., Guo, X., Polak, L., Lawton, L. N., Young, R. A., Zheng, D., et al. (2011). Genome-wide maps of histone modifications unwind in vivo chromatin states of the hair follicle lineage. *Cell Stem Cell* 9, 219–232. doi: 10.1016/j.stem.2011.07.015

Lim, X., Tan, S. H., Yu, K. L., Lim, S. B., and Nusse, R. (2016). Axin2 marks quiescent hair follicle bulge stem cells that are maintained by autocrine Wnt/beta-catenin signaling. *Proc. Natl. Acad. Sci. U.S.A.* 113, E1498–E1505.

Lin, H. (2002). The stem-cell niche theory: lessons from flies. *Nat. Rev. Genet.* 3, 931–940. doi: 10.1038/nrg952

Liu, Y., Lyle, S., Yang, Z., and Cotsarelis, G. (2003). Keratin 15 promoter targets putative epithelial stem cells in the hair follicle bulge. *J. Invest. Dermatol.* 121, 963–968. doi: 10.1046/j.1523-1747.2003.12600.x

Lo Celso, C., Prowse, D. M., and Watt, F. M. (2004). Transient activation of beta-catenin signalling in adult mouse epidermis is sufficient to induce new hair follicles but continuous activation is required to maintain hair follicle tumours. *Development* 131, 1787–1799. doi: 10.1242/dev.01052

Lowry, W. E., Blanpain, C., Nowak, J. A., Guasch, G., Lewis, L., and Fuchs, E. (2005). Defining the impact of beta-catenin/Tcf transactivation on epithelial stem cells. *Genes Dev.* 19, 1596–1611. doi: 10.1101/gad.1324905

Lu, C. P., Polak, L., Rocha, A. S., Pasolli, H. A., Chen, S. C., Sharma, N., et al. (2012). Identification of stem cell populations in sweat glands and ducts reveals roles in homeostasis and wound repair. *Cell* 150, 136–150. doi: 10.1016/j.cell.2012.04.045

Lyle, S., Christofidou-Solomidou, M., Liu, Y., Elder, D. E., Albelda, S., and Cotsarelis, G. (1998). The C8/144B monoclonal antibody recognizes cytokeratin 15 and defines the location of human hair follicle stem cells. *J. Cell Sci.* 111(Pt 21), 3179–3188.

Lyle, S., Christofidou-Solomidou, M., Liu, Y., Elder, D. E., Albelda, S., and Cotsarelis, G. (1999). Human hair follicle bulge cells are biochemically distinct and possess an epithelial stem cell phenotype. *J. Investig. Dermatol. Symp. Proc.* 4, 296–301. doi: 10.1038/sj.jidsp.5640233

Maini, P. K., Baker, R. E., and Chuong, C. M. (2006). Developmental biology. The turing model comes of molecular age. *Science* 314, 1397–1398. doi: 10.1126/science.1136396

Mardaryev, A. N., Ahmed, M. I., Vlahov, N. V., Fessing, M. Y., Gill, J. H., Sharov, A. A., et al. (2010). Micro-RNA-31 controls hair cycle-associated changes in gene expression programs of the skin and hair follicle. *FASEB J.* 24, 3869–3881. doi: 10.1096/fj.10-160663

Massague, J., Seoane, J., and Wotton, D. (2005). Smad transcription factors. *Genes Dev.* 19, 2783–2810. doi: 10.1101/gad.1350705

Mecklenburg, L., Tobin, D. J., Muller-Rover, S., Handjiski, B., Wendt, G., Peters, E. M. J., et al. (2000). Active hair growth (Anagen) is associated with angiogenesis. *J. Investig. Dermatol.* 114, 909–916. doi: 10.1046/j.1523-1747.2000.00954.x

Meinhardt, H., and Gierer, A. (2000). Pattern formation by local self-activation and lateral inhibition. *Bioessays* 22, 753–760. doi: 10.1002/1521-1878(200008)22:8<753::aid-bies9>3.0.co;2-z

Mende, I., Karsunky, H., Weissman, I. L., Engleman, E. G., and Merad, M. (2006). Flk2+ myeloid progenitors are the main source of Langerhans cells. *Blood* 107, 1383–1390. doi: 10.1182/blood-2005-05-1878

Merad, M., Manz, M. G., Karsunky, H., Wagers, A., Peters, W., Charo, I., et al. (2002). Langerhans cells renew in the skin throughout life under steady-state conditions. *Nat. Immunol.* 3, 1135–1141. doi: 10.1038/ni852

Merrill, B. J., Gat, U., DasGupta, R., and Fuchs, E. (2001). Tcf3 and Lef1 regulate lineage differentiation of multipotent stem cells in skin. *Genes Dev.* 15, 1688–1705. doi: 10.1101/gad.891401

Mesler, A. L., Veniaminova, N. A., Lull, M. V., and Wong, S. Y. (2017). Hair follicle terminal differentiation is orchestrated by distinct early and late matrix progenitors. *Cell. Rep.* 19, 809–821. doi: 10.1016/j.celrep.2017.03.077

Millar, S. E. (2002). Molecular mechanisms regulating hair follicle development. *J. Invest. Dermatol.* 118, 216–225. doi: 10.1046/j.0022-202x.2001.01670.x

Mira, H., Andreu, Z., Suh, H., Lie, D. C., Jessberger, S., Consiglio, A., et al. (2010). Signaling through BMPR-IA regulates quiescence and long-term activity of neural stem cells in the adult hippocampus. *Cell Stem Cell* 7, 78–89. doi: 10.1016/j.stem.2010.04.016

Morris, R. J., Liu, Y., Marles, L., Yang, Z., Trempus, C., Li, S., et al. (2004). Capturing and profiling adult hair follicle stem cells. *Nat. Biotechnol.* 22, 411–417. doi: 10.1038/nbt950

Morris, R. J., and Potten, C. S. (1999). Highly persistent label-retaining cells in the hair follicles of mice and their fate following induction of anagen. *J. Invest. Dermatol.* 112, 470–475. doi: 10.1046/j.1523-1747.1999.00537.x

Muller-Rover, S., Handjiski, B., van der Veen, C., Eichmuller, S., Foitzik, K., McKay, I. A., et al. (2001). A comprehensive guide for the accurate classification of murine hair follicles in distinct hair cycle stages. *J. Invest. Dermatol.* 117, 3–15. doi: 10.1046/j.0022-202x.2001.01377.x

Nguyen, H., Merrill, B. J., Polak, L., Nikolova, M., Rendl, M., Shaver, T. M., et al. (2009). Tcf3 and Tcf4 are essential for long-term homeostasis of skin epithelia. *Nat. Genet.* 41, 1068–1075. doi: 10.1038/ng.431

Nguyen, H., Rendl, M., and Fuchs, E. (2006). Tcf3 governs stem cell features and represses cell fate determination in skin. *Cell* 127, 171–183. doi: 10.1016/j.cell.2006.07.036

Nicu, C., Hardman, J. A., Pople, J., and Paus, R. (2019). Do human dermal adipocytes switch from lipogenesis in anagen to lipophagy and lipolysis during catagen in the human hair cycle? *Exp. Dermatol.* 28, 432–435. doi: 10.1111/exd.13904

Nijhof, J. G., Braun, K. M., Giangreco, A., van Pelt, C., Kawamoto, H., Boyd, R. L., et al. (2006). The cell-surface marker MTS24 identifies a novel population of follicular keratinocytes with characteristics of progenitor cells. *Development* 133, 3027–3037. doi: 10.1242/dev.02443

Niola, F., Zhao, X., Singh, D., Castano, A., Sullivan, R., Lauria, M., et al. (2012). Id proteins synchronize stemness and anchorage to the niche of neural stem cells. *Nat. Cell Biol.* 14, 477–487. doi: 10.1038/ncb2490

Nishimura, E. K., Jordan, S. A., Oshima, H., Yoshida, H., Osawa, M., Moriyama, M., et al. (2002). Dominant role of the niche in melanocyte stem-cell fate determination. *Nature* 416, 854–860. doi: 10.1038/416854a

Nowak, J. A., Polak, L., Pasolli, H. A., and Fuchs, E. (2008). Hair follicle stem cells are specified and function in early skin morphogenesis. *Cell Stem Cell* 3, 33–43. doi: 10.1016/j.stem.2008.05.009

Oliver, R. F., and Jahoda, C. A. (1988). Dermal-epidermal interactions. *Clin. Dermatol.* 6, 74–82. doi: 10.1016/0738-081x(88)90069-7

Osaka, N., Takahashi, T., Murakami, S., Matsuzawa, A., Noguchi, T., Fujiwara, T., et al. (2007). ASK1-dependent recruitment and activation of macrophages induce hair growth in skin wounds. *J. Cell Biol.* 176, 903–909. doi: 10.1083/jcb.200611015

Oshima, H., Rochat, A., Kedzia, C., Kobayashi, K., and Barrandon, Y. (2001). Morphogenesis and renewal of hair follicles from adult multipotent stem cells. *Cell* 104, 233–245. doi: 10.1016/s0092-8674(01)00208-2

Oshimori, N., and Fuchs, E. (2012). Paracrine TGF-beta signaling counterbalances BMP-mediated repression in hair follicle stem cell activation. *Cell Stem Cell* 10, 63–75. doi: 10.1016/j.stem.2011.11.005

Ouspenskaia, T., Matos, I., Mertz, A. F., Fiore, V. F., and Fuchs, E. (2016). WNT-SHH antagonism specifies and expands stem cells prior to niche formation. *Cell* 164, 156–169. doi: 10.1016/j.cell.2015.11.058

Panteleyev, A. A. (2018). Functional anatomy of the hair follicle: the secondary hair germ. *Exp. Dermatol.* 27, 701–720. doi: 10.1111/exd.13666

Panteleyev, A. A., Jahoda, C. A., and Christiano, A. M. (2001). Hair follicle predetermination. *J. Cell Sci.* 114, 3419–3431.

Paus, R., Ito, N., Takigawa, M., and Ito, T. (2003). The hair follicle and immune privilege. *J. Investig. Dermatol. Symp. Proc.* 8, 188–194.

Paus, R., van der Veen, C., Eichmuller, S., Kopp, T., Hagen, E., Muller-Rover, S., et al. (1998). Generation and cyclic remodeling of the hair follicle immune

system in mice. *J. Invest. Dermatol.* 111, 7–18. doi: 10.1046/j.1523-1747.1998.00243.x

Pena-Jimenez, D., Fontenete, S., Megias, D., Fustero-Torre, C., Grana-Castro, O., Castellana, D., et al. (2019). Lymphatic vessels interact dynamically with the hair follicle stem cell niche during skin regeneration in vivo. *EMBO J.* 38:e101688.

Petersson, M., Brylka, H., Kraus, A., John, S., Rappl, G., Schettina, P., et al. (2011). TCF/Lef1 activity controls establishment of diverse stem and progenitor cell compartments in mouse epidermis. *EMBO J.* 30, 3004–3018. doi: 10.1038/emboj.2011.199

Philippeos, C., Telerman, S. B., Oules, B., Pisco, A. O., Shaw, T. J., Elgueta, R., et al. (2018). Spatial and single-cell transcriptional profiling identifies functionally distinct human dermal fibroblast subpopulations. *J. Invest. Dermatol.* 138, 811–825. doi: 10.1016/j.jid.2018.01.016

Plikus, M., Wang, W. P., Liu, J., Wang, X., Jiang, T. X., and Chuong, C. M. (2004). Morpho-regulation of ectodermal organs: integument pathology and phenotypic variations in K14-Noggin engineered mice through modulation of bone morphogenic protein pathway. *Am. J. Pathol.* 164, 1099–1114. doi: 10.1016/s0002-9440(10)63197-5

Plikus, M. V., Baker, R. E., Chen, C. C., Fare, C., de la Cruz, D., Andl, T., et al. (2011). Self-organizing and stochastic behaviors during the regeneration of hair stem cells. *Science* 332, 586–589. doi: 10.1126/science.1201647

Plikus, M. V., Guerrero-Juarez, C. F., Ito, M., Li, Y. R., Dedhia, P. H., Zheng, Y., et al. (2017). Regeneration of fat cells from myofibroblasts during wound healing. *Science* 355, 748–752.

Plikus, M. V., Mayer, J. A., de la Cruz, D., Baker, R. E., Maini, P. K., Maxson, R., et al. (2008). Cyclic dermal BMP signalling regulates stem cell activation during hair regeneration. *Nature* 451, 340–344. doi: 10.1038/nature06457

Rabbani, P., Takeo, M., Chou, W., Myung, P., Bosenberg, M., Chin, L., et al. (2011). Coordinated activation of Wnt in epithelial and melanocyte stem cells initiates pigmented hair regeneration. *Cell* 145, 941–955. doi: 10.1016/j.cell.2011.05.004

Rahmani, W., Liu, Y., Rosin, N. L., Kline, A., Raharjo, E., Yoon, J., et al. (2018). Macrophages promote wound-induced hair follicle regeneration in a CX3CR1- and TGF-beta1-dependent manner. *J. Invest. Dermatol.* 138, 2111–2122. doi: 10.1016/j.jid.2018.04.010

Rendl, M., Lewis, L., and Fuchs, E. (2005). Molecular dissection of mesenchymal-epithelial interactions in the hair follicle. *PLoS Biol.* 3:e331. doi: 10.1371/journal.pbio.0030331

Rendl, M., Polak, L., and Fuchs, E. (2008). BMP signaling in dermal papilla cells is required for their hair follicle-inductive properties. *Genes Dev.* 22, 543–557. doi: 10.1101/gad.1614408

Rhee, H., Polak, L., and Fuchs, E. (2006). Lhx2 maintains stem cell character in hair follicles. *Science* 312, 1946–1949. doi: 10.1126/science.1128004

Rinkevich, Y., Walmsley, G. G., Hu, M. S., Maan, Z. N., Newman, A. M., Drukker, M., et al. (2015). Skin fibrosis. Identification and isolation of a dermal lineage with intrinsic fibrogenic potential. *Science* 348:aaa2151. doi: 10.1126/science.aaa2151

Rochat, A., Kobayashi, K., and Barrandon, Y. (1994). Location of stem cells of human hair follicles by clonal analysis. *Cell* 76, 1063–1073. doi: 10.1016/0092-8674(94)90383-2

Rodeheffer, M. S., Birsoy, K., and Friedman, J. M. (2008). Identification of white adipocyte progenitor cells in vivo. *Cell* 135, 240–249. doi: 10.1016/j.cell.2008.09.036

Rompolas, P., Deschene, E. R., Zito, G., Gonzalez, D. G., Saotome, I., Haberman, A. M., et al. (2012). Live imaging of stem cell and progeny behaviour in physiological hair-follicle regeneration. *Nature* 487, 496–499. doi: 10.1038/nature11218

Rompolas, P., Mesa, K. R., and Greco, V. (2013). Spatial organization within a niche as a determinant of stem-cell fate. *Nature* 502, 513–518. doi: 10.1038/nature12602

Salzer, M. C., Lafzi, A., Berenguer-Llergo, A., Youssif, C., Castellanos, A., Solanas, G., et al. (2018). Identity noise and adipogenic traits characterize dermal fibroblast aging *Cell* 175, 1575.e22–1590.e22.

Sato, N., Sanjuan, I. M., Heke, M., Uchida, M., Naef, F., and Brivanlou, A. H. (2003). Molecular signature of human embryonic stem cells and its comparison with the mouse. *Dev. Biol.* 260, 404–413. doi: 10.1016/s0012-1606(03)00256-2

Schmidt-Ullrich, R., and Paus, R. (2005). Molecular principles of hair follicle induction and morphogenesis. *Bioessays* 27, 247–261. doi: 10.1002/bies.20184

Schofield, R. (1978). The relationship between the spleen colony-forming cell and the haemopoietic stem cell. *Blood Cells* 4, 7–25.

Sharov, A. A., Mardaryev, A. N., Sharova, T. Y., Grachtchouk, M., Atoyan, R., Byers, H. R., et al. (2009). Bone morphogenetic protein antagonist noggin promotes skin tumorigenesis via stimulation of the Wnt and Shh signaling pathways. *Am. J. Pathol.* 175, 1303–1314. doi: 10.2353/ajpath.2009.090163

Shwartz, Y., Gonzalez-Celeiro, M., Chen, C. L., Pasolli, H. A., Sheu, S. H., Fan, S. M., et al. (2020). Cell types promoting goosebumps form a niche to regulate hair follicle stem cells. *Cell* 182, 578.e19–593.e19.

Snippert, H. J., Haegebarth, A., Kasper, M., Jaks, V., van Es, J. H., Barker, N., et al. (2010). Lgr6 marks stem cells in the hair follicle that generate all cell lineages of the skin. *Science* 327, 1385–1389. doi: 10.1126/science.1184733

Spradling, A., Drummond-Barbosa, D., and Kai, T. (2001). Stem cells find their niche. *Nature* 414, 98–104. doi: 10.1038/35102160

Strazzulla, L. C., Wang, E. H. C., Avila, L., Lo Sicco, K., Brinster, N., Christiano, A. M., et al. (2018). Alopecia areata: disease characteristics, clinical evaluation, and new perspectives on pathogenesis. *J. Am. Acad. Dermatol.* 78, 1–12. doi: 10.1155/2013/348546

Tabib, T., Morse, C., Wang, T., Chen, W., and Lafyatis, R. (2018). SFRP2/DPP4 and FMO1/LSP1 define major fibroblast populations in human skin. *J. Invest. Dermatol.* 138, 802–810. doi: 10.1016/j.jid.2017.09.045

Tanimura, S., Tadokoro, Y., Inomata, K., Binh, N. T., Nishie, W., Yamazaki, S., et al. (2011). Hair follicle stem cells provide a functional niche for melanocyte stem cells. *Cell Stem Cell* 8, 177–187. doi: 10.1016/j.stem.2010.11.029

Taylor, G., Lehrer, M. S., Jensen, P. J., Sun, T. T., and Lavker, R. M. (2000). Involvement of follicular stem cells in forming not only the follicle but also the epidermis. *Cell* 102, 451–461. doi: 10.1016/s0092-8674(00)00050-7

Trempus, C. S., Morris, R. J., Bortner, C. D., Cotsarelis, G., Faircloth, R. S., Reece, J. M., et al. (2003). Enrichment for living murine keratinocytes from the hair follicle bulge with the cell surface marker CD34. *J. Invest. Dermatol.* 120, 501–511. doi: 10.1046/j.1523-1747.2003.12088.x

Tumbar, T., Guasch, G., Greco, V., Blanpain, C., Lowry, W. E., Rendl, M., et al. (2004). Defining the epithelial stem cell niche in skin. *Science* 303, 359–363. doi: 10.1126/science.1092436

Turing, A. M. (1990). The chemical basis of morphogenesis. 1953. *Bull. Math. Biol.* 52, 153–197.

Udy, G. B., Towers, R. P., Snell, R. G., Wilkins, R. J., Park, S. H., Ram, P. A., et al. (1997). Requirement of STAT5b for sexual dimorphism of body growth rates and liver gene expression. *Proc. Natl. Acad. Sci. U.S.A.* 94, 7239–7244. doi: 10.1073/pnas.94.14.7239

Van Keymeulen, A., Mascre, G., Youseff, K. K., Harel, I., Michaux, C., De Geest, N., et al. (2009). Epidermal progenitors give rise to Merkel cells during embryonic development and adult homeostasis. *J. Cell Biol.* 187, 91–100. doi: 10.1083/jcb.200907080

Van Mater, D., Kolligs, F. T., Dlugosz, A. A., and Fearon, E. R. (2003). Transient activation of beta -catenin signaling in cutaneous keratinocytes is sufficient to trigger the active growth phase of the hair cycle in mice. *Genes Dev.* 17, 1219–1224. doi: 10.1101/gad.1076103

Vidal, V. P., Chaboissier, M. C., Lutzkendorf, S., Cotsarelis, G., Mill, P., Hui, C. C., et al. (2005). Sox9 is essential for outer root sheath differentiation and the formation of the hair stem cell compartment. *Curr. Biol.* 15, 1340–1351. doi: 10.1016/j.cub.2005.06.064

Wang, E. C. E., Dai, Z., Ferrante, A. W., Drake, C. G., and Christiano, A. M. (2019). A subset of TREM2(+) dermal macrophages secretes oncostatin M to maintain hair follicle stem cell quiescence and inhibit hair growth. *Cell Stem Cell* 24, 654.e6–669.e6.

Wang, L., Siegenthaler, J. A., Dowell, R. D., and Yi, R. (2016). Foxc1 reinforces quiescence in self-renewing hair follicle stem cells. *Science* 351, 613–617. doi: 10.1126/science.aad5440

Wang, X., Chen, H., Tian, R., Zhang, Y., Drutskaya, M. S., Wang, C., et al. (2017). Macrophages induce AKT/beta-catenin-dependent Lgr5(+) stem cell activation and hair follicle regeneration through TNF. *Nat. Commun.* 8:14091.

Wei, Z. G., Cotsarelis, G., Sun, T. T., and Lavker, R. M. (1995). Label-retaining cells are preferentially located in fornical epithelium - implications on conjunctival epithelial homeostasis. *Investig. Ophthalmol. Vis. Sci.* 36, 236–246.

Weinberg, W. C., Goodman, L. V., George, C., Morgan, D. L., Ledbetter, S., Yuspa, S. H., et al. (1993). Reconstitution of hair follicle development in vivo: determination of follicle formation, hair growth, and hair quality by dermal cells. *J. Invest. Dermatol.* 100, 229–236. doi: 10.1111/1523-1747.ep12468971

Winter, H., Langbein, L., Praetzel, S., Jacobs, M., Rogers, M. A., Leigh, I. M., et al. (1998). A novel human type II cytokeratin, K6hf, specifically expressed in the companion layer of the hair follicle. *J. Investig. Dermatol.* 111, 955–962. doi: 10.1046/j.1523-1747.1998.00456.x

Wu, Y. F., Wang, S. H., Wu, P. S., Fan, S. M., Chiu, H. Y., Tsai, T. H., et al. (2015). Enhancing hair follicle regeneration by nonablative fractional laser: assessment of irradiation parameters and tissue response. *Lasers Surg. Med.* 47, 331–341. doi: 10.1002/lsm.22330

Xiao, Y., Woo, W. M., Nagao, K., Li, W., Terunuma, A., Mukouyama, Y. S., et al. (2013). Perivascular hair follicle stem cells associate with a venule annulus. *J. Invest. Dermatol.* 133, 2324–2331. doi: 10.1038/jid.2013.167

Xie, T., and Spradling, A. C. (1998). decapentaplegic is essential for the maintenance and division of germline stem cells in the *Drosophila ovary*. *Cell* 94, 251–260. doi: 10.1016/s0092-8674(00)81424-5

Xin, T., Gonzalez, D., Rompolas, P., and Greco, V. (2018). Flexible fate determination ensures robust differentiation in the hair follicle. *Nat. Cell Biol.* 20, 1361–1369. doi: 10.1038/s41556-018-0232-y

Yang, H., Adam, R. C., Ge, Y., Hua, Z. L., and Fuchs, E. (2017). Epithelial-mesenchymal micro-niches govern stem cell lineage choices. *Cell* 169, 483.e13–496.e13.

Ying, Q. L., Nichols, J., Chambers, I., and Smith, A. (2003). BMP induction of Id proteins suppresses differentiation and sustains embryonic stem cell self-renewal in collaboration with STAT3. *Cell* 115, 281–292. doi: 10.1016/s0092-8674(03)00847-x

Yu, M., Kissling, S., Freyschmidt-Paul, P., Hoffmann, R., Shapiro, J., and McElwee, K. J. (2008). Interleukin-6 cytokine family member oncostatin M is a hair-follicle-expressed factor with hair growth inhibitory properties. *Exp. Dermatol.* 17, 12–19.

Zhang, B., Tsai, P. C., Gonzalez-Celeiro, M., Chung, O., Boumard, B., Perdigoto, C. N., et al. (2016). Hair follicles' transit-amplifying cells govern concurrent dermal adipocyte production through Sonic Hedgehog. *Genes Dev.* 30, 2325–2338. doi: 10.1101/gad.285429.116

Zhang, J., He, X. C., Tong, W. G., Johnson, T., Wiedemann, L. M., Mishina, Y., et al. (2006). Bone morphogenetic protein signaling inhibits hair follicle anagen induction by restricting epithelial stem/progenitor cell activation and expansion. *Stem Cells* 24, 2826–2839. doi: 10.1634/stemcells.2005-0544

Zhang, J., Niu, C., Ye, L., Huang, H., He, X., Tong, W. G., et al. (2003). Identification of the haematopoietic stem cell niche and control of the niche size. *Nature* 425, 836–841. doi: 10.1038/nature02041

Zhang, Y. V., Cheong, J., Ciapurin, N., McDermitt, D. J., and Tumbar, T. (2009). Distinct self-renewal and differentiation phases in the niche of infrequently dividing hair follicle stem cells. *Cell Stem Cell* 5, 267–278. doi: 10.1016/j.stem.2009.06.004

Zhang, Z., Shao, M., Hepler, C., Zi, Z., Zhao, S., An, Y. A., et al. (2019). Dermal adipose tissue has high plasticity and undergoes reversible dedifferentiation in mice. *J. Clin. Invest.* 129, 5327–5342. doi: 10.1172/jci130239

Zwick, R. K., Guerrero-Juarez, C. F., Horsley, V., and Plikus, M. V. (2018). Anatomical, physiological, and functional diversity of adipose tissue. *Cell Metab.* 27, 68–83. doi: 10.1016/j.cmet.2017.12.002

Conflict of Interest: The authors declare that the research was conducted in the absence of any commercial or financial relationships that could be construed as a potential conflict of interest.

Copyright © 2020 Daszczuk, Mazurek, Pieczonka, Olczak, Boryń and Kobielak. This is an open-access article distributed under the terms of the Creative Commons Attribution License (CC BY). The use, distribution or reproduction in other forums is permitted, provided the original author(s) and the copyright owner(s) are credited and that the original publication in this journal is cited, in accordance with accepted academic practice. No use, distribution or reproduction is permitted which does not comply with these terms.

frontiers in Cell and Developmental Biology

ORIGINAL RESEARCH
published: 14 December 2020
doi: 10.3389/fcell.2020.593638

miR-140-5p in Small Extracellular Vesicles From Human Papilla Cells Stimulates Hair Growth by Promoting Proliferation of Outer Root Sheath and Hair Matrix Cells

Yuxin Chen†, Junfei Huang†, Zhen Liu†, Ruosi Chen, Danlan Fu, Lunan Yang, Jin Wang, Lijuan Du, Lihong Wen, Yong Miao and Zhiqi Hu**

Department of Plastic and Aesthetic Surgery, Nanfang Hospital of Southern Medical University, Guangzhou, China

OPEN ACCESS

Edited by:
Mingxing Lei,
Chongqing University, China

Reviewed by:
Ping Wu,
University of Southern California, United States
Xuegang Xu,
The First Affiliated Hospital of China Medical University, China

***Correspondence:**
Zhiqi Hu
huzhiqidr163@i.smu.edu.cn
Yong Miao
miaoyong123@i.smu.edu.cn

† These authors have contributed equally to this work

Specialty section:
This article was submitted to Stem Cell Research, a section of the journal Frontiers in Cell and Developmental Biology

Received: *11 August 2020*
Accepted: *11 November 2020*
Published: *14 December 2020*

Citation:
Chen Y, Huang J, Liu Z, Chen R, Fu D, Yang L, Wang J, Du L, Wen L, Miao Y and Hu Z (2020) miR-140-5p in Small Extracellular Vesicles From Human Papilla Cells Stimulates Hair Growth by Promoting Proliferation of Outer Root Sheath and Hair Matrix Cells. Front. Cell Dev. Biol. 8:593638. doi: 10.3389/fcell.2020.593638

The application of dermal papilla cells to hair follicle (HF) regeneration has attracted a great deal of attention. However, cultured dermal papilla cells (DPCs) tend to lose their capacity to induce hair growth during passage, restricting their usefulness. Accumulating evidence indicates that DPCs regulate HF growth mainly through their unique paracrine properties, raising the possibility of therapies based on extracellular vesicles (EVs). In this study, we explored the effects of EVs from high- and low-passage human scalp follicle dermal papilla cells (DP-EVs) on activation of hair growth, and investigated the underlying mechanism. DP-EVs were isolated by ultracentrifugation and cultured with human scalp follicles, hair matrix cells (MxCs), and outer root sheath cells (ORSCs), and we found low-passage DP-EVs accelerated HF elongation and cell proliferation activation. High-throughput miRNA sequencing and bioinformatics analysis identified 100 miRNAs that were differentially expressed between low- (P3) and high- (P8) passage DP-EVs. GO and KEGG pathway analysis of 1803 overlapping target genes revealed significant enrichment in the BMP/TGF-β signaling pathways. BMP2 was identified as a hub of the overlapping genes. miR-140-5p, which was highly enriched in low-passage DP-EVs, was identified as a potential regulator of BMP2. Direct repression of BMP2 by miR-140-5p was confirmed by dual-luciferase reporter assay. Moreover, overexpression and inhibition of miR-140-5p in DP-EVs suppressed and increased expression of BMP signaling components, respectively, indicating that this miRNA plays a critical role in hair growth and cell proliferation. DP-EVs transport miR-140-5p from DPCs to epithelial cells, where it downregulates BMP2. Therefore, DPC-derived vesicular miR-140-5p represents a therapeutic target for alopecia.

Keywords: extracellular vesicles, hair growth, dermal papilla cells, microRNA, BMP signaling

INTRODUCTION

Hair loss is a widespread and progressive disorder that plagues a large number of people. The appearance of alopecia can be ameliorated by existing treatments, such as minoxidil and hair transplant surgery. However, the medications are only effective for mild-to-medium hair loss, and surgery is limited by the viability of hair follicles (HFs) in the donor scalp (Ho and Zito, 2019; Katzer et al., 2019).

Hair follicles are epidermal appendages that cycle between an active growth stage (anagen) and a quiescent stage (telogen), separated by an intermediate remodeling stage (catagen) (Plikus and Chuong, 2008). HF morphogenesis and cycling are regulated by complex and intricate interactions between the epithelial and mesenchymal cells, and require spatiotemporal integration of multiple stimulatory and inhibitory signals (Kishimoto et al., 2000; Baker and Murray, 2012; Veraitch et al., 2013; Kandyba and Kobielak, 2014). In this process, the dermal papilla (DP), a unique stem cell niche derived from the mesenchyme, serves as the signaling center that triggers hair cycling through a paracrine signaling mechanism (Inui and Itami, 2011; Leiros et al., 2012; Zhang et al., 2014). Extracellular vesicles (EVs) are thought to play a critical role in this process (Kwack et al., 2019; le Riche et al., 2019; Chen et al., 2020; Rajendran et al., 2020). These signal exchanges promote activation of cellular pathways that are essential for hair epithelial cell growth, differentiation, and function, such as inhibition and activation of the BMP/TGF-β and WNT signaling pathways (Jamora et al., 2003; Greco et al., 2009; Genander et al., 2014). However, cultured DPCs tend to lose their hair-inducing capacity during passage, and high-passage DPCs (≧P8) fail to trigger HFs when interacting with epidermal cells *in vivo* (Matsuzaki, 2008; Lin et al., 2016; Wang J. et al., 2018). Conditioned medium from low-passage DPCs, which contains DP-EVs, can stimulate DPC proliferation *in vitro* and mouse dorsal hair growth *in vivo* (Zhang et al., 2014, 2016). EVs secreted from DPCs can accelerate hair growth *in vivo* and *in vitro* (Zhou et al., 2018; Yan et al., 2019; Kwack et al., 2019; le Riche et al., 2019), but the mechanisms underlying this growth-promoting effect remain to be fully elucidated.

Extracellular vesicles are nano-vesicles secreted from various cell types that carry regulatory proteins, mRNAs, and microRNAs (miRNAs) (Mittelbrunn et al., 2011; Zhou et al., 2014). Several reports have documented the functional contributions of specific miRNAs to hair development, including miR-125b (Zhang et al., 2011), miR-24 (Amelio et al., 2013), miR-205 (Wang et al., 2013), and miR-31 (Mardaryev et al., 2010). Especially, a recent research has discovered that dermal exosomes containing miR-218-5p could promote hair regeneration by regulating β-catenin signaling in mice (Hu et al., 2020). These studies suggest that vesicular miRNAs might play an especially important role in governing cell-to-cell communication (Yu et al., 2016), silencing or promoting known genes and pathways related to HF regeneration, and could also serve as biomarkers (Carrasco et al., 2019; Yan et al., 2019). However, the specific miRNAs involved in this process are unclear, and very few studies have sought to identify the miRNAs in human DP-EVs by high-throughput RNA sequencing. In this study, we used a human scalp follicle organ culture model to explore the influence of low- and high-passage DP-EVs on hair growth and activation of lower outer root sheath cells (ORSCs) and hair matrix cells (MxCs). Using high-throughput miRNA sequencing, we selected the top 100 most differentially expressed miRNAs (DEMs) and analyzed the biological functions and networks of their predicted target genes. We identified miRNAs in DP-EVs that may be involved in the process of HF regeneration, providing insight into DP-EV–regulated HF regeneration at the molecular level. Quantitative real-time PCR (qRT-PCR), western blot, and immunofluorescence staining analysis of key target genes were also performed.

Abbreviations: EVs, extracellular vesicles; HF, hair follicle; DP, dermal papilla; DPC, dermal papilla cell; DP-EV, dermal papilla-derived extracellular vesicle; ORS, outer root sheath; MxC, hair matrix cell; IRS, inner root sheath; hDPC, human dermal papilla cell; miRNA, microRNA; MSC, mesenchymal stem cell; ALP, alkaline phosphatase; NCAM, neural cell adhesion molecule; α-SMA, α-smooth muscle actin; IF, immunofluorescence; NTA, nanoparticle tracking analysis; P3, passage 3; P8, passage 8; TGF-β, transforming growth factor-beta; WNT, wingless-type MMTV integration site family; BMP, bone morphogenetic protein; K15, keratoprotein 15; 3D, three-dimensional.

MATERIALS AND METHODS

Isolation and Culture of Human HFs

Occipital scalp skin samples were obtained from discarded tissue from elective cosmetic operations performed on healthy adults (five women aged 35–45 years). Ethical approval and an institutional review board exemption were obtained from the Medical Ethical Committee of Southern Medical University.

Hair follicles in anagen stage were microdissected from each sample under an MZ8 dissecting microscope (Leica Microsystems, Wetzlar, Germany) (Langan et al., 2015). The basic culture medium (Corning Glassworks, Corning, NY, United States) containing 300 μl basic culture medium: William's E medium supplemented with 10 ng/ml hydrocortisone, 10 μg/ml insulin, 10 U/ml penicillin, and 2 mM l-glutamine (Life Technologies, Paisley, United Kingdom) was supplemented with P3-DP-EVs (300 μg DP-EVs in 300 μl medium), P8-DP-EVs, or PBS (as a negative control). HFs were photographed using the Leitz Labovert inverted microscope (Leitz Labovert FS, Wetzlar, Germany), measured for length, and assessed for follicle bulb morphology every 24 h for 9 days. Unless specified, all materials were supplied by Sigma-Aldrich (Dorset, United Kingdom).

Preparation of Cells and Isolation of DP-Derived EVs

Human scalp follicles were separated, and hair bulbs were cut and collected using microsurgical scissors and microscope forceps under the microscope. Hair bulbs were incubated with 0.2% collagenase I (Sigma-Aldrich) in PBS for 1 h at 37°C. The pellet was cultured in DMEM containing 10% FBS in 5% CO_2 at 37°C. Media were collected from low (P3) and high (P8) passage hDPC cultures and stored at −20°C. EVs were isolated by ultracentrifugation (SW 32 Ti swinging-bucket rotor in a Beckman Coulter L8-80M Ultracentrifuge) as described previously (Rajendran et al., 2020). In brief, 500 ml hDPC

medium was centrifuged at 300 × *g* for 10 min and 2000 × *g* for 10 min to remove live cells and dead cells, respectively. The supernatant was then filtered with pressure through 0.22 μm membrane filters to remove cell debris and vesicles > 220 nm in diameter. Next, the supernatant was ultracentrifuged at 100,000 × *g* for 70 min. Finally, the pellet was washed and resuspended in PBS and stored at −80°C. The negative control was an equal volume of 1 × PBS, which was prepared in the same way as the actual EV samples.

Outer root sheath cells from the lower outer root sheath region were isolated and prepared as described previously (Lü et al., 2006; Zhou et al., 2018), the single-cell suspension was collected and cultured in Defined Keratinocyte serum-free medium (DK-SFM) (Gibco) at 37°C. Human MxCs were purchased from ScienCell Research Laboratories (ScienCell, San Diego, CA, United States; Cat. #2410) as previously described (Chen et al., 2020). As recommended by the provider, MxCs were cultured in MSC medium (ScienCell, Cat. #7501) with 5% exosome-free FBS, 1% stem cell growth supplement (ScienCell, Cat. #7562), and 1% penicillin–streptomycin. Cells were incubated in an atmosphere containing 5% CO_2 at 37°C.

Verification of DP-EVs

The particle size of DP-EVs was investigated by nanoparticle tracking analysis (NTA) on a NanoSight NS300 (Malvern Panalytical, Malvern, United Kingdom). Before acquisition, the highly concentrated samples were diluted in Milli-Q water (1:1000). Three individual measurements were obtained and analyzed using the NTA software version 2.3 (Malvern Panalytical).

Transmission electron microscopy (TEM) was used to characterize the morphology of DP-EVs. Briefly, DP-EVs were fixed in 3% glutaraldehyde for 2 h and washed twice with PBS. Ten micrograms of EV suspension was loaded onto formvar carbon-coated 200 mesh copper grids for 20 min at room temperature. Adsorbed DP-EVs were negatively stained with 1% phosphotungstic acid for 5 min. The grids were then washed three times with distilled water and examined on an H-600 transmission electron microscope (Hitachi, Tokyo, Japan) at 100 kV.

For DP-EV labeling and uptake assay, a 100 μl suspension of EVs was labeled using the PKH26 Red Fluorescent Cell Linker Kit for General Cell Membrane Labeling (DiI; Sigma-Aldrich, St. Louis, MO, United States) with a 20 min incubation at room temperature. To wash out the dye, the sample was ultracentrifuged twice at 100,000 × *g* for 1 h. As a negative control, an equal volume of PBS supernatant was mixed with DiI and then prepared in the same way as the actual exosome samples. The precipitate was resuspended in 100 μl PBS. For the DPC uptake assay, an appropriate amount of DP-EVs (as determined by BCA protein assay) was added to the cell culture. P3 lower ORSCs and MxCs were transfected with GFP and cultured with DiI-labeled DP-EVs for 24 h. Cells were fixed with 4% paraformaldehyde for 15 min and washed three times with PBST, and then the coverslips were mounted on glass slides using ProLong Diamond Antifade Mountant with DAPI (Life Technologies/Thermo Fisher Scientific, Waltham, MA, United States) prior to imaging on a confocal laser scanning microscope (LSM510; Carl Zeiss, Jena, Germany).

Western Blot Analysis

For identification of vesicular markers, protein extracts were isolated from EVs using RIPA protein lysis buffer containing 1 mM PMSF. Equal amounts of protein (10 μg/lane) were subjected to SDS-PAGE under non-reducing conditions, and the gels were blotted onto nitrocellulose membranes (Pierce, Waltham, MA, United States) in an electrophoretic transfer cell (Bio-Rad). The membrane was blocked with 5% non-fat milk at 4°C overnight and then probed with anti-CD63 (1:800 dilution; Abcam), anti-CD9 (1:800 dilution; Abcam), and anti-ALIX (1:800 dilution; Abcam) antibody for 1 h. The membrane was incubated with sheep anti-mouse IgG conjugated to HRP (NeoBioscience, Shenzhen, China) for 1 h. Band density was determined using the Bio-Rad Quality One Software. To detect the expression of key proteins in ORSCs and MxCs, total protein was extracted from human HF using RIPA lysis buffer and subjected to western blot analysis as described above. Antibodies against the following proteins were obtained from Abcam (Cambridge, United Kingdom): β-catenin (1:100 dilution), Lef-1 (1:100 dilution), Shh (1:100 dilution), Gli1 (1:100 dilution), Cyclin D1 (1:400 dilution), Cyclin E (1:400 dilution), BMP2 (1:800 dilution), and SMAD5 (1:400 dilution). p-SMAD5 was obtained from Millipore (1:800 dilution).

Histological Examination and Immunofluorescence Staining

Grafted follicles were taken on days 1, 10, 15, 20, and 30 after transplantation and embedded in paraffin blocks. Five micron-thick longitudinal sections were prepared, followed by hematoxylin and eosin (HE) staining. Images were taken by optical microscope. Follicle specimens were fixed in 4% paraformaldehyde at 4°C for 12 h. Following antigen retrieval using citrate buffer, the sample was blocked with 5% serum. Images were obtained on an IX61 FL fluorescence microscope (Olympus) and analyzed using Image-Pro Plus. Images were also obtained using an Olympus FLUOVIEW FV10i confocal laser scanning microscope. Eight images were taken of each sample, and a normalized average-intensity picture of images was used for analysis. Images were analyzed using the Image-Pro Plus software.

Processing of RNA-Seq Data, Target Gene Prediction and Functional Enrichment

Total miRNAs from DP-EVs (P3 and P8) were extracted and subjected to miRNA sequencing. RNA quality was verified on an Agilent 2100 BioAnalyzer (Agilent Technologies, Santa Clara, CA, United States). Quality control of raw sequence data was performed using the FastQC tool. RNA expression levels were expressed as reads per kilobase per million (RPKM) mapped reads. The DESeq package was used to detect DEMs between the DP-EVs (P3) and DP-EVs (P8). Genes with RPKM > 1 were included in the subsequent analyses. The threshold was set to a

twofold change and an FDR < 0.05. The top 100 differentially expressed DEMs were visualized on a heatmap. The heatmap and unsupervised cluster analysis of the top 100 DEMs were plotted using *z*-score normalization on OmicShare tools, an online platform for data analysis[1]. Target genes of DEMs were predicted using TargetScan[2] and miRDB[3] (Agarwal et al., 2015). Using OmicShare tools, GO analysis was performed to elucidate the concrete biological functions of specific genes (Ashburner et al., 2000), and KEGG pathway enrichment was used to identify the critical signal pathways (Kanehisa et al., 2017). To further elucidate the molecular mechanisms related to the predicted genes, TargetScan, miRanda, PicTar, PITA and DIANA-microT databases (Krek et al., 2005; Paraskevopoulou et al., 2013; Vejnar et al., 2013; Agarwal et al., 2015; Wong and Wang, 2015) were used in combination to predict the miRNAs responsible for regulating the predicted hub genes.

To screen PPIs (protein–protein interaction), the target genes of DEMs were mapped to the STRING database[4] (Franceschini et al., 2013), and networks were visualized using Cytoscape (Smoot et al., 2011). The most significant modules were identified with the plug-in MCODE of Cytoscape with a cutoff MCODE score of >5 (Bandettini et al., 2012). Hub genes were identified using the CytoHubba plug-in of Cytoscape, ranked by Maximal Clique Centrality (Chin et al., 2014). HF-related miR-140-5p targets were identified using TargetScan and based on their co-occurrence with the search term "hair follicle signaling" in the PubMed database (Liu et al., 2008; Rishikaysh et al., 2014; Akilli et al., 2015; Yi, 2017). Interactions between network genes were annotated using Cytoscape.

Dual-Luciferase Reporter Assay

For the purpose of verifying the binding relationship between miR-140-5p and BMP2, and to assess whether BMP2 is a direct target gene of miR-140-5p, ORSCs were seeded in 6-well plates (Guangzhou Jet Bio-Filtration Co., Ltd, TCP-010-006) at a density of 2.5×10^5 cells/well with the complete media. The artificially synthesized 3′-UTR of BMP2 was inserted into the pMIR-reporter vector (Yue Yang Biotechnology Co., Ltd., Beijing, China). A site-specific mutation was then introduced into the 3′-UTR fragment. One microgram of BMP2-wild type (WT) or BMP2-mutant type (MUT) was cotransfected into ORSCs with 50 nM miR-140-5p mimic or miR-NC. Transfections were performed using Lipofectamine 2000 (Invitrogen) with Opti-MEM (Thermo Fisher Scientific). After 48 h, the cells were lysed and subjected to luciferase assay using the dual-luciferase reporter assay reagent (GeneCopoeia, Rockville, MD, United States). Luciferase activity was detected using the Luciferase Assay kit (K801-200; Biovision, San Francisco, CA, United States) on a Glomax20/20 luminometer (Promega Corporation, Madison, WI, United States). The 3′-UTR of BMP2 was obtained from GeneCopoeia.

[1]www.omicshare.com/tools

[2]http://www.targetscan.org/

[3]http://mirdb.org/miRDB/

[4]https://string-db.org/

RNA Interference

The concentration of transfection units per milliliter (TU/mL) was calculated using the following formula: (% infected cells × cells used in the titration/100 × 1000 μl/μl virus added to the well) = TU/mL. The stable overexpression and inhibition of miR-140-5p in P3-DPCs were established by stable transduction with lentivirus (1E + 8 TU/mL) (Sino Biological) at a multiplicity of infection (MOI) of 10. In brief, DPCs (P3) were transfected with miRNA oligonucleotides containing an 50 nM miR-140-5p overexpression sequence and the corresponding negative control vector (miRNA-NC), or an 50 nM miR-140-5p inhibiting segment (si-miR-140-5p) and the corresponding negative control vector (si-miRNA-NC), all purchased from Sino Biological. In both the SiHa and C33a cell lines, the transfected cells were designated as miRNA-NC, miR-140-5p, si-miRNA-NC, and si-miR-140-5p, and DPCs treated with an equal volume of PBS were used as a blank control. After 12 h of culture, EVs (miRNA-NC-EV, miR-140-5p-EV, si-miRNA-NC-EV, and si-miR-140-5p-EV) were isolated from DPCs and used for subsequent experiments. An equal amount of PBS was used as a blank control.

Animal Model Experiments

All animal experiments were performed using 7-week-old female C57BL/6 mice. Animals were purchased from the Experimental Animal Centre at Southern Medical University (Guangzhou, China). Depilated mice were randomly injected with miRNA-NC-EVs, miR-140-5p-EVs, si-miRNA-NC-EVs, or si-miR-140-5p-EV (4 mg/ml dissolved in PBS, 1 ml per mouse) every 2 days, or PBS without EVs (as a negative control). Ethical approval for all experimental procedures was obtained from the Experimental Animal Centre at Southern Medical University.

Quantitative (q)RT-PCR

Total RNA from regenerative HFs was isolated using the Trizol reagent (Life Technologies), and cDNA was generated using the PrimeScript RT-PCR Kit (Takara, Dalian, China). qRT-PCR was performed using the SYBR PrimeScript RT-PCR Kit (Takara), Power SYBR Green PCR Master Mix (Life Technologies), and ABI Prism 7900HT Sequence Detection System (Life Technologies). PCR cycling conditions were as follows: denaturation for 10 min at 95°C, followed by 40 cycles of denaturation (95°C for 15 s), annealing (60°C for 20 s), and extension (72°C for 10 s). Fold-changes in relative gene expression were calculated using the $2^{-\Delta\Delta Ct}$ method. For miRNA quantification, total RNA was reverse-transcribed using the TaqMan advanced miRNA cDNA synthesis kit (Applied Biosystems). All specific primers for gene and miRNA expression were purchased from Applied Biosystems. Primer sequences used in this study are provided in **Supplementary Table S1**.

Statistical Analysis

Statistical analysis was performed using SPSS 16.0 software (SPSS, Inc, Chicago, IL, United States). All values are shown as means ± SD ANOVA was used for multiple comparisons. Comparisons between groups were performed using the Wilcoxon test and *t*-test. $p < 0.05$ was considered statistically

significant. Each experiment was repeated at least three times. For statistical assessment of cultured HFs, the mean value per donor under each treatment was determined before calculation of the sample mean, data from each experimental condition were analyzed for normal distribution using the Kolmogorov–Smirnoff test.

RESULTS

Difference Between Low- and High-Passage DPCs

To determine the biological difference between low- and high-passage DPCs, we isolated DPCs from human follicle dermal fibroblasts for culturing, and collected cells in P3 and P8 for observation. P3-DPCs exhibited the tendency to aggregate, whereas P8-DPCs lost this property (**Supplementary Figure S1A**). To characterize intrinsic properties relevant to HF inductivity in DPCs, distinct DP markers including alkaline phosphatase (ALP), neural cell adhesion molecule (NCAM), and α-smooth muscle actin (α-SMA) were monitored by IF, western blot, and RT-PCR analysis (Lin et al., 2016; Wang J. et al., 2018) (**Supplementary Figures S1B–E**). As illustrated in **Supplementary Figure S1**, expression of ALP and NCAM was higher in P3-DPCs than in P8-DPCs (**$p < 0.05$), but expression of α-SMA increased with increasing passage number. The results indicated that the molecular characteristics of human DPCs differed between high and low passage.

Preparation and Characterization of DP-EVs

Extracellular vesicles were isolated from low-passage (P3) and high-passage (P8) human DPCs by ultracentrifugation. The morphology of DP-EVs was analyzed by TEM, which revealed that they had a cup- or round-shaped form (**Figure 1A**). NTA revealed that the diameter of DP-EVs ranged from 58.8 to 255.0 nm, with an average diameter of 91.3 ± 18 nm (**Figure 1B**). Western blots showed that DP-EVs expressed EV-specific surface markers such as CD63, CD9, and ALIX (**Figure 1C**). To monitor the uptake of DP-EVs, we applied P3 human MxCs and ORSCs transfected with GFP, and labeled DP-EVs with DiI (red). Cells were cultured with DP-EVs for 24 h. Under the fluorescence microscope, DiI-labeled EVs were observed in the cytoplasm of MxCs and ORSCs (**Figure 1D**), whereas ORSCs in the negative control group had no DiI signaling in the cytoplasm (**Figure 1D**). These data suggested that we successfully isolated DP-EVs, which could be absorbed by MxCs and ORSCs, respectively.

The Therapeutic Effect of DP-EVs on Human HF Growth in Organ Culture

To determine whether DP-EVs could affect scalp HF growth, we grew isolated HFs in basic culture medium supplemented with various concentrations of DP-EVs and collected daily images to assess their morphology. HFs in basic culture medium produced hair fiber, inner root sheath (IRS), and ORS, but not the dermal sheath (**Figure 2A**). By day 4, some HFs exhibited a catagen-like morphology: pigmentation had ceased, and the DP was detached from the hair fiber and hair matrix (**Figure 2A**). Treatment with 0.01–1 μg/μl P3-DP-EV enhanced HF growth in a dose-dependent manner (**Supplementary Figure S2**). Treatment with 1 μg/μl DP-EVs had a significantly stronger anagen-prolonging effect than lower concentrations (0.1 and 0.01 μg/μl). Hence, we chose 1 μg/μl DP-EVs for subsequent experiments. We previously reported that DiI-labeled DP-EVs were absorbed by hair matrix (Chen et al., 2020). However, we found that DiI-labeled DP-EVs were also absorbed and integrated into the lower ORS region (**Figure 2B**).

To assess the therapeutic effect of DP-EVs in organ culture, we added DP-EVs from P3 and P8 DPCs to cultured human HFs; HFs treated with PBS were used as a negative control (**Figure 2C**). EVs from P3 DPCs accelerated human hair growth and prolonged hair anagen (**Figures 2C–F**). By day 9, the length of HFs cultured with DP-EVs (P3) increased by 1.93 ± 0.12 mm, whereas HFs cultured with DP-EVs (P8) and PBS increased by only 1.57 ± 016 mm and 1.58 ± 0.18 mm, respectively (**Figure 2D**). Following treatment with P3-DP-EVs, about 83.4% of HFs were in anagen on day 9, about 13% higher than in samples treated with DP-EVs (P8) or PBS (**Figure 2F**). We also assessed cell viability of human HFs on day 5 based on Ki67 immunofluorescence. The results revealed that HFs treated with DP-EVs (P3) had the most Ki67-positive cells in lower ORS and hair matrix ($p < 0.01$) (**Figures 2G,H**), indicating that HFs treated with low-passage DP-EVs significantly activated hair growth. Combined with the fluorescence staining results (**Figure 2B**), these observations indicate that EVs can be absorbed by HFs in the lower ORS and hair matrix region, and can activate proliferation of lower ORSCs and MxCs. We then performed double staining for K15 and Ki67. In the lower ORS region, K15 is highly expressed (Moll et al., 2008). Immunofluorescence staining revealed significant widening of the K15+-stained lower ORS region at day 5 in HFs treated with DP-EVs (P3) (**Figures 2G,H**), indicating that low-passage DP-EVs stimulated ORS cell proliferation in cultured human HFs.

Effect of DP-EVs on Human ORSCs

In a previous study, we showed that low-passage DP-EVs significantly promoted MxC proliferation (Chen et al., 2020). After treating lower ORSCs with low- or high-passage DP-EVs, we assessed their proliferation (**Figure 3A**). The results of CCK-8 and Ki67 immunofluorescence staining revealed that low-passage DP-EVs promoted cell proliferation, with a higher $Ki67^+$ cell ratio than P8-DP-EV treatment (**Figures 3B,C**).

We previously reported the stimulatory effect of MxCs, as well as inhibition of BMP signaling and promotion of Wnt signaling by DP-EVs (Chen et al., 2020). To investigate changes in hair growth regulators of ORSCs, we evaluated the expression levels of known follicle-regulatory genes in the Wnt, BMP, and Shh signaling pathways in ORSCs (Watt et al., 2008; Choi, 2018) by RT-PCR and western blot (**Figures 3D–F**). As shown in **Figure 3D**, at day 5 in cells treated with DP-EVs (P3), hub genes in the Wnt signaling pathway, including β-catenin, Lef-1, and Tcf3, were upregulated, whereas BMP2 was

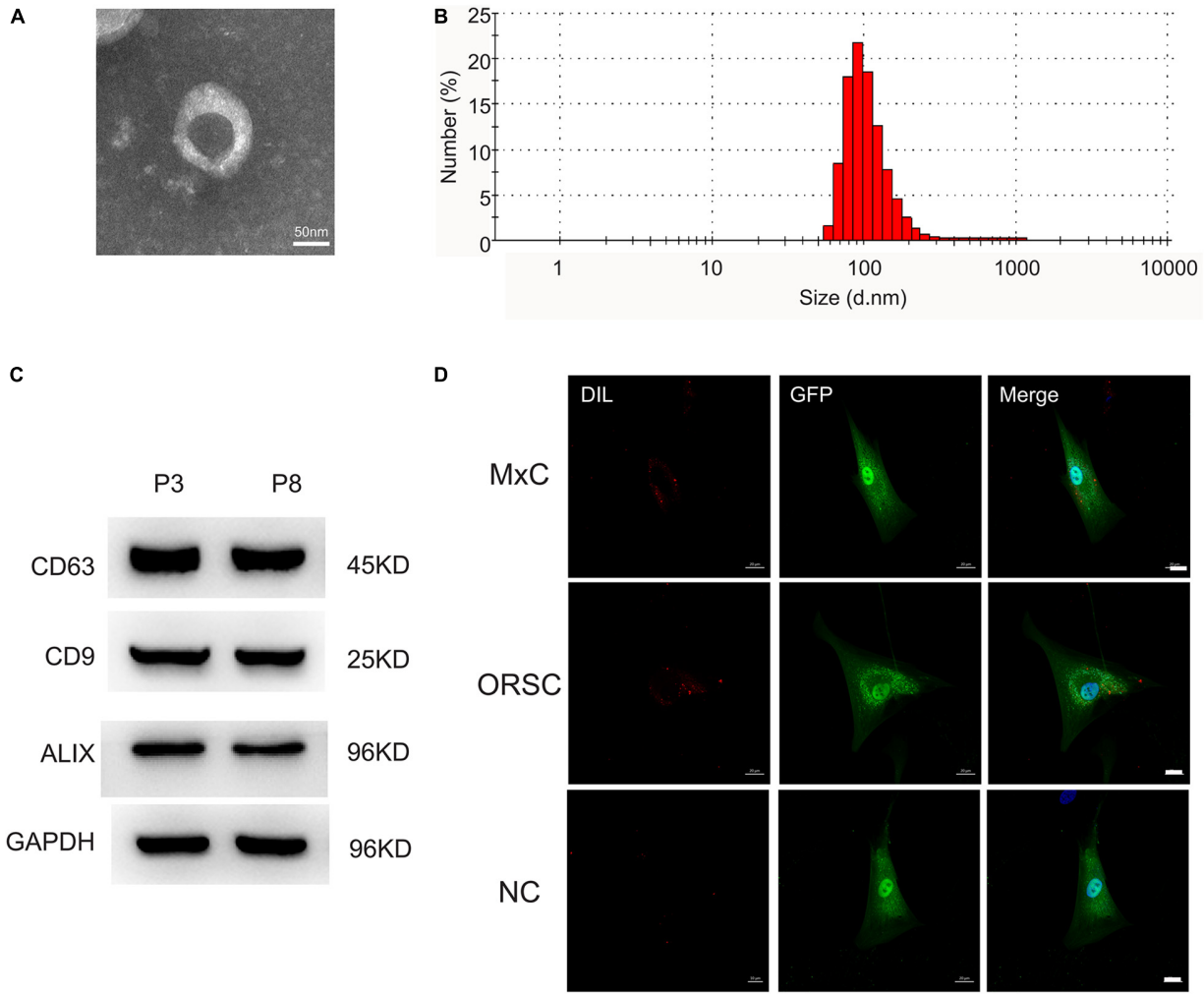

FIGURE 1 | Characterization of DP-EVs from P3 and P8 DPCs. **(A)** Transmission electron microscopy morphology of DP-EVs. **(B)** Vesicular size distribution, measured by NTA. Scale bar: 50 nm. **(C)** Western blots of DP-EVs to detect CD63, CD9, and ALIX; $n = 8$ for each group. **(D)** DP-EVs were labeled with DiI and taken up by GFP-transfected MxCs and ORSCs. As a negative control, an equal volume of PBS mixed with DIL was cultured with ORSCs. $n = 8$ for each group. Scale bar: 50 μm.

downregulated. Shh and Gli1 in the Shh signaling pathway were also upregulated (**Figure 3D**). In accordance with the results of RT-PCR, levels of components of the Wnt (β-catenin and Lef-1) and Shh signaling pathways (Shh and Gli1) increased after 5 days of low-passage DP-EV treatment, whereas the BMP2 level significantly decreased. These data indicated that low-passage DP-EVs may promote ORSC proliferation by up-regulating the Wnt and Shh pathways and down-regulating the BMP2 pathway.

Identification and Validation of Differentially Expressed miRNAs in Low- and High-Passage DP-EVs

Extracellular vesicles deliver various miRNAs to other cells and affect cellular functions (Witwer et al., 2013; Cobelli et al., 2017). Several lines of evidence suggest that miRNA might play a more important role in cell-to-cell communication (Carrasco et al., 2019; Hu et al., 2020), acting as promoters or suppressors by silencing or promoting known genes and pathways related to HF growth. To determine how low-passage DP-EVs augment hair growth, we deduced that the miRNAs in DP-EVs may be delivered to hair matrix and lower ORS to activate them and promote their proliferation. Therefore, we investigated the miRNA expression profiles of EVs derived from human DPCs at P3 and P8 by high-throughput sequencing; the datasets have been deposited in the Gene Expression Omnibus (GEO) database[5]. Of the 563 hsa-miRNAs screened (**Supplementary Table S2**), we identified the top 100 most DEMs (i.e., 50 upregulated and 50 downregulated) in P3 vs. P8 DP-EVs (cutoff: $p < 0.05$; fold change > 2.0) (**Supplementary Table S3**). To highlight differences between the two groups,

[5]https://www.ncbi.nlm.nih.gov/geo/query/acc.cgi?acc=GSE136241

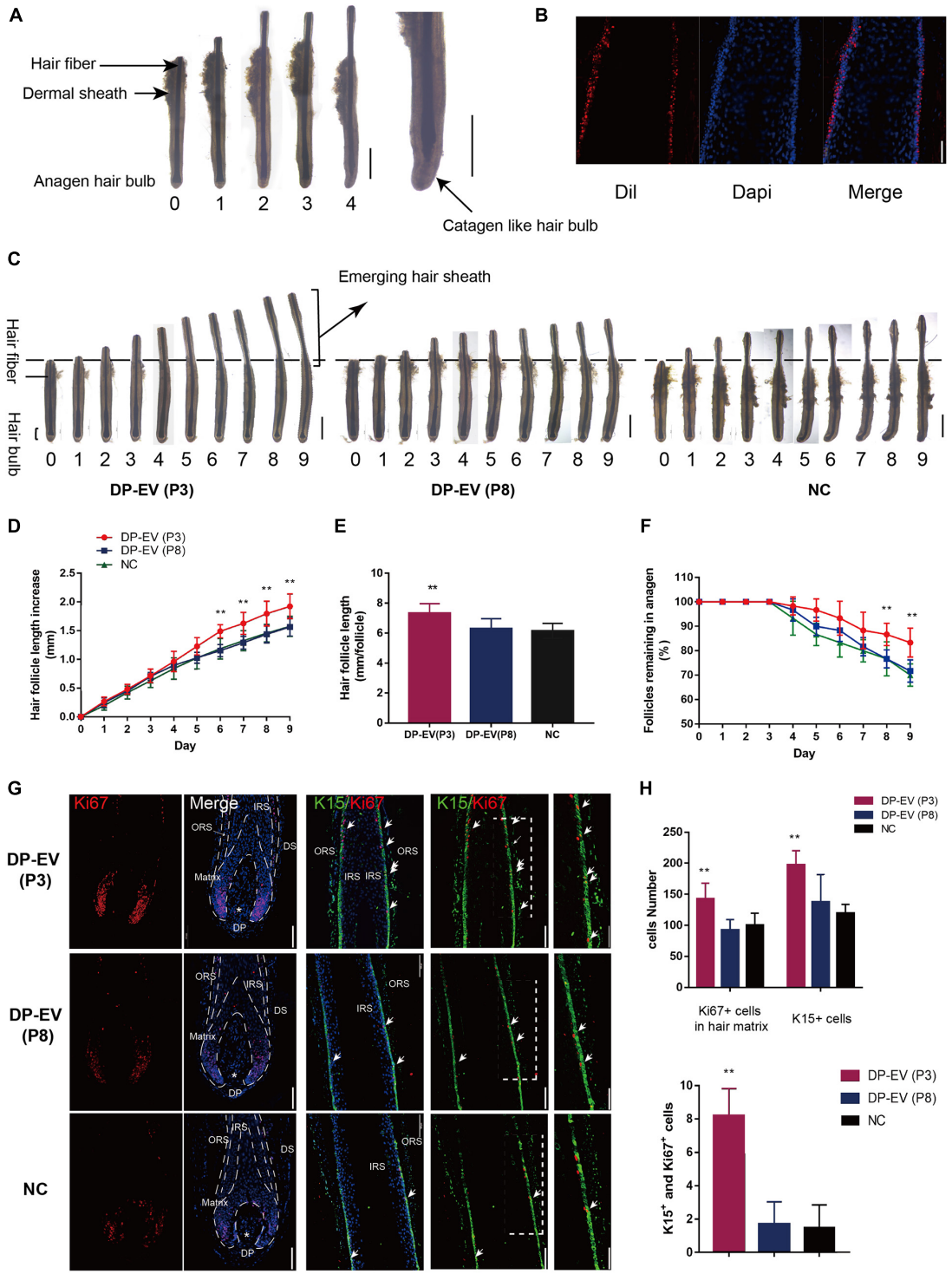

FIGURE 2 | The therapeutic effect of DP-EVs on human scalp HF growth in organ culture. **(A)** Sequential photomicrographs, taken every 24 h, of individual scalp follicles in organ culture under the indicated conditions. Scale bars: 1 mm. Some hair follicles exhibited a catagen-like morphology by day 4. Scale bars: 0.5 mm. **(B)** DiI-labeled DP-EVs were absorbed by HF lower ORS. Scale bar: 20 μm. **(C)** Hair follicles were cultured with P3- or P8-DP-EVs (containing 300 μg DP-EVs in 300 μl culture medium) or negative control medium. Scale bars: 1 mm. **(D–F)** Hair follicles in each group were assessed and measured daily for increase in hair length **(D)**, accumulated hair length **(E)**, and the percentage of hair follicles remaining in anagen **(F)**. **(G)** Immunofluorescence staining of Ki67 and K15 in the hair matrix and lower ORS region. Scale bar: 100 μm. **(H)** Quantitative analysis of the number of Ki67+, K15+, and Ki67+/K15+ double-staining cells in hair follicle. Data are expressed as means ± SD. $n = 60$ from give healthy female individuals (12 samples from each individual). $^{**}p < 0.01$ vs. PBS-treated group (NC). Statistical significance determined by one-way ANOVA with Bonferroni comparisons; $n = 5$ for each group.

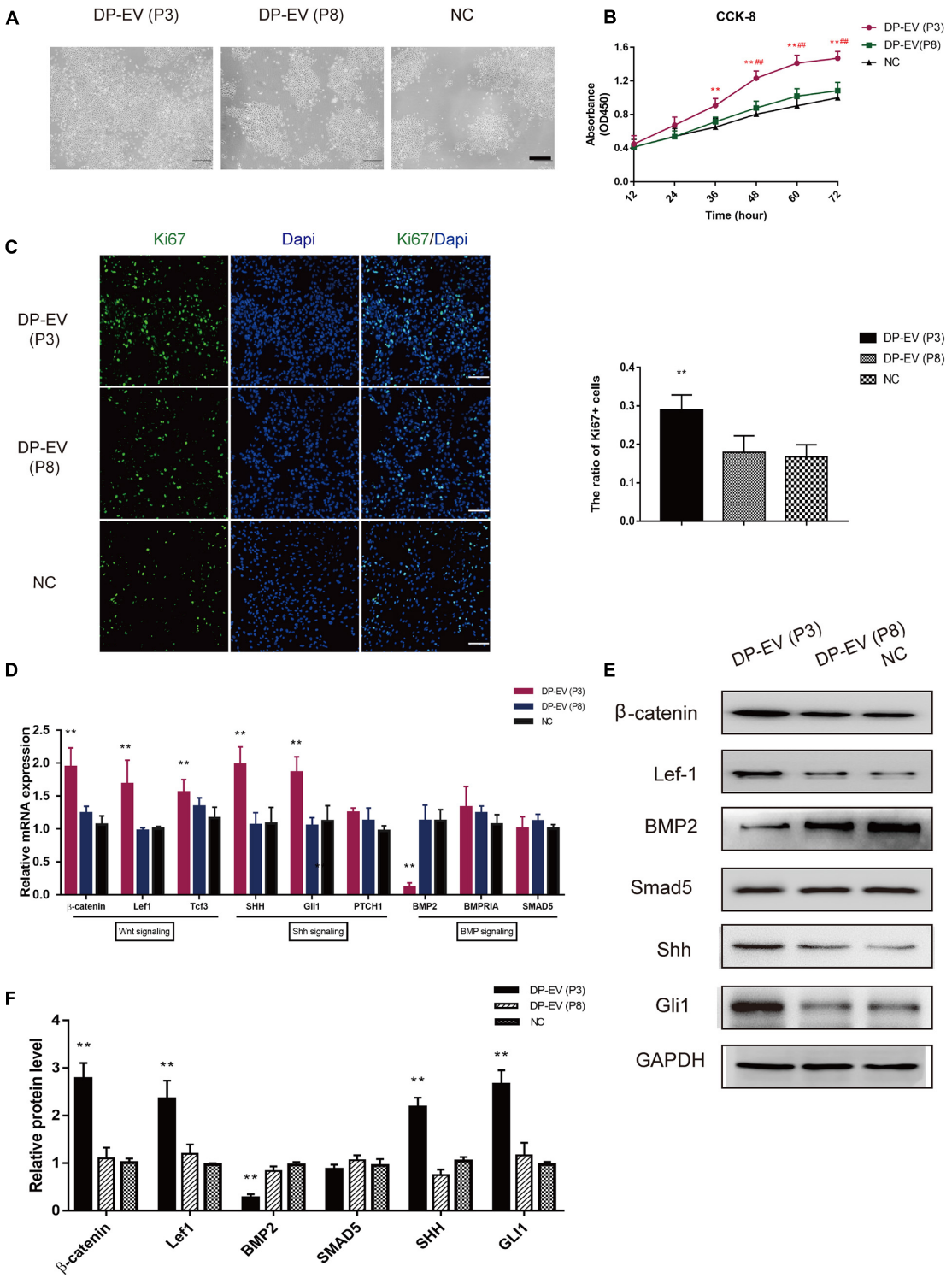

FIGURE 3 | Effect of DP-EVs on human hair follicle lower outer root sheath cells (ORSCs). **(A,B)** ORSCs were treated with DP-EVs from P3 and P8 human DPCs, and cell viability was examined by CCK-8 assay. **(C)** Immunofluorescence microscopy and quantitative analysis of the percentage of Ki67 + ORSCs treated with DP-EVs (P3), DP-EVs (P8), or PBS for 48 h. Scale bar: 100 μm. **(D)** RT-PCR analysis of known follicle-regulatory genes in ORSCs after DP-EV treatment for 5 days. **(E,F)** Western blot analysis of known follicle-regulatory proteins in ORSCs after DP-EV treatment for 5 days. Data are expressed as means ± SD. $^{**}p < 0.01$ vs. negative control (NC); $^{\#\#}p < 0.01$ vs. P8-DP-EV–treated group. Statistical significance was evaluated by one-way ANOVA with Bonferroni comparison; $n = 5$ for each group.

we then performed an unsupervised clustering analysis of the 100 DEMs (**Figure 4A**). In this analysis, relationships among genes and samples are represented by trees whose branch lengths reflect the degree of similarity between the variables. To validate the profiling data, we performed RT-PCR on the same RNA samples used for the miRNA-Seq and confirmed the altered expression of 10 randomly selected miRNAs that were strongly up- or downregulated. Consistent with the miRNA-Seq data, the results showed that miR-10b-5p, miR-454-3p, miR-140-5p, miR-18a-3p, and miR-23a-5p were upregulated and miR-28-3p, miR-31-5p, miR-342-3p, miR-382-5p, and miR-452-5p were downregulated in low-passage vs. high-passage DP-EVs ($p < 0.05$) (**Figure 4B**). In P3 DP-EVs, the five most abundant miRNAs (miR-1246, miR-21-5p, miR-140-5p, miR-122-5p, and miR-24-3p) accounted for 36.0% of the total miRNA reads (**Figure 4C**), and miR-140-5p and miR-24-3p were upregulated.

Identification of Target Genes and Functional Analysis

Each microRNA can regulate a large number of target genes, and several databases based on various algorithms are available for prediction of miRNA gene targets. We chose TargetScan and miRDB to predict the targets of the 100 DEMs, resulting in the identification of 1803 genes (**Figure 5A** and **Supplementary Table S4**). To analyze the biological classifications of the predicted target genes, we performed functional and pathway enrichment analyses. Using KEGG pathway analysis to mine canonical signaling pathways, we found that the predicted target genes were strongly associated with the TGF-β Signaling Pathway (**Figure 5B** and **Supplementary Table S5**) (BMP belongs to the TGF-β family). GO analysis revealed that changes in the biological processes (BP) of the predicted target genes were significantly associated with GO terms such as "chondrocyte differentiation," "BMP signaling pathway," and "positive regulation of bone mineralization" (**Figure 5C** and **Supplementary Table S6**). To explore interactions among the predicted target genes, we constructed a PPI network of the target genes and screened the most important modules using MCODE. The significant module with the highest score (7.75) included 9 nodes and 28 edges (**Figure 4D**). Genes often interact with each other through hub genes; indeed, CytoHubba identified BMP2 and SMAD5 as the most significant hub genes involved in this module (**Figure 4D**). As above, we focused subsequent studies on the BMP signaling pathway.

miR-140-5p Targets BMP2 and Negatively Correlates With BMP2

The screen identified BMP2 and its downstream target SMADs as the hubs of the regulated gene module (**Figure 4D**), and BMP2 was downregulated in ORSCs treated with low-passage DP-EVs, whereas expression of SMADS remained unchanged (**Figures 3D–F**). Hence, to explore the molecular mechanisms accounting for the BMP2-suppressive role of miRNAs in DP-EVs, we screened for miRNAs that regulate BMP2 using the PITA, miRmap, microT4, miRanda, PicTar, and TargetScan databases (**Supplementary Table S7**). The results (**Figure 4E**) revealed that among the 100 DEMs, only miR-140-5p (accounting for 6.96% of the total miRNA reads in passage 3 DP-EVs in **Figure 4C**) was scored as a potential regulator of BMP2 in all databases. The TargetScan website revealed the target binding sequences of miR-140-5p in the BMP2 mRNA (**Figure 4F**). In addition, we constructed an interaction network of miR-140-5p and its target genes (**Supplementary Table S8**). To refine the list of potential target genes downstream of miR-140-5p that might be specifically involved in HF growth, we identified targets of miR-140-5p within a HF-related gene network (**Figure 5D**). The predicted miR-140-5p network includes key genes that regulate multiple points in the TGF-β superfamily (to which BMP belongs), and the sizes of the nodes represent the binding score of miR-140-5p to target genes. Regulation of a target mRNA by an miRNA requires temporal and spatial coexpression. Therefore, we transfected ORSCs with a plasmid containing a luciferase-BMP2 3′ UTR construct to test the predicted miR-140-5p-target interactions. The luciferase reporter assay showed that co-transfection of miR-140-5p mimic or inhibitor along with the wild-type BMP2 reporter caused significant down-regulation or up-regulation, respectively, of luciferase reporter activity ($p < 0.01$) (**Figures 4G,H**). However, co-transfection of miR-140-5p mimic or inhibitor along with the mutant BMP2 reporter had no effect on reporter activity (**Figures 4G,H**). These results indicated that miR-140-5p in low-passage DP-EVs inhibits the expression of BMP2 in ORSCs.

DPC-Derived Vesicular miR-140-5p Promotes ORSC and MxCs Proliferation *in vitro*

Based on the bioinformatics analysis findings, we examined the pro-proliferation effect of DPC-derived vesicular miR-140-5p in ORSCs. First, we investigated whether EVs transferred miR-140-5p into ORSCs. To this end, we isolated overexpressing or inhibiting miR-140-5p DPCs established by lentivirus transfection. Real-time PCR analysis revealed an elevated miR-140-5p expression level in miR-140-5p–overexpressing DPCs, and a reduced miR-140-5p level in miR-140-5p–silenced (si-miR-140-5p) DPCs, relative to control cells (DPCs transfected with miR-NC or si-miR-Nc) and parental cells (**Figure 6A**; $^{**}p < 0.01$). A similar tendency was observed in EVs derived from DPCs (**Figure 6A**; $^{**}p < 0.01$). To confirm the role of EVs in transporting miR-140-5p to ORSCs, we incubated ORSCs miR-140-5p–overexpressing or –inhibited DP-EVs, and harvested the cells for qRT-PCR analysis at various times (0, 12, 24, and 36 h). As shown in **Figure 6B**, miR-140-5p levels in ORSCs were markedly upregulated after the cells were treated with miRNA-NC, miR-140-5p–overexpressing, or si-miRNA-NC DP-EVs for 12 h, but were most upregulated in miR-140-5p–overexpressing DP-EVs, indicating that DP-EVs transferred miR-140-5p into ORSCs. However, this effect was abolished by miR-140-5p silencing. ORSCs treated with an equal amount of PBS was used as a negative control. After 12 h of culture, EVs derived from the transfected DPCs were designated as miRNA-NC-EVs,

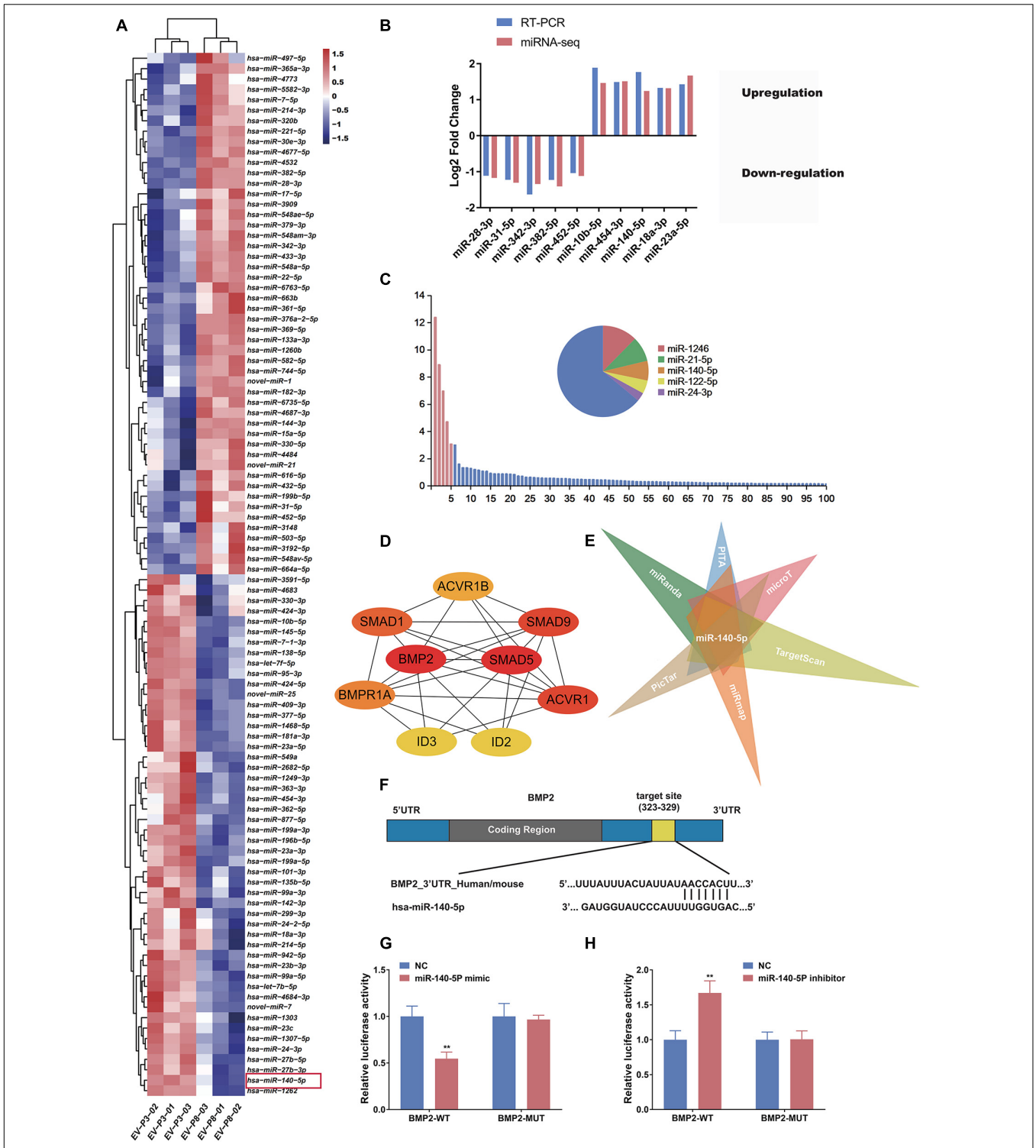

FIGURE 4 | miR-140-5p–enriched DP-EVs decrease the expression of BMP2. **(A)** Heatmap and unsupervised cluster analysis of DEMs between DP-EVs (P3) and DP-EVs (P8). RNA expression level is represented by colors: bright red indicates high values, and blue indicates low values. **(B)** Validation of RNA-Seq data. **(C)** Relative proportion of miRNAs in total miRNA reads of DP-EVs (P3). U6 was used as an endogenous control; $n = 8$ for each group. **(D)** The most significant module obtained from the PPI network had 9 nodes and 28 edges. Hub genes (*BMP2* and *SMAD5*) were identified by Cytohubba. **(E)** Potential miRNAs involved in regulation of BMP2, predicted using the TargetScan, miRanda, miRmap, PicTar, PITA, and DIANA-microT databases. **(F)** Schematic diagram of miR-145 binding site on the 3′UTR of *SMAD5* mRNA, according to the TargetScan website. **(G,H)** Transfection of ORSCs with 50 nM miR-140-5p mimic **(G)** and inhibitor **(H)** for 48 h altered luciferase activity of wild-type and mutant *BMP2* 3′ UTR construct. Error bars denote the standard error of the means of three experiments. $^{**}p < 0.01$ (two-tailed Student's *t*-test).

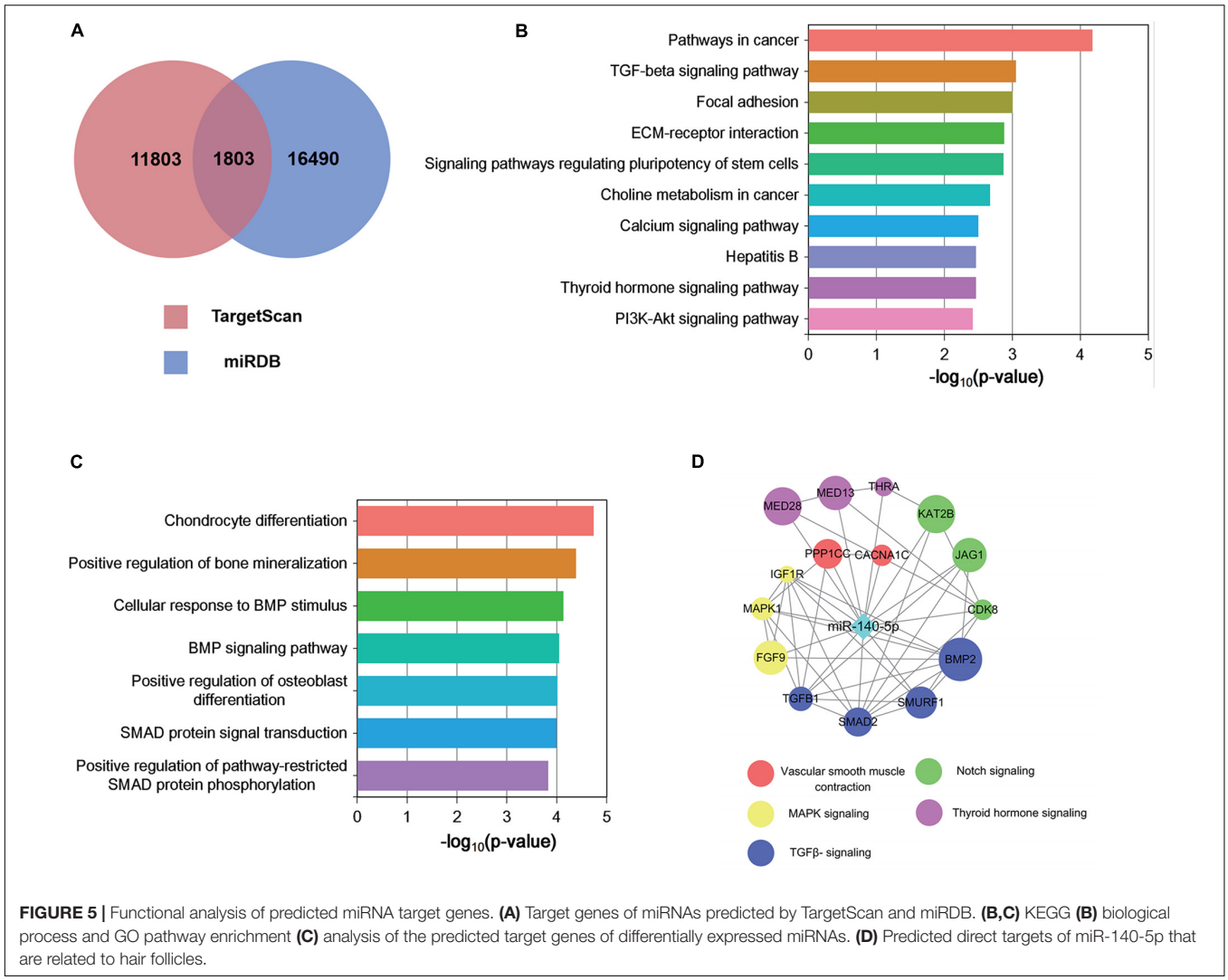

FIGURE 5 | Functional analysis of predicted miRNA target genes. **(A)** Target genes of miRNAs predicted by TargetScan and miRDB. **(B,C)** KEGG **(B)** biological process and GO pathway enrichment **(C)** analysis of the predicted target genes of differentially expressed miRNAs. **(D)** Predicted direct targets of miR-140-5p that are related to hair follicles.

miR-140-5p-EVs, si-miRNA-NC-EVs, or si-miR-140-5p-EVs and used for subsequent experiments.

To investigate the function of DPC-derived vesicular miR-140-5p in ORSCs, we examined the pro-proliferation activity of DP-EVs by Ki67 and CCK-8 assay in ORSCs (**Figures 6C–E**). As illustrated in **Figure 6C–E**, ORSCs treated with miR-140-5p–overexpressing EVs had the highest Ki67^{+} cell ratio and maximum absorbance at 450 nm at 48 h (**Figures 6C–E**; $^{**}p < 0.001$) (40 μg EVs were added to the medium on day 0 and day 3). The pro-proliferation effect of DP-EVs was eliminated in the miR-140-5p–silence group. These results indicated that vesicular miR-140-5p stimulates ORSC proliferation.

By bioinformatics analysis and luciferase activity assay (**Figures 4G,H**), we identified BMP2 as the most probable downstream target gene of miR-140-5p. To further confirm the regulatory effect of vesicular miR-140-5p on BMP2, we evaluated the expression of BMP2 and its downstream targets SMAD5 and p-SMAD5 in ORSCs treated with various DP-EVs. Western blot revealed that overexpression of miR-140-5p led to a reduction in the levels of BMP2 and p-SMAD5, but not SMAD5. By contrast, inhibition of miR-140-5p markedly reversed the DP-EV–induced reduction of BMP2 and p-SMAD5 in ORSCs (**Figures 6F,G**). The result also showed that ORSCs treated with miR-140-5p–overexpressing EVs on day 5 expressed the highest levels of Cyclin D1 and Cyclin E, which are key cell cycle-related proteins, suggesting that miR-140-5p–overexpressing EVs affected ORSC cell proliferation. By contrast, cells treated with miR-140-5p–silenced EVs expressed the lowest levels of Cyclin D1 and Cyclin E (**Figures 6F,G**).

Similar trends were also found in MxCs treated in the same way as ORSCs. As shown in **Supplementary Figure S3A**, we also observed that DP-EVs transferred miR-140-5p into MxCs. MxCs treated with miR-140-5p–overexpressing EVs had the highest Ki67 + cell ratio at 48 h (**Supplementary Figure S3B**; $^{**}p < 0.001$). These results indicated that vesicular miR-140-5p stimulates ORSC proliferation. Similar western blot results indicated that ORSCs treated with miR-140-5p–overexpressing EVs expressed the lowest levels of BMP2 and p-SMAD5, and the highest levels of Cyclin D1 and Cyclin E at day 5 (**Supplementary Figures S4A,B**). Together, these data

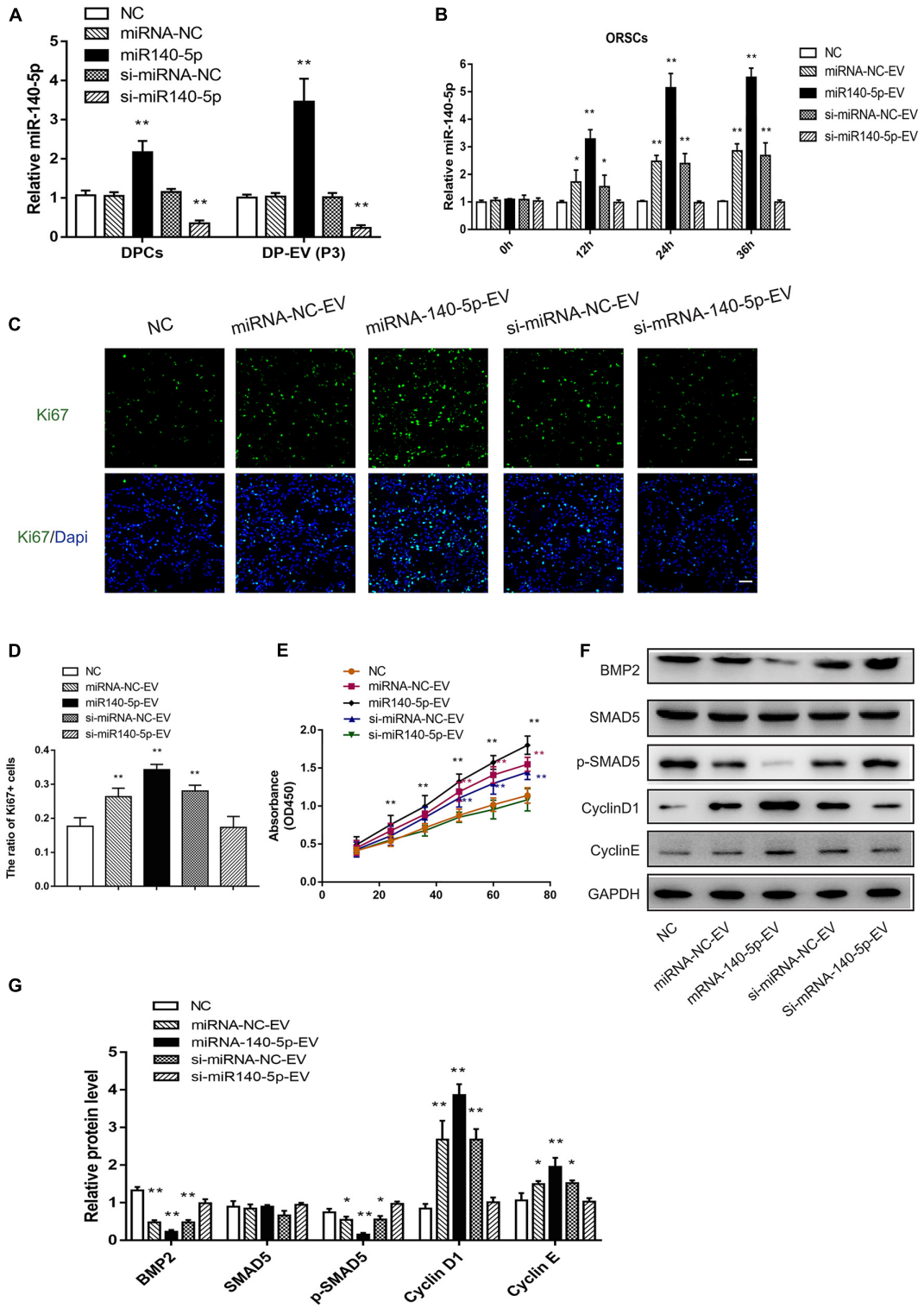

FIGURE 6 | Effect of DPC vesicular miR-140-5p on ORSCs *in vitro*. DP-EVs were isolated from DPCs overexpressing (miR-140-5p) or inhibiting miR-140-5p (si-miR-140-5p) for 48 h (concentration for miRNA mimics or inhibitor: 50 nM). The control group was transfected with an equal volume of control lentiviral vector (miR-NC, si-miR-NC) or PBS. **(A)** RT-PCR was performed to analyze the relative expression of miR-140-5p in DPCs and their EVs. **(B)** ORSCs were treated with DP-EVs for the indicated lengths of time (0, 12, 24, and 36 h), and then miR-140-5p was detected by RT-PCR. **(C,D)** Immunofluorescence microscopy and quantitative analysis of the percentage of Ki67 + ORSCs treated with DP-EVs or PBS for 48 h. Scale bar: 50 μm. **(E)** CCK-8 assay for cell viability of ORSCs treated with DP-EVs at the indicated time points. **(F,G)** Western blot and quantification of BMP regulatory proteins and cyclins in ORSCs after DP-EV treatment for 5 days. Data represent means ± SD of triplicates (*$p < 0.05$; **$p < 0.01$).

suggest that DP-EVs promote ORSCs and MxCs proliferation by delivering miR-140-5p, which targets BMP2 and further regulates phosphorylation of SMAD5. Prior studies have confirmed the strong relationship between BMP inhibition and epithelial cell proliferation (Kulessa et al., 2000). These results indicated that vesicular miR-140-5p stimulates ORSC proliferation by inhibiting the BMP signaling pathway.

DPC-Derived Vesicular miR-140-5p Promotes Hair Growth in Culture

Above, we showed that DPC vesicular miR-140-5p promoted ORSC and MxCs proliferation *in vitro*. However, the HF is a complex mini-organ. Hence, we investigated whether DPC vesicular miR-140-5p was also pro-proliferative in HFs. Specifically, we used a human scalp follicle culture system to investigate the function of vesicular miR-140-5p in HFs. In these experiments, 40 μg EVs (miRNA-NC-EVs, miR-140-5p-EVs, si-miRNA-NC-EVs, or si-miR-140-5p-EV) was added to the medium of cultured HFs every 3 days. After incubation for 9 days, we found that the administration of miR-140-5p-EV significantly promoted HF growth and prolonged anagen (**Supplementary Figure S5** and **Figures 7A,B**; $^{**}p < 0.01$). The HF length in the miR-140-5p-EV group increased 2.22 ± 0.21 mm, with about 86.67% of HFs remaining in anagen during EV treatment. By contrast, when miR-140-5p was silenced in EVs (si-miR-140-5p-EV), the growth of the HFs and the anagen-prolonging effect were repressed (**Figures 7A,B**; $^{*}p < 0.05$).

Cell proliferation in cultured HFs was evaluated at day 5 by IHC. We performed double staining for K15 (green) and Ki67 (red) to identify proliferative ORSCs and MxCs. **Figures 7C–F** shows that miR-140-5p-EVs significantly promoted lower ORSC proliferation and widened the ORS region relative to the control and miR-140-5p–silenced group. In hair matrix, HFs treated with miR-140-5p-EV contained large numbers of $Ki67^{+}$ cells ($^{**}p < 0.001$). These data indicated that vesicular miR-140-5p stimulated lower ORSC and MxC proliferation in cultured human HFs.

To confirm the downstream target of miR-140-5p in cultured HFs, we performed IF to analyze BMP2 and p-SMAD5 on day 5. Relative to si-miR-140-5p-EV treatment and the control, BMP2 and its downstream target p-SMAD5 expression decreased in response to miR-140-5p-EV treatment in both the hair matrix and lower ORS region, as demonstrated by immunofluorescence staining (**Figures 8A–E**; $^{**}p < 0.01$). However, silencing the expression of miR-140-5p in DP-EVs restored the expression of BMP2 and p-SMAD5 (**Figures 8A–E**; $^{**}p < 0.01$). These data indicated that BMP2 and SMAD5 levels were significantly downregulated in cultured HFs treated with miR-140-5p–overexpressing DP-EVs.

DPC-Derived Vesicular miR-140-5p Accelerate the Telogen-to-Anagen Transition in C57BL/6 Mice

We also investigated whether DPC vesicular miR-140-5p was pro-proliferative *in vivo*. For this purpose, we used C57BL/6 mice for treatment by depilating a patch of dorsal hair. After treatment with EVs (miRNA-NC-EVs, miR-140-5p-EVs, si-miRNA-NC-EVs, or si-miR-140-5p-EV) (4 mg/ml dissolved in PBS, 1 ml per mouse) or PBS (as a negative control) (**Supplementary Figure S6A**), the hair coverage rate at day 18 was ∼84.6% in the miR-140-5p-EV-treated group, which was about 1.77-fold higher than PBS-treated group. The results revealed that miR-140-5p-EVs were the most effective at accelerating the hair transition from the telogen to anagen phase (**Supplementary Figures S6B,D**; $^{**,\#\#,++}p < 0.01$). The skin thickness of miR-140-5p-EV-treated mice significantly increased relative to the PBS-treated group at day 12 (**Supplementary Figures S6C,E**). Moreover, miR-140-5p-EV treatment significantly increased the number of Ki67-positive cells ($P < 0.01$) on day 18, whereas the BMP2 level significantly decreased (**Supplementary Figures S6F–H**). These data revealed that miR-140-5p-EVs were the most effective at accelerating the hair transition from the telogen to anagen phase *in vivo*.

DISCUSSION

The HF, a mammalian mini-organ, has an intrinsic stem cell niche that regulates prominent physiological growth cycling, making it a valuable model for studying cellular and signaling mechanisms underlying organ regeneration (Wang et al., 2015), as well as disorders of stem cells and their niche, as abnormal secretion from these cells results in hair loss (Ojeh et al., 2015; Pratt et al., 2017; Katzer et al., 2019). Although this issue affects millions of people, the available means of treatment remain limited (Katzer et al., 2019).

The DP are considered to be the signaling center of the HF, which plays an important role in hair growth, cycling, and regeneration (Ojeh et al., 2015; Owczarczyk-Saczonek et al., 2018). It is well established that DPCs induce HF morphogenesis (Biernaskie et al., 2009; Ojeh et al., 2015; Owczarczyk-Saczonek et al., 2018): when mixed with infantile keratinocytes in a specific proportion, implanted DPCs can induce the growth of new HFs in rodents (Amici et al., 2009), and experiments in immune-deficient rats have shown that cells derived from the DP can be incorporated into existing DPs, giving rise to stronger HFs (Biernaskie et al., 2009). However, the HF induction capacity of DPCs decreases with passage (Zhang et al., 2014; Lin et al., 2016; Wang J. et al., 2018); the limited availability of donor hair, ethical concerns, and the risks of immunological rejection also restrict the clinical application of this approach (Zhu et al., 2017; Liu et al., 2018). Recent research has shown that paracrine signaling strongly contributes to the efficacy of cell-based therapies, and that changes in the biological information (such as proteins and miRNAs) carried by EVs may play a critical role in this phenomenon (Witwer et al., 2013). Although DP-EVs from low-passage DPCs can promote the catagen-to-anagen transition of HF and prolong anagen (Chen et al., 2020), we found that DP-EVs from high-passage DPCs lose their ability promote hair growth. The cause for this discrepancy remains unclear, and the underlying mechanism needs to be further investigated.

Hair follicle growth relies on a dermal–epidermal interaction in the HFs (Wang et al., 2015). In anagen, DPCs secrete various

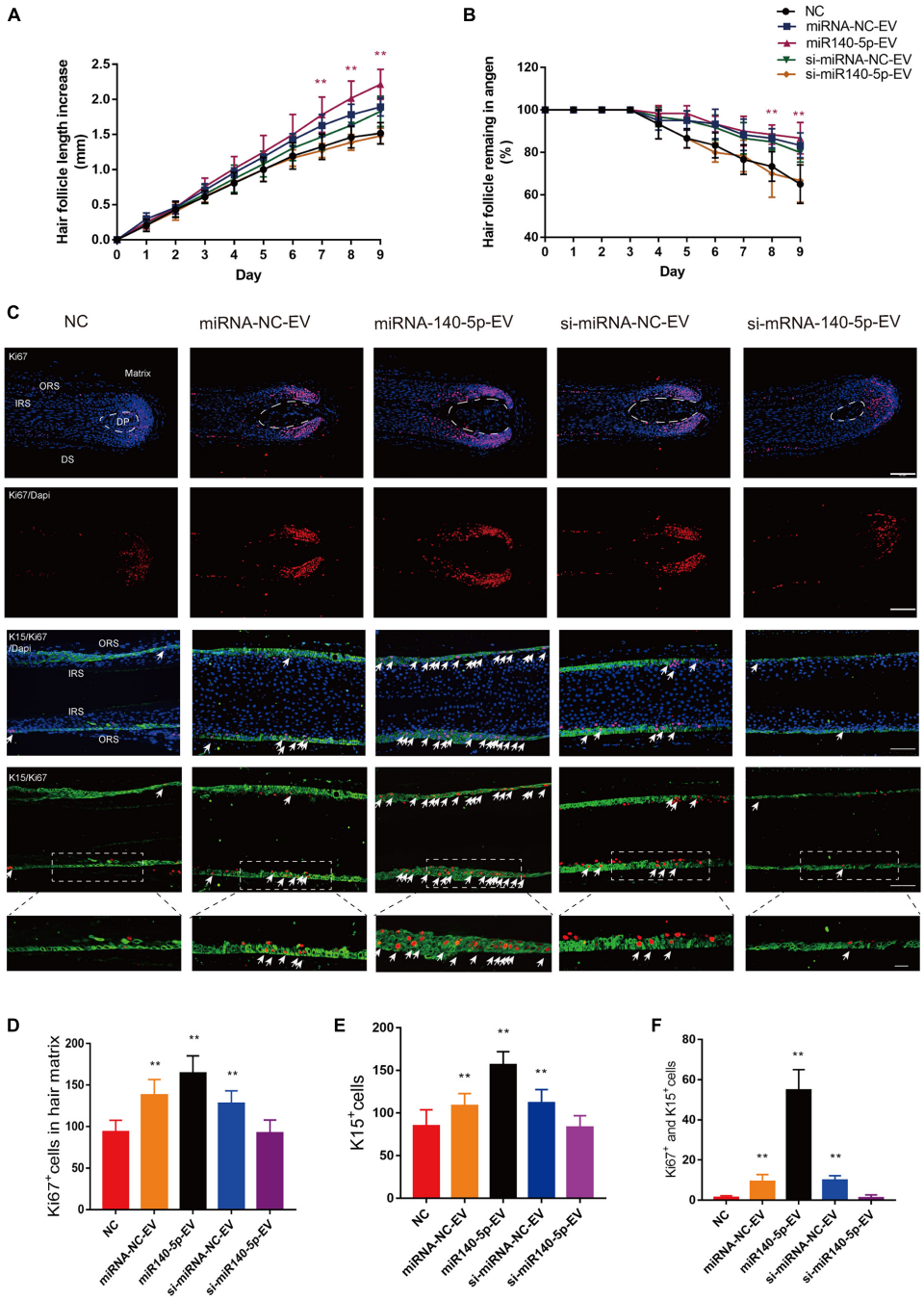

FIGURE 7 | Effect of DPC vesicular miR-140-5p on cultured hair follicles. Cultured human follicles were treated with EVs isolated from DPCs overexpressing (miR-140-5p) or inhibiting miR-140-5p (si-miR-140-5p) for 9 days. The control group was transfected with an equal volume of control Lentiviral vector (miR-NC, si-miR-NC) or PBS. **(A,B)** Hair follicles in each group were assessed and measured daily for increase in hair length **(A)** and the percentage of hair follicles remaining in anagen **(B)**. **(C–F)** Immunofluorescence staining of Ki67 and K15 in hair matrix and lower ORS. Scale bar: 100 μm. Quantitative analysis of the number of Ki67+ **(C,D)**, K15+ **(C,E)** and Ki67+/K15+ double-staining cells **(C,F)** in hair follicle. Data are expressed as means ± s.d. n = 60 from five healthy female individuals (12 samples from each individual). $^{**}p < 0.01$ vs. PBS-treated group (NC). Statistical significance was evaluated by one-way ANOVA with Bonferroni comparisons; $n = 5$ for each group.

activators to the HF epithelium (Yang and Cotsarelis, 2010). During this period, hair growth activation primarily relies on the proliferative activity of the hair matrix and hair ORS, which are located adjacent to DPs (Lee and Tumbar, 2012; Premanand and Reena, 2018). We previously reported that after treatment with DP-EVs, MxCs undergo rapid proliferation

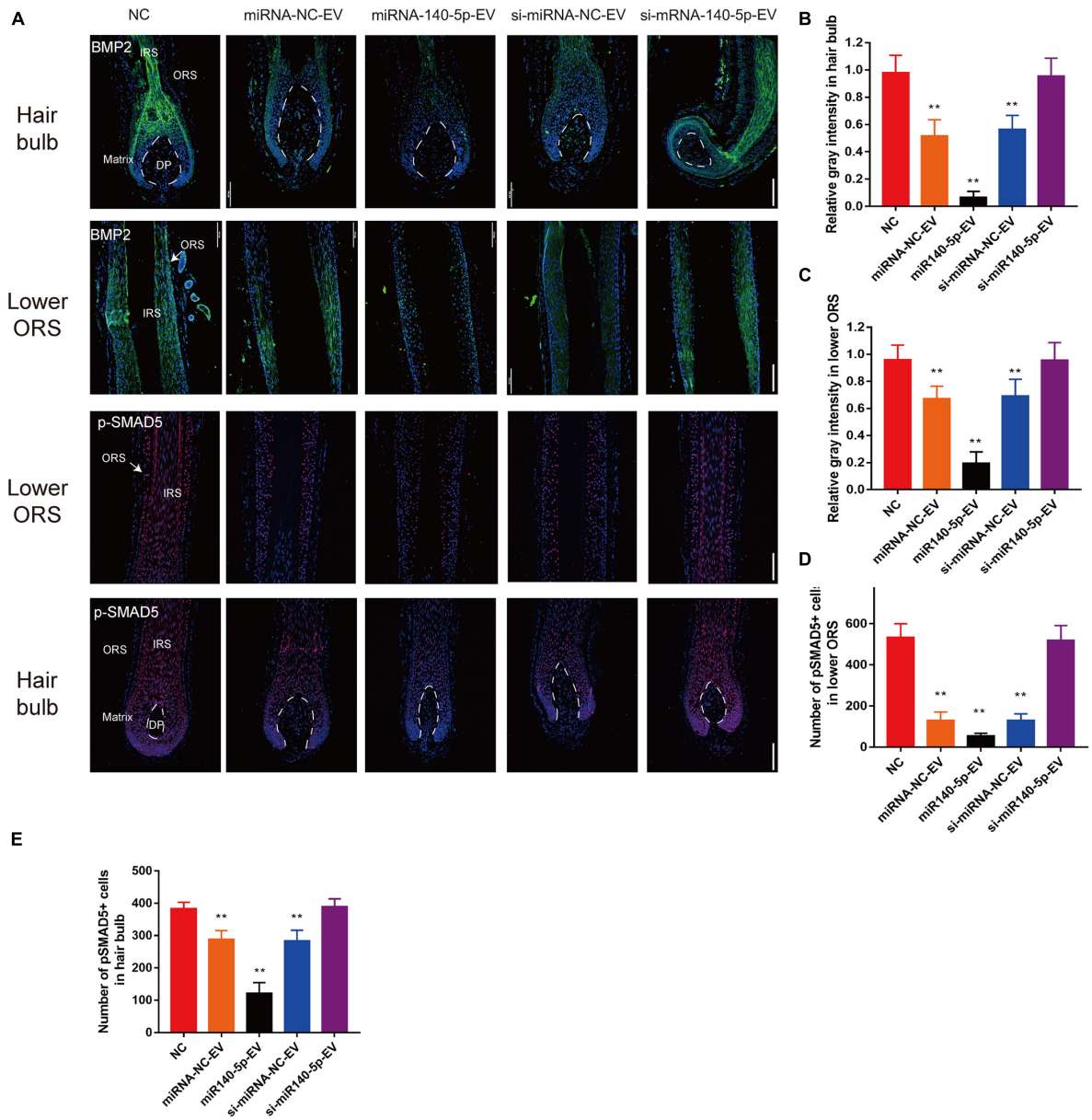

FIGURE 8 | DPC vesicular miR-140-5p downregulated BMP2 and p-SMAD5 in hair follicles. **(A)** Immunofluorescence staining of BMP2 and p-SMAD5 in hair follicle after treatment with DP-EVs for 9 days. Scale bar: 100 μm. **(B–D)** Quantitative analysis of the relative gray intensity level of BMP2 in hair bulb **(B)** and in lower ORS **(C)**, and the number of p-SMAD5^{+} cells in lower ORS **(D)** and hair bulb **(E)**. Data are expressed as means ± SD. $n = 60$ from five healthy female individuals (12 samples from each individual). $^{**}p < 0.01$ vs. PBS-treated group (NC). Statistical significance was evaluated by one-way ANOVA with Bonferroni comparisons; $n = 5$ for each group.

and then differentiate to form the hair fiber and IRS (Chen et al., 2020). However, it has not been demonstrated that hair matrix can affect the growth of ORS, and the reason for the accelerated growth of ORS has not been clarified. Several cellular pathways, including BMP/TGF-β, are essential for regulation of epithelial proliferation and differentiation (Kulessa et al., 2000; Lee and Tumbar, 2012; Huang et al., 2019). In the canonical SMAD-dependent BMP signaling pathway, the interactions between BMP2 and its receptors cause phosphorylation of their immediate downstream targets (SMAD proteins); BMP2 was originally defined by its ability to induce ectopic bone and cartilage formation *in vivo* (Reddi, 1992). In the hair formation process, BMP pathway inhibition is a distinguishing feature of the activation of proliferation by epithelial components (Greco et al., 2009; Genander et al., 2014) and can promote WNT signaling (Jamora et al., 2003). Hence, we then focused on whether biological functions differed between EVs derived from high- and low-passage DPCs. We successfully isolated DP-EVs, labeled EVs,

and removed excess dye to an undetectable level as previously described (Roberts-Dalton et al., 2017; Krause et al., 2018), and then observed the uptake of DP-EVs in the lower ORS and hair matrix in cultured HFs (Chen et al., 2020). Cell proliferation was stimulated in both cell populations by low-passage human DP-EVs *in vivo* and *in vitro*, but remained unchanged after treatment with high-passage DP-EVs. Hair matrix proliferation is intimately related to the regulatory function of DP, and determines hair shaft and IRS growth (Lee and Tumbar, 2012; Huang et al., 2019). Apart from MxCs, immunofluorescence staining and RT-PCR revealed that lower ORSCs were also dynamically activated after treatment with P3-DP-EVs, which explained the accelerated growth of the hair outer root sheath. We then examined known follicle-regulatory proteins in the process of EV treatment and found that Wnt signaling was upregulated, whereas BMP2 was downregulated, by P3-DP-EV treatment. One possible reason for this difference is that DPC-derived EVs can carry pro-proliferative and hair-inductive information from their parent cells, but this information is gradually lost over the course of serial passage (Biernaskie et al., 2009; Higgins et al., 2013).

The mRNA, miRNA, and protein composition of EVs differ from those of their originating cells. Accumulating evidence shows that miRNAs in EVs play major roles in cell-to-cell communication (Yu et al., 2016). Not only DP-specific markers, but also the whole transcriptome characteristics of DPCs change rapidly over the course of cell passage (Higgins et al., 2013), which may subsequently change the composition of DP-EVs. Thus, to identify the stimulatory factors responsible for EV-regulated HF regeneration that may change over the course of DP cell passage, we performed miRNA sequencing in DP-EVs from low- and high-passage DPCs. Analysis of the 100 most DEMs revealed that the predicted target genes were enriched in functions related to the BMP signaling pathway, and the most significant interaction module identified from among the predicted target genes consisted of BMP signaling components. BMP2 was identified as the hub regulatory gene of miR-140-5p, which accounted for 6.96% of the total miRNA reads in P3-DP-EVs. Although few studies have investigated the role of miR-140-5p in dermatology, miR-140-5p expression is known to promote proliferation in dental pulp stem cells (Sun et al., 2017), neural stem cells (Tseng et al., 2019), and chondrocytes (Tao et al., 2017; Wang Z. et al., 2018). We showed that overexpression of miR-140-5p in human HFs was confirmed to stimulate ORSC and MxCs proliferation by treatment with overexpressed vesicular miR-140-5p, but was restricted by vesicular miR-140-5p inhibition. We also got similar results in animal experiments.

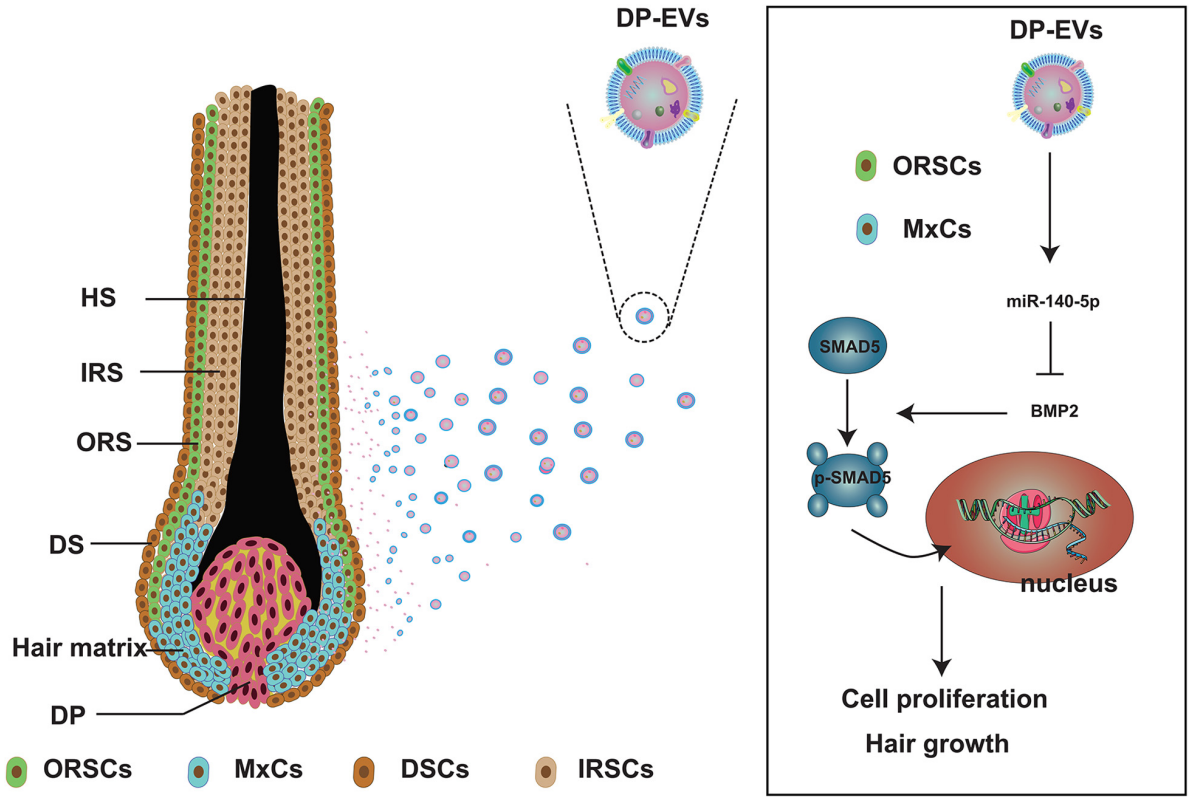

SCHEME 1 | Schematic illustration of low-passage DP-EVs inhibiting the BMP signaling pathway in ORSCs and MxCs. In cultured scalp follicles, miR-140-5p–enriched EVs derived from DPCs were transferred to ORSCs and MxCs. miR-140-5p could suppress the BMP pathway by directly binding to and repressing BMP2. Down-regulation of endogenous BMP2 resulted in inhibition of SMAD5 serine phosphorylation in ORSCs and MxCs, leading in turn to cell proliferation and hair growth. ORSC, outer root sheath cell; MxC, hair matrix cell; DSCs, dermal sheath cell; IRSC, inner root sheath cell; DPC, dermal papilla cell; DP-EV, dermal papilla-derived extracellular vesicle.

BMP2 is a BMP signal that is crucial for maintaining the hair cycle during telogen (Kobielak et al., 2007). Upon BMP inhibition, the HF tilts toward anagen (Greco et al., 2009; Kandyba et al., 2013). In the beginning of anagen, accumulated BMP-inhibitory and Wnt-/Shh-activating signals in HFs initiate a new round of hair growth (Jamora et al., 2003; Shimomura and Christiano, 2010; Hsu et al., 2014). The BMP pathway in HFs is largely antagonistic to the Wnt and Shh pathways: Wnt and Shh signaling are putative BMP targets in epithelial components. Reduced BMP signaling in ORS and hair matrix could lead to proliferation of ORSCs and MxCs (Kulessa et al., 2000; Kobielak et al., 2003), which may help to explain why both ORSC and MxCs proliferation is activated following DP-EV treatment. However, when BMP signaling was downregulated in cultured HFs, changes in the proportion of Wnt/BMP prolong proliferation and could delay differentiation (Plikus et al., 2008; Kandyba et al., 2013). As a result, the anagen stage is prolonged (Plikus et al., 2008). In this study, we demonstrated that BMP2 is a direct target of miR-140-5p, and that overexpression of miR-140-5p in ORSCs and MxCs downregulates BMP2. We then identified and validated bona fide downstream targets of SMAD5, whose phosphorylation is impacted by BMP signaling. Interestingly, gene expression of SMAD5 remained unchanged, but the levels of the phosphorylated product p-SMAD5 were elevated. These data suggested that miR-140-5p directly binds to and regulates BMP2 mRNA but not SMAD5 mRNA. Activation of BMP2 leads to phosphorylation of SMAD5, which ultimately promotes ORSC and MxCs proliferation and prolongs anagen (**Scheme 1**).

Recent research has discovered that dermal exosomes containing miR-218-5p could promote hair regeneration by regulating β-catenin signaling in mice (Hu et al., 2020). Consistent with our study, miR-140-5p was upregulated 1.64 ± 0.684 fold in 3D cultured DPCs compared with 2D cultured high-passage DPCs based on the previously published sequencing results (Hu et al., 2020). While there was no significant difference in miR-218-5p content in our sequencing results, which may because of the species differences in human and mice HFs, and/or because the miR-218-5p content in DP-EVs is mainly affected by DPC culture environment (3D or 2D) rather than the number of cell passages. It was previously reported that miR-218-5p directly targets SFRP2, and thus, it up-regulates the Wnt/β-catenin pathway in HF in mice (Zhao et al., 2019; Hu et al., 2020). Wnt signaling can also be upregulated in the epithelial population following BMP inhibition (Kulessa et al., 2000; Kandyba et al., 2013). This may help to explain why Wnt signaling in ORSCs and MxCs were also upregulated after treatment with low-passage DP-EVs in our study.

Although the mechanism underlying the therapeutic effects of DP-EVs has not been clarified, our data revealed that low-passage DP-EVs promote ORSC and MxCs proliferation and prolong anagen via vesicular miR-140-5p–mediated suppression of BMP2 signaling pathways. Further investigation is needed to determine whether vesicular proteins and miRNAs other than miR-140-5p impact HF growth and hair cycling. Overall, our findings suggested that DP-EVs could be further exploited as a therapeutic agent to treat hair loss.

DATA AVAILABILITY STATEMENT

The datasets presented in this study can be found in online repositories. The names of the repository/repositories and accession number(s) can be found in the article/**Supplementary Material**.

ETHICS STATEMENT

The studies involving human participants were reviewed and approved by Medical Ethical Committee of Southern Medical University. The patients/participants provided their written informed consent to participate in this study. The animal study was reviewed and approved by Experimental Animal Centre at Southern Medical University. Written informed consent was obtained from the individual(s) for the publication of any potentially identifiable images or data included in this article.

AUTHOR CONTRIBUTIONS

All authors contributed to writing the manuscript and given approval to the final version of the manuscript. YC, JH, and ZL were principal investigator of the study, conceptualized the research, collected the data, performed the data analysis, and drafted the manuscript. LY, DF, RC, LD, JW, and LW helped to conceive the study and assisted in development of data analysis. YM and ZH provided the supervision and suggestions.

FUNDING

This study was funded by the National Natural Science Foundation of China (Grant Nos. 81772104, 81701929, 81971889, and 81902013), the Natural Science Foundation of Guangdong Province (Grant No. 2017A030310120), Guangdong Basic and Applied Basic Research Foundation (Grant No. 2019A1515012170), Science and Technology Program of Guangzhou (Grant No. 201904010480), and Medical Scientific Research Foundation of Guangdong Province (Grant No. C2019112).

ACKNOWLEDGMENTS

We thank Guangdong Provincial Key Laboratory of Construction and Detection in Tissue Engineering for providing experimental instruments.

SUPPLEMENTARY MATERIAL

The Supplementary Material for this article can be found online at: https://www.frontiersin.org/articles/10.3389/fcell.2020.593638/full#supplementary-material

REFERENCES

Agarwal, V., Bell, G. W., Nam, J. W., and Bartel, D. P. (2015). Predicting effective microRNA target sites in mammalian mRNAs. *Elife* 4: e05005.

Akilli, O. O., Pakula, H., Chmielowiec, J., Qi, J., Stein, S., Lan, L., et al. (2015). Gab1 and Mapk signaling are essential in the hair cycle and hair follicle stem cell quiescence. *Cell Rep.* 13, 561–572. doi: 10.1016/j.celrep.2015.09.015

Amelio, I., Lena, A. M., Bonanno, E., Melino, G., and Candi, E. (2013). miR-24 affects hair follicle morphogenesis targeting Tcf-3. *Cell Death Dis.* 4:e922. doi: 10.1038/cddis.2013.426

Amici, A. W., Yamato, M., Okano, T., and Kobayashi, K. (2009). The multipotency of adult vibrissa follicle stem cells. *Differentiation* 77, 317–323. doi: 10.1016/j.diff.2008.10.010

Ashburner, M., Ball, C. A., Blake, J. A., Botstein, D., Butler, H., Cherry, J. M., et al. (2000). Gene ontology: tool for the unification of biology. The gene ontology consortium. *Nat. Genet.* 25, 25–29. doi: 10.1038/75556

Baker, R. E., and Murray, P. J. (2012). Understanding hair follicle cycling: a systems approach. *Curr. Opin. Genet. Dev.* 22, 607–612. doi: 10.1016/j.gde.2012.11.007

Bandettini, W. P., Kellman, P., Mancini, C., Booker, O. J., Vasu, S., Leung, S. W., et al. (2012). MultiContrast delayed enhancement (MCODE) improves detection of subendocardial myocardial infarction by late gadolinium enhancement cardiovascular magnetic resonance: a clinical validation study. *J. Cardiovasc. Magn. Reson.* 14:83. doi: 10.1186/1532-429X-14-83

Biernaskie, J., Paris, M., Morozova, O., Fagan, B. M., Marra, M., Pevny, L., et al. (2009). SKPs derive from hair follicle precursors and exhibit properties of adult dermal stem cells. *Cell Stem Cell* 5, 610–623. doi: 10.1016/j.stem.2009.10.019

Carrasco, E., Soto-Heredero, G., and Mittelbrunn, M. (2019). The role of extracellular vesicles in cutaneous remodeling and hair follicle dynamics. *Int. J. Mol. Sci.* 20:2758. doi: 10.3390/ijms20112758

Chen, Y., Huang, J., Chen, R., Yang, L., Wang, J., Liu, B., et al. (2020). Sustained release of dermal papilla-derived extracellular vesicles from injectable microgel promotes hair growth. *Theranostics* 10, 1454–1478. doi: 10.7150/thno.39566

Chin, C. H., Chen, S. H., Wu, H. H., Ho, C. W., Ko, M. T., and Lin, C. Y. (2014). cytoHubba: identifying hub objects and sub-networks from complex interactome. *BMC Syst. Biol.* 8(Suppl. 4):S11. doi: 10.1186/1752-0509-8-S4-S11

Choi, B. Y. (2018). Hair-growth potential of ginseng and its major metabolites: a review on its molecular mechanisms. *Int. J. Mol. Sci.* 19:2703. doi: 10.3390/ijms19092703

Cobelli, N. J., Leong, D. J., and Sun, H. B. (2017). Exosomes: biology, therapeutic potential, and emerging role in musculoskeletal repair and regeneration. *Ann. N. Y. Acad. Sci.* 1410, 57–67. doi: 10.1111/nyas.13469

Franceschini, A., Szklarczyk, D., Frankild, S., Kuhn, M., Simonovic, M., Roth, A., et al. (2013). STRING v9.1: protein-protein interaction networks, with increased coverage and integration. *Nucleic Acids Res.* 41, D808–D815. doi: 10.1093/nar/gks1094

Genander, M., Cook, P. J., Ramskold, D., Keyes, B. E., Mertz, A. F., Sandberg, R., et al. (2014). BMP signaling and its pSMAD1/5 target genes differentially regulate hair follicle stem cell lineages. *Cell Stem Cell* 15, 619–633. doi: 10.1016/j.stem.2014.09.009

Greco, V., Chen, T., Rendl, M., Schober, M., Pasolli, H. A., Stokes, N., et al. (2009). A two-step mechanism for stem cell activation during hair regeneration. *Cell Stem Cell* 4, 155–169. doi: 10.1016/j.stem.2008.12.009

Higgins, C. A., Chen, J. C., Cerise, J. E., Jahoda, C. A., and Christiano, A. M. (2013). Microenvironmental reprogramming by three-dimensional culture enables dermal papilla cells to induce de novo human hair-follicle growth. *Proc. Natl. Acad. Sci. U.S.A.* 110, 19679–19688. doi: 10.1073/pnas.1309970110

Ho, C. H., and Zito, P. M. (2019). *Androgenetic Alopecia*. Treasure Island, FL: StatPearls Publishing.

Hsu, Y. C., Li, L., and Fuchs, E. (2014). Transit-amplifying cells orchestrate stem cell activity and tissue regeneration. *Cell* 157, 935–949. doi: 10.1016/j.cell.2014.02.057

Hu, S., Li, Z., Lutz, H., Huang, K., Su, T., Cores, J., et al. (2020). Dermal exosomes containing miR-218-5p promote hair regeneration by regulating β-catenin signaling. *Sci. Adv.* 6:a1685.

Huang, W. Y., Lin, E. T., Hsu, Y. C., and Lin, S. J. (2019). Anagen hair follicle repair: timely regenerative attempts from plastic extra-bulge epithelial cells. *Exp. Dermatol.* 28, 406–412. doi: 10.1111/exd.13889

Inui, S., and Itami, S. (2011). Molecular basis of androgenetic alopecia: from androgen to paracrine mediators through dermal papilla. *J. Dermatol. Sci.* 61, 1–6. doi: 10.1016/j.jdermsci.2010.10.015

Jamora, C., DasGupta, R., Kocieniewski, P., and Fuchs, E. (2003). Links between signal transduction, transcription and adhesion in epithelial bud development. *Nature* 422, 317–322. doi: 10.1038/nature01458

Kandyba, E., and Kobielak, K. (2014). Wnt7b is an important intrinsic regulator of hair follicle stem cell homeostasis and hair follicle cycling. *Stem Cells* 32, 886–901. doi: 10.1002/stem.1599

Kandyba, E., Leung, Y., Chen, Y. B., Widelitz, R., Chuong, C. M., and Kobielak, K. (2013). Competitive balance of intrabulge BMP/Wnt signaling reveals a robust gene network ruling stem cell homeostasis and cyclic activation. *Proc. Natl. Acad. Sci. U.S.A.* 110, 1351–1356. doi: 10.1073/pnas.1121312110

Kanehisa, M., Furumichi, M., Tanabe, M., Sato, Y., and Morishima, K. (2017). KEGG: new perspectives on genomes, pathways, diseases and drugs. *Nucleic Acids Res.* 45, D353–D361. doi: 10.1093/nar/gkw1092

Katzer, T., Leite, J. A., Beck, R., and Da, S. C. (2019). Physiopathology and current treatments of androgenetic alopecia: going beyond androgens and anti-androgens. *Dermatol. Ther.* 32:e13059. doi: 10.1111/dth.13059

Kishimoto, J., Burgeson, R. E., and Morgan, B. A. (2000). Wnt signaling maintains the hair-inducing activity of the dermal papilla. *Genes Dev.* 14, 1181–1185.

Kobielak, K., Pasolli, H. A., Alonso, L., Polak, L., and Fuchs, E. (2003). Defining BMP functions in the hair follicle by conditional ablation of BMP receptor IA. *J. Cell Biol.* 163, 609–623. doi: 10.1083/jcb.200309042

Kobielak, K., Stokes, N., de la Cruz, J., Polak, L., and Fuchs, E. (2007). Loss of a quiescent niche but not follicle stem cells in the absence of bone morphogenetic protein signaling. *Proc. Natl. Acad. Sci. U.S.A.* 104, 10063–10068. doi: 10.1073/pnas.0703004104

Krause, M., Rak-Raszewska, A., Naillat, F., Saarela, U., Schmidt, C., Ronkainen, V. P., et al. (2018). Exosomes as secondary inductive signals involved in kidney organogenesis. *J. Extracell. Vesicles* 7:1422675. doi: 10.1080/20013078.2017.1422675

Krek, A., Grun, D., Poy, M. N., Wolf, R., Rosenberg, L., Epstein, E. J., et al. (2005). Combinatorial microRNA target predictions. *Nat. Genet.* 37, 495–500. doi: 10.1038/ng1536

Kulessa, H., Turk, G., and Hogan, B. L. (2000). Inhibition of BMP signaling affects growth and differentiation in the anagen hair follicle. *EMBO J.* 19, 6664–6674. doi: 10.1093/emboj/19.24.6664

Kwack, M. H., Seo, C. H., Gangadaran, P., Ahn, B. C., Kim, M. K., Kim, J. C., et al. (2019). Exosomes derived from human dermal papilla cells promote hair growth in cultured human hair follicles and augment the hair-inductive capacity of cultured dermal papilla spheres. *Exp. Dermatol.* 28, 854–857. doi: 10.1111/exd.13927

Langan, E. A., Philpott, M. P., Kloepper, J. E., and Paus, R. (2015). Human hair follicle organ culture: theory, application and perspectives. *Exp. Dermatol.* 24, 903–911. doi: 10.1111/exd.12836

le Riche, A., Aberdam, E., Marchand, L., Frank, E., Jahoda, C., Petit, I., et al. (2019). Extracellular vesicles from activated dermal fibroblasts stimulate hair follicle growth through dermal papilla-secreted Norrin. *Stem Cells* 37, 1166–1175. doi: 10.1002/stem.3043

Lee, J., and Tumbar, T. (2012). Hairy tale of signaling in hair follicle development and cycling. *Semin. Cell Dev. Biol.* 23, 906–916. doi: 10.1016/j.semcdb.2012.08.003

Leiros, G. J., Attorresi, A. I., and Balana, M. E. (2012). Hair follicle stem cell differentiation is inhibited through cross-talk between Wnt/beta-catenin and androgen signalling in dermal papilla cells from patients with androgenetic alopecia. *Br. J. Dermatol.* 166, 1035–1042. doi: 10.1111/j.1365-2133.2012.10856.x

Lin, B., Miao, Y., Wang, J., Fan, Z., Du, L., Su, Y., et al. (2016). Surface tension guided hanging-drop: producing controllable 3D spheroid of high-passaged human dermal papilla cells and forming inductive microtissues for hair-follicle

regeneration. *ACS Appl. Mater. Interfaces* 8, 5906–5916. doi: 10.1021/acsami.6b00202

Liu, J. Y., Peng, H. F., and Andreadis, S. T. (2008). Contractile smooth muscle cells derived from hair-follicle stem cells. *Cardiovasc. Res.* 79, 24–33. doi: 10.1093/cvr/cvn059

Liu, Y. R., Ortiz-Bonilla, C. J., and Lee, Y. F. (2018). Extracellular vesicles in bladder cancer: biomarkers and beyond. *Int. J. Mol. Sci.* 19:2822. doi: 10.3390/ijms19092822

Lü, Z. F., Cai, S. Q., Wu, J. J., and Zheng, M. (2006). Biological characterization of cultured dermal papilla cells and hair follicle regeneration in vitro and in vivo. *Chin. Med. J. (Engl.)* 119, 275–281.

Mardaryev, A. N., Ahmed, M. I., Vlahov, N. V., Fessing, M. Y., Gill, J. H., Sharov, A. A., et al. (2010). Micro-RNA-31 controls hair cycle-associated changes in gene expression programs of the skin and hair follicle. *FASEB J.* 24, 3869–3881. doi: 10.1096/fj.10-160663

Matsuzaki, T. (2008). [Technologies for hair reconstruction and their applicability for pharmaceutical research]. *Yakugaku Zasshi* 128, 11–20. doi: 10.1248/yakushi.128.11

Mittelbrunn, M., Gutierrez-Vazquez, C., Villarroya-Beltri, C., Gonzalez, S., Sanchez-Cabo, F., Gonzalez, M. A., et al. (2011). Unidirectional transfer of microRNA-loaded exosomes from T cells to antigen-presenting cells. *Nat. Commun.* 2:282. doi: 10.1038/ncomms1285

Moll, R., Divo, M., and Langbein, L. (2008). The human keratins: biology and pathology. *Histochem. Cell Biol.* 129, 705–733. doi: 10.1007/s00418-008-0435-6

Ojeh, N., Pastar, I., Tomic-Canic, M., and Stojadinovic, O. (2015). Stem cells in skin regeneration, wound healing, and their clinical applications. *Int. J. Mol. Sci.* 16, 25476–25501. doi: 10.3390/ijms161025476

Owczarczyk-Saczonek, A., Krajewska-Wlodarczyk, M., Kruszewska, A., Banasiak, L., Placek, W., Maksymowicz, W., et al. (2018). Therapeutic potential of stem cells in follicle regeneration. *Stem Cells Int.* 2018:1049641. doi: 10.1155/2018/1049641

Paraskevopoulou, M. D., Georgakilas, G., Kostoulas, N., Vlachos, I. S., Vergoulis, T., Reczko, M., et al. (2013). DIANA-microT web server v5.0: service integration into miRNA functional analysis workflows. *Nucleic Acids Res.* 41, W169–W173. doi: 10.1093/nar/gkt393

Plikus, M. V., and Chuong, C. M. (2008). Complex hair cycle domain patterns and regenerative hair waves in living rodents. *J. Invest. Dermatol.* 128, 1071–1080. doi: 10.1038/sj.jid.5701180

Plikus, M. V., Mayer, J. A., de la Cruz, D., Baker, R. E., Maini, P. K., Maxson, R., et al. (2008). Cyclic dermal BMP signalling regulates stem cell activation during hair regeneration. *Nature* 451, 340–344. doi: 10.1038/nature06457

Pratt, C. H., King, L. J., Messenger, A. G., Christiano, A. M., and Sundberg, J. P. (2017). Alopecia areata. *Nat. Rev. Dis. Primers* 3:17011. doi: 10.1038/nrdp.2017.11

Premanand, A., and Reena, R. B. (2018). Androgen modulation of Wnt/beta-catenin signaling in androgenetic alopecia. *Arch. Dermatol. Res.* 310, 391–399. doi: 10.1007/s00403-018-1826-8

Rajendran, R. L., Gangadaran, P., Seo, C. H., Kwack, M. H., Oh, J. M., Lee, H. W., et al. (2020). Macrophage-derived extracellular vesicle promotes hair growth. *Cells* 9:856. doi: 10.3390/cells9040856

Reddi, A. H. (1992). Regulation of cartilage and bone differentiation by bone morphogenetic proteins. *Curr. Opin. Cell Biol.* 4, 850–855. doi: 10.1016/0955-0674(92)90110-x

Rishikaysh, P., Dev, K., Diaz, D., Qureshi, W. M., Filip, S., and Mokry, J. (2014). Signaling involved in hair follicle morphogenesis and development. *Int. J. Mol. Sci.* 15, 1647–1670. doi: 10.3390/ijms15011647

Roberts-Dalton, H. D., Cocks, A., Falcon-Perez, J. M., Sayers, E. J., Webber, J. P., Watson, P., et al. (2017). Fluorescence labelling of extracellular vesicles using a novel thiol-based strategy for quantitative analysis of cellular delivery and intracellular traffic. *Nanoscale* 9, 13693–13706. doi: 10.1039/c7nr04128d

Shimomura, Y., and Christiano, A. M. (2010). Biology and genetics of hair. *Annu. Rev. Genomics Hum. Genet.* 11, 109–132. doi: 10.1146/annurev-genom-021610-131501

Smoot, M. E., Ono, K., Ruscheinski, J., Wang, P. L., and Ideker, T. (2011). Cytoscape 2.8: new features for data integration and network visualization. *Bioinformatics* 27, 431–432. doi: 10.1093/bioinformatics/btq675

Sun, D. G., Xin, B. C., Wu, D., Zhou, L., Wu, H. B., Gong, W., et al. (2017). miR-140-5p-mediated regulation of the proliferation and differentiation of human dental pulp stem cells occurs through the lipopolysaccharide/toll-like receptor 4 signaling pathway. *Eur. J. Oral Sci.* 125, 419–425. doi: 10.1111/eos.12384

Tao, S. C., Yuan, T., Zhang, Y. L., Yin, W. J., Guo, S. C., and Zhang, C. Q. (2017). Exosomes derived from miR-140-5p-overexpressing human synovial mesenchymal stem cells enhance cartilage tissue regeneration and prevent osteoarthritis of the knee in a rat model. *Theranostics* 7, 180–195. doi: 10.7150/thno.17133

Tseng, A. M., Chung, D. D., Pinson, M. R., Salem, N. A., Eaves, S. E., and Miranda, R. C. (2019). Ethanol exposure increases miR-140 in extracellular vesicles: implications for fetal neural stem cell proliferation and maturation. *Alcohol. Clin. Exp. Res.* 43, 1414–1426. doi: 10.1111/acer.14066

Vejnar, C. E., Blum, M., and Zdobnov, E. M. (2013). miRmap web: comprehensive microRNA target prediction online. *Nucleic Acids Res.* 41, W165–W168. doi: 10.1093/nar/gkt430

Veraitch, O., Kobayashi, T., Imaizumi, Y., Akamatsu, W., Sasaki, T., Yamanaka, S., et al. (2013). Human induced pluripotent stem cell-derived ectodermal precursor cells contribute to hair follicle morphogenesis in vivo. *J. Invest. Dermatol.* 133, 1479–1488. doi: 10.1038/jid.2013.7

Wang, D., Zhang, Z., O'Loughlin, E., Wang, L., Fan, X., Lai, E. C., et al. (2013). MicroRNA-205 controls neonatal expansion of skin stem cells by modulating the PI(3)K pathway. *Nat. Cell Biol.* 15, 1153–1163. doi: 10.1038/ncb2827

Wang, J., Miao, Y., Huang, Y., Lin, B., Liu, X., Xiao, S., et al. (2018). Bottom-up nanoencapsulation from single cells to tunable and scalable cellular spheroids for hair follicle regeneration. *Adv. Healthc. Mater.* 7:1700447. doi: 10.1002/adhm.201700447

Wang, X., Hsi, T. C., Guerrero-Juarez, C. F., Pham, K., Cho, K., McCusker, C. D., et al. (2015). Principles and mechanisms of regeneration in the mouse model for wound-induced hair follicle neogenesis. *Regeneration (Oxf.)* 2, 169–181. doi: 10.1002/reg2.38

Wang, Z., Hu, J., Pan, Y., Shan, Y., Jiang, L., Qi, X., et al. (2018). miR-140-5p/miR-149 affects chondrocyte proliferation, apoptosis, and autophagy by targeting FUT1 in osteoarthritis. *Inflammation* 41, 959–971. doi: 10.1007/s10753-018-0750-6

Watt, F. M., Estrach, S., and Ambler, C. A. (2008). Epidermal Notch signalling: differentiation, cancer and adhesion. *Curr. Opin. Cell Biol.* 20, 171–179. doi: 10.1016/j.ceb.2008.01.010

Witwer, K. W., Buzas, E. I., Bemis, L. T., Bora, A., Lasser, C., Lotvall, J., et al. (2013). Standardization of sample collection, isolation and analysis methods in extracellular vesicle research. *J. Extracell. Vesicles* 2:20360. doi: 10.3402/jev.v2i0.20360

Wong, N., and Wang, X. (2015). miRDB: an online resource for microRNA target prediction and functional annotations. *Nucleic Acids Res.* 43, D146–D152. doi: 10.1093/nar/gku1104

Yan, H., Gao, Y., Ding, Q., Liu, J., Li, Y., Jin, M., et al. (2019). Exosomal micro RNAs derived from dermal papilla cells mediate hair follicle stem cell proliferation and differentiation. *Int. J. Biol. Sci.* 15, 1368–1382. doi: 10.7150/ijbs.33233

Yang, C. C., and Cotsarelis, G. (2010). Review of hair follicle dermal cells. *J. Dermatol. Sci.* 57, 2–11. doi: 10.1016/j.jdermsci.2009.11.005

Yi, R. (2017). Concise review: mechanisms of quiescent hair follicle stem cell regulation. *Stem Cells* 35, 2323–2330. doi: 10.1002/stem.2696

Yu, X., Odenthal, M., and Fries, J. W. (2016). Exosomes as miRNA carriers: formation-function-future. *Int. J. Mol. Sci.* 17:2028. doi: 10.3390/ijms17122028

Zhang, H., Zhu, N. X., Huang, K., Cai, B. Z., Zeng, Y., Xu, Y. M., et al. (2016). iTRAQ-based quantitative proteomic comparison of early- and late-passage human dermal papilla cell secretome in relation to inducing hair follicle regeneration. *PLoS One* 11:e167474. doi: 10.1371/journal.pone.0167474

Zhang, L., Stokes, N., Polak, L., and Fuchs, E. (2011). Specific microRNAs are preferentially expressed by skin stem cells to balance self-renewal and early lineage commitment. *Cell Stem Cell* 8, 294–308. doi: 10.1016/j.stem.2011.01.014

Zhang, P., Kling, R. E., Ravuri, S. K., Kokai, L. E., Rubin, J. P., Chai, J. K., et al. (2014). A review of adipocyte lineage cells and dermal papilla cells in hair follicle regeneration. *J. Tissue Eng.* 5:1548681038. doi: 10.1177/2041731414556850

Zhao, B., Chen, Y., Yang, N., Chen, Q., Bao, Z., Liu, M., et al. (2019). miR-218-5p regulates skin and hair follicle development through Wnt/β-catenin signaling pathway by targeting SFRP2. *J. Cell. Physiol.* 234, 20329–20341. doi: 10.1002/jcp.28633

Zhou, L., Wang, H., Jing, J., Yu, L., Wu, X., and Lu, Z. (2018). Regulation of hair follicle development by exosomes derived from dermal papilla cells. *Biochem. Biophys. Res. Commun.* 500, 325–332. doi: 10.1016/j.bbrc.2018.04.067

Zhou, W., Fong, M. Y., Min, Y., Somlo, G., Liu, L., Palomares, M. R., et al. (2014). Cancer-secreted miR-105 destroys vascular endothelial barriers to promote metastasis. *Cancer Cell* 25, 501–515. doi: 10.1016/j.ccr.2014.03.007

Zhu, Y., Wang, Y., Zhao, B., Niu, X., Hu, B., Li, Q., et al. (2017). Comparison of exosomes secreted by induced pluripotent stem cell-derived mesenchymal stem cells and synovial membrane-derived mesenchymal stem cells for the treatment of osteoarthritis. *Stem Cell Res. Ther.* 8:64. doi: 10.1186/s13287-017-0510-9

Conflict of Interest: The authors declare that the research was conducted in the absence of any commercial or financial relationships that could be construed as a potential conflict of interest.

Copyright © 2020 Chen, Huang, Liu, Chen, Fu, Yang, Wang, Du, Wen, Miao and Hu. This is an open-access article distributed under the terms of the Creative Commons Attribution License (CC BY). The use, distribution or reproduction in other forums is permitted, provided the original author(s) and the copyright owner(s) are credited and that the original publication in this journal is cited, in accordance with accepted academic practice. No use, distribution or reproduction is permitted which does not comply with these terms.

frontiers in Cell and Developmental Biology

ORIGINAL RESEARCH
published: 11 January 2021
doi: 10.3389/fcell.2020.582282

Increased Expression of Zyxin and Its Potential Function in Androgenetic Alopecia

Qingmei Liu[1†], Xiangguang Shi[1†], Yue Zhang[1†], Yan Huang[2], Kai Yang[3], Yulong Tang[2], Yanyun Ma[2], Yuting Zhang[2], Ji'an Wang[1], Li Zhang[3], Qi Zhang[1], Xiao Liu[1], Jinran Lin[1], Jiucun Wang[2,4,5*] and Wenyu Wu[1,3*]*

[1] Department of Dermatology, Huashan Hospital, Fudan University, Shanghai, China, [2] State Key Laboratory of Genetic Engineering, Collaborative Innovation Center for Genetics and Development, School of Life Sciences, Fudan University, Shanghai, China, [3] Department of Dermatology, Jing'an District Central Hospital, Shanghai, China, [4] Human Phenome Institute, Fudan University, Shanghai, China, [5] Research Unit of Dissecting the Population Genetics and Developing New Technologies for Treatment and Prevention of Skin Phenotypes and Dermatological Diseases (2019RU058), Chinese Academy of Medical Sciences, Beijing, China

OPEN ACCESS

Edited by:
Mingxing Lei,
Chongqing University, China

Reviewed by:
Yuhong Li,
Army Medical University, China
Xingqi Zhang,
First Affiliated Hospital of Sun Yat-sen University, China
Julia Li Zhong,
Chongqing University, China

***Correspondence:**
Wenyu Wu
wuwenyu@huashan.org.cn
Jiucun Wang
jcwang@fudan.edu.cn
Jinran Lin
jinranlin@fudan.edu.cn

[†] These authors have contributed equally to this work

Specialty section:
This article was submitted to Stem Cell Research, a section of the journal Frontiers in Cell and Developmental Biology

Received: 11 July 2020
Accepted: 27 November 2020
Published: 11 January 2021

Citation:
Liu Q, Shi X, Zhang Y, Huang Y, Yang K, Tang Y, Ma Y, Zhang Y, Wang J, Zhang L, Zhang Q, Liu X, Lin J, Wang J and Wu W (2021) Increased Expression of Zyxin and Its Potential Function in Androgenetic Alopecia. Front. Cell Dev. Biol. 8:582282. doi: 10.3389/fcell.2020.582282

Androgenetic alopecia (AGA) is the most common progressive form of hair loss, occurring in more than half of men aged > 50 years. Hair follicle (HF) miniaturization is a feature of AGA, and dermal papillae (DP) play key roles in hair growth and regeneration by regulating follicular cell activity. Previous studies have revealed that adhesion signals are important factors in AGA development. Zyxin (ZYX) is an actin-interacting protein that is essential for cell adhesion and migration. The aim of this research was to investigate the expression and potential role of ZYX in AGA. Real-time polymerase chain reaction (RT-PCR) analysis revealed that ZYX expression was elevated in the affected frontal HF of individuals with AGA compared to unaffected occipital HF. Moreover, increased ZYX expression was also observed within DP using immunofluorescence staining. Our *in vivo* results revealed that ZYX knockout mice showed enhanced hair growth and anagen entry compared to wild-type mice. Reducing ZYX expression in *ex vivo* cultured HFs by siRNA resulted in the enhanced hair shaft production, delayed hair follicle catagen entry, increased the proliferation of dermal papilla cells (DPCs), and upregulated expression of stem cell-related proteins. These results were further validated in cultured DPCs *in vitro*. To further reveal the mechanism by which ZYX contributes to AGA, RNA-seq analysis was conducted to identify gene signatures upon ZYX siRNA treatment in cultured hair follicles. Multiple pathways, including focal adhesion and HIF-1 signaling pathways, were found to be involved. Collectively, we discovered the elevated expression of ZYX in the affected frontal hair follicles of AGA patients and revealed the effects of ZYX downregulation on *in vivo* mice, *ex vivo* hair follicles, and *in vitro* DPC. These findings suggest that ZYX plays important roles in the pathogenesis of AGA and stem cell properties of DPC and may potentially be used as a therapeutic target in AGA.

Keywords: androgenetic alopecia, Zyxin, hair follicle, dermal papilla cell, RNA-seq

INTRODUCTION

Androgenic alopecia (AGA) is a common chronic and progressive alopecia disease that can occur in both men and women. The incidence of AGA is higher in Caucasians than in other populations (Otberg et al., 2007). At the same time, the incidence of AGA has a certain age correlation (Severi et al., 2003). Although AGA is not life-threatening, it has a major impact on an individual's appearance and self-confidence and indirectly has a negative impact on the patient's life and social interactions. The main manifestations of AGA in males include frontotemporal hairline recession, whereas females mainly exhibit diffuse hair loss.

The hair cycle mainly consists of anagen, catagen, and telogen phases. In the normal population, the majority of hair is in the anagen phase and lasts the longest. However, in individuals with AGA, the anagen phase is shorter, while the telogen phase is longer. This change leads to the transformation of hair from terminal to vellus and hair follicle miniaturization in individuals with AGA (Lolli et al., 2017). Dermal papilla cells (DPC) exist in hair bulbs and play an important role in inducing hair follicle formation, as well as serve as the main site of androgen activity in hair follicles (Chew et al., 2016; Betriu et al., 2020). DPC can induce hair regeneration and maintain hair in the growth stage through its stem cell characteristics (Yang and Cotsarelis, 2010).

It is well-known that AGA is mainly caused by an increase in androgen levels regulated by genes, particularly dihydrotestosterone (DHT) in the local scalp, which makes the hair follicles smaller. A variety of signaling pathways are involved in the regulation of the hair cycle and hair follicle miniaturization, including Wnt/β-catenin, BMP, and JAK (Vasserot et al., 2019). There are differences in the protein expression level of some markers in the hair frontal parietal region and occipital region. Some inflammation-related markers are only expressed in the areas involved in AGA (Vogt et al., 2017). These differentially expressed genes are involved in several pathways, such as WNT/ β-catenin, androgen, and estrogen (Hochfeld et al., 2019). Differences in these pathways and gene expression levels affect the behavior of hair follicles, including DPC. DPC showed the characteristic of aggregated growth when cultured *in vitro*, which is closely related to the formation of hair follicles and the hair cycle. Previous studies have revealed that adhesion signals are important factors in AGA development. Focal adhesion and cell-to-cell adhesion play major roles in cell aggregation and the growth of DPC, and some extracellular matrices can also affect the aggregation and growth of DPC (Young et al., 2009; Yang et al., 2012).

Zyxin (ZYX), a cytoskeletal protein encoded by *ZYX*, was first described by Mary Beckerle in 1986 as an 82-kDa protein associated with adherent plaques such as focal adhesions (FAs) and actin filaments in cultured chicken embryo fibroblasts (Belgardt et al., 2020). Detailed studies have identified that ZYX is located in FAs and actin stress fibers (Crawford and Beckerle, 1991), and it is structurally and functionally bound to the cytoskeleton (Crawford and Beckerle, 1991). Under stable conditions, ZYX interacts with various integrins, actin-binding, and signaling molecules to affect cell adhesion, movement, and signal transduction. ZYX can also shuffle between the cytoplasm and the nucleus. In the nucleus, ZYX interacts with transcription factors to enhance gene expression (Wang and Gilmore, 2003). Moreover, ZYX constitutes a direct signaling pathway from cytoskeletal-plasma membrane networks to the nucleus, similar to the Wnt/β-catenin pathway and the AP-1 co-activator JAB1 (Wang and Gilmore, 2003). Furthermore, previous studies also revealed that ZYX could mediate the cooperation between Hippo and TGF-β signaling pathways (Ma et al., 2016). The Wnt/β-catenin, Hippo and TGF-β signaling pathways had been implicated in the development of AGA. Therefore, we hypothesize that ZYX plays an important role in AGA.

In the present study, we investigated the expression level and potential role of ZYX on AGA. First, we discovered the upregulated expression of ZYX in the affected frontal HF of AGA patients compared to the unaffected occipital HF. Then, we studied the effect of ZYX downregulation on dorsal hair growth in C57BL/6 mice, cultured hair follicles, and dermal papilla cells. Moreover, we conducted a transcriptome study to delineate the pathways regulated by ZYX. This study provides insights into the molecular mechanism of AGA and may facilitate in the development of novel strategies to control hair loss.

MATERIALS AND METHODS

Assessment of Hair Growth *in vivo*

Wild-type (WT) and ZYX-knockout C57BL/6 mice (6–8 weeks old) were used in the experiment and maintained according to the guidelines approved by the Institutional Animal Care and Use Committee of Fudan University. The dorsal hair of all of the mice was depilated by applying liquid rosin under anesthesia for observation and anagen induction. Baseline and subsequent hair growth were recorded by the same digital camera at a uniform angle and manner for subsequent comparison.

Human Hair Follicle Organ Dissection and Culture

The scalp hair follicle units of the bald region and non-bald region were obtained from 20 male hair transplant patients with ethical approval and informed consent. The average age of the patients was 30.85 ± 7.31 years, and the average duration of disease was 5.55 ± 2.44 years. According to the Norwood-Hamilton Scale, the degree of hair loss ranged from III V to VI (**Table 1**). Isolated anagen follicles were used in this study. The isolated human scalp hair follicles were cultured in Williams E medium (Gibco BRL, Grand Island, NY, USA) containing 2 mM glutamine, 10 ng/mL hydrocortisone, 100 U/mL penicillin, and 100 mg/mL streptomycin in 12-well plates at 37.0°C and 5% CO_2 atmosphere. For the *ex vivo* HF culture, HFs that grew to lengths of 0.3–0.5 mm after 24 h were selected for the subsequent experiment (Kwon et al., 2006).

Immunofluorescence Staining

The collected HF samples were embedded in paraffin sections. Then, the sections were sealed with bovine serum albumin and incubated overnight with the primary antibody at 4°C. The

TABLE 1 | Characteristics of all patients in this study.

Patient No.	Age (years)	Disease duration (years)	Classification (Norwood-Hamilton Scale)
1	22	3	IVA
2	25	5	IVA
3	27	5	VA
4	34	6	IV
5	28	6	V
6	30	5	V
7	27	5	V
8	28	3	IV
9	29	6	V
10	24	2	V
11	27	3	V
12	33	10	VI
13	47	12	V
14	50	6	IV
15	25	5	III V
16	30	5	IV
17	43	5	IV
18	27	10	VI
19	29	5	IV
20	32	4	III V

antibodies are ZYX (1:500, ab109316; Abcam, United Kingdom) and Ki67 (1:300, ab39012; Abcam). Then, the sections were incubated with a second antibody at room temperature for 1 h. After the second antibody was removed, the nuclei were counterstained with 4-amino-6-diamino-2-phenyl indole (DAPI, Beyotime Biotechnology, China). The stained sections were observed under a microscope (Olympus, Tokyo, Japan), and images were captured.

Isolation and Culture of hDPCs

DPCs were isolated from the isolated hair follicle bulb and transferred to a polystyrene Petri dish coated with bovine typeI collagen. The characteristics of the DPCs were assessed as shown in **Supplementary Figure 1**. Penicillin (100 U/mL), streptomycin (100 μg/mL), and 20% heat-inactivated fetal bovine serum were added at 37°C and in a 5% CO_2 humidified atmosphere and cultured in Dulbecco's modified Eagle's medium. The culture medium was changed every 3 days. The explants were maintained for several days, and when cell growth reached the subfusion state, the cells were harvested in Hank's equilibrium salt solution with 0.25% trypsin/10 mM EDTA and passaged at a ratio of 1:3. Then, the DP cells were cultured in DMEM containing 10% fetal bovine serum, and the third-generation cells were used in the experiment (Moon et al., 2013).

RNA Isolation, Reverse Transcription, and Real-Time PCR (qPCR)

RNA was extracted from DPCs using TRIzol (Invitrogen), and complementary DNA (cDNA) was synthesized using a high-capacity cDNA reverse transcriptase kit (Application Biosystems). Real-time PCR was performed in a 384-well format with SYBR Green I PCR Kit (Takara, Shiga, Japan) and analyzed in an ABI Prism 7900 detector system (Applied Biological System). The housekeeping gene *GADPH* was used as endogenous control, and the expression of related genes was calculated by the $^{\Delta\Delta}$Ct method (Livak and Schmittgen, 2001).

Cell Proliferation Assay

Cell proliferation was monitored using the xCELLigence system (Baselot in Switzerland and ACEA Biosciences in San Diego, CA, USA). First, the background impedance of E-plate 16 (Roche, East Sussex, UK) was measured using only the growth medium. Then, the 50 μL suspension cells were inoculated into the hole of E-plate 16 and placed in a CO_2 incubator. Real-time cell analysis (RTCA) software was used to calculate the growth parameters. The cell index was used to represent the percentage of cells in the pore.

Aggregation Detection of DPCs

First, 6×10^4 cells DPCs were seeded into a 12-plate per well and incubated for 24 h and 72 h for cell attachment. Cells were cultured in the completed DMEM. The aggregation behavior of DPCs was observed under a phase-contrast microscope.

RNA-seq Data Analysis

One to two micrograms of total RNA extracted from hair follicles was used to prepare sequencing libraries using a TruSeq RNA Prep Kit (Illumina, San Diego, CA, USA), and RNA-seq was performed using a genome analyzer HiSeq X Ten (Illumina). FastQC was used to investigate the sequence quality, and FASTX Toolkit was employed to remove low-quality reads. Kallisto (version 0.44.0) was used for transcriptional quantification without alignment, and tximport was employed to integrate abundance.h5 files to an expressed gene count file, which was used to detect differentially expressed genes (DEGs) using DESeq2 according to the analysis manual. Genes with a P-value < 0.05 and $|\log_2 \text{fold-change}| > 1$ were determined as DEGs. Kyoto Encyclopedia of Genes and Genomes (KEGG) and Reactome pathway analyses of DEGs were conducted with R Package cluster Profiler (version 3.8.1). The R package ggplot2 (version 3.0.0) was used to draw bar charts, dot plots, and volcano maps, whereas pheatmap (version 1.0.12) was employed to draw a heat map.

Statistical Analysis

All of the data were analyzed by SPSS 16.0 statistical software, and two independent t-tests or one-way ANOVA were used for comparison between groups. Differences with a $P < 0.05$ were deemed to be statistically significant.

RESULTS

ZYX Expression Is Upregulated in AGA HFs and Dermal Papilla Cells

To examine the expression levels of ZYX in AGA, 20 paired HF tissues from AGA patients were collected. HE staining showed that the AGA HFs from occipital nonbald and frontal bald

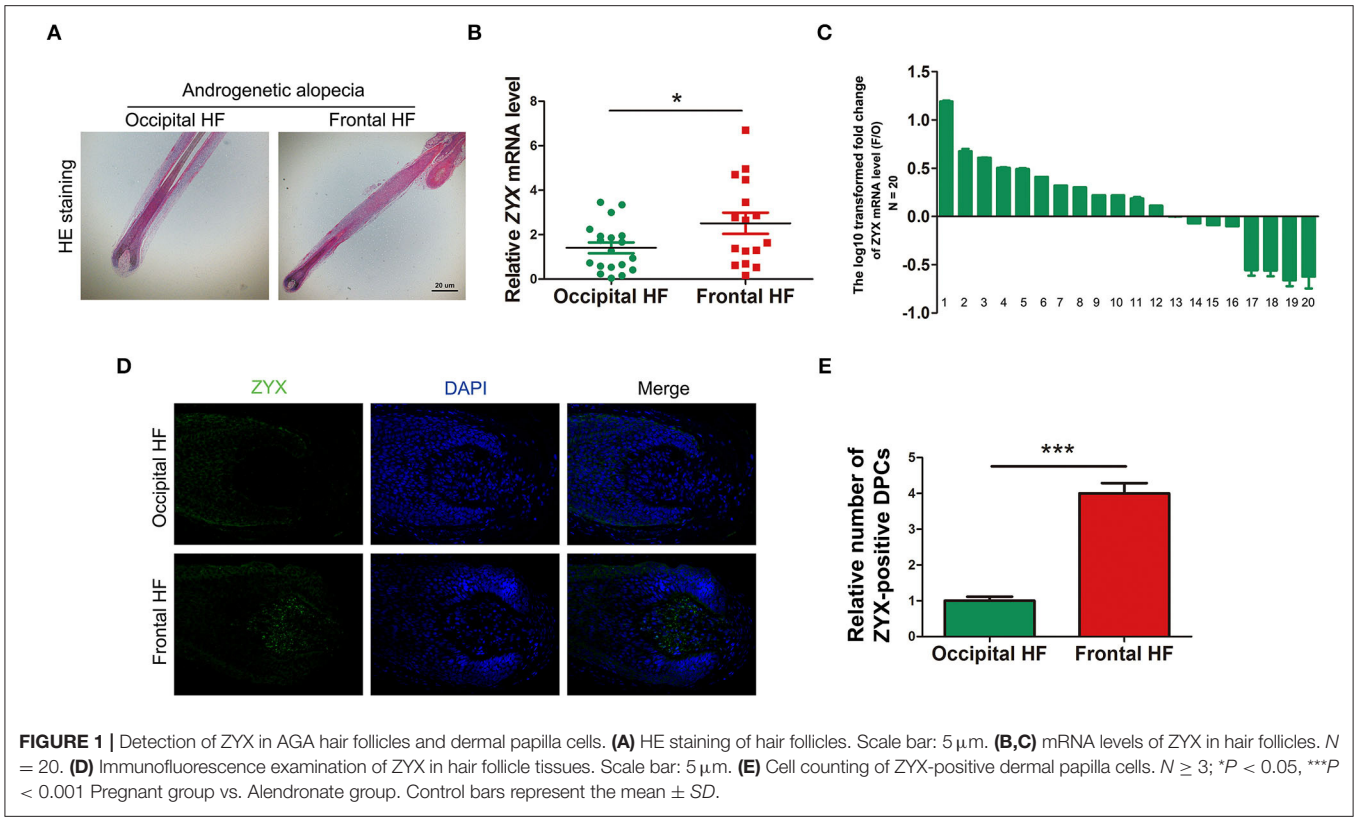

FIGURE 1 | Detection of ZYX in AGA hair follicles and dermal papilla cells. **(A)** HE staining of hair follicles. Scale bar: 5 μm. **(B,C)** mRNA levels of ZYX in hair follicles. $N = 20$. **(D)** Immunofluorescence examination of ZYX in hair follicle tissues. Scale bar: 5 μm. **(E)** Cell counting of ZYX-positive dermal papilla cells. $N \geq 3$; $^{*}P < 0.05$, $^{***}P < 0.001$ Pregnant group vs. Alendronate group. Control bars represent the mean ± *SD*.

region were anagen HFs (**Figure 1A**). Then, qPCR analysis was performed and the results showed that the mRNA levels of *ZYX* were significantly higher (∼2-fold) in the frontal HF compared to the unaffected occipital HF (**Figure 1B**). In addition, among the 20 paired tissues from the AGA HF, 12 frontal HFs (60%) showed a significant increase in *ZYX* mRNA expression when compared with paired occipital HFs (**Figure 1C**). An integrity HF is composed of various cell populations that contribute to the unique biology of HFs during HF formation. Therefore, an immunofluorescence staining assay was used to explore certain cell types that respond to the upregulation of ZYX in AGA HFs. Our results further showed that ZYX was widely expressed in every cell type, but specifically increased in dermal papilla cells (**Figure 1D**). Additionally, the number of ZYX-positive DP cells increased in the frontal HF group compared with the occipital HF group (**Figure 1E**). Collectively, we discovered that ZYX expression increased AGA HFs and DPs, which suggests that ZYX play a stimulatory role in AGA.

ZYX Deletion Promotes Hair Regrowth *in vivo*

Depilation is an ideal strategy for investigating hair growth. After hair removal, the HF cell cycle was synchronized and accumulated cells in the regrowth phase. To test whether ZYX plays a role in HF cell cycle, WT and *Zyx*-knockout (*Zyx*-/-) mice were depilated. Then, four parameters, namely, length, HF percentage and cycling score (HCS), diameter of hair bulbs, and skin thickness were evaluated to assess HF growth rate. At 24 days after hair removal, photos were taken from five WT and five KO mice; these showed that hair had grown and covered the back skin of the Zyx-/- group, while there were still some bare areas in the WT mice (**Figure 2A**). The hair shafts were longer and thicker in the *Zyx*-/- mice compared to the WT mice (**Figure 2B**). We then assessed the morphology of *Zyx*-/-HFs that had thicker skin, and histomorphometric analysis revealed that the subcutis was surrounded by more melanin and bulbs. However, the WT mice showed that most of the hair bulbs were at the dermis subcutis border (**Figure 2C**). Bulb diameter, skin thickness, and HCS were higher in *Zyx*-/- mice when compared to WT mice (**Figure 2D**). These results suggest that ZYX deletion facilitates hair regrowth.

ZYX Knockdown Promotes HF Growth *in vitro*

Cell cycle, apoptosis, and inductivity play important roles in the proliferation and regeneration of HFs. To access whether ZYX is essential for HF development and for phase transition in the HF cycle, human HFs obtained from the AGA patients were treated with *ZYX* siRNA. Histomorphometric analysis showed that ZYX knockdown significantly increased the length of hair shafts compared to the negative control (NC) (**Figure 3A**). Consistently, 75% of the HFs in the *ZYX* siRNA group was anagen and 25% was catagen, whereas the NC group was 40% anagen and 60% catagen, implying that ZYX deficiency retains the HF cycle in the anagen stage (**Figure 3B**). Furthermore, HE and immunofluorescence staining revealed larger bulb diameter and increased the number of Ki67-positive cells in *si-ZYX* HFs than that in NC HFs (**Figures 3C,D**). We next aimed to examine the cell apoptosis effect on *ZYX*-silenced HFs. We then observed

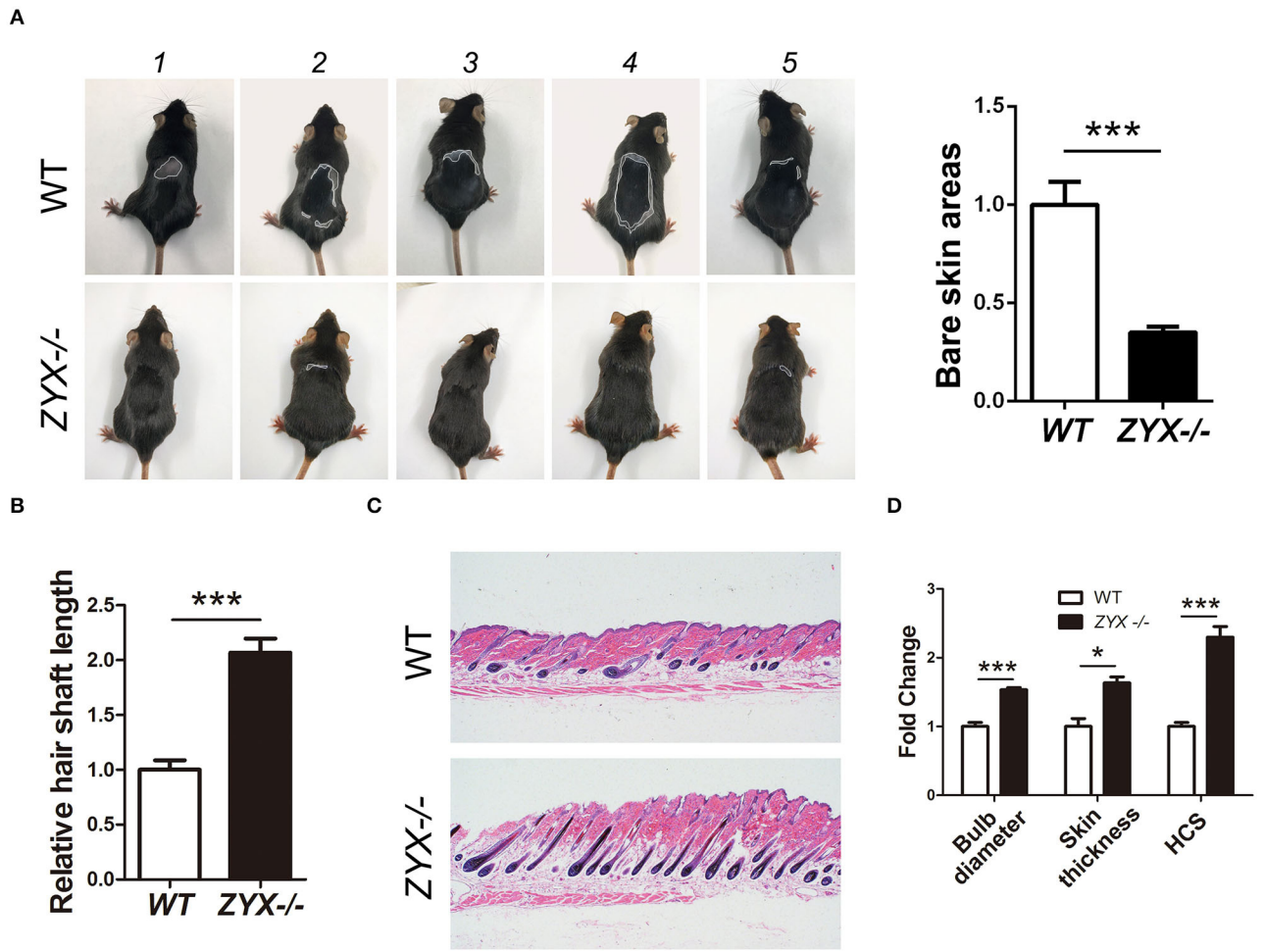

FIGURE 2 | Effect of ZYX on hair growth in mice. **(A)** Size of hair covered skin area in *Zyx-/-* and WT mice. Different morphology of hair shaft **(B)** and hair follicles **(C)** in *Zyx-/-* and WT mice. **(D)** HF percentage and cycling score in *Zyx-/-* and WT mice. Scale bar: 5 μm, $N = 6$ per group; $^{*}P < 0.05$, $^{***}P < 0.001$. Control bars represent the mean ± *SD*.

that HFs transfected with *si-ZYX* led to a significant reduction in TUNEL-positive cells (**Figure 3E**). These results suggested that ZYX inhibits HF growth by regulating fibroblast HF cycle and promoting cell apoptosis. To further define the protective role of *si-ZYX* in hair growth, we examined stem cell markers. As expected, si-ZYX significantly induced the expression of SOX2, CD133, and NOG (**Figure 3F**). Taken together, we concluded that *si-ZYX* promoted HF growth *in vitro* by delaying catagen entry, suppressing cell apoptosis, and sustaining the cell inductivity.

ZYX Knockdown Sustains the Aggregation Behavior and Facilitates the Proliferation of DP Cells *in vitro*

Based on the fact that dermal papilla cells (DPCs) play a critical role in HF growth, formation, inductivity sustainment, and cycling, we investigated the role of ZYX in DP cells. ZYX expression was first knocked down in DPCs by siRNA (**Figure 4A**). Then, an RTCA assay was performed, which showed that the cell index of DPCs subjected to *si-ZYX* treatment was significantly higher than the NC cells, suggesting that ZYX imparts anti-proliferative effects on DPCs (**Figures 4B,C**). Accordingly, DPCs treated with *si-ZYX* exhibited an increase in the percentage of cells in the S phase, which was accompanied by a decrease in the percentage of G1 phase cells (**Figures 4D,E**). Moreover, *si-ZYX* increased the mRNA levels of cell inductivity marker, including SOX2, CD133, and NOG (**Figure 4F**). Consistently, a cell aggregation assay further revealed that knocking down ZYX facilitated sphere formation (**Figure 4G**). Taken together, ZYX knockdown accelerated DPC growth by regulating the cell cycle and inducing the aggregation behavior of DPCs.

Gene Expression Profiles Validate the Growth-Promotional Effect of *si-ZYX* on HFs

To elucidate the potential mechanisms underlying the anti-proliferative role of ZYX in HFs, RNA sequencing (RNA-seq) was performed. Heat map analysis of all of the DEGs based on

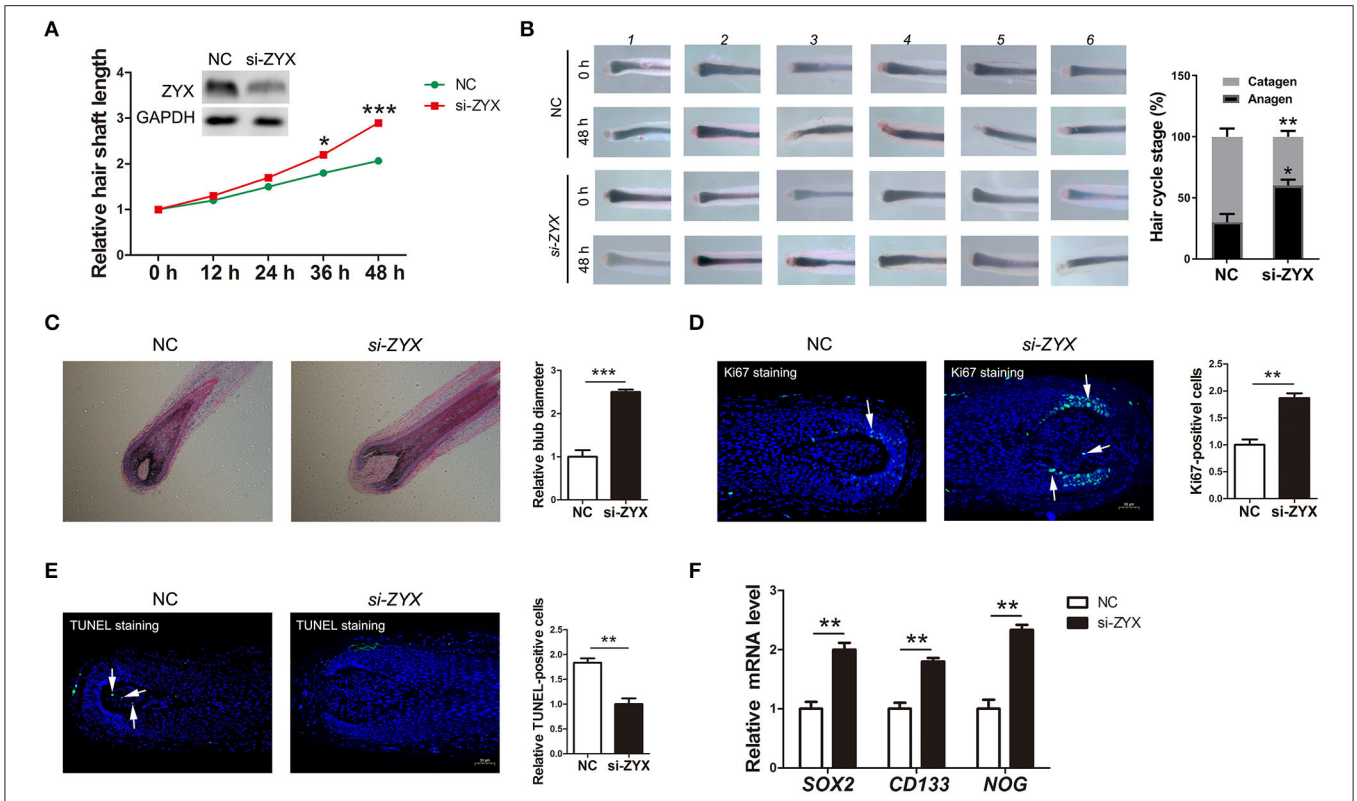

FIGURE 3 | The ratio of hair follicle growth after ZYX knockdown *in vitro*. **(A)** Measurement of the length of hair shaft in ZYX knockdown and negative control groups. **(B)** Distribution of hair follicle cycle in ZYX knockdown and control groups. **(C,D)** Bulb diameter and cell counting of Ki67-positive cells in si-ZYX HFs and NC HFs. **(E)** Evaluation of apoptosis using the TUNEL method after ZYX knockdown. **(F)** Inductivity marker expression in si-ZYX HFs. $^{*}P < 0.05$, $^{**}P < 0.01$, $^{***}P < 0.001$. Control bars represent the mean ± *SD*.

RNA-seq assay revealed that the gene expression profiles of the NC and ZYX siRNA treatment groups were distinct (**Figure 5A**). A total of 1,131 DEGs were identified between the two groups, with 576 upregulated DEGs and 555 down-regulated DEGs in *si-ZYX*, respectively (**Figure 5B**). Further cluster analysis showed that the upregulated DEGs are involved in cell cycle, apoptosis, and other metabolic pathways (e.g., glutathione and pyrimidine), whereas the downregulated DEGs are involved in focal adhesion, HIF-1, PI3K-Akt, MAPK, and other metabolic pathways (e.g., cholesterol and glycolysis) (**Figures 5C,D**). Taken together, the RNA-Seq data indicated that systemic changes in biopathways were induced by knocking down ZYX.

DISCUSSION

AGA is the most common form of hair loss in humans, and it is characterized by the miniaturization of hair follicles and gradual hair loss. AGA causes cosmetic problems and psychological distress in affected individuals. The key pathophysiological changes of AGA are limited to HFs in the bald and nonbald regions of the scalp. To date, numerous DEGs and pathways have been identified, including those related to WNT/β-catenin, androgen, hair cycle regulation, hair keratin production, estrogen, melatonin, ephrin, ErbB, and Hippo signaling pathways (Vogt et al., 2017; Hochfeld et al., 2019). An improved understanding of the differences between HF populations and its contribution to AGA pathobiology is thus desirable.

Previous studies have revealed that adhesion signals are important factors in HF and AGA development. For example, α-parvin, which is a FA protein that couples integrins to actin cytoskeleton, is indispensable to HF development (Altstaetter et al., 2020). Furthermore, there is cross-talk between FA/integrin and Wnt signaling pathways, which is one of the most important signaling pathways in AGA (Ridgway et al., 2012). Therefore, we hypothesized that ZYX, an important FA molecule, imparts important effects on HF and AGA development. The present work was designed to study the role of ZYX in AGA. We found that Zyxin is upregulated in the affected frontal HFs of AGA patients compared to the unaffected occipital HFs. To further study the effect of ZYX on HF and AGA, we conducted *in vivo* and *in vitro* studies using mice, cultured HFs, and dermal papilla cells. Using *in vivo* experiments, *ex vivo* cultured HFs and *in vitro* DPCs, we found that reduced ZYX expression enhances hair shaft production, delays HF catagen entry, and enhances DPC proliferation and inductivity. Higher activity of DPCs delays the process of hair miniaturization and promotes shaft elongation. Hair shaft elongation is apparently negatively correlated to hair

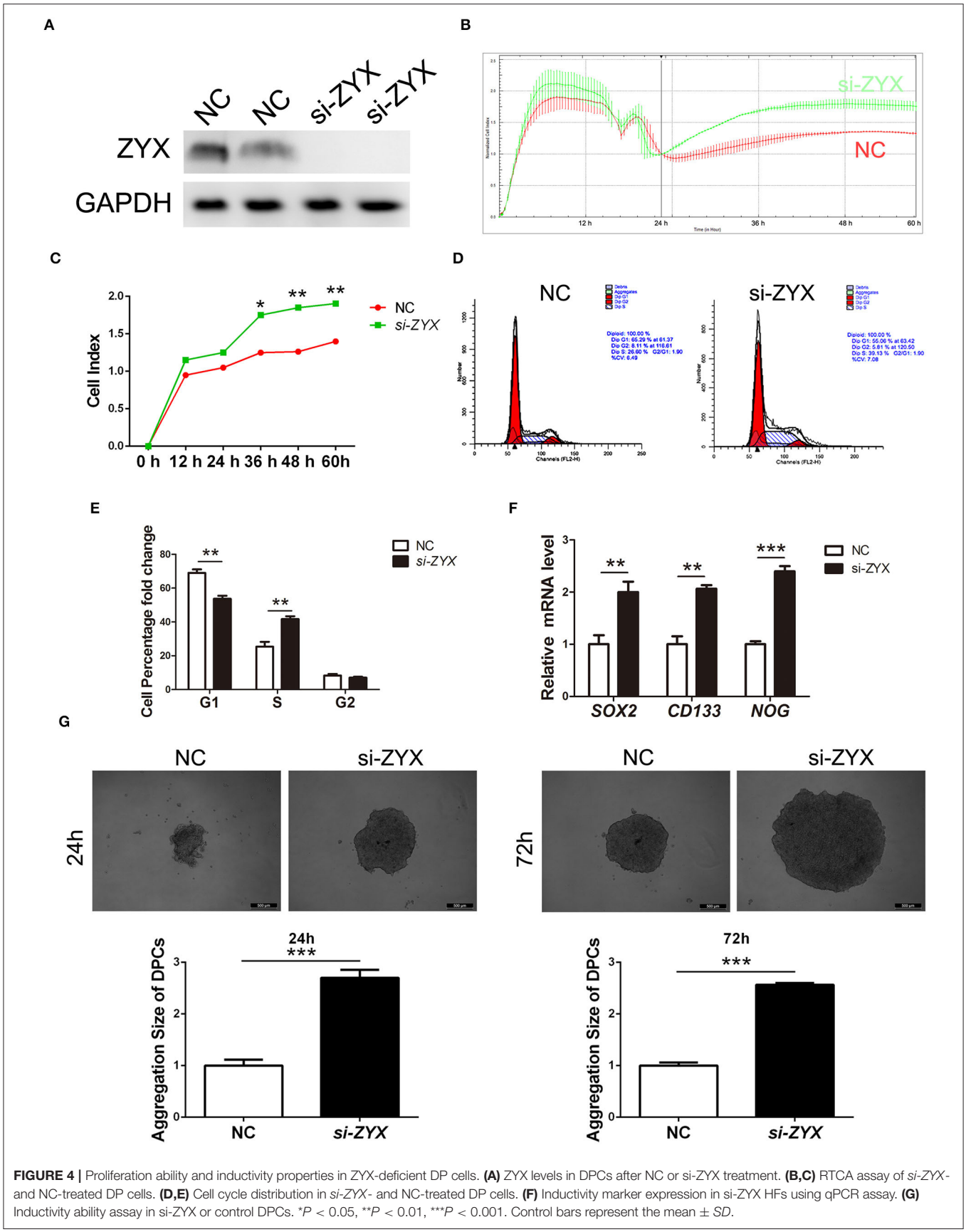

FIGURE 4 | Proliferation ability and inductivity properties in ZYX-deficient DP cells. **(A)** ZYX levels in DPCs after NC or si-ZYX treatment. **(B,C)** RTCA assay of *si-ZYX*- and NC-treated DP cells. **(D,E)** Cell cycle distribution in *si-ZYX*- and NC-treated DP cells. **(F)** Inductivity marker expression in si-ZYX HFs using qPCR assay. **(G)** Inductivity ability assay in si-ZYX or control DPCs. $^{*}P < 0.05$, $^{**}P < 0.01$, $^{***}P < 0.001$. Control bars represent the mean ± *SD*.

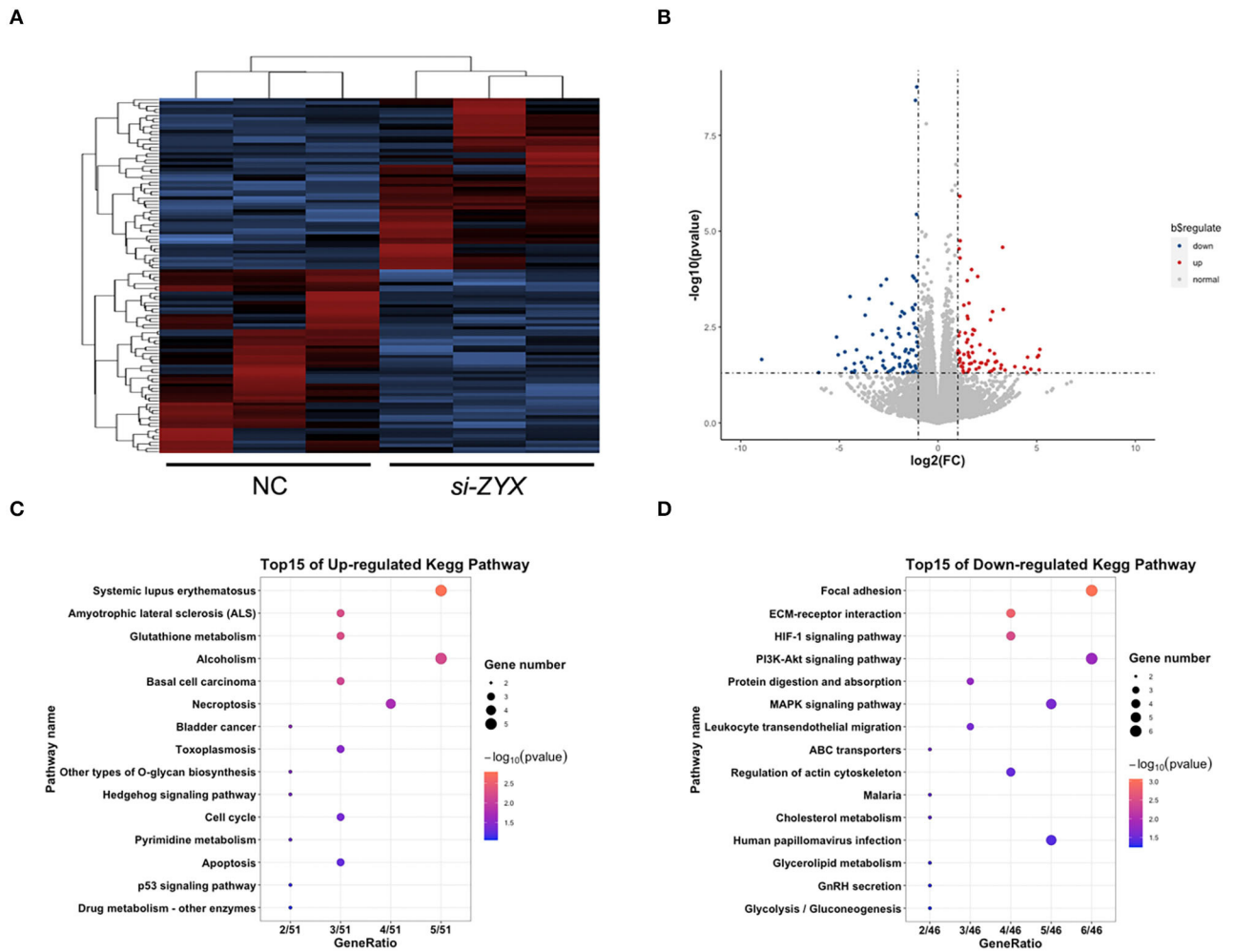

FIGURE 5 | Transcriptomics changes in ZYX-deficient DP cells. **(A)** Heat map of DEGs between ZYX knockdown and control DP cells. **(B)** List of the upregulated and downregulated DEGs. **(C,D)** KEGG analysis of the DEGs. $N = 3$ per group.

miniaturization. All of the above results show that ZYX plays an essential role in AGA, and ZYX inhibition might be an effective means for the treatment of AGA and the other hair loss diseases.

DPC stem cell properties play an important role in HF formation and hair growth cycle (Armstrong et al., 2006), and the augmentation of inductivity in DPCs could increase the rate of hair growth and control hair loss. A previous study revealed that the formation of stress fibers and FA complexes contribute to the activity of stem cells (Tucker et al., 2013), which in turn suggests that the FA signaling pathway plays a role in regulating cell inductivity. In the present study, we found that treatment of DPCs with ZYX siRNA significantly promotes cell proliferation. In addition, our real-time PCR analysis and immunocytochemistry staining revealed that ZYX knockdown by siRNA increased the mRNA and protein expression levels of stem cell markers, such as SOX2, CD133, and NOG, in cultured DPCs. Sox-2, a stem cell-related transcription factor, functions in pluripotency maintenance of DPCs. Sox-2 is a key regulator of hair growth that controls progenitor migration by fine-tuning BMP-mediated mesenchymal-epithelial crosstalk (Clavel et al., 2012). Moreover, the presence of stem cell protein markers such as CD133 is indicative of the inductive properties of DPCs. As previously reported, active treatments that induce or enhance stem cell properties of DPCs may be beneficial for hair loss therapeutics. Here, we discovered that ZYX downregulation enhances inductivity maintenance of cultured DPCs. These findings suggest that ZYX plays important roles in HFs and AGA by regulating the activity of DPC. The knowledge gained from our present study may be utilized in the development of novel strategies to control AGA hair loss.

RNA-seq detection was further performed to explore the mechanism of ZYX knockdown in AGA using cultured HFs. KEGG analysis revealed that cell cycle, apoptosis, focal adhesion, ECM-receptor interaction, HIF-1signaling pathway, and PI3K-AKT signaling pathways are the main regulatory pathways

that are related to the DEGs detected in ZYX siRNA-treated HFs. This study showed that si-ZYX promoted cultured HF growth, which led to a significant reduction of TUNEL-positive cells in HFs and facilitated DP cell proliferation (**Figures 3**, **4**). These findings also showed that cell cycle and apoptosis pathways are involved in the role of ZYX. Furthermore, RT-PCR was performed to detect changes in the expression level of pathway-related genes. **Supplementary Figure 2** shows that the expression levels of PLCB1 (metabolic pathway-related gene), ALDOC/TIMP1/LDHA (HIF-1 signaling pathway-related genes), and ITGB3 (focal adhesion-related gene) were altered after ZYX siRNA treatment. Therefore, we inferred that the effects of ZYX on HF and AGA are also related to FA, HIF-1, and metabolic signaling pathways. ZYX is a classical cytoskeletal protein that is related to FA. Cell adhesion molecules, including cadherins and integrins, are key regulators of stem cell growth and differentiation, for both hair follicle epithelia and epidermal keratinocytes (Akiyama et al., 2000). Integrins and cadherins play a major role in hair follicle growth and proliferation (Silva et al., 2020). A combination of activities simultaneously influences the HIF-1α pathway processes to increase hair density (Juchaux et al., 2020). Minoxidil, an FDA-approved topical drug for AGA treatment, activates an angiogenic pathway HIF-1-VEGF, a potential positive pharmacologic effect for hair growth. Treatment methods against the HIF-1 signaling pathway and hypoxia may be potentially used for the treatment of hair loss. However, we found that the HIF-1 signaling pathway was downregulated by siZYX in this study. Our *in vivo* and *in vitro* data indicated that ZYX plays a role in HF and AGA by regulating the FA signaling pathway via the ITGB1 and HIF-1 signaling pathways, although more research is needed to explore the underlying mechanisms.

CONCLUSION

This is the first report that describes the upregulated expression of ZYX in the affected frontal HF of AGA patients compared to the unaffected occipital HF. We found that reduced ZYX expression by siRNA enhances hair shaft production, delays HF catagen entry, and DPC proliferation and inductivity. These findings suggest that ZYX plays important roles in the pathogenesis of AGA and stem cell properties of DPCs, and thus ZYX may be potentially used as a therapeutic target in AGA.

DATA AVAILABILITY STATEMENT

The original contributions presented in the study are included in the article/**Supplementary Material**, further inquiries can be directed to the corresponding author/s.

ETHICS STATEMENT

The studies involving human participants were reviewed and approved by Huashan hospital, Fudan University. The patients/participants provided their written informed consent to participate in this study. The animal study was reviewed and approved by Fudan Universtiy.

AUTHOR CONTRIBUTIONS

WW, JiuW, and JL conceived and designed the work. QL, XS, YueZ, and YH performed research and collected and analyzed the data. QZ, YT, and YM analyzed the data. KY, Ji'aW, and LZ collected human tissue samples. QL, XS, and YutZ wrote the manuscript. XL modified the manuscript. All authors read and approved the final manuscript.

FUNDING

This study was supported by the grants from Shanghai Engineering Technology Research Center of Hair Medicine (19DZ2250500), Science and Technology Committee of Shanghai Municipality Guiding Fund (19411962400), Clinical Research Plan of SHDC (SHDC2020CR2033B), CAMS Innovation Fund for Medical Sciences (2019-I2M-5-066), National Science Foundation of China (81903203 and 81671550), Innovative research team of high-level local universities in Shanghai, and Shanghai Municipal Science and Technology Major Project (2017SHZDZX01).

SUPPLEMENTARY MATERIAL

The Supplementary Material for this article can be found online at: https://www.frontiersin.org/articles/10.3389/fcell.2020.582282/full#supplementary-material

REFERENCES

Akiyama, M., Smith, L. T., and Shimizu, H. (2000). Changing patterns of localization of putative stem cells in developing human hair follicles. *J. Invest. Dermatol.* 114, 321–327. doi: 10.1046/j.1523-1747.2000.00857.x

Altstaetter, J., Hess, M. W., Costell, M., and Montanez, E. (2020). alpha-parvin is required for epidermal morphogenesis, hair follicle development and basal keratinocyte polarity. *PLoS ONE* 15:e230380. doi: 10.1371/journal.pone.0230380

Armstrong, L., Hughes, O., Yung, S., Hyslop, L., Stewart, R., Wappler, I., et al. (2006). The role of PI3K/AKT, MAPK/ERK and NF kappa beta signalling in the maintenance of human embryonic stem cell pluripotency and viability highlighted by transcriptional profiling and functional analysis. *Hum. Mol. Genet* 15, 1894–1913. doi: 10.1093/hmg/ddl112

Belgardt, E., Steinberg, T., Husari, A., Dieterle, M. P., Hulter-Hassler, D., Jung, B., et al. (2020). Force-responsive Zyxin modulation in periodontal ligament cells is regulated by YAP rather than TAZ. *Cell. Signal* 72:109662. doi: 10.1016/j.cellsig.2020.109662

Betriu, N., Jarrosson-Moral, C., and Semino, C. E. (2020). Culture and differentiation of human hair follicle dermal papilla cells in a soft 3d self-assembling peptide scaffold. *Biomolecules* 10:684. doi: 10.3390/biom10050684

Chew, E. G. Y., Tan, J. H. J., Bahta, A. W., Ho, B. S. Y., Liu, X., Lim, T. C., et al. (2016). Differential expression between human dermal papilla cells from balding and non-balding scalps reveals new candidate genes for androgenetic alopecia. *J. Invest. Dermatol.* 136, 1559–1567. doi: 10.1016/j.jid.2016.03.032

Clavel, C., Grisanti, L., Zemla, R., Rezza, A., Barros, R., Sennett, R., et al. (2012). Sox2 in the Dermal papilla niche controls hair growth by fine-tuning BMP signaling in differentiating hair shaft progenitors. *Dev. Cell* 23, 981–994. doi: 10.1016/j.devcel.2012.10.013

Crawford, A. W., and Beckerle, M. C. (1991). Purification and characterization of zyxin, an 82,000-dalton component of adherens junctions. *J. Biol. Chem.* 266, 5847–5853

Hochfeld, L. M., Keller, A., Anhalt, T., Fricker, N., Nothen, M. M., Heilmann-Heimbach, S., et al. (2019). Insights into male androgenetic alopecia: differential gene expression profiling of plucked hair follicles and integration with genetic data. *J. Invest. Dermatol.* 139, 235–238. doi: 10.1016/j.jid.2018.06.182

Juchaux, F., Sellathurai, T., Perrault, V., Boirre, F., Delannoy, P., Bakkar, K., et al. (2020). A combination of pyridine-2, 4-dicarboxylic acid diethyl ester and resveratrol stabilizes hypoxia-inducible factor 1-alpha and improves hair density in female volunteers. *Int. J. Cosmet. Sci.* 42, 167–173. doi: 10.1111/ics.12600

Kwon, O. S., Oh, J. K., Kim, M. H., Park, S. H., Pyo, H. K., Kim, K. H., et al. (2006). Human hair growth *ex vivo* is correlated with *in vivo* hair growth: selective categorization of hair follicles for more reliable hair follicle organ culture. *Arch. Dermatol. Res.* 297, 367–371. doi: 10.1007/s00403-005-0619-z

Livak, K. J., and Schmittgen, T. D. (2001). Analysis of relative gene expression data using real-time quantitative PCR and the 2(-Delta Delta C(T)) method. *Methods* 25, 402–408. doi: 10.1006/meth.2001.1262

Lolli, F., Pallotti, F., Rossi, A., Fortuna, M. C., Caro, G., Lenzi, A., et al. (2017). Androgenetic alopecia: a review. *Endocrine* 57, 9–17. doi: 10.1007/s12020-017-1280-y

Ma, B., Cheng, H., Gao, R., Mu, C., Chen, L., Wu, S., et al. (2016). Zyxin-Siah2-Lats2 axis mediates cooperation between Hippo and TGF-beta signalling pathways. *Nat. Commun.* 7:11123. doi: 10.1038/ncomms11123

Moon, P.-G., Kwack, M. H., Lee, J.-E., Cho, Y.-E., Park, J.-H., Hwang, D., et al. (2013). Proteomic analysis of balding and non-balding mesenchyme-derived dermal papilla cells from androgenetic alopecia patients using on-line two-dimensional reversed phase-reversed phase LC-MS/MS. *J. Proteomics* 85, 174–191. doi: 10.1016/j.jprot.2013.04.004

Otberg, N., Finner, A. M., and Shapiro, J. (2007). Androgenetic alopecia. *Endocrinol. Metabol. Clin. North Am.* 36:379. doi: 10.1016/j.ecl.2007.03.004

Ridgway, R. A., Serrels, B., Mason, S., Kinnaird, A., Muir, M., Patel, H., et al. (2012). Focal adhesion kinase is required for beta-catenin-induced mobilization of epidermal stem cells. *Carcinogenesis* 33, 2369–2376. doi: 10.1093/carcin/bgs284

Severi, G., Sinclair, R., Hopper, J. L., English, D. R., McCredie, M. R. E., Boyle, P., et al. (2003). Androgenetic alopecia in men aged 40-69 years: prevalence and risk factors. *Br. J. Dermatol.* 149, 1207–1213. doi: 10.1111/j.1365-2133.2003.05565.x

Silva, L. M. A., Hsieh, R., Lourenco, S. V., Ottoni, V., Valente, N., and Fernandes, J. D. (2020). Immunoexpression of adhesion molecules during human fetal hair development. *Histol. Histopathol.* 35, 911–917. doi: 10.14670/HH-18-224

Tucker, R. P., Ferralli, J., Schittny, J. C., and Chiquet-Ehrismann, R. (2013). Tenascin-C and tenascin-W in whisker follicle stem cell niches: possible roles in regulating stem cell proliferation and migration. *J. Cell Sci.* 126, 5111–5115. doi: 10.1242/jcs.134650

Vasserot, A. P., Geyfman, M., and Poloso, N. J. (2019). Androgenetic alopecia: combing the hair follicle signaling pathways for new therapeutic targets and more effective treatment options. *Expert Opin. Ther. Targets*. 23, 755–771. doi: 10.1080/14728222.2019.1659779

Vogt, A., Pfannes, E. K. B., Fimmel, S., Hadam, S., Andruck, A., Kottner, J., et al. (2017). Infundibular protein and RNA microarray analyses from affected and clinically non-affected scalp in male androgenetic alopecia patients. *Exp. Dermatol.* 26, 518–521. doi: 10.1111/exd.13326

Wang, Y., and Gilmore, T. D. (2003). Zyxin and paxillin proteins: focal adhesion plaque LIM domain proteins go nuclear. *Biochim. Biophys. Acta Mol. Cell Res.* 1593, 115–120. doi: 10.1016/S0167-4889(02)00349-X

Yang, C.-C., and Cotsarelis, G. (2010). Review of hair follicle dermal cells. *J. Dermatol. Sci.* 57, 2–11. doi: 10.1016/j.jdermsci.2009.11.005

Yang, Y., Li, Y., Wang, Y., Wu, J., Yang, G., Yang, T., et al. (2012). Versican gene: regulation by the beta-catenin signaling pathway plays a significant role in dermal papilla cell aggregative growth. *J. Dermatol. Sci.* 68, 157–163. doi: 10.1016/j.jdermsci.2012.09.011

Young, T.-H., Tu, H.-R., Chan, C.-C., Huang, Y.-C., Yen, M.-H., Cheng, N.-C., et al. (2009). The enhancement of dermal papilla cell aggregation by extracellular matrix proteins through effects on cell-substratum adhesivity and cell motility. *Biomaterials* 30, 5031–5040. doi: 10.1016/j.biomaterials.2009.05.065

Conflict of Interest: The authors declare that the research was conducted in the absence of any commercial or financial relationships that could be construed as a potential conflict of interest.

Copyright © 2021 Liu, Shi, Zhang, Huang, Yang, Tang, Ma, Zhang, Wang, Zhang, Zhang, Liu, Lin, Wang and Wu. This is an open-access article distributed under the terms of the Creative Commons Attribution License (CC BY). The use, distribution or reproduction in other forums is permitted, provided the original author(s) and the copyright owner(s) are credited and that the original publication in this journal is cited, in accordance with accepted academic practice. No use, distribution or reproduction is permitted which does not comply with these terms.

frontiers in Cell and Developmental Biology

PERSPECTIVE
published: 12 January 2021
doi: 10.3389/fcell.2020.628114

Skin Cyst: A Pathological Dead-End With a New Twist of Morphogenetic Potentials in Organoid Cultures

Weiming Qiu[1†], Pei-Rong Gu[2†], Cheng-Ming Chuong[3] and Mingxing Lei[2,4*]*

[1] Department of Dermatology, General Hospital of Central Theater Command of Chinese People's Liberation Army, Wuhan, China, [2] Integrative Stem Cell Center, China Medical University Hospital, China Medical University, Taichung, Taiwan, [3] Department of Pathology, Keck School of Medicine, University of Southern California, Los Angeles, CA, United States, [4] "111" Project Laboratory of Biomechanics and Tissue Repair, Key Laboratory of Biorheological Science and Technology of the Ministry of Education, College of Bioengineering, Chongqing University, Chongqing, China

A cyst is a closed sac-like structure in which cyst walls wrap certain contents typically including air, fluid, lipid, mucous, or keratin. Cyst cells can retain multipotency to regenerate complex tissue architectures, or to differentiate. Cysts can form in and outside the skin due to genetic problems, errors in embryonic development, cellular defects, chronic inflammation, infections, blockages of ducts, parasites, and injuries. Multiple types of skin cysts have been identified with different cellular origins, with a common structure including the outside cyst wall engulfs differentiated suprabasal layers and keratins. The skin cyst is usually used as a sign in pathological diagnosis. Large or surfaced skin cysts affect patients' appearance and may cause the dysfunction or accompanying diseases of adjacent tissues. Skin cysts form as a result of the degradation of skin epithelium and appendages, retaining certain characteristics of multipotency. Surprisingly, recent organoid cultures show the formation of cyst configuration as a transient state toward more morphogenetic possibility. These results suggest, if we can learn more about the molecular circuits controlling upstream and downstream cellular events in cyst formation, we may be able to engineer stem cell cultures toward the phenotypes we wish to achieve. For pathological conditions in patients, we speculate it may also be possible to guide the cyst to differentiate or de-differentiate to generate structures more akin to normal architecture and compatible with skin homeostasis.

Keywords: skin homeostasis, stem cell, multipotency, regeneration, hair follicle, tissue engineering

OPEN ACCESS

Edited by:
Masatake Osawa, Gifu University, Japan

Reviewed by:
Hironobu Fujiwara, RIKEN, Japan
Krzysztof Kobielak, University of Warsaw, Poland

****Correspondence:***
Cheng-Ming Chuong
cmchuong@usc.edu
Mingxing Lei
mingxing@cqu.edu.cn

† These authors have contributed equally to this work

Specialty section:
This article was submitted to Stem Cell Research, a section of the journal Frontiers in Cell and Developmental Biology

Received: *11 November 2020*
Accepted: *17 December 2020*
Published: *12 January 2021*

Citation:
Qiu W, Gu P-R, Chuong C-M and Lei M (2021) Skin Cyst: A Pathological Dead-End With a New Twist of Morphogenetic Potentials in Organoid Cultures. Front. Cell Dev. Biol. 8:628114. doi: 10.3389/fcell.2020.628114

INTRODUCTION

Skin is the largest organ of the body in mammal. Along with the appendages, skin functions on regulating body temperature, defending against micro-organisms infection, and protecting the body from external harmful matters such as toxic substances and UV irradiation (Chuong et al., 2002). Skin is mainly composed of the epidermis and dermis. Epithelial-mesenchymal interactions allow development of several dynamic skin appendages such as hair follicle, sebaceous gland, sweat gland, etc., which play diverse roles in skin function (Lei et al., 2017a). Epithelial cells have apical-basal polarity and line up in a sheet. Cyst can form when epithelial cells fail to continue to the next

stages of morphogenesis. Progress has been made in the investigation of how skin cyst forms and why this structure can be developed. Interestingly, in skin organoid culture, we have observed cysts form transiently, but then they undergo further morphogenesis (Tang et al., 2002; Lei et al., 2017b). This makes us contemplate whether the cysts in the skin we have encountered are not bona fide dead-ends, but are structures stuck in a morphogenetic process that misses certain morphogenetic cues. Therefore, skin cysts may be rescuable with new twists as seen in the restoration of skin cells from adult mice that lose the regenerative ability to form hairs. Here we first review the more traditional knowledge of skin cyst pathology. Then we summarize recent progress on the formation of cyst configuration during tissue engineering of skin organoid formation. We present a new perspective that the skin cyst may be turned from a morphogenetic dead-end into a morphogenetic hub if we can explore its upstream and downstream events.

THE FORMATION OF CYST CONFIGURATIONS UNDER PHYSIOLOGICAL AND PATHOLOGICAL CONDITIONS

Classification of Skin Cyst

A skin cyst includes a basal epidermal layer surrounded by layers of dermal cells. The basal layer differentiates toward the inside of the cyst into the suprabasal layers which undergo terminal differentiation to produce keratin debris (**Figures 1A,B**). Skin cysts can be classified into five major types per cellular origins (Kaya and Saurat, 2018; **Figure 1C**). These include cysts with epithelial cells from infundibulum or interfollicular epidermis (epidermal cysts, comedo, milia, and eruptive vellus cysts) (Swygert et al., 2007), cysts with epithelial cells from outer root sheath (ORS) of the hair follicle (trichilemmal or pilar cysts), cysts with epithelial cells from the sebaceous duct (steatocystoma and cutaneous keratocyst), cysts with epithelial cells from sweat gland (hidrocystoma), cysts with epithelial cells from hair matrix (hair matrix cyst), and hamartomatous cysts (dermoid cyst, folliculosebaceous hamartoma and metabolizing acquired dioxin-induced skin hamartoma). Different cellular origins contribute to diverse skin cysts formation. Epidermal cyst is the most common cutaneous cysts present as nodules in the skin. The disruption of the hair follicle, implantation of the epithelium due to traumatic and penetrating injury, excessive ultraviolet (UV) radiation, infection with the human papillomavirus (HPV), medicine (e.g., imiquimod, cyclosporine, vemurafenib, etc.) (Ramagosa et al., 2008; Boussemart et al., 2013) and inherited diseases (e.g., Gardner's syndrome) all lead to the formation of epidermal cysts. These cystic lesions are usually asymptomatic. It consists of multilayer squamous epithelia and is filled with keratinized substances differentiated by the suprabasal epithelial cells. Some squamous epithelial cells form squamous eddies around the cysts.

Cysts Configurations Are Observed in Developmental and Physiological Conditions

Cyst formation is required in the early stage of embryogenesis and functional maintenances of organs. A blastocyst is a physical structure developed in the early development of mammals. A blastocyst contains the inner cell mass which subsequently develops the embryo and the outer layer which forms blastocele. An ovarian follicle, a spheroid cellular aggregation set, can influence stages of the menstrual cycle by secreting hormones. In every menstrual cycle, each ovarian follicle has the potential to release an egg cell for fertilization. Additionally, in adult tissues such as the thyroid gland, thyroid follicle consists of cuboidal epithelium and contents which contain colloid, thyroglobulin, and iodine. Thyroid follicles secret thyroid hormones to regulate body metabolism and growth.

Cyst Formation Under Pathological Conditions

Cysts can be observed in almost every organ such as skin, kidney, liver, ovary, lung, joint and mammary gland, ranging from microscopic scale to several centimeters in diameter. For example, renal cysts with fluid-filled contents can be observed in a single cyst and several polycystic kidney diseases (Ferro et al., 2019). Progressive dilatation of biliary micro-hamartomas promotes the development of simple hepatic cysts in the liver (Kimura et al., 1978; Jung et al., 2012). Ovarian cysts including functional cysts and non-functional cysts are usually filled by fluid or semiliquid material (Bottomley and Bourne, 2009). Ganglion cyst is often formed next to a joint and usually filled with excess joint fluid (Hsu et al., 2007). Breast cyst is a fluid-filled sac, and it is necessary to ensure whether breast cyst is benign or malignant. Cyst is also present in fibrosis which is an inherited disease. Cystic fibrosis can cause progressive damage to the respiratory system and chronic digestive system (Castellani and Assael, 2017).

PATHOGENESIS OF THE SKIN CYST

Imbalance of Skin Homeostasis Leads to Cyst Formation

Skin cysts can form due to mistakes during skin development. For example, variants in PLCD1 are detected in families with multiple trichilemmal cysts (Shimomura et al., 2019). Dermoid cysts form due to the sequestration of ectodermal tissues during embryonic closure. These cysts originated from ectoderm locate in the subcutaneous tissue, but still maintain the multipotency to develop fully differentiated ectopic structures, such as nails and dental, cartilage-like, and bone-like structures. This suggests

Abbreviations: iPSCs, induced pluripotent stem cells; ORS, outer root sheath; UV, ultraviolet; HPV, human papillomavirus; IL-1R, IL-1 receptor; IAP, inhibitor of apoptosis proteins; MADISH, metabolizing acquired dioxin-induced skin hamartomas; VDR, Vitamin D receptor; Dsc3, Desmocollin3; HFSCs, hair follicle stem cells; IRS, inner root sheath; APC, adenomatosis polyposis coli; GSK3, glycogen synthase kinase 3; CK1α, casein kinase 1α; Shh, Sonic Hedgehog; IC, intercellular domain; Adams, A disintegrin and metalloproteases; PCδ1, Phospholipase Cδ1.

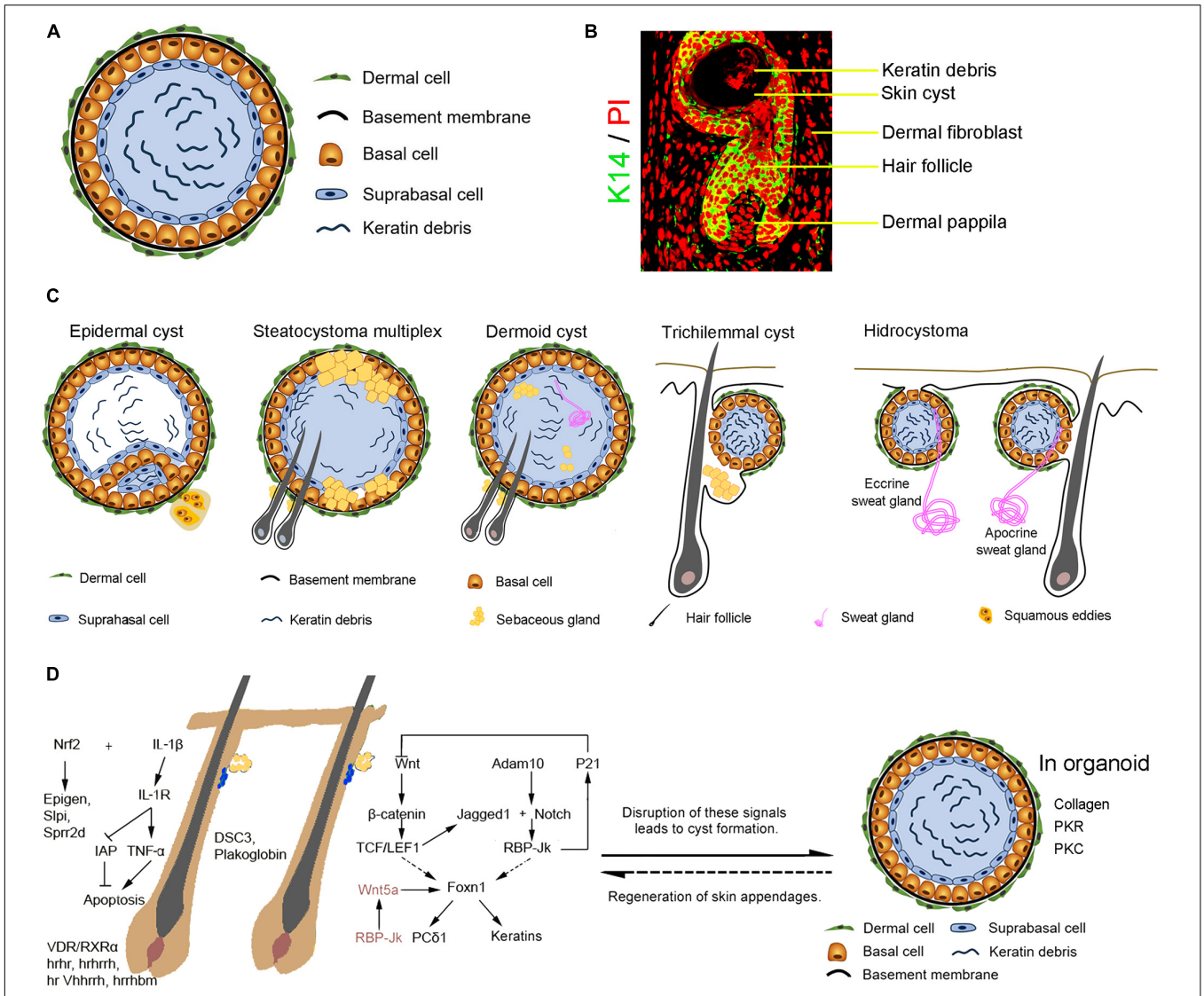

FIGURE 1 | The formation of the skin cyst as a sign in pathology. **(A)** The general characteristics of skin cysts. Skin cyst consists of a cyst wall of basal cells, suprabasal cells, and cyst contents (e.g., keratin debris, sebaceous gland, sweat gland, or hair). Some skin cysts are surrounded by layers of dermal cells and a basement membrane between dermal cells and basal epidermal cells. **(B)** Relationship with hair follicles. Hair follicle induction on the cyst wall upon epithelial-mesenchymal interaction mechanism. **(C)** Different types of skin cysts. Epidermal cyst is the most common cutaneous cyst which includes the general skin cyst components. Some epidermal cyst forms squamous eddies around the cyst. Steatocystoma multiplex originated from the outer root sheath of hair follicles contains sebaceous glands and can generate hair follicles. A dermoid cyst contains can form a sebaceous gland, hair follicle, or sweat gland when interacting with dermal cells surrounding the cyst. A trichilemmal cyst originates from the outer root sheath of hair follicles and produces abundant keratin material inside the cyst. The basal cells coalesce with the suprabasal layer without a clear boundary line. Hydrocystoma forms due to disorders of the sweat gland, including the eccrine sweat gland and the apocrine sweat gland. Eccrine hidrocystoma is filled with the residue of sweat, an inner columnar cell layer, an outer myoepithelial cells layer, a basement membrane, and dermal cells. Apocrine hidrocystoma consists of lipofuscin granules contents, an inner secretory columnar layer, an outer myoepithelial layer, basement membrane, and dermal cells. **(D)** Complex signalings balance skin and appendages homeostasis and cyst formation. Knockout of *IL-1/IL-1R* or activation of Nrf2 disrupts skin and hair follicle homeostasis, leading to skin cysts formation. Ablation of *hrhr, hrhr^{rh}, hr Vhhr^{rh}, hr^{rhbm}*, and *VDR/RXRα* results in hair loss and cyst formation. Disrupted expression of cell-cell adhesion molecules DSC3 or Plakoglobin results in skin cyst formation. Disruption of Wnt and Notch pathways which regulate hair growth causes the formation of skin cysts from hair follicles. Abnormality of RBP-Jk/Wnt5a signals in dermal papilla cells induces skin cyst formation. In addition, interactions between the basal epidermal cells of the skin cyst and surrounding dermal cells may result in skin appendage regeneration.

that the formation of cysts might be a self-protection response to mistakes during skin development.

Skin is constantly subjected to insults such as UV radiation, toxin, invasive pathogens, etc (Lei and Chuong, 2018). In response to these insults, skin epidermis initiates a rapid innate immune response by producing chemokine, antimicrobial peptides, and Toll-like receptors (Selleri et al., 2007; Reithmayer et al., 2009; Nagao et al., 2012). Skin keratinocytes produce IL-1β in response to UV radiation and infection (Dai et al., 2017). IL-1 receptor (IL-1R) or IL-1β knockout mice develop

multiple epidermal cysts when receiving chronic UVB exposure (Kulkarni et al., 2017). IL-1β signaling mediates UV-induced proinflammatory responses (Maelfait et al., 2008) and promotes UVB-induced apoptosis through driving TNF-α release and down-regulating inhibitor of apoptosis proteins (IAP) (Kothny-Wilkes et al., 1999). Knockout of IL-1R blocks the expression of TNF-α and promotes keratinocytes to be resistant to UVB-induced apoptosis, leading to the disruption of skin homeostasis and skin cysts formation. Transcription factor Nrf2 plays an important role in protecting skin from reactive oxygen species which are induced by the harmful insults from microorganisms, UV light, and toxic chemicals (Schafer et al., 2010; Tan and Wahli, 2014). Nrf2 activation in keratin 5 (K5)-positive skin epithelia leads to hair loss, infundibula dilatation, sebaceous gland enlargement, and cyst formation, with upregulation of Epigen, Slpi, and Sprr2d in the cyst (Tan and Wahli, 2014).

The inflammatory response to the grafted epidermal tissues during implantation can be important in the formation of skin cysts. To protect tissues from stimuli such as pathogens infection or damage in cells, inflammatory responses involving immune cells, blood vessels, and molecular mediators are mobilized to eliminate the necrotic cells and tissues to facilitate tissue repair (Ferrero-Miliani et al., 2007). Thus, after the implantation of ectopic epidermal tissues, inflammatory response can be activated to wrap these ectopic epidermal tissues, leading to cyst formation.

Cell-cell adhesion is the basis for forming tissue integrity. Conditional knockout of Desmocollin3 (Dsc3) in the skin epithelium destroys the cell-cell adhesion, causing intra-epidermal blistering, and cyst formation in the hair follicle (Chen et al., 2008). Another cell adhesion molecule Plakoglobin as a cytoplasmic constituent of the desmosome is involved in the intracellular signaling events essential for epidermal differentiation. Specific expression of N-terminally truncated plakoglobin in epidermis results in the formation of additional hair germs, hyperplastic hair follicles, dermal cysts, and even non-invasive hair follicle tumors (Teuliere et al., 2004). The epithelial cells of the cysts are derived from precortex and hair matrix cells and show hair follicle or epidermal characteristics by molecular characterization.

Different Types of Hair Follicle-Derived Skin Cysts Help Reveal the Molecular Control of Cyst Formation

A hair follicle is a complex micro-organ with multiple cellular components including the bulge, ORS, inner root sheath (IRS), hair bulb, and dermal papilla. Homeostasis of the hair follicle is maintained by the coordination of extracellular matrix signaling, autocrine signaling, paracrine signaling, systematic signaling, etc (Chueh et al., 2013). Abnormality in hair follicle development and regeneration often leads to cyst formation (Vidal et al., 2005).

Sonic Hedgehog (Shh), Transforming Growth Factors β (TGFβ), and Bone Morphogenetic Protein (BMP) signaling pathways are required in hair follicle morphogenesis and hair follicular growth (Adam et al., 2018; Lim et al., 2018; Rahmani et al., 2018). Specific deletion of Shh receptor Smoothened in skin epithelium causes a transformation of ORS to epidermis-like structure, hair loss, and cyst formation (Gritli-Linde et al., 2007). Specific deletion of TGFβ mediator Smad4 in basal skin epithelial cells results in epidermal and follicular hyperplasia, progressive hair loss, and cyst formation (Yang et al., 2005). Cyst formation is also observed in skin epithelia-*Bmpr1a* knockout and activation mice (Kobielak et al., 2003, 2007; Yuhki et al., 2004).

Wnt/β-catenin signaling largely influences hair follicle stem cells (HFSCs) behaviors including activating HFSCs during regeneration and promoting their differentiation during hair growth (Rabbani et al., 2011; Lei et al., 2013, 2014). Deletion of β-catenin in basal epidermal and hair follicular keratinocytes causes epidermal hyperplasia and cyst formation (Huelsken et al., 2001). K15 and integrin β1, markers of HFSCs, are expressed in the cyst wall, suggesting that the multipotency of epidermal stem cells may be partially maintained through the formation of cyst after epidermal deletion of β-catenin. Enhanced Wnt signaling also causes not only tumorigenesis but also skin cyst formation (Gat et al., 1998; Hassanein et al., 2003). Overexpression of truncated LEF1 without the β-catenin interacting domain in keratinocytes suppresses hair differentiation but induces sebaceous gland differentiation and causes cyst formation beneath the bulge region. These cysts exhibit a multipotency of epidermal stem cells or sebaceous gland stem cells (Merrill et al., 2001), suggesting that LEF1 may interact with transcriptional inhibitors and promote the progeny of HFSCs to transform into a population of cells with the multipotency of epidermal stem cells or sebaceous gland stem cells.

Notch signaling pathway is important in maintaining the homeostasis of hair follicles and epidermis. Specific deletion of Notch pathway genes such as *Jagged 1, Notch1, Notch2*, or *RBP-Jκ* in skin epithelia blocks the differentiation of IRS, induces the differentiation of ORS cells besides HFSCs, and causes the skin cyst formation (Demehri and Kopan, 2009). Moreover, conditional knockout of Adam10 in skin epithelia results in impaired expression of Notch pathway target genes *Hes* and *Hey* and causes hair loss, epidermal hyperproliferation, and epidermal cyst formation (Weber et al., 2011). Disruption of mesenchyme-derived signals also causes skin cyst formation. Deletion of CSL/RBP-Jκ, the effector of the canonical Notch pathway in dermal papilla cells and dermal fibroblasts causes the degeneration of hair follicles into epidermal cysts, with high levels of interfollicular marker expression (Hu et al., 2010). Mesenchymal deletion of RBP-Jκ results in a decreased expression of dermal papilla specific signatures, such as Wnt5a, Fgf7, Fgf10, and Noggin (Rendl et al., 2005). Hair follicle reconstruction assay by injecting *Wnt5a*-deficient dermal papilla cells and normal keratinocytes into the nude mice skin shows the development of skin cysts rather than hair follicles (Rendl et al., 2005). Besides, Notch1 can activate the *Wnt5a* promoter by RBP-Jκ (Rendl et al., 2005), suggesting that Wnt5a is a primary target gene of the activated RBP-Jk to control normal hair follicle development or cyst formation. Functioning downstream of Wnt5a, Foxn1 directly activates the Notch1 promoter by binding Notch1 promoter in mice (Cai et al., 2009), to regulate hair differentiation. This suggests that the Notch-Wnt5a-Foxn1

mesenchymal-epithelial signaling module functions as a positive feedback to regulate hair differentiation. Besides, deletion of Phospholipase C(δ1 (PCδ1), one of the target genes of Foxn1, also causes cyst formation (Nakamura et al., 2003).

Suppresion of histone modification-related enzymes can lead to the failure of hair follicles to regenerate properly, and therefore turn the hair follicles into cysts. For instance, *Hdac1* maintains the homeostasis of epidermis and hair follicles. Epithelium-specific knockout of *Hdac1* in mice causes hyperkeratosis, hair follicle dystrophy, extensive alopecia, and epithelial cyst-like structures (Hughes et al., 2014). However, Krt14 and Trp63 which mark the epidermal stem cells are expressed in the whole cyst wall. This suggests that hair follicle progenitor-derived cells retain certain multipotency properties of epidermal stem cells. The degeneration of hair follicles into epidermal stem cells is also present in other epidermal cysts (Demehri and Kopan, 2009; Kulkarni et al., 2017; Yang et al., 2020).

Perturbation of several genes or signaling pathways that are necessary for the skin homeostasis and hair follicle formation results in epidermal cysts formation. These genes include hairless (hrhr), hairless-rhino (hrhrrh), rhino (hr Vhhrrh), bald Mill Hill (hrrhbm) (Mann, 1971; Brancaz et al., 2004), Vitamin D receptor (VDR) (Keisala et al., 2009) and RXRα (Li et al., 2001), etc.

Mapping the molecular mechanisms by which these signaling pathways interact with each other to control the hair follicle homeostasis or skin cyst formation requires further bioinformatics approaches and functional tests. At least known studies have revealed that Wnt and Notch pathways are largely involved in this molecular regulatory network (**Figure 1D**).

THE FORMATION OF CYST CONFIGURATION IN ORGANOID CULTURES

Recent studies on organoid formation demonstrate that the cyst formation is a common and essential process to generate the mini-organs (Bredenoord et al., 2017; Dutta et al., 2017; Smith and Tabar, 2019; Lee et al., 2020). Most organoids are derived from embryonic stem cells, induced pluripotent stem cells (iPSCs), or primary cultured cells. The cells are guided or self-organize to form a cyst-like structure in most types of organoid culture before induction of the desired tissues/organs (Rossi et al., 2018). Some cells (like dissociated endothelial) form tubes when they are cultured. Different from formation of a tube which is a long hollow cylinder structure, involving tissue mechanics of ECM and cytoskeleton. It would be interesting to identify the driving forces of each arrow in the morphospace in **Figure 1B**, whether it is biochemical or biophysical based. We think this would be the challenge of next step in organoid study, to be able to guide the formation of desired tissues for application. Progress has been made in identifying the novel characteristics of the cyst formed *in vivo* and *in vitro*. Growing evidence shows that the cyst structure retains certain multipotency to self-renew and differentiate, and *de novo* regenerate mini-organs resembling those formed during the developmental processes. Cyst forms budded structure during intestinal organoid development, with involvement of fate-specific changes in osmatic and actomyosin forces, as well as Yap signaling pathway activation (Serra et al., 2019; Yang et al., 2020). This endows the cysts not only as a pathological structure but also with the potential to study how cells retain multipotency to generate new organs *in vivo* and *in vitro*.

Tissue-engineered skin represents a useful strategy for the treatment of skin injuries. Primary cultured skin cells, iPS-differentiated skin cells, embryonic stem cells-differentiated skin cells, etc., are used to generate fully functional skin with appendages formation. Accompanying with fully functional skin formation during the explant transplantation into the nude mice is the formation of skin cysts, which express the epidermal stem cell markers. Appendages such as hair follicles not only form from the regenerated skin but also the skin cysts (Zheng et al., 2005; Balana et al., 2015; Lei et al., 2017b; Lee et al., 2020).

Skin cyst formation also occurs when pluripotent stem cells are cultured *in vitro*, which is termed skin organoid culture (Lei et al., 2017b; Lee et al., 2018, 2020). The *in vitro* cultured organoids can form the fully functional skin with epidermis and dermis structures, as well as with regeneration of skin appendages such as hair follicle (**Figure 2**; Lei et al., 2017b; Lee et al., 2018), sebaceous gland (Feldman et al., 2019) and sweat gland (Diao et al., 2019). This indicates that though skin cyst is an abnormal structure to the organism, the formation of the skin cyst can be the other way for the tissue to retain sufficient multipotency. And importantly, the process of the cyst formation during the cell self-organization *in vitro* is required for further tissue regeneration. The reason why cells prefer to choose this more complex way to form fully functional skin requires further investigation. However, one possibility is that the easiest way for one to reach the destination from the beginning may not be through a straight

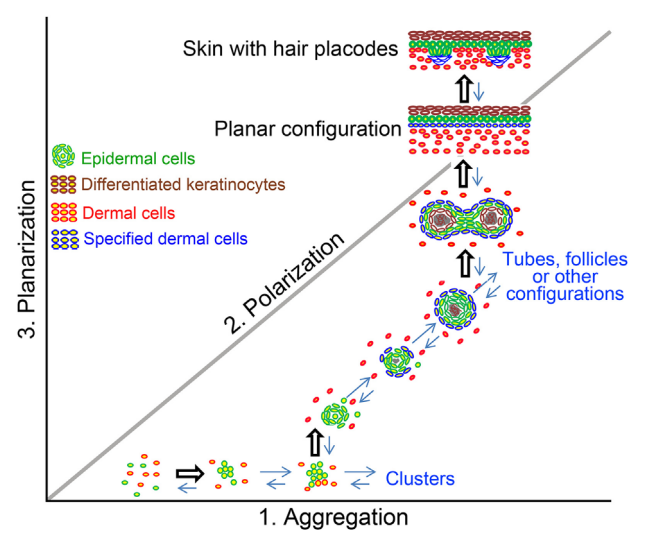

FIGURE 2 | The formation of cyst configuration in skin organoid culture. A morphospace of potential epidermal and dermal cell configuration is shown. Pattern diagram showing possible multicellular configurations during newborn skin cells organoid culture. Dissociated cells undergo a series of morphological transitions including aggregation, polarization, coalescence, and planarization, to form hair primordia [The figure is from Lei et al. (2017b)].

line but by consuming their lowest energy. Thus, the skin cells may use the same strategy to form fully functional skin by forming the skin cyst to maintain their multipotency. Indeed, adult cells with declined regenerative ability can be reactivated to form skin organoid through cyst formation by applying certain factors during culture and regenerate hair follicles upon regeneration (Lei et al., 2017b).

CONCLUSION AND NEW POSSIBILITIES

Here we show cyst form from the progenitor/stem cells who find their route to maintain multipotency and can regenerate the original tissues under pathological and skin organoid culture conditions. Cysts in pathological conditions are formed from complex tissue architectures by making closed sac-like tissue structures that contain simple or complex tissues depending on their origin and mutation type, with complex molecular regulatory networks largely involving Wnt and Notch pathways. They also tend to form during renewal conditions such as hair cycling. They failed to form complex structures and get "stuck" in the cyst stage. Organoids first form cysts with relatively homogeneous progenitors and tissue structures, and then start developing more complex tissue architectures with cell differentiation and tissue patterning, with the involvement of extracellular matrix and protein kinases C and R (**Figure 1D**). These lead to a new look of the skin cysts as potential new therapeutic possibilities.

However, several outstanding questions regarding skin cyst formation remain. For example, how to guide cyst in organoid cultures to continue morphogenesis? This can be achieved by modifying the molecular profiles of the cyst cells. The configuration may also be changed by 2-dimensional or 3-dimensional culture conditions. Activation or de-stabilization of the cyst can also be achieved by altering the physical properties of the surrounding environment, by affecting the affinity of ECM and cyst epithelial cells. What happens when the cyst configuration de-stabilization? Is it the loss of apical-basal cell polarity? Realignment of cell adhesion and neighboring cellular partners? Does the rigid structure enter a more fluid state similar to those observed in epithelial-mesenchymal transition?

With the organoid cultures as a platform to investigate the mechanism by which skin organoids undergo a morpho-space development, from aggregate to skin cyst, then to a planar skin with hair regeneration will help answer these questions. As researches on the topic of skin biology continue, understanding the control of cyst configuration, we hope to provide a theoretical basis for understanding the pathogenesis of skin cysts, improving the therapeutic methods of skin cysts, and producing more functional skin organoids for tissue regeneration.

DATA AVAILABILITY STATEMENT

The original contributions presented in the study are included in the article/Supplementary Material, further inquiries can be directed to the corresponding author/s.

AUTHOR CONTRIBUTIONS

C-MC and ML contributed to the conception and design of the manuscript. WQ, P-RG, C-MC, and ML wrote the article and approved the final version. All authors read and approved the final manuscript.

FUNDING

This work was supported by China Medical University Hospital in Taiwan, National Natural Science Foundation of China (82003384 and 81602782), Fundamental Research Funds for the Central Universities (2020CDJYGSG003) and Scientific Research Foundation from Chongqing University (02210011044110), and Joint Foundation of Health Commission of Hubei Province in China (WJ2019H098). C-MC was supported by NIH NIAMS AR60306, GM125322, and a collaborative grant between University of Southern California (USC) and China Medical University in Taiwan (CMU) (USC grant number 5351285884). C-MC is a paid science advisor of CMU.

REFERENCES

Adam, R. C., Yang, H., Ge, Y., Lien, W. H., Wang, P., Zhao, Y., et al. (2018). Temporal layering of signaling effectors drives chromatin remodeling during hair follicle stem cell lineage progression. *Cell Stem Cell* 22, 398–413.e7. doi: 10.1016/j.stem.2017.12.004

Balana, M. E., Charreau, H. E., and Leiros, G. J. (2015). Epidermal stem cells and skin tissue engineering in hair follicle regeneration. *World J. Stem Cells* 7, 711–727. doi: 10.4252/wjsc.v7.i4.711

Bottomley, C., and Bourne, T. (2009). Diagnosis and management of ovarian cyst accidents. *Best Pract. Res. Clin. Obstet. Gynaecol.* 23, 711–724. doi: 10.1016/j.bpobgyn.2009.02.001

Boussemart, L., Routier, E., Mateus, C., Opletalova, K., Sebille, G., Kamsu-Kom, N., et al. (2013). Prospective study of cutaneous side-effects associated with the BRAF inhibitor vemurafenib: a study of 42 patients. *Ann. Oncol.* 24, 1691–1697. doi: 10.1093/annonc/mdt015

Brancaz, M. V., Iratni, R., Morrison, A., Mancini, S. J., Marche, P., Sundberg, J., et al. (2004). A new allele of the mouse hairless gene interferes with Hox/LacZ transgene regulation in hair follicle primordia. *Exp. Mol. Pathol.* 76, 173–181. doi: 10.1016/j.yexmp.2003.10.003

Bredenoord, A. L., Clevers, H., and Knoblich, J. A. (2017). Human tissues in a dish: the research and ethical implications of organoid technology. *Science* 355:aaf9414. doi: 10.1126/science.aaf9414

Cai, J., Lee, J., Kopan, R., and Ma, L. (2009). Genetic interplays between Msx2 and Foxn1 are required for Notch1 expression and hair shaft differentiation. *Dev. Biol.* 326, 420–430. doi: 10.1016/j.ydbio.2008.11.021

Castellani, C., and Assael, B. M. (2017). Cystic fibrosis: a clinical view. *Cell. Mol. Life Sci.* 74, 129–140. doi: 10.1007/s00018-016-2393-2399

Chen, J., Den, Z., and Koch, P. J. (2008). Loss of desmocollin 3 in mice leads to epidermal blistering. *J. Cell Sci.* 121, 2844–2849. doi: 10.1242/jcs.031518

Chueh, S. C., Lin, S. J., Chen, C. C., Lei, M., Wang, L. M., Widelitz, R., et al. (2013). Therapeutic strategy for hair regeneration: hair cycle activation, niche

environment modulation, wound-induced follicle neogenesis, and stem cell engineering. *Expert. Opin. Biol. Ther.* 13, 377–391. doi: 10.1517/14712598.2013.739601

Chuong, C. M., Nickoloff, B. J., Elias, P. M., Goldsmith, L. A., Macher, E., Maderson, P. A., et al. (2002). What is the 'true' function of skin? *Exp. Dermatol.* 11, 159–187. doi: 10.1034/j.1600-0625.2002.00112.x

Dai, X., Tohyama, M., Murakami, M., and Sayama, K. (2017). Epidermal keratinocytes sense dsRNA via the NLRP3 inflammasome, mediating interleukin (IL)-1beta and IL-18 release. *Exp. Dermatol.* 26, 904–911. doi: 10.1111/exd.13334

Demehri, S., and Kopan, R. (2009). Notch signaling in bulge stem cells is not required for selection of hair follicle fate. *Development* 136, 891–896. doi: 10.1242/dev.030700

Diao, J., Liu, J., Wang, S., Chang, M., Wang, X., Guo, B., et al. (2019). Sweat gland organoids contribute to cutaneous wound healing and sweat gland regeneration. *Cell Death Dis.* 10:238. doi: 10.1038/s41419-019-1485-1485

Dutta, D., Heo, I., and Clevers, H. (2017). Disease modeling in stem cell-derived 3D organoid systems. *Trends Mol. Med.* 23, 393–410. doi: 10.1016/j.molmed.2017.02.007

Feldman, A., Mukha, D., Maor, I. I., Sedov, E., Koren, E., Yosefzon, Y., et al. (2019). Blimp1(+) cells generate functional mouse sebaceous gland organoids in vitro. *Nat. Commun.* 10:2348. doi: 10.1038/s41467-019-10261-10266

Ferrero-Miliani, L., Nielsen, O. H., Andersen, P. S., and Girardin, S. E. (2007). Chronic inflammation: importance of NOD2 and NALP3 in interleukin-1beta generation. *Clin. Exp. Immunol.* 147, 227–235. doi: 10.1111/j.1365-2249.2006.03261.x

Ferro, F., Vezzali, N., Comploj, E., Pedron, E., Di Serafino, M., Esposito, F., et al. (2019). Pediatric cystic diseases of the kidney. *J Ultrasound* 22, 381–393. doi: 10.1007/s40477-018-0347-349

Gat, U., DasGupta, R., Degenstein, L., and Fuchs, E. (1998). De Novo hair follicle morphogenesis and hair tumors in mice expressing a truncated beta-catenin in skin. *Cell* 95, 605–614. doi: 10.1016/s0092-8674(00)81631-81631

Gritli-Linde, A., Hallberg, K., Harfe, B. D., Reyahi, A., Kannius-Janson, M., Nilsson, J., et al. (2007). Abnormal hair development and apparent follicular transformation to mammary gland in the absence of hedgehog signaling. *Dev. Cell* 12, 99–112. doi: 10.1016/j.devcel.2006.12.006

Hassanein, A. M., Glanz, S. M., Kessler, H. P., Eskin, T. A., and Liu, C. (2003). beta-Catenin is expressed aberrantly in tumors expressing shadow cells: pilomatricoma, craniopharyngioma, and calcifying odontogenic cyst. *Am. J. Clin. Pathol.* 120, 732–736. doi: 10.1309/EALE-G7LD-6W71-67PX

Hsu, C. S., Hentz, V. R., and Yao, J. (2007). Tumours of the hand. *Lancet Oncol.* 8, 157–166. doi: 10.1016/S1470-2045(07)70035-70039

Hu, B., Lefort, K., Qiu, W., Nguyen, B. C., Rajaram, R. D., Castillo, E., et al. (2010). Control of hair follicle cell fate by underlying mesenchyme through a CSL-Wnt5a-FoxN1 regulatory axis. *Genes Dev.* 24, 1519–1532. doi: 10.1101/gad.1886910

Huelsken, J., Vogel, R., Erdmann, B., Cotsarelis, G., and Birchmeier, W. (2001). beta-Catenin controls hair follicle morphogenesis and stem cell differentiation in the skin. *Cell* 105, 533–545. doi: 10.1016/s0092-8674(01)00336-331

Hughes, M. W., Jiang, T. X., Lin, S. J., Leung, Y., Kobielak, K., Widelitz, R. B., et al. (2014). Disrupted ectodermal organ morphogenesis in mice with a conditional histone deacetylase 1, 2 deletion in the epidermis. *J. Invest. Dermatol.* 134, 24–32. doi: 10.1038/jid.2013.283

Jung, S. M., Seo, J. M., and Lee, S. K. (2012). The relationship between biliary amylase and the clinical features of choledochal cysts in pediatric patients. *World J. Surg.* 36, 2098–2101. doi: 10.1007/s00268-012-1619-1618

Kaya, G., and Saurat, J. H. (2018). Cutaneous adnexal cysts revisited: what we know and what we think we know. *Dermatopathology* 5, 79–85. doi: 10.1159/000488585

Keisala, T., Minasyan, A., Lou, Y. R., Zou, J., Kalueff, A. V., Pyykko, I., et al. (2009). Premature aging in vitamin D receptor mutant mice. *J. Steroid Biochem. Mol. Biol.* 115, 91–97. doi: 10.1016/j.jsbmb.2009.03.007

Kimura, K., Tsugawa, C., Ogawa, K., Matsumoto, Y., Yamamoto, T., Kubo, M., et al. (1978). Choledochal cyst: etiological considerations and surgical management in 22 cases. *Arch. Surg.* 113, 159–163. doi: 10.1001/archsurg.1978.01370140049010

Kobielak, K., Pasolli, H. A., Alonso, L., Polak, L., and Fuchs, E. (2003). Defining BMP functions in the hair follicle by conditional ablation of BMP receptor IA. *J. Cell Biol.* 3, 609–623. doi: 10.1083/jcb.200309042

Kobielak, K., Stokes, N., de la Cruz, J., Polak, L., and Funchs, E. (2007). Loss of a quiescent niche but not follicle stem cells in the absence of bone morphogenetic protein signaling. *Proc. Natl. Acad. Sci. U.S.A.* 24, 10063–10068. doi: 10.1073/pnas.0703004104

Kothny-Wilkes, G., Kulms, D., Luger, T. A., Kubin, M., and Schwarz, T. (1999). Interleukin-1 protects transformed keratinocytes from tumor necrosis factor-related apoptosis-inducing ligand- and CD95-induced apoptosis but not from ultraviolet radiation-induced apoptosis. *J. Biol. Chem.* 274, 28916–28921. doi: 10.1074/jbc.274.41.28916

Kulkarni, N. N., Adase, C. A., Zhang, L. J., Borkowski, A. W., Li, F., Sanford, J. A., et al. (2017). IL-1 Receptor-knockout mice develop epidermal cysts and show an altered innate immune response after exposure to UVB radiation. *J. Invest. Dermatol.* 137, 2417–2426. doi: 10.1016/j.jid.2017.07.814

Lee, J., Bscke, R., Tang, P. C., Hartman, B. H., Heller, S., and Koehler, K. R. (2018). Hair FOLLICLE development in mouse pluripotent stem cell-derived skin organoids. *Cell Rep.* 22, 242–254. doi: 10.1016/j.celrep.2017.12.007

Lee, J., Rabbani, C. C., Gao, H., Steinhart, M. R., Woodruff, B. M., Pflum, Z. E., et al. (2020). Hair-bearing human skin generated entirely from pluripotent stem cells. *Nature* 582, 399–404. doi: 10.1038/s41586-020-2352-2353

Lei, M., and Chuong, C. M. (2018). Epidermal darwinism and competitive equilibrium within the epidermis. *Cell Stem Cell* 23, 627–629. doi: 10.1016/j.stem.2018.10.019

Lei, M., Guo, H., Qiu, W., Lai, X., Yang, T., Widelitz, R. B., et al. (2014). Modulating hair follicle size with Wnt10b/DKK1 during hair regeneration. *Exp. Dermatol.* 23, 407–413. doi: 10.1111/exd.12416

Lei, M., Schumacher, L. J., Lai, Y. C., Juan, W. T., Yeh, C. Y., Wu, P., et al. (2017a). Self-organization process in newborn skin organoid formation inspires strategy to restore hair regeneration of adult cells. *Proc. Natl. Acad. Sci. U.S.A.* 114, E7101–E7110. doi: 10.1073/pnas.1700475114

Lei, M., Yang, L., and Chuong, C. M. (2017b). Getting to the core of the dermal papilla. *J. Invest. Dermatol.* 137, 2250–2253. doi: 10.1016/j.jid.2017.07.824

Lei, M. X., Chuong, C. M., and Widelitz, R. B. (2013). Tuning Wnt signals for more or fewer hairs. *J. Invest. Dermatol.* 133, 7–9. doi: 10.1038/jid.2012.446

Li, M., Chiba, H., Warot, X., Messaddeq, N., Gerard, C., Chambon, P., et al. (2001). RXR-alpha ablation in skin keratinocytes results in alopecia and epidermal alterations. *Development* 128, 675–688.

Lim, C. H., Sun, Q., Ratti, K., Lee, S. H., Zheng, Y., Takeo, M., et al. (2018). Hedgehog stimulates hair follicle neogenesis by creating inductive dermis during murine skin wound healing. *Nat. Commun.* 9:4903. doi: 10.1038/s41467-018-07142-7149

Maelfait, J., Vercammen, E., Janssens, S., Schotte, P., Haegman, M., Magez, S., et al. (2008). Stimulation of toll-like receptor 3 and 4 induces interleukin-1beta maturation by caspase-8. *J. Exp. Med.* 205, 1967–1973. doi: 10.1084/jem.20071632

Mann, S. J. (1971). Hair loss and cyst formation in hairless and rhino mutant mice. *Anat. Rec.* 170, 485–499. doi: 10.1002/ar.1091700409

Merrill, B. J., Gat, U., DasGupta, R., and Fuchs, E. (2001). Tcf3 and Lef1 regulate lineage differentiation of multipotent stem cells in skin. *Genes Dev.* 15, 1688–1705. doi: 10.1101/gad.891401

Nagao, K., Kobayashi, T., Moro, K., Ohyama, M., Adachi, T., Kitashima, D. Y., et al. (2012). Stress-induced production of chemokines by hair follicles regulates the trafficking of dendritic cells in skin. *Nat. Immunol.* 13, 744–752. doi: 10.1038/ni.2353

Nakamura, Y., Fukami, K., Yu, H., Takenaka, K., Kataoka, Y., Shirakata, Y., et al. (2003). Phospholipase Cdelta1 is required for skin stem cell lineage commitment. *EMBO J.* 22, 2981–2991. doi: 10.1093/emboj/cdg302

Rabbani, P., Takeo, M., Chou, W., Myung, P., Bosenberg, M., Chin, L., et al. (2011). Coordinated activation of Wnt in epithelial and melanocyte stem cells initiates pigmented hair regeneration. *Cell* 6, 941–955. doi: 10.1016/j.cell.2011.05.004

Rahmani, W., Liu, Y., Rosin, N. L., Kline, A., Raharjo, E., Yoon, J., et al. (2018). Macrophages promote wound-induced hair follicle regeneration in a CX3CR1- and TGF-beta1-dependent manner. *J. Invest. Dermatol.* 138, 2111–2122. doi: 10.1016/j.jid.2018.04.010

Ramagosa, R., de Villiers, E. M., Fitzpatrick, J. E., and Dellavalle, R. P. (2008). Human papillomavirus infection and ultraviolet light exposure as epidermoid inclusion cyst risk factors in a patient with Epidermodysplasia verruciformis?. *J. Am. Acad. Dermatol.* 58:S68.e1-6. doi: 10.1016/j.jaad.2007.01.032

Reithmayer, K., Meyer, K. C., Kleditzsch, P., Tiede, S., Uppalapati, S. K., Glaser, R., et al. (2009). Human hair follicle epithelium has an antimicrobial defence system that includes the inducible antimicrobial peptide psoriasin (S100A7) and RNase 7. *Br. J. Dermatol.* 161, 78–89. doi: 10.1111/j.1365-2133.2009.09154.x

Rendl, M., Lewis, L., and Fuchs, E. (2005). Molecular dissection of mesenchymal-epithelial interactions in the hair follicle. *PLoS Biol.* 3:e331. doi: 10.1371/journal.pbio.0030331

Rossi, G., Manfrin, A., and Lutolf, M. P. (2018). Progress and potential in organoid research. *Nat. Rev. Genet.* 19, 671–687. doi: 10.1038/s41576-018-0051-59

Schafer, M., Dutsch, S., Auf, D. K. U., Navid, F., Schwarz, A., Johnson, D. A., et al. (2010). Nrf2 establishes a glutathione-mediated gradient of UVB cytoprotection in the epidermis. *Genes Dev.* 24, 1045–1058. doi: 10.1101/gad.568810

Selleri, S., Arnaboldi, F., Palazzo, M., Gariboldi, S., Zanobbio, L., Opizzi, E., et al. (2007). Toll-like receptor agonists regulate beta-defensin 2 release in hair follicle. *Br. J. Dermatol.* 156, 1172–1177. doi: 10.1111/j.1365-2133.2007.07899.x

Serra, D., Mayr, U., Boni, A., Lukonin, I., Rempfler, M., Challet, M. L., et al. (2019). Self-organization and symmetry breaking in intestinal organoid development. *Nature* 569, 66–72. doi: 10.1038/s41586-019-1146-y

Shimomura, Y., O'Shaughnessy, R., and Rajan, N. (2019). PLCD1 and pilar cysts. *J. Invest. Dermatol.* 139, 2075–2077. doi: 10.1016/j.jid.2019.05.027

Smith, R. C., and Tabar, V. (2019). Constructing and deconstructing cancers using human pluripotent stem cells and organoids. *Cell Stem Cell* 24, 12–24. doi: 10.1016/j.stem.2018.11.012

Swygert, K. E., Parrish, C. A., Cashman, R. E., Lin, R., and Cockerell, C. J. (2007). Melanoma in situ involving an epidermal inclusion (infundibular) cyst. *Am. J. Dermatopathol.* 29, 564–565. doi: 10.1097/DAD.0b013e3181513e5c

Tan, N. S., and Wahli, W. (2014). The emerging role of Nrf2 in dermatotoxicology. *EMBO Mol. Med.* 6, 431–433. doi: 10.1002/emmm.201303797

Tang, L., Madani, S., Lui, H., and Shapiro, J. (2002). Regeneration of a new hair follicle from the upper half of a human hair follicle in a nude mouse. *J. Invest. Dermatol.* 119, 983–984. doi: 10.1046/j.1523-1747.2002.00009.x

Teuliere, J., Faraldo, M. M., Shtutman, M., Birchmeier, W., Huelsken, J., Thiery, J. P., et al. (2004). beta-catenin-dependent and -independent effects of DeltaN-plakoglobin on epidermal growth and differentiation. *Mol. Cell. Biol.* 24, 8649–8661. doi: 10.1128/MCB.24.19.8649-8661.2004

Vidal, V. P., Chaboissier, M. C., Lutzkendorf, S., Cotsarelis, G., Mill, P., Hui, C. C., et al. (2005). Sox9 is essential for outer root sheath differentiation and the formation of the hair stem cell compartment. *Curr. Biol.* 15, 1340–1351. doi: 10.1016/j.cub.2005.06.064

Weber, S., Niessen, M. T., Prox, J., Lullmann-Rauch, R., Schmitz, A., Schwanbeck, R., et al. (2011). The disintegrin/metalloproteinase Adam10 is essential for epidermal integrity and Notch-mediated signaling. *Development* 138, 495–505. doi: 10.1242/dev.055210

Yang, L., Mao, C., Teng, Y., Li, W., Zhang, J., Cheng, X., et al. (2005). Targeted disruption of Smad4 in mouse epidermis results in failure of hair follicle cycling and formation of skin tumors. *Cancer Res.* 65, 8671–8678. doi: 10.1158/0008-5472.CAN-05-0800

Yang, Q., Xue, S. L., Chan, C. J., Rempfler, M., Vischi, D., Gutierrez, F. M., et al. (2020). Cell fate coordinates mechano-osmotic forces in intestinal crypt morphogenesis. *bioRxiv* [Preprint], doi: 10.1101/2020.05.13.094359

Yuhki, M., Yamada, M., Kawano, M., Iwasato, T., Itohara, S., Yoshida, H., et al. (2004). BMPR1A signaling is necessary for hair follicle cycling and hair shaft differentiation in mice. *Development* 131, 1825–1833. doi: 10.1242/dev.01079

Zheng, Y., Du, X., Wang, W., Boucher, M., Parimoo, S., and Stenn, K. (2005). Organogenesis from dissociated cells: generation of mature cycling hair follicles from skin-derived cells. *J. Invest. Dermatol.* 124, 867–876. doi: 10.1111/j.0022-202X.2005.23716.x

Conflict of Interest: The authors declare that the research was conducted in the absence of any commercial or financial relationships that could be construed as a potential conflict of interest.

Copyright © 2021 Qiu, Gu, Chuong and Lei. This is an open-access article distributed under the terms of the Creative Commons Attribution License (CC BY). The use, distribution or reproduction in other forums is permitted, provided the original author(s) and the copyright owner(s) are credited and that the original publication in this journal is cited, in accordance with accepted academic practice. No use, distribution or reproduction is permitted which does not comply with these terms.

frontiers in Cell and Developmental Biology

ORIGINAL RESEARCH
published: 05 February 2021
doi: 10.3389/fcell.2021.633331

Rapamycin Protects Skin Fibroblasts From UVA-Induced Photoaging by Inhibition of p53 and Phosphorylated HSP27

Gen-Long Bai[1†], Ping Wang[1†], Xin Huang[2], Zi-Yue Wang[1], Di Cao[1], Chuan Liu[1], Yi-Yi Liu[1], Ruo-Lin Li[1] and Ai-Jun Chen[1]*

[1] Department of Dermatology, The First Affiliated Hospital of Chongqing Medical University, Yuzhong, China, [2] Prescriptions Department, College of Traditional Chinese Medicine, Chongqing Medical University, Yuzhong, China

OPEN ACCESS

Edited by:
Mingxing Lei,
Chongqing University, China

Reviewed by:
Songmei Geng,
Xi'an Jiaotong University, China
Xiao-Yong Man,
Zhejiang University, China
Xiang Chen,
Central South University, China

***Correspondence:**
Ai-Jun Chen
cajhx@aliyun.com

[†] These authors have contributed equally to this work

Specialty section:
This article was submitted to Stem Cell Research, a section of the journal Frontiers in Cell and Developmental Biology

Received: 25 November 2020
Accepted: 14 January 2021
Published: 05 February 2021

Citation:
Bai G-L, Wang P, Huang X, Wang Z-Y, Cao D, Liu C, Liu Y-Y, Li R-L and Chen A-J (2021) Rapamycin Protects Skin Fibroblasts From UVA-Induced Photoaging by Inhibition of p53 and Phosphorylated HSP27. Front. Cell Dev. Biol. 9:633331. doi: 10.3389/fcell.2021.633331

Skin aging caused by UV radiation is called photoaging is characterized by skin roughness and dryness accompanied by a significant reduction of dermal collagen. Rapamycin is a macrolide immunosuppressant which has been shown to exhibit "anti-aging" effects in cells and organisms, however, its roles in the skin photoaging remains unclear. Here, we investigate the role of rapamycin and HSP27, which we have previously identified as an inhibitor of UV-induced apoptosis and senescence in HaCat cells, in a UVA-induced photoaging model of primary human dermal fibroblasts (HDFs). Results from senescence-associated beta-galactosidase (SA-β-gal) staining revealed that rapamycin significantly reduced senescence in UVA-treated HDFs. In addition, treatment with rapamycin significantly increased cell autophagy levels, decreased the expression of p53 and phosphorylated HSP27, and reduced genotoxic and oxidative cellular stress levels in UVA-induced HDFs. Knockdown of HSP27 resulted in a significant increase of MMP-1 and MMP-3 as well as a decrease in type I collagen expression. Rapamycin mitigated these effects by activation of the classical TGF-β/Smad signaling pathway and increasing the transcriptional activity of MAPK/AP-1. Taken together, these results suggest that rapamycin may potentially serve as a preventive and therapeutic agent for UVA-induced photoaging of the skin.

Keywords: rapamycin, UVA, photoaging, human dermal fibroblasts, Hsp27, autophagy

INTRODUCTION

Photoaging is the result of premature aging of the skin caused by the destructive effects of ultraviolet (UV) radiation. Distinctive clinical features of photoaging include a coarse, dry skin texture, pigmentation disorders, increased wrinkles, and telangiectasia (Young et al., 2017). Pathohistologically, photoaging is characterized by a significant reduction in dermal collagen and the accumulation of abnormal elastin fibers (Han et al., 2014). While the exact pathomechanisms remain unclear, high expression levels and increased activity of matrix metalloproteinases (MMP)-1, 3, and 9 have long been thought to play important roles in the process of photoaging (Nakyai et al., 2017; Seo et al., 2018).

In addition to its role as a molecular chaperone, our previous work revealed a role for HSP27, a member of the small heat shock protein family, in the regulation of apoptosis during skin photoaging. We found that HSP27 can mediate apoptosis in HaCat cells through the mitochondrial caspase pathway by activation of the Akt-dependent phosphorylation pathway and inhibition of the p53/Bax/Bcl-2-dependent mitochondrial apoptosis pathway in order to regulate the subcellular localization of p21 and thereby exerting photoprotective effects (Liu et al., 2019a,b). However, the role of HSP27 in dermal tissue photoaging, especially in UVA-irradiated human dermal fibroblast (HDF) photoaging remains unclear.

Autophagy is an evolutionarily conserved cellular process that is thought to be an essential cell survival mechanism via the degradation of unnecessary or dysfunctional organelles and proteins (Yonekawa and Thorburn, 2013). Decreased or defective autophagy has been linked to a variety of pathological processes, including neurodegeneration, infection, cancer, and aging (Mizushima and Komatsu, 2011). It has been demonstrated that the activation of autophagy can exert anti-apoptotic effects by facilitating UVA-induced clearance of oxidized phospholipid and protein aggregates from keratinocytes (Zhao et al., 2013). More recently, it has been shown that UVA-induced photoaging in fibroblasts impairs lysosomal function and thereby inhibits degradation during autophagy (Huang et al., 2019).

Rapamycin is an inhibitor of mTOR, a serine/threonine protein kinase of the phosphatidylinositol 3-kinase-related kinase family. mTOR is sensitive to a variety of environmental and endocrine stimuli and has important regulatory functions in cell proliferation, metabolism, and the aging process (Arriola Apelo and Lamming, 2016). Rapamycin has previously been successfully used in mouse models of age-related diseases, including cancer and Alzheimer's disease, and it has been demonstrated to improve age-related cognitive decline and even rejuvenate aged hearts in mice (Wilkinson et al., 2012; Lin et al., 2017). A previous studies has suggested that the "anti-aging" effects of rapamycin are achieved by a reduction in reactive oxygen species (ROS) (Qin et al., 2018), however, the exact role and potential protective effects of rapamycin in UVA-induced photoaging of skin fibroblasts, as well as the role of HSP27 in protecting from photoaging, remain unclear.

Previously, we had used a UVB-induced photodamage model in HaCat cells which displayed a range of senescence phenotypes, including altered cell morphology, positive senescence-associated beta galactosidase (SA-β-gal) staining, and cell cycle arrest (Liu et al., 2019a). Here, to reveal the mechanisms underlying dermal photoaging induced by UVA, we investigated the role of rapamycin and HSP27 in a UVA irradiation human dermal fibroblasts (HDFs) photoaging model, focusing on cellular effects including UVA-irradiated cell autophagy.

MATERIALS AND METHODS

Cells

Healthy skin tissues were obtained from patients who underwent skin biopsies at our hospital from December 2018 to July 2020. All procedures were approved by the Ethics Committee of The First Affiliated Hospital of Chongqing Medical University, and all patients provided written informed consent. Healthy skin tissues were cut into fragments under aseptic conditions, and the epidermis and dermis were separated to obtain primary human dermal fibroblasts (HDFs). Tissues were digested with type II collagenase (Sigma-Aldrich, USA) and cultured in Dulbecco's modified Eagle medium (DMEM, Gibco, USA) with 10% fetal bovine serum (FBS, Absin, China) at 37°C under 5% CO_2. This study was conducted using two to four generations of fibroblasts.

Ultraviolet a (UVA) Irradiation Cell Model

For all experiments, HDFs with high cell viability and rapid proliferation were selected. In the UVA irradiation group, fibroblasts were irradiated with 5 J/cm² once per day for 8 days using a UVA lamp (TL10RS, Philips, Netherlands) with an emission spectrum between 320 and 400 nm. UVA irradiation was measured by a UVA 365 radiometer (Photoelectric Instrument Factory of Beijing Normal University, China). Control cells were exposed to the same conditions but not UVA-irradiated.

Evaluation of Cellular Viability

The viability of HDFs following exposure to different doses of UVA and different concentrations of rapamycin were assessed using the CCK-8 assay (MCE, USA). Cells were incubated with MTT solution for 1 h, and absorbance was measured at 450 nm using Multiskan Spectrum(ThermoFisher Scientific, USA).

RNA Isolation and Real Time PCR (RT-PCR)

Total RNA was extracted using the RNAiso Plus kit (TaKaRa, Japan) and converted to cDNA using the RT Master Mix for qPCR (MCE, USA). The SYBR Green qPCR Master Mix (MCE, USA) was used for RT-PCR. For each reaction, a total of 35 cycles were carried out. Primer sequences were as follows:

Name	Forward primer (5'->3')	Reverse primer (5'->3')
Collagen 1	AAGGTGTTGTGC GATGACG	GGTTTCTTGGTCG GTGGGT
MMP-1	GGCTGAAAGTGAC TGGGAAAC	CTTGGCAAATCT GGCGTG
MMP-3	CAATCCTACTG TTGCTGTGCG	CAAGGTTCATGC TGGTGTCC
MMP-9	TTTGACAGCGAC AAGAAGTGG	TCAGGGCGAGG ACCATAGAG
p62	TGAGTCCCTCTCC CAGATGCT	GGGGGATGCTTTG AATACTGG
HSP27	CCCACCCAAGT TTCCTCCT	GGCAGTCTCATC GGATTTTG
LC3 B	AAGGCGCTTACAG CTCAATG	ACACTGACAAT TTCATCCCGA
ACTB	AGAAAATCTGG CACCACACCT	GATAGCACAGCCT GGATAGCA

Western Blotting

RIPA lysis buffer (Beyotime Biotechnology, China), including Protease Inhibitor Cocktail (MCE, USA), was used to extract

proteins. The total protein concentration in each sample was assessed using the BCA assay (Beyotime Biotechnology, China). Proteins were separated on 10 and 12% polyacrylamide gels using SDS-PAGE and transferred to nitrocellulose membranes. Sequentially, the membranes were blocked in 7% skimmed milk for 1 h at room temperature and incubated with primary antibodies and secondary antibodies. Finally, protein bands were visualized using the SuperSignal™ West Femto Maximum Sensitivity Substrate kit (ThermoFisher Scientific, USA). Protein bands were quantified by densitometry and normalized to β-actin. The antibodies used in this study: HSP27(Abcam, UK), Phosphorylated-HSP27, beta-Actin, p53, COL1A1(Cell Signaling Technology, USA), p62, LC3 B, ATG5 (Bimake, USA).

siRNA Transfection

siRNAs were obtained from GenePharma (Shanghai, China). The siRNA sequences used to inhibit HSP27 expression were 5'-GGACGAGCAUGGCUACAUCTT-3' (sense strand) and 5'-GAUGUAGCCAUGCUCGUCCTT-3' (antisense strand). HDFs with good cell viability and rapid proliferation were selected for transfection. Fibroblasts were inoculated in 6-well plates and pre-cultured for 24 h, and experiments were performed after the cells were completely walled. The complete medium was then replaced by serum-free medium and siRNA and HiPerFect Transfection Reagent (Qiagen, Germany) were added. Transfection continued for 6 h before replacing serum-free medium with complete medium for subsequent experiments.

Senescence-Associated Beta-Galactosidase (SA-β-gal) Staining

Cells were stained using the Senescence β-Galactosidase Staining Kit (Beyotime Biotechnology, China) according to the manufacturer's instructions. At room temperature, the medium was discarded and cells were washed once with PBS and fixed with 4% polymethanol for 15 min. Cells were again washed three times with PBS and incubated with the staining solution overnight at 37°C. Samples were observed and counted under a reverse-phase microscope (200x) (Olympus, Japan), and five randomly collected images were used for quantification of senescent cells.

Histological Analysis

We selected pathological tissue specimens for immunohistochemical labeling and Masson staining from five patients with a clinical diagnosis of chronic actinic dermatitis and six patients have normal skin with cosmetic surgery. All the patients signed informed consent. Clinically removed skin specimen were fixed with 4% paraformaldehyde and then paraffin-embedded for sectioning. Each specimen was subjected to hematoxylin-eosin staining, Masson-trichrome staining, and immunohistochemical labeling. Under the microscope, five randomly selected fields of view were used to collect images for subsequent analysis.

Flow Cytometry to Detect Apoptosis

Twenty-four hours after the last UVA irradiation, cells grown in the 6-well plates as well as the supernatant were collected, labeled with Annexin V-fluorescein isothiocyanate and propidium iodide, and apoptotic cells were detected by flow cytometry (Beckman Coulter, UK). The number of apoptotic cells was analyzed using the Flowjo_v10 software.

Statistical Analysis

All experiments were repeated at least three times. Statistical analyses were performed using Graphpad Prism 8 (GraphPad Software Inc., USA) and SPSS v22.0 (IBM Corporation, USA), and data are presented as mean ± SD. Between-group comparisons were performed using ANOVA or student's *t*-test for statistical analysis. $p < 0.05$ was considered statistically significant.

RESULTS

Optimization of UVA and Rapamycin Dosage

Based on previously published work, we initially assessed the effect of 5, 10, and 20 J/cm² for our UVA-induced photoaging model in primary human dermal fibroblasts (Nakyai et al., 2017; Xu et al., 2018; Souza et al., 2020). As we observed a high level of cell death at 20 J/cm², we proceeded using 5 and 10 J/cm² for HDF treatment in subsequent experiments. As shown in **Figure 1A**, there were significantly more senescent (SA-β-gal positive) HDFs after UVA irritation, but there was no difference between the 5 and 10 J/cm² UVA irritation groups. Moreover, at the protein level, there was a significant increase in the expression of p-HSP27 and p62, and a decrease in LC3 II/LC3 I in both UVA irritation groups as compared to controls (**Figure 1B**). The same results were also reflected in the mRNA level (**Figures 1C–E**). Levels of ATG5 correspond to the early stages of autophagosome formation. These were not significantly altered after UVA irritation (**Figures 1B,F**), neither at mRNA nor protein level. As our results showed that a relatively low dose of UVA is sufficient to induce photoaging, we chose UVA irradiation of 5 J/cm² for our model.

To determine the optimal concentration of rapamycin for subsequent experiments, we evaluated the cytotoxic and anti-apoptotic effects of rapamycin on primary HDFs in the concentration range of 0–10 μM. Our results showed that there is no cytotoxic effect of rapamycin at 0–10 μM (**Figure 2C**), while 5 μM of rapamycin showed an anti-apoptotic efficacy in UVA-treated cells (**Figures 2A,B**).

Rapamycin Reduces UVA-Induced Cellular Senescence

HDFs in the UVA irradiation group showed a large degree of senescence in the UVA irritation group compared to the control group, but this increase in senescence could be reversed by rapamycin treatment (**Figures 2D,E**).

Rapamycin Promotes Autophagy in UVA-Irradiated HDFs

Light chain protein 3 (LC3) is a key molecule in the autophagy pathway. In the presence of autophagic activation, LC3I converts to LC3II and binds to the membrane of the autophagosome, thus the LC3II/LC3I ratio is widely used to assess autophagy

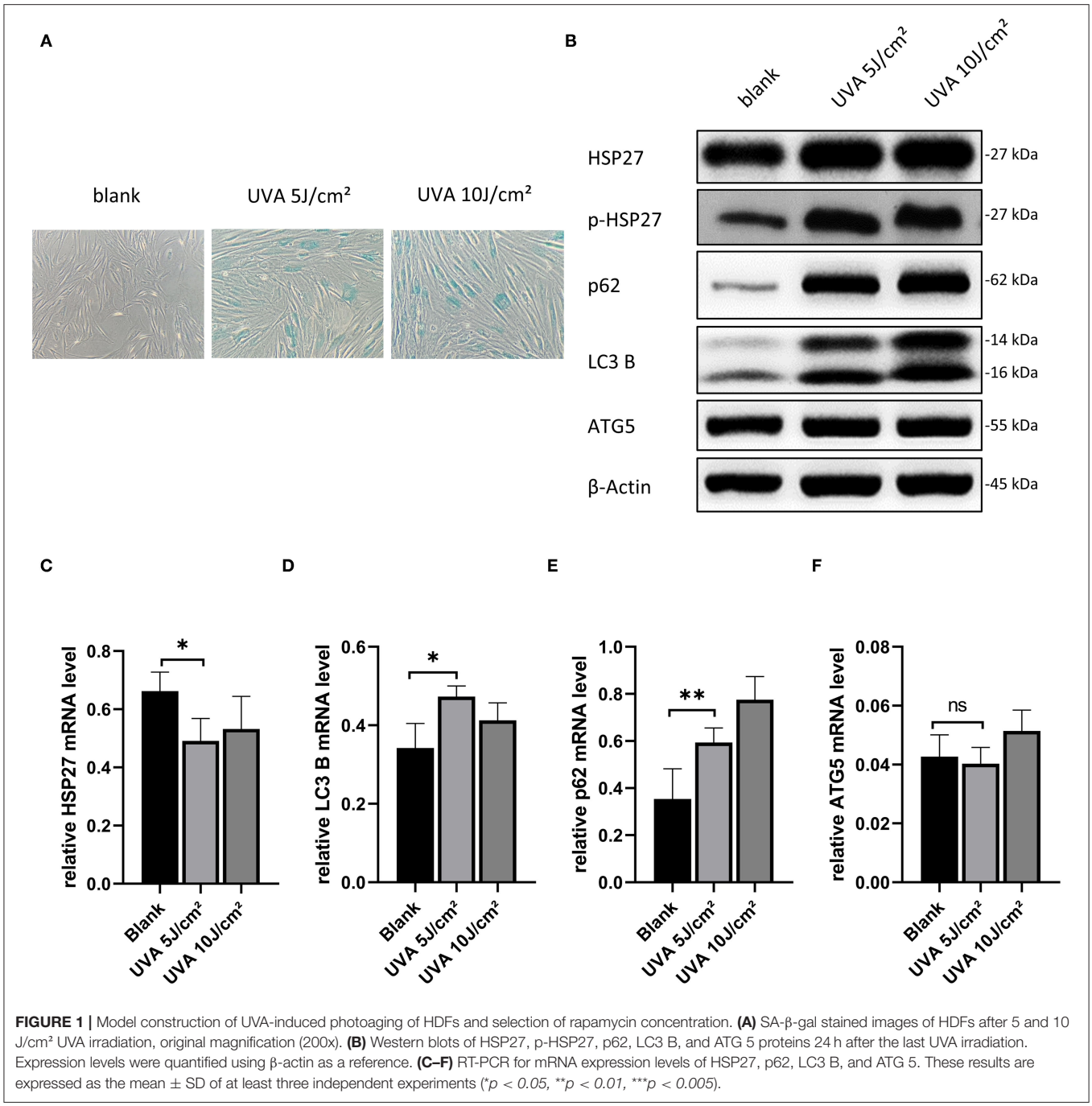

FIGURE 1 | Model construction of UVA-induced photoaging of HDFs and selection of rapamycin concentration. **(A)** SA-β-gal stained images of HDFs after 5 and 10 J/cm² UVA irradiation, original magnification (200x). **(B)** Western blots of HSP27, p-HSP27, p62, LC3 B, and ATG 5 proteins 24 h after the last UVA irradiation. Expression levels were quantified using β-actin as a reference. **(C–F)** RT-PCR for mRNA expression levels of HSP27, p62, LC3 B, and ATG 5. These results are expressed as the mean ± SD of at least three independent experiments (*$p < 0.05$, **$p < 0.01$, ***$p < 0.005$).

levels (Li et al., 2011). HDFs irradiated with UVA showed a significant decrease in LC3II/LC3I expression compared to the control group, while there was no significant change in p62, which is a substrate for the autophagic degradation phase (Lamark et al., 2017), indicating that UVA causes the cellular autophagic flow to stagnate in the degradation phase. However, the expression of both p53 and p-HSP27 was significantly increased, indicating that HDFs exhibited elevated stress levels in response to UVA. Both with and without UVA irradiation, the autophagic flux was significantly increased in rapamycin-treated HDFs, while the expression of both p53 and p-HSP27 was significantly decreased, suggesting that rapamycin may be able to counter UVA-induced increases in cellular stress levels. However, surprisingly, p62 levels following UVA irradiation remained unchanged even after activation of the autophagy pathway with rapamycin, further confirming that UVA irradiation induces an impairment of degradation during autophagy (**Figure 3**).

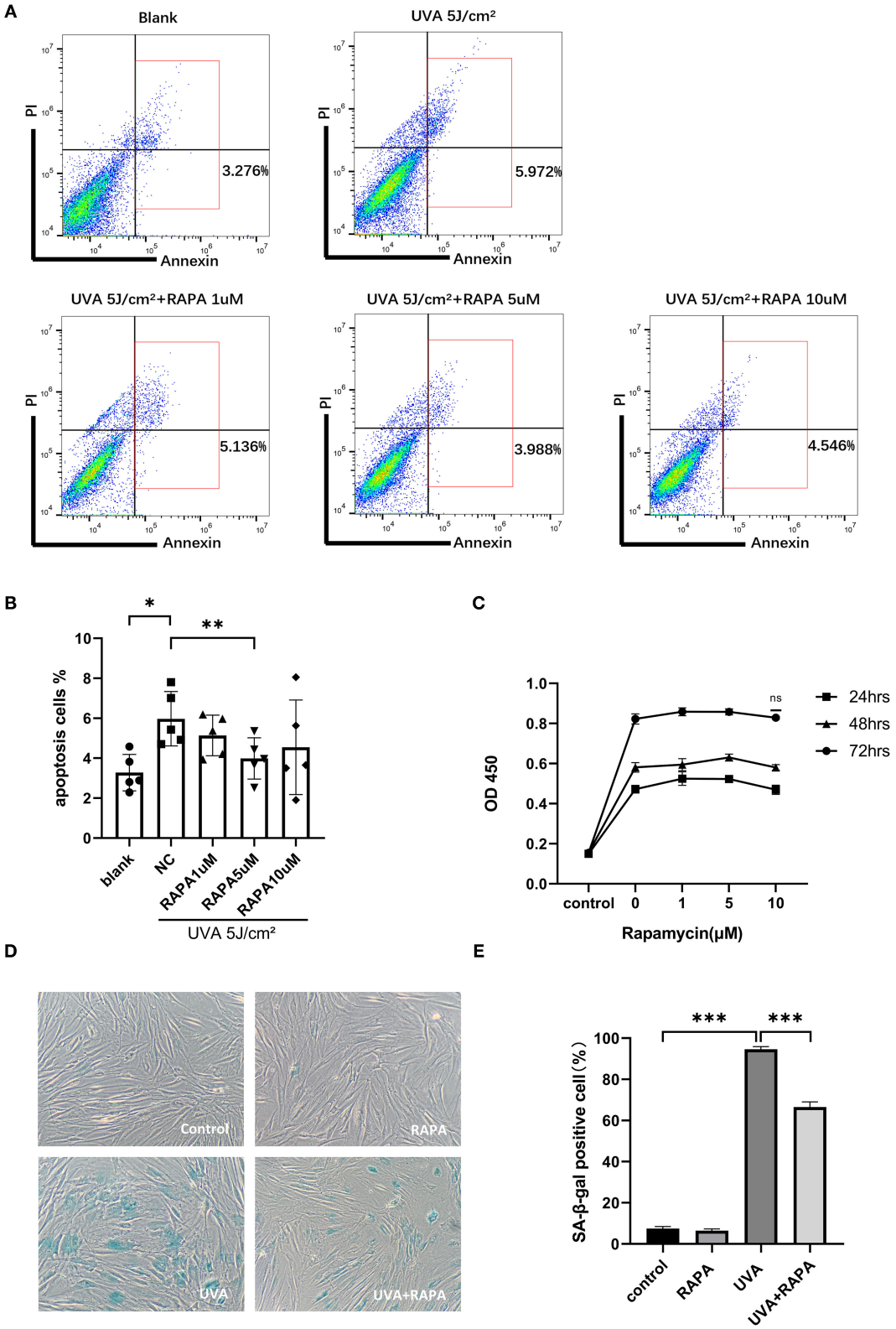

FIGURE 2 | Selection of rapamycin concentration and SA-β-gal staining of HDFs. **(A,B)** Flow cytometry showed that UVA significantly increased apoptosis in HDFs and 5 μM rapamycin was effective in reducing UVA-induced apoptosis of HDFs. **(C)** The proliferative activity of HDFs after 24, 48, and 72 h incubation with rapamycin (0–10 μM) was analyzed using the CCK-8 colorimetric assay, and results are expressed as OD ± SD. This revealed no statistical difference compared with the control

(Continued)

FIGURE 2 | group. **(D)** There were significantly more SA-β-gal(+) cells in the UVA group and fewer and lighter staining in the UVA+rapamycin group than in the UVA group. Few SA-β-gal(+) cells are seen in the control and rapamycin groups. **(E)** SA-β-gal positivity was calculated based on 400 cells counted per well. Results are expressed as mean ± SD of at least three independent experiments (*$p < 0.05$, **$p < 0.01$, ***$p < 0.005$).

Effect of Rapamycin on HDFs Following siRNA Knockdown of HSP27

To investigate the effect of HSP27 on autophagy in UVA-induced photoaging HDFs, as well as the role of rapamycin in HDFs, we constructed HSP27 knockdown HDFs by using HSP27 siRNA (**Figures 4A,D**).We subsequently detected the expression of autophagy-associated p62 and LC3B in the control and si-HSP27 group by western blotting, and found that HSP27 knockdown suppressed the expression LC3B expression regardless of UVA irradiation, while it increased the expression of p62 following UVA exposure (**Figures 4B,E,F**).

It has been reported that UVA can significantly decrease the expression of type I collagen and increase the expression of MMP-1, 2, 3, and 9 in photoaged cells (Pittayapruek et al., 2016), and we have previously observed similar results in our models. Interestingly, regardless of UVA exposure, we found a significant increase in the expression of MMP-1 and 3, as well as a significant decrease in type I collagen mRNA levels following knockdown of HSP27 in HDFs. However, this effect was alleviated in the rapamycin-treated group. Therefore, we hypothesize that HSP27 may be involved in the synthesis of MMPs and collagen degradation, and rapamycin could alleviate alterations induced by HSP27 deficiencies or dysfunction (**Figures 4B,C,G,H**).

Expression of Type I Collagen, HSP27 and Autophagy-Related Proteins in Clinical Tissues

To further investigate the relationship between HSP27, autophagy and type I collagen, we selected tissues from normal skin biopsies and from patients with a diagnosis of chronic actinic dermatitis (CAD) for Masson staining and immunohistochemical labeling of HSP27, LC3 B, p62, and Collagen I. Compared to normal patients, skin tissue from patients with photoaged dermatitis expressed lower levels of HSP27, LC3 B, and Collagen I, while p62 expression showed diffuse flaky positive foci. Masson staining revealed that the dermal collagen in CAD patients was partially pale, disorganized and loose, and the collagen fibers were significantly reduced. These results suggested that photoaged skin exhibits lower levels of autophagy and collagen fibers than normal skin, which was consistent with our *in vitro* experiments (**Figure 5**).

DISCUSSION

Dermal fibroblasts are the major cellular component of the dermis, producing collagen, fibronectin, glycosaminoglycans and other extracellular matrix components which support the dermal structure and help to maintain skin elasticity and moisture (Thulabandu et al., 2018). UVA is a potent form of UV radiation that can damage dermal fibroblasts. UVA exposure leads to fibroblast cell cycle arrest, apoptosis, dysfunction of secretion and synthesis and skin aging (Wlaschek et al., 2001). The skin of the head and face is particularly susceptible to photoaging due to its continuous and long-term exposure to the environment. In order to avoid intrinsic photoaging, we selected skin tissues from non-exposed regions for our primary fibroblast culture in this study. There is currently no "gold standard" for *in vitro* modeling of UVA-induced fibroblast photoaging. Based on the literature and previous studies conducted in our group, we initially tested irradiation with 5, 10, and 20 J/cm² UVA on HDFs, respectively, to identify the appropriate irradiation dose. This revealed that, with the exception of 20 J/cm² UVA irradiation which induced significant cell death, both 5 and 10 J/cm² UVA caused significant senescent morphological changes in HDFs as well as positive SA-β-gal staining. As we aimed to model chronic photoaging in this project, we chose the lower dose of 5 J/cm² of UVA as the irradiation dose for our experimental model. Hereby, we provide a new *in vitro* model of UVA-induced fibroblast photoaging.

HSP27 has previously been considered as an adaptive cellular response protein that helps the organism to survive due to its protective effects against heat-induced cellular damage and its primary function as a molecular chaperone involved in protein folding and a variety of cellular processes (Singh et al., 2017). Additionally, the phosphorylated form of HSP27 can interact with denatured and aggregated proteins to protect cells against severe damage from stress (Kampinga et al., 1994; Trott et al., 2009). In previous studies, we have demonstrated that HSP27 is significantly elevated in photoaged rat skin and HaCaT cells and exerts protective effects against photoaging by modulating anti-apoptotic pathways (Liu et al., 2019a,b). In our UVA photoaging model, we found no significant increase in the expression of HSP27, while phosphorylated HSP27 increased significantly. This suggested that p-HSP27 may be more important for protection from photoaging in HDFs.

Rapamycin is a classical activator of autophagy which acts by inhibiting the activity of mTOR (Arriola Apelo and Lamming, 2016). Autophagy is activated following UVA-induced genotoxic stress and elevated ROS levels (Galati et al., 2019). Rapamycin has been reported to reduce UVB-induced ROS accumulation and promote the antioxidant capacities of cells (Qin et al., 2018). In our study, p-HSP27 was significantly decreased after rapamycin treatment, which also seems to suggest that rapamycin reduced the level of UVA-induced oxidative stress on cells. The tumor suppressor p53 is involved in a variety of cellular processes such as apoptosis, necrosis, aging and autophagy, and is also a major constituted of the DNA damage response pathway (Mrakovcic and Frohlich, 2018). In our UVA-induced photoaging model of HDFs, a significant elevation of p53 was accompanied by activation of the autophagy pathway, and treatment with rapamycin inhibited the sustained increase in p53 expression despite elevated levels of cellular autophagy,

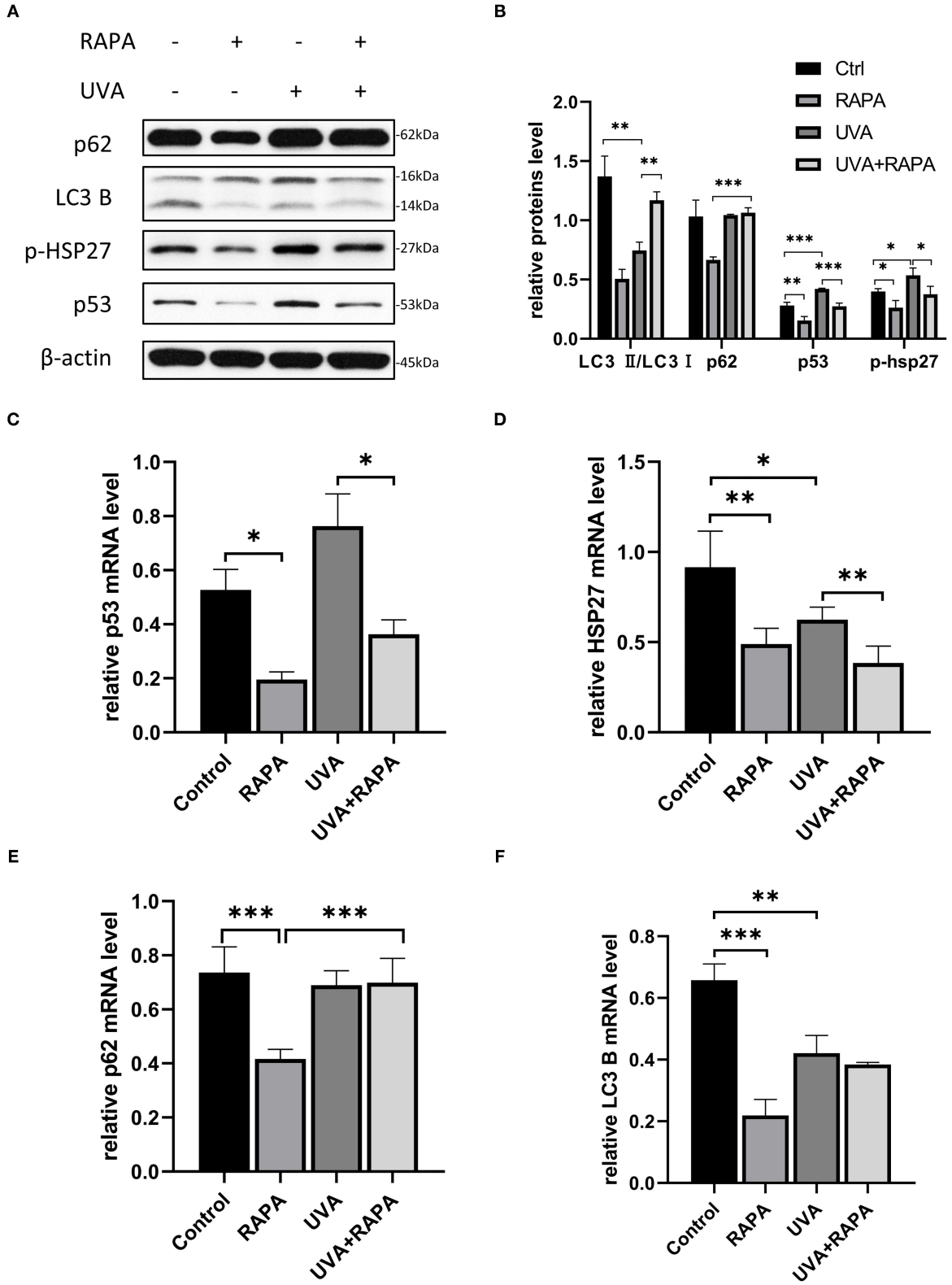

FIGURE 3 | 5μM Rapamycin treatment of UVA-induced photoaged HDFs promoted increased autophagy, reduced the expression of p-HSP27 and p53, and decreased the stress levels of cells. **(A,B)** Western blots of p62, LC3 B, p-HSP27, and p53 expression after 24 h of rapamycin treatment. Proteins were quantified using β-actin as reference and expressed as a fold change in protein levels compared to control cells. Results are expressed as mean ± SD of at least three

(Continued)

FIGURE 3 | experiments (*$p < 0.05$, **$p < 0.01$, ***$p < 0.005$). **(C–F)** RT-PCR for mRNA expression levels of p62, LC3 B, p-HSP27 and p53. Results are expressed as mean ± SD of at least three assays (*$p < 0.05$, **$p < 0.01$, ***$p < 0.005$).

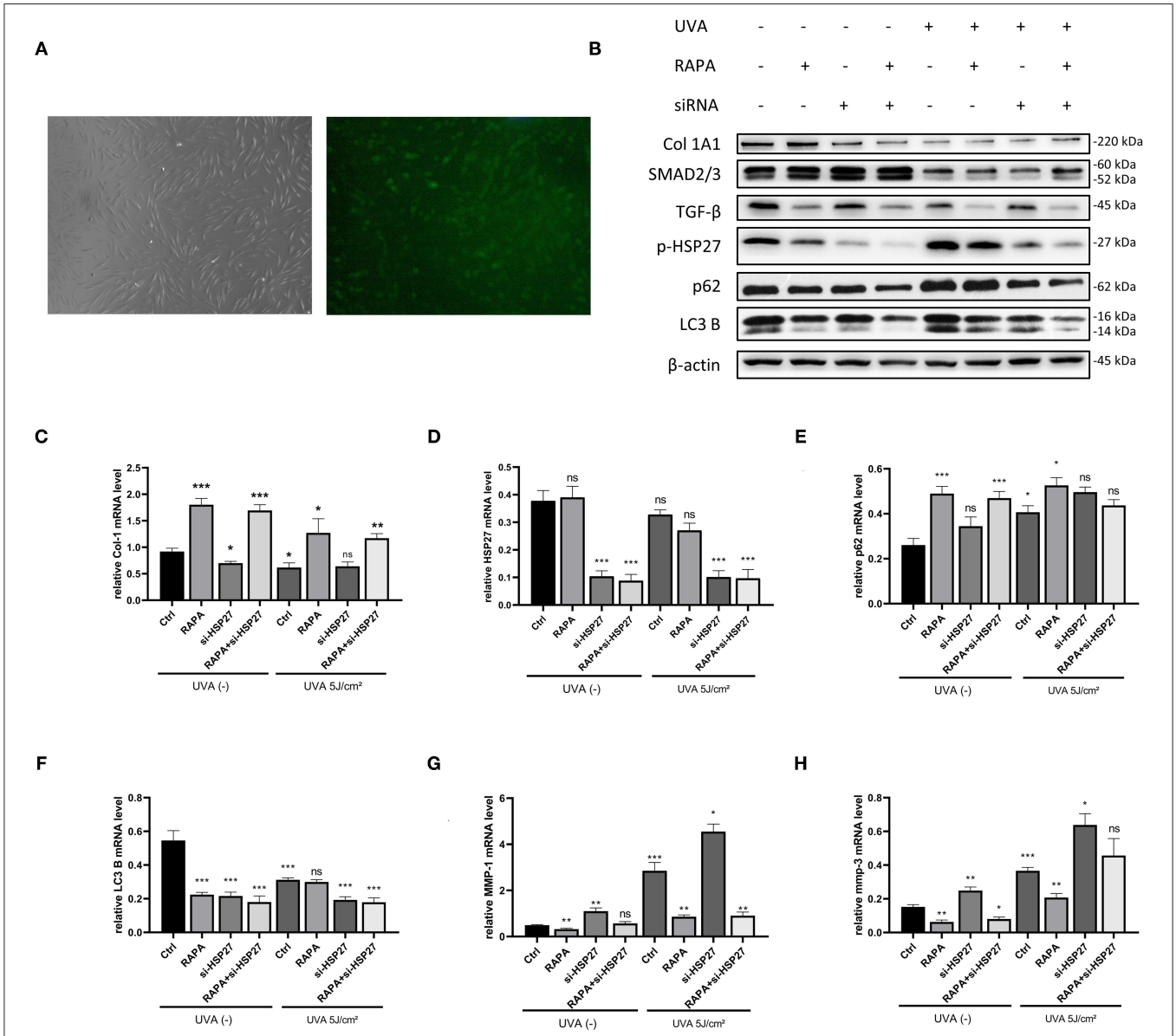

FIGURE 4 | 5μM Rapamycin treatment of UVA-induced photoaged si-HSP27 HDFs reduced the collagen reduction and MMP-1 and 3 expression following UVA irradiation and knockdown of HSP27. **(A)** Fluorescence microscopy of FAM-labeled HSP27 siRNA-transfected fibroblasts at original magnification (40x), transfection efficiency around 80%. **(B)** Western blot of Collagen I, TGF-β,SMAD2/3,p-HSP27, p62, and LC3 B expression of knockdown HSP27 HDFs after 24 h of rapamycin treatment. Proteins were quantified using β-actin as reference and expressed as a fold change in protein levels compared to control cells. Results are expressed as mean ± SD of at least three assays (*$p < 0.05$, **$p < 0.01$, ***$p < 0.005$). **(C–H)** RT-PCR was performed to detect the mRNA expression levels of Collagen I, p-HSP27, p62, and LC3 B. The mRNA expression levels of Collagen I, p-HSP27, p62, and LC3 B were determined by RT-PCR. Results are expressed as mean ± SD of at least three assays (*$p < 0.05$, **$p < 0.01$, ***$p < 0.005$).

preventing programmed cell death due to over-activation of autophagy. Taken together, these results indicate a potential of rapamycin to protect against oxidative and genotoxic stress, and despite the many well-documented adverse effects of rapamycin as an immunosuppressant, our experimental results suggest it may be suitable as a anti-photoaging agent.

Repeated exposure to sunlight causes skin photoaging, which is characterized by coarse, dry skin texture, pigmentation disorders, increased wrinkles, and capillary dilatation. The mechanisms underlying skin photoaging have been suggested to involve alterations in cellular composition, a significant reduction in dermal collagen, accumulation of abnormal elastic

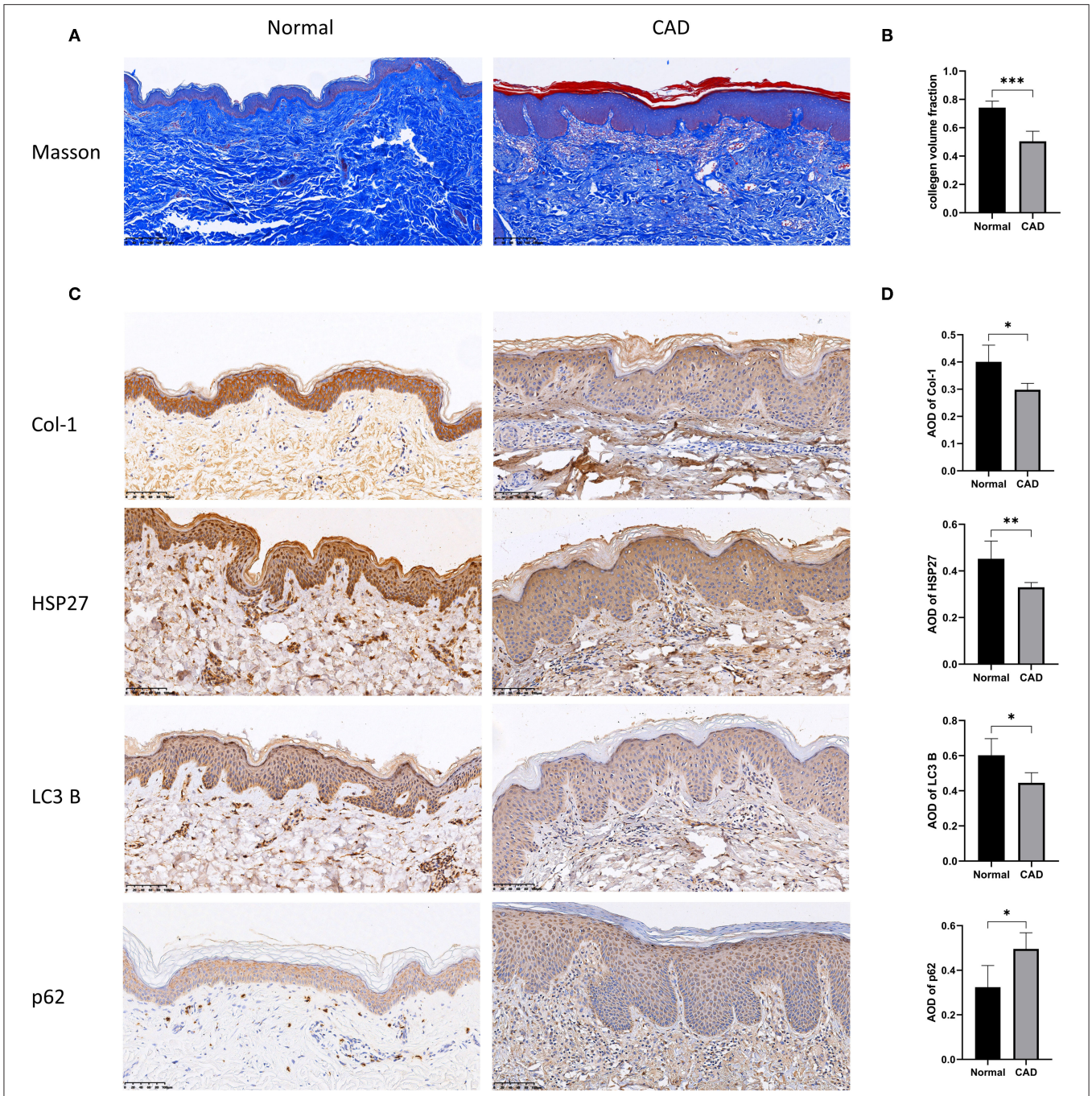

FIGURE 5 | Histopathological results of the skin of normal and photoaged groups using Masson trichrome staining and immunohistochemical labeling. **(A,B)** Histopathological results of Masson staining of skin from normal and photoaged groups. The collagen volume fraction was calculated, which is expressed as mean ± SD of at least three measurements (*$p < 0.05$, **$p < 0.01$, ***$p < 0.005$). **(C,D)** Immunohistochemical markers for Collagen I, HSP27, p62 and LC3 B and quantification of Average Optical Density (AOD) were performed on normal and photoaged skin, and the results are expressed as mean ± SD of at least three measurements (*$p < 0.05$, **$p < 0.01$, ***$p < 0.005$).

fibers, and degradation of extracellular matrix components (Amano, 2016). It has been shown that UVA-induced photoaging increases the expression of MMPs and inhibits the synthesis of type I collagen (Varani et al., 2001), which we were able to confirm in this study as the expression of MMP-1 and MMP-3 was significantly increased, while the expression of type I collagen was significantly decreased in UVA-irradiated HDFs. Interestingly, when HSP27 was knocked down, a further exacerbation of the

UVA-induced increase in MMPs expression and degradation of type I collagen was observed. This may suggest that HSP27 is involved in the regulation of MMPs and collagen, and exerts its effects in anti-photoaging, at least in part, via these cellular components. After rapamycin treatment, the effects of UVA irradiation and knocked down HSP27 were abolished: the expression of MMPs was decreased and an increased synthesis of type I collagen was observed. These effects of rapamycin might be achieved via activation of the classical TGF-β/Smad signaling pathway and the transcriptional activation of MAPK/AP-1 (Wu et al., 2018). However, in our results, rapamycin was not shown to increase the expression of TGF-β, but significantly decreased it. Rapamycin has been reported to directly activate the TGF-β receptor (Miyakawa et al., 2018), thus activating the TGF-β/SMAD pathway and increasing the expression of type I collagen.

Despite promising findings in this study, we have not yet been able to determine in what way rapamycin regulates HSP27 to exert its anti-photoaging effects and can thus far only speculate about the potential pathways by which this regulation may occur. In future studies, we will continue to explore the mechanisms of the regulation of autophagy and anti-photoaging by HSP27 in depth.

DATA AVAILABILITY STATEMENT

The original contributions generated for the study are included in the article/supplementary material, further inquiries can be directed to the corresponding author/s.

ETHICS STATEMENT

The studies involving human participants were reviewed and approved by The first affiliated hospital of Chongqing Medical University of ethics committee. The patients/participants provided their written informed consent to participate in this study.

AUTHOR CONTRIBUTIONS

G-LB and PW performed all experiments, wrote the manuscript, and interpreted the data. XH and A-JC provided technical support for this study. Z-YW, DC, CL, Y-YL, and R-LL reviewed the literature. G-LB and PW contributed equally to this work. All authors examined the manuscript and approved the conclusions.

FUNDING

This work was financially supported by National Natural Science Foundation of China (Nos. 81874238 and 81573027) and Natural Science Foundation Project of CQ (No. cstc2016jcyjA0430).

ACKNOWLEDGMENTS

We thank the Laboratory Research Center of the First Affiliated Hospital of Chongqing Medical University and the Department of dermatology of the First Affiliated Hospital of Chongqing Medical University for Technical Support.

REFERENCES

Amano, S. (2016). Characterization and mechanisms of photoageing-related changes in skin. Damages of basement membrane and dermal structures. *Exp. Dermatol*. 25(Suppl. 3), 14–19. doi: 10.1111/exd.13085

Arriola Apelo, S. I., and Lamming, D. W. (2016). Rapamycin: an InhibiTOR of aging emerges from the soil of easter island. *J. Gerontol. A Biol. Sci. Med. Sci*. 71, 841–849. doi: 10.1093/gerona/glw090

Galati, S., Boni, C., Gerra, M. C., Lazzaretti, M., and Buschini, A. (2019). Autophagy: a player in response to oxidative stress and DNA damage. *Oxid. Med. Cell. Longev*. 2019:5692958. doi: 10.1155/2019/5692958

Han, A., Chien, A. L., and Kang, S. (2014). Photoaging. *Dermatol. Clin*. 32, 291–299. doi: 10.1016/j.det.2014.03.015

Huang, Y., Li, Y., Qu, Y., Zheng, Y., Ouyang, M., Zhang, Y., et al. (2019). UVA-induced photoaging inhibits autophagic degradation by impairing lysosomal function in dermal fibroblasts. *Biochem. Biophys. Res. Commun*. 518, 611–618. doi: 10.1016/j.bbrc.2019.08.103

Kampinga, H. H., Brunsting, J. F., Stege, G. J., Konings, A. W., and Landry, J. (1994). Cells overexpressing Hsp27 show accelerated recovery from heat-induced nuclear protein aggregation. *Biochem. Biophys. Res. Commun*. 204, 1170–1177. doi: 10.1006/bbrc.1994.2586

Lamark, T., Svenning, S., and Johansen, T. (2017). Regulation of selective autophagy: the p62/SQSTM1 paradigm. *Essays Biochem*. 61, 609–624. doi: 10.1042/EBC20170035

Li, M., Hou, Y., Wang, J., Chen, X., Shao, Z. M., and Yin, X. M. (2011). Kinetics comparisons of mammalian Atg4 homologues indicate selective preferences toward diverse Atg8 substrates. *J. Biol. Chem*. 286, 7327–7338. doi: 10.1074/jbc.M110.199059

Lin, A. L., Jahrling, J. B., Zhang, W., DeRosa, N., Bakshi, V., Romero, P., et al. (2017). Rapamycin rescues vascular, metabolic and learning deficits in apolipoprotein E4 transgenic mice with pre-symptomatic Alzheimer's disease. *J. Cereb. Blood Flow Metab*. 37, 217–226. doi: 10.1177/0271678X15621575

Liu, C., Huang, X., Wang, P., Pan, Y., Cao, D., Liu, Y. Y., et al. (2019a). Interference of Hsp27 results in apoptosis induced by photodamage via regulation of subcellular localization of p21 in immortalized human keratinocytes. *Med. Sci. Monit*. 25, 7557–7566. doi: 10.12659/MSM.917164

Liu, Y., Huang, X., Wang, P., Pan, Y., Cao, D., Liu, C., et al. (2019b). The effects of HSP27 against UVB-induced photoaging in rat skin. *Biochem. Biophys. Res. Commun*. 512, 435–440. doi: 10.1016/j.bbrc.2019.03.076

Miyakawa, A., Girão-Silva, T., Krieger, J., and Edelman, E. (2018). Rapamycin activates TGF receptor independently of its ligand: implications for endothelial dysfunction. *Clin. Sci*. 132, 437–447. doi: 10.1042/CS20171457

Mizushima, N., and Komatsu, M. (2011). Autophagy: renovation of cells and tissues. *Cell* 147, 728–741. doi: 10.1016/j.cell.2011.10.026

Mrakovcic, M., and Frohlich, L. F. (2018). p53-Mediated Molecular Control of Autophagy in Tumor Cells. *Biomolecules* 8:14. doi: 10.3390/biom8020014

Nakyai, W., Saraphanchotiwitthaya, A., Viennet, C., Humbert, P., and Viyoch, J. (2017). An *in vitro* model for fibroblast photoaging comparing single and repeated UVA irradiations. *Photochem. Photobiol*. 93, 1462–1471. doi: 10.1111/php.12801

Pittayapruek, P., Meephansan, J., Prapapan, O., Komine, M., and Ohtsuki, M. (2016). Role of matrix metalloproteinases in photoaging and photocarcinogenesis. *Int. J. Mol. Sci*. 17:868. doi: 10.3390/ijms17060868

Qin, D., Ren, R., Jia, C., Lu, Y., Yang, Q., Chen, L., et al. (2018). Rapamycin protects skin fibroblasts from ultraviolet B-induced photoaging by suppressing the production of reactive oxygen species. *Cell. Physiol. Biochem*. 46, 1849–1860. doi: 10.1159/000489369

Seo, S. W., Park, S. K., Oh, S. J., and Shin, O. S. (2018). TLR4-mediated activation of the ERK pathway following UVA irradiation contributes to increased cytokine

and MMP expression in senescent human dermal fibroblasts. *PLoS ONE* 13:e0202323. doi: 10.1371/journal.pone.0202323

Singh, M. K., Sharma, B., and Tiwari, P. K. (2017). The small heat shock protein Hsp27: present understanding and future prospects. *J. Therm. Biol.* 69, 149–154. doi: 10.1016/j.jtherbio.2017.06.004

Souza, C., Monico, D. A., and Tedesco, A. C. (2020). Implications of dichlorofluorescein photoinstability for detection of UVA-induced oxidative stress in fibroblasts and keratinocyte cells. *Photochem. Photobiol. Sci.* 19, 40–48. doi: 10.1039/C9PP00415G

Thulabandu, V., Chen, D., and Atit, R. P. (2018). Dermal fibroblast in cutaneous development and healing. *Wiley Interdiscip. Rev. Dev. Biol.* 7:e307. doi: 10.1002/wdev.307

Trott, D., McManus, C. A., Martin, J. L., Brennan, B., Dunn, M. J., and Rose, M. L. (2009). Effect of phosphorylated hsp27 on proliferation of human endothelial and smooth muscle cells. *Proteomics* 9, 3383–3394. doi: 10.1002/pmic.200800961

Varani, J., Spearman, D., Perone, P., Fligiel, S. E., Datta, S. C., Wang, Z. Q., et al. (2001). Inhibition of type I procollagen synthesis by damaged collagen in photoaged skin and by collagenase-degraded collagen *in vitro*. *Am. J. Pathol.* 158, 931–942. doi: 10.1016/S0002-9440(10)64040-0

Wilkinson, J. E., Burmeister, L., Brooks, S. V., Chan, C. C., Friedline, S., Harrison, D. E., et al. (2012). Rapamycin slows aging in mice. *Aging Cell* 11, 675–682. doi: 10.1111/j.1474-9726.2012.00832.x

Wlaschek, M., Tantcheva-Poor, I., Naderi, L., Ma, W., Schneider, L. A., Razi-Wolf, Z., et al. (2001). Solar UV irradiation and dermal photoaging. *J. Photochem. Photobiol. B. Biol.* 63, 41–51. doi: 10.1016/S1011-1344(01)00201-9

Wu, Y., Wang, W., Peng, X. M., He, Y., Xiong, Y. X., Liang, H. F., et al. (2018). Rapamycin upregulates connective tissue growth factor expression in hepatic progenitor cells through TGF-beta-Smad2 dependent signaling. *Front. Pharmacol.* 9:877. doi: 10.3389/fphar.2018.00877

Xu, X., Zheng, Y., Huang, Y., Chen, J., Gong, Z., Li, Y., et al. (2018). Cathepsin D contributes to the accumulation of advanced glycation end products during photoaging. *J. Dermatol. Sci.* 90, 263–275. doi: 10.1016/j.jdermsci.2018.02.009

Yonekawa, T., and Thorburn, A. (2013). Autophagy and cell death. *Essays Biochem.* 55, 105–117. doi: 10.1042/bse0550105

Young, A. R., Claveau, J., and Rossi, A. B. (2017). Ultraviolet radiation and the skin: photobiology and sunscreen photoprotection. *J. Am. Acad. Dermatol.* 76, S100–S109. doi: 10.1016/j.jaad.2016.09.038

Zhao, Y., Zhang, C. F., Rossiter, H., Eckhart, L., Konig, U., Karner, S., et al. (2013). Autophagy is induced by UVA and promotes removal of oxidized phospholipids and protein aggregates in epidermal keratinocytes. *J. Invest. Dermatol.* 133, 1629–1637. doi: 10.1038/jid.2013.26

Conflict of Interest: The authors declare that the research was conducted in the absence of any commercial or financial relationships that could be construed as a potential conflict of interest.

Copyright © 2021 Bai, Wang, Huang, Wang, Cao, Liu, Liu, Li and Chen. This is an open-access article distributed under the terms of the Creative Commons Attribution License (CC BY). The use, distribution or reproduction in other forums is permitted, provided the original author(s) and the copyright owner(s) are credited and that the original publication in this journal is cited, in accordance with accepted academic practice. No use, distribution or reproduction is permitted which does not comply with these terms.

frontiers in Cell and Developmental Biology

BRIEF RESEARCH REPORT
published: 05 February 2021
doi: 10.3389/fcell.2021.571474

Dietary Vitamin A Impacts Refractory Telogen

*Liye Suo[1], Christine VanBuren[2], Eylul Damla Hovland[2], Natalia Y. Kedishvili[3], John P. Sundberg[4] and Helen B. Everts[1,2]**

[1] Department of Human Nutrition, The Ohio State University, Columbus, OH, United States, [2] Department of Nutrition and Food Sciences, Texas Woman's University, Denton, TX, United States, [3] Department of Biochemistry and Molecular Genetics, Schools of Medicine and Dentistry, University of Alabama at Birmingham, Birmingham, AL, United States, [4] The Jackson Laboratory, Bar Harbor, ME, United States

Hair follicles cycle through periods of growth (anagen), regression (catagen), rest (telogen), and release (exogen). Telogen is further divided into refractory and competent telogen based on expression of bone morphogenetic protein 4 (BMP4) and wingless-related MMTV integration site 7A (WNT7A). During refractory telogen hair follicle stem cells (HFSC) are inhibited. Retinoic acid synthesis proteins localized to the hair follicle and this localization pattern changed throughout the hair cycle. In addition, excess retinyl esters arrested hair follicles in telogen. The purpose of this study was to further define these hair cycle changes. BMP4 and WNT7A expression was also used to distinguish refractory from competent telogen in C57BL/6J mice fed different levels of retinyl esters from two previous studies. These two studies produced opposite results; and differed in the amount of retinyl esters the dams consumed and the age of the mice when the different diet began. There were a greater percentage of hair follicles in refractory telogen both when mice were bred on an unpurified diet containing copious levels of retinyl esters (study 1) and consumed excess levels of retinyl esters starting at 12 weeks of age, as well as when mice were bred on a purified diet containing adequate levels of retinyl esters (study 2) and remained on this diet at 6 weeks of age. WNT7A expression was consistent with these results. Next, the localization of vitamin A metabolism proteins in the two stages of telogen was examined. Keratin 6 (KRT6) and cellular retinoic acid binding protein 2 (CRABP2) localized almost exclusively to refractory telogen hair follicles in study 1. However, KRT6 and CRABP2 localized to both competent and refractory telogen hair follicles in mice fed adequate and high levels of retinyl esters in study 2. In mice bred and fed an unpurified diet retinol dehydrogenase SDR16C5, retinal dehydrogenase 2 (ALDH1A2), and cytochrome p450 26B1 (CYP26B1), enzymes and proteins involved in RA metabolism, localized to BMP4 positive refractory telogen hair follicles. This suggests that vitamin A may contribute to the inhibition of HFSC during refractory telogen in a dose dependent manner.

Keywords: vitamin A, retinoid metabolism, hair cycle, stem cells, telogen

OPEN ACCESS

Edited by:
Sung-Jan Lin,
National Taiwan University, Taiwan

Reviewed by:
Chao-Chun Yang,
National Cheng Kung University, Taiwan
Katerina Strati,
University of Cyprus, Cyprus

***Correspondence:**
Helen B. Everts
heverts@twu.edu

Specialty section:
This article was submitted to Stem Cell Research, a section of the journal Frontiers in Cell and Developmental Biology

Received: *10 June 2020*
Accepted: *13 January 2021*
Published: *05 February 2021*

Citation:
Suo L, VanBuren C, Hovland ED, Kedishvili NY, Sundberg JP and Everts HB (2021) Dietary Vitamin A Impacts Refractory Telogen. Front. Cell Dev. Biol. 9:571474. doi: 10.3389/fcell.2021.571474

INTRODUCTION

The hair follicle has a self-cycling ability. It goes through a regeneration phase (anagen), a degenerative phase (catagen) involving the apoptosis and loss of the lower two-thirds of the hair follicle, a resting phase (telogen), and a release phase (exogen) (Chase et al., 1951; Milner et al., 2002). The transition from telogen to anagen requires the activation and proliferation of stem cells of the hair follicle bulge (HFSC) (Cotsarelis et al., 1990). Telogen hair follicles can be divided into two stages, refractory and competent telogen, based on the expression of bone morphogenetic protein 2 and 4 (BMP2 and BMP4) (Plikus et al., 2008). During refractory telogen BMP2, BMP4, BMP6, and fibroblast growth factor 18 (FGF18) keep HFSC in the quiescent state (Chen and Chuong, 2012; Hsu and Fuchs, 2012). During competent telogen these inhibitory factors are themselves inhibited. Transforming growth factor beta (TGFB) and the BMP inhibitor Noggin inhibit BMP signaling to trigger anagen initiation (Botchkarev et al., 1999, 2001; Oshimori and Fuchs, 2012). WNT7A and WNT7B are also directly inhibited by BMP signaling and relief of this inhibition is important for the initiation of the new hair cycle (Kandyba et al., 2013; Kandyba and Kobielak, 2014). According to this theory, anagen initiation can only occur if the hair follicle is in competent telogen. BMP6 and FGF18 are secreted from inner bulge cells, which are marked by keratin 6 (KRT6) (Hsu et al., 2011). This KRT6 layer has also been called suprabasal bulge cells (Wang et al., 2016), companion layer of the club hair, and trichilemmal keratin (Higgins et al., 2009). Hsu et al. (2011) showed that these cells are derived from the outer root sheath (ORS) and contain many stem cell regulators. Thus, they are neither companion layer nor simply differentiated ORS. The term inner bulge cells will be used throughout to define this layer. These inner bulge KRT6 positive cells also anchor the hair follicle to the club hair and are involved in shedding hair during late exogen (Higgins et al., 2009, 2011).

Retinoids is a general term for both synthetic and natural forms of vitamin A. The dietary form of vitamin A is retinyl esters. Retinyl esters are important for healthy hair (Everts, 2012); since both too much or too little retinyl esters leads to alopecia (hair loss) in humans and other mammals (Wolbach and Howe, 1925; Anzano et al., 1979; Berth-Jones and Hutchinson, 1995; Bleasel et al., 1999; Shih et al., 2009; Baldwin et al., 2012; Ocon et al., 2012; Duncan et al., 2013; Everts et al., 2013; Suo et al., 2015). Synthetic retinoids, such as acitretin and etretinate, cause alopecia at doses between 25 and 75 mg/d (Gupta et al., 1989; Murray et al., 1991; Katz et al., 1999). This retinoid-associated alopecia is dose-dependent and hair loss is reversible after significant reduction of retinoid dose or cessation of the systemic therapy (Gupta et al., 1989; Murray et al., 1991; Berth-Jones and Hutchinson, 1995; Katz et al., 1999). Retinoid-induced alopecia results in an arrest of hair follicles in telogen combined with an anchorage defect in the follicle during telogen (Berth-Jones and Hutchinson, 1995). Retinoid-induced alopecia also reduced anagen in cultured human hair follicles by inducing TGFB2 and triggering catagen (Foitzik et al., 2005). The mechanisms by which vitamin A regulates HFSC during the transition from telogen to anagen are still unknown.

The active form of vitamin A is retinoic acid (RA). RA is synthesized at or near the site of action (Duester, 2013; Obrochta et al., 2014), by a few key enzymes (Napoli, 2012). In the cell, retinol is either esterified to retinyl ester for storage by the enzymes lecithin:retinol acyltransferase and diglyceride acyltransferase 1 (DGAT1) (MacDonald and Ong, 1988; Orland et al., 2005); or retinol is reversibly oxidized to retinal by retinol dehydrogenases (Rexer and Ong, 2002; Napoli, 2012; Kedishvili, 2013). Five retinol dehydrogenases localize to the skin including: dehydrogenase reductase SDR family member 9 (DHRS9) (Rexer and Ong, 2002; Markova et al., 2003; Nadauld et al., 2005; Everts et al., 2007), retinol dehydrogenase 1/16 (RDH1/16) (Jurukovski et al., 1999; Karlsson et al., 2003), retinol dehydrogenases short-chain dehydrogenase/reductase family 16C members 5 and 6 (SDR16C5 and SDR16C6) (Belyaeva et al., 2012; Adams et al., 2017), and retinol dehydrogenase 10 (RDH10) (Wu et al., 2002; Lee et al., 2011). Retinal is further irreversibly oxidized to RA by retinal dehydrogenases 1–3 (ALDH1A1–3) (Napoli, 1999). RA binds cellular retinoic acid binding proteins (CRABPs) that transport RA throughout the cell (Ong, 1987). CRABP2-bound RA is transported into the nucleus and delivered to retinoic acid receptors (RARA, RARB, and RARG) (Dong et al., 1999; Sessler and Noy, 2005). RA and its receptors activate the transcription of over 500 genes involved in proliferation and differentiation (Giguere et al., 1987; Balmer and Blomhoff, 2002). Both CRABP1 and CRABP2 also transport RA into the endoplasmic reticulum to cytochrome P450 family members (CYP26A1, CYP26B1, and CYP26C1) that degrade RA and protect cells from vitamin A toxicity (Boylan and Gudas, 1992; Chen et al., 2003; Isoherranen and Zhong, 2019).

In a previous study in C57BL/6J (B6) mice, retinyl esters dose dependently altered the hair cycle (Everts et al., 2013). Feeding B6 mice an unpurified diet containing up to 28 IU retinyl esters/g diet during breeding and then excess levels of retinyl esters (56 IU/g diet) at 12 weeks of age resulted in more hair follicles in telogen (Study 1). However, when B6 mice were fed adequate retinyl esters (4 IU/g diet) during breeding and then excess levels of retinyl esters at 6 weeks of age there was no difference in the hair cycle (Study 2). Excess RA in *Dgat1*^{tm1Far} null mice also altered the hair cycle by both lengthening the first anagen and shortening the second telogen (Shih et al., 2009).

Abbreviations: Mouse genes/transcripts, first letter capitalized all subsequent letters lower case and all in italics; Proteins, all capital letters no italics; ANOVA, analysis of variance; BMP2, 4, 6, bone morphogenic protein 2, 4, 6; HFSC, hair follicle stem cell; SDR16C5, 6, retinol dehydrogenase short-chain dehydrogenase/reductase family 16C members 5 and 6; RDH10, retinol dehydrogenase 10; ALDH1A1, 2, 3, aldehyde dehydrogenase family member 1A1, 2, 3; CRABP2, cellular retinoic acid binding protein II; CYP26A1, B1, C1, cytochrome P450 family member 26A1, B1, C1; B6, C57BL/6J; FGF18, fibroblast growth factor 18; KRT6, keratin 6; ORS, outer root sheath; TGFB2, transforming growth factor beta 2; RA, retinoic acid; DGAT1, diglyceride acyltransferase 1; DHRS9, dehydrogenase/reductase SDR family 9; RDH1/16, retinol dehydrogenase 1/16; IU, international unit; NIH, national institutes of health; AIN, American Institute of Nutrition; IHC, immunohistochemistry; LHX2, LIM homeobox protein 2; NFAT1C, nuclear factor of activated T cells, cytoplasmic, calcineurin dependent 1; FOXC1, forkhead box c1; ATAC-seq, Assay for transposase accessible chromatin then sequencing; SMAD, RARA, RARB, RARG, retinoic acid receptors alpha, beta, and gamma; CCCA, central centrifugal cicatricial alopecia; AA, alopecia areata.

These effects were partially reversed when the mice were fed a retinyl ester deficient diet. Excess RA in *Cyp26b1*^{tm1Hh} null mice blocked embryonic hair development; but the hair cycle could not be examined due to perinatal lethality (Okano et al., 2012). Conditional deletion of *Cyp26b1* in the dermal papilla and dermis (*En1Cre;Cyp26b1*^{tm1Hh}) reduced zig-zag hairs, but did not block hair development. Recently, reduced retinal synthesis in *Del(4Sdr16c5-Sdr16c6)1Nyk* double null mice altered the hair cycle (Wu et al., 2019). These mice entered anagen at a younger age than controls; however, a complete analysis of the hair cycle was not performed. Initial localization studies done before the discovery of two telogen stages observed ALDH1A2 and CRABP2 localized to some, but not all telogen hair follicles (Everts et al., 2007). In contrast, DHRS9 did not localize to the hair follicle until anagen. This study was done to better define the effects of retinyl ester on the hair cycle.

MATERIALS AND METHODS

Animals

Mice

The Jackson Laboratory (Bar Harbor, ME, United States) Institutional Animal Care and Use Committee approved all procedures. C57BL/6J (Stock number 664; hereafter referred to as B6) mice (The Jackson Laboratory, Bar Harbor, ME, United States) were used.

Hair Cycle Localization Study

B6 Dams and female pups were fed the NIH 31 diet (LabDiet 5K52, Purina Mills, St. Louis, MO, United States) throughout this study. Only females were used because they fight less, which reduces wounds. Wounds by themselves will initiate anagen, which would interfere with this study (Sundberg et al., 2018). Mice were sacrificed and skin collected at 70, 77, 80, 83, 84, 85, 86, 88, 90, 91, 93, 97, and 100 days of age to obtain hair follicles in all stages of the hair cycle without manipulation. Skin from one to three regions of the back (interscapular, thoracolumbar, and lumbar regions) from one to five mice were collected at each time point, Skin was fixed overnight in Fekete's solution (61% ethanol, 3.2% formaldehyde, and 0.75 N acetic acid), and processed routinely for histology and immunohistochemistry (Everts et al., 2007). Approximately 60 hair follicles were analyzed per section of skin collected. The guide suggested by Muller-Rover et al. (2001) was used to stage hair follicles based on histology (Muller-Rover et al., 2001).

Study 1

B6 Dams and female pups were fed the NIH 31 diet (LabDiet 5K52, Purina Mills, St Louis, MO) until 12 weeks of age, and then switched to an American Institute of Nutrition (AIN)93 maintenance diet containing 4 ($n = 8$), 28 ($n = 9$), or 56 ($n = 10$) IU retinyl acetate/g diet (Research Diets, Inc., New Brunswick, NJ, United States) for 16 weeks (**Figure 1G**) (Everts et al., 2013). All mice with telogen hair follicles were analyzed. Only females were used to avoid wounds (Sundberg et al., 2018). In addition, female mice are more prone to central centrifugal cicatricial alopecia (CCCA), which was the focus of the initial diet study (Sundberg et al., 1994a). The first study was done to test the hypothesis that high retinyl esters worsens CCCA in B6 mice, since we saw an increased expression of RA synthesis proteins in both patients with CCCA and the B6 mouse model. The doses were chosen based on recommendations and measuring retinyl ester levels in the diet fed mice at The Jackson Laboratory production facility. The AIN and National Research Council recommend 4 IU/g diet; and 28 IU/g diet was the highest level measured in the standard diets at The Jackson Laboratory. We chose 56 as two times the highest level. However, this is not what we saw. None of the mice fed the highest level of retinyl esters had hair loss and they all had the majority of their hair follicles in telogen. There was an increased severity of disease in mice fed the 28 versus 4 IU diet. There was no specific reason for starting study one when the mice were 12 weeks old. These results lead us to perform a second study to reduce the level of retinyl esters and see how that impacted CCCA in the B6 mice. Breeding mice for three generations on the AIN93 growth diet reduced RA in several tissues (Obrochta et al., 2014) and reduced skin RA levels in *Dgat1*^{tm1Far} null mice (Shih et al., 2009).

Study 2

B6 Dams and their first and second-generation female pups were fed an AIN93 growth diet containing 4 IU retinyl acetate/g diet (Research Die, Inc., New Brunswick, NJ, United States). Second generation female pups were used in this study (**Figure 1J**). Six-week-old B6 mice were fed an AIN93 Maintenance diet containing 4 ($n = 7$), 28 ($n = 10$), or 56 ($n = 6$) IU retinyl acetate/g diet (Research Diets, Inc., New Brunswick, NJ, United States) for 12 weeks (Everts et al., 2013). At 6 weeks of age B6 mice are adults and have hair follicles in telogen. All mice with telogen hair follicles were analyzed.

Immunohistochemistry (IHC)

Immunohistochemistry was performed in serial sections as described previously (Everts et al., 2007). Primary antibodies to the following proteins were purchased: BMP4 (Abcam, Cambridge, MA, United States; Vector Labs, Burlingame, CA, United States), WNT7A (Abcam, Cambridge, MA, United States), CYP26B1 (ACRIS, Rockville, MD, United States), KRT6 (Covance/BioLegend, Dedham, MA, United States), and RDH10 (Proteintech, Rosemont, IL, United States). Antibodies against ALDH1A2 and CRABP2 were made in the Ong laboratory (Everts et al., 2007). The antibody against SDR16C5 was made in the Kedishvili laboratory (Wu et al., 2019). The Vector anti-BMP4 antibody was made in mice. All other primary antibodies were made in rabbits. Biotinylated anti-rabbit or anti-mouse antibodies (Jackson ImmunoResearch Laboratories, Inc., West Grove, PA, United States) was used second, followed by a horseradish peroxidase conjugated anti-biotin antibody (Bethyl Laboratories, Inc., Montgomery, TX, United States). The red 3-amino-9-ethylcarbazole plus enhancers (AEC+; Dako, Carpinteria, CA, United States) substrate chromogen was used followed by counterstaining with Gils Hematoxylin III (Poly Scientific, Bay Shore, NY, United States) and mounting

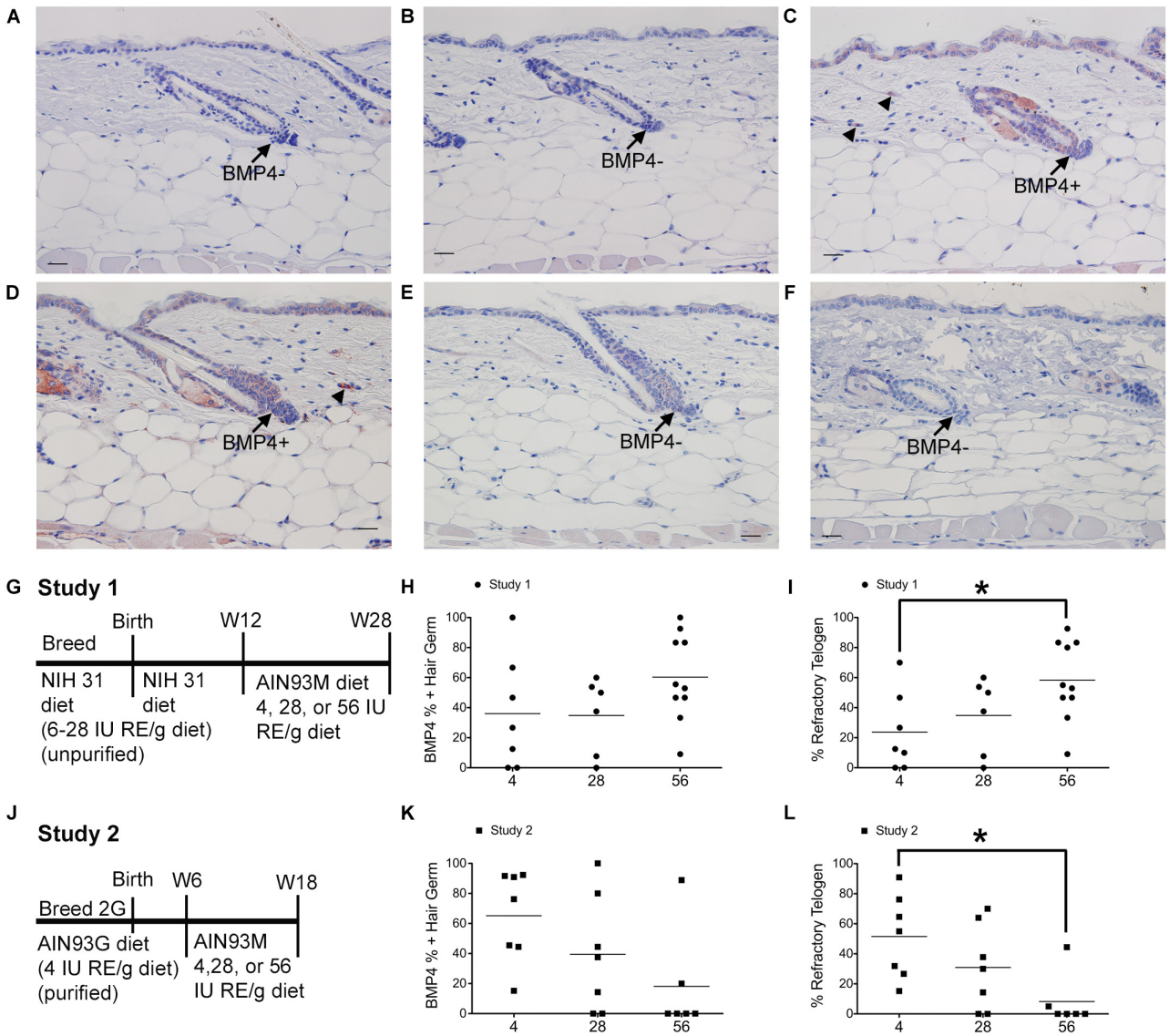

FIGURE 1 | Dietary vitamin A impacts the percent of BMP4 positive refractory telogen hair follicles. C57BL/6J wild type Dams and female pups were fed either the NIH 31 diet containing 6–28 IU retinyl esters (RE)/g diet **(A–C,G–I)** or the AIN93G diet containing 4IU retinyl acetate/g diet **(D–F,J–L)** for two generations (2G). At either 12 **(A–C,G–I)** or 6 **(D–F,J–L)** weeks (W) of age these mice were switched to the AIN93M diet containing 4 (**A,D**, $n = 7$–8), 28 (**B,E**, $n = 9$–10), or 56 (**C,F**, $n = 6$–10) IU retinyl acetate/g diet for either 16 **(A–C,G–I)** or 12 **(D–F,J–L)** weeks. **(G,J)** show the feeding protocol for the two studies. Immunohistochemistry (IHC) was performed with antibodies against BMP4 (Abcam) in all skin containing telogen hair follicles. Telogen hair germs were counted as either positive or negative for BMP4. An average of 37 telogen hair germs per mouse were scored (3–70). The fraction of BMP4 positive telogen hair germs was calculated by dividing the number of BMP4 positive telogen hair germs by the total number of telogen hair germs. This fraction was then multiplied by either 100 to get the percent of positive hair germs **(H,K)** or the percentage of telogen follicles calculated in the original diet studies (Everts et al., 2013) to determine the percentage of hair follicle in refractory telogen **(I,L)**. A 2 × 3 ANOVA revealed an interaction between study and diet. $^*p < 0.05$, by a one-way ANOVA performed on the interaction variable followed by Tukey *post-hoc* test. Bar = 25.2 μm. Arrow, hair germ; arrowhead, dermal cell.

in aquamount (Dako, Carpinteria, CA, United States). Images were captured on either an Olympus BX51 microscope with the DP71 camera (Olympus, Tokyo, Japan) or Nikon Eclipse i80 microscope with the DS-Ri2 camera (Nikon Instruments Inc., Melville, NY, United States). Images were sized, cropped, and composite figures were created in Adobe Photoshop CS3 or Elements (San Francisco, CA, United States). Most figures are using unaltered images. For **Figure 3** the whole images were minimally altered in Photoshop Elements using the exposure and balance settings in the "Quick" menu. Unaltered images are in **Supplementary Figure 3**.

Bone morphogenetic protein 4 positive and negative telogen hair germs and dermal cells were counted from mice fed various levels of vitamin A in studies 1 and 2. The percent of hair follicles in refractory telogen was calculated in two steps. First, the number of BMP4 positive telogen hair germs was divided

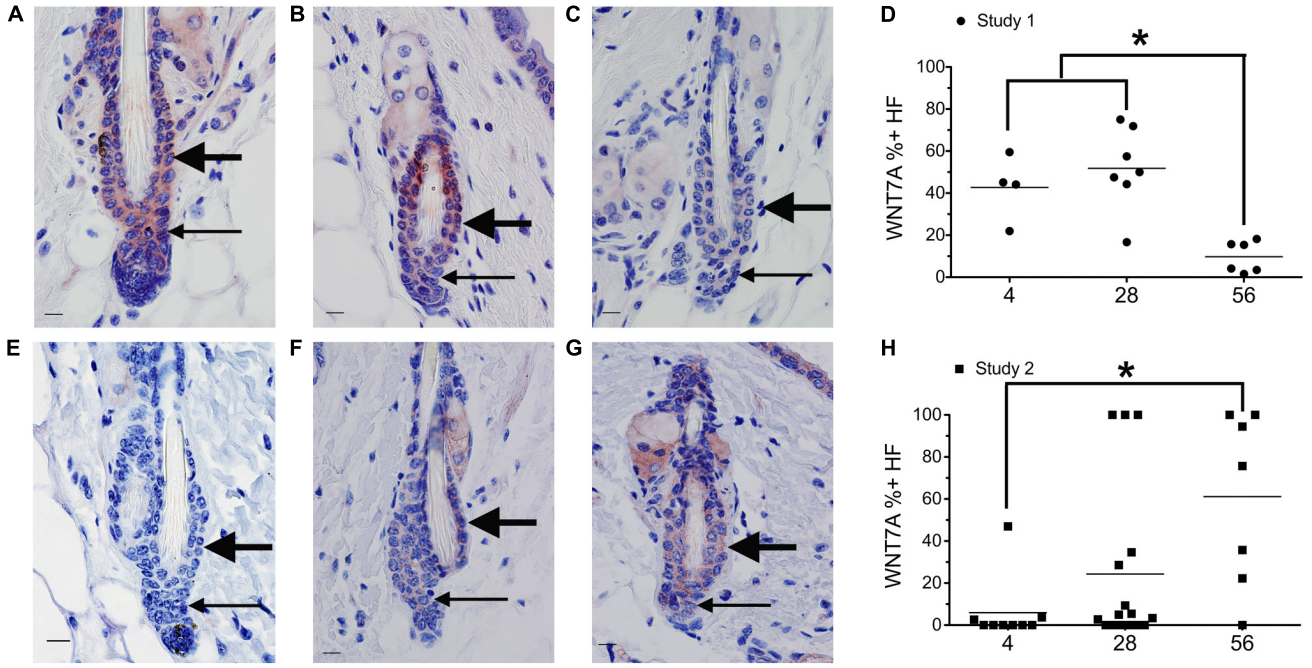

FIGURE 2 | Dietary vitamin A regulates WNT7A. Mice from study 1 **(A–D)** or study 2 **(E–H)** were switched to the AIN93M diet containing 4 (**A,E**, $n = 4$–9), 28 (**B,F**, $n = 7$–16), or 56 (**C,G**, $n = 6$–7) IU retinyl acetate/g diet. Immunohistochemistry (IHC) was performed with antibodies against WNT7A in all skin containing telogen hair follicles. WNT7A positive and negative immunoreactivity in the club hair, bulge, and hair germ were counted together as hair follicles and the percent of positive hair follicles calculated **(D,H)**. An average of 29 (range of 1–72) telogen hair follicles per mouse were scored. $^*p < 0.05$, by a one-way ANOVA followed by Tukey *post-hoc* test for study 1 and Kruskal–Wallis test followed by Mann–Whitney *U* test for study 2. Bar = 10.1 μm. Large arrow, club hair; small arrow, hair germ.

by the total number of telogen hair follicles to get the fraction of telogen hair germs in refractory telogen. Second, this fraction was multiplied by the percentage of telogen follicles calculated in the original diet studies (Everts et al., 2013) because skin that contained only anagen or catagen hair follicles were not analyzed for BMP4. This percent of hair follicles in refractory telogen was subtracted from the total percent of telogen follicles to get the percent of follicles in competent telogen. An average of 37 telogen hair follicles per mouse were scored for BMP4 (3–70). Materials are available upon request.

Co-immunofluorescence (Co-IFA)

Co-immunofluorescence was performed using a two-antibody co-localization system in frozen dorsal skin sections as previously described (Duncan et al., 2013). Primary antibodies against the following proteins were used with the indicated concentrations: ALDH1A2 (Rabbit, produced in the Ong laboratory), CRABP2 (Rabbit, produced in the Ong laboratory), CYP26B1 (Rabbit, ACRIS, Chapel Hill, NC, United States), BMP4 (Mouse, Vector Lab, Burlingame, CA, United States), and CD34 (Rat, BD Biosciences Pharmingen, San Jose, CA, United States). Secondary antibodies (anti-rat, anti-rabbit, anti-mouse, Invitrogen, Carlsbad, CA, United States) conjugated with Alexa Fluor 488 or Alexa Fluor 594 were used. Nuclei were stained with DAPI (Invitrogen, Carlsbad, CA, United States) for 1 min and subsequently the sections were washed and cover slipped with Prolong Gold anti-fade reagent (Molecular Probes, Eugene, OR, United States). Pictures were taken at 20X and 60X magnification (Nikon ACT-1, Tokyo) and processed in Adobe Photoshop CS4 (San Francisco, CA, United States).

Co-IHC

Immunohistochemistry was first performed with antibodies against KRT6 and CRABP2 using AEC+ (red) as described above with additional blocking steps using the streptavidin, biotin blocking kit (Vector Labs, Burlingame, CA, United States). IHC was then performed with the Vector mouse anti-BMP4 antibody using the Mouse on Mouse ImmPRESS Peroxidase kit with some modifications (Vector Labs, Burlingame, CA, United States). First, we doubled the concentration of blocking reagent and incubated the slides for 2 h. Second, we diluted the ImmPRESS reagent 1:1 in the provided 2.5% normal horse serum. Slides were then treated with DAB Eq (brown) for 10 min, counterstained and mounted as described above. The number of hair follicles with positive KRT6 or CRABP2 plus or minus dermal BMP4 was counted. The percent of positive KRT6 or CRABP2 hair follicles with dermal BMP4 was then calculated separately from the percent of KRT6 or CRABP2 hair follicles without dermal BMP4. An average of 26 hair follicles (range of 2–54) were scored per mouse. Four to seven mice per diet were analyzed. Images were taken with the Nikon Eclipse i80 microscope with the DS-Ri2 camera (Nikon Instruments Inc., Melville, NY, United States). Images were sized, cropped, composite figures were created, and whole images were adjusted for brightness, contrast, and

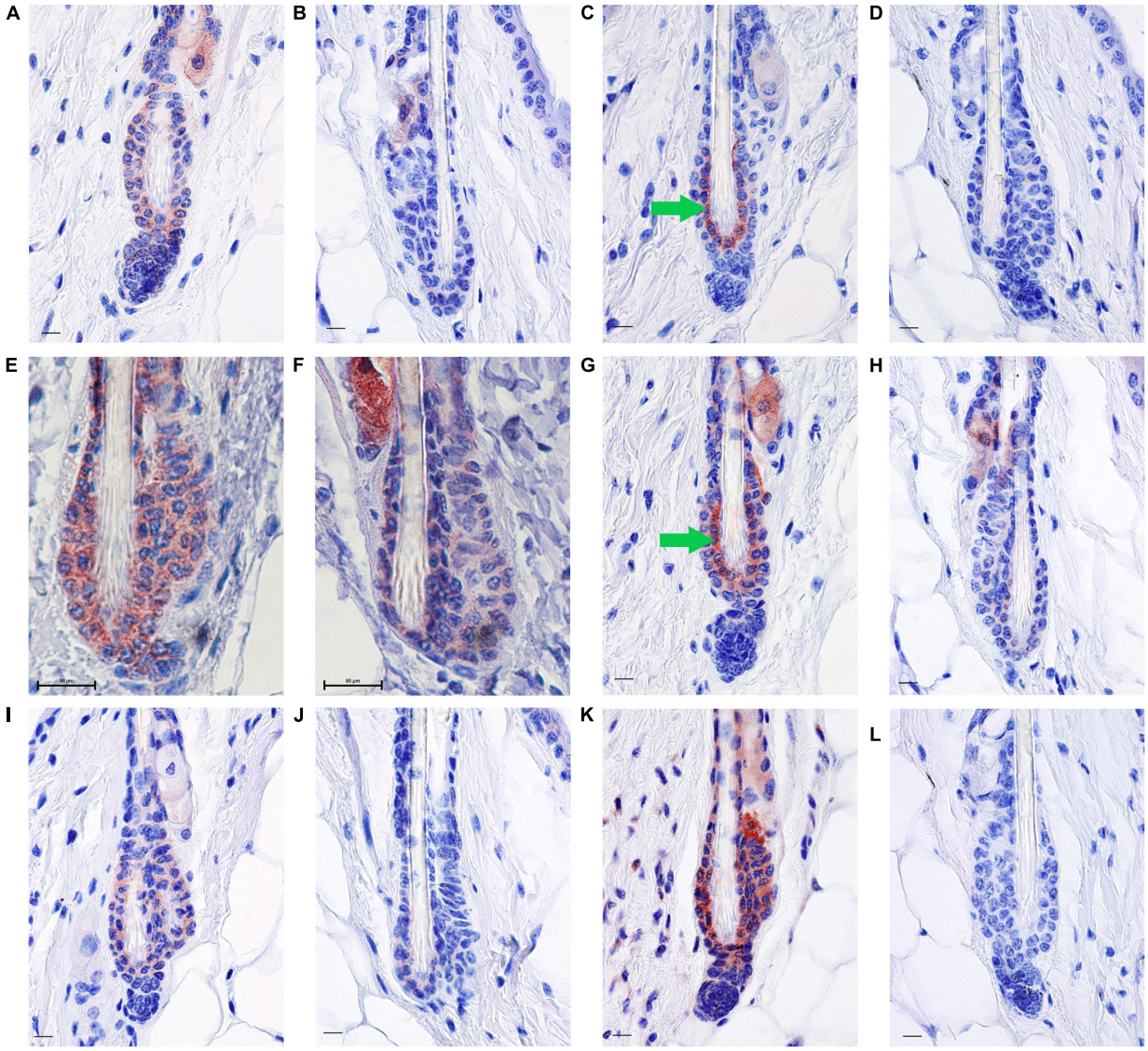

FIGURE 3 | RA synthesis and degradation enzymes localize to BMP4 positive refractory telogen hair follicles. Skin from female C57BL/6J wild type mice fed an unpurified diet was collected at 70–101 days of age (n = 1–5 mice/time point). One to three regions of skin were collected per mouse. Immunohistochemistry (IHC) was performed with antibodies against BMP4 **(A,B)**, KRT6 **(C,D)**, SDR16C5 **(E,F)**, CRABP2 **(G,H)**, ALDH1A2 **(I,J)**, and CYP26B1 **(K,L)** using a red chromagen. Hair follicles that match the BMP4+ hair germ are on the left of each pair **(A,C,E,G,I,K)**, while hair follicles that match the BMP4– hair germ are on the right of each pair **(B,D,F,H,J,L)**. Details of these match ups are in **Supplementary Figures 3, 4**. An average of 60 hair follicles were examined per region of skin. Bar = 50 mm in **(E,F)**, and Bar = 10.1 μm in all other images. Images were cropped around the lower hair follicle. Whole images were minimally altered in Photoshop Elements using the exposure and balance settings in the "Quick" menu. Unaltered images are in **Supplementary Figure 1**. Green arrow, inner bulge cells.

color balance in Adobe Photoshop CS3. Unaltered images are in **Supplementary Figure 6**.

Statistical Analysis

Equal variance was first confirmed using Levene's test of equality of error variances using SPSS version 24 (IMB SPSS Statistics, Chicago, IL, United States). Comparison among experimental groups was analyzed by univariate analysis of variance using a 2 × 3 full factorial model followed by Tukey *post-hoc* test when significant treatments effects were seen. When there was a significant interaction between study and diet a one-way ANOVA was performed on the interaction variable followed by Tukey *post-hoc* test. When equal variances were not seen, each study was analyzed by Kruskal–Wallis followed by Mann–Whitney U test. P value < 0.05 is defined as statistical significance.

RESULTS

Mice from study 1 (**Figure 1G**) on the 56 IU diet had 98% of their hair follicles in telogen when analyzed histologically

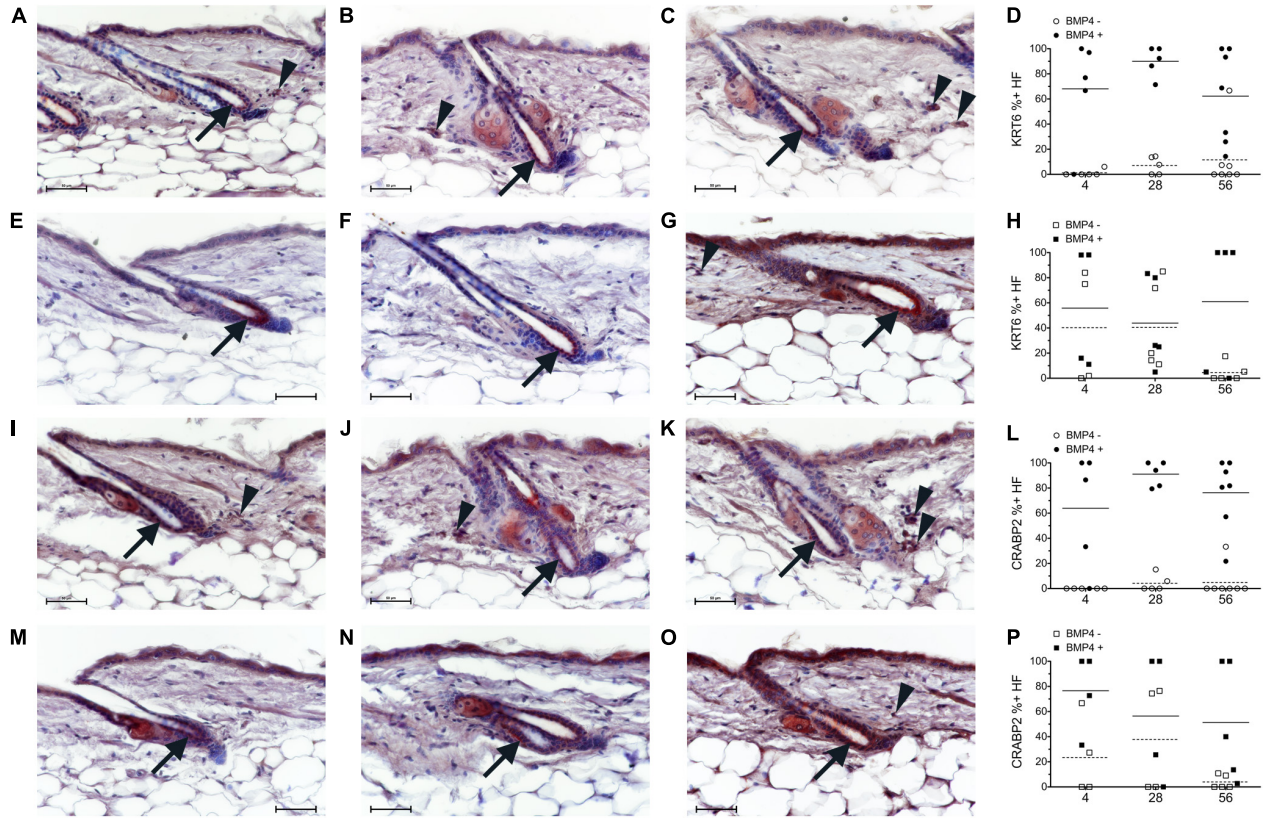

FIGURE 4 | Breeding mice on AIN93G diet altered the localization pattern of KRT6 and CRABP2. Study 1 (**A–D,I–L**, circles) or study 2 (**E–H,M–P**, squares) mice were switched to the AIN93M diet containing 4 (**A,E,I,M** $n = 4$–5), 28 (**B,F,J,N**, $n = 5$), or 56 (**C,G,K,O**, $n = 5$–7) IU retinyl acetate/g diet. Co-Immunohistochemistry (IHC) was performed with antibodies against KRT6 and CRABP2 (red) with BMP4 (brown, Vector) in skin containing telogen hair follicles. Hair follicles with KRT6 and CRABP2 positive and negative localization in the inner bulge cells were counted separately for hair follicles with strong BMP4 positive cells in the dermis (Filled) and hair follicles without strong BMP4 positive cells in the dermis (open). The background brown in the arrector pili and dermal fat was ignored. The percent of positive KRT6 and CRABP2 hair follicles with and without BMP4 was calculated **(D,H,L,P)**. An average of 26 (range of 2–54) telogen hair follicles per mouse were scored. Whole images were minimally altered in Photoshop CS3. Unaltered images are in **Supplementary Figure 6**. Bar = 50 μm. Arrow, inner bulge cells; arrowhead, strong BMP4 positive dermal cells.

(Everts et al., 2013). To better define how dietary vitamin A altered the hair cycle, we first examined the expression of several regulators of the hair cycle. Using an antibody from Vector Labs we found that retinyl esters increased the number of dermal BMP4 positive cells in both studies (**Supplementary Figure 1**). Because we were not sure that the red immunoreactivity we were seeing in the dermis was really within the dermal cells, we repeated the study with a different antibody against BMP4. The Abcam antibody against BMP4 had immunoreactivity within the hair germ and epidermis in addition to the dermis, similar to BMP4-Lacz reporter mice (**Figure 1**; Plikus et al., 2008). Quantifying the percent of hair follicles with positive expression in the hair germ we saw a similar trend in study 1 as was seen with the other antibody (**Figures 1A–C,H**). However, in study 2 there was a trend for a drop in the percent of positive BMP4 hair germs as the amount of retinyl esters in the diet increased (**Figures 1D–F,K**). Using the BMP4 positive hair germ to indicate refractory telogen, we also calculated the percent of hair follicles in refractory telogen. BMP4 is high during refractory telogen and negative during competent telogen. **Figure 1I** shows that mice from study 1 fed the 56 IU diet had the majority of their hair follicles in refractory telogen. This was significantly greater than mice fed the 4 IU diet in study 1. Retinyl esters had no significant effect on the hair cycle in study 2 when analyzed histologically. **Figure 1L** shows that when these mice were fed the 56 IU diet significantly fewer hair follicles were in refractory telogen than mice fed 4 IU diet. WNT7A increases as hair follicles transition from competent telogen to anagen. **Figure 2** shows that fewer WNT7A positive hair follicles were seen in both the 56 IU diet group of study 1 and the 4 IU diet group of study 2. This further supports the findings that these hair follicles are in refractory telogen.

Next, we attempted to determine the localization pattern of vitamin A metabolism proteins during telogen using BMP4 to mark refractory telogen. Dorsal skin was collected from B6 mice fed an unpurified diet at 70–101 days of age and IHC performed in serial sections with antibodies against BMP4 (Abcam), KRT6, SDR16C5, RDH10, ALDH1A2, CRABP2, and CYP26B1. Using the Abcam antibody, all proteins localized to BMP4 positive telogen hair follicles (**Figure 3** and **Supplementary Figures 2, 3**).

SDR16C5 and ALDH1A2 were also seen in BMP4 negative telogen hair follicles, but at a lower level (**Figure 3** and **Supplementary Figures 2, 4**). However, CRABP2 and CYP26B1 were barely detectable and KRT6 was negative in BMP4 negative follicles. CYP26B1 also localized to the dermis surrounding the BMP4 positive hair follicle, but not the BMP4 negative hair follicles. In addition, CRABP2 localized to the inner KRT6 positive bulge cells (**Figures 3C,G**, green arrows). RDH10 localized to all telogen hair follicles at similar levels (data not shown). This expression pattern contrasted the Co-IFA performed on frozen sections from a few mice from the retinyl ester diet studies using the Vector Labs antibody (**Supplementary Figure 5**). Thus, we ran Co-IHC with the Vector Labs BMP4 antibody, KRT6 and CRABP2 on samples from all of the diets in the retinyl ester feeding studies. We found that both KRT6 and CRABP2 localized to the inner bulge only when BMP4 was in the dermis in all but one mouse in study 1 (**Figures 4A–D,I–L** arrow and arrowhead and **Supplementary Figure 6**). However, when mice from study 2 were fed either the 4 or 28 IU diet KRT6 and CRABP2 localized to the inner bulge in both the presence and absence of dermal BMP4 (**Figures 4E–H,M–P**). All of the data are presented in the figures and **Supplementary Data Sheet 1**.

DISCUSSION

This study was done to better define the impact retinyl esters have on the hair cycle. In mice bred on an unpurified diet, excess (pharmacological) levels of retinyl esters lead to a greater percentage of hair follicles in refractory telogen. Regardless of retinyl ester level fed, KRT6 and CRABP2 localized to the inner bulge cells almost exclusively in refractory telogen in these mice. SDR16C5, ALDH1A2, and CYP26B1 also localized to the hair follicle at greater intensities during refractory telogen in mice bred and fed an unpurified diet. In contrast, when mice were bred on a purified diet containing recommended (physiological) levels of retinyl esters the percent of hair follicles in refractory telogen decreased as retinyl ester levels increased. In addition, KRT6 and CRABP2 localized to the inner bulge cells during both competent and refractory telogen in adult mice fed recommended (4IU) and high (28IU) levels of retinyl esters. These data suggest that vitamin A may regulate HFSC in a dose and time dependent manner.

Bone morphogenetic protein 2, BMP4, and BMP6 inhibit HFSCs during refractory telogen (Plikus et al., 2008; Hsu et al., 2011). BMP2 and 4 are secreted from adipocytes, while BMP6 localizes to KRT6 positive inner bulge cells (Hsu et al., 2011; Wang et al., 2016; Yi, 2017). KRT6 positive cells also express LIM homeobox protein 2 (LHX2), NFAT1C, and FGF18 during telogen that also inhibit HFSC to maintain telogen (Hsu et al., 2011; Kimura-Ueki et al., 2012; Yi, 2017). HFSC inhibition (quiescence) also requires forkhead box c1 (FOXC1) signaling during early anagen (Wang et al., 2016). FOXC1 directly increased NFATC1 and BMP6. RNA-seq in postnatal day 30 B6;SJL-Tg(*Krt1-15crePGR)22Cot/J/Foxc1*^{tm1Blh} null mice identified increased *Aldh1a2* expression. Assay for transposase accessible chromatin then sequencing (ATAC-seq) analysis of the promoters of differentially expressed genes revealed a SMAD binding motif in the promoter of *Aldh1a2*, but not NFATC1 or FOXC1 binding sites. This suggests that BMP signaling may increase ALDH1A2 and RA synthesis during refractory telogen to contribute to HFSC quiescence.

Retinoic acid may also regulate HFSC quiescence. Excess RA in the *Cyp26b1*^{tm1Hh} null mice decreased *Lhx2* at embryonic day E16.5 and E18.5 along with altering several other HFSC regulatory genes and blocked hair follicle development (Okano et al., 2012). However, defective hair development was not seen in dermal papilla and dermal directed *En1*$^{tm2(cre)Wrst}$;*Cyp26b1*^{tm1Hh} null mice. The finding that CYP26B1 localized to the HFSC and inner bulge in addition to the dermis in this study suggests that reduced RA may be critical within the HFSC and/or inner bulge cells but not the dermal papilla. CRABP2 shuttles RA to both RARs and CYP26B1 (Dong et al., 1999; Nelson et al., 2016). This suggests that a low dose of RA may be necessary specifically in the inner bulge cells, while reduced RA is critical in the HFSC and dermis during refractory telogen. Further evidence for a role of RA in HFSC quiescence include: premature anagen entry with both reduced RA in *Del(4Sdr16c5-Sdr16c6)1Nyk* double null mice and excess RA in *Dgat1*^{tm1Far} null mice; and an increase of hair follicles in refractory telogen following excess retinyl esters in study 1, reduced retinyl esters in study 2, and pharmacological doses of synthetic retinoids in the clinic.

Retinoic acid synthesis proteins localizing to the KRT6 positive inner bulge cells during telogen is similar to what was seen in the inner cell layer and companion layer during anagen (Everts et al., 2007). ALDH1A3 localized to the KRT6 positive companion layer in the suprabulbar region, ALDH1A2 localized to the inner layer of the ORS in the isthmus and at a lower intensity in the companion layer in the suprabulbar region, and CRABP2 localized to the inner layer of the ORS in the infundibulum. The intensity of the immunoreactivity seems slightly higher in anagen than telogen, however, other methods besides IHC are needed to quantitate this small difference. The inner layer next to the anagen bulge expressed DHRS9, ALDH1A3, CRABP2, and RARA. This suggests that RA is important for these layers of the hair follicle throughout the hair cycle. Future studies are needed to determine the exact roles of RA in these cells; however, RA directly increases the expression of KRT6 (Navarro et al., 1995).

Keratin 6 positive inner bulge cells are also important for anchoring the club hair to the follicle, regulating the release of the club hair during exogen, and providing a reservoir of HFSC in the old hair follicle (Higgins et al., 2009, 2011; Wang et al., 2016). Microarray analysis revealed that *Cyp26b1* expression decreased in these inner bulge cells in late exogen verses early exogen (Higgins et al., 2011). A reduction of CYP26B1 would increase RA levels, suggesting that RA may also regulate hair shedding during exogen. High RA in *Dgat1*^{tm1Far} null mice lead to cyclical alopecia characterized by excess shedded hair during anagen, which is consistent with excess exogen or anagen effluvium (Shih et al., 2009). This alopecia was reduced when mice were fed a retinyl ester deficient diet. Thus, RA synthesis within the KRT6 positive inner bulge cells may impact exogen in addition to altering the telogen to anagen transition.

The cause of the elevated refractory telogen with low retinyl esters in study 2 is unclear. The two retinyl ester feeding studies had both different diets during breeding and different times when the diets where changed. This likely resulted in changes in retinyl esters at different stages of the hair cycle that were of different doses. Studies with both B6;SJL-Tg(*Krt1-15crePGR)22Cot/J, Foxc1*^{tm1Blh} null mice and FGF18 injections revealed opposite effects based on the stage of the hair cycle the follicle was in at the time (Kimura-Ueki et al., 2012; Wang et al., 2016). The dissociation of KRT6 from BMP4 expression in study 2 suggests that the hair cycle stage may be important. Also note that most studies that examine HFSC regulation are done on mice fed an unpurified diet.

The dose of retinyl esters may also play a significant role in the U-shaped dose response curve seen in these studies. When low amounts of retinyl esters are consumed or not absorbed, vitamin A deficiency results in follicular hyperkeratosis and alopecia in both rats and humans (Wolbach and Howe, 1925; Anzano et al., 1979; Bleasel et al., 1999; Girard et al., 2006; Ocon et al., 2012). Excessive consumption of retinoids through retinyl ester supplementation or retinoid treatments also leads to alopecia (Gupta et al., 1989; Murray et al., 1991; Berth-Jones and Hutchinson, 1995; Katz et al., 1999; Shih et al., 2009). Vitamin A deficiency and pharmacological levels of RA also inhibit sebum production in the sebaceous gland (Zouboulis et al., 1993; Thiboutot et al., 2009; Barbieri et al., 2019). This is due to the hormesis effects of RA production (Napoli, 2020). As consumption of retinyl ester increases, the concentration of RA rises and provides increasing beneficial effects until the optimal concentration is reached. After this point, however, the benefits of retinyl ester supplementation decrease and then cease altogether. At high concentrations, RA is toxic and has deleterious effects on the organism. These data suggest that pharmacological doses of retinoids may arrest hair follicles in refractory telogen as a toxic effect of increased RA synthesis during this time. However, physiological doses of retinoids may play a greater role in anagen induction. Future studies are needed to tease out whether this is an effect of retinyl ester dose or timing of the retinyl ester.

The hair cycle impacts alopecia in different ways. In the context of central centrifugal cicatricial alopecia (CCCA, B6 dermatitis), arresting hair follicles in refractory telogen is a good thing. This is because CCCA in mice only occurs when hair follicles are in anagen (Sundberg et al., 2011). No mice fed the 56 IU diet in study 1 had alopecia in the previous study (Everts et al., 2013). Anagen hair follicles are also the target of immune attach in alopecia areata (AA) (Sundberg et al., 1994b). Thus, arresting hair follicles in refractory telogen can prevent some types of alopecia (CCCA, AA), while facilitating others such as telogen effluvium. Retinoids in different contexts and doses may impact the various forms of alopecia differently.

DATA AVAILABILITY STATEMENT

The original contributions presented in the study are included in the article/**Supplementary Material**, further inquiries can be directed to the corresponding author.

ETHICS STATEMENT

The animal study was reviewed and approved by The Jackson Laboratory (Bar Harbor, ME, United States) Institutional Animal Care and Use Committee.

AUTHOR CONTRIBUTIONS

HE and JS conceptualized, acquired funding, provided resources, provided supervision, and reviewed and edited the manuscript. HE administered the project and curated the data. LS, CV, EH, and HE performed the analyses. LS wrote the original draft. CV wrote the first draft of the revision. NK provided resources. All authors contributed to the article and approved the submitted version.

FUNDING

This work was funded by grants from the National Institutes of Health (AR052009 to JS; AR052710 to HE; AR076924 to NK and HE) and Texas Woman's University Research Enhancement Program and their Teaching and Research Grant for Equipment and Technology to HE.

ACKNOWLEDGMENTS

The authors thank Kathleen Silva for feeding the mice in the vitamin A study and collecting all of the mice in this study.

SUPPLEMENTARY MATERIAL

The Supplementary Material for this article can be found online at: https://www.frontiersin.org/articles/10.3389/fcell.2021.571474/full#supplementary-material

REFERENCES

Adams, M. K., Lee, S. A., Belyaeva, O. V., Wu, L. Z., and Kedishvili, N. Y. (2017). Characterization of human short chain dehydrogenase/reductase SDR16C family members related to retinol dehydrogenase 10. *Chem. Biol. Interact.* 276, 88–94. doi: 10.1016/j.cbi.2016.10.019

Anzano, M. A., Lamb, A. J., and Olson, J. A. (1979). Growth, appetite, sequence of pathological signs and survival following the induction of rapid, synchronous vitamin A deficiency in the rat. *J. Nutr.* 109, 1419–1431. doi: 10.1093/jn/109.8.1419

Baldwin, T. J., Rood, K. A., Kelly, E. J., and Hall, J. O. (2012). Dermatopathy in juvenile Angus cattle due to vitamin A deficiency. *J. Vet. Diagn. Invest.* 24, 763–766. doi: 10.1177/1040638712445767

Balmer, J. E., and Blomhoff, R. (2002). Gene expression regulation by retinoic acid. *J. Lipid. Res.* 43, 1773–1808. doi: 10.1194/jlr.r100015-jlr200

Barbieri, J. S., Spaccarelli, N., Margolis, D. J., and James, W. D. (2019). Approaches to limit systemic antibiotic use in acne: Systemic alternatives, emerging topical therapies, dietary modification, and laser and light-based treatments. *J. Am. Acad. Dermatol.* 80, 538–549. doi: 10.1016/j.jaad.2018.09.055

Belyaeva, O. V., Lee, S. A., Adams, M. K., Chang, C. B., and Kedishvili, N. Y. (2012). Short chain dehydrogenase/reductase Rdhe2 is a novel retinol dehydrogenase essential for frog embryonic development. *J. Biol. Chem.* 287, 9061–9071. doi: 10.1074/jbc.m111.336727

Berth-Jones, J., and Hutchinson, P. E. (1995). Novel cycle changes in scalp hair are caused by etretinate therapy. *Br. J. Dermatol.* 132, 367–375. doi: 10.1111/j.1365-2133.1995.tb08669.x

Bleasel, N. R., Stapleton, K. M., Lee, M. S., and Sullivan, J. (1999). Vitamin A deficiency phrynoderma: due to malabsorption and inadequate diet. *J. Am. Acad. Dermatol.* 41, 322–324. doi: 10.1016/s0190-9622(99)70375-0

Botchkarev, V. A., Botchkareva, N. V., Nakamura, M., Huber, O., Funa, K., Lauster, R., et al. (2001). Noggin is required for induction of the hair follicle growth phase in postnatal skin. *FASEB. J.* 15, 2205–2214. doi: 10.1096/fj.01-0207com

Botchkarev, V. A., Botchkareva, N. V., Roth, W., Nakamura, M., Chen, L. H., Herzog, W., et al. (1999). Noggin is a mesenchymally derived stimulator of hair-follicle induction. *Nat. Cell Biol.* 1, 158–164. doi: 10.1038/11078

Boylan, J. F., and Gudas, L. J. (1992). The level of Crabp-I expression influences the amounts and types of all-*trans*-retinoic acid metabolites in F9 teratocarcinoma stem-cells. *J. Biol. Chem.* 267, 21486–21491. doi: 10.1016/s0021-9258(19)36635-9

Chase, H. B., Rauch, H., and Smith, V. W. (1951). Critical stages of hair development and pigmentation in the mouse. *Physiol. Zool.* 24, 1–7. doi: 10.1086/physzool.24.1.30152098

Chen, A. C., Yu, K., Lane, M. A., and Gudas, L. J. (2003). Homozygous deletion of the CRABPI gene in AB1 embryonic stem cells results in increased CRABPII gene expression and decreased intracellular retinoic acid concentration. *Arch. Biochem. Biophys.* 411, 159–173. doi: 10.1016/s0003-9861(02)00732-4

Chen, C. C., and Chuong, C. M. (2012). Multi-layered environmental regulation on the homeostasis of stem cells: The saga of hair growth and alopecia. *J. Dermatol. Sci.* 66, 3–11. doi: 10.1016/j.jdermsci.2012.02.007

Cotsarelis, G., Sun, T. T., and Lavker, R. M. (1990). Label-retaining cells reside in the bulge area of pilosebaceous unit: implications for follicular stem cells, hair cycle, and skin carcinogenesis. *Cell* 61, 1329–1337. doi: 10.1016/0092-8674(90)90696-c

Dong, D., Ruuska, S. E., Levinthal, D. J., and Noy, N. (1999). Distinct roles for cellular retinoic acid-binding proteins I and II in regulating signaling by retinoic acid. *J. Biol. Chem.* 274, 23695–23698. doi: 10.1074/jbc.274.34.23695

Duester, G. (2013). Retinoid signaling in control of progenitor cell differentiation during mouse development. *Sem. Cell. Dev. Biol.* 24, 694–700. doi: 10.1016/j.semcdb.2013.08.001

Duncan, F. J., Silva, K. A., Johnson, C., King, B., Szatkiewicz, J. P., Kamdar, S., et al. (2013). Endogenous retinoids in the pathogenesis of alopecia areata. *J. Invest. Dermatol.* 133, 334–343.

Everts, H. B. (2012). Endogenous retinoids in the hair follicle and sebaceous gland. *Biochim. Biophys. Acta* 1821, 222–229. doi: 10.1016/j.bbalip.2011.08.017

Everts, H. B., Silva, K. A., Montgomery, S., Suo, L., Menser, M., Valet, A., et al. (2013). Retinoid metabolism is altered in human and mouse cicatricial alopecia. *J. Invest. Dermatol.* 133, 325–333. doi: 10.1038/jid.2012.393

Everts, H. B., Sundberg, J. P., King, L. E. Jr., and Ong, D. E. (2007). Immunolocalization of enzymes, binding proteins, and receptors sufficient for retinoic acid synthesis and signaling during the hair cycle. *J. Invest. Dermatol.* 127, 1593–1604. doi: 10.1038/sj.jid.5700753

Foitzik, K., Spexard, T., Nakamura, M., Halsner, U., and Paus, R. (2005). Towards dissecting the pathogenesis of retinoid-induced hair loss: All-*trans* retinoic acid induces premature hair follicle regression (catagen) by upregulation of transforming growth factor-beta 2 in the dermal papilla. *J. Invest. Dermatol.* 124, 1119–1126. doi: 10.1111/j.0022-202x.2005.23686.x

Giguere, V., Ong, E. S., Segui, P., and Evans, R. M. (1987). Identification of a receptor for the morphogen retinoic acid. *Nature* 330, 624–629. doi: 10.1038/330624a0

Girard, C., Dereure, O., Blatiere, V., Guillot, B., and Bessis, D. (2006). Vitamin A deficiency phrynoderma associated with chronic giardiasis. *Pediatr. Dermatol.* 23, 346–349. doi: 10.1111/j.1525-1470.2006.00261.x

Gupta, A. K., Goldfarb, M. T., Ellis, C. N., and Voorhees, J. J. (1989). Side-effect profile of acitretin therapy in psoriasis. *J. Am. Acad. Dermatol.* 20, 1088–1093. doi: 10.1016/s0190-9622(89)70138-9

Higgins, C. A., Westgate, G. E., and Jahoda, C. A. B. (2009). From telogen to exogen: mechanisms underlying formation and subsequent loss of the hair club fiber. *J. Invest. Dermatol.* 129, 2100–2108. doi: 10.1038/jid.2009.66

Higgins, C. A., Westgate, G. E., and Jahoda, C. A. B. (2011). Modulation in proteolytic activity is identified as a hallmark of exogen by transcriptional profiling of hair follicles. *J. Invest. Dermatol.* 131, 2349–2357. doi: 10.1038/jid.2011.227

Hsu, Y. C., and Fuchs, E. (2012). A family business: stem cell progeny join the niche to regulate homeostasis. *Nat. Rev. Mole. Cell Biol.* 13, 103–114. doi: 10.1038/nrm3272

Hsu, Y. C., Pasolli, H. A., and Fuchs, E. (2011). Dynamics between stem cells, niche, and progeny in the hair follicle. *Cell* 144, 92–105. doi: 10.1016/j.cell.2010.11.049

Isoherranen, N., and Zhong, G. (2019). Biochemical and physiological importance of the CYP26 retinoic acid hydroxylases. *Pharmacol. Therapeut.* 204:e107400.

Jurukovski, V., Markova, N. G., Karaman-Jurukovska, N., Randolph, R. K., Su, J., Napoli, J. L., et al. (1999). Cloning and characterization of retinol dehydrogenase transcripts expressed in human epidermal keratinocytes. *Mol. Genet. Metabol.* 67, 62–73. doi: 10.1006/mgme.1999.2840

Kandyba, E., and Kobielak, K. (2014). Wnt7b Is an Important Intrinsic Regulator of Hair Follicle Stem Cell Homeostasis and Hair Follicle Cycling. *Stem Cells* 32, 886–901.

Kandyba, E., Leung, Y., Chen, Y. B., Widelitz, R., Chuong, C. M., and Kobielak, K. (2013). Competitive balance of intrabulge BMP/Wnt signaling reveals a robust gene network ruling stem cell homeostasis and cyclic activation. *Proc. Nat. Acad. Sci. U. S. A.* 110, 1351–1356. doi: 10.1073/pnas.1121312110

Karlsson, T., Vahlquist, A., Kedishvili, N., and Torma, H. (2003). 13-*cis*-Retinoic acid competitively inhibits 3 alpha-hydroxysteroid oxidation by retinol dehydrogenase RoDH-4: a mechanism for its anti-androgenic effects in sebaceous glands? *Biochem. Biophys. Res. Commun.* 303, 273–278. doi: 10.1016/s0006-291x(03)00332-2

Katz, H. I., Waalen, J., and Leach, E. E. (1999). Acitretin in psoriasis: an overview of adverse effects. *J. Am. Acad. Dermatol.* 41, S7–S12.

Kedishvili, N. Y. (2013). Enzymology of retinoic acid biosynthesis and degradation. *J. Lipid. Res.* 54, 1744–1760. doi: 10.1194/jlr.r037028

Kimura-Ueki, M., Oda, Y., Oki, J., Komi-Kuramochi, A., Honda, E., Asada, M., et al. (2012). Hair cycle resting phase is regulated by cyclic epithelial FGF18 signaling. *J. Invest. Dermatol.* 132, 1338–1345. doi: 10.1038/jid.2011.490

Lee, S.-A., Belyaeva, O. V., Wu, L., and Kedishvili, N. Y. (2011). Retinol dehydrogenase 10 but not retinol/sterol dehydrogenase(s) regulates the expression of retinoic acid-responsive genes in human transgenic skin raft culture. *J. Biol. Chem.* 286, 13550–13560.

MacDonald, P. N., and Ong, D. E. (1988). A lecithin:retinol acyltransferase activity in human and rat liver. *Biochem. Biophys. Res. Commun.* 156, 157–163. doi: 10.1016/s0006-291x(88)80818-0

Markova, N. G., Pinkas-Sarafova, A., Karaman-Jurukovska, N., Jurukovski, V., and Simon, M. (2003). Expression pattern and biochemical characteristics of a major epidermal retinol dehydrogenase. *Mol. Genet. Metab.* 78, 119–135. doi: 10.1016/s1096-7192(02)00226-3

Milner, Y., Sudnik, J., Filippi, M., Kizoulis, M., Kashgarian, M., and Stenn, K. (2002). Exogen, shedding phase of the hair growth cycle: characterization of a mouse model. *J. Invest. Dermatol.* 119, 639–644. doi: 10.1046/j.1523-1747.2002.01842.x

Muller-Rover, S., Handjiski, B., van der Veen, C., Eichmuller, S., Foitzik, K., McKay, I. A., et al. (2001). A comprehensive guide for the accurate classification of murine hair follicles in distinct hair cycle stages. *J. Invest. Dermatol.* 117, 3–15. doi: 10.1046/j.0022-202x.2001.01377.x

Murray, H. E., Anhalt, A. W., Lessard, R., Schacter, R. K., Ross, J. B., Stewart, W. D., et al. (1991). A 12-month treatment of severe psoriasis with acitretin: results of a Canadian open multicenter study. *J. Am. Acad. Dermatol.* 24, 598–602. doi: 10.1016/0190-9622(91)70091-f

Nadauld, L. D., Shelton, D. N., Chidester, S., Yost, H. J., and Jones, D. A. (2005). The zebrafish retinol dehydrogenase, rdh1l, is essential for intestinal development and is regulated by the tumor suppressor adenomatous polyposis coli. *J. Biol. Chem.* 280, 30490–30495. doi: 10.1074/jbc.m504973200

Napoli, J. L. (1999). Retinoic acid: its biosynthesis and metabolism. *Prog. Nucleic Acid Res. Mol. Biol.* 63, 139–188. doi: 10.1016/s0079-6603(08)60722-9

Napoli, J. L. (2012). Physiological insights into all-*trans*-retinoic acid biosynthesis. *Biochim. Biophys. Acta* 1821, 152–167. doi: 10.1016/j.bbalip.2011.05.004

Napoli, J. L. (2020). Post-natal all-trans-retinoic acid biosynthesis. *Methods Enzymol.* 637, 27–54. doi: 10.1016/bs.mie.2020.02.003

Navarro, J. M., Casatorres, J., and Jorcano, J. L. (1995). Elements controlling the expression and induction of the skin hyperproliferation-associated keratin K6. *J. Biol. Chem.* 270, 21362–21367. doi: 10.1074/jbc.270.36.21362

Nelson, C. H., Peng, C. C., Lutz, J. D., Yeung, C. K., Zelter, A., and Isoherranen, N. (2016). Direct protein-protein interactions and substrate channeling between cellular retinoic acid binding proteins and CYP26B1. *FEBS Lett.* 590, 2527–2535. doi: 10.1002/1873-3468.12303

Obrochta, K. M., Kane, M. A., and Napoli, J. L. (2014). Effects of diet and strain on mouse serum and tissue retinoid concentrations. *PLoS One* 9:e99435. doi: 10.1371/journal.pone.0099435

Ocon, J., Cabrejas, C., Altemir, J., and Moros, M. (2012). Phrynoderma: a rare dermatologic complication of bariatric surgery. *J. Parenter. Enteral. Nutr.* 36, 361–364. doi: 10.1177/0148607111422067

Okano, J., Levy, C., Lichti, U., Sun, H. W., Yuspa, S. H., Sakai, Y., et al. (2012). Cutaneous retinoic acid levels determine hair follicle development and downgrowth. *J. Biol. Chem.* 287, 39304–39315. doi: 10.1074/jbc.m112.397273

Ong, D. E. (1987). Cellular retinoid-binding proteins. *Arch. Dermatol.* 123, 1693–1695a.

Orland, M. D., Anwar, K., Cromley, D., Chu, C. H., Chen, L. P., Billheimer, J. T., et al. (2005). Acyl coenzyme A dependent retinol esterification by acyl coenzyme A : diacylglycerol acyltransferase 1. *Biochim. Biophys. Acta* 1737, 76–82. doi: 10.1016/j.bbalip.2005.09.003

Oshimori, N., and Fuchs, E. (2012). Paracrine TGF-beta signaling counterbalances BMP-mediated repression in hair follicle stem cell activation. *Cell Stem Cell* 10, 63–75. doi: 10.1016/j.stem.2011.11.005

Plikus, M. V., Mayer, J. A., de la Cruz, D., Baker, R. E., Maini, P. K., Maxson, R., et al. (2008). Cyclic dermal BMP signalling regulates stem cell activation during hair regeneration. *Nature* 451, 340–344. doi: 10.1038/nature06457

Rexer, B. N., and Ong, D. E. (2002). A novel short-chain alcohol dehydrogenase from rats with retinol dehydrogenase activity, cyclically expressed in uterine epithelium. *Biol. Rep.* 67, 1555–1564. doi: 10.1095/biolreprod.102.007021

Sessler, R. J., and Noy, N. (2005). A ligand-activated nuclear localization signal in cellular retinoic acid binding protein-II. *Mol. Cell* 18, 343–353. doi: 10.1016/j.molcel.2005.03.026

Shih, M. Y. S., Kane, M. A., Zhou, P., Yen, C. L. E., Streeper, R. S., Napoli, J. L., et al. (2009). Retinol esterification by DGAT1 is essential for retinoid homeostasis in murine skin. *J. Biol. Chem.* 284, 4292–4299. doi: 10.1074/jbc.m807503200

Sundberg, J. P., Booth, C. J., Nanney, L. B., Fleckman, P., and King, L. E. (2018). "Skin and adnexa," in *Comparative anatomy and histology A mouse, rat, and human atlas. Second*, eds P. Treuting, S. M. Dintzis, C. W. Frevert, D. Liggitt, and K. S. Montine (Amsterdam: Elsevier), 511–542. doi: 10.1016/b978-0-12-802900-8.00024-5

Sundberg, J. P., Brown, K. S., and McMahon, W. M. (1994a). "Chronic ulcerative dermatitis in black mice," in *Handbook of Mouse Mutations With Skin and Hair Abnormalities: Anumal Models and Biomedical Tools*, ed. J. P. Sundberg (Boca Raton, FL: CRC Press), 485–492. doi: 10.1201/9781003068952-67

Sundberg, J. P., Cordy, W. R., and King, L. E. Jr. (1994b). Alopecia areata in aging C3H/HeJ mice. *J. Invest. Dermatol.* 102, 847–856. doi: 10.1111/1523-1747.ep12382416

Sundberg, J. P., Taylor, D., Lorch, G., Miller, J., Silva, K. A., Sundberg, B. A., et al. (2011). Primary follicular dystrophy with scarring dermatitis in C57BL/6 mouse substrains resembles central centrifugal cicatricial alopecia in humans. *Vet. Pathol.* 48, 513–524. doi: 10.1177/0300985810379431

Suo, L., Sundberg, J. P., and Everts, H. B. (2015). Dietary vitamin A regulates wingless-related MMTV integration site signaling to alter the hair cycle. *Exp. Biol. Med.* 240, 618–623. doi: 10.1177/1535370214557220

Thiboutot, D., Gollnick, H., Bettoli, V., Dreno, B., Kang, S. W., Leyden, J. J., et al. (2009). New insights into the management of acne: An update from the Global Alliance to Improve Outcomes in Acne Group. *J. Am. Acad. Dermatol.* 60, S1–S50.

Wang, L., Siegenthaler, J. A., Dowell, R. D., and Yi, R. (2016). Foxc1 reinforces quiescence in self-renewing hair follicle stem cells. *Science* 351, 613–617. doi: 10.1126/science.aad5440

Wolbach, S. B., and Howe, P. R. (1925). Tissue changes following deprivation of fat-soluble A vitamin. *J. Exp. Med.* 42, 753–777. doi: 10.1084/jem.42.6.753

Wu, B. X., Chen, Y. M., Chen, Y., Fan, C., Rohrer, B., Crouch, R. K., et al. (2002). Cloning and characterization of a novel all-*trans* retinol short-chain dehydrogenase/reductase from the RPE. *Invest. Ophthalmol. Vis. Sci.* 43, 3365–3372.

Wu, L. Z., Belyaeva, O., Adams, M. K., Klyuyeva, A. V., Lee, S. A., Goggans, K. R., et al. (2019). Mice lacking the epidermal retinol dehydrogenases SDR16C5 and SDR16C6 display accelerated hair growth and enlarged meibomian glands. *J. Biol. Chem.* 294, 17060–17074. doi: 10.1074/jbc.ra119.010835

Yi, R. (2017). Concise review: mechanisms of quiescent hair follicle stem cell regulation. *Stem Cells* 35, 2323–2330. doi: 10.1002/stem.2696

Zouboulis, C. C., Korge, B. P., Mischke, D., and Orfanos, C. E. (1993). Altered proliferation, synthetic activity, and differentiation of cultured human sebocytes in the absence of vitamin-A and their modulation by synthetic retinoids. *J. Invest. Dermatol.* 101, 628–633. doi: 10.1111/1523-1747.ep12366092

Conflict of Interest: The authors declare that the research was conducted in the absence of any commercial or financial relationships that could be construed as a potential conflict of interest.

Copyright © 2021 Suo, VanBuren, Hovland, Kedishvili, Sundberg and Everts. This is an open-access article distributed under the terms of the Creative Commons Attribution License (CC BY). The use, distribution or reproduction in other forums is permitted, provided the original author(s) and the copyright owner(s) are credited and that the original publication in this journal is cited, in accordance with accepted academic practice. No use, distribution or reproduction is permitted which does not comply with these terms.

frontiers in Cell and Developmental Biology

REVIEW
published: 11 February 2021
doi: 10.3389/fcell.2021.598717

UVA-Triggered Drug Release and Photo-Protection of Skin

Vega Widya Karisma[1], Wei Wu[1], Mingxing Lei[1], Huawen Liu[2], Muhammad Farrukh Nisar[3], Matthew D. Lloyd[4], Chararеh Pourzand[5,6] and Julia Li Zhong[1]**

[1] Key Laboratory of Biorheological Science and Technology, Ministry of Education, Bioengineering College, Chongqing University, Chongqing, China, [2] Three Gorges Central Hospital, Chongqing, China, [3] Department of Physiology and Biochemistry, Cholistan University of Veterinary and Animal Sciences (CUVAS), Bahawalpur, Pakistan, [4] Drug and Target Discovery, Department of Pharmacy and Pharmacology, University of Bath, Bath, United Kingdom, [5] Medicines Design, Department of Pharmacy and Pharmacology, University of Bath, Bath, United Kingdom, [6] Medicines Development, Centre for Therapeutic Innovation, University of Bath, Bath, United Kingdom

Light has attracted special attention as a stimulus for triggered drug delivery systems (DDS) due to its intrinsic features of being spatially and temporally tunable. Ultraviolet A (UVA) radiation has recently been used as a source of external light stimuli to control the release of drugs using a "switch on- switch off" procedure. This review discusses the promising potential of UVA radiation as the light source of choice for photo-controlled drug release from a range of photo-responsive and photolabile nanostructures *via* photo-isomerization, photo-cleavage, photo-crosslinking, and photo-induced rearrangement. In addition to its clinical use, we will also provide here an overview of the recent UVA-responsive drug release approaches that are developed for phototherapy and skin photoprotection.

Keywords: caged iron chelators, drug delivery systems (DDS), skin photo-protection, smart sunscreens, up-conversion nanoparticles, UVA-triggered drug release

OPEN ACCESS

Edited by:
Sung-Jan Lin,
National Taiwan University, Taiwan

Reviewed by:
Michael R. Hamblin,
Massachusetts General Hospital and Harvard Medical School, United States
Zi-Bing Jin,
Capital Medical University, China

***Correspondence:**
Julia Li Zhong
jlzhong@cqu.edu.cn
Chararеh Pourzand
C.A.Pourzand@bath.ac.uk

Specialty section:
This article was submitted to Stem Cell Research, a section of the journal Frontiers in Cell and Developmental Biology

Received: *25 August 2020*
Accepted: *13 January 2021*
Published: *11 February 2021*

Citation:
Karisma VW, Wu W, Lei M, Liu H, Nisar MF, Lloyd MD, Pourzand C and Zhong JL (2021) UVA-Triggered Drug Release and Photo-Protection of Skin. Front. Cell Dev. Biol. 9:598717. doi: 10.3389/fcell.2021.598717

INTRODUCTION

The introduction of targeted drug delivery systems (DDS) has greatly enhanced the bioavailability of the drugs while substantially reducing their side effects. This is because DDS enable the highly selective delivery of the drug to the lesion site whilst minimizing its premature loss (Bahrami et al., 2017; Breitsamer and Winter, 2019; Huang et al., 2019). It also provides flexibility by controlling the timing, duration and the level of drug release while combining the attainment of a therapeutic drug concentration with on-demand release (Davoodi et al., 2018). The ability to control drug delivery has become a very important goal during drug development since it maximizes therapeutic efficiency whilst minimizing undesirable effects. This is achieved with either internal or external stimuli (Bhowmik et al., 2012; Senapati et al., 2018). The use of DDS responding to external stimuli offers a promising approach for the controlled release of drugs since their spatiotemporal properties allow flexible control of drug dosage, timing, and duration of treatment (Yao et al., 2016; Wang and Kohane, 2017; Rwei et al., 2018) according to the patients' needs, with consequent reduction in side-effects and an increase in therapeutic efficacy.

It is becoming possible to use either UV or near-infrared (NIR) radiation as an external stimuli in DDS. Light can be used either as a single-dose or a multi-switchable stimulus. The single-light dose stimulus can trigger an irreversible change in the photo-responsive drug carrier which results in the release of the drug. The multi-switchable stimulus allows the drug to be released from its carrier in a pulsatile manner (Alvarez-Lorenzo et al., 2009). Light as a stimulus has

been the subject of special attention because it allows release of a wide range of therapeutic compounds with spatial and temporal control (Bagheri et al., 2016). By selecting an appropriate wavelength, it may be possible to accurately fine-tune the power and focus of the light, depending on the energy it bears and its ability to penetrate the body tissues (Barhoumi and Kohane, 2015). The nanostructure-based DDS may open or close upon irradiation (Liu et al., 2016; Shim et al., 2017). In fact, light is an attractive trigger for drug delivery due to its ability to facilitate spatiotemporal drug release using photo-degradation, photo-thermal effects, or photo-induced hydrophobicity transfer (Yu et al., 2014; Son et al., 2019). The presence of light can induce irreversible or reversible structure changes through bond cleavage, isomerization, switchable electrostatic attraction and molecular rearrangement (Kamaly et al., 2016). Activation can occur by a one or two-photon absorption processes (Liu G. et al., 2013).

Ultraviolet A (UVA, 320–400 nm) comprises more than 95% of the UV radiation reaching earth and is responsible for oxidative damage to the skin and eyes. This damage results in premature photo-aging, and contributes to skin carcinogenesis, ocular pathologies and affects the balance between cellular repair and apoptosis (Svobodova et al., 2006; Amaro-Ortiz et al., 2014; Kim and He, 2014). As the longest wavelength of UV radiation, UVA can penetrate to the dermis and subcutaneous layer and 1% of UVA can penetrate to the blood (up to ∼150 μm in depth) and can cause oxidative damage to cellular constituents notably DNA, proteins and lipids due to its ability to generate reactive oxygen species (ROS) *via* intracellular chromophores (Seité et al., 2010; D'Orazio et al., 2013; Karran and Brem, 2016; Brem et al., 2017; Lan et al., 2019; Moreno et al., 2019), which may lead to the cell death (apoptosis or necrosis depending on the severity of the insult) (Pourzand and Tyrrell, 1999; Marionnet et al., 2011; Jaszewska et al., 2013; Burke, 2018; Dunaway et al., 2018). UVA irradiation also directly accelerates skin aging by promoting the formation of wrinkles, reducing elasticity and loss of skin pigmentation due to upregulation of collagen levels and matrix metalloproteinases (MMPs) (Seité et al., 2010; Marionnet et al., 2011; Dunaway et al., 2018).

Despite the adverse effects of solar UV radiation, its energy especially UVB is absorbed by the epidermis layer through 7-dehydrocholesterol to convert the energy photon into provitamin D_3 and isomerized into vitamin D_3 to regulate the Ca^{2+} metabolism of the skin (Wexler et al., 2005; Passeron et al., 2019). In dermatology, UVA is routinely used for photo-therapy in combination with topical treatment due to its low side effects and ease of use for many skin conditions (Vangipuram and Feldman, 2016). Nevertheless, UVA irradiation may contribute to skin cancer (Wexler et al., 2005). Long wave UVA1 (340–400 nm) has an effect on localized atopic dermatitis and scleroderma, and exerts its therapeutic effect through T cell apoptosis, collagenase induction, and angiogenesis (Lee et al., 2013; Teske and Jacobe, 2016). The UVA therapy and its combination with psoralen also known as PUVA (Psoralen-UVA) is currently used for the treatment of diseases such as psoriasis, vitiligo, and cutaneous T-cell lymphoma (Tippisetty et al., 2013; Tsai-Turton, 2014). PUVA triggers the delayed reaction of erythemal ∼96 h after UVA radiation of the psoralen-sensitized skin (Ibbotson, 2018). The antiproliferative activity of the treatment occurs via the arrangement of DNA monoadduct and inter-strand cross-links (ICLs) in the irradiated cells (Derheimer et al., 2009).

As an attractive light stimulus, the controlled spatiotemporal use of UVA radiation offers the possibility of activating nanostructure-based DDS following irradiation and the release of the medicine at a specific side (Breuckmann et al., 2004; Jiang et al., 2005; Agasti et al., 2009; Jin et al., 2011; Prasad et al., 2020) (see **Figure 1**). Some photo-activated substances and functional groups are relatively inert to NIR light but react upon irradiation with UV light, thereby causing chemical and/or physical changes (Jayakumar et al., 2012; Tong et al., 2012). Among several light triggers, UV light has been considered for the controlled release of drugs, proteins, and DNA as well as for other applications in signaling agents (Sreejivungsa et al., 2016).

The UV-responsive drug-carrying nanoparticles allow the release of their cargo following UV radiation *via* various mechanisms of UV-triggered drug delivery systems (Tong et al., 2012; Mura et al., 2013; Barhoumi et al., 2015). Most of the light-responsive materials respond to UV light, leading to significant release of their cargo to targeted site (Zhao et al., 2019). Nanoparticles are capable of discharging their payload at the higher range and farther diffusion through the corneal tissue and collagen gel upon the irradiation with UV light (Tong et al., 2012). The UV light also provides high energy per photon to break the covalent bonds, thus initiating drug-release by photo-isomerization, photo-cleavage, photo-crosslinking or rearrangement (Linsley and Wu, 2017; Zhao et al., 2019). These advantageous matters are considered to utilize UV light in controlling drug delivery. Nevertheless, the high phototoxicity and shorter tissue penetration (up to 100–150 μm) limit the utilization of UV light resulting in tissue damage and low drug release from the DDS (Liu et al., 2016; Zhao et al., 2019). In this regard, a strategy has been established to overcome the challenge of UV light limitation by the use of up-conversion nanoparticles (UCNPs). The use of a combination of NIR and UV to produce UCNPs is an attractive alternative as it minimizes the adverse effects of UV penetration since UCNPs can convert NIR light into UV and visible light (Cho et al., 2015).

Various studies investigating UV-induced drug release are getting considerable attention. For example, Cabane et al. (2011) studied the potential of photo-responsive polymersomes using a photo-cleavable amphiphilic block copolymer (PMLC-2-nitrobenzyl-polyacrylic acid), which degraded upon exposure to UV radiation (365 nm) in a dose-dependent manner. Similarly, Wang et al. (2014) designed micelles incorporating spiropyran within the polymer. Upon irradiation the micelle diameter decreased with consequent release of the drug. A photo-responsive liposome based on 1,2-bis(10,12-tricosadiynoyl)-sn-glycero-3-phosphocholine (DC-8,9-PC) fabricated by Li et al. (2015) targeted to CD20 underwent intermolecular cross-linking *via* its di-acetylenic groups upon UV irradiation. Wang et al. (2015) combined mesoporous titanium dioxide (TiO_2) with polyethyleneimine (PEI) to produce nanoparticles, which released folic acid and paclitaxel upon UV irradiation thereby facilitating

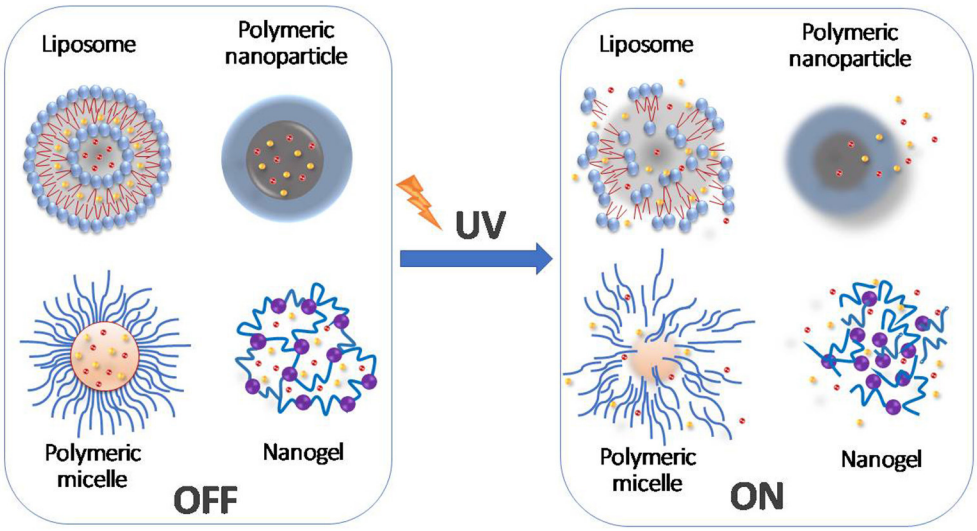

FIGURE 1 | Schematic diagram representing the controlled drug release mediated by the UV light-induced changes to molecular structures.

controlled release of the anticancer drug and promoting cancer cell-specific uptake.

UVA-controlled release can also be a promising alternative strategy for protecting the skin from the effects of UV radiation (Vogt et al., 2016). Previous research by us demonstrated that the UVA-controlled release of caged iron chelators can protect the skin against UVA-induced oxidative damage and the ensuing necrotic cell death (Yiakouvaki et al., 2006). This is due to the ability of the caged iron chelators to sequester excess harmful labile iron release in skin cells caused by radiation in a dose- and context-dependent manner (Zhong et al., 2004; Kitazawa et al., 2006). The UVA-mediated labile iron release can be mitigated by the use of an iron chelator thus reducing the associated photo-aging and photo-carcinogenesis (Pouillot et al., 2013) using photo-controlled and activatable-caged iron chelators (Reelfs et al., 2010). Our approach provided the possibility of formulating sunscreens with light-activated iron chelators as their main UVA-activatable ingredient to protect the skin against the oxidizing UVA component of sunlight.

This review highlights the mechanisms underlying drug release following photoactivation of various drug-loaded nanoparticles with UV (specifically UVA) and NIR for clinical use or skin photoprotection.

MECHANISMS OF UVA-INDUCED DRUG RELEASE

In order to use UVA light as a trigger for DDS, specific molecular mechanisms are required. Controlled drug release can be achieved through a number of different mechanisms, including photo-isomerization, photo-cleavage, photo-crosslinking, and photo-induced rearrangement (Barhoumi et al., 2015), as summarized in **Figure 2** and discussed below.

Photo-Isomerization

Photo-isomerization is the interconversion of two metastable forms upon light irradiation, which results in a conformational change due to the two forms having different physical and chemical properties (Stranius and Börjesson, 2017). This photo-isomerization can be reversible (Li et al., 2016). Some isomerization mechanisms involve the breaking of the chemical structure and its conversion into the lowest energy phase following photo-isomerization. These changes can be reversible as seen with spiropyran (Olejniczak et al., 2015). Other molecules such as azobenzene can undergo a reversible *cis*/*trans* isomerization (Shao et al., 2008) without bond breakage (Barhoumi et al., 2015).

The photo-isomerizations of azobenzene and their derivatives have been extensively studied for their use as photochromic compounds in drug-release systems (Gao et al., 2014). Azobenzene can exist as both *cis* and *trans* (*Z*-and *E*-) isomers. The *trans* to *cis* isomerization occurs upon irradiation with UV whilst the reverse *cis*- to *trans*-isomerization is catalyzed by visible light, mechanical stress or electrostatic stimulation (Bandara and Burdette, 2012; Zhang et al., 2019). Compared to many photo-responsive moieties, azobenzene has better light-responsive properties by virtue of its ability to undergo reversible isomerization between the non-polar *trans* and polar *cis* configurations in many solvents (Zhang et al., 2019). Consequently, it has been widely used in liposomes, mesoporous silica, and micellar DDS (Olejniczak et al., 2015). Azobenzene absorbs at two wavelengths, in visible light as a weak band (~430 nm in *n*-hexane) associated with the excitation of the formally dipole-forbidden $^1B_{2g}(n\pi^*)$ transition, and as a strong band in the UV region (~320 nm in *n*-hexane) linked to absorption of dipole-allowed $^1B_{1u}(\pi\pi^*)$ transition (Tan et al., 2015). Therefore, the isomerization from *trans* to *cis* geometry occurs upon irradiation with UV light (320–365 nm) and is reversed by exposure to blue light (400–450 nm) or heat, thus

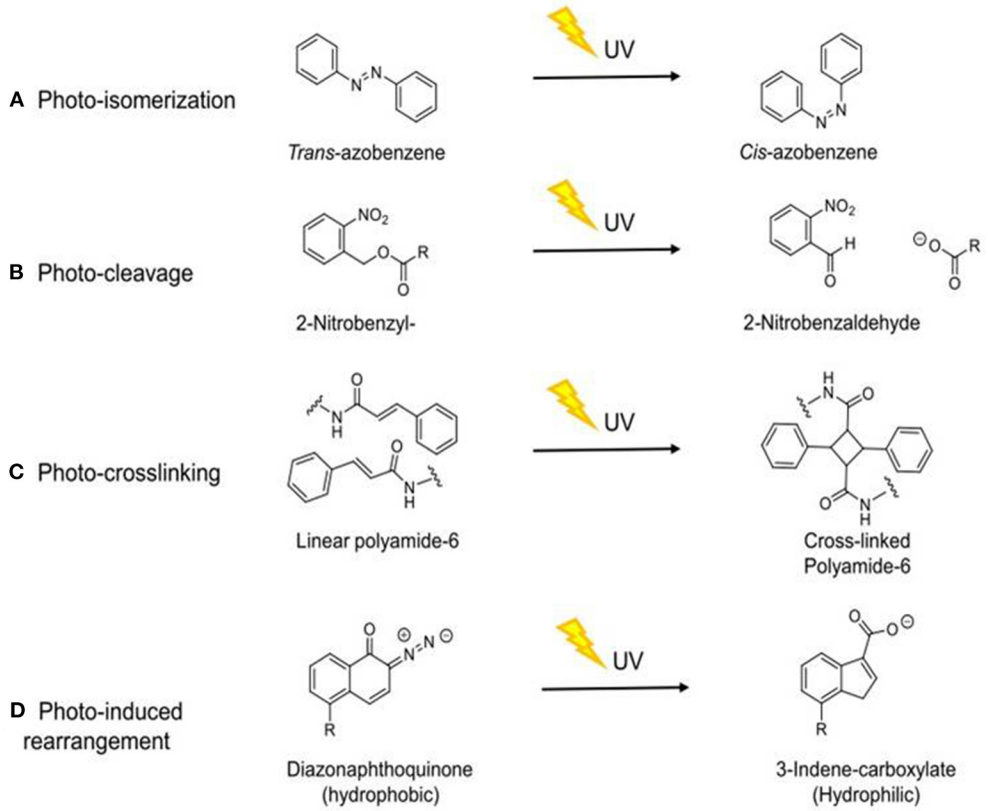

FIGURE 2 | Schematic diagram of the molecular mechanisms by which UVA induces drug release through different mechanisms. **(A)** Photo-isomerization (Stranius and Börjesson, 2017); **(B)** Photo-cleavage (Kauscher et al., 2019); **(C)** Photo-crosslinking (Tunc et al., 2014); **(D)** Photo-induced rearrangement (Olejniczak et al., 2015). R = aliphatic group.

changing molecule geometry, polarity, and electronic features (Tylkowski et al., 2017).

A study from Galante et al. (2019) investigated bridging of silsesquioxane with azobenzene moieties in order to produce a self-healing material upon UV-irradiation. They demonstrated that UV irradiation effectively changed the intra-molecular conformation of the azo-chromophores resulting from a *trans* to *cis* isomerization. UV irradiation increased the mobility of the material allowing it follow into damaged areas which was followed by reestablishment of hydrogen bonds. Another study from Zhang P. et al. (2019) prepared shape-memory materials (SMMs) incorporating azobenzene derivative 4-cyano-4′-pentyloxyazobenzene (5CAZ) and UCNPs. These mechanically stretched materials could be deformed by the UV/vis/NIR light irradiation due to the presence of the UCNPs. Irradiation of nanoparticles with NIR light (980 nm) causes the emission of photons within the UV/vis region and their absorption by photo-responsive azobenzene derivative resulting in photo-isomerization and hence changes in the UCNP structure (Liu J. et al., 2013).

Liposomes have also been established as an effective light-responsive drug delivery system, as irradiation can induce bilayer isomerization leading to structural changes (Lajunen et al., 2016; Deng et al., 2018). Liu and An (2019) enhanced the photo-responsiveness of liposomes by preparing liposomes that incorporated 4-butylazobenzene-4-hexyloxy-trimethyl-ammoniumtrifluoroacetate (BHA) as a photo-responsive element. Reversible structural isomerization was used to release the entrapped curcumin payload upon irradiation (**Figure 3**). Similarly, Uda et al. (2016) investigated the release of molecules from liposomes in response to light. The copolymer of poly(vinyl alcohol) carrying a malachite green moiety (PVA-MG) was inert under dark condition but associated with liposomes upon irradiation, causing the release of the encapsulated compound.

Photo-Cleavage

The implementation of photosensitive drug release through a photo-cleavable linker can be achieved using coumarin or 2-nitrobenzyl-derivatives, dendrimersomes or other known cleavable units (Kauscher et al., 2019). Photo-cleavage occurs due to the breakdown of covalent bonds following light irradiation (between 320 and 400 nm), effecting fast degradation of molecule structures and allowing the release of payloads or the release an immobilized molecule (Huang et al., 2014; Grim et al., 2015; Olejniczak et al., 2015). Absorbance of high energy photons by

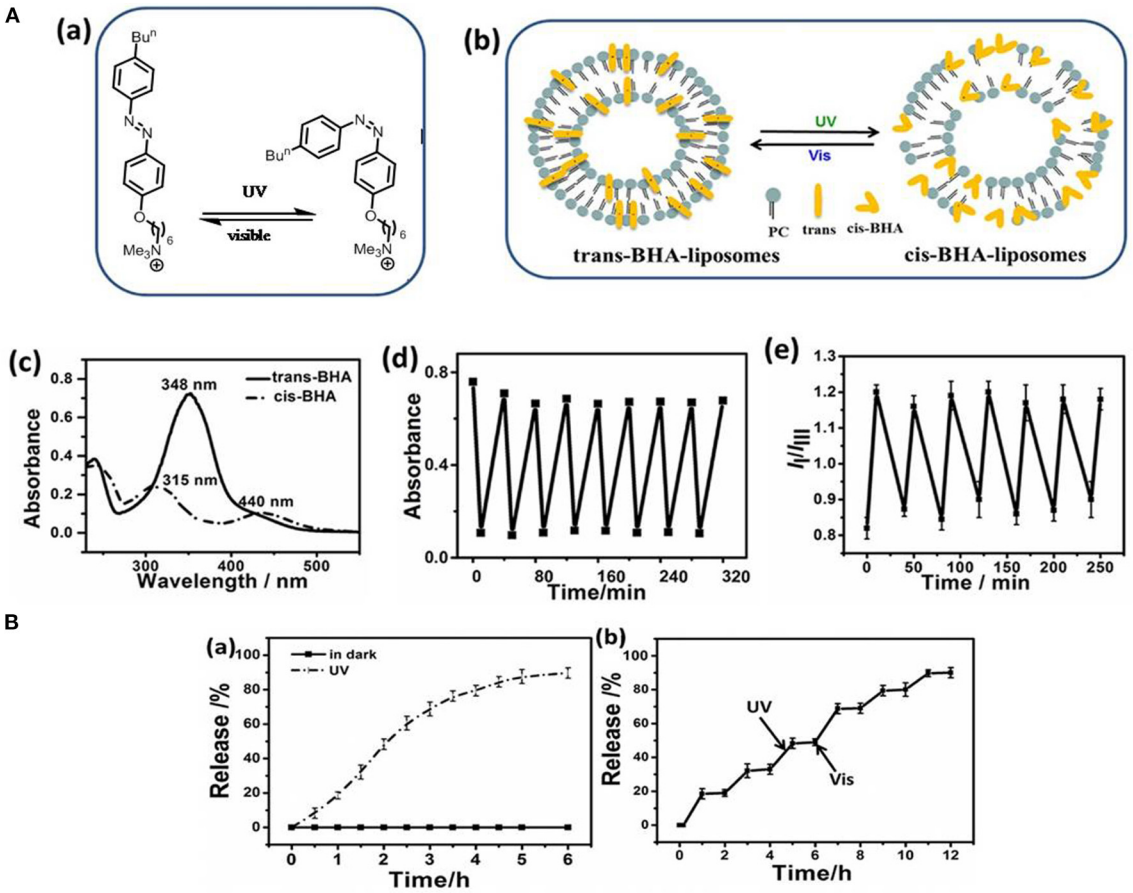

FIGURE 3 | (A) Photo-isomerization of BHA-liposome (a) Chemical structure and photo-isomerization of BHA; (b) The microstructure schematic of the trans- and *cis*-BHA-liposome; (c) The UV-visible spectra of BHA-liposomes showing changes upon isomerization; (d) Changes in the absorbance of the BHA-liposome at 348 nm during alternating cycles of UV and visible light; (e) I_I/I_{III} values for the BHA-liposome with time upon alternating irradiation with UV and visible light. **(B)** Drug release from a liposome: (a) Curcumin release from liposomes in the dark (black line) and upon UV irradiation (red line); (b) The accumulated release of curcumin from BHA-curcumin-liposomes upon alternate irradiation by UV and visible light. Reproduced with permission (Liu and An, 2019). Copyright 2018, Elsevier. BHA, 4-butylazobenzene-4-hexyloxy-trimethyl-ammonium trifluoroacetate.

the pro-drug are required to induce photo-cleavage of bonds (Härtner et al., 2007). 2-Nitrobenzyl and coumarin moieties are photo-cleavable linkers commonly incorporated into polymers, micelles, or in low molecular compounds (Härtner et al., 2007) used to construct the drug delivery systems. Photo-cleavage can be achieved either by UV radiation (between 320 and 400 nm) or NIR light (Liu G. et al., 2013).

Kim and Diamond (2006) investigated 2-nitrobenzyl and 2-nitrophenylethyl derivatives experiencing photo-decomposition upon irradiation with long-wavelength UV light (UVA, 365 nm) in DDS. These studies revealed that the rate of decomposition for 2-nitrobenzylderivatives were particularly suitable for use in DDS. Choi et al. (2012) designed a drug release system activated by UVA irradiation using 2-nitrobenzyl as the photo-cleavable linker for the light-mediated release of methotrexate. They also used 2-nitrobenzyl linkers to extend the release of methotrexate from a fifth-generation poly(amidoamine) dendrimer carrier. Hu and colleagues (Hu et al., 2017) developed photo- and chemo-cleavable compounds by combining a 2-nitrobenzyl ester moiety as a photo-cleavable linker within multi-block polystyrenes. These polymers could be cleaved not only using UVA light but also by ester group hydrolysis.

Another commonly used linker for photo-cleavage linker is coumarin and its derivatives, since faster release rates are achieved compared to 2-nitrobenzyl (Beauté et al., 2019). Coumarin derivatives possess longer absorption wavelengths, larger molar extinction coefficients, higher stability, and biocompatibility, and strong fluorescent properties (Gao et al., 2017). Jiang et al. (2017) investigated three different coumarin dimer isomers using time-resolved transient absorption spectroscopy in order to verify the mechanism of photo-cleavage. This revealed that the cleavage mechanism was *via* a non-fluorescent, short-lived (<200 fs) singlet reaction state. Chung et al. (2013) also analyzed the effect of coumarin on polymer model stating that the increase in coumarin functionality resulted in decreasing nanoparticle size and polydispersity and increased the stability of the polymer in water. Hence, Soares et al. (2017) examined light-sensitive moieties

for releasing bioactive molecules by combining coumarin with oxazoles using butyric acid resulting in a shorter irradiation time at a longer wavelength (11 min, at 350 nm), thus demonstrating coumarin can enhance the photo-cleavage of the prodrug. A combination of coumarin with (6-bromo-7-methoxycoumarin)-nicotinamide reported by Bourbon et al. (2013) also showed photo-cleavage upon irradiation. Nazemi and Gillies (2014) reported the synthesis of polyester dendrimers incorporating 2-nitrobenzyl photo-cleavable linkers. Complete photolytic cleavage of the dendrimer backbone without formation of macromolecular byproducts was observed upon illumination with UV light. Liu et al. (2019) reported a low-molecular-weight hydrogelator (LMWG) that contained coumarin derivatives. The hydrogel underwent photo-cleavage at the C-N bond in 7-aminocoumarin upon irradiation at 365 nm. Alam et al. (2015) also modified the liposomes to enable photo-induced cleavage by synthesized photo-cleavable lipid analogs with 2-nitrobenzyl moiety close to the head-group of the lipid backbone to maximize bio-conjunction efficiency and photo-release (**Figure 4**). Delivery of the liposome containing the photo-cleavable lipid to live cells was also demonstrated. Another study by Radl et al. (2015) combined an epoxy-based polymer with a 2-nitrobenzyl ester (*o*-NBE). They successfully demonstrated the efficiency of photo-cleavage upon UV radiation and this technology could be applied to thin composite materials.

Photo-Crosslinking

Photo-crosslinking occurs through irradiation of polymerizable double bond either directly or by use of a sensitizer or radical initiator with consequent release of molecules (Fomina et al., 2012; Tunc et al., 2014). This mechanism has been used in drug delivery systems utilizing nanoparticles and stabilizing therapeutic nanocarriers such as nano-capsules and liposomes (Barhoumi et al., 2015). Photochemical crosslinking of polymers occurs upon UV irradiation at 364 nm, and de-crosslinking at 254 nm, affecting a decrease in nanoparticles size for cargo release from nanocarriers (Karimi et al., 2017). Photo-crosslinking is usually used in the formation of nanoparticles but it can be utilized in photo-triggered drug release (Fomina et al., 2012).

Some photo-crosslinking materials need radical initiators to perform crosslinking under UV irradiation. For example, Chesterman et al. (2018) compared cinnamoyl groups and coumarin within functionalized copolymers. The coumarin functionalized aliphatic polycarbonates demonstrating effective crosslinking upon UVA irradiation at wavelengths between 320 and 400 nm with the maximum intensity being 365 nm. Ding et al. (2011) analyzed some copolymers incorporating the cinnamyloxy group by synthesizing poly(ethylene glycol monomethyl ether)-β-poly(*L*-glutamic acid-co-γ-cinnamyl-*L*-glutamate) [mPEG-β-P(LGA/CLG)] and poly(*L*-glutamic acid-co-γ-cinnamyl-*L*-glutamate)-β-poly(ethylene glycol)-β-poly(*L*-glutamic acid-co-γ-cinnamyl-*L*-glutamate) (P(LGA/CLG)-β-PEG-β-P(LGA/CLG)) by using ring-opening polymerization (ROP) of γ-benzyl-*L*-glutamate-N-carboxy anhydride (BLG-NCA) monomer with a PEG-based macro-initiator. The results revealed the micelle polymer [P(LGA/CLG)] core block was able to crosslink under UVC irradiation at 254 nm wavelength due to cinnamyloxy photo-dimerization. Similarly, Teixeira et al. (2013) used benzophenone to induce photo-crosslinking during their synthesis of water-based poly(ethylene oxide) (PEO) polymers and successfully demonstrated photo-crosslinking upon UV radiation.

Liposomes are an alternative drug delivery system when using photo-induced crosslinking of lipids to enhance drug release efficiency. This results from the liposome lipid bilayer undergoing crosslinking upon UV irradiation (Leung and Romanowski, 2012). This mechanism is illustrated by research conducted by Yavlovich et al. (2009), in which they designed a light-triggered liposome from photo-polymerizable phospholipid DC-8,9-PC (1,2-bis(tricosa-10,12-diynoyl)-sn-glycero-3-phosphocholine) and 1,2-dipalmitoyl-sn-glycero-3-phosphocholine, which was used to encapsulate the fluorescent dye calcein. Exposure of this liposome to UV irradiation at 254 nm resulted in DC-8,9-PC cross-linking and release of the fluorescent dye. This finding proved that UV light-induced crosslinking of the liposome lipid bilayer resulted in release of its contents (Yavlovich et al., 2009). Photo-crosslinking of the liposome resulting in drug release occurred not only at 254 nm but also at 514 nm. At 254 nm, the photo-crosslinking resulted in liposome membrane disruption and polymerization, while at 514 nm the mechanism was related to ROS production (Miranda and Lovell, 2016). Liposomes containing DC-8,9-PC loaded with doxorubicin have been used to demonstrate their potential *in vitro* and in cell-based assays (Puri, 2014). Significantly, irradiation at 514 nm resulted in increased cytotoxicity compared to irradiation at 254 nm. Although the exact mechanism for doxorubicin release was not determined (Miranda and Lovell, 2016), it appears to be related to a type I photo-reaction involving electron transfer and generations of O_2^- and H_2O_2 (Yavlovich et al., 2013).

Photo-Induced Rearrangement

Exposure to light causes Wolff rearrangement of some molecules, and this has been used to trigger drug release from micelles either using NIR at 800 nm or UV radiation at 350 or 365 nm (Olejniczak et al., 2015). For a Wolff rearrangement to occur, α-diazocarbonyl compounds eliminate nitrogen and form a ketene intermediate, which subsequently reacts with nucleophiles such as water, alcohols, or amines to form the corresponding carboxylic acids, esters or amides, respectively. Ketenes can also undergo [2+2] cycloaddition to form compounds with four-membered rings (Cui and Thiel, 2013; Barhoumi et al., 2015).

Liu et al. (2012) conducted research using a dextran-graft-(2-diazo-1,2-naphthoquinone) (Dex-DNQ) amphiphilic copolymer in which the hydrophilic dextran moiety was modified with the hydrophobic DNQ. The DNQ undergoes Wolff rearrangement upon UV irradiation, triggering drug release from Dex-DNQ micelles. Similarly, Sun et al. (2014) designed light-responsive linear-dendritic amphiphiles (PEO-D3DNQ) complexed with DNQ. The DNQ absorption was reduced upon irradiation at 365 nm, suggesting that the Wolff rearrangement had occurred. Upon UV irradiation, the PEO-D3DNQ polymer was disrupted releasing the encapsulated drug *via* conversion of the hydrophobic DNQ

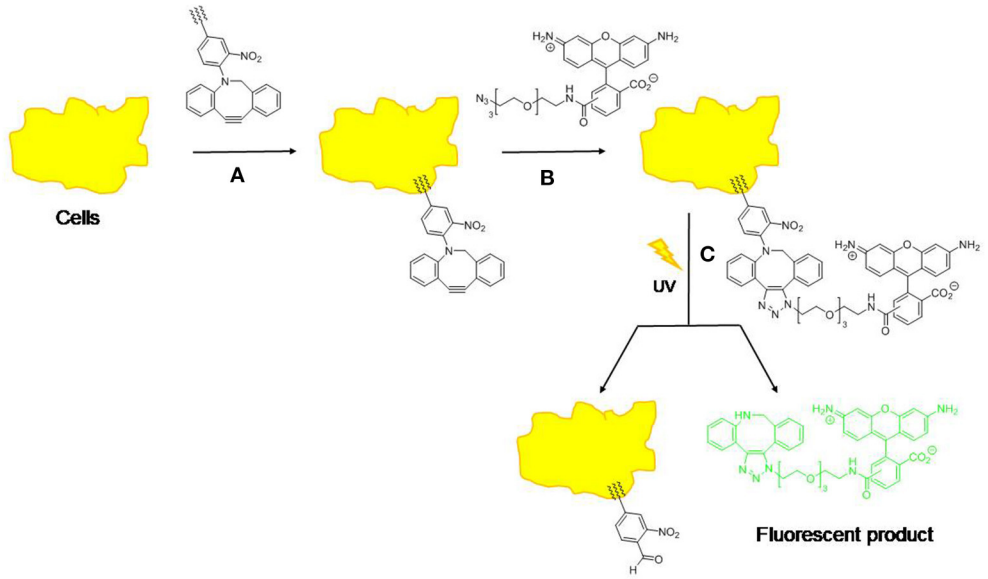

FIGURE 4 | Approach to the analysis of cell membrane delivery and release using copper-free "click" chemistry and a photo-cleavage. (1) Cells are treated with lipid-tethered compound; (2) Cells are treated with "azide fluor 448" to give 'clicked' compound; (3) Cells are treated with UV light to effect photo-cleavage and release fluorophore (λ_{em} = 501 nm, λ_{ex} = 525 nm).

into hydrophilic indene-3-carboxylic acid. Recently, Li et al. (2018) combined UV/NIR light and pH to effect controlled release using amphiphilic polymers of poly(ethyleneglycol)-block-poly(dimethylaminoethyl methacrylate) modified with DNQ (PEG-PDMAEMA-DNQ). Upon irradiation with UVA (365 nm), DNQ was converted into indene-3-carboxylic acid to release coumarin from micelles (Chesterman et al., 2018). This study reveals that the combination of UV light and pH-responsiveness can be used to trigger drug release.

APPLICATION OF UVA-TRIGGERED DRUG RELEASE

UV light is able to stimulate drug release through mechanisms such as photo-isomerization, photo-cleavage, photo-crosslinking, and photo-induced rearrangement. This typically triggers a conformational change in the DDS, releasing the drug (Barhoumi et al., 2015). Compared to other light-triggers, short-wavelength UV light possesses higher energy which is able to break down molecular structures such as covalent bonds or promotes isomerization between different conformations, and achieves a much better response (Yang et al., 2017). Herein, the application of UVA drug release as a strategy for photo-therapy, photo-protection, and caged iron chelators is discussed for use in smart sunscreens and other DDS.

Photo-Therapy

Considering the utility of UVA-triggered drug release, many studies are focusing on combining light-triggered release to enhance the advantages of photo-therapy especially in the use of photodynamic therapy (PDT) or photo-thermal therapy (PTT) (Cao et al., 2018). Since UCNPs have been established to exploit UV, many studies employ the combination of UCNPs with photo-therapy (Qiu et al., 2018). UCNPs provide the strategy of up-conversion to utilize the low toxicity and deep penetration of NIR (Silva et al., 2019) to overcome the limitations of photo-toxicity and low depth tissue penetration (around 10 mm) (Mura et al., 2013) by UV light. The two or multiple photons with low energy from NIR light are converted into high energy of one emitted photon in UV light (Zhong et al., 2014; Jafari and Rezvanpour, 2019). Thus, the approach appears to overcome the limitations of using UV in photo-therapy and photo-drug release (Marturano et al., 2019). The application of UCNPs also offers the possibility of using NIR irradiation energy to elicit photo-chemistry which usually requires UV or visible light. Hence some UCNPs contain Yb^{3+} and Tm^{3+} as a converter to emit UV light upon NIR excitation at 980 nm to improve their ability to release drug (Wang et al., 2013). Since NIR light provides deep tissue penetration, the conversion of NIR to UV light allows more effective and efficient drug release from UCNPs, whilst minimizing tissue damage and cell death (Lee and Park, 2018) by reducing light scattering within the biological sample (Raza et al., 2019).

Hou et al. (2015) revealed that the combination of UCNPs@TiO_2-based NIR light-mediated PDT triggers cancer cell death through the mitochondria-apoptosis pathway. As reported, their UCNPs had a TiO_2 shell with a NaYF4:Yb^{3+}core (see **Figure 5**). The use of Tm^{3+}@NaGdF4:Yb^{3+} enhanced the up-conversion of NIR into UV upon irradiation of TiO_2 (photosensitizer) to form extracellular and intracellular ROS which in turn induced tumor inhibition. Similarly, Hou et al. (2017) introduced UCNPs@mSiO_2-(azo+RB) (azobenzene +

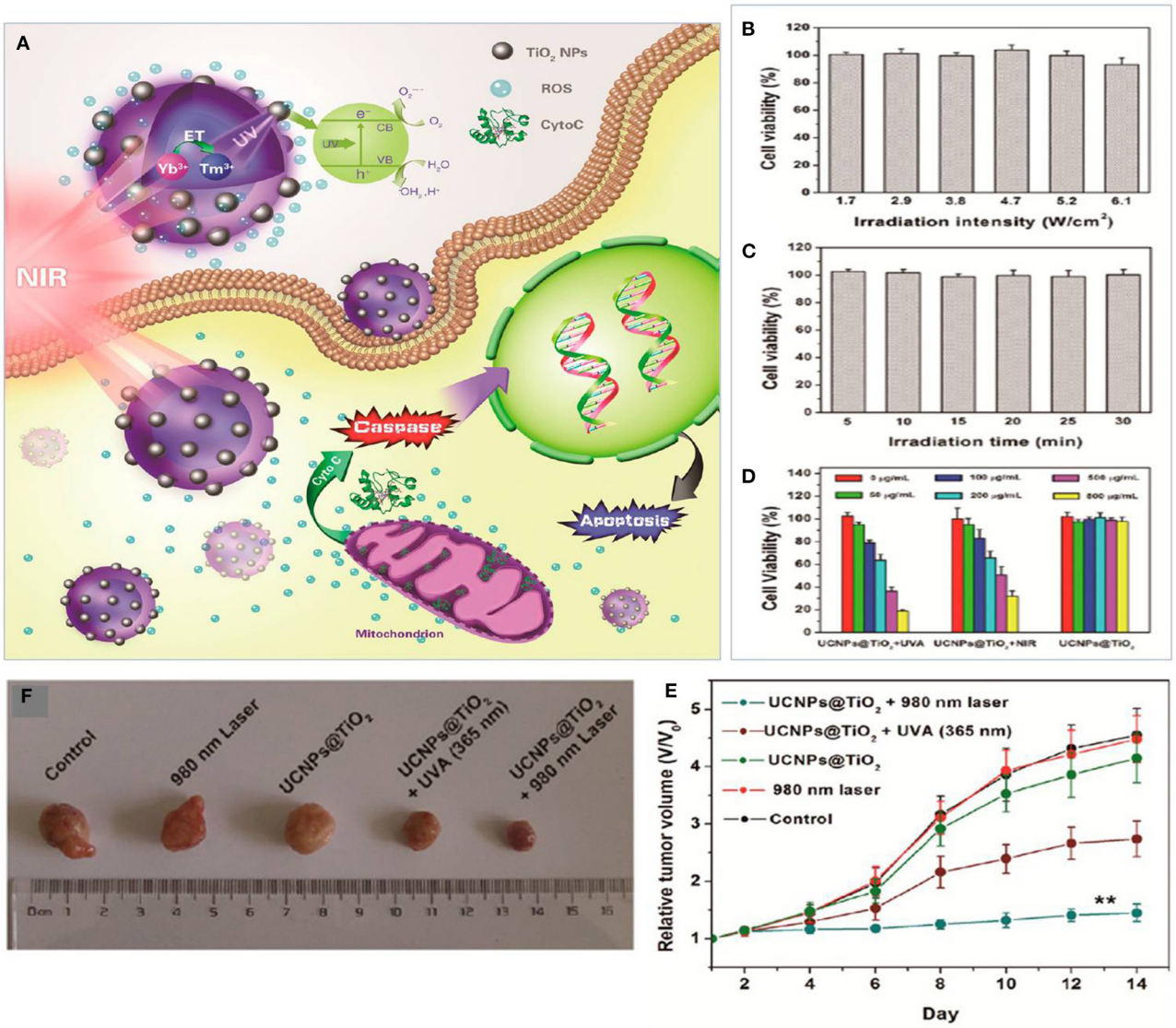

FIGURE 5 | (A) Plot for the potential molecular mechanism of inducing apoptosis with UCNPs@TiO2-based NIR light-mediated PDT treatment. **(B)** Cell viability after 980 nm laser irradiation for different intensities for 30 min (5 min break after 10 min of irradiation). **(C)** After UV light irradiation at 365 nm for different irradiation times. **(D)** *In vitro* viability of HeLa cells treated with UCNPs@TiO2 NCs. **(E)** *In vitro* tumor volume changes of tumor-bearing mice in different groups after various treatments. **(F)** Digital photograph of excised tumors from representative mice after various treatments. Data for **(B–E)** are means ± SD, n = 3. Adapted with permission from Hou et al. (2015). Copyright 2015, American Chemical Society.

Rose Bengal) nano-impellers which utilized the UCNP core to release doxorubicin (DOX) and generate ROS in a combination of chemotherapy and PDT. Based on their study, NIR light at 980 nm was used to produce UV light within the UCNPs core-shell, which activated azobenzene with consequent release of doxorubicin and activation of Rose Bengal as a photosensitizer for the generation of cytotoxic ROS to maximize the treatment.

Recently, Bi et al. (2018) investigated photo-therapy treatment by combining PDT and PTT utilizing UCNPs composed of graphene oxide and $ZnFe_2O_4$. They used Tm^{3+} at the core of the UCNPs to convert NIR into UV emission, which activated graphene oxide and $ZnFe_2O_4$to achieve PTT. Moreover, this strategy triggered $ZnFe_2O_4$ to generate ROS and other toxic radicals by reaction with H_2O_2 in the tumor microenvironment. This strategy was able to overcome one of the limitations of drug release using UV light, since these UCNPs had reduced cytotoxicity to normal cells and highly cytotoxic to cancer cells.

Huang et al. (2017) focused on the utilization of nanoscale ZnO because of its potential as a smart drug delivery system due to its biocompatibility, ease of modification, and good properties and structures as well as low cost. A previous study on ZnO and benzophenone-3 (Huang et al., 2013) demonstrated the cyclic hydrophobic to hydrophilic switching and *vice versa* under UV and dark exposure. Building on this, Huang et al.

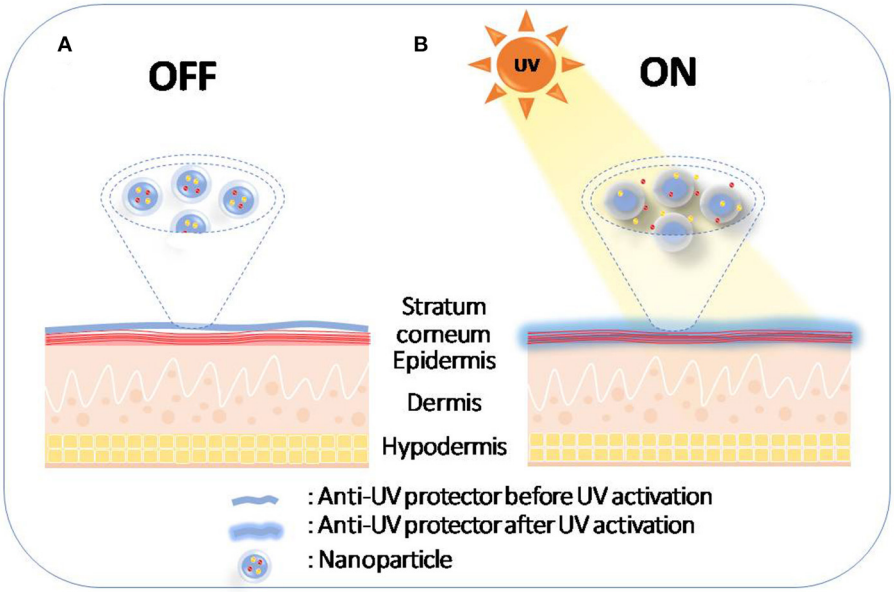

FIGURE 6 | Schematic diagram of photo-protection by UVA-induced drug release on the skin. **(A)** Nanoparticles remain on stratum corneum before sun exposure; **(B)** Nanoparticles release the drug after sun exposure.

(2015) developed nanocomposites of Fe_3O_4@ZnO core-shell to load docetaxel and encapsulate the epidermal growth factor (EGF) on the polymer. Upon stimulation with UV irradiation, the chemical structure of ZnO was rearranged to release docetaxel and EGF, resulting in obstruction of the growth of cancer cells (Huang et al., 2015). In further research, they designed a photo-responsive multifunctional drug delivery by combining Fe_3O_4@ZnO core-shell and amphipathic polymer of P(BA-co-HBA)-loaded docetaxel which was able to boost chemotherapy effects by UV stimulation to trigger the ZnO hydrophilic / hydrophobic transition to release the drug and to prompt the amphipathic polymer to adsorb and encapsulate EGF (Huang et al., 2016). Later, Kong et al. (2017) used the same multifunctional DDS to decrease the growth of skin cancer by giving a low dose of UV to release docetaxel and absorb EGF. A study from Huang et al. (2016) also demonstrated that UV-mediated drug release would be able to control docetaxol release with simultaneous EGF adsorption resulting in reduced proliferation and metastasis of cancer cells.

Photo-Protection

UV radiation contributes to 65% of melanoma cases and almost 90% of non-melanoma skin cancers and has gained much attention as it triggers other hazardous effects including acute and chronic skin damage, photo-aging, and immune system effects (Amaro-Ortiz et al., 2014; Kim and He, 2014; Gilbertz et al., 2018). It is becoming essential to protect body parts from exposure to UV radiation as a preventive strategy using sunscreens for photo-protection (Yeager and Lim, 2019), which contain UV filters to reflect, absorb, and disperse the energy of solar illumination (Geoffrey et al., 2019). A new sophisticated technology allows the utilization of the drug delivery systems in skin protection. Since human skin is an exposed surface, external stimuli such as heat, visible light or UV light can be used to control drug release on the skin for protection and to treat inflammation (Vogt et al., 2016). This idea offers the possibility of activating drug release upon UV exposure to protect the skin when it is most needed (Geoffrey et al., 2019) (**Figure 6**).

Previously, Huang et al. (2015) studied a smart drug release system for skin protection by using ZnO nanoparticles as a UV filter loaded with benzophenone-3. The system was tested on keratinocytes and skin fibroblasts to investigate drug release upon UV irradiation. The ZnO NPs were able to interconvert between hydrophobic and hydrophilic states upon light and dark exposure, respectively. Almost all benzophenone-3 was released after 2 h of UV exposure ($\sim$100 kJ/m^2) with light switch on and off each 30 min, and low cytotoxicity for the nanoparticles was observed for human keratinocytes and fibroblasts. Their findings demonstrated the UV-triggered drug release as a skin protection strategy which initiated further studies. In a follow-up study (Huang et al., 2020), the same group investigated acetyl-11-keto-β-boswellic acid (AKBA)-loaded ZnO nanoparticles for UVA (160 kJ/m^2) protection. AKBA possesses outstanding anti-inflammatory and antioxidant effects, and the nanoparticles had low cytotoxicity to HaCaT cells.

Similarly, Aparici-Espert et al. (2018) introduced photo-caged sunscreens for UV responsive release by combining the nonsteroidal anti-inflammatory drug diclofenac with avobenzone as a solar filter utilizing a phenacylavobenzone pro-drug. Photolysis of the dyad in a hydrogen-donor solvent resulted in simultaneous release of diclofenac and avobenzone. Another study from Suh et al. (2019) formulated a smart

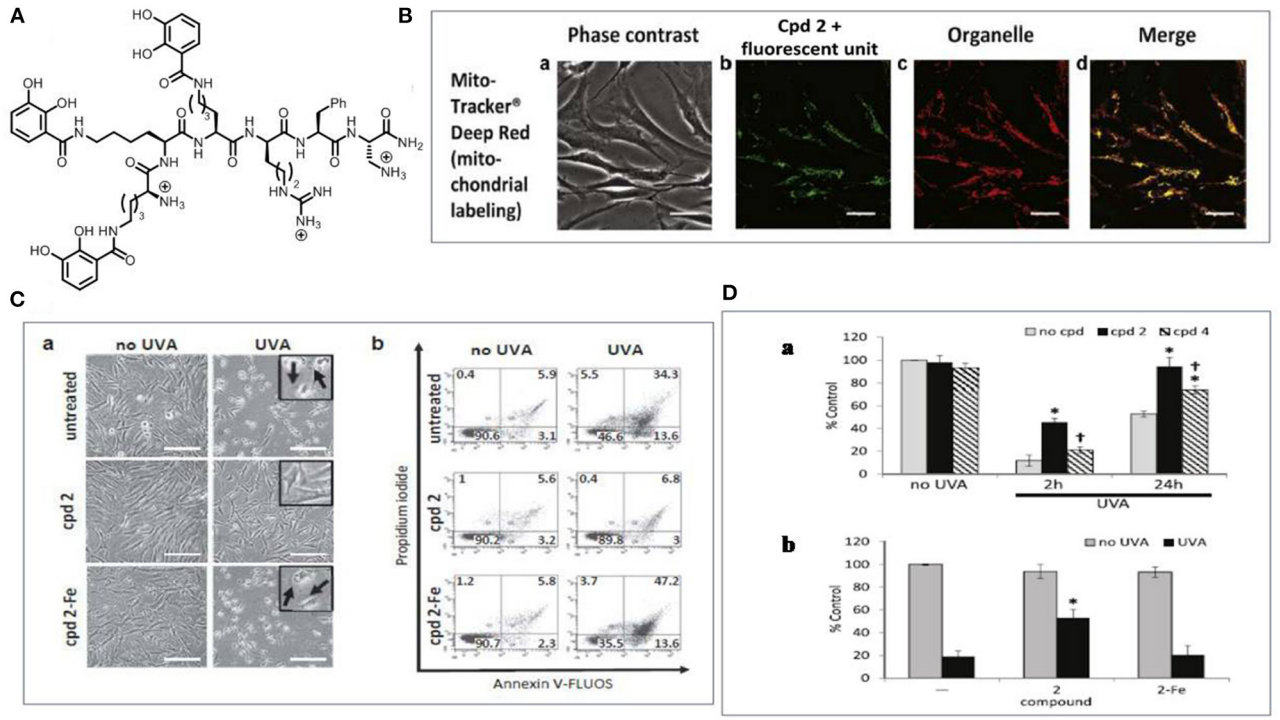

FIGURE 7 | The use of mitochondrial targeted tricatechol iron chelator for skin photoprotection. **(A)** The structure of the chelator (compound 2). **(B)** Microscopy analysis of the subcellular localization of compound 2 tagged with a fluorescent unit (a) Phase contrast; (b) Compound 2 with the fluorescent unit; (c) Mitochondria stained with mito tracker (d) Merged data. Scale bar = 10 μm; **(C)** Compound 2 protects FEK4 cells from UVA-induced cell death (a) Bright-field images were captured 24 h after treatment. Swelling (arrow in insert) is indicative of cell death by necrosis and is visible after UVA treatment alone or in the combination of compound 2-Fe. Scale bar = 50 μm; (b) Cells analyzed by flow cytometry. Live cells are defined as Annexin V-negative/PI-negative (lower left-hand quadrant). **(D)** Compound 2 significantly reduces UVA-induced damage to mitochondria membrane (a) Bar chart of the results of TMRM staining experiment; (b) FEK4 cells were pre-treated with either compound 2 alone or as a complex with iron. Data are means ± SD, n = 3-5. TMRM, tetramethylrhodamine methyl ester; UVA, ultraviolet A. Adapted with permission under the terms of CC BY 4.0 license (Reelfs et al., 2016). Copyright 2016, The Authors. Published by Elsevier.

sunscreen by encapsulating padimate O UVB filters within biodegradable nanoparticles BNPs consisted of poly($_{D,L}$-lactic acid)-hyperbranched polyglycerol containing avobenzone and octocrylene. This study found that the incorporation of a UV filter within nanoparticles offered filter stabilization and optimized drug release upon UV irradiation. The result also showed water-resistance of formulated sunscreen to be around 85% particle retention after 3 h. The results indicated biodegradable nanoparticles were able to protect and release the drug upon UV illumination to protect the skin.

Caged Iron Chelators

Irradiation of human skin cells with physiological doses (up to 250 kJ/m^2) of UVA also result in release of labile iron from stores with consequent generation of ROS that contribute to skin photo-aging and photo-carcinogenesis (Bissett et al., 1991; Pourzand et al., 1999). The increased levels of ROS foster oxidative stress in subcellular compartments notably lysosomes, mitochondria, plasma membranes, and even nuclear membranes (Reelfs et al., 2004; Aroun et al., 2012). In skin fibroblasts, UVA-induced damage to mitochondrial membranes leads to immediate ATP depletion which in conjunction with damage to plasma membranes promote necrotic cell death (Zhong et al., 2004; Aroun et al., 2012). It is necessary to protect the skin cells from iron overload by regulating and restricting the absorption of iron as well as regulating iron-binding to proteins such as ferritin, transferrin, and hemoglobin (Powers and Buchanan, 2019; Katsarou and Pantopoulos, 2020). However, upon UVA radiation, the iron homeostasis is severely compromised in skin cells due to proteolytic degradation of the iron storage protein ferritin which contributes to accumulation of potentially damaging intracellular labile iron observed immediately after UVA irradiation. Therefore, iron chelators can be used to remove the UVA-mediated excess labile iron within the cell and consequently suppress the production of higher amounts of ROS via Fenton chemistry (Jomova and Valko, 2011; Cabantchik, 2014; Abbate and Hider, 2017; Koppenol and Hider, 2019). However, iron chelators need to be used carefully in order to remove excess iron without disrupting the essential iron homeostasis within the cells (Reelfs et al., 2010; Powers and Buchanan, 2019; Zhou et al., 2019).

To avert excessive depletion of iron by chelators, it is imperative to design a smart chelating agent as a prodrug which is released only upon UV irradiation of the skin

(Reelfs et al., 2010). As mentioned previously, our group (Yiakouvaki et al., 2006) introduced a series of light-activated iron chelators salicylaldehyde isonicotinoyl hydrazone (SIH) and pyridoxal isonicotinoylhydrazone (PIH) which were caged using the 1-(2-nitrophenyl)ethyl group. Under normal/dark conditions (without UVA exposure), the caged iron chelator was stable and did not deplete the labile iron pool within the cell. In contrast, upon exposure to UVA radiation the chelator was released, which protected the skin cells and prevented the UVA-induced necrosis. These results support the application of UVA-induced drug release as a future skin photoprotection strategy.

Pelle et al. (2011) extended the previous study by examining (2-nitrophenyl)ethyl pyridoxal isonicotinoyl hydrazone (2-PNE-PIH) as an iron chelator pro-drug that was activated upon UVA irradiation whilst minimizing the effect on essential iron metabolism. The prodrug was activated by UVA irradiation to release the active chelator PIH which sequestered the excess labile iron which was concomitantly produced by UVA in keratinocytes. This provoked a dose- and context-dependent protection against UVA damage in keratinocytes. The light-activated iron chelators have therefore a great potential as powerful sunscreen ingredients with superior effectiveness than antioxidants. The antioxidants only neutralize one cycle of ROS formation without affecting the harmful labile iron that will continue to catalyze the formation of harmful ROS (Wang et al., 2014). Franks et al. (2015) also synthesized a multifunctional caged compound PC-HAPI [2-((E)-1-(2-isonicotinoyl hydrazono) ethyl) phenyl *trans*-3-(2,4-dihydroxyphenyl) acrylate] with a caging moiety based on trans-(*o*-hydroxy) cinnamate ester which was photocleavable upon UVA exposure to release a coumarin-based natural antioxidant umbelliferone, and an aroylhydrazone metal chelator, HAPI [N′-[1-(2-hydroxyphenyl)ethyliden] isonicotinoylhydrazide]. The latter light-activatable compound was used to tackle the dual damaging effects of UVA component of sunlight by neutralizing the ROS and harmful labile iron released by the radiation in the skin cells (Pourzand and Tyrrell, 1999; Pourzand et al., 1999). Since unprotected iron-chelators represent a risk of toxicity due to non-targeted iron depletion, multifunctional pro-chelators that have little or no affinity for iron until activated by external stimuli (e.g., ROS) have gained ground as cardio-protective and neuroprotective agents (Jansová and Šimunek, 2019; Wu et al., 2020).

Another challenge in using iron chelators for skin photoprotection is to target the chelating agent to the heart of oxidative damage. The mitochondrial-targeted iron chelators are reported (Reelfs et al., 2016) to provide unprecedented protection against UVA-induced damage in skin fibroblasts. The design of mitochondria-targeted chelators was based on the observation that mitochondria were a significant source of ROS whilst maintaining iron homeostasis (Levi and Rovida, 2009; Aroun et al., 2012). We designed a mitochondria-targeted hexadentate iron chelator based on the tricatechol motif (compound 2) (**Figure 7**). Upon UVA irradiation, the mitochondria-targeted iron chelator protected the skin cells from damage by reducing the organelles' labile iron levels and consequent ROS levels. The above studies support the development of UVA-induced caged iron chelators to protect the skin from the detrimental effect of sunlight as a promising strategy for skin protection.

CONCLUSIONS AND PERSPECTIVES

The introduction of light-controlled drug delivery systems has greatly improved the targeted delivery since the use of an external stimulus such as light gives many benefits. The intrinsic properties of light mean that spatially and temporally controlled release in a wide range of therapeutic applications can be easily achieved. Hence, it provides the possibility of controlling the power of the stimulus and the ability to focus it onto a specific area and penetrate into body tissues by choosing an appropriate wavelength of light (Barhoumi and Kohane, 2015; Bagheri et al., 2016; Liu et al., 2016; Shim et al., 2017).

UVA in the range of 320–400 nm has been used in some treatments of skin conditions and also in DDS. Despite the photo-toxicity of UVA resulting in damage to the cell, UVA shows significant potential as a stimulus for drug release. The higher energy of the UVA light means that it is possible to breakdown covalent bonds within molecular structures and hence some materials are highly responsive to UV light (Breuckmann et al., 2004; Svobodova et al., 2006; Jin et al., 2011). In order to achieve optimum usage of UVA for photo-triggered drug delivery, mechanisms such as photo-isomerization, photo-cleavage, photo-crosslinking, and photo-induced rearrangement can be utilized. These mechanisms induce changes in covalent bonding of the material or other conformational changes.

More recently, some applications in clinical photo-therapy such as PDT and PTT have been established to capitalize on the benefits of the controlled-release drugs by UV. Some systems also utilize up-conversion to improve therapeutic outcomes by converting NIR to UV light since NIR light can penetrate deeply into tissues and is much less harmful than UV light (Qiu et al., 2018; Jafari and Rezvanpour, 2019; Marturano et al., 2019). It is also possible to utilize UVA-induced drug release to release a photo-protective agent upon exposure to sunlight (Vogt et al., 2016; Geoffrey et al., 2019; Yeager and Lim, 2019). Since UVA-induced drug release is only activated upon UV irradiation, the use of these pro-drugs within sunscreens offer a promising approach for skin protection during the exposure to daily sunlight. The discovery of caged iron chelators is a more recent development in the area of UVA-activated drug release in smart sunscreens, minimizing damage by preventing ROS formation whilst also minimizing non-specific iron depletion (Basu-Modak et al., 2006; Yiakouvaki et al., 2006; Levi and Rovida, 2009; Reelfs et al., 2016).

Taking all of these aspects into consideration, UVA-induced drug release shows great promise as a means of controlling drug release with many potential applications. These include the use of UV radiation for controlled drug release and the use of smart sunscreens to protect the skin cells against sunlight-mediated UV damage.

AUTHOR CONTRIBUTIONS

VK, WW, CP, and JZ contributed on conceptualized of the study. VK and MN wrote the manuscript, ML, HL, MDL, and JZ assisted in writing of the manuscript. WW, ML, HL, MDL, CP, and JZ contributed to the revision of the manuscript for important intellectual content. All authors contributed to the writing of this manuscript and approved the final version to be published and agree to be accountable for all aspects of this work.

FUNDING

This work is financially supported by The National Science Foundation of China (No. 82003384, 81271776, and 81573073), The Fundamental Research Funds for the Central Universities (Project No. 2020CDJYGSG001 and 2020CDJYGSG003), Chongqing Talents Program (CQYC2020058022), Scientific Research Foundation from Chongqing University (02210011044110), and the 111 Project of Biomechanics and Tissue Repair (B605). This work was also supported by Series of Evidence-Based Study on Hot Spring Wellness, Chongqing Municipal Commission of Culture and Tourism Development (to JZ). Key projects of Chongqing Municipal Science and Technology Commission (cstc2017jcyjbx0044), and a Welcome Trust Showcase Award, UK (Contract No. 067653/Z/02/Z), and a Biotechnology and Biological Sciences Research Council (BBSRC, Grant No. BB/J005223/1), UK.

REFERENCES

Abbate, V., and Hider, R. (2017). Iron in biology. *Metallomics* 9, 1467–1469. doi: 10.1039/C7MT90039B

Agasti, S. S., Chompoosor, A., You, C.-C., Ghosh, P., Kim, C. K., and Rotello, V. M. (2009). Photoregulated release of caged anticancer drugs from gold nanoparticles. *J. Am. Chem. Soc.* 131, 5528–5729. doi: 10.1021/ja900591t

Alam, S., Alves, D. S., Whitehead, S. A., Bayer, A. M., McNitt, C. D., Popik, V. V., et al. (2015). A clickable and photocleavable lipid analogue for cell membrane delivery and release. *Bioconjug. Chem.* 26, 1021–1031. doi: 10.1021/acs.bioconjchem.5b00044

Alvarez-Lorenzo, C., Bromberg, L., and Concheiro, A. (2009). Light-sensitive intelligent drug delivery systems. *Photochem. Photobiol.* 85, 848–860. doi: 10.1111/j.1751-1097.2008.00530.x

Amaro-Ortiz, A., Yan, B., and D'Orazio, J. A. (2014). Ultraviolet radiation, aging and the skin: prevention of damage by topical cAMP manipulation. *Molecules* 19, 6202–6219. doi: 10.3390/molecules19056202

Aparici-Espert, I., Miranda, M. A., and Lhiaubet-Vallet, V. (2018). Sunscreen-based photocages for topical drugs: a photophysical and photochemical study of a diclofenac-avobenzone dyad. *Molecules* 23, 1–11. doi: 10.3390/molecules23030673

Aroun, A., Zhong, J. L., Tyrrell, R. M., and Pourzand, C. (2012). Iron, oxidative stress and the example of solar ultraviolet A radiation. *Photochem. Photobiol. Sci.* 11, 118–134. doi: 10.1039/C1PP05204G

Bagheri, A., Arandiyan, H., Boyer, C., and Lim, M. (2016). Lanthanide-doped upconversion nanoparticles: emerging intelligent light-activated drug delivery systems. *Adv. Sci.* 3, 1–25. doi: 10.1002/advs.201500437

Bahrami, B., Hojjat-Farsangi, M., Mohammadi, H., Anvari, E., Ghalamfarsa, G., Yousefi, M., et al. (2017). Nanoparticles and targeted drug delivery in cancer therapy. *Immunol. Lett.* 190, 64–83. doi: 10.1016/j.imlet.2017.07.015

Bandara, H. D., and Burdette, S. C. (2012). Photoisomerization in different classes of azobenzene. *Chem. Soc. Rev.* 41, 1809–1825. doi: 10.1039/C1CS15179G

Barhoumi, A., and Kohane, D. S. (2015). "Light-controlled nanoparticulate drug delivery systems" in *Applications of Nanoscience in Photomedicine*, eds Hamblin, M. R., and Avci, P (Chandos Publishing), 393–413. doi: 10.1533/9781908818782.393

Barhoumi, A., Liu, Q., and Kohane, D. S. (2015). Ultraviolet light-mediated drug delivery: principles, applications, and challenges. *J. Controlled Release*. 219, 31–42. doi: 10.1016/j.jconrel.2015.07.018

Basu-Modak, S., Ali, D., Gordon, M., Polte, T., Yiakouvaki, A., Pourzand, C., et al. (2006). Suppression of UVA-mediated release of labile iron by epicatechin-a link to lysosomal protection. *Free Radic. Biol. Med.* 41, 1197–1204. doi: 10.1016/j.freeradbiomed.2006.06.008

Beauté, L., McClenaghan, N., and Lecommandoux, S. (2019). Photo-triggered polymer nanomedicines: from molecular mechanisms to therapeutic applications. *Adv. Drug Deliv. Rev.* 138, 148–166. doi: 10.1016/j.addr.2018.12.010

Bhowmik, D., Gopinath, H., Kumar, B. P., Duraivel, S., and Kumar, K. S. (2012). Controlled release drug delivery systems. *Pharma Innov.* 1(10 Pt A):24.

Bi, H., He, F., Dai, Y., Xu, J., Dong, Y., Yang, D., et al. (2018). Quad-model imaging-guided high-efficiency phototherapy based on upconversion nanoparticles and $ZnFe_2O_4$ integrated graphene oxide. *Inorg. Chem.* 57, 9988–9998. doi: 10.1021/acs.inorgchem.8b01159

Bissett, D. L., Chatterjee, R., and Hannon, D. P. (1991). Chronic ultraviolet radiation-induced increase in skin iron and the photoprotective effect of topically applied iron chelators 1. *Photochem. Photobiol.* 54, 215–223. doi: 10.1111/j.1751-1097.1991.tb02009.x

Bourbon, P., Peng, Q., Ferraudi, G., Stauffacher, C., Wiest, O., and Helquist, P. (2013). Development of carbamate-tethered coumarins as phototriggers for caged nicotinamide. *Bioorg. Med. Chem. Lett.* 23, 6321–6324. doi: 10.1016/j.bmcl.2013.09.067

Breitsamer, M., and Winter, G. (2019). Vesicular phospholipid gels as drug delivery systems for small molecular weight drugs, peptides and proteins: State of the art review. *Int. J. Pharm.* 557, 1–8. doi: 10.1016/j.ijpharm.2018.12.030

Brem, R., Guven, M., and Karran, P. (2017). Oxidatively-generated damage to DNA and proteins mediated by photosensitized UVA. *Free Radic. Biol. Med.* 107, 101–109. doi: 10.1016/j.freeradbiomed.2016.10.488

Breuckmann, F., Gambichler, T., Altmeyer, P., and Kreuter, A. (2004). UVA/UVA1 phototherapy and PUVA photochemotherapy in connective tissue diseases and related disorders: a research based review. *BMC Dermatol.* 4:11. doi: 10.1186/1471-5945-4-11

Burke, K. E. (2018). Mechanisms of aging and development - A new understanding of environmental damage to the skin and prevention with topical antioxidants. *Mech. Ageing Dev.* 172, 123–130. doi: 10.1016/j.mad.2017.12.003

Cabane, E., Malinova, V., Menon, S., Palivan, C. G., and Meier, W. (2011). Photoresponsive polymersomes as smart, triggerable nanocarriers. *Soft Matter*. 7, 9167–9176. doi: 10.1039/c1sm05880k

Cabantchik, Z. I. (2014). Labile iron in cells and body fluids: physiology, pathology, and pharmacology. *Front. Pharmacol.* 5:45. doi: 10.3389/fphar.2014.00045

Cao, J., Chen, Z., Chi, J., Sun, Y., and Sun, Y. (2018). Recent progress in synergistic chemotherapy and phototherapy by targeted drug delivery systems for cancer treatment. *Artif. Cells Nanomed. Biotechnol.* 46, 817–830. doi: 10.1080/21691401.2018.1436553

Chesterman, J. P., Hughes, T. C., and Amsden, B. G. (2018). Reversibly photo-crosslinkable aliphatic polycarbonates functionalized with coumarin. *Eur. Polym. J.* 105, 186–193. doi: 10.1016/j.eurpolymj.2018.05.038

Cho, H. J., Chung, M., and Shim, M. S. (2015). Engineered photo-responsive materials for near-infrared-triggered drug delivery. *J. Ind. Eng. Chem.* 31, 15–25. doi: 10.1016/j.jiec.2015.07.016

Choi, S. K., Verma, M., Silpe, J., Moody, R. E., Tang, K., Hanson, J. J., et al. (2012). A photochemical approach for controlled drug release in targeted drug delivery. *Bioorg. Med. Chem.* 20, 1281–1290. doi: 10.1016/j.bmc.2011.12.020

Chung, J. W., Neikirk, C., and Priestley, R. D. (2013). Investigation of coumarin functionality on the formation of polymeric nanoparticles. *J. Colloid Interface Sci.* 396, 16–22. doi: 10.1016/j.jcis.2013.01.038

Cui, G., and Thiel, W. (2013). Photoinduced ultrafast wolff rearrangement: a non-adiabatic dynamics perspective. *Angew. Chem*. 125, 451–454. doi: 10.1002/ange.201207628

Davoodi, P., Lee, L. Y., Xu, Q., Sunil, V., Sun, Y., Soh, S., et al. (2018). Drug delivery systems for programmed and on-demand release. *Adv. Drug Deliv. Rev*. 132, 104–138. doi: 10.1016/j.addr.2018.07.002

Deng, W., Chen, W., Clement, S., Guller, A., Zhao, Z., Engel, A., et al. (2018). Controlled gene and drug release from a liposomal delivery platform triggered by X-ray radiation. *Nat. Commun*. 9, 1–11. doi: 10.1038/s41467-018-05118-3

Derheimer, F. A., Hicks, J. K., Paulsen, M. T., Canman, C. E., and Ljungman, M. (2009). Psoralen-induced DNA interstrand cross-links block transcription and induce p53 in an ataxia-telangiectasia and rad3-related-dependent manner. *Mol. Pharmacol*. 75, 599–607. doi: 10.1124/mol.108.051698

Ding, J., Zhuang, X., Xiao, C., Cheng, Y., Zhao, L., He, C., et al. (2011). Preparation of photo-cross-linked pH-responsive polypeptide nanogels as potential carriers for controlled drug delivery. *J. Mater. Chem*. 21, 11383–11391. doi: 10.1039/c1jm10391a

D'Orazio, J., Jarrett, S., Amaro-Ortiz, A., and Scott, T. (2013). UV radiation and the skin. *Int. J. Mol. Sci*. 14, 12222–12248. doi: 10.3390/ijms140612222

Dunaway, S., Odin, R., Zhou, L., Ji, L., Zhang, Y., and Kadekaro, A. L. (2018). Natural antioxidants: multiple mechanisms to protect skin from solar radiation. *Front. Pharmacol*. 9, 1–14. doi: 10.3389/fphar.2018.00392

Fomina, N., Sankaranarayanan, J., and Almutairi, A. (2012). Photochemical mechanisms of light-triggered release from nanocarriers. *Adv. Drug Deliv. Rev*. 64, 1005–1020. doi: 10.1016/j.addr.2012.02.006

Franks, A. T., Wang, Q., and Franz, K. J. (2015). A multifunctional, light-activated prochelator inhibits UVA-induced oxidative stress. *Bioorg. Med. Chem. Lett*. 25, 4843–4847. doi: 10.1016/j.bmcl.2015.06.048

Galante, M. J., Zucchi, I. A., Oyanguren, P. A., and Sáiz, L. M. (2019). Light-induced healing in azobenzene bridged silsesquioxanes. *Eur. Polym. J*. 117, 382–390. doi: 10.1016/j.eurpolymj.2019.05.025

Gao, A.-H., Li, B., Zhang, P.-Y., and Liu, J. (2014). Photochemical dynamics simulations for trans-cis photoisomerizations of azobenzene and bridged azobenzene. *Comput. Theor. Chem*. 1031, 13–21. doi: 10.1016/j.comptc.2013.12.029

Gao, Z., Yuan, P., Wang, D., Xu, Z., Li, Z., and Shao, X. (2017). Photo-controlled release of fipronil from a coumarin triggered precursor. *Bioorg. Med. Chem. Lett*. 27, 2528–2535. doi: 10.1016/j.bmcl.2017.03.091

Geoffrey, K., Mwangi, A., and Maru, S. (2019). Sunscreen products: rationale for use, formulation development and regulatory considerations. *Saudi Pharm. J*. 27, 1009–1018. doi: 10.1016/j.jsps.2019.08.003

Gilbertz, K.-P., Placzek, M., and Hotz, M. E. (2018). Ultraviolet exposure: health effects. *Encyclopedia of Environmental Health*. 2nd ed (Elsevier). doi: 10.1016/B978-0-12-409548-9.11267-9

Grim, J. C., Marozas, I. A., and Anseth, K. S. (2015). Thiol-ene and photo-cleavage chemistry for controlled presentation of biomolecules in hydrogels. *J. Controlled Release*. 219, 95–106. doi: 10.1016/j.jconrel.2015.08.040

Härtner, S., Kim, H. C., and Hampp, N. (2007). Phototriggered release of photolabile drugs via two-photon absorption-induced cleavage of polymer-bound dicoumarin. *J. Polym. Sci. Part A Polym. Chem*. 45, 2443–2452. doi: 10.1002/pola.22007

Hou, B., Yang, W., Dong, C., Zheng, B., Zhang, Y., Wu, J., et al. (2017). Controlled co-release of doxorubicin and reactive oxygen species for synergistic therapy by NIR remote-triggered nanoimpellers. *Mater. Sci. Eng C*. 74, 94–102. doi: 10.1016/j.msec.2017.02.016

Hou, Z., Zhang, Y., Deng, K., Chen, Y., Li, X., Deng, X., et al. (2015). UV-emitting upconversion-based TiO2 photosensitizing nanoplatform: near-infrared light mediated *in vivo* photodynamic therapy via mitochondria-involved apoptosis pathway. *ACS Nano*. 9, 2584–2599. doi: 10.1021/nn506107c

Hu, X., Chen, F., Li, N., Bai, W., and Bai, R. (2017). One-pot strategy for preparation of photo-and chemo-cleavable polystyrene containing o-nitrobenzyl ester moieties. *Polym. Degrad. Stability*. 142, 55–61. doi: 10.1016/j.polymdegradstab.2017.05.014

Huang, P., Wang, X., Liang, X., Yang, J., Zhang, C., Kong, D., et al. (2019). Nano-, micro-, and macroscale drug delivery systems for cancer immunotherapy. *Acta Biomater*. 85, 1–26. doi: 10.1016/j.actbio.2018.12.028

Huang, X., Lu, J., Yue, D., Fan, Y., Yi, C., Wang, X., et al. (2015). Fe_3O_4@ZnO core-shell nanocomposites for efficient and repetitive removal of low density lipoprotein in plasma and on blood vessel. *Nanotechnology*. 26:125101. doi: 10.1088/0957-4484/26/12/125101

Huang, X., Nisar, M. F., Wang, M., Wang, W., Chen, L., Lin, M., et al. (2020). UV-responsive AKBA@ ZnO nanoparticles potential for polymorphous light eruption protection and therapy. *Mater. Sci. Eng C*. 107:110254. doi: 10.1016/j.msec.2019.110254

Huang, X., Wang, X., Wang, S., Yang, J., Zhong, L., and Pan, J. (2013). UV and dark-triggered repetitive release and encapsulation of benzophenone-3 from biocompatible ZnO nanoparticles potential for skin protection. *Nanoscale* 5, 5596–5601. doi: 10.1039/c3nr00090g

Huang, X., Zheng, X., Xu, Z., and Yi, C. (2017). Zno-based nanocarriers for drug delivery application: from passive to smart strategies. *Int. J. Pharm*. 534, 190–194. doi: 10.1016/j.ijpharm.2017.10.008

Huang, X., Zheng, X., Yi, C., and Yin, S. P. (2016). (BA-co-HBA) coated Fe_3O_4@ZnO nanoparticles as photo-responsive multifunctional drug delivery systems for safer cancer therapy. *Nano* 11:1650057. doi: 10.1142/S1793292016500570

Huang, Y., Dong, R., Zhu, X., and Yan, D. (2014). Photo-responsive polymeric micelles. *Soft Matter*. 10, 6121–6138. doi: 10.1039/C4SM00871E

Ibbotson, S. H. (2018). A perspective on the use of NB-UVB phototherapy vs. PUVA photochemotherapy. *Front. Med*. 5:184. doi: 10.3389/fmed.2018.00184

Jafari, M., and Rezvanpour, A. (2019). Upconversion nano-particles from synthesis to cancer treatment: a review. *Adv. Powder Technol*. 30, 1731–1753. doi: 10.1016/j.apt.2019.05.027

Jansová, H., and Šimunek, T. (2019). Cardioprotective potential of iron chelators and prochelators. *Curr. Med. Chem*. 26, 288–301. doi: 10.2174/0929867324666170920155439

Jaszewska, E., Soin, M., Filipek, A., and Naruszewicz, M. (2013). UVA-induced ROS generation inhibition by *Oenothera paradoxa* defatted seeds extract and subsequent cell death in human dermal fibroblasts. *J. Photochem. Photobiol. B Biol*. 126, 42–46. doi: 10.1016/j.jphotobiol.2013.07.001

Jayakumar, M. K. G., Idris, N. M., and Zhang, Y. (2012). Remote activation of biomolecules in deep tissues using near-infrared-to-UV upconversion nanotransducers. *Proc. Natl. Acad. Sci. U. S. A*. 109, 8483–8488. doi: 10.1073/pnas.1114551109

Jiang, J., Tong, X., and Zhao, Y. (2005). A new design for light-breakable polymer micelles. *J. Am. Chem. Soc*. 127, 8290–8291. doi: 10.1021/ja0521019

Jiang, M., Paul, N., Bieniek, N., Buckup, T., Hampp, N., and Motzkus, M. (2017). Photocleavage of coumarin dimers studied by femtosecond UV transient absorption spectroscopy. *Phys. Chem. Chem. Phys*. 19, 4597–4606. doi: 10.1039/C6CP08076F

Jin, Q., Mitschang, F., and Agarwal, S. (2011). Biocompatible drug delivery system for photo-triggered controlled release of 5-fluorouracil. *Biomacromolecules* 12, 3684–3691. doi: 10.1021/bm2009125

Jomova, K., and Valko, M. (2011). Importance of iron chelation in free radical-induced oxidative stress and human disease. *Curr. Pharm. Des*. 17, 3460–3473. doi: 10.2174/138161211798072463

Kamaly, N., Yameen, B., Wu, J., and Farokhzad, O. C. (2016). Degradable controlled-release polymers and polymeric nanoparticles: mechanisms of controlling drug release. *Chem. Rev*. 116, 2602–2663. doi: 10.1021/acs.chemrev.5b00346

Karimi, M., Sahandi Zangabad, P., Baghaee-Ravari, S., Ghazadeh, M., Mirshekari, H., and Hamblin, M. R. (2017). Smart nanostructures for cargo delivery: uncaging and activating by light. *J. Am. Chem. Soc*. 139, 4584–4610. doi: 10.1021/jacs.6b08313

Karran, P., and Brem, R. (2016). Protein oxidation, UVA and human DNA repair. *DNA Repair*. 44, 178–185. doi: 10.1016/j.dnarep.2016.05.024

Katsarou, A., and Pantopoulos, K. (2020). Basics and principles of cellular and systemic iron homeostasis. *Mol. Aspects Med*. 75:100866. doi: 10.1016/j.mam.2020.100866

Kauscher, U., Holme, M. N., Björnmalm, M., and Stevens, M. M. (2019). Physical stimuli-responsive vesicles in drug delivery: Beyond liposomes and polymersomes. *Adv. Drug Deliv. Rev*. 138, 259–275. doi: 10.1016/j.addr.2018.10.012

Kim, I., and He, Y.-Y. (2014). Ultraviolet radiation-induced non-melanoma skin cancer: regulation of DNA damage repair and inflammation. *Genes Dis*. 1, 188–198. doi: 10.1016/j.gendis.2014.08.005

Kim, M. S., and Diamond, S. L. (2006). Photocleavage of o-nitrobenzyl ether derivatives for rapid biomedical release applications. *Bioorg. Med. Chem. Lett*. 16, 4007–4010. doi: 10.1016/j.bmcl.2006.05.013

Kitazawa, M., Iwasaki, K., and Sakamoto, K. (2006). Iron chelators may help prevent photoaging. *J. Cosmet. Dermatol*. 5, 210–217. doi: 10.1111/j.1473-2165.2006.00218.x

Kong, F., Huang, X., Yue, D., and Pan, J. (2017). A biocompatible and magnetic nanocarrier with a safe UV-initiated docetaxel release and cancer secretion removal properties increases therapeutic potential for skin cancer. *Mater. Sci. Eng. C*. 76, 579–585. doi: 10.1016/j.msec.2017.03.078

Koppenol, W. H., and Hider, R. (2019). Iron and redox cycling. Do's and don'ts. *Free Radic. Biol. Med*. 133, 3–10. doi: 10.1016/j.freeradbiomed.2018.09.022

Lajunen, T., Nurmi, R., Kontturi, L., Viitala, L., Yliperttula, M., Murtomäki, L., et al. (2016). Light activated liposomes: functionality and prospects in ocular drug delivery. *J. Controlled Release* 244, 157–166. doi: 10.1016/j.jconrel.2016.08.024

Lan, C.-C. E., Hung, Y.-T., Fang, A.-H., and Ching-Shuang, W. (2019). Effects of irradiance on UVA-induced skin aging. *J. Dermatol. Sci*. 94, 220–228. doi: 10.1016/j.jdermsci.2019.03.005

Lee, C.-H., Wu, S.-B., Hong, C.-H., Yu, H.-S., and Wei, Y.-H. (2013). Molecular mechanisms of UV-induced apoptosis and its effects on skin residential cells: the implication in UV-based phototherapy. *Int. J. Mol. Sci*. 14, 6414–6435. doi: 10.3390/ijms14036414

Lee, G., and Park, Y. I. (2018). Lanthanide-doped upconversion nanocarriers for drug and gene delivery. *Nanomaterials* 8:511. doi: 10.3390/nano8070511

Leung, S. J., and Romanowski, M. (2012). Light-activated content release from liposomes. *Theranostics* 2:1020. doi: 10.7150/thno.4847

Levi, S., and Rovida, E. (2009). The role of iron in mitochondrial function. *Biochim. Biophys. Acta* 1790, 629–636. doi: 10.1016/j.bbagen.2008.09.008

Li, H., Guo, K., Wu, C., Shu, L., Guo, S., Hou, J., et al. (2015). Controlled and targeted drug delivery by a UV-responsive liposome for overcoming chemo-resistance in non-hodgkin lymphoma. *Chem. Biol. Drug Des*. 86, 783–794. doi: 10.1111/cbdd.12551

Li, L., Pan, S., Ou, E., Hu, K., Yin, X., Li, Y., et al. (2016). Morphological patterns of controlled particle dispersion by photoisomerization of spiropyrans. *Mater. Lett*. 180, 291–294. doi: 10.1016/j.matlet.2016.05.182

Li, Q., Cao, Z., and Wang, G. (2018). Diazonaphthoquinone-based amphiphilic polymer assemblies for NIR/UV light-and pH-responsive controlled release. *Polym. Chem*. 9, 463–471. doi: 10.1039/C7PY01822C

Linsley, C. S., and Wu, B. M. (2017). Recent advances in light-responsive on demand drug-delivery systems. *Ther. Deliv*. 8, 89–107. doi: 10.4155/tde-2016-0060

Liu, D., Yang, F., Xiong, F., and Gu, N. (2016). The smart drug delivery system and its clinical potential. *Theranostics* 6:1306. doi: 10.7150/thno.14858

Liu, G., Liu, W., and Dong, C.-M. (2013). UV-and NIR-responsive polymeric nanomedicines for on-demand drug delivery. *Polym. Chem*. 4, 3431–3443. doi: 10.1039/c3py21121e

Liu, G.-Y., Chen, C.-J., Li, D.-D., Wang, S.-S., and Ji, J. (2012). Near-infrared light-sensitive micelles for enhanced intracellular drug delivery. *J. Mater. Chem*. 22, 16865–16871. doi: 10.1039/c2jm00045h

Liu, J., Bu, W., Pan, L., and Shi, J. (2013). NIR-triggered anticancer drug delivery by upconverting nanoparticles with integrated azobenzene-modified mesoporous silica. *Angew. Chem*. 125, 4471–4475. doi: 10.1002/ange.201300183

Liu, Q., Wang, H., Li, G., Liu, M., Ding, J., Huang, X., et al. (2019). A photocleavable low molecular weight hydrogel for light-triggered drug delivery. *Chin. Chem. Lett*. 30, 485–488. doi: 10.1016/j.cclet.2018.06.009

Liu, Y., and An, X. (2019). Preparation, microstructure and function of liposome with light responsive switch. *Colloids Surf. B Biointerfaces* 178, 238–244. doi: 10.1016/j.colsurfb.2018.10.068

Marionnet, C., Grether-Beck, S., Seité S., Marini, A., Jaenicke, T., Lejeune, F., et al. (2011). A broad-spectrum sunscreen prevents UVA radiation-induced gene expression in reconstructed skin in vitro and in human skin *in vivo*. *Exp. Dermatol*. 20, 477–482. doi: 10.1111/j.1600-0625.2011.01265.x

Marturano, V., Kozlowska, J., Bajek, A., Giamberini, M., Ambrogi, V., Cerruti, P., et al. (2019). Photo-triggered capsules based on lanthanide-doped upconverting nanoparticles for medical applications. *Coord. Chem. Rev*. 398:213013. doi: 10.1016/j.ccr.2019.213013

Miranda, D., and Lovell, J. F. (2016). Mechanisms of light-induced liposome permeabilization. *Bioeng. Transl. Med*. 1, 267–276. doi: 10.1002/btm2.10032

Moreno, N. C., Garcia, C. C. M., Munford, V., Rocha, C. R. R., Pelegrini, A. L., Corradi, C., et al. (2019). The key role of UVA-light induced oxidative stress in human xeroderma pigmentosum variant cells. *Free Radic. Biol. Med*. 131, 432–442. doi: 10.1016/j.freeradbiomed.2018.12.012

Mura, S., Nicolas, J., and Couvreur, P. (2013). Stimuli-responsive nanocarriers for drug delivery. *Nat. Mater*. 12, 991–1003. doi: 10.1038/nmat3776

Nazemi, A., and Gillies, E. R. (2014). Dendrimersomes with photodegradable membranes for triggered release of hydrophilic and hydrophobic cargo. *Chem. Commun*. 50, 11122–11125. doi: 10.1039/C4CC05161K

Olejniczak, J., Carling, C.-J., and Almutairi, A. (2015). Photocontrolled release using one-photon absorption of visible or NIR light. *J. Controlled Release*. 219, 18–30. doi: 10.1016/j.jconrel.2015.09.030

Passeron, T., Bouillon, R., Callender, V., Cestari, T., Diepgen, T., Green, A. C., et al. (2019). Sunscreen photoprotection and vitamin D status. *Br. J. Dermatol*. 181, 916–931. doi: 10.1111/bjd.17992

Pelle, E., Jian, J., Declercq, L., Dong, K., Yang, Q., Pourzand, C., et al. (2011). Protection against ultraviolet A-induced oxidative damage in normal human epidermal keratinocytes under post-menopausal conditions by an ultraviolet A-activated caged-iron chelator: a pilot study. *Photodermatol. Photoimmunol. Photomed*. 27, 231–235. doi: 10.1111/j.1600-0781.2011.00604.x

Pouillot, A., Polla, A., and Polla, B. S. (2013). Iron and iron chelators: a review on potential effects on skin aging. *Curr. Aging Sci*. 6, 225–231. doi: 10.2174/18746098112059990037

Pourzand, C., and Tyrrell, R. M. (1999). Apoptosis, the role of oxidative stress and the example of solar UV radiation. *Photochem. Photobiol*. 70, 380–390. doi: 10.1111/j.1751-1097.1999.tb08239.x

Pourzand, C., Watkin, R. D., Brown, J. E., and Tyrrell, R. M. (1999). Ultraviolet A radiation induces immediate release of iron in human primary skin fibroblasts: the role of ferritin. *Proc. Natl. Acad. Sci. U. S. A*. 96, 6751–6756. doi: 10.1073/pnas.96.12.6751

Powers, J. M., and Buchanan, G. R. (2019). Disorders of iron metabolism: new diagnostic and treatment approaches to iron deficiency. *Hematol. Oncol. Clin*. 33, 393–408. doi: 10.1016/j.hoc.2019.01.006

Prasad, S., Coias, J., Chen, H. W., and Jacobe, H. (2020). Utilizing UVA-1 phototherapy. *Dermatol. Clin*. 38, 79–90. doi: 10.1016/j.det.2019.08.011

Puri, A. (2014). Phototriggerable liposomes: current research and future perspectives. *Pharmaceutics*. 6, 1–25. doi: 10.3390/pharmaceutics6010001

Qiu, H., Tan, M., Ohulchanskyy, T. Y., Lovell, J. F., and Chen, G. (2018). Recent progress in upconversion photodynamic therapy. *Nanomaterials* 8:344. doi: 10.3390/nano8050344

Radl, S., Kreimer, M., Griesser, T., Oesterreicher, A., Moser, A., Kern, W., et al. (2015). New strategies towards reversible and mendable epoxy based materials employing [4πs+ 4πs] photocycloaddition and thermal cycloreversion of pendant anthracene groups. *Polymer* 80, 76–87. doi: 10.1016/j.polymer.2015.10.043

Raza, A., Hayat, U., Rasheed, T., Bilal, M., and Iqbal, H. M. (2019). "Smart" materials-based near-infrared light-responsive drug delivery systems for cancer treatment: a review. *J. Mater. Res. Technol*. 8, 1497–1509. doi: 10.1016/j.jmrt.2018.03.007

Reelfs, O., Abbate, V., Hider, R. C., and Pourzand, C. (2016). A powerful mitochondria-targeted iron chelator affords high photoprotection against solar ultraviolet a radiation. *J. Invest. Dermatol*. 136, 1692–1700. doi: 10.1016/j.jid.2016.03.041

Reelfs, O., Tyrrell, R. M., and Pourzand, C. (2004). Ultraviolet A radiation-induced immediate iron release is a key modulator of the activation of NF-κB in human skin fibroblasts. *J. Invest. Dermatol*. 122, 1440–1447. doi: 10.1111/j.0022-202X.2004.22620.x

Reelfs, O. M., Eggleston, I., and Pourzand, C. (2010). Skin protection against UVA-induced iron damage by multiantioxidants and iron chelating drugs/prodrugs. *Curr. Drug Metab*. 11, 242–249. doi: 10.2174/138920010791196265

Rwei, A. Y., Wang, B., Ji, T., and Kohane, D. S. (2018). Predicting the tissue depth for remote triggering of drug delivery systems. *J. Controlled Release* 286, 55–63. doi: 10.1016/j.jconrel.2018.07.033

Seité, S., Fourtanier, A., Moyal, D., and Young, A. R. (2010). Photodamage to human skin by suberythemal exposure to solar ultraviolet radiation can be attenuated by sunscreens: a review. *Br. J. Dermatol*. 163, 903–914. doi: 10.1111/j.1365-2133.2010.10018.x

Senapati, S., Mahanta, A. K., Kumar, S., and Maiti, P. (2018). Controlled drug delivery vehicles for cancer treatment and their performance. *Signal Trans. Target. Therapy* 3, 1–19. doi: 10.1038/s41392-017-0004-3

Shao, J., Lei, Y., Wen, Z., Dou, Y., and Wang, Z. (2008). Nonadiabatic simulation study of photoisomerization of azobenzene: detailed mechanism and load-resisting capacity. *J. Chem. Phys*. 129:164111. doi: 10.1063/1.3000008

Shim, G., Ko, S., Kim, D., Le, Q.-V., Park, G. T., Lee, J., et al. (2017). Light-switchable systems for remotely controlled drug delivery. *J. Controlled Release* 267, 67–79. doi: 10.1016/j.jconrel.2017.09.009

Silva, J. M., Silva, E., and Reis, R. L. (2019). Light-triggered release of photocaged therapeutics-Where are we now? *J. Controlled Release* 298, 154–176. doi: 10.1016/j.jconrel.2019.02.006

Soares, A. M., Hungerford, G., Costa, S. P., and Gonçalves, M. S. T. (2017). Photoactivatable prodrugs of butyric acid based on new coumarin fused oxazole heterocycles. *Dyes Pigm*. 137, 91–100. doi: 10.1016/j.dyepig.2016.10.001

Son, J., Yi, G., Yoo, J., Park, C., Koo, H., and Choi, H. S. (2019). Light-responsive nanomedicine for biophotonic imaging and targeted therapy. *Adv. Drug Deliv. Rev*. 138, 133–147. doi: 10.1016/j.addr.2018.10.002

Sreejivungsa, K., Suchaichit, N., Moosophon, P., and Chompoosor, A. (2016). Light-regulated release of entrapped drugs from photoresponsive gold nanoparticles. *J. Nanomater*. 2016:4964693. doi: 10.1155/2016/4964693

Stranius, K., and Börjesson, K. (2017). Determining the photoisomerization quantum yield of photoswitchable molecules in solution and in the solid state. *Sci. Rep*. 7, 1–9. doi: 10.1038/srep41145

Suh, H. W., Lewis, J., Fong, L., Ramseier, J. Y., Carlson, K., Peng, Z. H., et al. (2019). Biodegradable bioadhesive nanoparticle incorporation of broad-spectrum organic sunscreen agents. *Bioeng. Transl. Med*. 4, 129–140. doi: 10.1002/btm2.10092

Sun, L., Zhu, B., Su, Y., and Dong, C.-M. (2014). Light-responsive linear-dendritic amphiphiles and their nanomedicines for NIR-triggered drug release. *Polym. Chem*. 5, 1605–1613. doi: 10.1039/C3PY00533J

Svobodova, A., Walterova, D., and Vostalova, J. (2006). Ultraviolet light induced alteration to the skin. *Biomed. Pap. Palacky Univ. Olomouc* 150:25. doi: 10.5507/bp.2006.003

Tan, E. M., Amirjalayer, S., Smolarek, S., Vdovin, A., Zerbetto, F., and Buma, W. J. (2015). Fast photodynamics of azobenzene probed by scanning excited-state potential energy surfaces using slow spectroscopy. *Nat. Commun*. 6, 1–7. doi: 10.1038/ncomms6860

Teixeira, R. S., Correa, R. J., Belvino, A., and Nascimento, R. S. (2013). UV Irradiation-induced crosslinking of aqueous solution of poly (ethylene oxide) with benzophenone as initiator. *J. Appl. Polym. Sci*. 130, 2458–2467. doi: 10.1002/app.39381

Teske, N. M., and Jacobe, H. T. (2016). Phototherapy for sclerosing skin conditions. *Clin. Dermatol*. 34, 614–622. doi: 10.1016/j.clindermatol.2016.05.012

Tippisetty, S., Goudi, D., Mohammed, A. W., and Jahan, P. (2013). Repair efficiency and PUVA therapeutic response variation in patients with vitiligo. *Toxicol. In Vitro*. 27, 438–440. doi: 10.1016/j.tiv.2012.08.003

Tong, R., Hemmati, H. D., Langer, R., and Kohane, D. S. (2012). Photoswitchable nanoparticles for triggered tissue penetration and drug delivery. *J. Am. Chem. Soc*. 134, 8848–8855. doi: 10.1021/ja211888a

Tsai-Turton, M. (2014). *PUVA*. doi: 10.1016/B978-0-12-386454-3.00052-X

Tunc, D., Le Coz, C., Alexandre, M., Desbois, P., Lecomte, P., and Carlotti, S. (2014). Reversible cross-linking of aliphatic polyamides bearing thermo- and photoresponsive cinnamoyl moieties. *Macromolecules* 47, 8247–8254. doi: 10.1021/ma502083p

Tylkowski, B., Trojanowska, A., Marturano, V., Nowak, M., Marciniak, L., Giamberini, M., et al. (2017). Power of light-functional complexes based on azobenzene molecules. *Coord. Chem. Rev*. 351, 205–217. doi: 10.1016/j.ccr.2017.05.009

Uda, R. M., Kato, Y., and Takei, M. (2016). Photo-triggered release from liposomes without membrane solubilization, based on binding to poly (vinyl alcohol) carrying a malachite green moiety. *Colloids Surf. B Biointerfaces* 146, 716–721. doi: 10.1016/j.colsurfb.2016.07.018

Vangipuram, R., and Feldman, S. (2016). Ultraviolet phototherapy for cutaneous diseases: a concise review. *Oral Dis*. 22, 253–259. doi: 10.1111/odi.12366

Vogt, A., Wischke, C., Neffe, A. T., Ma, N., Alexiev, U., and Lendlein, A. (2016). Nanocarriers for drug delivery into and through the skin-do existing technologies match clinical challenges? *J. Controlled Release* 242, 3–15. doi: 10.1016/j.jconrel.2016.07.027

Wang, B., Chen, K., Yang, R., Yang, F., and Liu, J. (2014). Stimulus-responsive polymeric micelles for the light-triggered release of drugs. *Carbohydr. Polym*. 103, 510–519. doi: 10.1016/j.carbpol.2013.12.062

Wang, C., Cheng, L., and Liu, Z. (2013). Upconversion nanoparticles for photodynamic therapy and other cancer therapeutics. *Theranostics* 3:317. doi: 10.7150/thno.5284

Wang, T., Jiang, H., Wan, L., Zhao, Q., Jiang, T., Wang, B., et al. (2015). Potential application of functional porous TiO_2 nanoparticles in light-controlled drug release and targeted drug delivery. *Acta Biomater*. 13, 354–363. doi: 10.1016/j.actbio.2014.11.010

Wang, Y., and Kohane, D. S. (2017). External triggering and triggered targeting strategies for drug delivery. *Nat. Rev. Mater*. 2, 1–14. doi: 10.1038/natrevmats.2017.20

Wexler, P., Anderson, B. D., Gad, S. C., Hakkinen, P. B., Kamrin, M., De Peyster, A., et al. (2005). *Encyclopedia of Toxicology*. Cambridge, MA: Academic Press.

Wu, Z., Palanimuthu, D., Braidy, N., Salikin, N. H., Egan, S., Huang, M. L., et al. (2020). Novel multifunctional iron chelators of the aroyl nicotinoyl hydrazone class that markedly enhance cellular NAD+/NADH ratios. *Br. J. Pharmacol*. 177, 1967–1987. doi: 10.1111/bph.14963

Yang, Y., Mu, J., and Xing, B. (2017). Photoactivated drug delivery and bioimaging. *Wiley Interdiscipl. Rev. Nanomed. Nanobiotechnol*. 9:e1408. doi: 10.1002/wnan.1408

Yao, J., Feng, J., and Chen, J. (2016). External-stimuli responsive systems for cancer theranostic. *Asian J. Pharm. Sci*. 11, 585–595. doi: 10.1016/j.ajps.2016.06.001

Yavlovich, A., Singh, A., Tarasov, S., Capala, J., Blumenthal, R., and Puri, A. (2009). Design of liposomes containing photopolymerizable phospholipids for triggered release of contents. *J. Therm. Anal. Calorim*. 98, 97–104. doi: 10.1007/s10973-009-0228-8

Yavlovich, A., Viard, M., Gupta, K., Sine, J., Vu, M., Blumenthal, R., et al. (2013). Low-visibility light-intensity laser-triggered release of entrapped calcein from 1,2-bis (tricosa-10,12-diynoyl)-sn-glycero-3-phosphocholine liposomes is mediated through a type I photoactivation pathway. *Int. J. Nanomed*. 2013, 2575–2587. doi: 10.2147/IJN.S44993

Yeager, D. G., and Lim, H. W. (2019). What's new in photoprotection: a review of new concepts and controversies. *Dermatol. Clin*. 37, 149–157. doi: 10.1016/j.det.2018.11.003

Yiakouvaki, A., Savović J., Al-Qenaei, A., Dowden, J., and Pourzand, C. (2006). Caged-iron chelators a novel approach towards protecting skin cells against UVA-induced necrotic cell death. *J. Invest. Dermatol*. 126, 2287–2295. doi: 10.1038/sj.jid.5700373

Yu, J., Chu, X., and Hou, Y. (2014). Stimuli-responsive cancer therapy based on nanoparticles. *Chem. Commun*. 50, 11614–11630. doi: 10.1039/C4CC03984J

Zhang, L., Zhao, L., Ling, Y., and Tang, H. (2019). Unusual light-tunable thermoresponsive behavior of OEGylated homopolypeptide with azobenzene and thioether spacers. *Eur. Polym. J*. 111, 38–42. doi: 10.1016/j.eurpolymj.2018.12.013

Zhang, P., Wu, B., Huang, S., Cai, F., Wang, G., and Yu, H. (2019). UV-vis-NIR light-induced bending of shape-memory polyurethane composites doped with azobenzene and upconversion nanoparticles. *Polymer* 178:121644. doi: 10.1016/j.polymer.2019.121644

Zhao, W., Zhao, Y., Wang, Q., Liu, T., Sun, J., and Zhang, R. (2019). Remote light-responsive nanocarriers for controlled drug delivery: advances and perspectives. *Small* 15, 1–34. doi: 10.1002/smll.201903060

Zhong, J. L., Yiakouvaki, A., Holley, P., Tyrrell, R. M., and Pourzand, C. (2004). Susceptibility of skin cells to UVA-induced necrotic cell death reflects

the intracellular level of labile iron. *J. Invest. Dermatol*. 123, 771–780. doi: 10.1111/j.0022-202X.2004.23419.x

Zhong, Y., Tian, G., Gu, Z., Yang, Y., Gu, L., Zhao, Y., et al. (2014). Elimination of photon quenching by a transition layer to fabricate a quenching-shield sandwich structure for 800 nm excited upconversion luminescence of Nd 3+-sensitized nanoparticles. *Adv. Mater*. 26, 2831–2837. doi: 10.1002/adma.201304903

Zhou, T., Kong, X.-L., and Hider, R. C. (2019). Synthesis and iron chelating properties of hydroxypyridinone and hydroxypyranone hexadentate ligands. *Dalton Trans*. 48, 3459–3466. doi: 10.1039/C8DT05014G

Conflict of Interest: The authors declare that the research was conducted in the absence of any commercial or financial relationships that could be construed as a potential conflict of interest.

Copyright © 2021 Karisma, Wu, Lei, Liu, Nisar, Lloyd, Pourzand and Zhong. This is an open-access article distributed under the terms of the Creative Commons Attribution License (CC BY). The use, distribution or reproduction in other forums is permitted, provided the original author(s) and the copyright owner(s) are credited and that the original publication in this journal is cited, in accordance with accepted academic practice. No use, distribution or reproduction is permitted which does not comply with these terms.

frontiers in Cell and Developmental Biology

PERSPECTIVE
published: 19 February 2021
doi: 10.3389/fcell.2021.635340

Tissue Mechanics in Haired Murine Skin: Potential Implications for Skin Aging

Hans I-Chen Harn[1,2], Chih-Chiang Chen[3,4,5], Sheng-Pei Wang[1,2], Mingxing Lei[6,7] and Cheng-Ming Chuong[1]**

[1] Department of Pathology, Keck School of Medicine, University of Southern California, Los Angeles, CA, United States, [2] International Research Center of Wound Repair and Regeneration (iWRR), National Cheng Kung University, Tainan, Taiwan, [3] Department of Dermatology, Taipei Veterans General Hospital, Taipei, Taiwan, [4] Institute of Clinical Medicine, National Yang-Ming University, Taipei, Taiwan, [5] Department of Dermatology, National Yang-Ming University, Taipei, Taiwan, [6] 111 Project Laboratory of Biomechanics and Tissue Repair, College of Bioengineering, Chongqing University, Chongqing, China, [7] Key Laboratory of Biorheological Science and Technology of the Ministry of Education, College of Bioengineering, Chongqing University, Chongqing, China

OPEN ACCESS

Edited by:
Masatake Osawa,
Gifu University, Japan

Reviewed by:
Ilja L. Kruglikov,
Wellcomet GmbH, Germany
Desmond Tobin,
University College Dublin, Ireland

***Correspondence:**
Hans I-Chen Harn
harnhnv@gmail.com
Cheng-Ming Chuong
cmchuong@med.usc.edu

Specialty section:
This article was submitted to Stem Cell Research, a section of the journal Frontiers in Cell and Developmental Biology

Received: 30 November 2020
Accepted: 01 February 2021
Published: 19 February 2021

Citation:
Harn HI, Chen CC, Wang SP, Lei M and Chuong CM (2021) Tissue Mechanics in Haired Murine Skin: Potential Implications for Skin Aging. Front. Cell Dev. Biol. 9:635340. doi: 10.3389/fcell.2021.635340

During aging, the skin undergoes changes in architecture and composition. Skin aging phenotypes occur due to accumulated changes in the genome/epigenome, cytokine/cell adhesion, cell distribution/extracellular matrix (ECM), etc. Here we review data suggesting that tissue mechanics also plays a role in skin aging. While mouse and human skin share some similarities, their skin architectures differ in some respects. However, we use recent research in haired murine skin because of the available experimental data. Skin suffers from changes in both its appendages and inter-appendage regions. The elderly exhibit wrinkles and loose dermis and are more likely to suffer from wounds and superficial abrasions with poor healing. They also have a reduction in the number of skin appendages. While telogen is prolonged in aging murine skin, hair follicle stem cells can be rejuvenated to enter anagen if transplanted to a young skin environment. We highlight recent single-cell analyses performed on epidermis and aging human skin which identified new basal cell subpopulations that shift in response to wounding. This may be due to alterations of basement membrane stiffness which would change tissue mechanics in aging skin, leading to altered homeostatic dynamics. We propose that the extracellular matrix (ECM) may play a key role as a chemo-mechanical integrator of the multi-layered senescence-associated signaling pathways, dictating the tissue mechanical landscape of niche microenvironments in aging phenotypes. We show examples where failed chemo-mechanical signaling leads to deteriorating homeostasis during skin aging and suggest potential therapeutic strategies to guide future research to delay the aging processes.

Keywords: skin aging, extracellular matrix, macroenvironment, hair regeneration, skin tension, tissue mechanics, tensional homeostasis, microenvironment

INTRODUCTION

As skin ages, it undergoes physiological and pathological changes causing a decline in both structure and function (Gilchrest, 1989; Tobin, 2017). These changes affect many aspects of skin biology, including (1) compromised barrier function and mechanical protection, (2) dampened immune responses, (3) impaired thermoregulation, (4) decreased sweat and sebum production, (5) delayed hair cycling (Chueh et al., 2013; Chen et al., 2016), and (6) delayed wound healing (Gosain and DiPietro, 2004). Aging is complex involving both intrinsic and extrinsic factors. Earlier work by Hayflick suggests cells have a fixed cellular lifespan, leading to the identification of roles of telomere in aging (Kameda et al., 2020). Recent epigenetic studies identified unique age-related methylome changes associated with the aging epigenome (Zhang et al., 2020). Environmental stresses such as somatic mutations, free radical damage, senescence-associated secretory phenotype, autophagy, chronic inflammation, etc. can also promote senescence (Di Micco et al., 2020; Tabibzadeh, 2021). These findings have identified new concepts and therapeutic targets fostering the hope that aging can be delayed and perhaps tissues can be rejuvenated by modifying the epigenome (Guarasci et al., 2019) or by activating resident tissue stem cells (Fuchs and Blau, 2020). While these are important aspects of the aging process, in this mini-review, we discuss the role of tissue mechanics in the aging skin. Tensional homeostasis, a process that balances the extracellular forces exerted on cells by extracellular matrix (ECM) or neighboring cells and the reciprocal forces, is essential to maintain cell function and tissue remodeling. While we consider this concept has a role in both human and mouse aging skin, we will focus more on the haired murine skin because of the available reports. During mouse skin aging, the tissue mechanics landscape shifts greatly, as skin homeostasis declines. Based on these reports, we suggest some potential therapeutic strategies at the end.

THE AGING SKIN

Manifestations of the aging skin include rough skin textures, wrinkles, laxity, atrophy, pigmentary changes, loss of underlying fat, dry and itchy skin, inability to perspire sufficiently, hair graying, hair loss, thinning of nail plates amongst others (Farage et al., 2013). Recent reports show these traits are affected by both intrinsic (chronological) and extrinsic (non-genetic) factors (Parsons, 1996; Gunn et al., 2009; Tobin, 2017).

Human Skin Aging and Related Diseases

Intrinsically aged skin appears dry and pale with fine wrinkles and increased laxity. This results from gradual physiologic changes include reductions of cell number, collagen production, blood flow, lipids, and rete ridges (Montagna et al., 1989; Tobin, 2017). Extrinsic human skin aging entails changes caused by environmental factors, including ultraviolet light (UV). UV damage upregulates matrix metalloproteases (MMP) (Fisher et al., 1996; Quan et al., 2013) and impacts collagen degradation and synthesis (Varani et al., 2006), as well as the production of elastotic materials in the skin. This creates a microenvironment of fragmented collagen and leads to aberrant collagen homeostasis. There is controversy regarding the effect of aging, whether intrinsic or extrinsic, on epidermal thickness (El-Domyati et al., 2002). Some studies have suggested that intrinsic aging tends to cause a slight overall thinning of the viable epidermis (Lavker, 1979; Lavker and Kligman, 1988; Branchet et al., 1990), while others have found that extrinsic aging tends to cause irregular thickening of the epidermis (Gilchrest, 1989). Recently, single-cell RNA analyses revealed a progressive accumulation of photoaging-related changes and increased chronic inflammation in aging human eyelid skin (Zou et al., 2020). Hair follicular stem cells (HFSC) were shown to be nearly normal in human androgenetic alopecia; the problem is the failure of the niche to convert bulge stem cells (SC) into hair germs, hence resulting in prolonged telogen (Garza et al., 2011). These changes also contribute to hair follicle miniaturization and lowered hair density (Matsumura et al., 2016) and the competition of HFSC fates (Liu et al., 2019).

Solar elastosis, characterized by the replacement of normal elastic fibers with a disordered mass of elastotic material near the dermal-epidermal junction, is the hallmark of photodamaged dermis (Yaar and Gilchrest, 2007). Senile purpura, characterized by recurrent formation of ecchymoses on the sun-exposed extensor surfaces of the extremities, is another disease related to reduction of connective tissue in the dermis. Age-related skin thinning and sun-induced damage of the dermal connective tissue results in inadequate support, increased fragility and rupture of the microvasculature (Fenske and Lober, 1986) as well as decreased wound tensile strength (Thomas, 2001); its cosmetic concerns can negatively impact a patient's quality of life (McKnight et al., 2015).

Structural and Functional Changes in Aging Skin

Within the aging mouse skin, the cell number and turnover rate decrease across all cell types (Farage et al., 2013), which impacts epidermal thickness and barrier integrity (Minematsu et al., 2011). Langerhans cells also decrease in number, leading to impaired immune responses (Wulf et al., 2004). Melanocytes lose their enzyme activity, resulting in uneven pigmentation (Nishimura et al., 2005). The flattening of the dermo-epidermal junction alters the epidermal anchoring system (Le Varlet et al., 1998), and hence the skin becomes more vulnerable to dermo-epidermal separation. In the aging dermis, the cellularity, vascularity, innervation, and ECM content also decrease (Makrantonaki and Zouboulis, 2007). The structure of sweat glands becomes distorted and the number of functional sweat glands decreases (Fenske and Lober, 1986). The loss of adipose tissue hinders thermoregulatory function and other signaling roles (Zwick et al., 2018). Interestingly, aging-associated decreases in dermal thickness corresponds with increases in dermal white adipose tissue (dWAT) thickness (Kruglikov et al., 2019b; Zhang et al., 2021). Mature dermal adipocytes de-differentiate and release free fatty acids into the surrounding ECM, which further changes the metabolism and

strongly modulates the physiology of adjacent dermal fibroblasts, significantly influencing their collagen expression (Kruglikov and Scherer, 2016). The reduced number and activity of fibroblasts were implicated as the cause of decreased dermal ECM synthesis, leading to deranged ECM support and adequate functions for the skin and skin appendages (Cole et al., 2018). Low fibroblast activity also affects collagen fibril crosslinking (Yang et al., 2008), resulting in a rigid but weakened dermis (Silver et al., 2003). Disorganized ECM also decreases the amount of mechanical loading experienced by the dermal fibroblasts and a possibly diminished ability of the skin to respond to mechanical stimuli, creating a vicious cycle that further deteriorates the homeostasis and physiological functioning of the aged skin (Wu et al., 2011). The structural changes in aging skin and the multilayer control of skin homeostasis (**Figures 1A,B**), wound healing, and HFSC interaction with the surrounding ECM will be further discussed.

Factors Underlying How Aging Changes the Murine Skin

Adult skin SC are vital for replacing cells in tissues, but their capacity declines with age. SC are regulated by both macroenvironmental signals (Chen and Chuong, 2012; Chen et al., 2016) and their microenvironmental niche (Ge et al., 2020). On the macroenvironment level, the hair cycle in aged mouse skin shows higher and longer expression of HFSC activation inhibitors such as BMPs, DKK1, and SFRPs in the dermis (Chen et al., 2014). On the cellular level, HFSC from aged skin show defects in Nfatc1 (Keyes et al., 2013) and FoxC1 (Lay et al., 2016; Wang et al., 2016). Microenvironmental factors including ECM (Ge et al., 2020), immune, sensory nerves and arrector pili (Shwartz et al., 2020) all take part in regulating HFSC activity. Expression and maintenance of the hemidesmosome component Col17A1 are critical for skin homeostasis and skin epithelial stem cell retention (Matsumura et al., 2016; Liu et al., 2019). Tenascin C (Tnc), an element of the ECM, is shown to promote ECM integrity and is reduced in aged skin (Choi et al., 2020). Thus, both intrinsic and extrinsic factors play a role in the aging of HFSC (Lei and Chuong, 2016).

TENSIONAL HOMEOSTASIS: BALANCED TISSUE MECHANICS

Tissue mechanics (Kenedi et al., 1975; Hsu et al., 2018a) can provide a new approach in contemplating stem cell regeneration in the aged skin.

ECM/MMP and Tissue Mechanics in the Skin

The skin cells interact dynamically with the basement membrane (BM), ECM, and the dermis to shape the structure and function of the skin (Fiore et al., 2020). The dermis contains the greatest volume of ECM, which interacts with the dermal cells that generate contractile forces, especially in face of injury (Hsu et al., 2018a; Harn et al., 2019). The amount, content, and organization of ECM being synthesized and remodeled by the MMPs in the dermis is in an intricate balance to maintain the homeostasis of the skin and in aging (Naylor et al., 2011; Tracy et al., 2016). In turn, the ECM provides not only biochemical but also mechanical cues to impact cell behavior (Watt and Fujiwara, 2011). Cells sense mechanical stimuli via mechanosensors (e.g., integrin, hemidesmosomes, adherent junctions, stretch-sensitive ion channels) and translocate these signals into the nucleus for transcriptional response in the mechanotransduction process (Wong et al., 2011). Tensional homeostasis, a concept introduced by Weaver and colleagues to describe the balance between the extracellular forces exerted on the cells by neighboring cells, ECM and reciprocal forces generated by the cells (Paszek et al., 2005), is also essential for maintaining cell function and tissue remodeling in the skin (Harn et al., 2019).

Heterogeneity of the Basal Layer and HF Niche

Recent single-cell analyses identify new sub-populations of basal cells that specifically localize at the top or bottom of rete ridges (Wang et al., 2020), suggesting a mechanical control. Interfollicular epithelial cell differentiation is best described as a single step gradualistic process with a large number of transition cells between the basal and spinous layer (Lin et al., 2020). Their homeostatic states also shift in response to wounding into four different cell states that govern cell proliferation or differentiation (Haensel et al., 2020). We speculate this flexibility of cell states shown during homeostasis is also reflected on cell mechanics; the dynamic changes of cell states also create physical changes to cellular forces that drive cell migration and collective morphological changes.

Rete ridge reductions and tissue mechanical landscape changes in aging skin can either be the cause or consequence of changes in these basal layer sub-populations. Additionally, the basement membrane (BM) adjacent to HFSC serves as an arrector pili muscle (APM) niche (Fujiwara et al., 2011), which together with the sympathetic nerve can form a dual-component niche to modulate HFSC activity (Shwartz et al., 2020). ECM dysregulation that accumulates during skin aging could also affect BM properties chemically and mechanically, which in turn alters APM homeostasis and HFSC regulation.

Tissue Mechanics in Aging Skin: ECM Dysregulation, Wrinkling, and Wound Healing

The changes in ECM synthesis, assembly and dampened cellular response to mechanical stimuli in aged skin lead to low proliferation, discontinued migration, prolonged cell-cycle arrest, and eventually cell death (Sherratt, 2009; Wu et al., 2011). Kruglikov and Scherer reported wrinkling as a mechanical phenomenon where the mismatch of mechanical modules between adjacent epidermal-dermal or dermal-subcutaneous junctions, leads to structural instabilities inside the skin (Kruglikov and Scherer, 2018). We view wrinkles as an excessively stiff apical surface area (stratified epidermis) with a decreased basal dimension and resistance (reduced ECM,

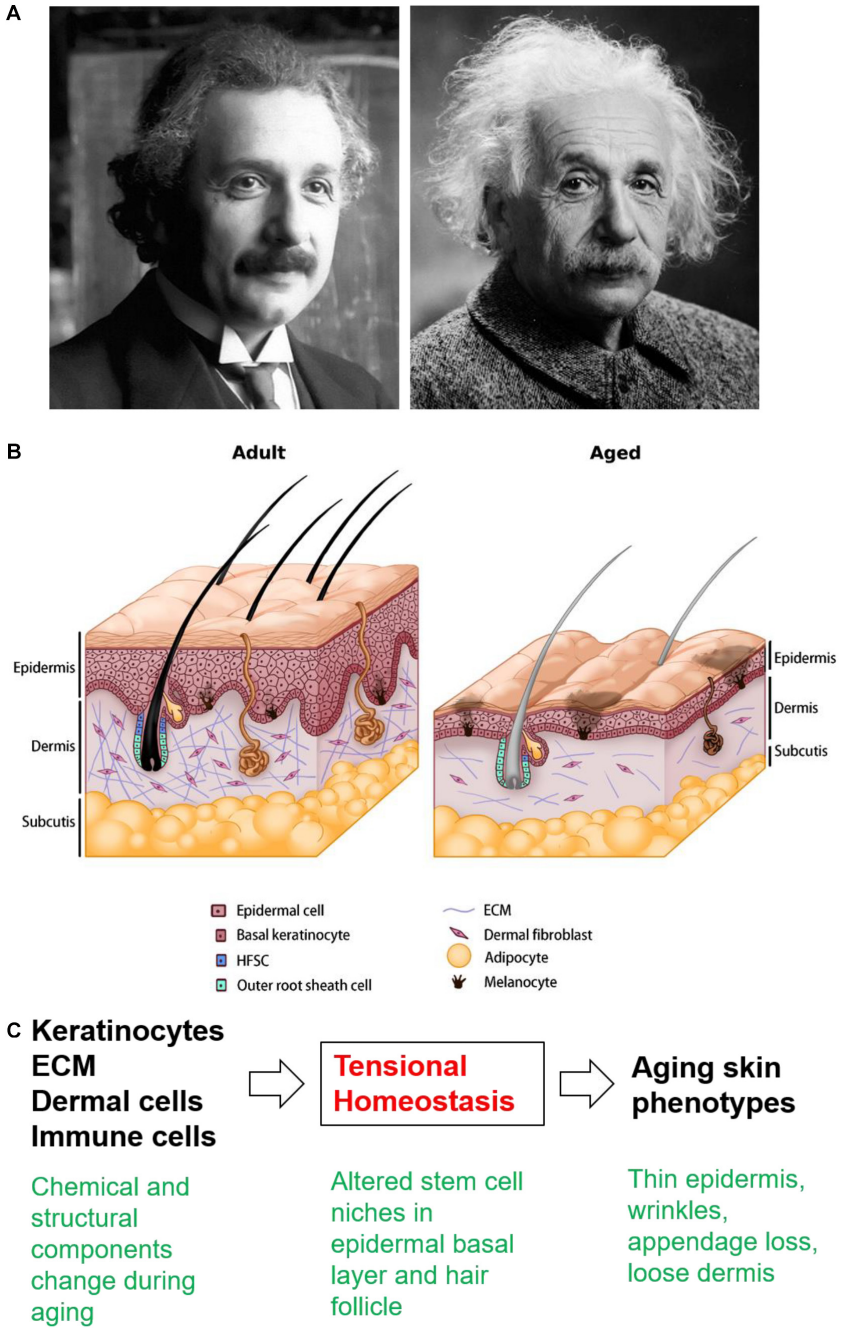

FIGURE 1 | The aging skin. **(A)** Young and old Albert Einstein used to illustrate the changes in the appearance of aging skin. Source: Pixabay. **(B)** Schematic drawing showing skin architecture in the adult and aged skin. In aged skin, the overall thickness decreases progressively across all layers, accompanied by wrinkles, pigmentary changes, loss of underlying fat, hair graying, hair loss, and decreased sebaceous gland function. The reduced number and altered activity of fibroblasts have been implicated as the underlying cause of decreased dermal ECM synthesis, leading to deranged ECM support and affects collagen fibril crosslinking. The changes in decreasing cell numbers and altered ECM production and assembly also contribute to hair follicle miniaturization and lowered hair density in aged skin. **(C)** Cellular/molecular events reviewed in the text present potential new therapeutic targets.

dermal cell, adipose tissue) that leads to tissue folding (Varner and Nelson, 2014). In multilayered epithelial tissue, softening, and enhanced remodeling of the BM promote tumor budding, while stiffening of the BM promotes tissue folding (Fiore et al., 2020). In parallel, what factors could contribute to the reduced rete ridges and increased wrinkles in aging skin? We propose 3 possible scenarios: (1) BM stiffness increases in aging skin, (2) loss of Col17A1 causes an increase in the ratio of differentiated cells to basal progenitor cells, and (3) decreases in dermis stiffness and length force the attached apical epidermis to

bend and fold upward. The precise mechanical changes of these constituents in aging skin remains to be investigated.

Wound healing in a healthy, aged individual is delayed but not defective (Gerstein et al., 1993). This is due to their dampened cellular activity and asynchronization of pro and anti-inflammatory responses to injury (Ashcroft et al., 2002). The reduced number, activity, and migration of keratinocytes and fibroblasts in aged skin lead to delayed re-epithelialization, wound closure, and tissue reformation (Moulin et al., 2000; Ashcroft et al., 2002). On the other hand, although aged skin shows little capacity to regenerate, it is less prone to form hypertrophic scars and keloids (Hsu et al., 2018b), whose etiology is mechanically sensitive (Harn et al., 2015, 2016). Aging skin is characterized by reduced ECM deposition brought about by (1) low skin tension, (2) dampened cellular responses to mechanical stimuli coupled with (3) low pro-inflammatory signaling, and (4) the reduced capacity of dermal adipocytes to transdifferentiate into myofibroblasts (Varani et al., 2006; Zhang et al., 2019) which could underlie reduced scarring after wounding.

IMPACTS WITH PERTURBED TENSIONAL HOMEOSTASIS

Perturbation to tissue mechanics or disruption of tensional homeostasis impacts physiological functioning of the skin, including hair cycling and wound healing (Hsu et al., 2018a; Harn et al., 2019).

Skin Tension and Scarring vs. Regeneration

Generally, increasing skin tension or stiffness leads to higher cell activity and ECM synthesis. Molecules responsible for mechanotransduction are also important in regulating tensional homeostasis. Epidermal-specific deletion of integrin or focal adhesion kinase (FAK) results in disfigured hair follicles and dysregulated hair cycle propagation (Essayem et al., 2006). Activation of TRPV1, a transient receptor potential cation channel involved in mechano-transduction, inhibits hair shaft lengthening and induces premature catagen (Biro et al., 2006). Tension across the wound has been demonstrated as a key inducer of scarring in hypertrophic scars and keloids (Harn et al., 2019). FAK and integrins could be important mediators of these mechanotransduction processes (Wong et al., 2012), although the reduced capacity of dermal adipocytes to de- and transdifferentiate into myofibroblasts could also be an underlying factor (Zhang et al., 2019). In contrast, the African Spiny mice skin expresses a high collagen III to I ratio producing an exceptionally soft substrate (Seifert et al., 2012). Spiny mice can regenerate their skin and all of their appendages after full-thickness wounding (Jiang et al., 2019).

Cyclic Stretch of the Dorsal Murine Skin Activates HFSC

The impact of skin "loosening" during aging can be deduced from the effects of mechanical force on the homeostasis of HFSC. The amount and duration of skin mechanical stretching result in HFSC proliferation (Chu et al., 2019). This depends on three major components. First, the counterbalance between Wnt and BMP-2; second, M2 subtype macrophage polarization; third, growth factor secretion, especially HGF and IGF-1 (Chu et al., 2019). However, this mechanical activation of hair cells seems compromised in the stiff and less extendable aged mice skin (Lynch et al., 2017; Meador et al., 2020) which has difficulty in eliciting a desirable regeneration response via stretching. How mechanical force, ECM and immune cells contribute to aging skin's inadequate regenerative activity remains to be explored.

Hair Plucking in the Dorsal Murine Skin Triggers a Regenerative Immune Response

External mechanical forces such as hair plucking can also trigger the immune response-mediated regenerative process. Properly arranged hair plucking can trigger an efficient regenerative response mediated through a two-step immune response cascade, called quorum sensing (Chen et al., 2015). These examples demonstrate the importance of tissue mechanics on maintaining homeostasis of the skin and its response to injury.

RECENT DISCOVERIES FOR THERAPEUTIC STRATEGIES AGAINST AGING SKIN

Although currently there is no prominent strategy for developing new drugs against skin aging, there are a few chemical and mechanical approaches that have demonstrated potential.

Chemical-Based Approach: PRP, Follistatin, HES1, ADSC, and dWAT

Platelet-rich plasma (PRP) has been adopted to treat many degenerative disorders including hair loss (Li et al., 2012; Khatu et al., 2014) with reasonable success despite variations in current protocols (Ayatollahi et al., 2017; Picard et al., 2017). In principle, this approach is based on the various growth factors released (Gentile et al., 2017); however, its precise mechanism has not been elucidated. Charles-de-Sa et al. demonstrated that dWAT completely disappears after PRP injection and is replaced by fibrotic tissue, which is very similar to the effect observed after Bleomycin injection (Charles-de-Sa et al., 2018).

Replenishing effective growth factors or activating specific downstream genes such as Wnt-follistatin and follistatin-like 1 protein have been tested as a treatment for alopecia (Zimber et al., 2011; Chen et al., 2014). Pharmacological activation of HES1 alleviated the cellular senescence of aged dermal fibroblasts (Zou et al., 2020). Adipose-derived stem cells (ADSC) have shown effects related to dermal fibroblast activation via secretion of growth factors (Kim et al., 2011). Subcutaneous injection of ADSC significantly increased collagen density, dermal thickness, and fibroblast number in hairless mice (Fukuoka et al., 2017), and also stimulated collagen synthesis of human dermal fibroblasts (Kim et al., 2009).

TABLE 1 | Comparison of key differences between young and aged skin.

Category	Young skin	Aged skin	References
Structural features	Moist, smooth skin surface. Rete ridges, and sufficient subcutaneous fat, normal perspire function. Normal hair density and pigmentation.	Decrease thickness, dry, fine wrinkles, pigmentary changes. Reduced rete ridges and underlying fat, inability to perspire sufficiently, hair graying, hair loss, decrease sebaceous gland function, thinning of nail plates.	Farage et al., 2013; Tobin, 2017
Macroenvironment	Regulated hair cycle, homeostasis, normal physiological function, ECM and MMP balance, regulated expression of inhibitory and activating factors. Normal wound healing.	Prolonged telogen, deteriorated homeostasis and physiological function. Higher expression of MMPs. Longer expression of BMPs, DKK1, SFRP, downregulation of follistatin. Delayed wound healing. Somatic mutation, free radical damage, senescence-associated secretory phenotype, autophagy, chronic inflammation.	Chen et al., 2014; Fuchs and Blau, 2020; Kameda et al., 2020
Microenvironment	Normal HFSC and dermal cell number and function. Low DNA damage. Normal Nfatc1, FoxC1 expression. Normal and proper ECM production and crosslinking. COL17A1 maintenance. High Tnc expression.	Reduced HFSC and dermal cell number. Accumulated DNA damage. Defect Nfatc1 and FoxC1 expression. Reduced ECM production and deranged crosslinking. Increased COL17A1 proteolysis. Reduced Tnc expression. Aging epigenome.	Keyes et al., 2013; Lay et al., 2016; Matsumura et al., 2016; Wang et al., 2016; Guarasci et al., 2019; Liu et al., 2019; Choi et al., 2020; Di Micco et al., 2020; Zhang et al., 2020; Tabibzadeh, 2021
Tissue mechanics	Prone to hypertrophic scar and keloid. Activation of TRPV1 induces premature catagen. Cyclic stretch induces anagen re-entry. Hair plucking triggers a regenerative immune response.	Rigid dermis, less resistant to shearing force. Dampened cellular activity to mechanical stimuli. Less prone to scaring.	Chen et al., 2015; Chu et al., 2019; Harn et al., 2019

Summary of changes during the aging of haired murine skin, the micro- and macroenvironmental signals contributing to HFSC maintenance.

The adipocytes in the dWAT have high plasticity and undergo reversible dedifferentiation, in which adipocyte-derived preadipocytes trans-differentiate into myoblasts and are involved not only in the physiological hair cycle but also under pathological conditions such as hypertrophic scarring, systemic sclerosis and androgenetic alopecia (Zhang et al., 2019). During proliferation, differentiation and dedifferentiation, various extracellular vesicles are secreted to the nearby HF and in turn stimulate its hair cycle (Kruglikov et al., 2019b). Lastly, Caveolin-1 (Cav-1) is upregulated in aged skin and is associated with altered dermal thickness, dWAT expansion and ECM expression, which sequentially influences the mechanical properties of the skin layers (Kruglikov et al., 2019a,b). This makes Cav-1 a potential candidate for anti-aging treatment especially since Mevastatin has been shown to target Cav-1 as an effective treatment for chronic wound healing (Sawaya et al., 2019).

Mechanical Approach: Stretching and ECM/MMP Perturbation

Although the effectiveness of stretching-induced HF activation is less pronounced in aging mice (Chu et al., 2019), interestingly, subcutaneous injection of cross-linked hyaluronic acid stimulates collagen synthesis and partially restores dermal ECM that are lost in photodamaged skin (Bukhari et al., 2018; Yamada and Prow, 2020). It is speculated that this effect is achieved by mechanical stretching of the dermis and the activation of dermal fibroblasts (Chu et al., 2019). It also was demonstrated that cross-linked HA can significantly influence dWAT and subcutaneous WAT which modifies the dermal-subcutaneous junction (Kruglikov and Wollina, 2015), and directly but differentially affects the mature adipocytes and preadipocytes (Nadra et al., unpublished). Other studies have also focused on securing collagen integrity via suppressing MMP production and activity (Oh et al., 2020a), particularly in alleviating UVA-mediated suppression of collagen expression by stimulating TGF-β/Smad signaling (Oh et al., 2020b).

SUMMARY

We review the physiological changes associated with skin aging (**Table 1** and **Figure 1C**) and highlight the potential role of tensional homeostasis. Utilizing and providing a chemically or mechanically induced young environment might rescue aging phenotypes in the skin. This approach could potentially rescue basal layer homeostasis to control (1) epidermal thickness, (2) wound healing, (3) activation of HFSC, and (4) cell reprogramming during wound-induced hair neogenesis (Bhoopalam et al., 2020). While the haired murine skin provides an experimental model that reveals new molecular understanding summarized here, aging human skin has features that do not exist in the mouse model and await further exploration.

DATA AVAILABILITY STATEMENT

The original contributions presented in the study are included in the article/supplementary material, further inquiries can be directed to the corresponding author/s.

ETHICS STATEMENT

Written informed consent was not obtained from the individual(s) for the publication of any potentially identifiable images or data included in this article.

AUTHOR CONTRIBUTIONS

CCC and SPW contributed more to the clinical aspect. HICH, ML, and CMC contributed more to the basic research elements. All authors contributed to the writing, organization, and editing of the manuscript. The manuscript was proofread by Dr. R. B. Widelitz.

FUNDING

HICH was supported by the Featured Areas Research Center Program within the framework of the Higher Education Sprout Project by the Ministry of Education (MOE), The Excellent Research Center Program by the Ministry of Science and Technology (MOST 107-3017-F-006-002) in Taiwan, and NIGMS, NIH. CCC was funded by Ministry of Science and Technology (109-2314-B-010 -014 -MY3). ML was supported by the National Natural Science Foundation of China (82003384), Fundamental Research Funds for the Central Universities (2020CDJYGSG003), Chongqing Talents Program (CQYC2020058022), and Scientific Research Foundation from Chongqing University (02210011044110). CMC was funded by NIGMS, NIH (5R01GM 125322-02).

REFERENCES

Ashcroft, G. S., Mills, S. J., and Ashworth, J. J. (2002). Ageing and wound healing. *Biogerontology* 3, 337–345. doi: 10.1023/a:1021399228395

Ayatollahi, A., Hosseini, H., Gholami, J., Mirminachi, B., Firooz, F., and Firooz, A. (2017). Platelet rich plasma for treatment of non-scarring hair loss: systematic review of literature. *J. Dermatolog. Treat*. 28, 574–581. doi: 10.1080/09546634.2017.1303571

Bhoopalam, M., Garza, L. A., and Reddy, S. K. (2020). Wound induced hair neogenesis – a novel paradigm for studying regeneration and aging. *Front. Cell Dev. Biol*. 8:582346. doi: 10.3389/fcell.2020.582346

Biro, T., Bodo, E., Telek, A., Geczy, T., Tychsen, B., Kovacs, L., et al. (2006). Hair cycle control by vanilloid receptor-1 (TRPV1): evidence from TRPV1 knockout mice. *J. Invest. Dermatol*. 126, 1909–1912. doi: 10.1038/sj.jid.5700321

Branchet, M. C., Boisnic, S., Frances, C., and Robert, A. M. (1990). Skin thickness changes in normal aging skin. *Gerontology* 36, 28–35. doi: 10.1159/000213172

Bukhari, S. N. A., Roswandi, N. L., Waqas, M., Habib, H., Hussain, F., Khan, S., et al. (2018). Hyaluronic acid, a promising skin rejuvenating biomedicine: a review of recent updates and pre-clinical and clinical investigations on cosmetic and nutricosmetic effects. *Int. J. Biol. Macromol*. 120(Pt B), 1682–1695. doi: 10.1016/j.ijbiomac.2018.09.188

Charles-de-Sa, L., Gontijo-de-Amorim, N. F., Takiya, C. M., Borojevic, R., Benati, D., Bernardi, P., et al. (2018). Effect of use of platelet-rich plasma (PRP) in skin with intrinsic aging process. *Aesthet. Surg. J*. 38, 321–328. doi: 10.1093/asj/sjx137

Chen, C. C., and Chuong, C. M. (2012). Multi-layered environmental regulation on the homeostasis of stem cells: the saga of hair growth and alopecia. *J. Dermatol. Sci*. 66, 3–11. doi: 10.1016/j.jdermsci.2012.02.007

Chen, C. C., Murray, P. J., Jiang, T. X., Plikus, M. V., Chang, Y. T., Lee, O. K., et al. (2014). Regenerative hair waves in aging mice and extra-follicular modulators follistatin, dkk1, and sfrp4. *J. Invest. Dermatol*. 134, 2086–2096. doi: 10.1038/jid.2014.139

Chen, C. C., Plikus, M. V., Tang, P. C., Widelitz, R. B., and Chuong, C. M. (2016). The modulatable stem cell niche: tissue interactions during hair and feather follicle regeneration. *J. Mol. Biol*. 428, 1423–1440. doi: 10.1016/j.jmb.2015.07.009

Chen, C. C., Wang, L., Plikus, M. V., Jiang, T. X., Murray, P. J., Ramos, R., et al. (2015). Organ-level quorum sensing directs regeneration in hair stem cell populations. *Cell* 161, 277–290. doi: 10.1016/j.cell.2015.02.016

Choi, Y. E., Song, M. J., Hara, M., Imanaka-Yoshida, K., Lee, D. H., Chung, J. H., et al. (2020). Effects of tenascin C on the integrity of extracellular matrix and skin aging. *Int. J. Mol. Sci*. 21:8693. doi: 10.3390/ijms21228693

Chu, S. Y., Chou, C. H., Huang, H. D., Yen, M. H., Hong, H. C., Chao, P. H., et al. (2019). Mechanical stretch induces hair regeneration through the alternative activation of macrophages. *Nat. Commun*. 10:1524. doi: 10.1038/s41467-019-09402-8

Chueh, S. C., Lin, S. J., Chen, C. C., Lei, M., Wang, L. M., Widelitz, R., et al. (2013). Therapeutic strategy for hair regeneration: hair cycle activation, niche environment modulation, wound-induced follicle neogenesis, and stem cell engineering. *Expert Opin. Biol. Ther*. 13, 377–391. doi: 10.1517/14712598.2013.739601

Cole, M. A., Quan, T., Voorhees, J. J., and Fisher, G. J. (2018). Extracellular matrix regulation of fibroblast function: redefining our perspective on skin aging. *J. Cell Commun. Signal*. 12, 35–43. doi: 10.1007/s12079-018-0459-1

Di Micco, R., Krizhanovsky, V., Baker, D., and d'Adda di Fagagna, F. (2020). Cellular senescence in ageing: from mechanisms to therapeutic opportunities. *Nat. Rev. Mol. Cell Biol*. 22, 75–95. doi: 10.1038/s41580-020-00314-w

El-Domyati, M., Attia, S., Saleh, F., Brown, D., Birk, D. E., Gasparro, F., et al. (2002). Intrinsic aging vs. photoaging: a comparative histopathological, immunohistochemical, and ultrastructural study of skin. *Exp. Dermatol*. 11, 398–405. doi: 10.1034/j.1600-0625.2002.110502.x

Essayem, S., Kovacic-Milivojevic, B., Baumbusch, C., McDonagh, S., Dolganov, G., Howerton, K., et al. (2006). Hair cycle and wound healing in mice with a keratinocyte-restricted deletion of FAK. *Oncogene* 25, 1081–1089. doi: 10.1038/sj.onc.1209130

Farage, M. A., Miller, K. W., Elsner, P., and Maibach, H. I. (2013). Characteristics of the aging skin. *Adv. Wound Care (New Rochelle)* 2, 5–10. doi: 10.1089/wound.2011.0356

Fenske, N. A., and Lober, C. W. (1986). Structural and functional changes of normal aging skin. *J. Am. Acad. Dermatol*. 15(4 Pt 1), 571–585. doi: 10.1016/s0190-9622(86)70208-9

Fiore, V. F., Krajnc, M., Quiroz, F. G., Levorse, J., Pasolli, H. A., Shvartsman, S. Y., et al. (2020). Mechanics of a multilayer epithelium instruct tumour architecture and function. *Nature* 585, 433–439. doi: 10.1038/s41586-020-2695-9

Fisher, G. J., Datta, S. C., Talwar, H. S., Wang, Z. Q., Varani, J., Kang, S., et al. (1996). Molecular basis of sun-induced premature skin ageing and retinoid antagonism. *Nature* 379, 335–339. doi: 10.1038/379335a0

Fuchs, E., and Blau, H. M. (2020). Tissue stem cells: architects of their niches. *Cell Stem Cell* 27, 532–556. doi: 10.1016/j.stem.2020.09.011

Fujiwara, H., Ferreira, M., Donati, G., Marciano, D. K., Linton, J. M., Sato, Y., et al. (2011). The basement membrane of hair follicle stem cells is a muscle cell niche. *Cell* 144, 577–589. doi: 10.1016/j.cell.2011.01.014

Fukuoka, H., Narita, K., and Suga, H. (2017). Hair regeneration therapy: application of adipose-derived stem cells. *Curr. Stem Cell Res. Ther*. 12, 531–534. doi: 10.2174/1574888X12666170522114307

Garza, L. A., Yang, C. C., Zhao, T., Blatt, H. B., Lee, M., He, H., et al. (2011). Bald scalp in men with androgenetic alopecia retains hair follicle stem cells but lacks CD200-rich and CD34-positive hair follicle progenitor cells. *J. Clin. Invest*. 121, 613–622. doi: 10.1172/JCI44478

Ge, Y., Miao, Y., Gur-Cohen, S., Gomez, N., Yang, H., Nikolova, M., et al. (2020). The aging skin microenvironment dictates stem cell behavior. *Proc. Natl. Acad. Sci. U.S.A*. 117, 5339–5350. doi: 10.1073/pnas.1901720117

Gentile, P., Cole, J. P., Cole, M. A., Garcovich, S., Bielli, A., Scioli, M. G., et al. (2017). evaluation of not-activated and activated PRP in hair loss treatment: role of growth factor and cytokine concentrations obtained by different collection systems. *Int. J. Mol. Sci*. 18:408. doi: 10.3390/ijms18020408

Gerstein, A. D., Phillips, T. J., Rogers, G. S., and Gilchrest, B. A. (1993). Wound healing and aging. *Dermatol. Clin*. 11, 749–757.

Gilchrest, B. A. (1989). Skin aging and photoaging: an overview. *J. Am. Acad. Dermatol*. 21(3 Pt 2), 610–613. doi: 10.1016/s0190-9622(89)70227-9

Gosain, A., and DiPietro, L. A. (2004). Aging and wound healing. *World J. Surg*. 28, 321–326. doi: 10.1007/s00268-003-7397-6

Guarasci, F., D'Aquila, P., Montesanto, A., Corsonello, A., Bellizzi, D., and Passarino, G. (2019). Individual DNA methylation profile is correlated with age and can be targeted to modulate healthy aging and longevity. *Curr. Pharm. Des*. 25, 4139–4149. doi: 10.2174/1381612825666191112095655

Gunn, D. A., Rexbye, H., Griffiths, C. E., Murray, P. G., Fereday, A., Catt, S. D., et al. (2009). Why some women look young for their age. *PLoS One* 4:e8021. doi: 10.1371/journal.pone.0008021

Haensel, D., Jin, S., Sun, P., Cinco, R., Dragan, M., Nguyen, Q., et al. (2020). Defining epidermal basal cell states during skin homeostasis and wound healing using single-cell transcriptomics. *Cell Rep*. 30, e3932–e3936. doi: 10.1016/j.celrep.2020.02.091

Harn, H. I., Hsu, C. K., Wang, Y. K., Huang, Y. W., Chiu, W. T., Lin, H. H., et al. (2016). Spatial distribution of filament elasticity determines the migratory behaviors of a cell. *Cell Adh. Migr*. 10, 368–377. doi: 10.1080/19336918.2016.1156825

Harn, H. I., Ogawa, R., Hsu, C. K., Hughes, M. W., Tang, M. J., and Chuong, C. M. (2019). The tension biology of wound healing. *Exp. Dermatol*. 28, 464–471. doi: 10.1111/exd.13460

Harn, H. I., Wang, Y. K., Hsu, C. K., Ho, Y. T., Huang, Y. W., Chiu, W. T., et al. (2015). Mechanical coupling of cytoskeletal elasticity and force generation is crucial for understanding the migrating nature of keloid fibroblasts. *Exp. Dermatol*. 24, 579–584. doi: 10.1111/exd.12731

Hsu, C. K., Lin, H. H., Harn, H. I., Hughes, M. W., Tang, M. J., and Yang, C. C. (2018a). Mechanical forces in skin disorders. *J. Dermatol. Sci*. 90, 232–240. doi: 10.1016/j.jdermsci.2018.03.004

Hsu, C. K., Lin, H. H., Harn, H. I., Ogawa, R., Wang, Y. K., Ho, Y. T., et al. (2018b). Caveolin-1 controls hyperresponsiveness to mechanical stimuli and fibrogenesis-associated RUNX2 activation in keloid fibroblasts. *J. Invest. Dermatol*. 138, 208–218. doi: 10.1016/j.jid.2017.05.041

Jiang, T. X., Harn, H. I., Ou, K. L., Lei, M., and Chuong, C. M. (2019). Comparative regenerative biology of spiny (*Acomys cahirinus*) and laboratory (*Mus musculus*) mouse skin. *Exp. Dermatol*. 28, 442–449. doi: 10.1111/exd.13899

Kameda, M., Mikawa, T., Yokode, M., Inagaki, N., and Kondoh, H. (2020). Senescence research from historical theory to future clinical application. *Geriatr. Gerontol. Int*. doi: 10.1111/ggi.14121 [Epub Ahead of Print].

Kenedi, R. M., Gibson, T., Evans, J. H., and Barbenel, J. C. (1975). Tissue mechanics. *Phys. Med. Biol*. 20, 699–717. doi: 10.1088/0031-9155/20/5/001

Keyes, B. E., Segal, J. P., Heller, E., Lien, W. H., Chang, C. Y., Guo, X., et al. (2013). Nfatc1 orchestrates aging in hair follicle stem cells. *Proc. Natl. Acad. Sci. U.S.A*. 110, E4950–E4959. doi: 10.1073/pnas.1320301110

Khatu, S. S., More, Y. E., Gokhale, N. R., Chavhan, D. C., and Bendsure, N. (2014). Platelet-rich plasma in androgenic alopecia: myth or an effective tool. *J. Cutan. Aesthet. Surg*. 7, 107–110. doi: 10.4103/0974-2077.138352

Kim, J. H., Jung, M., Kim, H. S., Kim, Y. M., and Choi, E. H. (2011). Adipose-derived stem cells as a new therapeutic modality for ageing skin. *Exp. Dermatol*. 20, 383–387. doi: 10.1111/j.1600-0625.2010.01221.x

Kim, W. S., Park, B. S., Park, S. H., Kim, H. K., and Sung, J. H. (2009). Antiwrinkle effect of adipose-derived stem cell: activation of dermal fibroblast by secretory factors. *J. Dermatol. Sci*. 53, 96–102. doi: 10.1016/j.jdermsci.2008.08.007

Kruglikov, I. L., and Scherer, P. E. (2016). Dermal adipocytes: from irrelevance to metabolic targets? *Trends Endocrinol. Metab*. 27, 1–10. doi: 10.1016/j.tem.2015.11.002

Kruglikov, I. L., and Scherer, P. E. (2018). Skin aging as a mechanical phenomenon: the main weak links. *Nutr. Healthy Aging* 4, 291–307. doi: 10.3233/NHA-170037

Kruglikov, I. L., and Wollina, U. (2015). Soft tissue fillers as non-specific modulators of adipogenesis: change of the paradigm? *Exp. Dermatol*. 24, 912–915. doi: 10.1111/exd.12852

Kruglikov, I. L., Zhang, Z., and Scherer, P. E. (2019a). Caveolin-1 in skin aging – from innocent bystander to major contributor. *Ageing Res. Rev*. 55:100959. doi: 10.1016/j.arr.2019.100959

Kruglikov, I. L., Zhang, Z., and Scherer, P. E. (2019b). The role of immature and mature adipocytes in hair Cycling. *Trends Endocrinol. Metab*. 30, 93–105. doi: 10.1016/j.tem.2018.11.004

Lavker, R. M. (1979). Structural alterations in exposed and unexposed aged skin. *J. Invest. Dermatol*. 73, 59–66. doi: 10.1111/1523-1747.ep12532763

Lavker, R. M., and Kligman, A. M. (1988). Chronic heliodermatitis: a morphologic evaluation of chronic actinic dermal damage with emphasis on the role of mast cells. *J. Invest. Dermatol*. 90, 325–330. doi: 10.1111/1523-1747.ep12456193

Lay, K., Kume, T., and Fuchs, E. (2016). FOXC1 maintains the hair follicle stem cell niche and governs stem cell quiescence to preserve long-term tissue-regenerating potential. *Proc. Natl. Acad. Sci. U.S.A*. 113, E1506–E1515. doi: 10.1073/pnas.1601569113

Le Varlet, B., Chaudagne, C., Saunois, A., Barre, P., Sauvage, C., Berthouloux, B., et al. (1998). Age-related functional and structural changes in human dermo-epidermal junction components. *J. Investig. Dermatol. Symp. Proc*. 3, 172–179. doi: 10.1038/jidsymp.1998.34

Lei, M., and Chuong, C. M. (2016). Stem cells. aging, alopecia, and stem cells. *Science* 351, 559–560. doi: 10.1126/science.aaf1635

Li, Z. J., Choi, H. I., Choi, D. K., Sohn, K. C., Im, M., Seo, Y. J., et al. (2012). Autologous platelet-rich plasma: a potential therapeutic tool for promoting hair growth. *Dermatol. Surg*. 38(7 Pt 1), 1040–1046. doi: 10.1111/j.1524-4725.2012.02394.x

Lin, Z., Jin, S., Chen, J., Li, Z., Lin, Z., Tang, L., et al. (2020). Murine interfollicular epidermal differentiation is gradualistic with GRHL3 controlling progression from stem to transition cell states. *Nat. Commun*. 11:5434. doi: 10.1038/s41467-020-19234-6

Liu, N., Matsumura, H., Kato, T., Ichinose, S., Takada, A., Namiki, T., et al. (2019). Stem cell competition orchestrates skin homeostasis and ageing. *Nature* 568, 344–350. doi: 10.1038/s41586-019-1085-7

Lynch, B., Bonod-Bidaud, C., Ducourthial, G., Affagard, J. S., Bancelin, S., Psilodimitrakopoulos, S., et al. (2017). How aging impacts skin biomechanics: a multiscale study in mice. *Sci. Rep*. 7:13750. doi: 10.1038/s41598-017-13150-4

Makrantonaki, E., and Zouboulis, C. C. (2007). Molecular mechanisms of skin aging: state of the art. *Ann. N. Y. Acad. Sci*. 1119, 40–50. doi: 10.1196/annals.1404.027

Matsumura, H., Mohri, Y., Binh, N. T., Morinaga, H., Fukuda, M., Ito, M., et al. (2016). Hair follicle aging is driven by transepidermal elimination of stem cells via COL17A1 proteolysis. *Science* 351:aad4395. doi: 10.1126/science.aad4395

McKnight, B., Seidel, R., and Moy, R. (2015). Topical human epidermal growth factor in the treatment of senile purpura and the prevention of dermatoporosis. *J. Drugs Dermatol*. 14, 1147–1150.

Meador, W. D., Sugerman, G. P., Story, H. M., Seifert, A. W., Bersi, M. R., Tepole, A. B., et al. (2020). The regional-dependent biaxial behavior of young and aged mouse skin: a detailed histomechanical characterization, residual strain analysis, and constitutive model. *Acta Biomater*. 101, 403–413. doi: 10.1016/j.actbio.2019.10.020

Minematsu, T., Yamamoto, Y., Nagase, T., Naito, A., Takehara, K., Iizaka, S., et al. (2011). Aging enhances maceration-induced ultrastructural alteration of the epidermis and impairment of skin barrier function. *J. Dermatol. Sci*. 62, 160–168. doi: 10.1016/j.jdermsci.2011.03.005

Montagna, W., Kirchner, S., and Carlisle, K. (1989). Histology of sun-damaged human skin. *J. Am. Acad. Dermatol*. 21(5 Pt 1), 907–918. doi: 10.1016/s0190-9622(89)70276-0

Moulin, V., Auger, F. A., Garrel, D., and Germain, L. (2000). Role of wound healing myofibroblasts on re-epithelialization of human skin. *Burns* 26, 3–12. doi: 10.1016/s0305-4179(99)00091-1

Naylor, E. C., Watson, R. E., and Sherratt, M. J. (2011). Molecular aspects of skin ageing. *Maturitas* 69, 249–256. doi: 10.1016/j.maturitas.2011.04.011

Nishimura, E. K., Granter, S. R., and Fisher, D. E. (2005). Mechanisms of hair graying: incomplete melanocyte stem cell maintenance in the niche. *Science* 307, 720–724. doi: 10.1126/science.1099593

Oh, J. H., Joo, Y. H., Karadeniz, F., Ko, J., and Kong, C. S. (2020a). Syringaresinol inhibits UVA-induced MMP-1 expression by suppression of MAPK/AP-1 Signaling in HaCaT keratinocytes and human dermal fibroblasts. *Int. J. Mol. Sci*. 21:3981. doi: 10.3390/ijms21113981

Oh, J. H., Karadeniz, F., Kong, C. S., and Seo, Y. (2020b). Antiphotoaging effect of 3,5-dicaffeoyl-epi-quinic acid against UVA-induced skin damage by protecting human dermal fibroblasts in vitro. *Int. J. Mol. Sci*. 21:7756. doi: 10.3390/ijms21207756

Parsons, P. A. (1996). The limit to human longevity: an approach through a stress theory of ageing. *Mech. Ageing Dev*. 87, 211–218. doi: 10.1016/0047-6374(96)01710-1

Paszek, M. J., Zahir, N., Johnson, K. R., Lakins, J. N., Rozenberg, G. I., Gefen, A., et al. (2005). Tensional homeostasis and the malignant phenotype. *Cancer Cell* 8, 241–254. doi: 10.1016/j.ccr.2005.08.010

Picard, F., Hersant, B., Niddam, J., and Meningaud, J. P. (2017). Injections of platelet-rich plasma for androgenic alopecia: a systematic review. *J. Stomatol. Oral Maxillofac. Surg*. 118, 291–297. doi: 10.1016/j.jormas.2017.06.011

Quan, T., Little, E., Quan, H., Qin, Z., Voorhees, J. J., and Fisher, G. J. (2013). Elevated matrix metalloproteinases and collagen fragmentation in photodamaged human skin: impact of altered extracellular matrix microenvironment on dermal fibroblast function. *J. Invest. Dermatol*. 133, 1362–1366. doi: 10.1038/jid.2012.509

Sawaya, A. P., Jozic, I., Stone, R. C., Pastar, I., Egger, A. N., Stojadinovic, O., et al. (2019). Mevastatin promotes healing by targeting caveolin-1 to restore EGFR signaling. *JCI Insight* 4:e129320. doi: 10.1172/jci.insight.129320

Seifert, A. W., Kiama, S. G., Seifert, M. G., Goheen, J. R., Palmer, T. M., and Maden, M. (2012). Skin shedding and tissue regeneration in African spiny mice (*Acomys*). *Nature* 489, 561–565. doi: 10.1038/nature11499

Sherratt, M. J. (2009). Tissue elasticity and the ageing elastic fibre. *Age (Dordr)* 31, 305–325. doi: 10.1007/s11357-009-9103-6

Shwartz, Y., Gonzalez-Celeiro, M., Chen, C. L., Pasolli, H. A., Sheu, S. H., Fan, S. M., et al. (2020). Cell types promoting goosebumps form a niche to regulate hair follicle stem cells. *Cell* 182, 578–593.e19. doi: 10.1016/j.cell.2020.06.031

Silver, F. H., Siperko, L. M., and Seehra, G. P. (2003). Mechanobiology of force transduction in dermal tissue. *Skin Res. Technol*. 9, 3–23. doi: 10.1034/j.1600-0846.2003.00358.x

Tabibzadeh, S. (2021). Cell-centric hypotheses of aging. *Front. Biosci. (Landmark Ed.)* 26, 1–49. doi: 10.2741/4888

Thomas, D. R. (2001). Age-related changes in wound healing. *Drugs Aging* 18, 607–620. doi: 10.2165/00002512-200118080-00005

Tobin, D. J. (2017). Introduction to skin aging. *J. Tissue Viability* 26, 37–46. doi: 10.1016/j.jtv.2016.03.002

Tracy, L. E., Minasian, R. A., and Caterson, E. J. (2016). Extracellular matrix and dermal fibroblast function in the healing wound. *Adv. Wound Care (New Rochelle)* 5, 119–136. doi: 10.1089/wound.2014.0561

Varani, J., Dame, M. K., Rittie, L., Fligiel, S. E., Kang, S., Fisher, G. J., et al. (2006). Decreased collagen production in chronologically aged skin: roles of age-dependent alteration in fibroblast function and defective mechanical stimulation. *Am. J. Pathol*. 168, 1861–1868. doi: 10.2353/ajpath.2006.051302

Wang, L., Siegenthaler, J. A., Dowell, R. D., and Yi, R. (2016). Foxc1 reinforces quiescence in self-renewing hair follicle stem cells. *Science* 351, 613–617. doi: 10.1126/science.aad5440

Wang, S., Drummond, M. L., Guerrero-Juarez, C. F., Tarapore, E., MacLean, A. L., Stabell, A. R., et al. (2020). Single cell transcriptomics of human epidermis identifies basal stem cell transition states. *Nat. Commun*. 11:4239. doi: 10.1038/s41467-020-18075-7

Watt, F. M., and Fujiwara, H. (2011). Cell-extracellular matrix interactions in normal and diseased skin. *Cold Spring Harb. Perspect. Biol*. 3:a005124. doi: 10.1101/cshperspect.a005124

Wong, V. W., Akaishi, S., Longaker, M. T., and Gurtner, G. C. (2011). Pushing back: wound mechanotransduction in repair and regeneration. *J. Invest. Dermatol*. 131, 2186–2196. doi: 10.1038/jid.2011.212

Wong, V. W., Longaker, M. T., and Gurtner, G. C. (2012). Soft tissue mechanotransduction in wound healing and fibrosis. *Semin. Cell Dev. Biol*. 23, 981–986. doi: 10.1016/j.semcdb.2012.09.010

Wu, M., Fannin, J., Rice, K. M., Wang, B., and Blough, E. R. (2011). Effect of aging on cellular mechanotransduction. *Ageing Res. Rev*. 10, 1–15. doi: 10.1016/j.arr.2009.11.002

Wulf, H. C., Sandby-Moller, J., Kobayasi, T., and Gniadecki, R. (2004). Skin aging and natural photoprotection. *Micron* 35, 185–191. doi: 10.1016/j.micron.2003.11.005

Yaar, M., and Gilchrest, B. A. (2007). Photoageing: mechanism, prevention and therapy. *Br. J. Dermatol*. 157, 874–887. doi: 10.1111/j.1365-2133.2007.08108.x

Yamada, M., and Prow, T. W. (2020). Physical drug delivery enhancement for aged skin, UV damaged skin and skin cancer: translation and commercialization. *Adv. Drug Deliv. Rev*. 153, 2–17. doi: 10.1016/j.addr.2020.04.008

Yang, L., van der Werf, K. O., Fitie, C. F., Bennink, M. L., Dijkstra, P. J., and Feijen, J. (2008). Mechanical properties of native and cross-linked type I collagen fibrils. *Biophys. J*. 94, 2204–2211. doi: 10.1529/biophysj.107.111013

Zhang, W., Qu, J., Liu, G. H., and Belmonte, J. C. I. (2020). The ageing epigenome and its rejuvenation. *Nat. Rev. Mol. Cell Biol*. 21, 137–150. doi: 10.1038/s41580-019-0204-5

Zhang, Z., Kruglikov, I., Zhao, S., Zi, Z., Gliniak, C. M., Li, N., et al. (2021). Dermal adipocytes contribute to the metabolic regulation of dermal fibroblasts. *Exp. Dermatol*. 30, 102–111. doi: 10.1111/exd.14181

Zhang, Z., Shao, M., Hepler, C., Zi, Z., Zhao, S., An, Y. A., et al. (2019). Dermal adipose tissue has high plasticity and undergoes reversible dedifferentiation in mice. *J. Clin. Invest*. 129, 5327–5342. doi: 10.1172/JCI130239

Zimber, M. P., Ziering, C., Zeigler, F., Hubka, M., Mansbridge, J. N., Baumgartner, M., et al. (2011). Hair regrowth following a Wnt- and follistatin containing treatment: safety and efficacy in a first-in-man phase 1 clinical trial. *J. Drugs Dermatol*. 10, 1308–1312.

Zou, Z., Long, X., Zhao, Q., Zheng, Y., Song, M., Ma, S., et al. (2020). A single-cell transcriptomic atlas of human skin aging. *Dev. Cell* doi: 10.1016/j.devcel.2020.11.002 [Epub Ahead of Print].

Zwick, R. K., Guerrero-Juarez, C. F., Horsley, V., and Plikus, M. V. (2018). Anatomical, physiological, and functional diversity of adipose tissue. *Cell Metab*. 27, 68–83. doi: 10.1016/j.cmet.2017.12.002

Conflict of Interest: The authors declare that the research was conducted in the absence of any commercial or financial relationships that could be construed as a potential conflict of interest.

Copyright © 2021 Harn, Chen, Wang, Lei and Chuong. This is an open-access article distributed under the terms of the Creative Commons Attribution License (CC BY). The use, distribution or reproduction in other forums is permitted, provided the original author(s) and the copyright owner(s) are credited and that the original publication in this journal is cited, in accordance with accepted academic practice. No use, distribution or reproduction is permitted which does not comply with these terms.

frontiers in Cell and Developmental Biology

ORIGINAL RESEARCH
published: 05 March 2021
doi: 10.3389/fcell.2021.632882

Establishment of an Efficient Primary Culture System for Human Hair Follicle Stem Cells Using the Rho-Associated Protein Kinase Inhibitor Y-27632

Lihong Wen[1†], Yong Miao[1†], Zhexiang Fan[1], Jiarui Zhang[1], Yixuan Guo[2], Damao Dai[1], Junfei Huang[1], Zhen Liu[1], Ruosi Chen[1] and Zhiqi Hu[1]**

[1] Department of Plastic and Aesthetic Surgery, Nanfang Hospital, Southern Medical University, Guangzhou, China,
[2] Department of Plastic and Burn Surgery, Shenzhen Hospital, Southern Medical University, Shenzhen, China

OPEN ACCESS

Edited by:
Mingxing Lei,
Chongqing University, China

Reviewed by:
Luis Villa-Diaz,
Oakland University, United States
Xunwei Wu,
Shandong University, China

***Correspondence:**
Ruosi Chen
chenrscy@hotmail.com
Zhiqi Hu
huzhiqidr163@i.smu.edu.cn

† These authors have contributed equally to this work

Specialty section:
This article was submitted to Stem Cell Research, a section of the journal Frontiers in Cell and Developmental Biology

Received: *24 November 2020*
Accepted: *15 February 2021*
Published: *05 March 2021*

Citation:
Wen L, Miao Y, Fan Z, Zhang J, Guo Y, Dai D, Huang J, Liu Z, Chen R and Hu Z (2021) Establishment of an Efficient Primary Culture System for Human Hair Follicle Stem Cells Using the Rho-Associated Protein Kinase Inhibitor Y-27632. Front. Cell Dev. Biol. 9:632882. doi: 10.3389/fcell.2021.632882

Background: Hair follicle tissue engineering is a promising strategy for treating hair loss. Human hair follicle stem cells (hHFSCs), which play a key role in the hair cycle, have potential applications in regenerative medicine. However, previous studies did not achieve efficient hHFSC expansion *in vitro* using feeder cells. Therefore, there is a need to develop an efficient primary culture system for the expansion and maintenance of hHFSCs.

Methods: The hHFSCs were obtained by two-step proteolytic digestion combined with microscopy. The cell culture dishes were coated with human fibronectin and inoculated with hHFSCs. The hHFSCs were harvested using a differential enrichment procedure. The effect of Rho-associated protein kinase (ROCK) inhibitor Y-27632, supplemented in keratinocyte serum-free medium (K-SFM), on adhesion, proliferation, and stemness of hHFSCs and the underlying molecular mechanisms were evaluated.

Results: The hHFSCs cultured in K-SFM, supplemented with Y-27632, exhibited enhanced adhesion and proliferation. Additionally, Y-27632 treatment maintained the stemness of hHFSCs and promoted the ability of hHFSCs to regenerate hair follicles *in vivo*. However, Y-27632-induced proliferation and stemness in hHFSCs were conditional and reversible. Furthermore, Y-27632 maintained propagation and stemness of hHFSCs through the ERK/MAPK pathway.

Conclusion: An efficient short-term culture system for primary hHFSCs was successfully established using human fibronectin and the ROCK inhibitor Y-27632, which promoted the proliferation, maintained the stemness of hHFSCs and promoted the ability to regenerate hair follicles *in vivo*. The xenofree culturing method used in this study provided a large number of high-quality seed cells, which have applications in hair follicle tissue engineering and stem cell therapy.

Keywords: human hair follicle stem cells, hair follicle tissue engineering, Y-27632, primary culture system, ERK/MAPK pathway

INTRODUCTION

Alopecia results from various factors that decrease the regeneration ability of hair follicles and disrupt the hair cycle (York et al., 2020). Hair transplantation is one of the treatment strategies for hair loss. However, hair transplantation does not provide satisfactory therapeutic outcomes for large-scale hair loss (Vasserot et al., 2019). Although surgical procedures can redistribute hair follicles, they cannot reconstruct the hair follicles. Recent advances in hair tissue engineering have enabled effective treatment of hair loss, especially in cases of large-scale hair loss with insufficient donor hair follicles (Coelho et al., 2012; Owczarczyk-Saczonek et al., 2018). A prerequisite for efficient hair tissue engineering is the availability of seed cell source (Mistriotis and Andreadis, 2013).

Hair follicle stem cells (HFSCs), which are located at the base of the upper permanent portion of the follicular outer root sheath, are involved in mediating the different stages of the hair cycle, namely catagen, telogen, and anagen stages (Ohyama et al., 2006; Jimenez et al., 2011; Myung and Ito, 2012). In the human hair follicles, the HFSCs are characterized by the expression of various immunohistochemical markers, including cytokeratin-15 (CK15), cytokeratin-19 (CK19), and CD200 (Owczarczyk-Saczonek et al., 2018). HFSCs, which are located in easily accessible locations of the human body, exhibit innate characteristics of complete self-renewal and multipotency (ability to differentiate into various lineages) (Myung et al., 2009a,b; Yang et al., 2017). The important characteristic makes HFSCs valuable candidates for regenerative medicine beyond hair and skin regeneration, and wound healing (Mistriotis and Andreadis, 2013; Lim et al., 2018).

Several researchers have been culturing stem cells on 3T3 feeder layers, a technique established by Barrandon and Green (1987), for the last several decades. HFSCs, which are quiescent *in vivo*, rapidly proliferate upon *in vitro* culturing on feeder layers. However, the *in vitro* culturing of HFSCs results in the rapid loss of stem cell characteristics (Blanpain et al., 2004). Some studies have defined the culturing conditions that allow the expansion and maintenance of HFSCs (Chacon-Martinez et al., 2017). The primary culturing of HFSCs in the presence of epithelial growth factor is the most common approach to culture pluripotent cells. However, the cells cultured under these conditions have a poor proliferative ability and tend to differentiate after several passages *in vitro*. Only a little studies have focused on culturing HFSCs from human occipital scalp skin. The use of feeder layers and other matrix Matrigel extracted from mouse sarcoma is associated with the risk of transmission of unknown zoonoses and consequently limits clinical application (Limat et al., 1989). Therefore, there is a need to develop a new culture model for propagating human hair follicle stem cells (hHFSCs).

Rho GTPases and their downstream effectors, such as Rho kinases, are involved in cell adhesion, proliferation, migration, differentiation, and apoptosis through the regulation of the cell microenvironment (David et al., 2012). The Rho-associated protein kinase (ROCK) inhibitor Y-27632 is reported to exert diverse effects on cellular behavior by competing with ATP to bind to the Rho kinase adenosine triphosphate (ATP)-binding pocket (Takahara et al., 2003). Y-27632 can enhance the survival of stem cells from a variety of sources and protect the cultured stem cells from death during cell passage (Watanabe et al., 2007; Terunuma et al., 2010; Wen et al., 2018). Recently, Chapman et al. (2010) demonstrated that culturing human keratinocytes in the presence of Y-27632 markedly increased their proliferation and promoted immortalization. Pakzad et al. (2010) suggested the application of Y-27632, an inhibitor of Rho that regulates various cellular functions, including apoptosis and promoting the interaction of stem cells, to culture the pluripotent stem cells.

To the best of our knowledge, only one study has investigated the Y-27632-mediated regulation of HFSCs isolated from mouse vibrissae. Currently, there are no studies that have evaluated the effects of Y-27632 on the behaviors of HFSCs sourced from human occipital scalp skin (An et al., 2018). In contrast to murine HFSCs that are enriched with CD34-positive stem cells, CD34 is not the major stem cell marker in hHFSCs (Trempus et al., 2003). The hHFSCs express several markers, including CK15, CK19, and CD200 (Owczarczyk-Saczonek et al., 2018). Therefore, the studies on mouse HFSCs cannot be translated to the clinic for treating human diseases, due to the difference in the behaviors of hHFSCs and murine HFSCs. Here, we investigated the effects of Y-27632 on the proliferation, stemness maintenance of hHFSCs and ability to regenerate hair follicles *in vivo* and the underlying mechanisms. This study aimed to establish a novel culture model for hHFSCs using a ROCK inhibitor and to examine the potential application of Y-27632 for the efficient expansion of hHFSCs in hair tissue engineering.

MATERIALS AND METHODS

Tissue Specimens

The occipital scalp skin samples were obtained from discarded tissue of healthy adults (20 men and 3 women; aged 22–39 years old) who underwent selective cosmetic surgery. Ethical approval were obtained from the Medical Ethical Committee of Southern Medical University.

Animals

Female adult (4–6 weeks old) athymic nude mice (Balb/cAJcl-nu) and newborn C57BL/6J mice were purchased from the Experimental Animal Center of Southern Medical University (Guangzhou, China). All animal studies were conducted under the approval of the Animal Care and Use Committee at the International Medical Center to reduce suffering and provide for the full protection of animal welfare.

Culturing of hHFSCs

The human scalp samples were rinsed thrice with phosphate-buffered saline (PBS) and the bulge of the hair follicle between the isthmus and the upper part of the hair bulb was separated using microscissors under an MZ8 dissecting microscope (Leica Microsystems, Wetzlar, Germany). The isolated bulge tissue was treated with 0.1% Dispase (Invitrogen, Carlsbad, CA, United States) for 45 min following a previously published

protocol (Roh et al., 2005; Garza et al., 2011; Call et al., 2018). The epidermis and dermis were separated and the individual hair shafts, surrounding follicles, and surrounding interfollicular epidermis were simultaneously removed. The isolated epidermis was then washed with PBS and treated with 0.025% trypsin (Gibco, Gaithersburg, MD, United States) for 10 min at 37°C. The samples were vortexed and filtered through a 70 μm filter (Corning, Corning, NY, United States). Next, the filtered samples were centrifuged at 200 *g* for 5 min, seeded in six-well plates coated with 10 μg/mL human fibronectin (Sigma-Aldrich, St. Louis, MO, United States), and cultured in defined keratinocyte serum-free medium (K-SFM, Gibco) (Hakala et al., 2009). The hHFSCs were purified from a mixed population of outer root sheath cells using a differential enrichment procedure. Briefly, the suspended cells were plated onto culture dishes and incubated for 15 min. The cells in the culture medium that exhibited delayed attachment were transferred to a new culture dish.

To passage the cells, the cells were digested using 0.025% trypsin and centrifuged at 300 × g for 5 min after the culture reached a confluency of 80%. The cell pellets were suspended in the corresponding medium and plated onto other cell culture dishes.

Flow Cytometry

Single-cell suspensions were prepared from the cultured cells as described above. The cells were rinsed once with PBS and incubated with anti-ITGα6 (1:200, eBioscience, San Diego, CA, United States) and anti-CD200 (1:200, eBioscience) antibodies for 30 min on ice. Next, the cells were washed twice with fluorescent-activated cell sorting buffer (2% fetal calf serum and 2 mM ethylenediaminetetraacetic acid in PBS), and analyzed using an LSRFortessa (BD Biosciences, San Jose, CA, United States) flow cytometer. The flow cytometric data were analyzed using FlowJo software version 10 (BD Biosciences).

Cell Adhesion Assay

To each well of the 24-well plates, 10 μg/mL of fibronectin was added and the plates were incubated at 4°C overnight. The plates were washed thrice with PBS. Next, PBS containing 1% bovine serum albumin (BSA, Sigma) was added to each well and the plate was incubated at 37°C for 1 h. The plates were then washed thrice with PBS. The hHFSCs (1×10^5) were seeded in 24-well plates and treated with 0, 5, 10, or 20 μM Y-27632 (Targetmol, Wellesley Hills, MA, United States) in K-SFM at 37°C for 1 h. The medium containing the non-adherent cells was aspirated. The adherent cells were gently washed with PBS, fixed with methyl alcohol (Solarbio, Beijing, China), and stained with crystal violet (Solarbio). Images were captured using a microscope (Axio Zoom V16, Zeiss, Jena, Germany).

Cytotoxicity Assay

The hHFSCs were cultured in cell culture dishes, as described above, for 24 h. The culture medium was removed and the cells were treated with 0, 5, 10, or 20 μM Y-27632 in fresh K-SFM for 72 h. The cytotoxicity of Y-27632 was examined using the LIVE/DEAD® Viability/Cytotoxicity kit (Invitrogen) according to the manufacturer's instructions. The images were captured using a fluorescence microscope (IX73 FL, Olympus, Tokyo, Japan).

Cell Proliferation Assay

The effect of Y-27632 on hHFSC proliferation was examined using the 5-ethynyl-2′-deoxyuridine (EdU) labeling assay. The hHFSCs (2×10^5 cells per well) seeded in a 24-well plate were treated with 0, 5, 10, or 20 μM Y-27632 in K-SFM for 3 days. Next, the cells were treated with EdU (Ribobio Co., Ltd., Guangzhou, China) for 12 h, fixed, and stained with 1X Apollo567 for 30 min in the dark. The cells were counterstained with Hoechst and imaged using a fluorescence microscope (IX73 FL, Olympus) equipped with a camera. The proliferation rate was assessed by counting the proportion of EdU-positive nuclei (red) among the nuclei exhibiting blue fluorescence (six random microscopic fields were evaluated in each well). The data were obtained from five independent experiments.

Colony Formation Assay

The hHFSCs (1×10^4 cells per well) seeded in six-well plates were stimulated with 0, 5, 10, or 20 μM Y-27632 for 5 days. The cells were fixed in 4% paraformaldehyde (Solarbio) for 30 min. The total number of colonies was counted after staining with crystal violet for 15 min. The ability of hHFSCs, subjected to different treatments, to form colonies (groups of 50 or more adhering cells derived from the same mother cell) was assessed.

Immunocytochemistry and Immunohistochemistry

The cells were seeded (1×10^4 cells per well) in 24-well plates and cultured until approximately 30% confluency. Next, the cells were fixed in 4% paraformaldehyde and permeabilized with 0.1% Triton X-100 (Solarbio) in PBS for 10 min at room temperature. Further, the cells were blocked with 3% BSA in PBS and incubated with anti-CK15 (1:200, Abcam) and anti-CK19 (1:200, Abcam) antibodies in 1% BSA overnight at 4°C, followed by incubation with Cy3 anti-mouse secondary antibodies (1:500, Beyotime Institute of Biotechnology, Jiangsu, China) or Alexa Fluor® 488-labeled anti-rabbit secondary antibodies (1:500, Abcam) in the dark for 1 h at room temperature. The nuclei were stained with 4, 6-diamino-2-phenylindole (1:200, eBioscience). The images were captured using a fluorescent microscope (BX63, Olympus) equipped with a digital camera. The negative control comprised cells incubated with secondary antibody alone. The consecutive human scalp sections were immunohistochemically stained with anti-cytokeratin 15 (1:50, Abcam) antibody, following a previously described protocol (Inoue et al., 2009).

Histochemical Staining

The explanted hair follicles with attached surrounding tissue were fixed in 10% buffered formalin and embedded in paraffin wax. Next, the 5 μm thick sections were stained with hematoxylin and eosin (Solarbio) following standard procedures for visual identification and assessment of structural integrity of hair follicles, using a microscope (BX51, Olympus).

Quantitative Real-Time Polymerase Chain Reaction (qRT-PCR)

Total RNA was extracted from the cells subjected to different treatments, using Trizol (Takara, Tokyo, Japan). The mRNA was reverse-transcribed to complementary DNA (cDNA) using the PrimeScript RT-PCR kit (Takara) according to the manufacturer's s instructions. The qRT-PCR analysis was performed with SYBR Premix Ex Taq II (Tli RNaseH Plus; Takara) in a Light Cycle Roche 480 II Real-time PCR system (Roche, Basel Switzerland) in triplicate. The primer sequences used for qRT-PCR analysis are listed in **Table 1**. The expression levels of target genes were normalized to those of *GAPDH*. The relative expression level was calculated using the $2^{-\Delta\Delta Ct}$ method.

Western Blotting

Total proteins were extracted from cells using radioimmunoprecipitation assay (RIPA) lysis buffer (Beyotime, Shanghai, China) supplemented with protease and phosphatase inhibitor cocktail (Roche), following the manufacturer's instructions. The protein concentration was determined using the bicinchoninic acid protein assay kit (Thermo Scientific). The protein sample mixed with sodium dodecyl sulfate-polyacrylamide gel electrophoresis (SDS-PAGE) loading buffer was subjected to denaturation at 100°C for 5 min. Equal amounts of proteins (20 μg) were subjected to SDS-PAGE. The resolved proteins were transferred to a polyvinylidene fluoride membrane (Millipore). The membrane was blocked with non-fat dry milk for 1 h and incubated with the following primary antibodies overnight at 4°C: mouse anti-CK15 (1:1,000; Abcam), rabbit anti-CK19 (1:1,000; Abcam), rabbit anti-ERK1/2 (1:1,000; Cell Signaling Technology), rabbit anti-phospho-ERK1/2 (1:1,000; Cell Signaling Technology), and anti-GAPDH (1:10,000; Proteintech) antibodies. Next, the membrane was incubated with horseradish peroxidase-labeled secondary antibodies (1:2,000; Beyotime) for 1 h at room temperature. The membrane was washed thrice with tris-buffered saline containing 1% Tween-20. The immunoreactive bands were visualized using enhanced chemiluminescence reagents (Millipore). The level of target proteins was normalized to that of GAPDH before statistical analysis. The Image J 1.44 software (NIH, Bethesda, Maryland, United States) was used to quantify protein expression.

In vivo Hair Regeneration

Neonatal epidermal cells and dermal cells were prepared as described previously (Xiao et al., 2016). Briefly, the trunk skin of neonatal C57BL/6J mice was mechanically separated and digested with 0.1% Dispase at 37°C for 1 h. The skin specimen was then divided into epidermis and dermis using forceps. The epidermis was minced and digested in 0.025% trypsin at 37°C for 10 min and the dermis was minced and digested in 0.2% collagenase (Sigma-Aldrich, St. Louis, MO, United States) at 37°C for 1 h. After digestion, an equal volume of 10% FBS in DMEM was added to terminate the reaction, and the samples were filtered through 70 μm strainers. Following centrifugation and washing, murine neonatal epidermal cells and dermal cells were obtained.

For *in vivo* implantation, five groups were arranged for this experiment as (1) pre-prepared murine neonatal dermal cells alone (as negative control), (2) a mixture of murine neonatal epidermal cells and murine neonatal dermal cells (as positive control), (3 and 4) a mixture of P1 hHFSCs with or without 10 μM Y-27632 and pre-prepared murine neonatal dermal cells and (5) a mixture of P3 hHFSCs with 10 μM Y-27632 and pre-prepared murine neonatal dermal cells. Unless otherwise stated for each intracutaneous injection, 1×10^6 dermal cells and 5×10^5 epidermal cells or hHFSCs were resuspended (50 μL of DMEM) and injected (29-gauge needle, BD Biosciences) into the hypodermis of nude mice, forming a bleb. After 3 weeks, the skin at the injection spot was dissected. The number of hair follicles formed was quantified by microscopic photography and morphometry. The hair reconstruction by hHFSCs was confirmed in Paraffin section via immunohistochemically stained by the human-specific marker (anti-HLAA, 1:100, Abcam).

TABLE 1 | Primer sequences for qRT-PCR.

Gene	Forward primer (5′–3′)	Reverse primer (5′–3′)
GAPDH	GCACCGTCAAGGCTGAGAAC	TGGTGAAGACGCCAGTGGA
CK15	GACGGAGATCACAGACCTGAG	CTCCAGCCGTGTCTTTATGTC
CK19	AACGGCGAGCTAGAGGTGA	GGATGGTCGTGTAGTAGTGGC
Nanog	CAGAAGGCCTCACACCTAC	ATTGTTCCAGGTCTGGTTGC
Oct4	CACTGTACTCCTCGGTCCCTTTC	CAGGCACCTCAGTTTGAATGC

Statistical Analysis

All statistical analyses were performed using the GraphPad Prism 8 software (GraphPad Software, Inc., La Jolla, CA, United States). The data are expressed as mean ± standard deviation. Data from each experimental condition were analyzed for normality using the Kolmogorov–Smirnov test. The data were analyzed using the Wilcoxon test and *t*-test. The difference was considered significant at $p < 0.05$. Each experiment was repeated at least three times.

RESULTS

Primary Culture of hHFSCs From the Occipital Scalp Skin

The bulge zone of human hair follicles from the occipital scalp skin was identified based on CK15 and CK19 immunoreactivities. As described previously, the bulge zone was identified below the entrance of the sebaceous duct into the follicle at an average depth of 1 mm below the skin surface extending to a depth of 1.8 mm just below the arrector pili muscle insertion (Oh et al., 2011; **Figures 1A–C**). Differential interference contrast microscopy and histological examinations revealed that the plucked human hair follicles were intact with minimal dermal contamination. The follicular epithelium was trypsinized and filtered to obtain a single-cell suspension containing cells of varying sizes and shapes. The dissociated single cells were harvested using centrifugation, cultured in K-SFM, and purified using a differential enrichment procedure. After 3 days, the pre-attached cells appeared as clustered colonies comprising cells

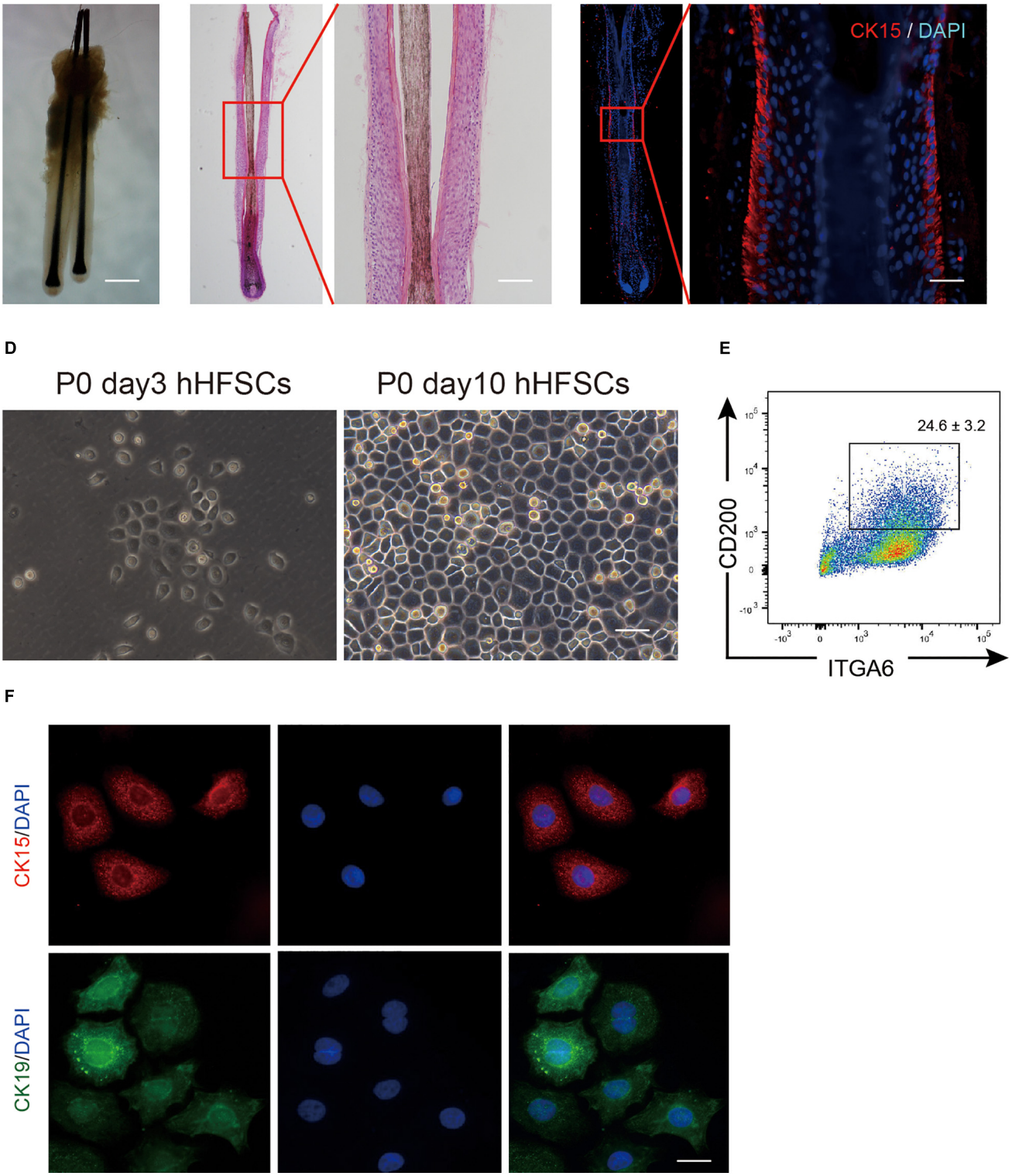

FIGURE 1 | Isolation and cultivation of hHFSCs. **(A)** Morphology of intact human hair follicles from the occipital scalp skin. Scale bars: 200 μm. **(B)** Morphology of an intact human hair follicle examined using H&E staining. Scale bars: 100 μm. **(C)** Section immunostained with anti-CK15 antibody showing the biological bulge zone. Scale bars: 50 μm. **(D)** Morphology of P0 hHFSCs cultured for 3 and 10 days. Scale bars: 100 μm. **(E)** Representative flow cytometry plots of P0 hHFSCs cultured in K-SFM. **(F)** Immunofluorescence analysis of CK15 and CK19 in the attached hHFSCs. Scale bars: 25 μm. All data are presented as mean ± standard deviation from at least three independent experiments. hHFSCs, human hair follicle stem cells; H&E, hematoxylin and eosin, K-SFM, keratinocyte serum-free medium.

with keratinocyte-like morphology with a large nucleus and a high nuclear-to-cytoplasmic ratio (**Figure 1D**). The P0 hHFSCs from occipital scalp skin comprised 24.6 ± 3.2% $CD200^+$ ITGα 6^+ HFSCs (**Figure 1E**). Immunofluorescence staining identified the stem cell markers CK15 and CK19 in hHFSCs (**Figure 1F**).

Y-27632 Promotes Cell Adhesion of hHFSCs in Primary Culture

Most single cells did not adhere to the plate and gradually died at the initial stages of the primary culture of hHFSCs. A few cells attached to the plate and continued to grow slowly as a monolayer. To investigate the effect of Y-27632 on the adhesion of hHFSCs, P0 hHFSCs were cultured in K-SFM supplemented with 0, 5, 10, or 20 μM Y-27632, for 1 h. The results of the cell adhesion assay indicated that Y-27632 dose-dependently promoted the adhesion of hHFSCs. The adhesion of hHFSCs treated with 10 and 20 μM of Y-27632 was not significantly different. However, the adhesion of hHFSCs treated with 10 μM Y-27632 was higher than that of hHFSCs treated with 5 μM Y-27632 (**Figures 2A,B**).

Y-27632 Promoted the Proliferation of hHFSCs

The cytotoxicity of different concentrations of Y-27632 against hHFSCs was determined using the LIVE/DEAD kit. Treatment with 0, 5, 10, or 20 μM of Y-27632 did not significantly affect the viability of hHFSCs (**Figures 2C,D**). The results of the EdU labeling assay revealed that the proportion of EdU-positive cells in the hHFSCs treated with 5, 10, and 20 μM Y-27632 (7.65 ± 0.63, 11.35 ± 1.17, and 10.28 ± 1.26%, respectively) was significantly higher than that in the negative control group (5.84 ± 0.96%; $p < 0.01$). The optimal concentrations of Y-27632 to promote hHFSC proliferation were 10 and 20 μM (**Figures 2E,F**).

Treatment with Y-27632 significantly increased the number of colony-forming units of hHFSCs (>50 cells/colony). Additionally, the colonies exhibited an enlarged morphology (>100 cells/colony) (**Figures 2G,H**). The number of colonies derived from cells treated with 10 μM Y-27632 (123.30 ± 7.57 colonies/well) was not significantly different from that derived from cells treated with 20 μM Y-27632 (115.30 ± 5.03 colonies/well) ($p > 0.001$). This indicated that 10 and 20 μM Y-27632 significantly promoted the proliferation of hHFSCs. For further experiments, 10 μM Y-27632 was used.

Y-27632 Maintained the Stemness of hHFSCs

The effect of Y-27632 on the stemness of hHFSCs was analyzed by examining the two stemness markers using immunocytochemistry. Compared with the control group, treatment with 5, 10, and 20 μM Y-27632 significantly increased the number of CK15-labeled hHFSCs ($p < 0.01$). Furthermore, the expression of CK15 in the cells treated with 10 μM and 20 μM Y-27632 was higher than that in the control group (**Figures 3A,B**). The expression of markers in hHFSCs was also detected using qRT-PCR and western blotting. The expression levels of CK15 and CK19 in the cells treated with Y-27632 were significantly higher than those in the control group (**Figure 3C**). The results of qRT-PCR analysis were consistent with those of western blotting (**Figure 3D**). Nanog and Oct4 are reported to contribute to the self-renewal of stem cells (Yu et al., 2006; Liu et al., 2019; Lu et al., 2019). The qRT-PCR analysis showed that the expression levels of Nanog and Oct4 in the cells treated with Y-27632 were significantly higher than those in the control group (**Figure 3E**).

Effect of Y-27632 on hHFSCs Was Conditional

Next, the effect of continuous ROCK inhibition on the proliferation of hHFSCs was examined. The cells were cultured in the presence of Y-27632 for 3 days and the inhibitor was removed thereafter. In the absence of Y-27632, the hHFSCs exhibited a delayed growth and reached senescence quickly, as evidenced by the disintegration of the nuclear membrane. However, the hHFSCs treated with 10 μM Y-27632 exhibited logarithmic growth (**Figure 4A**). The EdU labeling assay was performed to detect the effect of Y-27632 removal from the culture medium on the proliferation of hHFSCs. The proportion of EdU-positive cells among the cells cultured in the absence of Y-27632 was lower than that among the cells cultured in the presence of 10 μM Y-27632 (**Figures 4B,C**). Immunocytochemistry analysis was performed 3 days after the removal of Y-27632 to examine the expression of stemness markers of hHFSCs. The expression levels of CK15 and CK19 were downregulated in the clustered colonies at 72 h post-Y-27632 withdrawal (**Figures 4D,E**).

Conversely, Y-27632 was added to hHFSCs that had been cultured for 3 days in the absence of Y-27632. The rate of proliferation increased immediately even in the cells that were only a few cell divisions from reaching senescence (**Figures 4B,C**). The expression levels of CK15 and CK19 were also upregulated (**Figure 4F**). These results suggest that ROCK inhibition is necessary for the propagation and maintenance of hHFSCs *in vitro*.

Y-27632 Maintained hHFSCs Propagation and Stemness Through the ERK Signaling Pathway

Next, we examined the signaling pathways that mediate the mechanisms underlying Y-27632-induced cell proliferation and stemness maintenance. The mitogen-activated protein kinase (MAPK) cascades are central signaling elements that regulate cell proliferation and differentiation. The Y-27632-induced proliferation of hHFSCs was significantly inhibited upon treatment with 2.5, 5, or 10 μM of U0126, an inhibitor of extracellular signal-regulated kinase 1/2 (ERK) (**Figures 5A,B**). Then, we tested whether 10 μM of U0126 could downregulated the expression of stemness marker induced by Y-27632 on hHFSCs using qRT-PCR and western blotting. The results showed that the increased CK15 and CK19 expression induced by Y-27632 was blocked by U0126 (**Figures 5C–E**).

The mechanism underneath on the effect of Y-27632 was examined using western blotting. The hHFSCs were stimulated

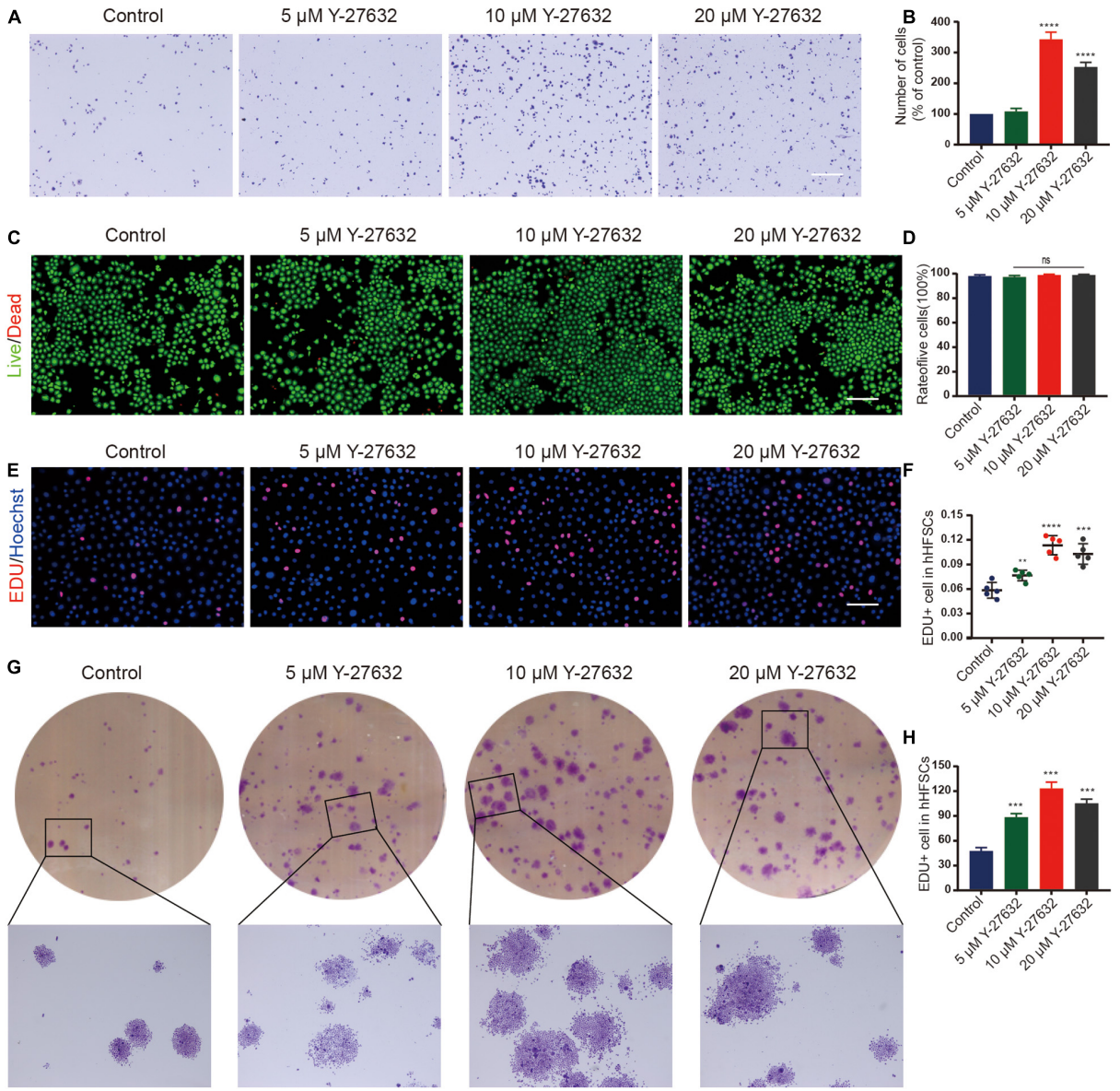

FIGURE 2 | Y-27632 promoted the adhesion and proliferation of hHFSCs. **(A,B)** The hHFSCs treated with 0, 5, 10, or 20 μM of Y-27632 were subjected to cell adhesion assay. Scale bars: 250 μm. **(C)** Live/dead staining of hHFSCs on day 5 of culturing. Live and dead cells are shown in green and red, respectively; Scale bars: 100 μm. **(D)** The proportion of live hHFSCs was not significantly different among the treatment groups ($p > 0.05$). **(E)** The hHFSCs treated with or without Y-27632 were subjected to the EdU labeling assay [EdU-positive (red); Hoechst (blue)]. Scale bars: 50 μm. **(F)** The proportion of EdU-positive cells in the Y-27632-treated group was significantly higher than that in the control group. **(G,H)** Colony formation assays further confirmed that the proliferation of hHFSCs was significantly upregulated upon treatment with Y-27632. All data are presented as mean ± standard deviation from at least three independent experiments. Student's *t*-test. ns, not significant; hHFSCs, human hair follicle stem cells; EdU, 5-ethynyl-2′-deoxyuridine. $^{**}p < 0.01$, $^{***}p < 0.001$, and $^{****}p < 0.0001$.

with 10 μM Y-27632 for 0, 10, 20, and 30 min. Y-27632 upregulated ERK phosphorylation at 10 min post-stimulation with a peak level at 20 min and gradually downregulated ERK phosphorylation thereafter (**Figure 5F**). The effect of U0126 on Y-27632-induced ERK activity was examined by evaluating ERK phosphorylation in the presence or absence of 10 μM U0126. Western blotting analysis revealed that the phosphorylation level of ERK decreased upon treatment with 10 μM U0126 (**Figure 5G**). These results indicate that the ERK/MAPK signaling pathways mediate Y-27632-induced hHFSC proliferation and stemness maintenance.

Y-27632 Promoted hHFSCs on the Capability of Regenerating Hair Follicles *in vivo*

We further performed functional analysis on the hHFSCs with Y-27632 using a reconstitution assay, which tests the ability

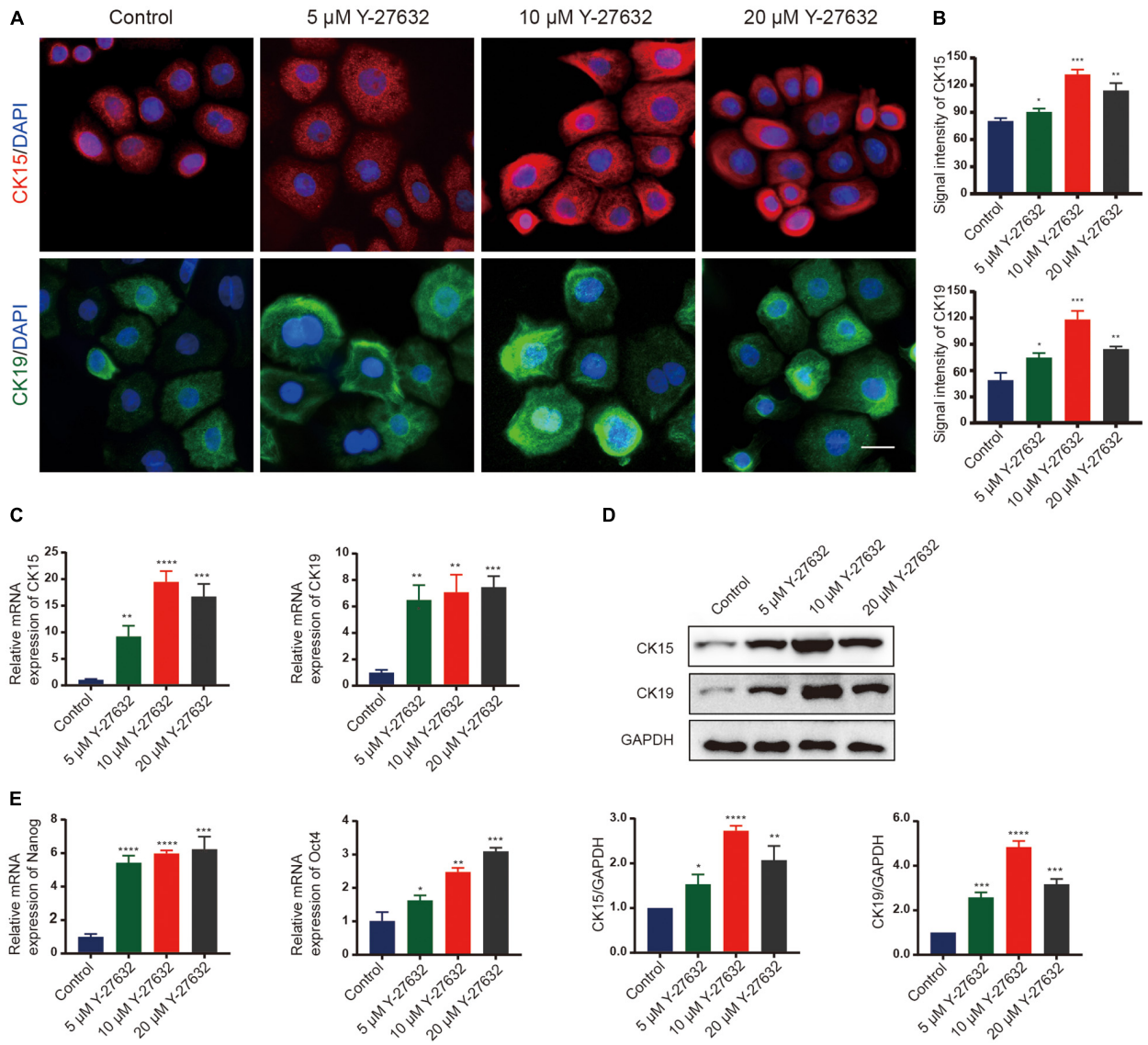

FIGURE 3 | Y-27632 maintained the stemness of hHFSCs. **(A)** Immunofluorescence staining of P1 hHFSCs was performed on day 5 of culturing. Scale bars: 25 μm. **(B)** The signal intensities of CK15 and CK19 in hHFSCs in the Y-27632-treated group were significantly higher than those in the control group. **(C)** Y-27632 upregulated the expression levels of CK15 and CK19 after 5 days of treatment. **(D)** Western blotting analysis of CK15 and CK19 expression levels. **(E)** The qRT-PCR analysis of Nanog and Oct4 mRNA expression. The qRT-PCR results are shown as fold-change relative to the expression in Y-27632-treated hHFSCs. hHFSCs, human hair follicle stem cells; qRT-PCR, quantitative real-time polymerase chain reaction. $^{*}p < 0.05$, $^{**}p < 0.01$, $^{***}p < 0.001$, and $^{****}p < 0.0001$.

of hHFSCs to regenerate hair follicles. We observed that the negative control groups which were only grafted with neonatal dermal cells did not exhibit new hair formation. Similar to positive control groups, *de novo* hair shafts were induced in recipient sites after 3 weeks of implantation in experimental groups which were grafted with a mixture of hHFSCs with or without Y-27632 and neonatal dermal cells. From stereoscopic observation, both P1 hHFSCs cultured in general medium and P1 hHFSCs treated with Y-27632 could induced hair follicles (**Figure 6A**). The morphology of the *de novo* hair follicles were intact, including the dermal papilla, matrix cells and other epithelial tissue (**Figure 6C**). Obviously, significantly more hair follicles formed in the group treated with Y-27632 than those in the control group (**Figures 6A,B**). Furthermore, Y-27632 maintained the multipotency of hHFSCs after several passages. The results showed that P3 hHFSCs with Y-27632 can also displayed an ideal HF inductivity (**Figures 6A,B**).

To investigate the internal structures of the reconsitituted skin, we performed tissue sectioning and HE staining. Histologic sectioning exhibited that a large number of mature HFs distributed within the hypodermic layer in the positive group and experimental groups (**Figure 6D**). Immunohistochemically staining showed positive expression of human-specific marker in the hair follicle cells differentiated by hHFSCs (**Figure 6E**).

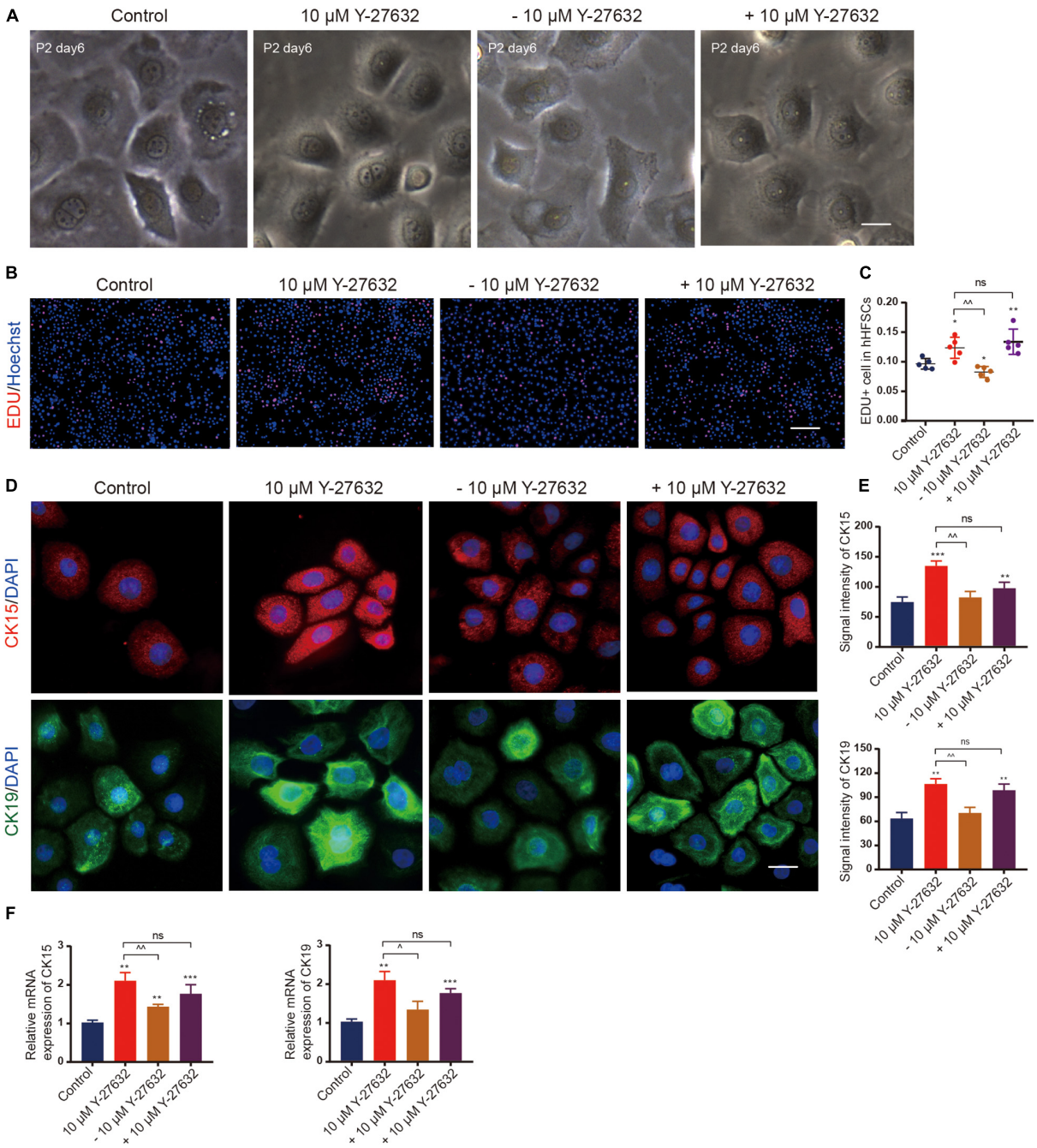

FIGURE 4 | The effect of Y-27632 on hHFSCs was conditional. **(A)** Morphology of P2 hHFSCs cultured for 6 days with or without Y-27632. Scale bars: 25 μm. **(B)** The hHFSCs treated with or without Y-27632 were subjected to the EdU labeling assay [EdU-positive (red); Hoechst (blue)]. Scale bars: 100 μm. **(C)** The proportion of EdU-positive cells in the Y-27632-treated group was significantly higher than that in the control group or Y-27632 withdrawal group. **(D)** Immunofluorescence staining of P2 hHFSCs was performed on day 5 of culturing. Scale bars: 50 μm. **(E)** The signal intensities of CK15 and CK19 in the Y-27632-treated group were significantly higher than those in the control group or Y-27632 withdraw group. **(F)** The qRT-PCR analysis of CK15 and CK19 mRNA expression. ns, not significant; hHFSCs, human hair follicle stem cells; EdU, 5-ethynyl-2′-deoxyuridine; qRT-PCR, quantitative real-time polymerase chain reaction. *compared with the control group; ^Y-27632-treated group vs. other experimental groups. *$p < 0.1$, **$p < 0.01$, ***$p < 0.001$, ^$p < 0.1$, ^^$p < 0.01$, and ^^^$p < 0.001$.

DISCUSSION

An ideal stem cell culture system should preserve the viability, promote proliferation, and maintain the stemness of hHFSCs, which are the major requirements for obtaining high-quality seed cells in hair follicle tissue engineering. In this study, we successfully established a xenofree primary culture system for hHFSCs. The hHFSCs cultured in K-SFM supplemented

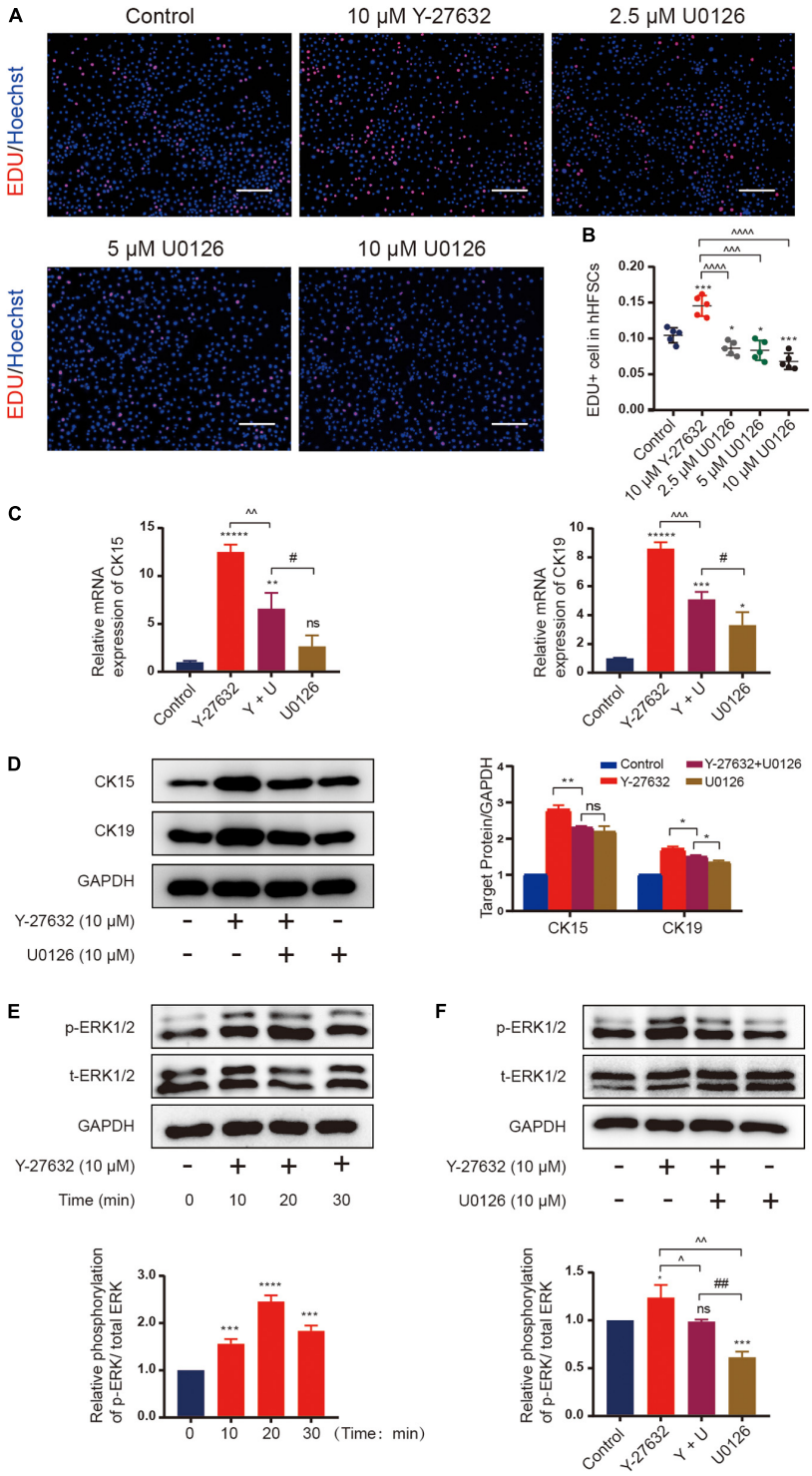

FIGURE 5 | Y-27632 maintained hHFSCs propagation and stemness through the ERK signaling pathway. **(A)** The hHFSCs treated with Y-27632 (10 μM) and 2.5, 5, or 10 μM U0126 (ERK inhibitor) for 72 h were subjected to the EdU labeling assay. Scale bars: 100 μm. **(B)** The proportion of EdU-positive cells significantly decreased upon treatment with U0126. **(C)** The increased mRNA expression of CK15 and CK19 induced by 10 μM Y-27632 was blocked by 10 μM U0126. **(D)** Western blotting analysis of CK15 and CK19 expression levels. **(E)** The hHFSCs were treated with 10 μM Y-27632 for 0, 10, 20, and 30 min and subjected to western blotting analysis to examine the level of p-ERK. **(F)** The p-ERK level was evaluated in the presence or absence of 10 μM U0126. U0126 attenuated Y-27632-induced ERK activity. hHFSCs, human hair follicle stem cells; EdU, 5-ethynyl-2′-deoxyuridine; qRT-PCR, quantitative real-time polymerase chain reaction. Data are presented as the mean ± standard error of mean from three independent experiments. *Compared with the control group; ˆY-27632-treated group vs. other experimental groups; #U0126-treated group vs. other experimental groups. $^{*}p < 0.05$, $^{**}p < 0.01$, $^{***}p < 0.001$, $^{****}p < 0.0001$, $^{*****}p < 0.00001$, $\hat{}p < 0.1$, $\hat{\hat{}}p < 0.01$, $\hat{\hat{}}\hat{}p < 0.001$, $\hat{\hat{}}\hat{\hat{}}p < 0.0001$, and $^{\#\#}p < 0.01$.

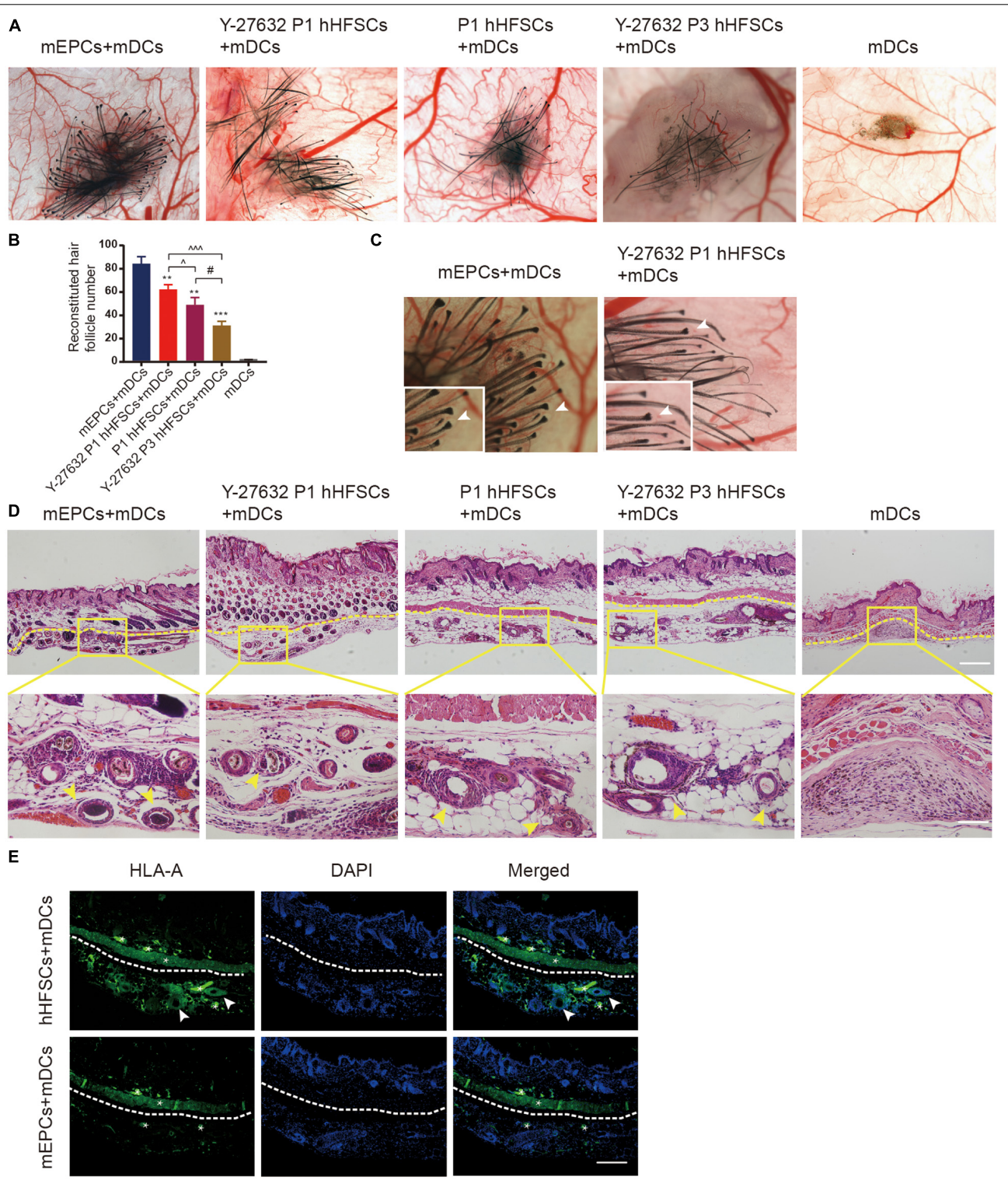

FIGURE 6 | Y-27632 promoted hHFSCs on the capability of regenerating hair follicles *in vivo*. **(A)** Stereoscopic images of recipient sites after 3 weeks post-transplant. **(B)** Analysis of the reconstituted hair follicle number among the negative group, the positive group and experimental groups. **(C)** The morphology of the *de novo* hair follicles were intact. **(D)** Histochemical staining of reconsitituted skin (the yellow dotted line divides the injection area and mouse skin) exhibited a large number of mature HFs in the positive group and experimental groups. Scale bars: 100 μm. **(E)** Immunohistochemically staining showed positive expression of human-specific marker in the hair follicle cells differentiated by hHFSCs. *non-specificity staining. Scale bars: 100 μm. mEPCs, murine neonatal epidermal cells; mDCs, murine neonatal dermal cells; hHFSCs, human hair follicle stem cells. *compared with the positive control group; ^Y-27632-treated P1 group vs. other experimental groups; #Y-27632-treated P3 group vs. other experimental groups. $^{**}p < 0.01$, $^{***}p < 0.001$, $^{\wedge}p < 0.1$, $^{\wedge\wedge\wedge}p < 0.001$, $^{\#}p < 0.1$.

with Y-27632 exhibited enhanced adhesion and proliferation. Moreover, Y-27632 maintained the stemness of hHFSCs and the ability of hHFSCs to regenerate hair follicles *in vivo*. The Y-27632-induced proliferation and stemness in hHFSCs were conditional and reversible. Furthermore, Y-27632 maintained hHFSCs propagation and stemness through the ERK/MAPK pathway (**Scheme 1**).

The hHFSCs have potential applications in hair follicle regenerative medicine, as they can undergo complete self-renewal and exhibit multipotency (differentiate into various lineages) (Yang et al., 2017). However, an efficient *in vitro* primary culture system for hHFSCs is currently not established. The main factors affecting the proliferation and biological characteristics of an adherent culture *in vitro* are the coated culture dishes and culture medium (Hong et al., 2019; Hashimoto et al., 2020). In this study, we obtained hHFSCs using a two-step proteolytic digestion combined with microscopy. The culture dishes were coated with an animal origin-free coating matrix, containing the human extracellular matrix, before culturing hHFSCs. The hHFSCs were then purified using a differential enrichment procedure, which utilizes the delayed adhesion of hHFSCs to the surface of a culture dish. Compared with the 3T3 feeder cells, mouse collagen type IV, and basement membrane matrix Matrigel extracted from mouse sarcoma in the traditional culture system, human fibronectin can prevent the transmission of unknown zoonoses, which is critical for the clinical application of hHFSCs (Limat et al., 1989; Li et al., 2015; Call et al., 2018).

The use of K-SFM, which was optimized for the isolation and expansion of hHFSCs, prevents the potential contamination derived from fibroblasts. However, the expression of CK15 was rapidly downregulated upon culturing the hHFSCs in K-SFM for a prolonged period (Blanpain et al., 2004). Some studies have suggested that the addition of serum may prevent the downregulation of CK15. However, the use of serum may contribute to the transmission of unknown zoonoses and the induction of immunological reactions after clinical transplantation (Limat et al., 1989). The small molecule Y-27632 can reprogram and modulate the state of stem cells and is considered as one of the alternatives to serum and macromolecular proteins for *in vitro* culturing (Li et al., 2015).

Y-27632, an inhibitor of ROCK, modulates various cellular functions, including actin cytoskeleton organization, cell adhesion, cell motility, and apoptosis (David et al., 2012). Additionally, Y-27632, which was developed as an inhibitor of the calcium-sensitization pathway involved in smooth muscle contraction, inhibits RhoA-induced formation of stress fibers and focal adhesions (Uehata et al., 1997). Watanabe et al. (2007) first applied Y-27632 to inhibit apoptosis of dissociated single human embryonic stem cells in adherent cultures. Treatment with Y-27632 enhanced the adhesion and survival of human embryonic stem cells in adherent cultures during passage, by inducing cytoskeletal changes. Consistent with these results, this study demonstrated that only a few cells attached to the plate and slowly formed a monolayer in the primary culture of hHFSCs. Most cells underwent apoptosis as they did not attach to the culture plate. The dissociated single cells exhibited enhanced survival upon treatment with Y-27632. Moreover, Y-27632 dose-dependently increased the adhesion of hHFSCs.

The hallmarks of hHFSCs are enhanced proliferation and multipotency. The supplementation of Y-27632 can regulate

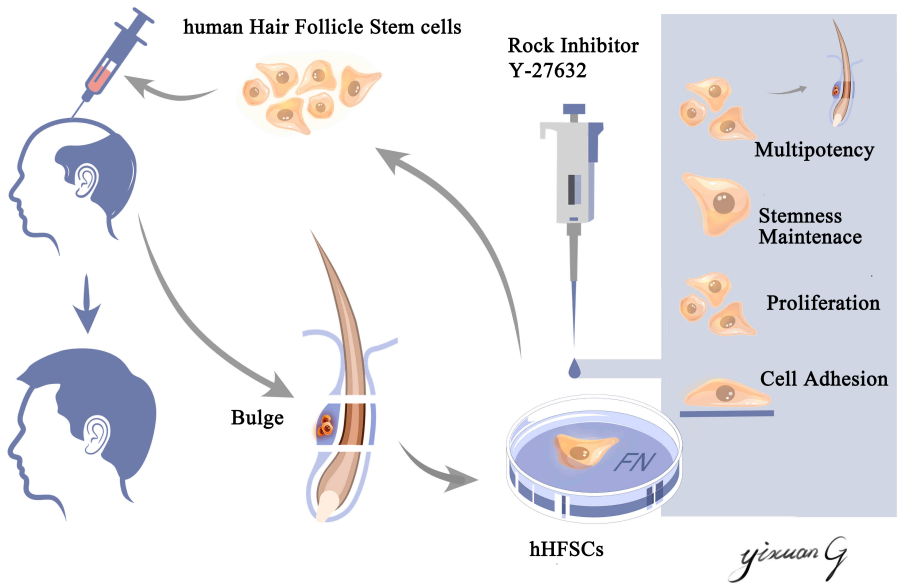

SCHEME 1 | Schematic illustration of an efficient primary culture system for human hair follicle stem cells isolated from occipital scalp skin using human fibronectin and ROCK inhibitor Y-27632. This culture model facilitated the proliferation, maintained the stemness of human hair follicle stem cells and the capability of regenerating hair follicles *in vivo*. This culture model may aid in obtaining an increased number of high-quality seed cells, which have applications in hair follicle tissue engineering and stem cell therapy.

the ability of stem cells to self-renew and differentiate into derivatives of all three germ layers (Sivasubramaiyan et al., 2009; Kurosawa, 2012). The use of Y-27632 during primary cultures offers a simple and effective way to prepare a large number of human epithelial stem cells from skin tissues (Terunuma et al., 2010; Wen et al., 2018). In this study, 10 and 20 μM Y-27632 significantly promoted the proliferation of primary hHFSCs. The challenges associated with *in vitro* culture of hHFSCs are low adhesion ratio and poor proliferation during passaging. The colony formation rate is an important indicator for evaluating the reattachment rate and the proliferation ability of hHFSCs. The number of clones directly affects the scale of cell expansion. In this study, the hHFSC colonies in K-SFM supplemented with Y-27632 were larger and more clustered than those in the control groups. These results suggest that Y-27632 facilitates the proliferation of hHFSCs.

Passage is one of the important indicators for evaluating the effectiveness of culture system. Y-27632 promotes the long-term proliferation of primary human keratinocytes and these cells efficiently bypassed senescence and became immortal (Chapman et al., 2010). However, passage and long-term proliferation is still a challenges in the culture of hHFSCs *in vitro* because of the different biological behavior of mouse and human stem cells (Yu et al., 2006; An et al., 2018). In our research, we found that both hHFSCs with or without Y-27632 at early passages (P1-2) were actively dividing and appeared small, cuboidal, and homogeneous. However, less cells could reattached onto culture dishes and became senescence with the flat and heterogeneous morphology at later passages (P3) in the untreated group. The hHFSCs with Y-27632 can be continuously cultured for at least 5 passages with a healthy status. Unfortunately only approximately 50% of the treated cells escaped senescence at passage 6 (**Supplementary Figure S1**). This data shown indicated that the culturing system we established is suit to short-term culture.

Self-renewal and multipotency (ability to differentiate into various lineages) are innate characteristics of HFSCs (Myung et al., 2009a). The supplementation of Y-27632 in K-SFM significantly upregulated the expression of hHFSC stemness markers (CK15 and CK19) and pluripotent markers (Nanog and Oct4). This was consistent with the results of previous studies, which demonstrated that Y-27632 upregulated Oct-3/4 expression in small colonies of human embryonic stem cells and spatiotemporally altered the balance between pluripotency and early differentiation events (Peerani et al., 2007; Sivasubramaniyan et al., 2010).

Our study further demonstrates the culture of hHFSCs in Y-27632 medium maintained their differentiation potential *in vivo*. *de novo* hair shafts were induced in recipient sites after 3 weeks of implantation with a mixture of hHFSCs and neonatal dermal cells. The culture system with Y-27632 appear to have stabilized the hair potential of the cells. Obviously, nearly 1.5-fold change more hair follicles formed in the group treated with Y-27632, compared with the control group. And we also demonstrated that Y-27632 maintained the multipotency of hHFSCs after several passages. Though there are some evidences that normal keratinocytes isolated from human tissue, for instance, isolated from fetal and newborn human foreskin epidermal cells combined with neonatal murine dermal cells could regenerate hair follicles *in vivo*, it involved the ethics of fetal-derived cells (Wu et al., 2014; Abaci et al., 2018). hHFSCs, which are located in easily accessible locations of human body, exhibit complete self-renewal and ability to differentiate to various lineages. These characteristic makes hHFSCs valuable seeder for hair follicle regeneration.

Chapman et al. (2014) demonstrated that the supplementation of ROCK inhibitor to the keratinocyte culture system promoted indefinite cellular proliferation, which was conditional and reversible. The removal of the ROCK inhibitor delayed cell growth and senescence after a few passages. However, Gao et al. (2019) demonstrated that treatment with Y-27632 enhanced the survival and adhesion of human embryonic stem cells but induced detachment and apoptosis of the attached cells. The authors suggested that the use of Y-27632 should be limited to 24 h to optimize its pro-survival effects. This may be because Y-27632 exerted different effects in different cell types and culture conditions. Therefore, it is important to determine the effect of long-term applications of Y-27632 in the culture medium of hHFSCs. The Y-27632-induced proliferation and stemness maintenance were reversible. The morphology of hHFSCs rapidly changed into a senescence phenotype and they exhibited a flat and heterogeneous morphology with an enlarged cytoplasmic volume after the removal of the ROCK inhibitor. Additionally, the removal of the ROCK inhibitor decreased the proliferation and reversed the stemness of hHFSCs. These results suggest that Y-27632 should be used in both the primary and short-term culture of hHFSCs routinely. This was consistent with the findings of Pakzad et al., who reported that the ROCK inhibitor, which regulates multiple cellular functions, should be routinely used in pluripotent stem cell culture (Pakzad et al., 2010).

Several studies have demonstrated that ROCK inhibitors regulate cell proliferation by activating different growth-regulatory proteins and triggering different signals in different cells (Yu et al., 2012; Wang et al., 2017). The MAPK cascades are central signaling elements that regulate various physiological processes, including cell proliferation, apoptosis, and stress response (Guo et al., 2020). ERK belongs to the MAPK family, which regulates the signaling cascades and transmits extracellular signals to intracellular targets (Garcia-Gomez et al., 2018). Previous studies have demonstrated that the ERK/MAPK signaling pathway is involved in the Y-27632-induced proliferation of periodontal ligament stem cells and Y-27632 maintained the balance of keratinocyte proliferation and differentiation through regulation of ERK activity (Wang et al., 2017; Zhang et al., 2019). Therefore, we examined the signaling pathways to determine the underlying mechanisms of Y-27632-induced proliferation and stemness maintenance of hHFSCs. Y-27632 dose-dependently enhanced cell proliferation within the concentration range of 5–20 μM. Treatment with U0126, an ERK inhibitor, mitigated the Y-27632-induced hHFSC proliferation and downregulated the expression of stemness marker induced by Y-27632. Meanwhile, western blotting analysis revealed that Y-27632 significantly increased the phosphorylation of ERK in the hHFSCs, which was mitigated upon treatment with U0126. These results indicate that Y-27632 maintained the

proliferation and stemness of hHFSCs through the ERK/MAPK signaling pathway.

CONCLUSION

We successfully established a xenofree short-term culture model for primary hHFSCs and demonstrated that the supplementation of Y-27632 in K-SFM promoted the adhesion, proliferation, stemness of hHFSCs and promoted the ability to regenerate hair follicles *in vivo*. Compared with the traditional method, the coating matrix and small molecule inhibitors used in the culture system could avoid the risk of heterogeneous gene contamination. These findings may aid in obtaining an increased number of high-quality seed cells, which have applications in hair follicle tissue engineering and stem cell therapy.

DATA AVAILABILITY STATEMENT

The original contributions presented in the study are included in the article/**Supplementary Material**, further inquiries can be directed to the corresponding author/s.

ETHICS STATEMENT

The studies involving human participants were reviewed and approved by the Medical Ethical Committee of Southern Medical University. The patients/participants provided their written informed consent to participate in this study. The animal study was reviewed and approved by the Experimental Animal Centre at Southern Medical University.

AUTHOR CONTRIBUTIONS

LW, JZ, and YG performed all the experiments and prepared the figures and tables. ZF, DD, JH, and ZL provided with the statistical assistance. LW wrote the first draft of the manuscript. RC and YM revised the manuscript for important intellectual content. ZH and RC contributed to the conception and design of the study. All authors contributed to manuscript revision, read, and approved the submitted version.

FUNDING

This study was funded by the National Natural Science Foundation of China (Grant Nos. 81971889, 81772104, and 81902013), the Natural Science Foundation of Guangdong Province (Grant Nos. 2020A1515010565 and 2020A1515110037), the Science and Technology Program of Guangzhou (Grant No. 201904010480), and the President Foundation of Nanfang Hospital, Southern Medical University (Grant No. 2019B015).

ACKNOWLEDGMENTS

We thank the Guangdong Provincial Key Laboratory of Clinical Medicine Experimental Research Center, Nanfang Hospital, Southern Medical University for providing experimental instruments. We thank the Department of Plastic and Aesthetic Surgery, Nanfang Hospital of Southern Medical University Guangzhou for providing scalp tissue. We also would like to thank Editage (www.editage.cn) for English language editing.

SUPPLEMENTARY MATERIAL

The Supplementary Material for this article can be found online at: https://www.frontiersin.org/articles/10.3389/fcell.2021.632882/full#supplementary-material

Supplementary Figure 1 | Y-27632 promoted the effective passages on short-term culture of hHFSCs. Both hHFSCs with or without Y-27632 at early passages (P1-2) were actively dividing and appeared small, cuboidal, and homogeneous. However, less cells could reattached onto culture dishes and became senescence with the flat and heterogeneous morphology at later passages (P3-4) in the untreated group. The hHFSCs with Y-27632 can be continuously cultured for at least 5 passages with a healthy status. Unfortunately only approximately 50% of the treated cells escaped senescence at passage 6. Scale bars: 100 μm.

REFERENCES

Abaci, H. E., Coffman, A., Doucet, Y., Chen, J., Jackow, J., Wang, E., et al. (2018). Tissue engineering of human hair follicles using a biomimetic developmental approach. *Nat. Commun.* 9:5301. doi: 10.1038/s41467-018-07579-y

An, L., Ling, P., Cui, J., Wang, J., Zhu, X., Liu, J., et al. (2018). ROCK inhibitor Y-27632 maintains the propagation and characteristics of hair follicle stem cells. *Am. J. Transl. Res.* 10, 3689–3700.

Barrandon, Y., and Green, H. (1987). Three clonal types of keratinocyte with different capacities for multiplication. *Proc. Natl. Acad. Sci. U.S.A.* 84, 2302–2306. doi: 10.1073/pnas.84.8.2302

Blanpain, C., Lowry, W. E., Geoghegan, A., Polak, L., and Fuchs, E. (2004). Self-renewal, multipotency, and the existence of two cell populations within an epithelial stem cell niche. *Cell* 118, 635–648. doi: 10.1016/j.cell.2004.08.012

Call, M., Meyer, E. A., Kao, W. W., Kruse, F. E., and Schlotzer-Schrehardt, U. (2018). Hair follicle stem cell isolation and expansion. *Bio Protoc.* 8:e2848. doi: 10.21769/BioProtoc.2848

Chacon-Martinez, C. A., Klose, M., Niemann, C., Glauche, I., and Wickstrom, S. A. (2017). Hair follicle stem cell cultures reveal self-organizing plasticity of stem cells and their progeny. *EMBO J.* 36, 151–164. doi: 10.15252/embj.201694902

Chapman, S., Liu, X., Meyers, C., Schlegel, R., and McBride, A. A. (2010). Human keratinocytes are efficiently immortalized by a Rho kinase inhibitor. *J. Clin. Invest.* 120, 2619–2626. doi: 10.1172/JCI42297

Chapman, S., McDermott, D. H., Shen, K., Jang, M. K., and McBride, A. A. (2014). The effect of Rho kinase inhibition on long-term keratinocyte proliferation is rapid and conditional. *Stem Cell Res. Ther.* 5:60. doi: 10.1186/scrt449

Coelho, M. B., Cabral, J. M., and Karp, J. M. (2012). Intraoperative stem cell therapy. *Annu. Rev. Biomed. Eng.* 14, 325–349. doi: 10.1146/annurev-bioeng-071811-150041

David, M., Petit, D., and Bertoglio, J. (2012). Cell cycle regulation of Rho signaling pathways. *Cell Cycle* 11, 3003–3010. doi: 10.4161/cc.21088

Gao, L., Nath, S. C., Jiao, X., Zhou, R., Nishikawa, S., Krawetz, R., et al. (2019). Post-passage rock inhibition induces cytoskeletal aberrations and apoptosis in human embryonic stem cells. *Stem Cell Res.* 41:101641. doi: 10.1016/j.scr.2019.101641

Garcia-Gomez, R., Bustelo, X. R., and Crespo, P. (2018). Protein-protein interactions: emerging oncotargets in the RAS-ERK pathway. *Trends Cancer* 4, 616–633. doi: 10.1016/j.trecan.2018.07.002

Garza, L. A., Yang, C. C., Zhao, T., Blatt, H. B., Lee, M., He, H., et al. (2011). Bald scalp in men with androgenetic alopecia retains hair follicle stem cells but lacks CD200-rich and CD34-positive hair follicle progenitor cells. *J. Clin. Invest.* 121, 613–622. doi: 10.1172/JCI44478

Guo, Y. J., Pan, W. W., Liu, S. B., Shen, Z. F., Xu, Y., and Hu, L. L. (2020). ERK/MAPK signalling pathway and tumorigenesis. *Exp. Ther. Med.* 19, 1997–2007. doi: 10.3892/etm.2020.8454

Hakala, H., Rajala, K., Ojala, M., Panula, S., Areva, S., Kellomaki, M., et al. (2009). Comparison of biomaterials and extracellular matrices as a culture platform for multiple, independently derived human embryonic stem cell lines. *Tissue Eng. Part A* 15, 1775–1785. doi: 10.1089/ten.tea.2008.0316

Hashimoto, K., Yamashita, K., Enoyoshi, K., Dahan, X., Takeuchi, T., Kori, H., et al. (2020). The effects of coating culture dishes with collagen on fibroblast cell shape and swirling pattern formation. *J. Biol. Phys.* 46, 351–369. doi: 10.1007/s10867-020-09556-3

Hong, H. K., Pyo, D. H., Kim, T. W., Yun, N. H., Lee, Y. S., Song, S. J., et al. (2019). Efficient primary culture model of patientderived tumor cells from colorectal cancer using a Rhoassociated protein kinase inhibitor and feeder cells. *Oncol. Rep.* 42, 2029–2038. doi: 10.3892/or.2019.7285

Inoue, K., Aoi, N., Sato, T., Yamauchi, Y., Suga, H., Eto, H., et al. (2009). Differential expression of stem-cell-associated markers in human hair follicle epithelial cells. *Lab. Invest.* 89, 844–856. doi: 10.1038/labinvest.2009.48

Jimenez, F., Izeta, A., and Poblet, E. (2011). Morphometric analysis of the human scalp hair follicle: practical implications for the hair transplant surgeon and hair regeneration studies. *Dermatol. Surg.* 37, 58–64. doi: 10.1111/j.1524-4725.2010.01809.x

Kurosawa, H. (2012). Application of Rho-associated protein kinase (ROCK) inhibitor to human pluripotent stem cells. *J. Biosci. Bioeng.* 114, 577–581. doi: 10.1016/j.jbiosc.2012.07.013

Li, Z., Han, S., Wang, X., Han, F., Zhu, X., Zheng, Z., et al. (2015). Rho kinase inhibitor Y-27632 promotes the differentiation of human bone marrow mesenchymal stem cells into keratinocyte-like cells in xeno-free conditioned medium. *Stem Cell Res. Ther.* 6:17. doi: 10.1186/s13287-015-0008-2

Lim, C. H., Sun, Q., Ratti, K., Lee, S. H., Zheng, Y., Takeo, M., et al. (2018). Hedgehog stimulates hair follicle neogenesis by creating inductive dermis during murine skin wound healing. *Nat. Commun.* 9:4903. doi: 10.1038/s41467-018-07142-9

Limat, A., Hunziker, T., Boillat, C., Bayreuther, K., and Noser, F. (1989). Postmitotic human dermal fibroblasts efficiently support the growth of human follicular keratinocytes. *J. Invest. Dermatol.* 92, 758–762. doi: 10.1111/1523-1747.ep12722530

Liu, F., Shi, J., Zhang, Y., Lian, A., Han, X., Zuo, K., et al. (2019). NANOG attenuates hair follicle-derived mesenchymal stem cell senescence by upregulating PBX1 and activating AKT signaling. *Oxid. Med. Cell. Longev.* 2019:4286213. doi: 10.1155/2019/4286213

Lu, Y., Qu, H., Qi, D., Xu, W., Liu, S., Jin, X., et al. (2019). OCT4 maintains self-renewal and reverses senescence in human hair follicle mesenchymal stem cells through the downregulation of p21 by DNA methyltransferases. *Stem Cell Res. Ther.* 10:28. doi: 10.1186/s13287-018-1120-x

Mistriotis, P., and Andreadis, S. T. (2013). Hair follicle: a novel source of multipotent stem cells for tissue engineering and regenerative medicine. *Tissue Eng. Part B Rev.* 19, 265–278. doi: 10.1089/ten.TEB.2012.0422

Myung, P., Andl, T., and Ito, M. (2009a). Defining the hair follicle stem cell (Part I). *J. Cutan. Pathol.* 36, 1031–1034. doi: 10.1111/j.1600-0560.2009.01396.x

Myung, P., Andl, T., and Ito, M. (2009b). Defining the hair follicle stem cell (Part II). *J. Cutan. Pathol.* 36, 1134–1137. doi: 10.1111/j.1600-0560.2009.01412.x

Myung, P., and Ito, M. (2012). Dissecting the bulge in hair regeneration. *J. Clin. Invest.* 122, 448–454. doi: 10.1172/JCI57414

Oh, J. H., Mohebi, P., Farkas, D. L., and Tajbakhsh, J. (2011). Towards expansion of human hair follicle stem cells in vitro. *Cell Prolif.* 44, 244–253. doi: 10.1111/j.1365-2184.2011.00754.x

Ohyama, M., Terunuma, A., Tock, C. L., Radonovich, M. F., Pise-Masison, C. A., Hopping, S. B., et al. (2006). Characterization and isolation of stem cell-enriched human hair follicle bulge cells. *J. Clin. Invest.* 116, 249–260. doi: 10.1172/JCI26043

Owczarczyk-Saczonek, A., Krajewska-Wlodarczyk, M., Kruszewska, A., Banasiak, L., Placek, W., Maksymowicz, W., et al. (2018). Therapeutic potential of stem cells in follicle regeneration. *Stem Cells Int.* 2018:1049641. doi: 10.1155/2018/1049641

Pakzad, M., Totonchi, M., Taei, A., Seifinejad, A., Hassani, S. N., and Baharvand, H. (2010). Presence of a ROCK inhibitor in extracellular matrix supports more undifferentiated growth of feeder-free human embryonic and induced pluripotent stem cells upon passaging. *Stem Cell Rev. Rep.* 6, 96–107. doi: 10.1007/s12015-009-9103-z

Peerani, R., Rao, B. M., Bauwens, C., Yin, T., Wood, G. A., Nagy, A., et al. (2007). Niche-mediated control of human embryonic stem cell self-renewal and differentiation. *EMBO J.* 26, 4744–4755. doi: 10.1038/sj.emboj.7601896

Roh, C., Tao, Q., Photopoulos, C., and Lyle, S. (2005). In vitro differences between keratinocyte stem cells and transit-amplifying cells of the human hair follicle. *J. Invest. Dermatol.* 125, 1099–1105. doi: 10.1111/j.0022-202X.2005.23958.x

Sivasubramaiyan, K., Totey, S., Bhat, V., Totey, S. M., and Deb, K. (2009). Y-27632 enhances differentiation of blastocyst like cystic human embryoid bodies to endocrinologically active trophoblast cells on a biomimetic platform. *J. Biomed. Sci.* 16:88. doi: 10.1186/1423-0127-16-88

Sivasubramaniyan, K., Pal, R., Totey, S., Bhat, V. S., and Totey, S. (2010). Rho kinase inhibitor y27632 alters the balance between pluripotency and early differentiation events in human embryonic stem cells. *Curr. Stem Cell Res. Ther.* 5, 2–12. doi: 10.2174/157488810790442769

Takahara, A., Sugiyama, A., Satoh, Y., Yoneyama, M., and Hashimoto, K. (2003). Cardiovascular effects of Y-27632, a selective Rho-associated kinase inhibitor, assessed in the halothane-anesthetized canine model. *Eur. J. Pharmacol.* 460, 51–57. doi: 10.1016/s0014-2999(02)02929-1

Terunuma, A., Limgala, R. P., Park, C. J., Choudhary, I., and Vogel, J. C. (2010). Efficient procurement of epithelial stem cells from human tissue specimens using a Rho-associated protein kinase inhibitor Y-27632. *Tissue Eng. Part A* 16, 1363–1368. doi: 10.1089/ten.TEA.2009.0339

Trempus, C. S., Morris, R. J., Bortner, C. D., Cotsarelis, G., Faircloth, R. S., Reece, J. M., et al. (2003). Enrichment for living murine keratinocytes from the hair follicle bulge with the cell surface marker CD34. *J. Invest. Dermatol.* 120, 501–511. doi: 10.1046/j.1523-1747.2003.12088.x

Uehata, M., Ishizaki, T., Satoh, H., Ono, T., Kawahara, T., Morishita, T., et al. (1997). Calcium sensitization of smooth muscle mediated by a Rho-associated protein kinase in hypertension. *Nature* 389, 990–994. doi: 10.1038/40187

Vasserot, A. P., Geyfman, M., and Poloso, N. J. (2019). Androgenetic alopecia: combing the hair follicle signaling pathways for new therapeutic targets and more effective treatment options. *Exp. Opin. Ther. Targets* 23, 755–771. doi: 10.1080/14728222.2019.1659779

Wang, T., Kang, W., Du, L., and Ge, S. (2017). Rho-kinase inhibitor Y-27632 facilitates the proliferation, migration and pluripotency of human periodontal ligament stem cells. *J. Cell. Mol. Med.* 21, 3100–3112. doi: 10.1111/jcmm.13222

Watanabe, K., Ueno, M., Kamiya, D., Nishiyama, A., Matsumura, M., Wataya, T., et al. (2007). A ROCK inhibitor permits survival of dissociated human embryonic stem cells. *Nat. Biotechnol.* 25, 681–686. doi: 10.1038/nbt1310

Wen, J., Zu, T., Zhou, Q., Leng, X., and Wu, X. (2018). Y-27632 simplifies the isolation procedure of human primary epidermal cells by selectively blocking focal adhesion of dermal cells. *J. Tissue Eng. Regen. Med.* 12, e1251–e1255. doi: 10.1002/term.2526

Wu, X., Scott, L. J., Washenik, K., and Stenn, K. (2014). Full-thickness skin with mature hair follicles generated from tissue culture expanded human cells. *Tissue Eng. Part A* 20, 3314–3321. doi: 10.1089/ten.TEA.2013.0759

Xiao, S., Hu, Z., Jiang, J., Miao, Y., and Feng, C. (2016). Neonatal murine skin-derived cells transplanted using a mini-chamber model produce robust and normal hair. *J. Tissue Eng. Regen. Med.* 10, E286–E293. doi: 10.1002/term.1802

Yang, H., Adam, R. C., Ge, Y., Hua, Z. L., and Fuchs, E. (2017). Epithelial-mesenchymal micro-niches govern stem cell lineage choices. *Cell* 169, 483.e–496.e. doi: 10.1016/j.cell.2017.03.038

York, K., Meah, N., Bhoyrul, B., and Sinclair, R. (2020). A review of the treatment of male pattern hair loss. *Exp. Opin. Pharmacother* 21, 603–612. doi: 10.1080/14656566.2020.1721463

Yu, H., Fang, D., Kumar, S. M., Li, L., Nguyen, T. K., Acs, G., et al. (2006). Isolation of a novel population of multipotent adult stem cells from human hair follicles. *Am. J. Pathol.* 168, 1879–1888. doi: 10.2353/ajpath.2006.051170

Yu, Z., Liu, M., Fu, P., Xie, M., Wang, W., and Luo, X. (2012). ROCK inhibition with Y27632 promotes the proliferation and cell cycle progression of cultured astrocyte from spinal cord. *Neurochem. Int.* 61, 1114–1120. doi: 10.1016/j.neuint.2012.08.003

Zhang, X., Qin, J., Xie, Z., Liu, C., Su, Y., Chen, Z., et al. (2019). Y-27632 preserves epidermal integrity in a human skin organ-culture (hSOC) system by regulating AKT and ERK signaling pathways. *J. Dermatol. Sci.* 96, 99–109. doi: 10.1016/j.jdermsci.2019.10.006

Conflict of Interest: The authors declare that the research was conducted in the absence of any commercial or financial relationships that could be construed as a potential conflict of interest.

Copyright © 2021 Wen, Miao, Fan, Zhang, Guo, Dai, Huang, Liu, Chen and Hu. This is an open-access article distributed under the terms of the Creative Commons Attribution License (CC BY). The use, distribution or reproduction in other forums is permitted, provided the original author(s) and the copyright owner(s) are credited and that the original publication in this journal is cited, in accordance with accepted academic practice. No use, distribution or reproduction is permitted which does not comply with these terms.

frontiers in Cell and Developmental Biology

ORIGINAL RESEARCH
published: 02 August 2021
doi: 10.3389/fcell.2021.590333

Human iPS Cell-Derived Cell Aggregates Exhibited Dermal Papilla Cell Properties in *in vitro* Three-Dimensional Assemblage Mimicking Hair Follicle Structures

Masahiro Fukuyama[1], Aki Tsukashima[1], Momoko Kimishima[1], Yoshimi Yamazaki[1], Hideyuki Okano[2] and Manabu Ohyama[1]*

[1] Department of Dermatology, Kyorin University Faculty of Medicine, Tokyo, Japan, [2] Department of Physiology, Keio University School of Medicine, Tokyo, Japan

OPEN ACCESS

Edited by:
Atsushi Asakura,
University of Minnesota Twin Cities,
United States

Reviewed by:
Young Kwan Sung,
Kyungpook National University,
South Korea
Thomas Andl,
University of Central Florida,
United States

****Correspondence:***
Manabu Ohyama
manabuohy@ks.kyorin-u.ac.jp

Specialty section:
This article was submitted to Stem Cell Research, a section of the journal Frontiers in Cell and Developmental Biology

Received: *01 August 2020*
Accepted: *07 July 2021*
Published: *02 August 2021*

Citation:
Fukuyama M, Tsukashima A, Kimishima M, Yamazaki Y, Okano H and Ohyama M (2021) Human iPS Cell-Derived Cell Aggregates Exhibited Dermal Papilla Cell Properties in in vitro Three-Dimensional Assemblage Mimicking Hair Follicle Structures. Front. Cell Dev. Biol. 9:590333. doi: 10.3389/fcell.2021.590333

Current approaches for human hair follicle (HF) regeneration mostly adopt cell-autonomous tissue reassembly in a permissive murine intracorporeal environment. This, together with the limitation in human-derived trichogenic starting materials, potentially hinders the bioengineering of human HF structures, especially for the drug discovery and treatment of hair loss disorders. In this study, we attempted to reproduce the anatomical relationship between an epithelial main body and the dermal papilla (DP) within HF *in vitro* by three-dimensionally assembling columnarly molded human keratinocytes (KCs) and the aggregates of DP cells and evaluated how HF characteristics were reproduced in the constructs. The replaceability of human-induced pluripotent stem cell (hiPSC)-derived DP substitutes was assessed using the aforementioned reconstruction assay. Human DP cell aggregates were embedded into Matrigel as a cluster. Subsequently, highly condensed human KCs were cylindrically injected onto DP spheroids. After 2-week culture, the structures visually mimicking HFs were obtained. KC-DP constructs partially reproduced HF microanatomy and demonstrated differential keratin (KRT) expression pattern in HFs: KRT14 in the outermost part and KRT13, KRT17, and KRT40, respectively, in the inner portion of the main body. KC-DP constructs tended to upregulate HF-related genes, *KRT25*, *KRT33A*, *KRT82*, *WNT5A*, and *LEF1*. Next, DP substitutes were prepared by exposing hiPSC-derived mesenchymal cells to retinoic acid and subsequently to WNT, BMP, and FGF signal activators, followed by cell aggregation. The resultant hiPSC-derived DP substitutes (iDPs) were combined with KCs in the invented assay. KC-iDP constructs morphologically resemble KC-DP constructs and analogously mimicked KRT expression pattern in HF. iDP in the constructs expressed DP-related markers, such as vimentin and versican. Intriguingly, KC-iDP constructs more intensely expressed *KRT33A*, *KRT82*, and *LEF1*, which were stepwisely upregulated by the addition of WNT ligand and the mixture of WNT, SHH, and EDA signaling activators, supporting the idea that iDP exhibited biological properties analogous to DP cell aggregates in the constructs *in vitro*. These preliminary

findings suggested the possibility of regenerating DP equivalents with *in vitro* hair-inductive capacity using hiPSC-derived cell composites, which potentially reduce the necessity of human tissue-derived trichogenic cell subset and eventually allow xeno-free bioengineering of human HFs.

Keywords: hair follicle, regeneration, epithelial–mesenchymal interactions, dermal papilla, human induced pluripotent stem cells, WNT signaling

INTRODUCTION

The hair follicle (HF) is a multifunctional mammalian skin appendage, providing a physical barrier against external insults, facilitating thermoregulation, and transmitting tactile sense (Stenn and Paus, 2001; Schneider et al., 2009; Nagao et al., 2012; Zimmerman et al., 2014). In the case of humans, hairstyles greatly influence one's appearance and therefore vast demand exists for the treatment of hair loss disorders (Saed et al., 2017; Ohyama, 2019). Establishment of a methodology to experimentally regenerate human HFs is of major significance in the management of hair loss conditions as a way of preparing therapeutic materials for hair transplantation and supplying an experimental platform for drug discovery (Ohyama, 2019). Considering the structural and functional complexity of HF for a small dimension miniorgan, HF bioengineering, especially that achieved *in vitro*, may provide a platform for the regeneration of other large-sized tissue or organs.

The HF is a cylindric structure composed of the epithelial main body consisting of keratinocytes (KCs) including stem cells and the mesenchymal structures; the dermal papilla (DP), a specialized hair-inductive dermal cell aggregate located at the bottom (bulb) of the HF, and the dermal sheath (DS) surrounding the main body (Yang and Cotsarelis, 2010; Ohyama, 2019). The HF continuously self-renews throughout life *via* the hair cycle (Stenn and Paus, 2001). Both HF morphogenesis and regeneration are enabled by well-orchestrated epithelial–mesenchymal interactions (EMIs) *via* biological signaling pathways, such as WNT, BMP, Sonic hedgehog (SHH), and Ectodysplasin A (EDA) pathways (St-Jacques et al., 1998; Millar, 2002; Zhang et al., 2009; Mikkola, 2011; Sennett and Rendl, 2012; Ohyama, 2019). To achieve successful HF regeneration, sufficient folliculogenic EMIs need to be elicited and maintained between receptive KCs and inductive DP (Millar, 2002; Sennett and Rendl, 2012; Ohyama, 2019).

To date, experimental HF regeneration has been attempted mainly by co-transplantation of KCs and trichogenic DP cells into an *in vivo* environment represented by the intracorporeal spaces of immunodeficient mice (Weinberg et al., 1993; Zheng et al., 2005; Ehama et al., 2007; Kobayashi et al., 2010). The transplanted cells evoke EMIs and cell-autonomously reassemble HF structures, which is constantly successful for murine cells and has recently been stabilized for human cells (Thangapazham et al., 2014a,b; Yoshida et al., 2019). Obviously, use of xeno-free environment is far more preferable considering the direct application of regenerated structures for regenerative medicine purposes (e.g., transplantation to hair loss areas). Adopting 3D-printing technology to precast HF-shape cavities in vascularized collagen gel that were filled with DP cell (DPC) aggregates and KCs, Abaci et al. recently bioengineered HF structures from human cells with the hair shaft diameter fairly comparable to that of human intermediate-vellus hairs, opening the door for mass production of bioengineered human HFs for regenerative medicine and pharmaceutical investigations (Abaci et al., 2018). At the same time, the approach requires advanced technologies and still not readily available for most laboratories. For drug discovery, a simpler platform allowing the regeneration of HF-like structures partially recapitulating pivotal HF characteristics would be beneficial.

Efficiency of experimental human HF regeneration in the abovementioned approaches can also be influenced by the biological properties of starting materials; for KCs, those derived from neonatal or juvenile individuals (Ehama et al., 2007; Thangapazham et al., 2014a), and for dermal cells, DP or DS cells expressing high levels of hair inductive markers (McElwee et al., 2003; Driskell et al., 2009; Ohyama et al., 2012; Higgins et al., 2013) have been considered to be preferable. Of note, preparation of DP cells with potent trichogenicity has been recognized to be a gold standard for such application (Yang and Cotsarelis, 2010; Ohyama, 2019). However, HF-derived DP cells collectable from hair loss patients are limited. In addition, DP lose their intrinsic properties after *in vitro* expansion, representing another major hurdle in human HF regeneration (Weinberg et al., 1993; Rendl et al., 2008; Ohyama et al., 2012; Higgins et al., 2013; Ohyama, 2019). Establishment of alternative material sources of DP cells should resolve such difficulties.

Human-induced pluripotent stem cells (hiPSCs) hold promise as a substituting cell source (Ohyama and Okano, 2014). Past studies demonstrated that hiPSCs could be differentiated into KC precursors or DP substituting cells and contribute to regeneration of HF-like structures in *in vivo* HF reconstitution assays (Veraitch et al., 2013, 2017). Imperfectness of regenerated structures and low efficiency of reproduction highlight the necessity of further improvements. In addition, whether hiPSC-derived cells exhibit analogous trichogenicity *in vitro* remains unknown.

In this study, we attempted to establish a simple assay in which highly condensed human KCs and the aggregates of DP cells were three-dimensionally assembled *in vitro* mimicking their anatomical association in HFs and cultured for 2 weeks. Histological and molecular biological analyses of regenerated structures were conducted to assess the resemblance of regenerated structures to HFs. hiPSC-derived mesenchymal cells were exposed to retinoic acid and subsequently to WNT, BMP, and FGF signal activators, followed by cell aggregation, expecting to elicit DP properties. The replaceability of hiPSC-derived DP substituting cell aggregates with DPs was assessed

using the assay developed. Effects of folliculogenic signaling pathway activation on the regenerated structures by WNT, SHH, and EDA agonists were also evaluated.

MATERIALS AND METHODS

Preparation of KCs, DP Cells, and Fibroblasts

Human KCs and DP cells were purchased from CELLnTECH Advanced Cell systems AG (Bern, Switzerland) and PromoCELL (Heidelberg, Germany), respectively, or isolated from adult human scalp samples obtained from surgery of benign scalp tumors as previously described. Human fibroblasts were purchased from PromoCELL (Heidelberg, Germany). All donors provided written informed consent in accordance with the Declaration of Helsinki. KCs at passages 3–6, fibroblasts at passage 5, and DP cells at passages 2–4 were used. KCs, fibroblasts, and DP cells were, respectively, cultured in CnT-PR (CELLnTECH Advanced Cell systems AG, Bern, Switzerland), Dulbecco's Modified Eagle's Medium (DMEM; Sigma-Aldrich, St. Louis, MO, United States) containing 10% fetal bovine serum (FBS; Biowest, Nuaillé, France), and follicle dermal papilla cell medium (DP medium; PromoCELL, Heidelberg, Germany) at 37°C in a 5% CO_2 prior to HF reconstruction assay. Culture medium was changed every 2 days.

Generation of Cell Aggregates From hiPSC-Derived DP Substituting Cells

hiPSC-derived DP substituting cells (iDPSCs) were generated following the previously published protocol with minor modifications (Veraitch et al., 2017). Three lines of hiPSCs generated by retroviral introduction of four Yamanaka factors into dermal fibroblasts [201B7 (Takahashi et al., 2007) and WD39 (Imaizumi et al., 2012)] or by gene delivery using a single, synthetic self-replicating VEE-RF RNA replicon into endothelial progenitor cells [RPChiPS771-2 (ReproCELL Inc., Yokohama, Japan)] were maintained on feeder-free culture dish filled with StemFit^{TM} (AJINOMOTO, Tokyo, Japan) following the manufacturer's protocol. For hiPSC-derived mesenchymal stem cell-like cell (iMC) induction, 6.5×10^4 hiPSCs/well in a six-well plate were placed onto a humanized substrate (CELLstart CTS; Life Technologies, Carlsbad, CA, United States). When a well was approximately 80% confluent, mesenchymal cell induction was initiated using Stempro MSC-SFM CTS (Life Technologies, Carlsbad, CA, United States) for 9–11 days. iMCs were then incubated in DMEM (Sigma-Aldrich, St. Louis, MO, United States) containing 10% FBS (Biowest, Nuaillé, France) with 10 μM all-trans retinoic acid (Sigma-Aldrich, St. Louis, MO, United States) for 4 days, and subsequently in DP cell-activating culture (DPAC) medium (Ohyama et al., 2012); 10% FBS-DMEM supplemented with 1 μM 6-bromoindirubin-3'-oxime (Sigma-Aldrich, St. Louis, MO, United States), 20 ng/ml bFGF (Peprotech, Rocky Hill, NJ, United States), and 200 ng/ml human recombinant BMP2 (R&D Systems, Minneapolis, MN, United States) for 7 days to obtain iDPSCs.

Preparation of DP Cell or iDPSC Aggregates

A total of 1×10^6 DP cells or iDPSCs were suspended in DP medium and stained with CellBrite^{TM} Orange Cytoplasmic Membrane Dye (Biotium, Hayward, CA, United States) following the manufacturer's protocol (Veraitch et al., 2017). After washing three times with DP medium, 5×10^3 DP cells or iDPSCs were seeded into each well of non-cell binding 96-well plate (Thermo Fisher Scientific, Rockford, IL, United States) containing DP medium. The plates were centrifuged at 500 rpm for 2 min and incubated at 37°C, 5% CO_2 with medium changes every 5 days to form DP-like cell aggregates.

Reconstitution of HF-Like Structure *in vitro*

Using dissection microscopes and a micropipette, 12 DP cell or iDPSC aggregates were placed in a group within 3 ml of Matrigel matrix (CORNING, Corning, NY, United States) in a cell culture insert for a six-well cell culture plate (Gibco, Rockford, IL, United States). Subsequently, 5 μl of highly condensed human KCs (23.4×10^6 on average per experiment) suspended in 500 μl of CnT-PR was cylindrically injected onto aggregated DP cell or iDPSC spheres embedded in Matrigel matrix, while pulling a micropipette outward, to form a structure mimicking HF architecture (**Figure 1A**). A fragment of guide nylon wire (BEAR Medical, Ibaraki, Japan) was inserted within KC composites as a scaffold (**Figure 1A**). The Matrigel matrix containing HF-like structures was submerged in the 1:1 mixture of CnT-PR and Amnio MAX-C100 (Gibco, Rockford, IL, United States) and incubated at 37°C, 5% CO_2 for 2 weeks. The medium was changed on alternate days.

Stimulation of Folliculogenic Signaling by Agonists

To activate HF morphogenesis associated WNT, SHH, and EDA signaling pathways in HF-like constructs, 2 μM CHIR99021 [the glycogen synthase kinase (GSK) 3β inhibitor (a WNT signal agonist) (Ring et al., 2003); Cayman Chemical, Ann Arbor, MI, United States], 2 μM purmorphamine [the Smo receptor agonist (a SHH signal agonist) (Sinha and Chen, 2006); FUJIFILM Wako Pure Chemical Co., Osaka, Japan], and 10 ng/ml EDA (recombinant ectodysplasin A1; R&D Systems, Minneapolis, MN, United States) were singly or jointly added to culture medium at the generation of HF-like structure and continued during 2-week culture.

Quantitative Reverse Transcription-Polymerase Chain Reaction

Total RNA was extracted using the RNeasy Mini Kit (Qiagen, Hilden, Germany) and cDNA was synthesized using the Superscript III First Strand Synthesis SuperMix (Invitrogen, Carlsbad, CA, United States) according to the manufacturers' instructions. All the used primer sequences are shown in

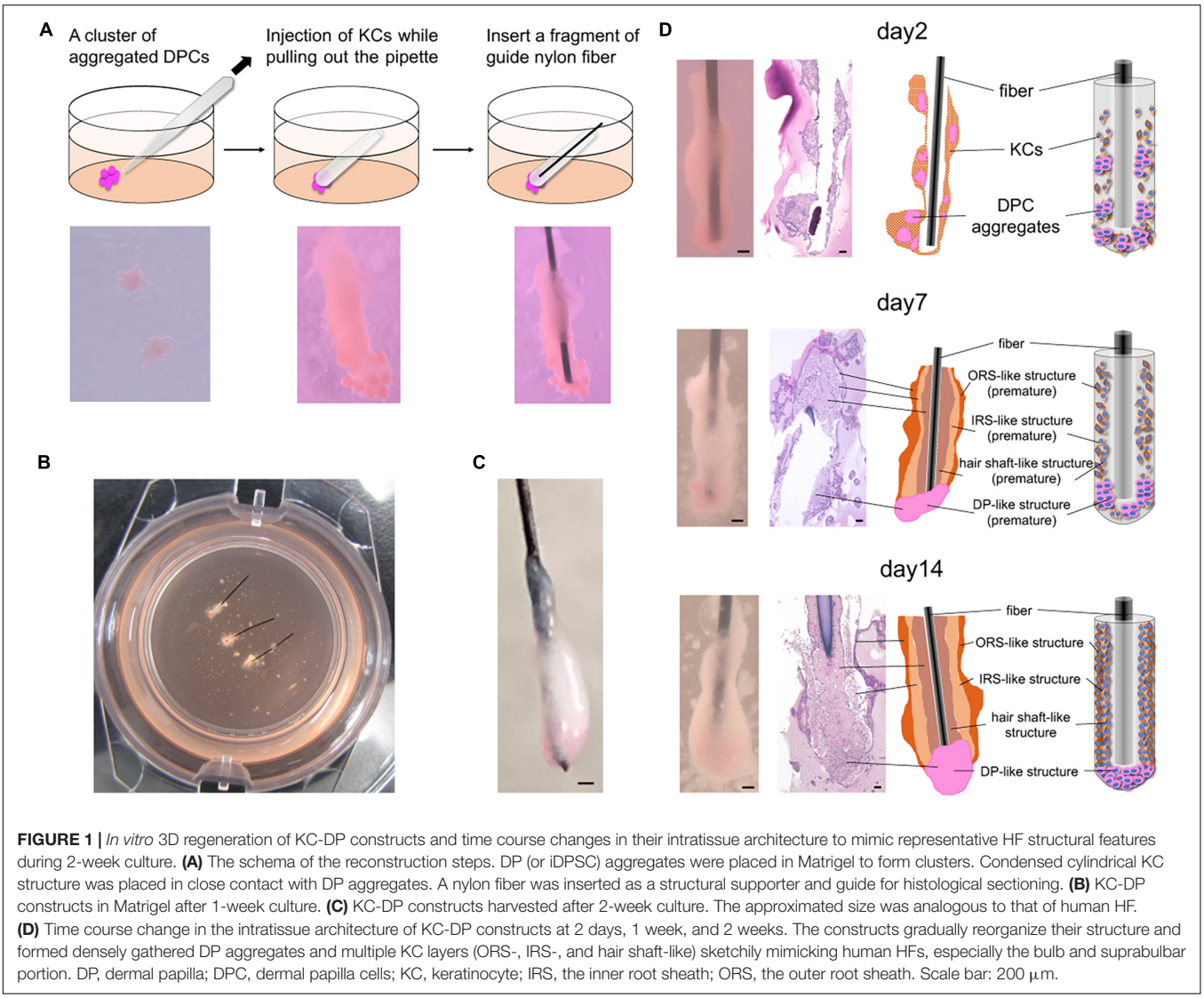

FIGURE 1 | *In vitro* 3D regeneration of KC-DP constructs and time course changes in their intratissue architecture to mimic representative HF structural features during 2-week culture. **(A)** The schema of the reconstruction steps. DP (or iDPSC) aggregates were placed in Matrigel to form clusters. Condensed cylindrical KC structure was placed in close contact with DP aggregates. A nylon fiber was inserted as a structural supporter and guide for histological sectioning. **(B)** KC-DP constructs in Matrigel after 1-week culture. **(C)** KC-DP constructs harvested after 2-week culture. The approximated size was analogous to that of human HF. **(D)** Time course change in the intratissue architecture of KC-DP constructs at 2 days, 1 week, and 2 weeks. The constructs gradually reorganize their structure and formed densely gathered DP aggregates and multiple KC layers (ORS-, IRS-, and hair shaft-like) sketchily mimicking human HFs, especially the bulb and suprabulbar portion. DP, dermal papilla; DPC, dermal papilla cells; KC, keratinocyte; IRS, the inner root sheath; ORS, the outer root sheath. Scale bar: 200 μm.

Supplementary Table 1. Real-time reverse transcription-polymerase chain reaction (RT-PCR) analyses were conducted using the PowerUp^{TM} SYBR^{TM} Green PCR Master Mix and the StepOne Real-Time PCR system (Applied Biosystems, Foster City, CA, United States). Cycling conditions consisted of an initial activation of 2 min at 95°C, then 40 cycles of denaturing at 95°C for 15 s, and annealing and extension at 60°C for 1 min. Messenger RNA expression levels were normalized to β-actin expression level adopting the ΔCT method and calculated based on $2^{-\Delta CT}$.

Histological and Immunohistochemical Analysis

Harvested HF-like constructs were fixed by 10% formalin and embedded in paraffin. For histological staining, paraffin-embedded tissue sections were deparaffinized and stained with Carrazzi's hematoxylin and counterstaining with eosin before mounted in malinol. For immunohistochemical analyses, the deparaffinized sections were pretreated in an autoclave (121°C, 5–10 min, pH 6), blocked endogenous peroxidase by 3% hydrogen peroxide at RT for 10 min, and incubated overnight at 4°C with the following primary antibodies: mouse anti-human cytokeratin 13 (KRT13) monoclonal antibody (Ks13.1; 1:100; PROGEN, Heidelberg, Germany), mouse anti-human cytokeratin 14 (KRT14) monoclonal antibody (LL002; 1:500; Abcam, Cambridge, MA, United States), rabbit anti-human cytokeratin 17 (KRT17) polyclonal antibody (ab53707; 1:200; Abcam, Cambridge, MA, United States), mouse anti-human cytokeratin 19 (KRT19) monoclonal antibody (Ks19.1; 1:200; Biocare Medical, Pacheco, CA, United States), mouse anti-human hair cortex cytokeratin/K40 (KRT40) monoclonal antibody (AE13; 1:50; Abcam, Cambridge, MA, United States), rabbit anti-human cytokeratin 75 (KRT75) polyclonal antibody (ab254740; 1:200; Abcam, Cambridge, MA, United States), rabbit anti-human GATA binding protein 3 (GATA3) polyclonal antibody (GTX109654; Gene Tex, Irvine, CA, United States), rabbit anti-human dickkopf 4 polyclonal antibody (DKK4; 1:100;

Abcam, Cambridge, MA, United States), rabbit anti-human sex determining region Y-box 2 (SOX2) monoclonal antibody (ab92494; 1:100; Abcam, Cambridge, MA, United States), rabbit anti-human lymphoid enhancer binding factor 1 (LEF1) monoclonal antibody (ab137872; 1:100; Abcam, Cambridge, MA, United States), mouse anti-human vimentin (VIM) monoclonal antibody (V9; 1:1; DAKO, Glostrup, Denmark), and mouse anti-human smooth muscle actin (SMA) monoclonal antibody (1A4; 1:1; DAKO, Glostrup, Denmark). For versican (VCAN) staining, the sections were incubated 2 h at RT with rabbit anti-human VCAN polyclonal antibody (versican V0, V1 neo; 1:100; Thermo Fisher Scientific, Rockford, IL, United States). After washing by tris-buffered saline, samples were incubated with secondary anti-mouse or rabbit antibodies (ENVISION Dual link system; DAKO, Glostrup, Denmark) for 30 min at RT. Subsequently, the sections were visualized by incubation with 3-amino-9-ethylcarbazole (AEC; DAKO, Glostrup, Denmark) and nuclei were counterstained by Mayer's hematoxylin.

Alkaline Phosphatase Staining

Frozen tissue sections were fixed with acetone for 10 min at 4°C. After washing with tris-buffered saline for 5 min, sections were exposed to 1 mg/ml alkaline phosphatase (ALP) Fast Blue RR salt (F0500; Sigma-Aldrich, St. Louis, MO, United States) in 0.2 mol/L 2-amino-2-methyl-1,3-propanediol-HCl buffer solution (pH 8.6) (A9754; Sigma-Aldrich, St. Louis, MO, United States) containing 0.05 mg/ml naphthol AS-MX phosphate disodium salt phosphatase substrate (N5000; Sigma-Aldrich, St. Louis, MO, United States) and 2% N,N-dimethylformamide (D4254; Sigma-Aldrich, St. Louis, MO, United States) for 45 min at 37°C. Subsequently, sections were counterstained by nuclear fast red (Muto Chemical KK, Tokyo, Japan) for 10 min.

Immunofluorescent Analysis

The samples were embedded in OCT and kept at -80°C before sectioning. The cryopreserved sections were defrosted, fixed with acetone at 4°C for 10 min, washed twice with PBS, and incubated with mouse anti-human vimentin (VIM) monoclonal antibody (V9; 1:1; DAKO, Glostrup, Denmark) for 30 min at RT, washed, and then incubated with Alexa Flour 488 goat anti-mouse IgG (H + L) polyclonal secondary antibody (A11029; 1:100; Invitrogen, Carlsbad, CA, United States) for 40 min at RT. The nuclei were stained by 4',6-diamidino-2-phenylindole (1:1,500; Dojindo Molecular Technologies, Inc., Kumamoto, Japan). After washing, specimens were mounted with PermaFluor Aqueous Mounting Medium (Thermo Fisher Scientific, Rockford, IL, United States). The images were obtained using BZ-X710 (KEYENCE, Osaka, Japan).

Statistical Analysis

Statistical analysis in this study was performed by Wilcoxon signed-rank test using SPSS version 25 (IBM, Armonk, NY, United States). A *p*-value of less than 0.05 was considered as statistically significant.

RESULTS

Normal KC and DP-Derived Constructs Reorganized Intratissue Architecture to Mimic Representative HF Structural Features During 2-Week Culture

Immediately after DP aggregates and condensed KCs were placed in Matrigel to reproduce their anatomical locations in HFs, individual cell components were in close contact with each other but clearly distinguishable (**Figure 1A**). In our pilot study, the constructs were generated and cultured without any auxiliary structural material, leading to the loss of distinct morphological characteristics and difficulty in preparation of histological sections under the absence of a direction indicator (**Supplementary Figure 1**). Being inspired by the work of Toyoshima et al. (2012), a nylon fiber was inserted into the main body of the KC-DP construct, which sustained the structural integrity at the time of reconstitution (**Figures 1A–C**).

During 2-week culture, the constructs grew and reformed gross morphology to a cudgel-like appearance with smoother surface visually mimicking human HFs, especially the suprabulbar (stem) and bulb portion (**Figures 1B–D**). Histological analysis of KC-DP constructs is technically challenging because of their smallness and fragility and illustrations were provided for each panel (**Figure 1D**). In 2-day cultured constructs, DP aggregates remained unfused, distributing around the end of the structures. A week later, the fundamental morphology was unchanged; however, the diameter of cylindrical body increased. Interestingly, DP aggregates seemed to relocate themselves to more densely distribute at the end portion. After 2 weeks, the end portion of the reconstructed structure usually enlarged resembling the bulb portion of the HF (**Figures 1C,D**). The orange-tinted end reflects dense accumulation of dye-stained DP aggregates, suggesting cell-autonomous self-reorganization (**Figure 1D**). The main body of KC-DP constructs consisted of major components subdivided by nylon fibers, individually consisting of three histologically distinct KC layers with differential eosin staining intensities (**Figure 1D**). This architecture resembled the arrangement of the outer and inner root sheath (ORS and IRS), and the hair shaft within HF (**Figure 1D** and **Supplementary Figure 2**). Human fibroblasts could be aggregated to form spheroid structure resembling DP aggregates (**Supplementary Figure 3A**); however, constructs generated with KC and fibroblast aggregates failed to form KC layers analogous to those observed in KC-DP constructs (**Supplementary Figure 3B**).

When KC-DP constructs cultured for 4 weeks were compared to those cultured for 2 weeks, morphologically analogous structures were formed; however, dyskeratotic cell-like changes with homogenous eosinophilic cytoplasm were observed in the constructs cultured for 4 weeks (**Supplementary Figure 4**).

These findings suggested that KC-DP constructs reorganized intratissue architecture to mimic representative HF structural features, especially those of the suprabulbar to bulb portion, during 2-week culture, possibly *via* trichogenic EMI between KC and DP components.

KC-DP Constructs Sketchily Reproduced Compartmental HF Characteristics in Immunohistochemistry

The HF is biochemically characterized by its distinct keratin and mesenchymal marker expression profiles. In normal human HFs, keratin (KRT) 13 is expressed in IRS, while KRT14 is detected in ORS. KRT17 is expressed in the inner aspect of ORS and KRT19 is diffusely detectable in ORS from the bulge to bulb. Immunoreactivity of KRT40, a representative hair hard keratin, is specifically observed in the hair shaft. VIM is a global mesenchymal marker expressed in the dermal portion of the HF. Expression levels of VCAN and SMA have been reported to correlate with DP and DS cell properties, including hair inductive property (Jahoda et al., 1991; Kishimoto et al., 1999; Kishimoto et al., 2000). These markers are preferentially expressed in the proximal portion of the dermal sheath and partially in the DP (Ohyama et al., 2010) (**Supplementary Figure 5**).

Time course immunohistochemical analyses suggested that KC-DP constructs gradually recapitulated microanatomical keratin and mesenchymal marker expression patterns of normal human HFs during 2-week culture (**Figure 2A**). In 2-day constructs, KRT13 demonstrated a weak and diffuse expression pattern in the KC compartment. However, KRT13 expression was confined to the inner layer of 1-week constructs, which became more intense and broader in 2-week constructs. At the beginning of the culture, KRT14 diffusely expressed in KC compartment in 2-day constructs, which localized to the layer next to that expressing KRT13, analogous to the HF. KRT17 was rather non-specifically expressed from the beginning of the assay, while KRT19 expression increased in the KRT14 expressed area similarly to normal HFs (Fukuyama et al., 2017). Interestingly, KRT40 expression, which is specific to the hair shaft and highlighted by AE13-positive immunoreactivity (**Supplementary Figure 5**), was initially negative but started to become detectable in KC strands located adjacent to the KRT13 expression area extending from the interface between DP aggregates after 1-week culture, which was maintained at 2 weeks.

VIM and VCAN were consistently detected in DP aggregates, providing a useful marker to distinguish dermal cells from KCs and implying that DP properties were maintained to some extent in the constructs (**Figure 2A**). The expression level of SMA, which rather represents a dermal sheath marker than that of DP (**Supplementary Figure 5**), gradually decreased in DP aggregates during the assay (**Figure 2A**).

These findings suggested that KC-DP constructs sketchily reproduced biochemical characteristics of individual HF compartments in a time-dependent manner during the 2-week assay.

Reconstituted HF-Like Structures Upregulated HF-Related Epithelial Genes While Downregulating WNT Signaling Genes

When compared to cultured human KCs, KC-DP constructs tendentiously upregulated *KRT33A* (hair shaft cortex keratin), *KRT82* (hair shaft cuticle keratin), and *KRT25* (IRS keratin) (Langbein et al., 2006; Schweizer et al., 2007), respectively, by 5.9-fold ($p = 0.095$), 15.1-fold ($p = 0.095$), and 14-fold ($p = 0.095$) on average. In contrast, representative HF-related WNT signaling genes *WNT5A* (DP marker) and *LEF1* (DP > HF-epithelial marker) were downregulated in KC-DP constructs compared to DPCs by 1.9-fold ($p = 0.095$) and 25-fold ($p < 0.01$), respectively (**Figure 2B**).

These observations suggested that folliculogenic EMIs between KC and DP components were elicited in the constructs and that the magnitude of EMI was insufficient because of the loss of DP properties *in vitro*.

Activation of WNT, SHH, and EDA Signaling Improved HF-Related Marker Expression in KC-DP Constructs

WNT signaling pathway has been reported to play key roles in HF morphogenesis and regeneration (Millar, 2002; Sennett and Rendl, 2012). Addition of WNT signaling agonists has been shown to sustain or ameliorate impaired intrinsic properties of human cultured DP cells (Ohyama et al., 2012; Soma et al., 2012). When exposed to a WNT agonist, CHIR99021 (Ring et al., 2003), KC-DP constructs did not markedly change their morphology. VIM, VCAN, and SMA immunoreactivity were maintained; however, gene expression analysis detected that HF-related genes, *KRT33A*, *KRT82*, *KRT25, WNT5A,* and *LEF1*, tended to be upregulated by the WNT agonist (**Figures 3A,B**).

Sonic hedgehog (SHH) and EDA signaling pathways are also crucial in folliculogenic EMIs (St-Jacques et al., 1998; Zhang et al., 2009; Mikkola, 2011). A recent study suggested that WNT, SHH, and EDA signaling agonists synergistically enhanced HF-related gene expression in cultured three-dimensional skin equivalent (Fukuyama et al., 2020). Based on this observation, the mixture of WNT, SHH, and EDA agonists was supplemented to the culture medium during the assay. Despite the fact that KRT40 immunoreactivity seemed to be mildly intensified, an increase in immunoreactivity of VIM, VCAM, and SMA was not evident in the mixture-treated KC-DP constructs. In contrast, further enhancement of HF-related keratin and WNT gene expression levels was noted when compared to those in untreated and WNT agonist-treated KC-DP constructs (**Figures 3A,B**).

Despite the fact that the extent of amelioration was moderate by the aforementioned combination, these findings favored the combined use of folliculogenic signaling activators for the quality improvement of KC-DP constructs.

iDPSC Aggregates Partially Recapitulated DP Properties *in vitro*

A past study reported that hiPSC-derived DP substituting cells (iDPSCs) share some biological characteristics of human intact DP cells, including hair inductive capacity, as demonstrated by *in vivo* HF reconstruction assay (Veraitch et al., 2017). Use of iDPSC aggregates for the replacement of DP aggregates in KC-DP constructs would be a reasonable approach to assess iDPSC properties *ex vivo*. Accordingly, three lines of hiPSCs were, respectively, induced into mesenchymal cells (iMCs) and

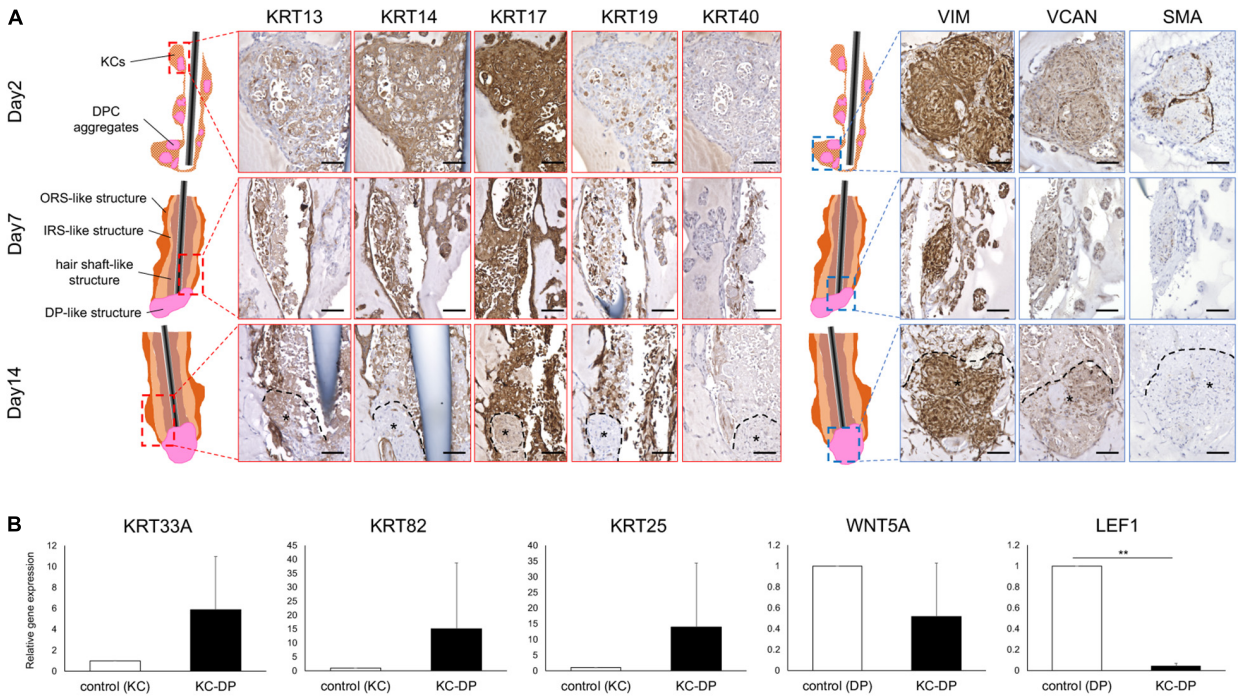

FIGURE 2 | Immunohistochemical and gene expression analysis of HF marker expression in KC-DP construct. **(A)** Time course immunohistochemical analyses revealed that the constructs regenerated with keratinocytes and dermal papilla cells (KC-DP) gradually recapitulated hair follicle (HF) marker expression patterns resembling those in human HF (see **Supplementary Figure S6**) during 2-week culture. KRT13 is expressed in the inner portion, while KRT14 is detected in the outer portion. KRT17 is diffusedly expressed in the main body, while KRT19 gradually became detectable in the inner and outermost portion. Linear immunoreactivity of KRT40 extended from DP. VIM, VCAN, and SMA were detected in DP. *: DP aggregates. **(B)** The expression levels of HF-related genes in KC-DP constructs (Mean ± SEM; $n = 5$, triplicate for each experimentation; $^{**}p < 0.01$, Wilcoxon signed-rank test). DP, dermal papilla; DPC, dermal papilla cells; KC, keratinocyte; KRT, keratin; VIM, vimentin; VCAN, versican; SMA, smooth muscle actin. Scale bar: 200 μm.

further differentiated into iDPSCs and subsequently aggregated based on the previously established protocol (Ohyama et al., 2012) (**Figure 4A**).

Spheroid formation adopting low cell-binding plate yielded DP and iDPSC aggregates with respective efficiency. Non-induced hiPSCs failed to form spheroids, suggesting that deviation into mesenchymal lineage is required in this methodology (**Supplementary Figure 6**). DP and WD39-hiPSC-derived iDPSCs successfully formed spheroid structures with a smooth surface (**Figure 4A**). Unexpectedly, 201B7-hiPSC- or RPC-hiPS771-2-derived iDPSC gave rise to cells that formed less compactly or irregularly aggregated structures (**Supplementary Figure 7**). Thus, WD39-hiPSC-derived iDPSC aggregates, hereafter termed as iDPs, were predominantly used for downstream experimentations.

A previous study reported the upregulation of selected DP markers during iDPSC induction from iMCs using the same protocol, but hiPSCs were maintained on feeders (Veraitch et al., 2017). In the present study adopting feeder-free hiPSCs, DP biomarkers, *NOG*, *SPRY4*, and *LRP4*, tended to be upregulated in iDPSCs compared to iMCs. Other DP or WNT signaling markers, *ALPL*, *WNT5A*, and *LEF1* (Ohyama et al., 2012), were downregulated in iDPSCs when compared to iMCs (**Figure 4B**). The expression levels of *ALPL*, *SPRY4*, and *WNT5A* were moderately restored by aggregating iDPSCs.

iDPs aggregates were able to locate at the bottom of HF-like structures during 2-week culture similarly to DP aggregates in KC-DP constructs. iDPs were less intensely stained with CellBrite^{TM} dye than DP aggregates and distinguishable (**Figure 4C**).

KC-iDP Constructs Reproduced Architectural/Biochemical Characteristics and Gene Expression Profile of KC-DP Constructs

When combined with cylindrically condensed KCs, iDPs formed structures morphologically analogous to KC-DP constructs (**Figure 5A**). Histologically, KC-iDP constructs reproduced architectural characteristics of KC-DP constructs, partially mimicking HF structures (**Figures 5B,C**).

Immunohistochemical examination demonstrated that KC-iDP constructs expressed HF-related markers in the same manner as KC-DP constructs (**Figure 5D**). Of note, intense immunoreactivity of hair shaft keratin, KRT40, as detected by AE13 monoclonal antibody, was observed in some KC-iDP constructs (**Figure 5D**). Expression levels of DP markers, VIM, VCAN, and SMA, in iDP aggregates were also comparable to those in KC-DP constructs (**Figures 2C, 5E**).

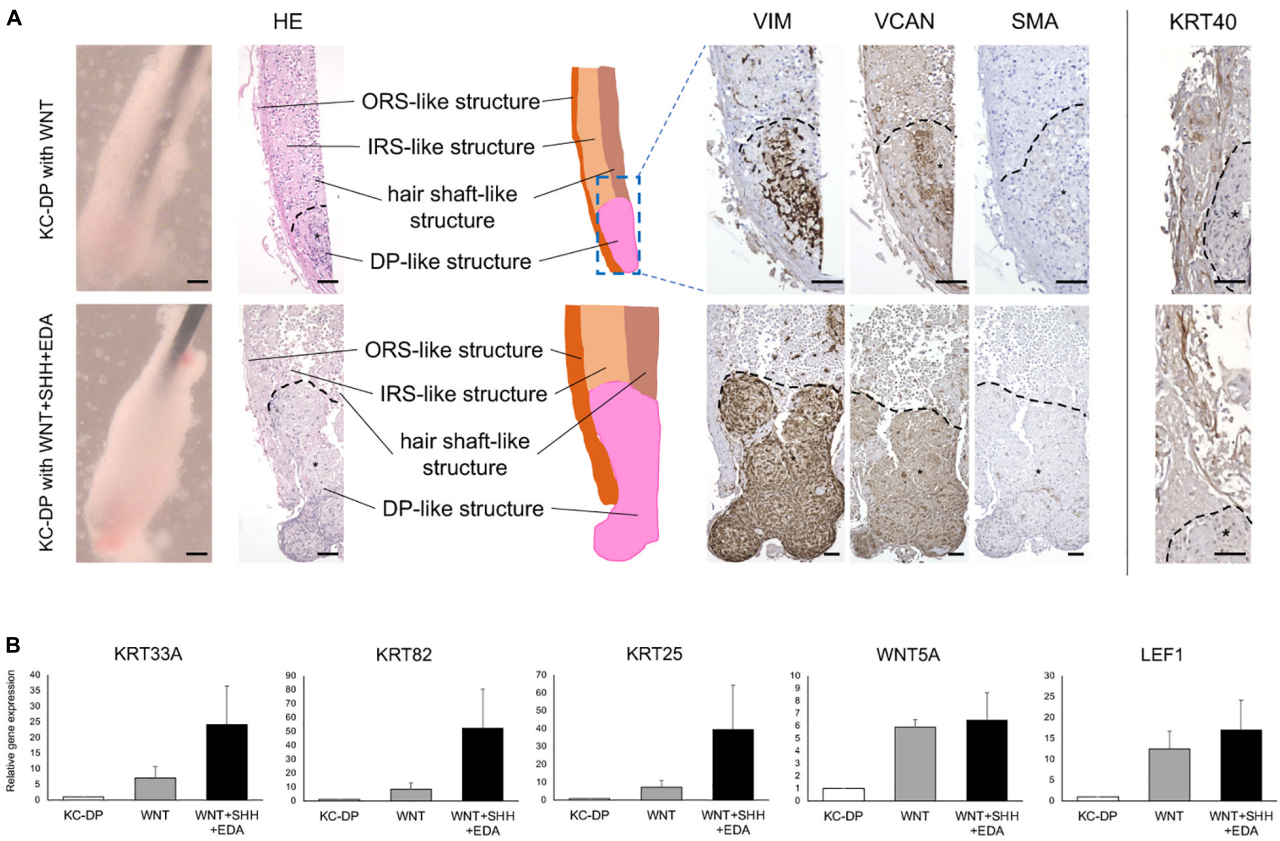

FIGURE 3 | Activation of WNT, SHH, and EDA signaling improved HF-related marker expression in KC-DP constructs. **(A)** Addition of the activators of signaling pathways involved in HF morphogenesis did not evidently ameliorate immunohistochemically detected HF marker expression in KC-DP constructs. *DP aggregates. **(B)** HF-related gene expression levels analyzed by qRT-PCR in KC-DP constructs tended to be increased by a WNT agonist (WNT) treatment, which tended to be further enhanced by the treatment by the mixture of agonists (WNT + SHH + EDA) (Mean ± SEM; $n = 3$, triplicate for each experimentation; Wilcoxon signed-rank test). KC, keratinocyte; DP, dermal papilla, Scale bar: 200 μm.

Intriguingly, hair shaft and IRS keratin genes, *KRT25*, *KRT33A*, and *KRT82*, were more intensely expressed in KC-iDP constructs than in KC-DP constructs (**Figure 6A**). *WNT5A* was almost equally expressed between KC-iDP and KC-DP constructs, while *LEF1* was upregulated by 8.7-fold in KC-iDP constructs (**Figure 6A**).

These findings suggested that iDPs improved their insufficiency in DP properties potentially *via* intercompartmental interaction with KCs within the constructs.

KC-iDP Constructs Responded to WNT, SHH, and EDA Agonists to Upregulate HF-Related Markers

To evaluate functional resemblances between KC-DP and KC-iDP constructs, a WNT activator alone or the mixture of WNT, SHH, and EDA activators were added to the culture of KC-iDP constructs. The resultant structures were morphologically comparable to non-treated KC-DP and KC-iDP constructs with analogous HF marker expression patterns (**Supplementary Figure 8**). A readily distinguishable HF-like bulb structure was reproduced in a representative WNT + SHH + EDA agonist mixture-treated KC-iDP construct (**Supplementary Figure 8**).

Intriguingly, KC-iDP constructs tended to express higher levels of HF keratin genes, *KRT33A*, *KRT82*, and *KRT25*, than those in KC-DP constructs. When treated by a WNT agonist, KC-iDP constructs significantly upregulated these HF keratin genes, which were further enhanced by the activation of WNT, SHH, and EDA signaling pathways ($p < 0.05$; **Figure 6A**). *WNT5A* was upregulated by the addition of WNT activator alone or by the combination of triple factors in KC-iDP constructs to the level in KC-DP constructs. *LEF1* expression was the most intense in WNT-treated KC-iDP constructs among all constructs examined, which was greater in triple factor-treated KC-iDP constructs than in non-treated KC-DP or KC-iDP constructs ($p < 0.05$; **Figure 6A**).

Further HF marker expression assessment in KC and DP/iDP compartment in the constructs was conducted by immune or enzyme histochemistry (**Figure 6B**). Immunoreactivity of KRT75, a marker of HF companion layer, was detected in the inner KC compartment of KC-DP constructs, which was more intense in KC-iDP constructs (**Figure 6C**). GATA3, a representative IRS marker (Chikh et al., 2007), was positively

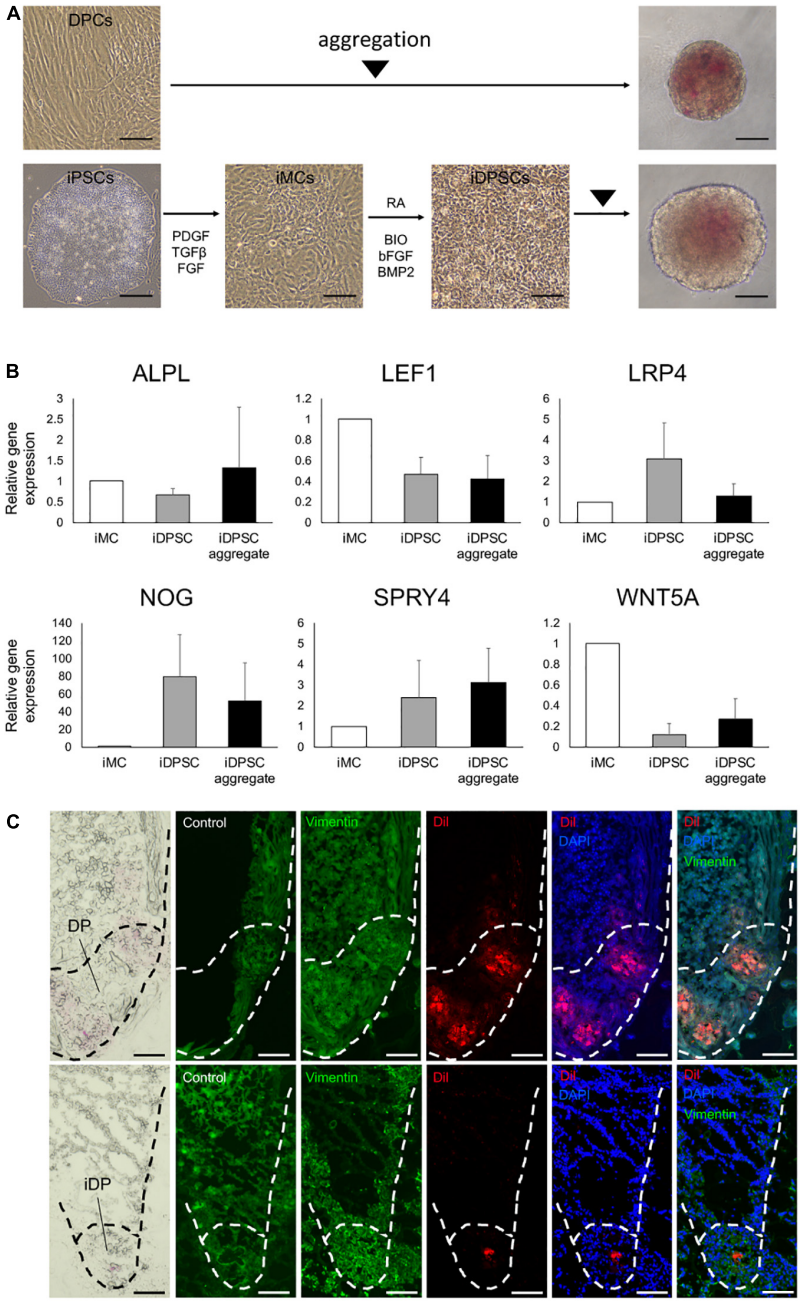

FIGURE 4 | Generation of hiPSC-derived dermal papilla substituting cell aggregates. **(A)** Aggregation of dermal papilla cells (DPCs) and the stepwise induction of human-induced pluripotent stem cell (hiPSC)-derived DP substituting cells (iDPSCs) from hiPSC-derived mesenchymal cells (iMCs) and the generation of iDPSC aggregates (iDPs). Scale bar: 100 μm. **(B)** Change in DP marker gene expression analyzed by qRT-PCR during iDP aggregate preparation from iMCs. (Mean ± SEM; $n = 3$, triplicate for each experimentation; Wilcoxon signed-rank test). **(C)** Immunofluorescent images of KC-DP (upper panels) and KC-iDP constructs (lower panels). Low dyeability to cytoplasmic membrane dyes distinguished iDPs from DPs. Scale bar: 200 μm.

stained in KC-DP and KC-iDP constructs (**Figure 6C**). DKK4, which is expressed in the hair placode and the hair shaft and partially in IRS of HF (Fliniaux et al., 2008), was observed in inner KC layers in KC-DP and KC-iDP constructs (**Figure 6B**). Furthermore, SOX2, LEF1, and ALP, which were expressed in the bulb, especially in DPs (**Supplementary Figure 5**), were more strongly stained in iDPs of KC-iDP constructs compared to those in KC-DP constructs (**Figure 6C**).

These findings suggested that iDPs would be functionally sufficient to replace DPs in KC-DP constructs, at least, to reproduce HF characteristics examined in the aforementioned three-dimensional culture protocol.

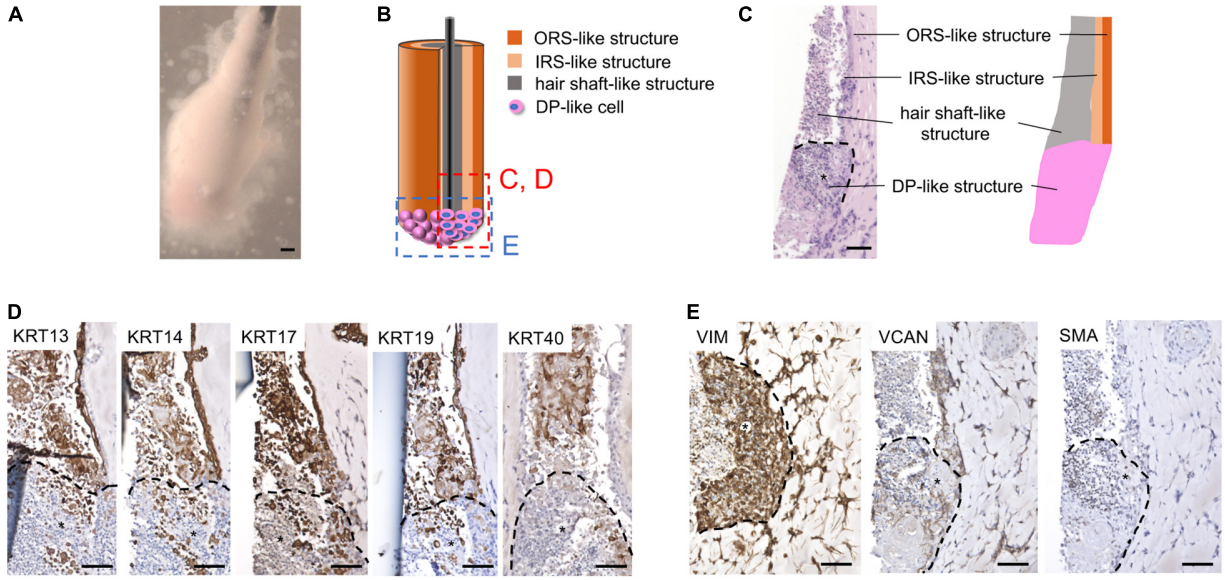

FIGURE 5 | KC-iDP constructs reproduced architectural/biochemical characteristics and gene expression profile of KC-DP constructs. **(A)** Morphology of KC-iDP constructs. Scale bar: 200 μm. **(B)** The schema illustrating the intratissue structure of KC-iDP constructs. **(C)** Histological characteristics of KC-iDP constructs resembling those of KC-DP constructs (see **Figure 2**). *: iDP aggregates. Scale bar: 200 μm. **(D)** Immunohistochemical analysis revealed that HF keratin distribution was almost indistinguishable between KC-DP and KC-iDP constructs (see **Figure 2**). KRT40-positive cells rearranged in the center of the main body mimicking the hair shaft without being splitted by a nylon fiber (the rightmost panel). *: iDP aggregates. Scale bar: 200 μm. **(E)** Immunoreactivities for mesenchymal markers in KC-iDP constructs. *: iDP aggregates. Scale bar: 200 μm; DP, dermal papilla; KC, keratinocyte; KRT, keratin; HF, hair follicle; iDP, human induced pluripotent cell-derived dermal papilla substituting cell aggregate; IRS, inner root sheath; ORS, outer root sheath; SMA, smooth muscle actin; VCAN, versican; VIM, vimentin.

DISCUSSION

The HF is a mini-organ consisting of multiple dynamically interacting epithelial and dermal components. Their anatomical relationships were crucial to elicit optimal EMIs to maintain the HF homeostasis represented by the hair cycle (Toyoshima et al., 2012; Abaci et al., 2018). Accordingly, microanatomical reproduction of HF architecture is pivotal to bioengineer structures fully reproducing HF architecture, let alone major functions (Abaci et al., 2018). Folliculogenic EMIs can partially be induced *in vitro* by the spheroid culture of HF-related epithelial and dermal cell mixtures (e.g., KCs and DP cells), which would not allow full recapitulation of three-dimensional (intercompartmental and directional) features of EMIs (Havlickova et al., 2009; Yen et al., 2010). Recent approaches took advantage of artificially assembling epithelial and mesenchymal components prior to *in vitro* or *in vivo* incubation *via* cell compartmentalization or molding to direct EMIs in a similar manner as in the HF (Toyoshima et al., 2012; Abaci et al., 2018). Adopting this strategy with substantial simplification, the methodology in the current study was invented.

Past studies demonstrated that cell aggregation ameliorated biological properties of cultured DP cells (Osada et al., 2007; Higgins et al., 2010; Kang et al., 2012; Ohyama et al., 2012; Higgins et al., 2013). The hair shaft has been reported to correlate with that of DP (Chi et al., 2013), suggesting that the magnitude of folliculogenic EMIs can be influenced by the size of regenerated DP cell aggregates. We initially attempted to generate larger DP cell aggregates; however, at least with our hands and the microenvironment of the assay developed, the central portion of DP aggregates with the size of human DPs tended to necrotize. Therefore, multiple smaller DP aggregates were generated and embedded as clusters in Matrigel. The DP aggregates did not completely fuse with each other but gradually gather together to form the assemblages during the 2-week culture. As the shape of the assemblages was hardly uniform among regenerated KC-DP constructs with the current approach, the magnitude of EMIs elicited in the KC-DP interface would be variable, which, together with the difference in biological properties of DP cells used for each experimentation, might account for the variance in HF-related keratin gene expression levels among KC-DP constructs. As HF markers, *WNT5A* and *LEF1*, were downregulated in KC-DP constructs than in control DP cells, the improvement in DP cell preparation is indispensable. Use of the dermal papilla activation culture condition (DPAC) (Ohyama et al., 2012) combined with an alternative aggregation protocol, e.g., the hanging drop culture (Higgins et al., 2013), may facilitate the preparation of more potent and larger DP cell spheroids replacing DP aggregates adopted in this study.

Using the protocol published by Toyoshima et al. as a reference, a nylon fiber was inserted into the center of KC-DP constructs. Originally, the investigators adopted this methodology for "*in vivo* transplantation of the bioengineered hair germ to prevent epithelial cyst formation and allow the bioengineered HF epithelium connected to that of the host

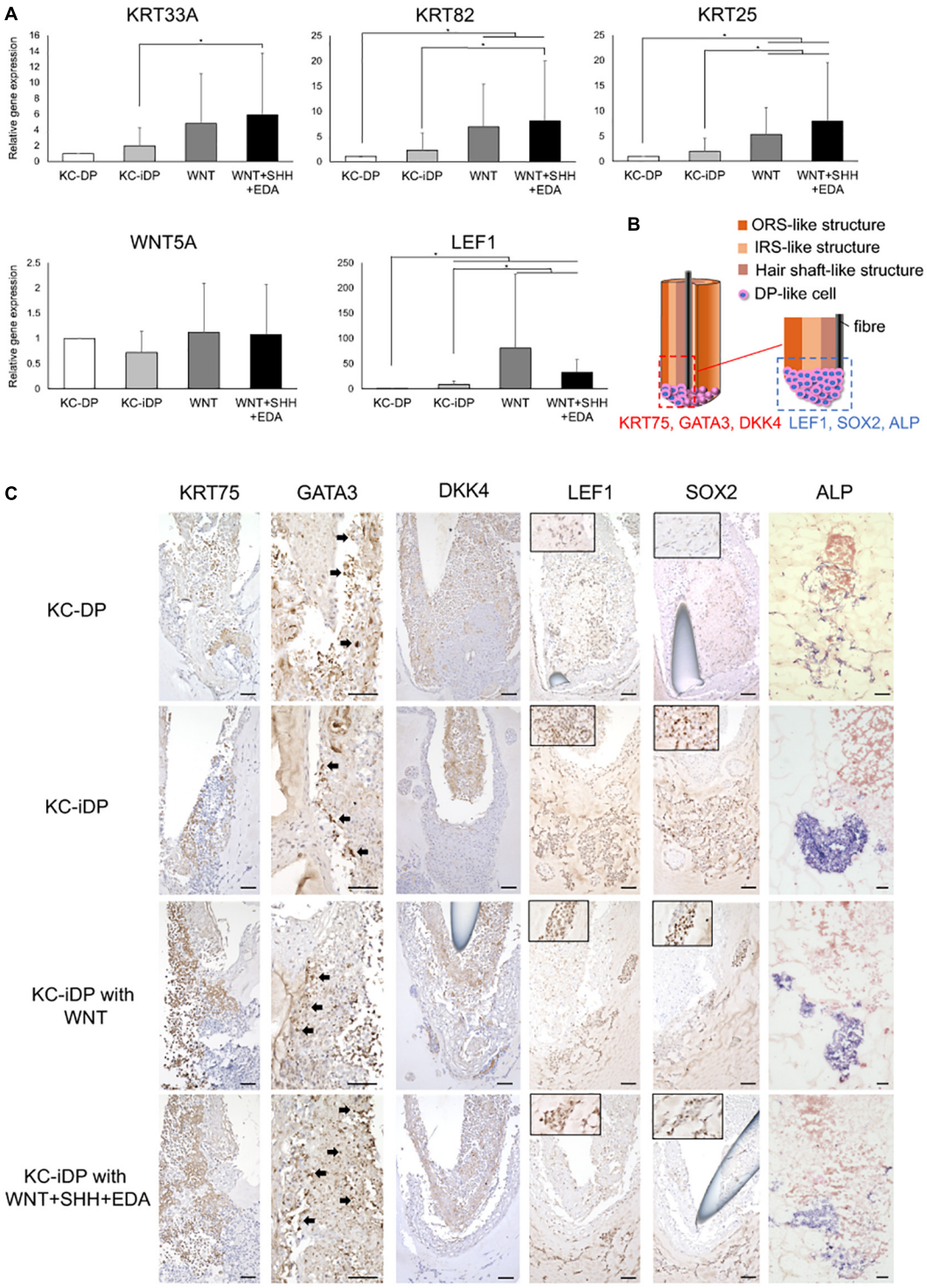

FIGURE 6 | KC-iDP constructs responded to WNT, SHH, and EDA agonists to upregulate HF-related markers. **(A)** A WNT agonist increased HF keratin gene and *LEF1* expression in KC-iDP constructs, which was further enhanced by the simultaneous activation of WNT, SHH, and EDA signaling pathways (Mean ± SEM; $n = 5$, triplicate for each experimentation; $^*p < 0.05$, Wilcoxon signed-rank test). **(B)** The schema illustrating the intratissue distribution of examined hair follicle markers within KC-iDP constructs. **(C)** Immunoreactivities for hair follicle epithelial (KRT75, GATA3, and DKK4) and mesenchymal (LEF1, SOX2, and ALP) markers in non-treated, WNT agonist-treated, and triple agonist-treated KC-iDP constructs in comparison to those in KC-DP constructs. KRT75, SOX2, and LEF1 immunoreactivities were more intense in KC-iDP constructs, when compared to those in KC-DP constructs. Scale bar: 200 μm. ALP, alkaline phosphatase; DKK4, dickkopf 4; DP, dermal papilla; GATA3, GATA binding protein 3; iDP, keratinocyte-human induced pluripotent cell-derived dermal papilla substituting cell aggregate; KC, keratinocyte; KRT, keratin; LEF1, lymphoid enhancer binding factor 1; SOX2, sex determining region Y-box 2.

animals leaving the hair canal for the emerging hair shaft" (Toyoshima et al., 2012). In the current study, the fiber is rather used to regulate the directionality of EMIs and maintain HF-like morphology by avoiding cell-autonomous migration/aggregation with resultant deformity of the *in vitro* regenerated constructs. In the assay developed, nylon fiber insertion is unfavorable as it vertically divides the KC-DP interface, leading to the split in EMIs. KC-DP constructs generated without a nylon fiber failed to sustain structural integrity, suggesting the necessity of some device to preserve morphological characteristics in the *in vitro* assay.

During the 2-week culture, KCs intercompartmentally differentiated or rearranged themselves to form multiple layers with a distinct histological characteristic and keratin expression pattern. As the constructs made of KCs and fibroblast aggregates failed to form stratified KC layers, EMIs between DP aggregates and adjacent KCs are speculated to have contributed to the formation of such layered structures. Cylindrical injection of KCs alone with the 2-week culture yielded KRT13 or KRT14 expressing outermost bilayers analogous to that observed in KC-DP constructs with central necrosis in the KC compartment (data not shown), suggesting that the microenvironment by itself, putatively *via* extracellular matrix contact or nutrition, pH, and hypoxia gradient, could also play roles in the recapitulation of HF-like keratin distribution in KC-DP constructs. Based on the change in KRT19 and KRT40 in KCs and VCAN and SMA expression in the dermal component, 2 weeks would be an optimal time for harvesting the culture product. At least with the current culture condition, further follicular differentiation by extending cultivation period cannot be expected. Histological examination of 4-week cultured KC-DP constructs detected robust intracompartmental necrosis. Incorporation of fibroblasts or vascular endothelial cells in Matrigel (Abaci et al., 2018) may extend the life span of the constructs. At the same time, such modifications complicate the protocol and can moderate the handiness of the assay.

Upregulation of HF-related keratins and mesenchymal markers by the addition of a WNT agonist or the mixture of WNT, SHH, and EDA agonists to the KC-DP construct culture implied an alternative approach to improve the assay by modulating the intensity of signaling pathways involved in HF morphogenesis. The concentrations for individual activators have been optimized for three-dimensional skin equivalent culture (Fukuyama et al., 2020), not for the current HF reconstitution assay. Other signaling pathways, represented by BMP and FGF signaling, plays pivotal roles in HF formation and regeneration (Rendl et al., 2008; Biggs et al., 2018) and therefore the addition of agonists of such signaling pathways to the activator mixture potentially enhance ameliorative effects on KC-DP constructs. The change in the content of culture supplements/additives minimally affects the complexity of the assay, and therefore, further optimization of the agonist mixture composition represents an important next step.

Unexpectedly, generation of iDPs morphologically analogous to DPs was only possible with WD39-derived iDPSCs. Less aggregative behavior observed in other hiPSC lines, together with the observation that non-induced hiPSCs failed to form spheroid in the adopted condition, suggested incomplete induction of DP properties in hiPSC lines other than WD39. Our past observation supports that the WD39 line is intrinsically mesenchymal-prone (Veraitch et al., 2013). This might have resulted in differential expression of cell adhesion molecules or extracellular matrices and enabled WD39 to form usable iDPs. Recent studies suggested roles of Hox genes and extracellular matrix in the determination of dermal cell phenotype, including that of DP cells (Driskell et al., 2013; Jiang et al., 2018; Yu et al., 2018). Thus, as a next step, it would be important to examine whether the expression of such potential determinants is different between WD39- and other hiPSC-derived iDPSCs to explain this observation, which emphasizes the importance of assessing the biological properties of hiPSC lines prior to downstream applications. WD39-derived iDPs moderately expressed DP markers. Low dyeability to cytoplasmic membrane dyes also distinguished iDPs from DPs. Such findings had implied functional inferiority of iDPs compared to DPs. Unexpectedly, HF-related keratin and WNT signaling gene expression levels were comparable to or more intense in KC-iDP constructs than those in KC-DP constructs. Moreover, markedly positive immunoreactivity of KRT40 could occasionally be observed in the KC-iDP construct. These observations suggested that iDPs intensified their DP properties to levels analogous to those in DPs putatively *via* the interaction with KCs *in vitro*.

The stepwise increase in HF-related keratin gene expression by a WNT agonist or the mixture of WNT, SHH, and EDA agonists was observed in the KC-iDP construct, which is also in favor of the acquisition of DP properties by iDPs *in vitro*. The magnitudes of upregulation by the addition of SHH and EDA activators were lesser in KC-iDP constructs compared to those generated with KCs and DPs. This might be explained by an intrinsically intense WNT activation state in KC-iDPs constructs as demonstrated by *LEF1* upregulation. Considering that the activation of WNT pathway alone and triple pathways did not result in major morphological or biochemical differences in KC-iDP constructs, additional modification to the culture condition, presumably *via* supplementation of extra signaling activators (e.g., SHH and BMP agonist), is mandated for further quality improvement of the KC-iDP construct.

We are aware of the limitations of the current study. Preparation of histological sections, especially frozen sections, was technically challenging because of the smallness and fragility of regenerated structures, which sometimes hampers accurate evaluation or comparisons. Manual reconstruction would not allow precisely consistent assembly of the constructs, potentially resulting in the variance in the size of the KC-DP or KC-iDP interface area, which could have affected the intensity of EMIs and result in differential expression of HF-related markers among the samples. Because of this inconsistency and the restriction in the amount of collectable samples, global gene expression analysis can hardly be conducted. The current protocol for DP induction can be applicable to selected hiPSC lines. However, these drawbacks also highlight the key elements indispensable

for successful *in vitro* bioengineering of human miniorgans adopting hiPSCs: preassessment of starting materials, importance of induction and cultivation period, microenvironment, intrastructurally directed EMls, and sufficient activation of pivotal signaling pathways.

The methodology developed in this study can provide a less complicated *in vitro* platform to assess the functionalities of tested mesenchymal components to elicit folliculogenic EMIs in an architecture sketchily resembling HFs, by which the possibility of using hiPSC-derived cell subsets for HF bioengineering was implied. With further modifications to the current protocol and hiPSC usage, the necessity of human tissue-derived trichogenic cell subsets, especially DPs, for regenerative medicine and drug discovery for hair loss disorders can be reduced.

DATA AVAILABILITY STATEMENT

The raw data supporting the conclusions of this article will be made available by the authors, without undue reservation.

ETHICS STATEMENT

The studies involving human participants were reviewed and approved by The Institutional Review Board of Kyorin University (Protocol Nos. H27-022, H28-131, and H29-116). The patients/participants provided their written informed consent to participate in this study.

AUTHOR CONTRIBUTIONS

MO designed the experiments. MF, AT, MK, YY, and MO performed the experiments and analyzed the data. HO supervised the project and provided materials and technical support. MF, HO, and MO drafted the manuscript. All authors contributed to the completion of the manuscript.

FUNDING

This work was supported by the JSPS KAKENHI Grant Number JP 16H05370 (to MO).

ACKNOWLEDGMENTS

We thank the donors for providing precious human scalp samples.

SUPPLEMENTARY MATERIAL

The Supplementary Material for this article can be found online at: https://www.frontiersin.org/articles/10.3389/fcell.2021.590333/full#supplementary-material

Supplementary Figure 1 | Morphology of KC-DP constructs generated without nylon fibers. Despite some constructs maintained club-like morphology, most constructs lost their structural characteristics to form less organized cell aggregates. Scale bar: 200 μm.

Supplementary Figure 2 | Histology of normal human hair follicle. The main body consisted of multiple keratinocyte layers with the dermal papilla at its proximal end. Scale bar: 200 μm.

Supplementary Figure 3 | The constructs consisted of KCs and aggregated fibroblasts failed to form multiple KC layers. When human fibroblasts-aggregates were combined with condensed columlar keratinocytes (KCs), multiple KC layers were not clearly formed unlike those in KC-DP constructs. Scale bar: 200 μm.

Supplementary Figure 4 | Morphological and histological findings of KC-DP constructs cultured for 4 weeks. The constructs were mainly consisted of necrotic cells and was surrounded by denucleated keratotic cells (arrowhead). Scale bar: 200 μm.

Supplementary Figure 5 | Keratins and dermal papilla-related marker expression pattern in human hair follicles. Keratin (KRT)13 is expressed in IRS, while KRT14 is detected in ORS. KRT17 is expressed in the inner aspect of ORS, while KRT19 is diffusely detectable in ORS from the bulge to the bulb. Immunoreactivity of KRT40, is specifically observed in the hair shaft. KRT75 is expressed in the companion layer. GATA3 is detected in IRS. DKK4 is weakly expressed in the hair shaft and in the root sheaths. VIM is a mesenchymal marker expressed in the dermal portion of the HF. VCAN and SMA are expressed in DS and DP. LEF1, SOX2, and ALP can be detected in DP. ALP, alkaline phosphatase; DKK4, dickkopf 4; DP, dermal papilla; DS, dermal sheath; GATA3, GATA binding protein 3; IRS, inner root sheath; KRT, keratin; LEF1, lymphoid enhancer binding factor 1; ORS, outer root sheath; SMA, smooth muscle actin; SOX2, sex determining region Y-box 2; VCAN, versican; VIM, vimentin. Scale bar: 200 μm.

Supplementary Figure 6 | WD39 hiPSCs failed to form cell Keratin aggregates in sphere formation. Unlike induced hiPSC-derived dermal papilla substituting cells, non-induced WD39 hiPSCs were unable to form spheres in cell aggregation protocol adopted. Scale bar: 100 μm.

Supplementary Figure 7 | Morphological comparison of WD39-, 201B7-hiPSC, and RPC-hiPS771-2-derived dermal papilla substituting aggregates. Note that 201B7 hiPSC formed less condensed fragile spheres, while RPC-hiPS771-2-hiPSCs hardly formed aggregates. hiPSC, human induced pluripotent stem cells. Scale bar: 100 μm.

Supplementary Figure 8 | Morphological, histological, and immunohistochemical analyses of KC-iDP constructs treated with a WNT agonist or the mixture of WNT, SHH, and EDA agonists. Gross morphology, histological characteristics, and immunohistological staining profiles of KC-iDP constructs were analogous to that of non-treated KC-iDP constructs presented in **Figure 5**. The main body was consisted of multiple KC layers showing respective positive immunoreactivity of KRT13, 14, 17, 19, and 40. iDP compartment was positive for VIM, VCAN, and SMA staining. KC, keratinocyte; KRT, keratin; iDP, human induced pluripotent stem cell-derived dermal papilla substituting cell aggregates; SMA, smooth muscle actin; VIM, vimentin; VCAN, versican Scale bar: 200 μm.

Supplementary Table 1 | Primer sequences for real-time PCR.

REFERENCES

Abaci, H. E., Coffman, A., Doucet, Y., Chen, J., Jackow, J., Wang, E., et al. (2018). Tissue engineering of human hair follicles using a biomimetic developmental approach. *Nat. Commun.* 9:5301. doi: 10.1038/s41467-018-07579-y

Biggs, L. C., Mäkelä, O. J., Myllymäki, S. M., Das Roy, R., Närhi, K., Pispa, J., et al. (2018). Hair follicle dermal condensation forms via Fgf20 primed cell cycle exit, cell motility, and aggregation. *Elife* 7:e36468. doi: 10.7554/eLife.36468

Chi, W., Wu, E., and Morgan, B. A. (2013). Dermal papilla cell number specifies hair size, shape and cycling and its reduction causes follicular decline. *Development* 140, 1676–1683. doi: 10.1242/dev.090662

Chikh, A., Sayan, E., Thibaut, S., Lena, A. M., DiGiorgi, S., Bernard, B. A., et al. (2007). Expression of GATA-3 in epidermis and hair follicle: relationship to p63. *Biochem. Biophys. Res. Commun.* 361, 1–6. doi: 10.1016/j.bbrc.2007.06.069

Driskell, R. R., Giangreco, A., Jensen, K. B., Mulder, K. W., and Watt, F. M. (2009). Sox2-positive dermal papilla cells specify hair follicle type in mammalian epidermis. *Development* 136, 2815–2823. doi: 10.1242/dev.038620

Driskell, R. R., Lichtenberger, B. M., Hoste, E., Kretzschmar, K., Simons, B. D., Charalambous, M., et al. (2013). Distinct fibroblast lineages determine dermal architecture in skin development and repair. *Nature* 504, 277–281. doi: 10.1038/nature12783

Ehama, R., Ishimatsu-Tsuji, Y., Iriyama, S., Ideta, R., Soma, T., Yano, K., et al. (2007). Hair follicle regeneration using grafted rodent and human cells. *J. Invest. Dermatol.* 127, 2106–2115. doi: 10.1038/sj.jid.5700823

Fliniaux, I., Mikkola, M. L., Lefebvre, S., and Thesleff, I. (2008). Identification of dkk4 as a target of Eda-A1/Edar pathway reveals an unexpected role of ectodysplasin as inhibitor of Wnt signalling in ectodermal placodes. *Dev. Biol.* 320, 60–71. doi: 10.1016/j.ydbio.2008.04.023

Fukuyama, M., Sato, Y., Yamazaki, Y., and Ohyama, M. (2017). Immunohistochemical dissection of cystic panfolliculoma focusing on the expression of multiple hair follicle lineage markers with an insight into the pathogenesis. *J. Cutan. Pathol.* 44, 861–866. doi: 10.1111/cup.12992

Fukuyama, M., Tsukashima, A., Kimishima, M., Yamazaki, Y., and Ohyama, M. (2020). Activators of WNT, sonic hedgehog and ectodysplasin A signaling pathways exert synergetic influence on folliculogenic epithelial-mesenchymal interactions in 3-D skin equivalents: an implication for regenerative medicine. *J. Dermatol.* 47, 1195–1197. doi: 10.1111/1346-8138.15523

Havlickova, B., Bíró, T., Mescalchin, A., Tschirschmann, M., Mollenkopf, H., Bettermann, A., et al. (2009). A human folliculoid microsphere assay for exploring epithelial- mesenchymal interactions in the human hair follicle. *J. Invest. Dermatol.* 129, 972–983. doi: 10.1038/jid.2008.315

Higgins, C. A., Chen, J. C., Cerise, J. E., Jahoda, C. A., and Christiano, A. M. (2013). Microenvironmental reprogramming by three-dimensional culture enables dermal papilla cells to induce de novo human hair-follicle growth. *Proc. Natl. Acad. Sci. U.S.A.* 110, 19679–19688. doi: 10.1073/pnas.1309970110

Higgins, C. A., Richardson, G. D., Ferdinando, D., Westgate, G. E., and Jahoda, C. A. (2010). Modelling the hair follicle dermal papilla using spheroid cell cultures. *Exp. Dermatol.* 19, 546–548. doi: 10.1111/j.1600-0625.2009.01007.x

Imaizumi, Y., Okada, Y., Akamatsu, W., Koike, M., Kuzumaki, N., Hayakawa, H., et al. (2012). Mitochondrial dysfunction associated with increased oxidative stress and α-synuclein accumulation in PARK2 iPSC-derived neurons and postmortem brain tissue. *Mol. Brain* 5:35. doi: 10.1186/1756-6606-5-35

Jahoda, C. A., Reynolds, A. J., Chaponnier, C., Forester, J. C., and Gabbiani, G. (1991). Smooth muscle alpha-actin is a marker for hair follicle dermis in vivo and in vitro. *J. Cell Sci.* 99(Pt 3), 627–636. doi: 10.1242/jcs.99.3.627

Jiang, D., Correa-Gallegos, D., Christ, S., Stefanska, A., Liu, J., Ramesh, P., et al. (2018). Two succeeding fibroblastic lineages drive dermal development and the transition from regeneration to scarring. *Nat. Cell Biol.* 20, 422–431. doi: 10.1038/s41556-018-0073-8

Kang, B. M., Kwack, M. H., Kim, M. K., Kim, J. C., and Sung, Y. K. (2012). Sphere formation increases the ability of cultured human dermal papilla cells to induce hair follicles from mouse epidermal cells in a reconstitution assay. *J. Invest. Dermatol.* 132, 237–239. doi: 10.1038/jid.2011.250

Kishimoto, J., Burgeson, R. E., and Morgan, B. A. (2000). Wnt signaling maintains the hair-inducing activity of the dermal papilla. *Genes Dev.* 14, 1181–1185.

Kishimoto, J., Ehama, R., Wu, L., Jiang, S., Jiang, N., and Burgeson, R. E. (1999). Selective activation of the versican promoter by epithelial- mesenchymal interactions during hair follicle development. *Proc. Natl. Acad. Sci. U.S.A.* 96, 7336–7341. doi: 10.1073/pnas.96.13.7336

Kobayashi, T., Iwasaki, T., Amagai, M., and Ohyama, M. (2010). Canine follicle stem cell candidates reside in the bulge and share characteristic features with human bulge cells. *J. Invest. Dermatol.* 130, 1988–1995. doi: 10.1038/jid.2010.68

Langbein, L., Rogers, M. A., Praetzel-Wunder, S., Helmke, B., Schirmacher, P., and Schweizer, J. (2006). K25 (K25irs1), K26 (K25irs2), K27 (K25irs3), and K28 (K25irs4) represent the type I inner root sheath keratins of the human hair follicle. *J. Invest. Dermatol.* 126, 2377–2386. doi: 10.1038/sj.jid.5700494

McElwee, K. J., Kissling, S., Wenzel, E., Huth, A., and Hoffmann, R. (2003). Cultured peribulbar dermal sheath cells can induce hair follicle development and contribute to the dermal sheath and dermal papilla. *J. Invest. Dermatol.* 121, 1267–1275. doi: 10.1111/j.1523-1747.2003.12568.x

Mikkola, M. L. (2011). The Edar subfamily in hair and exocrine gland development. *Adv. Exp. Med. Biol.* 691, 23–33. doi: 10.1007/978-1-4419-6612-4_3

Millar, S. E. (2002). Molecular mechanisms regulating hair follicle development. *J. Invest. Dermatol.* 118, 216–225. doi: 10.1046/j.0022-202x.2001.01670.x

Nagao, K., Kobayashi, T., Moro, K., Ohyama, M., Adachi, T., Kitashima, D. Y., et al. (2012). Stress-induced production of chemokines by hair follicles regulates the trafficking of dendritic cells in skin. *Nat. Immunol.* 13, 744–752. doi: 10.1038/ni.2353

Ohyama, M. (2019). Use of human intra-tissue stem/progenitor cells and induced pluripotent stem cells for hair follicle regeneration. *Inflamm. Regen.* 39:4. doi: 10.1186/s41232-019-0093-1

Ohyama, M., and Okano, H. (2014). Promise of human induced pluripotent stem cells in skin regeneration and investigation. *J. Invest. Dermatol.* 134, 605–609. doi: 10.1038/jid.2013.376

Ohyama, M., Kobayashi, T., Sasaki, T., Shimizu, A., and Amagai, M. (2012). Restoration of the intrinsic properties of human dermal papilla in vitro. *J. Cell Sci.* 125, 4114–4125. doi: 10.1242/jcs.105700

Ohyama, M., Zheng, Y., Paus, R., and Stenn, K. S. (2010). The mesenchymal component of hair follicle neogenesis: background, methods and molecular characterization. *Exp. Dermatol.* 19, 89–99. doi: 10.1111/j.1600-0625.2009.00935.x

Osada, A., Iwabuchi, T., Kishimoto, J., Hamazaki, T. S., and Okochi, H. (2007). Long-term culture of mouse vibrissal dermal papilla cells and de novo hair follicle induction. *Tissue Eng.* 13, 975–982. doi: 10.1089/ten.2006.0304

Rendl, M., Polak, L., and Fuchs, E. (2008). BMP signaling in dermal papilla cells is required for their hair follicle-inductive properties. *Genes Dev.* 22, 543–557. doi: 10.1101/gad.1614408

Ring, D. B., Johnson, K. W., Henriksen, E. J., Nuss, J. M., Goff, D., Kinnick, T. R., et al. (2003). Selective glycogen synthase kinase 3 inhibitors potentiate insulin activation of glucose transport and utilization in vitro and in vivo. *Diabetes* 52, 588–595. doi: 10.2337/diabetes.52.3.588

Saed, S., Ibrahim, O., and Bergfeld, W. F. (2017). Hair camouflage: a comprehensive review. *Int. J. Womens Dermatol.* 3, S75–S80. doi: 10.1016/j.ijwd.2017.02.016

Schneider, M. R., Schmidt-Ullrich, R., and Paus, R. (2009). The hair follicle as a dynamic miniorgan. *Curr. Biol.* 19, R132–R142. doi: 10.1016/j.cub.2008.12.005

Schweizer, J., Langbein, L., Rogers, M. A., and Winter, H. (2007). Hair follicle-specific keratins and their diseases. *Exp. Cell Res.* 313, 2010–2020. doi: 10.1016/j.yexcr.2007.02.032

Sennett, R., and Rendl, M. (2012). Mesenchymal-epithelial interactions during hair follicle morphogenesis and cycling. *Semin. Cell Dev. Biol.* 23, 917–927. doi: 10.1016/j.semcdb.2012.08.011

Sinha, S., and Chen, J. K. (2006). Purmorphamine activates the Hedgehog pathway by targeting Smoothened. *Nat. Chem. Biol.* 2, 29–30. doi: 10.1038/nchembio753

Soma, T., Fujiwara, S., Shirakata, Y., Hashimoto, K., and Kishimoto, J. (2012). Hair-inducing ability of human dermal papilla cells cultured under Wnt/β-catenin signalling activation. *Exp. Dermatol.* 21, 307–309. doi: 10.1111/j.1600-0625.2012.01458.x

Stenn, K. S., and Paus, R. (2001). Controls of hair follicle cycling. *Physiol. Rev.* 81, 449–494. doi: 10.1152/physrev.2001.81.1.449

St-Jacques, B., Dassule, H. R., Karavanova, I., Botchkarev, V. A., Li, J., Danielian, P. S., et al. (1998). Sonic hedgehog signaling is essential for hair development. *Curr. Biol.* 8, 1058–1068. doi: 10.1016/s0960-9822(98)70443-9

Takahashi, K., Tanabe, K., Ohnuki, M., Narita, M., Ichisaka, T., Tomoda, K., et al. (2007). Induction of pluripotent stem cells from adult human fibroblasts by defined factors. *Cell* 131, 861–872. doi: 10.1016/j.cell.2007.11.019

Thangapazham, R. L., Klover, P., Li, S., Wang, J. A., Sperling, L., and Darling, T. N. (2014a). A model system to analyse the ability of human keratinocytes to form hair follicles. *Exp. Dermatol.* 23, 443–446. doi: 10.1111/exd.12424

Thangapazham, R. L., Klover, P., Wang, J. A., Zheng, Y., Devine, A., Li, S., et al. (2014b). Dissociated human dermal papilla cells induce hair follicle neogenesis in grafted dermal-epidermal composites. *J. Invest. Dermatol.* 134, 538–540. doi: 10.1038/jid.2013.337

Toyoshima, K. E., Asakawa, K., Ishibashi, N., Toki, H., Ogawa, M., Hasegawa, T., et al. (2012). Fully functional hair follicle regeneration through the rearrangement of stem cells and their niches. *Nat. Commun.* 3:784. doi: 10.1038/ncomms1784

Veraitch, O., Kobayashi, T., Imaizumi, Y., Akamatsu, W., Sasaki, T., Yamanaka, S., et al. (2013). Human induced pluripotent stem cell-derived ectodermal precursor cells contribute to hair follicle morphogenesis in vivo. *J. Invest. Dermatol.* 133, 1479–1488. doi: 10.1038/jid.2013.7

Veraitch, O., Mabuchi, Y., Matsuzaki, Y., Sasaki, T., Okuno, H., Tsukashima, A., et al. (2017). Induction of hair follicle dermal papilla cell properties in human induced pluripotent stem cell-derived multipotent LNGFR(+)THY-1(+) mesenchymal cells. *Sci. Rep.* 7:42777. doi: 10.1038/srep42777

Weinberg, W. C., Goodman, L. V., George, C., Morgan, D. L., Ledbetter, S., Yuspa, S. H., et al. (1993). Reconstitution of hair follicle development in vivo: determination of follicle formation, hair growth, and hair quality by dermal cells. *J. Invest. Dermatol.* 100, 229–236. doi: 10.1111/1523-1747.ep12468971

Yang, C. C., and Cotsarelis, G. (2010). Review of hair follicle dermal cells. *J. Dermatol. Sci.* 57, 2–11. doi: 10.1016/j.jdermsci.2009.11.005

Yen, C. M., Chan, C. C., and Lin, S. J. (2010). High-throughput reconstitution of epithelial-mesenchymal interaction in folliculoid microtissues by biomaterial-facilitated self-assembly of dissociated heterotypic adult cells. *Biomaterials* 31, 4341–4352. doi: 10.1016/j.biomaterials.2010.02.014

Yoshida, Y., Soma, T., Matsuzaki, T., and Kishimoto, J. (2019). Wnt activator CHIR99021-stimulated human dermal papilla spheroids contribute to hair follicle formation and production of reconstituted follicle-enriched human skin. *Biochem. Biophys. Res. Commun.* 516, 599–605. doi: 10.1016/j.bbrc.2019.06.038

Yu, Z., Jiang, K., Xu, Z., Huang, H., Qian, N., Lu, Z., et al. (2018). Hoxc-Dependent mesenchymal niche heterogeneity drives regional hair follicle regeneration. *Cell Stem Cell* 23, 487–500.e486. doi: 10.1016/j.stem.2018.07.016

Zhang, Y., Tomann, P., Andl, T., Gallant, N. M., Huelsken, J., Jerchow, B., et al. (2009). Reciprocal requirements for EDA/EDAR/NF-kappaB and Wnt/beta-catenin signaling pathways in hair follicle induction. *Dev. Cell* 17, 49–61. doi: 10.1016/j.devcel.2009.05.011

Zheng, Y., Du, X., Wang, W., Boucher, M., Parimoo, S., and Stenn, K. (2005). Organogenesis from dissociated cells: generation of mature cycling hair follicles from skin-derived cells. *J. Invest. Dermatol.* 124, 867–876. doi: 10.1111/j.0022-202X.2005.23716.x

Zimmerman, A., Bai, L., and Ginty, D. D. (2014). The gentle touch receptors of mammalian skin. *Science* 346, 950–954. doi: 10.1126/science.1254229

Conflict of Interest: MO is a scientific advisor of Taisho Pharmaceutical Co. Ltd., Rhoto Pharmaceutical Co. Ltd., Pfizer R&D Inc., and Ili Lilly Japan K.K. and receives research grants from Shiseido Co. and Maruho Co. for the topics not related to this study. HO is a member of the scientific advisory boards of San Bio Co. Ltd., Eisai Co. Ltd., and Daiichi Sankyo Co. Ltd.

The remaining authors declare that the research was conducted in the absence of any commercial or financial relationships that could be construed as a potential conflict of interest.

Publisher's Note: All claims expressed in this article are solely those of the authors and do not necessarily represent those of their affiliated organizations, or those of the publisher, the editors and the reviewers. Any product that may be evaluated in this article, or claim that may be made by its manufacturer, is not guaranteed or endorsed by the publisher.

Copyright © 2021 Fukuyama, Tsukashima, Kimishima, Yamazaki, Okano and Ohyama. This is an open-access article distributed under the terms of the Creative Commons Attribution License (CC BY). The use, distribution or reproduction in other forums is permitted, provided the original author(s) and the copyright owner(s) are credited and that the original publication in this journal is cited, in accordance with accepted academic practice. No use, distribution or reproduction is permitted which does not comply with these terms.

frontiers in Cell and Developmental Biology

ORIGINAL RESEARCH
published: 17 September 2021
doi: 10.3389/fcell.2021.724310

Transcriptome Analysis Reveals an Inhibitory Effect of Dihydrotestosterone-Treated 2D- and 3D-Cultured Dermal Papilla Cells on Hair Follicle Growth

Yufan Zhang†, Junfei Huang†, Danlan Fu, Zhen Liu, Hailin Wang, Jin Wang, Qian Qu, Kaitao Li, Zhexiang Fan, Zhiqi Hu and Yong Miao**

Department of Plastic and Aesthetic Surgery, Nanfang Hospital of Southern Medical University, Guangzhou, China

OPEN ACCESS

Edited by:
Mingxing Lei, Chongqing University, China

Reviewed by:
Ekaterina Vorotelyak, Koltzov Institute of Developmental Biology, Russian Academy of Sciences, Russia
Ai-hua Wei, Capital Medical University, China
Martin Alphonse, The Johns Hopkins Hospital, Johns Hopkins Medicine, United States

***Correspondence:**
Yong Miao
miaoyong123@i.smu.edu.cn
Zhiqi Hu
huzhiqidr163@i.smu.edu.cn

† These authors have contributed equally to this work

Specialty section:
This article was submitted to Stem Cell Research, a section of the journal Frontiers in Cell and Developmental Biology

Received: *12 June 2021*
Accepted: *31 August 2021*
Published: *17 September 2021*

Citation:
Zhang Y, Huang J, Fu D, Liu Z, Wang H, Wang J, Qu Q, Li K, Fan Z, Hu Z and Miao Y (2021) Transcriptome Analysis Reveals an Inhibitory Effect of Dihydrotestosterone-Treated 2D- and 3D-Cultured Dermal Papilla Cells on Hair Follicle Growth. Front. Cell Dev. Biol. 9:724310. doi: 10.3389/fcell.2021.724310

Dermal papillae are a target of androgen action in patients with androgenic alopecia, where androgen acts on the epidermis of hair follicles in a paracrine manner. To mimic the complexity of the dermal papilla microenvironment, a better culture model of human dermal papilla cells (DPCs) is needed. Therefore, we evaluated the inhibitory effect of dihydrotestosterone (DHT)-treated two-dimensional (2D)- and 3D-cultured DPCs on hair follicle growth. 2D- and 3D-cultured DPC proliferation was inhibited after co-culturing with outer root sheath (ORS) cells under DHT treatment. Moreover, gene expression levels of β-catenin and neural cell adhesion molecules were significantly decreased and those of cleaved caspase-3 significantly increased in 2D- and 3D-cultured DPCs with increasing DHT concentrations. ORS cell proliferation also significantly increased after co-culturing in the control-3D model compared with the control-2D model. Ki67 downregulation and cleaved caspase-3 upregulation in DHT-treated 2D and 3D groups significantly inhibited ORS cell proliferation. Sequencing showed an increase in the expression of genes related to extracellular matrix synthesis in the 3D model group. Additionally, the top 10 hub genes were identified, and the expression of nine chemokine-related genes in DHT-treated DPCs was found to be significantly increased. We also identified the interactions between transcription factor (TF) genes and microRNAs (miRNAs) with hub genes and the TF–miRNA coregulatory network. Overall, the findings indicate that 3D-cultured DPCs are more representative of *in vivo* conditions than 2D-cultured DPCs and contribute to our understanding of the molecular mechanisms underlying androgen-induced alopecia.

Keywords: RNA-seq, 3D model, dermal papilla cells, dihydrotestosterone, androgenic alopecia, chemokines

INTRODUCTION

Hair follicle development and growth depends on reciprocal epithelial–mesenchymal interactions, and the starting point of the initial signals is thought to originate from the mesenchymal dermis (Dhouailly, 1973). The dermal papillae, a cluster of mesenchymal cells at the base of the hair follicle, are considered to play an important role in the hair cycle by regulating the growth and activity of

various cells in hair follicles through the secretion of diffusible proteins to the epidermis of hair follicles (Andl et al., 2002).

Androgen alopecia (AGA), also known as male hair loss, affects 50% of men worldwide and is the most common form of hair loss in men (McElwee and Shapiro, 2012). AGA is characterized by the gradual miniaturization of hair follicles and a premature transition from anagen to catagen induced by androgens (Jahoda, 1998). The dermal papilla cells (DPCs) of bald scalp contain more 5-α-reductase, leading to the conversion of peripheral testosterone into a more active dihydrotestosterone (DHT), which has an affinity that is five times as strong as that of testosterone. DHT binds to androgen receptors (ARs) in the nucleus, initiating a cascade of reactions and triggering this effect (Dallob et al., 1994). Overall, DPCs are the targets of androgen action in AGA hair follicles. Androgen drives DPCs to act on themselves in a paracrine manner in hair follicle epithelial cells, resulting in the miniaturization of hair follicles and changes in the hair follicle cycle (Randall et al., 2001). Thus, altering the expression of DPC-related genes under DHT treatment may be a key factor in androgen-potentiated balding.

To elucidate the regulatory effect of DHT-treated DPCs on epidermal cells of hair follicles, a co-culture model was established in 1995 in which outer root sheath (ORS) cells were cultured in the upper compartment and DPCs in the lower compartment of Transwell culture dishes (Itami et al., 1995). Subsequently, several scientists have used this co-culture model to explore the mechanism of AGA. Kwack et al. (2008) found that DHT-mediated Dickkopf Wnt signaling pathway inhibitor 1 (DKK1), secreted by DPCs, is involved in DHT-driven balding. Kitagawa et al. (2009) observed that DHT inhibited the proliferation of keratinocytes, which was induced by Wnt3a through Wnt/β-catenin signaling. Leirós et al. (2017) reported that DHT activates GSK-3β in DPCs, inhibiting the differentiation of hair follicle stem cells by phosphorylating β-catenin (Kitagawa et al., 2009); they also found that DHT could downregulate the expression of Wnt5a and Wnt10b by stimulating DPCs from patients with AGA. Inui et al. (2002) examined the role of androgen-induced transforming growth factor-β (TGF-β1) derived from DPCs in AGA, which is involved in the growth inhibition of epithelial cells in a co-culture system. Kwack et al. (2012) reported that DHT-inducible IL-6 inhibits the proliferation of human follicular keratinocytes. The above findings were obtained using the co-culture model of DPCs and hair follicle epidermal cells.

In previous studies, the DPCs were cultured in two-dimensional (2D) monolayers of co-culture systems; however, DPCs *in vivo* are surrounded by an extracellular matrix (ECM), clustered into a special 3D spherical and structured dermal papilla. Therefore, the 2D model has some limitations because it is unable to mimic the complexity of the hair follicle microenvironment. Compared with 2D culture conditions, a significant advantage of 3D culture is that it reduces the differences between cell models *in vitro* and *in vivo*. Additionally, 3D cultured cells are more representative of the complexity of *in vivo* conditions (Thippabhotla et al., 2019). With respect to DPCs in particular, previous studies have reported that 3D-cultured DPCs possess a greater hair follicle regenerating ability than 2D-cultured DPCs (Lin G. et al., 2020), indicating considerable differences in 2D- and 3D-cultured DPCs. Hair inductivity sharply decreases when DPCs are expanded in 2D culture because of the absence of the 3D microenvironment (Ohyama et al., 2012; Abaci et al., 2018). Several different approaches have been employed to construct DP spheroids in an attempt to restore the inductive characteristics of DPCs, such as hanging drop culture (Lin et al., 2016), low adhesion biomaterial surfaces (Osada et al., 2007), and hydrogel culture (Tan et al., 2019). In this study, we used a low adhesion biomaterial surface approach to culture DPCs in 3D and speculated that DHT-induced 2D- and 3D-cultured DPCs may secrete different kinds of proteins, inhibiting the proliferation of hair follicle epidermal cells by activating different pathways.

RNA sequencing (RNA-seq) is a relatively new method for analyzing eukaryotic transcripts, and it is cheaper and more effective for identifying previously unknown gene signatures compared with microarray and Sanger sequencing technology (Nagalakshmi et al., 2008). In the present study, we used RNA-seq to identify differentially expressed genes (DEGs) in 2D- and 3D-cultured DPCs under DHT treatment.

MATERIALS AND METHODS

In vitro Dermal Papilla Cells Cultured in 2D

Human hair follicles were taken from the balding (frontal) area of male patients undergoing hair transplantation surgery. Ethical approval and informed consent were obtained preoperatively from Nanfang Hospital of Southern Medical University. Dermal papillae were isolated from the bulbs of hair follicles, plated in a cell culture flask (Corning Inc., NY, United States) and cultured in Dulbecco's Modified Eagle Medium (DMEM; Gibco, MA, United States) supplemented with 1% (v/v) penicillin–streptomycin and 20% (v/v) fetal bovine serum (FBS; Gibco) at 37°C and 5% CO_2. Once the outgrowth reached 80% confluence, human DPCs were harvested by incubating with 0.25% (w/v) trypsin/EDTA (Gibco) and transferring to new culture dishes at a split ratio of 1:2.

In vitro Outer Root Sheath Cells Cultured in 2D

Outer root sheath cells were isolated from the same hair specimens mentioned above. The hair follicle bulb was separated using microscissors and treated with 0.1% dispase (Invitrogen, CA, United States) for 45 min. The dermal sheaths were separated and removed under a stereoscope, and the epidermis was treated with 0.05% trypsin (Gibco) for 10 min. After terminating digestion, the samples were filtered through a 70-μm strainer (Corning Inc.) and cultured with defined keratinocyte-SFM (KSFM; Gibco) in flasks that were pre-coated with 10 μg/mL human fibronectin (Sigma-Aldrich, MO, United States).

In vitro Dermal Papilla Cells Cultured in 3D

For 3D culture, DPCs were seeded in an ultra-low attachment 96-well plate (Corning Inc.) with DMEM, supplemented with 1% (v/v) penicillin–streptomycin and 10% (v/v) FBS. Spheroids were formed 1 day after seeding and were used in the further assays.

MTT Assay

Two-dimensional- and 3D-cultured DPCs (8×10^3 cells per well) were seeded into 96-well plates and cultured for two days with DHT at different concentrations. MTT (20 μL; 5 mg/mL) was added to each well, and the cells were incubated for 4 h at 37°C; subsequently 200 μL of dimethyl sulfoxide was added to dissolve the formazan after removing the supernatant products. Proliferation of DPCs was determined spectrophotometrically at 570 nm using an ELISA reader (TECAN Infinite F50, Männedorf, Switzerland).

Co-culture of Dermal Papilla Cells and Outer Root Sheath Cells

Two-dimensional-cultured DPCs were harvested by incubation with 0.25% (w/v) trypsin/EDTA from the cell culture flask and plated at a density of 1×10^4 cells/cm^2 in the upper compartment of Transwell culture dishes (Corning Inc.). Dermal papillae spheres of the same quantity as the 2D-cultured cells were also transferred to the upper compartment of another Transwell culture dish. ORS cells (4×10^3 cells/well), which were cultured in FBS-free DMEM on the day before co-culture, were added to the lower compartment of each dish and co-cultured with 2D- and 3D-cultured DPCs. After 1 day, the medium was changed and 10 μM DHT was added to the co-culture system. The number of ORS cells was counted after 3 days.

Western Blotting Analysis

Protein extracts were isolated from DPCs using a RIPA protein lysis buffer containing a protease inhibitor cocktail (Roche, Switzerland). Protein concentrations were determined using a BCA protein assay kit (Pierce, IL, United States), measuring the absorbance at 562 nm. Total protein (20 μg) was subjected to SDS-PAGE, and the separated proteins were transferred to a polyvinylidene fluoride membrane (Millipore, MA, United States). The membrane was blocked in 5% bovine serum albumin (BSA) for 1 h and probed with appropriate primary antibodies overnight at 4°C. Primary antibodies against the following proteins were used: AR (1:2,000; ab133273, Abcam, Cambridge, United Kingdom), neural cell adhesion molecule (NCAM; 1:2,000, ab75813, Abcam), β-catenin (1:2,000; ab32572, Abcam), Ki67 (1:2,000; ab16667, Abcam), cleaved caspase-3 (1:2,000; ab32042, Abcam), β-actin (1:5,000; ab8226, Abcam), and alpha-tubulin (1:5,000; AC007, ABclonal, MA, United States). After washing with Tris Buffered saline Tween, the blots were incubated with the corresponding secondary antibody (1:1,000; ab150077, Abcam) for 1 h at 20–25°C and photographed using an Odyssey infrared fluorescent scanning imager (Bio-Rad, CA, United States).

Immunofluorescence

Dermal papilla cells were washed once with PBS and fixed in 4% paraformaldehyde for 20 min at approximately 23°C. Then, the samples were rinsed with PBS three times, permeated with 0.3% Triton X-100 (Solarbio, Beijing, China), and blocked with 3% BSA (Solarbio). Subsequently, the samples were stained with primary antibodies against AR (1:200; Abcam) at 4°C overnight. The next day, DPCs were incubated with Alexa Fluor-568 conjugated anti-rabbit secondary antibody (1:200; Abcam) and 2-(4-amidinophenyl)-6-indolecarbamidine dihydrochloride (DAPI; 1:200; Abcam) for 1 h at 20–25°C. Finally, the samples were imaged using a fluorescence microscope (IX71 FL; Olympus, Tokyo, Japan).

RNA Extraction, Library Construction, and Sequencing

For RNA-seq analysis, 2D- and 3D-cultured DPCs were treated with or without DHT for 3 days. Samples were collected from 2D and 3D treated and control groups, and total RNA was extracted using a TRIzol kit (Invitrogen), according to the manufacturer's instructions. RNA quality was evaluated using Agilent 2100 Bioanalyzer (Agilent Technologies, CA, United States) and examined using RNase-free agarose gel electrophoresis. After total RNA extraction, eukaryotic mRNAs were enriched using oligomeric (dT) beads, and prokaryotic mRNAs were enriched by removing rRNAs using the Ribo-Zero^{TM} magnetic kit (Epicenter, WI, United States). The enriched mRNAs were then fragmented into short sequences using fragmentation buffer and reverse transcribed into cDNA using random primers. Second strand cDNA was synthesized using DNA polymerase I, RNase H, dNTP, and buffer. The QiaQuick PCR extraction kit (Qiagen, Venlo, Holland) was used to purify the cDNA fragments, repair base ends, and connect the Illumina sequencing adapters. The sizes of the ligated products were determined using agarose gel electrophoresis. The products were amplified by using PCR and sequenced using the Illumina NovaSeq 6000 by Gene Denovo Biotechnology Co. (Guangzhou, China). Gene expression analysis of identified transcripts was performed using the DESeq2 package in R software. Genes with changes in expression of $p < 0.05$ and $|\log2 FC| > 1$ were considered to be DEGs.

Correlation Analysis of Replicates

Correlation analysis of the three parallel experiments was performed using R software[1] to evaluate the reliability and operational stability of the experimental results. The repeatability was evaluated by calculating the correlation coefficient among the three replicates: the closer the correlation coefficient to 1, the stronger the repeatability among the three parallel experiments.

Principal Component Analysis

Principal component analysis (PCA) was performed using an omicshare tool.[2] We performed PCA to reveal the structure or relationship of the samples.

[1] http://www.r-project.org/

[2] https://www.omicshare.com

Identification of Differentially Expressed Genes

RNA differential expression analysis of the four groups (DHT-2D, control-2D, DHT-3D, and control-3D) was performed using DESeq2 (Love et al., 2014) software. Genes/transcripts with p-value [false discovery rate (FDR)] < 0.05, and logarithmic fold change value (log2FC) > 1 were considered to be DEGs. Overlapping genes between two comparison groups (DHT-2D vs. control-2D and DHT-3D vs. control-3D) were presented using Venn diagrams. DEGs were annotated using Gene Ontology (GO) and the Kyoto Encyclopedia of Genes and Genomes (KEGG) databases.

Gene Ontology and Kyoto Encyclopedia of Genes and Genomes Enrichment Analysis

To further identify section "Advantages of Control-3D Over Control-2D in Simulating Dermal Papilla Cells *in vivo*," we used KEGG[3] to specify relevant molecular processes of control-2D and control-3D. Subsequently, KEGG and GO were performed using The Database for Annotation, Visualization, and Integrated Discovery (DAVID; version 6.8[4]) to analyze the associated cellular pathways. Specifically, biological classification and molecular function enrichment were assessed for the DEGs in the control-2D vs. DHT-2D, and control-3D vs. DHT-3D, as well as overlapping DEGs between the two comparison groups (Huang et al., 2007).

Gene Set Enrichment Analysis

To determine statistically significant gene sets among the four groups, the genes were analyzed using Gene Set Enrichment Analysis (GSEA) software v3.0, available from the Broad Institute.[5] The dataset was input with the annotation file "hallmark gene sets." Enriched gene sets were identified based on $p < 0.05$ and FDR $q < 0.25$.

Construction of a Protein–Protein Interaction Network and Analysis of Module

The Search Tool for the Retrieval of Interacting Genes (STRING[6]) is an online database for analyzing protein–protein interaction (PPI) networks of genes (Szklarczyk et al., 2017), which determines genes as nodes and interactions as lines in a network. In the present study, the STRING database was used to construct the PPI network of overlapping DEGs between DHT-2D vs. control-2D and DHT-3D vs. control-3D. Networks with a combined score >0.4 were defined as statistically significant interactions. Cytoscape (v3.7.1) software was used to visualize the network file and present core and hub gene biological interactions. The plugin Molecular Complex Detection (MCODE) (version 1.4.2) of Cytoscape is an application for clustering a given network based on topology to find densely connected regions. The PPI networks were depicted using Cytoscape, and the most significant module in the PPI networks was identified using MCODE. The standard for selection was as follows: MCODE scores >5, degree cut-off $= 2$, node score cut-off $= 0.2$, max depth $= 100$, and node k-score $= 2$.

Hierarchical Clustering

Unsupervised hierarchical cluster analysis was performed on the ECM–receptor related genes, reported AGA-related genes, and overlapping DEGs in the two comparison groups (control-2D vs. DHT-2D and control-3D vs. DHT-3D). Raw z-scores were first calculated from counts of the four groups and then subjected to agglomerative hierarchical clustering analysis based on Ward's method and Euclidean distance. Bioinformatics analysis was performed, and heat maps were generated using an omicshare program (see text footnote 2).

Hub Genes Selection and Analysis

Hub genes were obtained from an application plugin in Cytoscape called CytoHubba. After constructing the network of genes, the top 10 genes with degree ≥ 10 were identified as hub genes. The Biological Networks Gene Oncology tool (BiNGO) (version 3.0.3), another APP plugin in Cytoscape, calculates overrepresented GO terms by GO_full analysis in the network and displays them as a network of significant GO terms. The term "GO_full analysis" is an option in the BiNGO settings that includes biological processes, cellular components, and molecular functions.

Quantitative Real-Time Reverse Transcription Polymerase Chain Reaction

Total RNA was extracted using a TRIzol reagent (Invitrogen) to evaluate expression levels of the 10 hub genes. cDNA was reverse transcribed from 2 mg of RNA using the SYBR Prime-Script RT-PCR Kit (TaKaRa Bio, Japan). Quantitative real-time reverse transcription polymerase chain reaction (qRT-PCR) was performed using the ABI Prism 7900HT Sequence Detection System (Life Technologies, CA, United States), according to the manufacturer's protocol. Relative gene expression levels were calculated using the $2^{-\Delta\Delta Ct}$ method.

Transcription Factor-Gene and MicroRNA Interactions With Hub Genes and Transcription Factor–MicroRNA Coregulatory Network

The NetworkAnalyst[7] platform was used to identify transcription factor (TF)-gene and microRNA (miRNA) interactions with hub genes and the TF–miRNA coregulatory network.

Statistical Analysis

Statistical analysis was conducted using one-way ANOVA and two-tailed Student's t-test in GraphPad Prism 8 (GraphPad

[3]https://www.kegg.jp/

[4]http://david.ncifcrf.gov

[5]http://software.broadinstitute.org/gsea/index.jsp

[6]http://string-db.org; version 10.5

[7]https://www.networkanalyst.ca/

Software Inc., CA, United States). Results are presented as the mean ± standard deviation (SD), and statistical significance was set at $p \leq 0.05$. Heat maps were used to display the hierarchical groupings of the gene expression profiles of the samples using R package. Each experiment was repeated at least three times.

RESULTS

Selection of Dermal Papilla Cells With Relatively High Expression of Androgen Receptor for Co-Culture Model

The results of immunofluorescence staining of DPCs at passage (P)2, P4, P6, and P8 showed that the AR protein was significantly expressed in P2 and P4 compared with that in P6 and P8 (**Figure 1A**). Similarly, western blotting analysis showed that the AR protein of the DPCs decreased during passage (**Figures 1B,C**), and the differences between the P2 group and the other groups were statistically significant. Additionally, when DPCs were treated with 10 μm DHT, immunofluorescence staining revealed that the AR had been transferred from the original cytoplasm to the nucleus (**Figures 1D,E**). We selected P2 DPCs with relatively high AR expression for the co-culture model.

Establishment of 2D and 3D Dermal Papilla Cell Co-Culture Models With Outer Root Sheath Cells for Androgen Alopecia

The construction process of 2D and 3D co-culture models is shown in **Figure 2**. DPCs are located within a complex ECM environment that involves wide-ranging intermolecular interactions. The 3D co-culture model thus offers a way to simulate the *in vivo* morphology and normal physiological function of these cells. DHT inhibited the proliferation of 2D-cultured DPCs in a dose-dependent manner after 2 days of treatment ($p < 0.0001$); however, only 10 μm DHT significantly inhibited the proliferation of 3D-cultured DPCs (**Figure 3A**). Additionally, there was a significant decrease in NCAM and β-catenin expression and a significant increase in cleaved caspase-3 expression in the 2D- (**Figures 3D–G**) and 3D-cultured DPCs (**Figures 3H–K**) with increasing DHT concentration. The number of ORS cells in the 3D co-culture model was nearly 1.5-times that of the 2D co-culture model. However, there was a decrease in the quantity of ORS cells in both the 2D and 3D co-culture models with an increase in DHT concentration (**Figure 3B**). DHT did not have an inhibitory effect on ORS cells that were not co-cultured with DPCs, suggesting that the negative effect of DHT on ORS cells (**Figure 3C**) was mediated indirectly

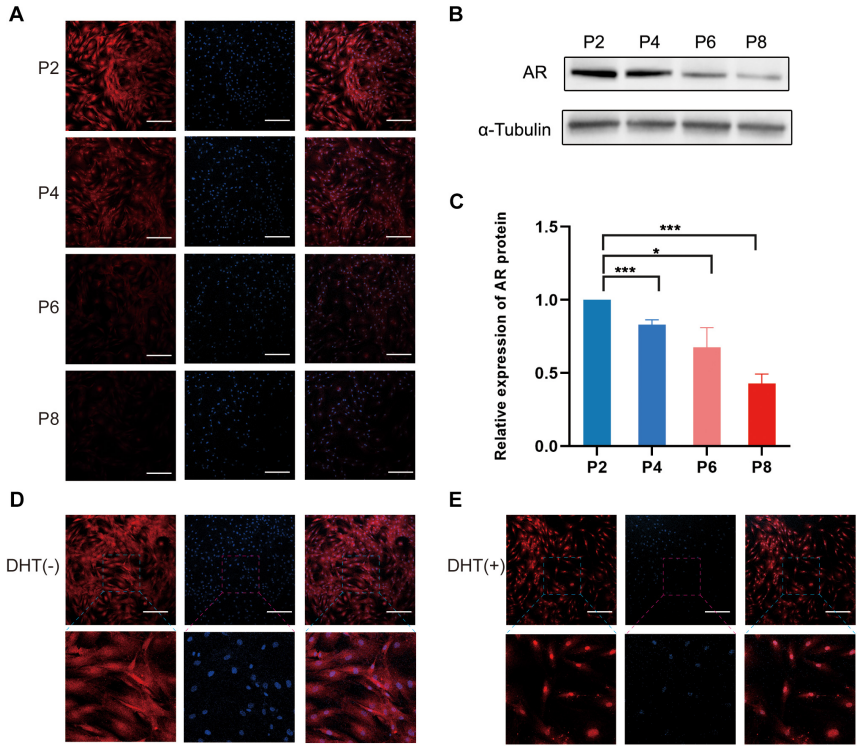

FIGURE 1 | Expression of androgen receptor in cultured DPCs and AR translocation from the cytoplasm to nucleus following DHT treatment. **(A)** Immunofluorescence images of AR expression of DPCs in different passages. Scale bar = 200 μm. **(B)** Western blotting analysis of AR in different passages. **(C)** Relative expression of AR protein in P2, P4, P6, and P8. Immunofluorescence images of AR expression **(D)** in the cytoplasm in the absence of DHT, and **(E)** in the nucleus in the presence of DHT. Results are presented as mean ± SD. $^{*}p < 0.05$; $^{***}p < 0.001$, compared with P2 group by one-way ANOVA and Student's *t*-test. AR, androgen receptor; DHT, dihydrotestosterone; DPC, dermal papilla cells.

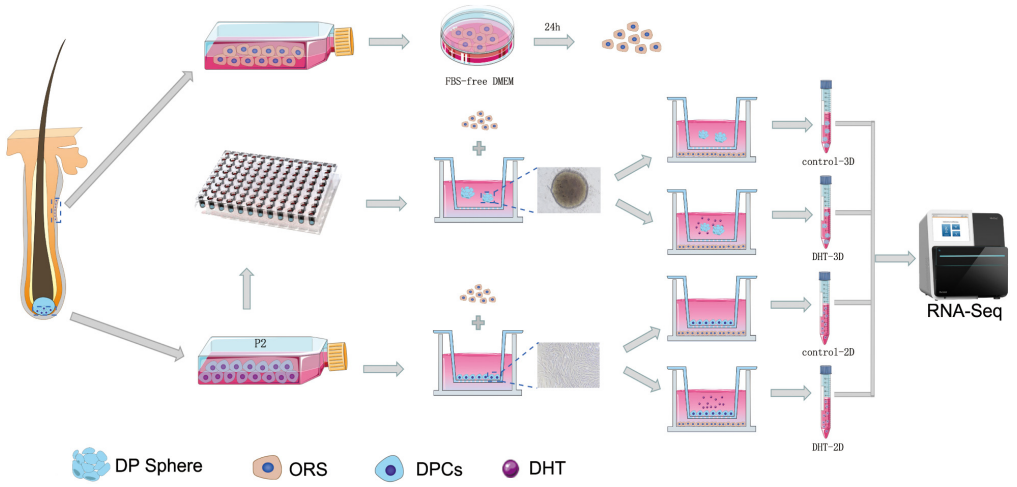

FIGURE 2 | Construction process for the 2D and 3D co-cultured models. The schematic shows the construction process of the 2D and 3D co-culture models containing DPCs and ORS cells. The specific steps are mentioned in section "Materials and Methods." DPCs and ORS cells were seeded, respectively, in the upper and lower compartments of Transwell culture dishes, with or without of DHT (10 μM). DHT, dihydrotestosterone; DPC, dermal papilla cell; ORS, outer root sheath.

by DPCs. There was a significant decrease in Ki67 (**Figures 3L–N**) and cleaved caspase-3 (**Figures 3L,O,P**) expression in ORS cells with increasing DHT concentration.

Clear Separation of Transcriptional Signatures of Inter-Groups and High Reproducibility of Intra-Groups

High-throughput sequencing technology was used to investigate the mRNA profiles of genes in the control-2D, DHT-2D, control-3D, and DHT-3D groups. A total of 12 DPC samples were collected from the models, with three samples from each group. Furthermore, Pearson's correlation analysis was performed to examine the similarity and discrepancy between the four groups using the normalized fragment counts as the distance between genes. The results showed that samples in the same group were highly similar, while samples from different groups were distinct. The correlation coefficients of the four groups ranged 0.85–0.88 for control-2D and control-3D, 0.96–0.97 for control-2D and DHT-2D, and 0.96–0.98 for control-3D and DHT-3D samples (**Figure 4A**). PCA results showed that 88.4% of gene expression variation (PC1: 70.1%, PC2: 18.3%) could be explained by the first two PCs (**Figure 4B**). Two of the four groups in the PCA projection showed a significant distance in the PC space, indicating that the significant variations in gene expression of the different treatment groups can be attributed to the DHT treatment and cell morphological changes in 2D- and 3D-cultured DPCs. A short distance in the intra-group analysis prompted minute variations and high biological replication among the three samples within one group. To directly observe gene abundance at any location in each sample, we used a violin plot to display the degree of dispersion of gene expression (y-axis) and data distribution of a vertical coordinate position (x-axis). We found that the interquartile distance, median, and gene expression distribution in the intra-group were nearly the same, indicating that the parallel samples had high reproducibility (**Figure 4C**). The correlation heatmap, PCA analysis, and violin plot demonstrated a clear separation of transcriptional signatures between the four groups and confirmed high-quality RNA-seq data for further functional analysis.

Advantages of Control-3D Over Control-2D in Simulating Dermal Papilla Cells *in vivo*

To demonstrate that the 3D model is more representative of the *in vivo* situation than the 2D model. The results of the analysis showed that there were 1,652 upregulated genes and 1,343 downregulated genes in the control-2D vs. control-3D group (**Figure 5A**). KEGG analysis of the DEGs indicates that the DEGs were mainly enriched in ECM–receptor interaction, with the gene number/total gene number (gene ratio) close to 0.5. Among 22 genes enriched in ECM–receptor interaction, unsupervised hierarchical clustering showed that 20 were upregulated and two were downregulated (**Figure 5B**), suggesting that the ECM was more abundant in the control-3D group (**Figure 5C**). Additionally, β-catenin expression was significantly higher in the control-3D than that in the control-2D group (**Figure 5D**), indicating the involvement of the canonical Wnt/β−catenin pathway, owing to 3D aggregation of DPCs. The expression of NCAM and β-catenin was confirmed by western blotting analysis (**Figures 5E–G**). The upregulated expression of NCAM in the 3D-control showed that the 3D model could exhibit, to some extent, the characteristics of hair follicle development *in vivo*.

Identification of Differentially Expressed Genes in Two Comparison Groups and Reliability of the Models

To further characterize DEGs in the control-2D vs. DHT-2D and control-3D vs. DHT-3D groups, gene expression analysis

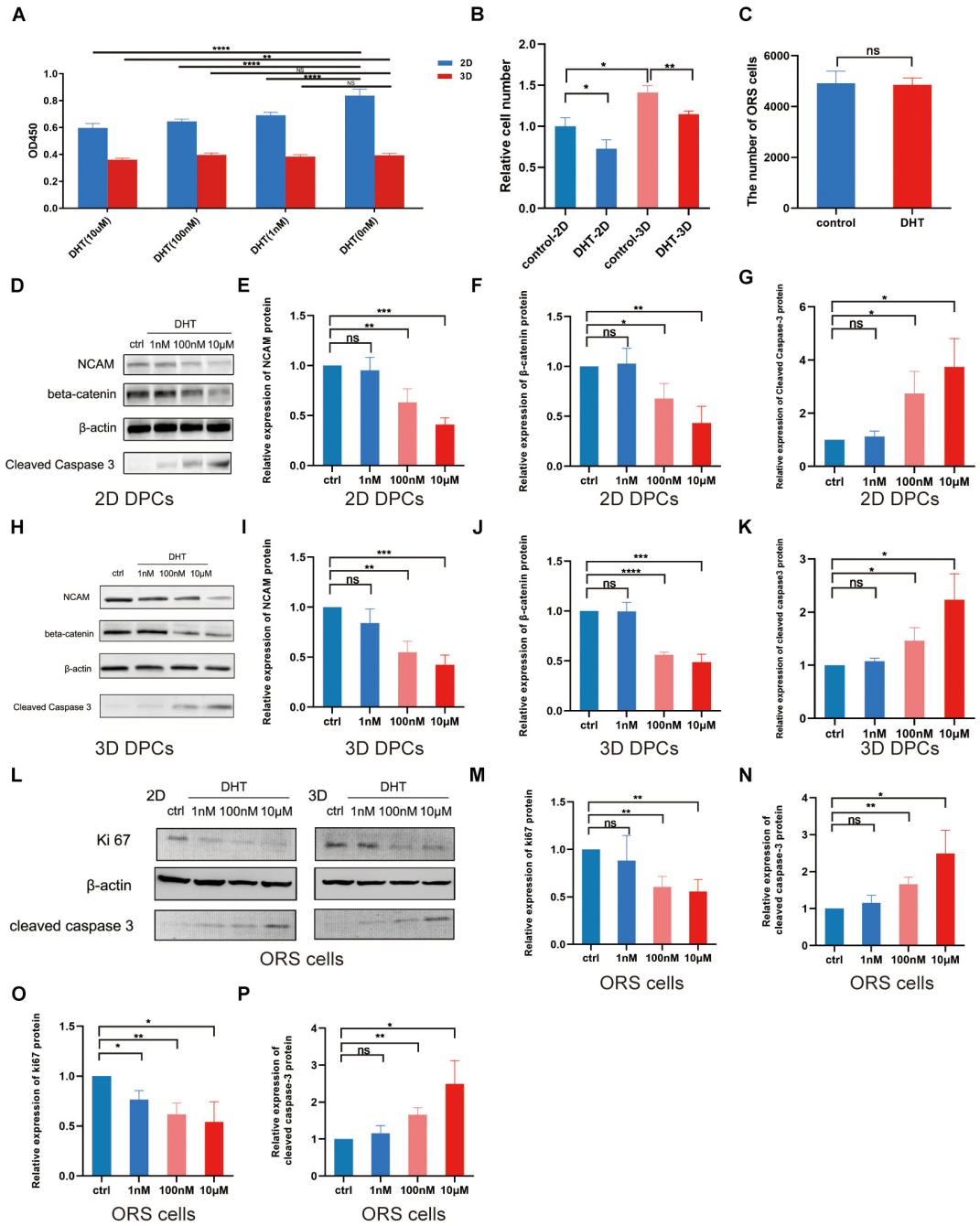

FIGURE 3 | Effect of dihydrotestosterone on outer root sheath cells regulated by dermal papilla cells in 2D and 3D co-culture models. **(A)** Effect of different concentrations of DHT on the proliferation of 2D- and 3D-cultured DPCs. **(B)** Relative ORS cell number in the four groups (control-2D, DHT-2D, control-3D, and DHT-3D). **(C)** Quantity of ORS cells cultured alone in the absence or presence of DHT (10 μM). Western blotting analysis of NCAM, β–catenin, and cleaved caspase-3 in the 2D- **(D)** and 3D-cultured **(H)** DPCs at 0 nM (control), 1 nM, 100 nM, and 10 μM DHT **(D)**. Relative expression of NCAM, β–catenin **(F)**, and cleaved caspase-3 in 2D **(E–G)** and 3D **(I–K)** DPCs. **(L)** Western blotting analysis of Ki67 and cleaved caspase-3 in 2D- and 3D-co-cultured ORS cells at 0 nM (control), 1 nM, 100 nM, and 10 μM DHT. Relative expression of Ki67 and cleaved caspase-3 in 2D **(M,N)** and 3D **(O,P)** ORS cells. The results were obtained using three replicates and presented as mean ± SD. ns, not significant; $^{*}p < 0.05$; $^{**}p < 0.01$; $^{***}p < 0.001$; and $^{****}p < 0.0001$ compared with the respective controls by one-way ANOVA and Student's *t*-test. DHT, dihydrotestosterone; DPC, dermal papilla cell; NCAM, neural cell adhesion molecule; ORS, outer root sheath.

was conducted on the transcripts (19,727 identified genes) from the two comparison groups (**Figures 6A,C**). A total of 3,331 DEGs were identified (1,891 in control-2D vs. DHT-2D and 1,440 in control-3D vs. DHT-3D), among which 1,175 were upregulated and 776 were downregulated in control-2D vs. DHT-2D samples, while 845 were upregulated and

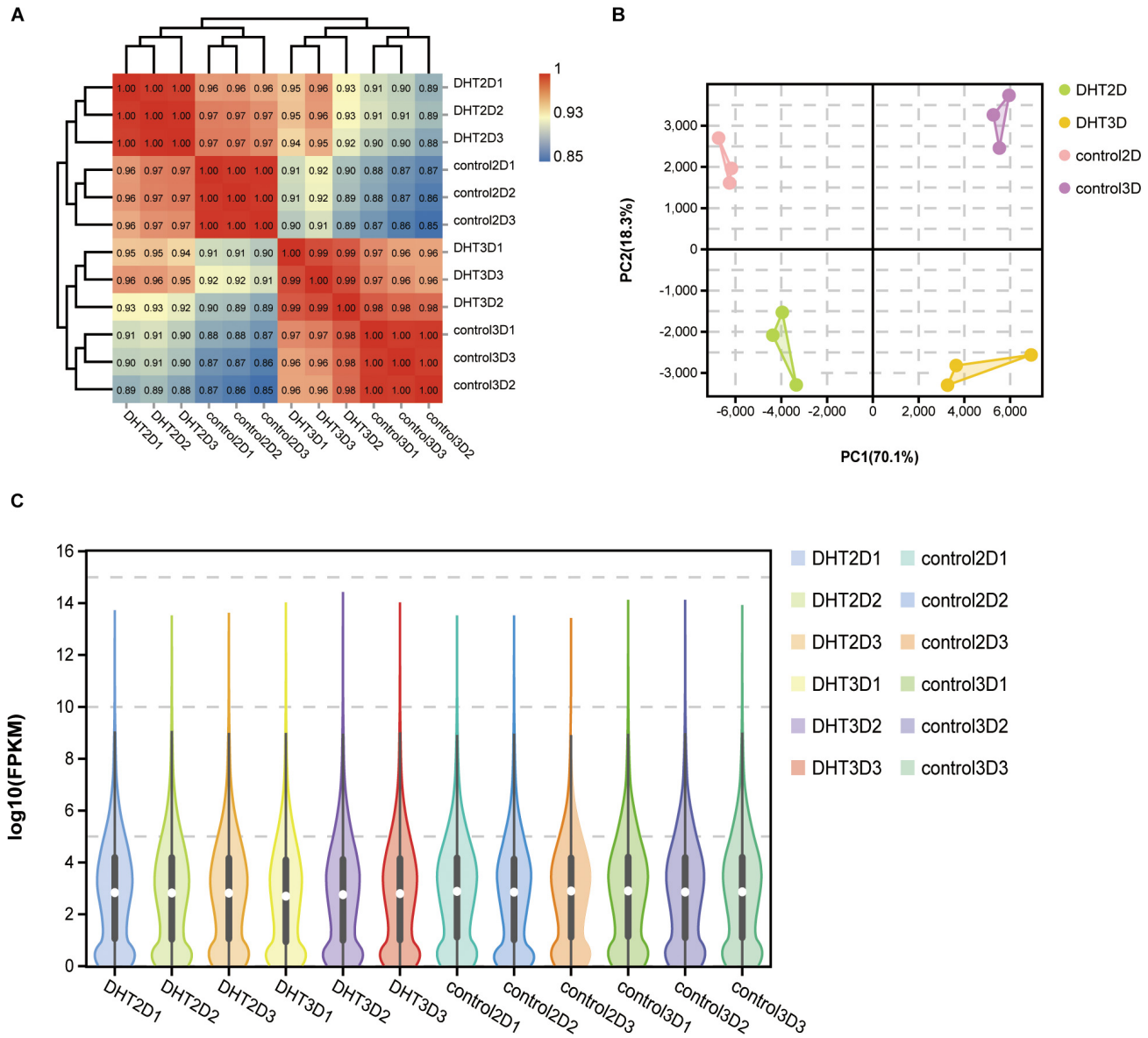

FIGURE 4 | Correlation analysis between samples. **(A)** Logarithm-transformed counts from RNA-seq dataset of control-2D, DHT-2D, control-3D, and DHT-3D used for Pearson's correlation analysis. R^2 values from Pearson's correlation analysis were plotted inside the grids of the heatmap. **(B)** PCA analysis. Percentages in PCA axis indicate the proportional variance explained by each PC. Control-2D samples are labeled pink, DHT-2D samples are labeled green, control-3D samples are labeled purple, and DHT-3D samples are labeled yellow, representative of conditions located in the upper right part of plot. **(C)** Violin plot visualizing data density at any location of all genes in each sample, indicating gene abundance expression. White dots represent the median, the black rectangle represents the lower quartile (Q1) range to the upper quartile (Q3), and black lines running through the violin chart represent the confidence interval. The outer shape of the black rectangle is the kernel density estimation, the length of the longitudinal axis of the figure represents the degree of gene dispersion, and the length of the horizontal axis represents the amount of gene expression distribution in a certain ordinate position. DHT, dihydrotestosterone; PCA, principal component analysis.

595 were downregulated in control-3D vs. DHT-3D samples (**Figure 6E**). To verify that the model can accurately reflect the effect of DPCs on ORS under androgen stimulation, an unsupervised hierarchical clustering was conducted using six genes (*IGF-1*, *DKK1*, *IL-6*, *TGF-β1*, *PTGDS*, and *CXXC5*) (**Figures 6B,D**). A hierarchical heatmap indicated that IGF-1 expression was downregulated in both the 2D and 3D models by DHT, while the expression levels of *DKK1*, *IL-6*, *TGF-β1*, *PGD2*, and *CXXC5* were upregulated in both models by DHT.

Gene Ontology functional annotation and KEGG pathway analysis of the DEGs in the control-2D vs. DHT-2D and control-3D vs. DHT-3D (1,891 and 1,440 genes) groups were performed using the DAVID online tool. KEGG analysis revealed that alterations in metabolism were significantly altered during steroid biosynthesis in DEGs identified in the comparison

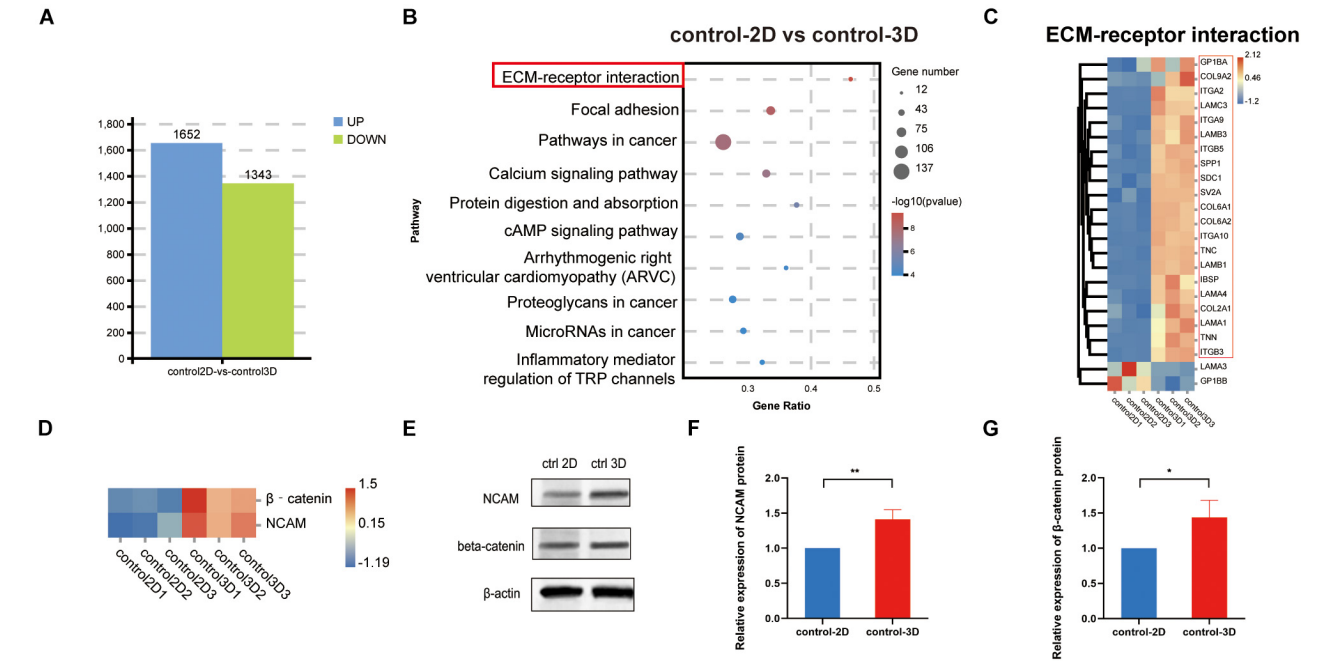

FIGURE 5 | Identification and comparison of 2D and 3D co-culture models in the absence of dihydrotestosterone. **(A)** Quantity of DEGs in control-2D vs. control-3D groups, displayed as a bar chart. Blue represents upregulation and green represents downregulation. **(B)** KEGG analysis of DEGs between control-2D and control-3D. The size of the bubble represents gene number, color depth represents the *p*-value, and the rich ratio represents the gene number/total gene number on the *y*-axis. **(C)** DEGs (22) in the control-2D and control-3D related to the ECM–receptor interaction are depicted as a heatmap. Red indicates upregulation and blue indicates downregulation. **(D)** Expression of β–catenin and NCAM of control-2D and control-3D depicted as a heatmap. Red indicates upregulation and blue indicates downregulation. **(E)** Western blotting analysis of expression of NCAM and β–catenin and the relative expression of NCAM **(F)** and β–catenin **(G)** in control-2D and control-3D DPCs. DEGs, differentially expressed genes; DPC, dermal papilla cell; ECM, extracellular matrix; NCAM, neural cell adhesion molecule. $^{*}p < 0.05$; $^{**}p < 0.01$.

groups. Meanwhile, in the 2D group, DEGs enriched in environmental information processing were primarily activated in the ECM–receptor interaction, Ras signaling pathway, PI3K-Akt signaling pathway, Wnt signaling pathway, and cell adhesion molecules (**Figure 7A**). The MAPK signaling pathway, TNF signaling pathway, ECM–receptor interaction, cytokine–cytokine receptor interaction, Rap1 signaling pathway, and PI3K–Akt signaling pathway were enriched in the 3D group (**Figure 8A**). Changes in the cellular processes of DEGs in the two comparison groups were related to focal adhesion in both groups. Additionally, DEGs in the 2D group were related to cell cycle, p53 signaling pathway, and oocyte meiosis. The KEGG network (**Supplementary Figure 1**) showed 10 nodes and 14 edges (black lines) in 3D groups, and the possible core pathways were the MAPK signaling pathway (six edges) and PI3K–Akt signaling pathway (five edges). However, fewer interactions between enriched pathways were established in the 2D network, with only four nodes and one edge. Based on the node size, the pathways enriched in the 2D model contained fewer genes than that in the 3D model. GO analysis revealed that DEGs in the 2D group were mainly enriched in condensed chromosomes, centromeric regions, ECMs, extracellular spaces in cell components (CC) and ECM organization, mitotic nuclear division, and extracellular structure organization in biological processes (BP) (**Figure 7B**). In the 3D group, changes in CC of DEGs were mainly enriched in the ECM, and changes in BP of DEGs were significantly enriched in ECM organization, nuclear division, extracellular structure organization, and organelle fission (**Figure 8B**).

Gene Set Enrichment Analysis of the Gene Expression Files in Dihydrotestosterone-3D vs. Control-3D and Dihydrotestosterone-2D vs. Control-2D

As KEGG and GO analyses are mainly dependent on DEGs and ignore genes that do not meet the threshold, we performed GSEA to examine the functional analysis of all of the genes identified in this study. Based on the results of GSEA, two new significant gene sets were identified in the 2D and 3D groups, which were not identified by KEGG and GO analyses. Overall, G2M checkpoint and E2F targets and mTORC1 signaling and inflammatory response were significantly enriched in the 2D and 3D groups, respectively. GSEA was employed to identify the enriched gene sets between the control-3D and DHT-3D, including two datasets. G2M checkpoints [normalized enrichment score (NES) $= -2.7017$, $p = 0$, FDR $= 0$], E2F targets (NES $= -2.7155$, $p = 0$, FDR $= 0$) (**Figures 9A,C,D**), mTORC1 signaling (NES $= 2.0349$, $p = 0$, FDR $= 0$), and inflammatory

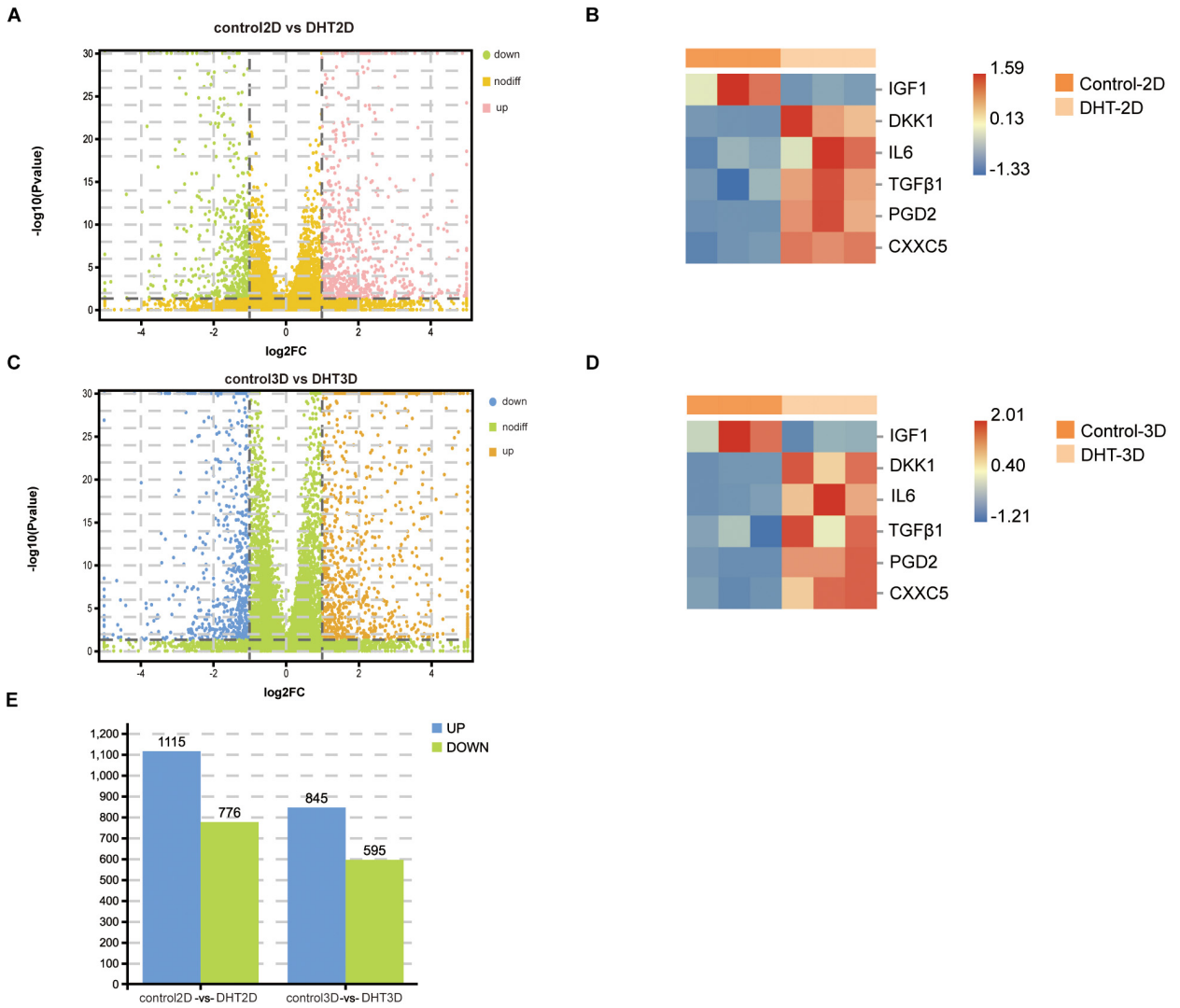

FIGURE 6 | Identification of differentially expressed genes in control-2D vs. dihydrotestosterone-2D and control-3D vs. dihydrotestosterone-3D, and the expression of proven genes. Volcano plot used to determine the DEGs in control-2D vs. DHT-2D **(A)** and control-3D vs. DHT-3D **(C)** using the following criteria: $p < 0.05$ and $\log2|FC| > 1$. Heatmap depicting the expression of six genes in control-2D vs. DHT-2D **(B)** and control-3D vs. DHT-3D **(D)**. Red indicates upregulation and blue indicates downregulation. **(E)** Quantity of DEGs in control-2D vs. DHT-2D and control-3D vs. DHT-3D. Blue represents upregulation and green represents downregulation. DEGs, differentially expressed genes; DHT, dihydrotestosterone.

responses (NES = 1.8069, $p = 0$, FDR = 0.0003) were enriched in the 3D group (**Figures 9B,E,F**).

Identification of Overlapping Differentially Expressed Genes Between Dihydrotestosterone-3D vs. Control-3D and Dihydrotestosterone-2D vs. Control-2D

After DEGs in the two comparison groups (1,891 in DHT-2D vs. control-2D and 1,440 in DHT-3D vs. control-3D) were identified, a Venn diagram (**Figure 10A**) was constructed to identify overlapping DEGs between the two comparison groups. Overall, 501 DEGs were common to both groups. Next, the DEGs were subjected to unsupervised hierarchical clustering and illustrated using an expression heatmap (**Figure 10B**).

Kyoto Encyclopedia of Genes and Genomes and Gene Ontology Enrichment Analysis of Overlapping Genes

Kyoto Encyclopedia of Genes and Genomes pathway analysis (**Figure 10H**) revealed that the overlapping DEGs were mainly enriched in focal adhesion, transcriptional misregulation in cancers, ECM–receptor interaction, and metabolic pathways. GO analysis (**Figure 10I**) showed that the DEGs were significantly

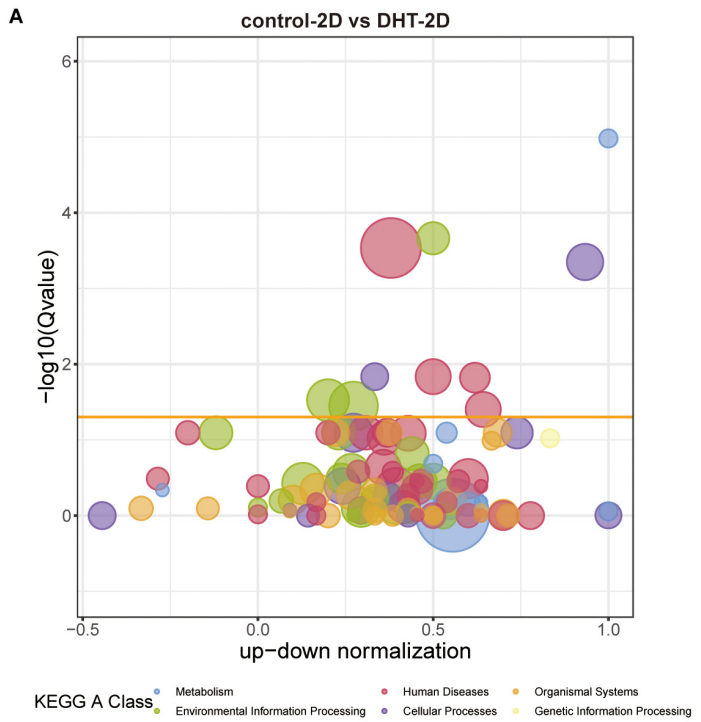

Pathway Top 20

ID	Descrption
ko00100	Steroid biosynthesis
ko04512	ECM−receptor interaction
ko04014	Ras signaling pathway
ko04151	PI3K−Akt signaling pathway
ko04310	Wnt signaling pathway
ko04514	Cell adhesion molecules (CAMs)
ko04110	Cell cycle
ko04115	p53 signaling pathway
ko04510	Focal adhesion
ko04114	Oocyte meiosis
ko05200	Pathways in cancer
ko05418	Fluid shear stress and atherosclerosis
ko05222	Small cell lung cancer
ko05206	MicroRNAs in cancer
ko05226	Gastric cancer
ko05215	Prostate cancer
ko05412	Arrhythmogenic right ventricular cardiomyopathy (ARVC)
ko04914	Progesterone−mediated oocyte maturation
ko04974	Protein digestion and absorption
ko04610	Complement and coagulation cascades

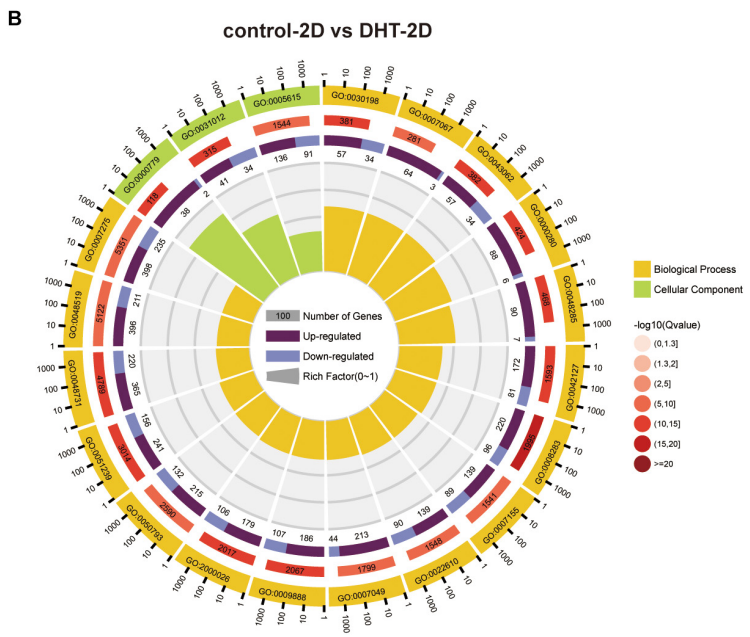

ID	Descrption
GO:0000779	condensed chromosome, centromeric region
GO:0031012	extracellular matrix
GO:0005615	extracellular space
GO:0008283	cell proliferation
GO:0042127	regulation of cell proliferation
GO:0030198	extracellular matrix organization
GO:0043062	extracellular structure organization
GO:0000280	nuclear division
GO:0048731	system development
GO:0051239	regulation of multicellular organismal process
GO:0009888	tissue development
GO:0048285	organelle fission
GO:2000026	regulation of multicellular organismal development
GO:0007275	multicellular organism development
GO:0050793	regulation of developmental process
GO:0022610	biological adhesion
GO:0007155	cell adhesion
GO:0007067	mitotic nuclear division
GO:0007049	cell cycle
GO:0048519	negative regulation of biological process

FIGURE 7 | Kyoto Encyclopedia of Genes and Genomes and GO analysis of differentially expressed genes in 2D cultured dermal papilla cells. **(A)** Blue and red circles indicate metabolism and human diseases, respectively. The green circle indicates environmental information processing, whereas the brown circle represents organismal systems. The purple and yellow circles indicate cellular processes and genetic information processing, respectively. The size of the bubble represents the rich factor (gene number/total gene number), the *y*-axis represents –log10(*Q*-value), and the *x*-axis represents the normalized number of upregulated genes minus downregulated genes. **(B)** GO analysis of DEGs in 2D. Yellow represents biological process, whereas green represents cellular components. From the exterior to interior; the first lap indicates the top 20 GO terms and the coordinate ruler with the number of genes is presented outside the lap; the second lap indicates the total number of genes in the GO term and –log10(*Q*-value), wherein the greater number of genes, the longer the strip, and the larger the –log10(*Q*-value), the darker the color shade; the third lap represents the upregulation/downregulation gene ratio, wherein dark purple represents the upregulated gene proportion, light purple represents the downregulated gene proportion, and the specific value is shown below; and the fourth lap represents the rich factor of each term (number of genes/total number of genes), and each small cell of the background auxiliary line represents 0.1. The chart on the right shows the gene symbols corresponding to the top 20 GO IDs. DEGs, differentially expressed genes.

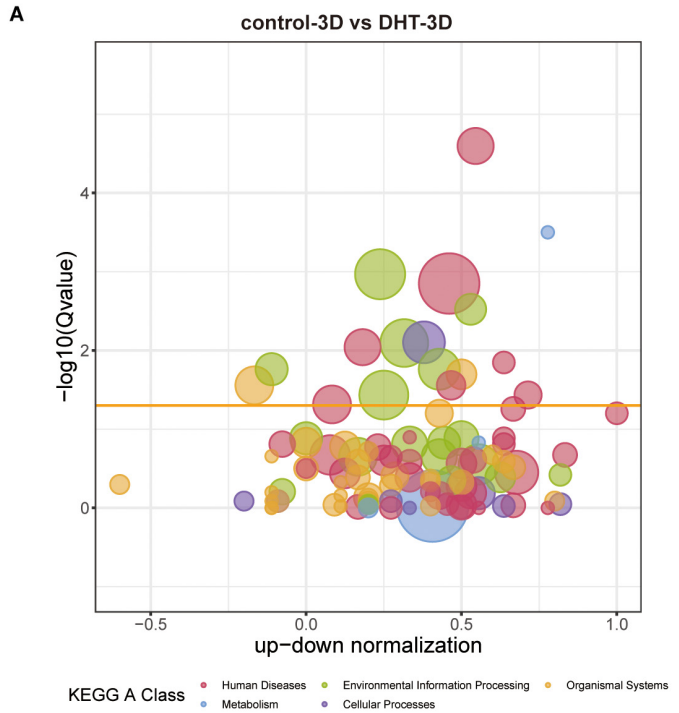

Pathway Top 20

ID	Descrption
ko00100	Steroid biosynthesis
ko04010	MAPK signaling pathway
ko04512	ECM−receptor interaction
ko04060	Cytokine−cytokine receptor interaction
ko04015	Rap1 signaling pathway
ko04668	TNF signaling pathway
ko04151	PI3K−Akt signaling pathway
ko04510	Focal adhesion
ko05323	Rheumatoid arthritis
ko05200	Pathways in cancer
ko05418	Fluid shear stress and atherosclerosis
ko05144	Malaria
ko05414	Dilated cardiomyopathy (DCM)
ko05410	Hypertrophic cardiomyopathy (HCM)
ko05202	Transcriptional misregulation in cancers
ko05140	Leishmaniasis
ko05321	Inflammatiory bowel disease (IBD)
ko04640	Hematopoietic cell lineage
ko04360	Axon guidance
ko04974	Protein digestion and absorption

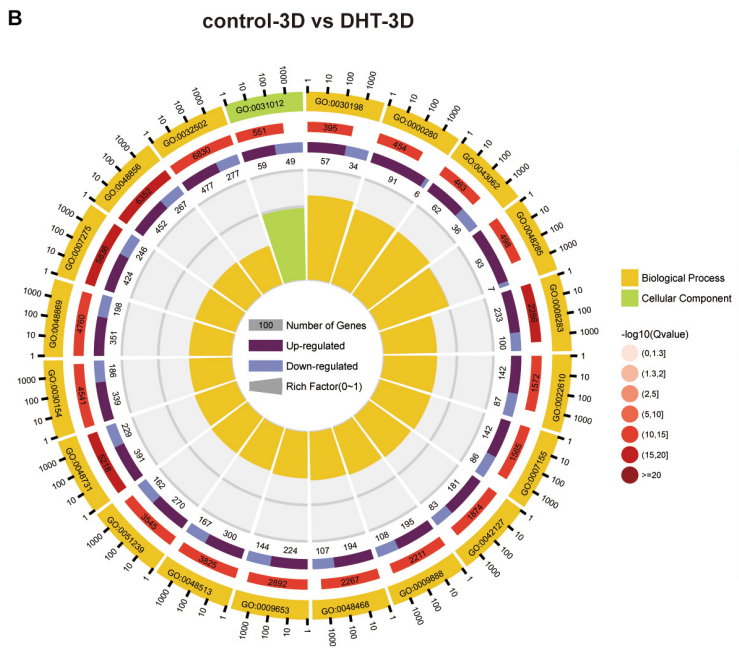

ID	Descrption
GO:0031012	extracellular matrix
GO:0008283	cell proliferation
GO:0048731	system development
GO:0048856	anatomical structure development
GO:0007275	multicellular organism development
GO:0032502	developmental process
GO:0030198	extracellular matrix organization
GO:0048513	animal organ development
GO:0009888	tissue development
GO:0000280	nuclear division
GO:0043062	extracellular structure organization
GO:0042127	regulation of cell proliferation
GO:0009653	anatomical structure morphogenesis
GO:0022610	biological adhesion
GO:0007155	cell adhesion
GO:0051239	regulation of multicellular organismal process
GO:0048869	cellular developmental process
GO:0048285	organelle fission
GO:0048468	cell development
GO:0030154	cell differentiation

FIGURE 8 | Kyoto Encyclopedia of Genes and Genomes and GO analysis of differentially expressed genes in 3D cultured dermal papilla cells. **(A)** Blue and red circles indicate metabolism and human diseases, respectively. The green circle indicates environmental information processing, whereas the brown circle represents organismal systems. The purple and yellow circles indicate cellular processes and genetic information processing, respectively. The size of the bubble represents the rich factor (gene number/total gene number), the *y*-axis represents –log10(*Q*-value), and the *x*-axis represents the normalized number of upregulated genes minus downregulated genes. **(B)** GO analysis of DEGs in 3D. Yellow: biological process, green: cellular component. From exterior to interior: first layer indicates the top 20 GO terms with the coordinate ruler indicating the number of genes presented external to the circle. Second layer (red): total number of genes in the GO term and –log10(*Q*-value), wherein a higher number of genes corresponds to a longer section, larger –log10(*Q*-value), and darker shade of red. Third layer: upregulation/downregulation gene ratio bar chart, wherein dark purple represents the upregulated gene proportion, light purple represents the downregulated gene proportion, and the specific value is shown below. Fourth layer: enrichment factor for each term (number of genes/total number of genes), with each small cell of the background auxiliary line representing 0.1. The chart on the right shows the gene symbols corresponding to the top 20 GO IDs. DEGs, differentially expressed genes.

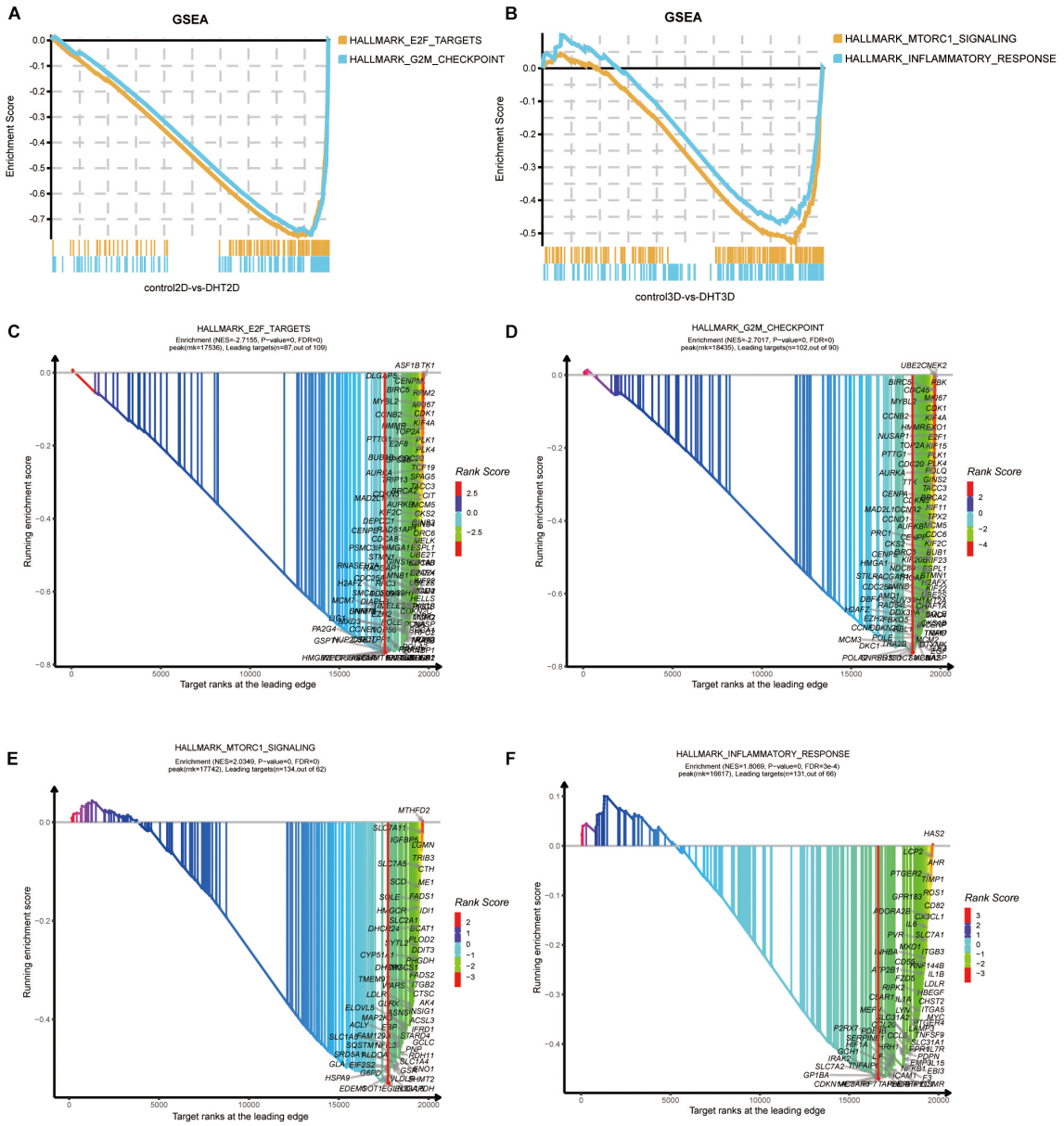

FIGURE 9 | Gene Set Enrichment Analysis of all genes. The overall results of GSEA for 2D and 3D groups are depicted in **(A,B)**, respectively. Each plot shows the running ESs (*y*-axes) and the position of the members of each gene set in the ranked list of genes between control-3D and DHT-3D or control-2D and DHT-3D (*x*-axes). Each vertical bar corresponds to one gene under the gene set, and the peak represents the ES of this gene set. GSEA results of four gene sets by xGSEAdotplot function: E2F targets **(C)** and G2M checkpoint **(D)** in 2D, and mTORC1 signaling **(E)** and inflammatory response **(F)** in 3D. The title of the plot has two rows, wherein the first row is the name of the dataset, and the second row represents the ES information. The peak (red vertical bar) divides the curve into two sides; the right side is called the leading edge and the genes on the surface are called leading targets (candidate genes). The *x*-axis represents target ranks and the *y*-axis represents ES. DHT, dihydrotestosterone; ES, enrichment score; GSEA, Gene Set Enrichment Analysis.

enriched in molecular function, including receptor binding and growth factor receptor binding.

Construction of a Protein–Protein Interaction Network and Module Analysis

A PPI network of the DEGs was constructed using Cytoscape, and the most significant module, with 45 nodes and 540 edges, was obtained (**Figure 10D**) using the MCODE application. Then, GO and KEGG analyses of the DEGs, which included functional classification and enrichment analyses, were performed using the DAVID online tool. The results showed that the chemokine signaling pathway was significantly enriched by nine DEGs, including *CXCL8*, *CXCL5*, *CX3CL1*, *CCL5*, *CCL28*, *CCL20*, *ADCY7*, *ADCY5*, and *ADCY4* (**Figures 11A,B**).

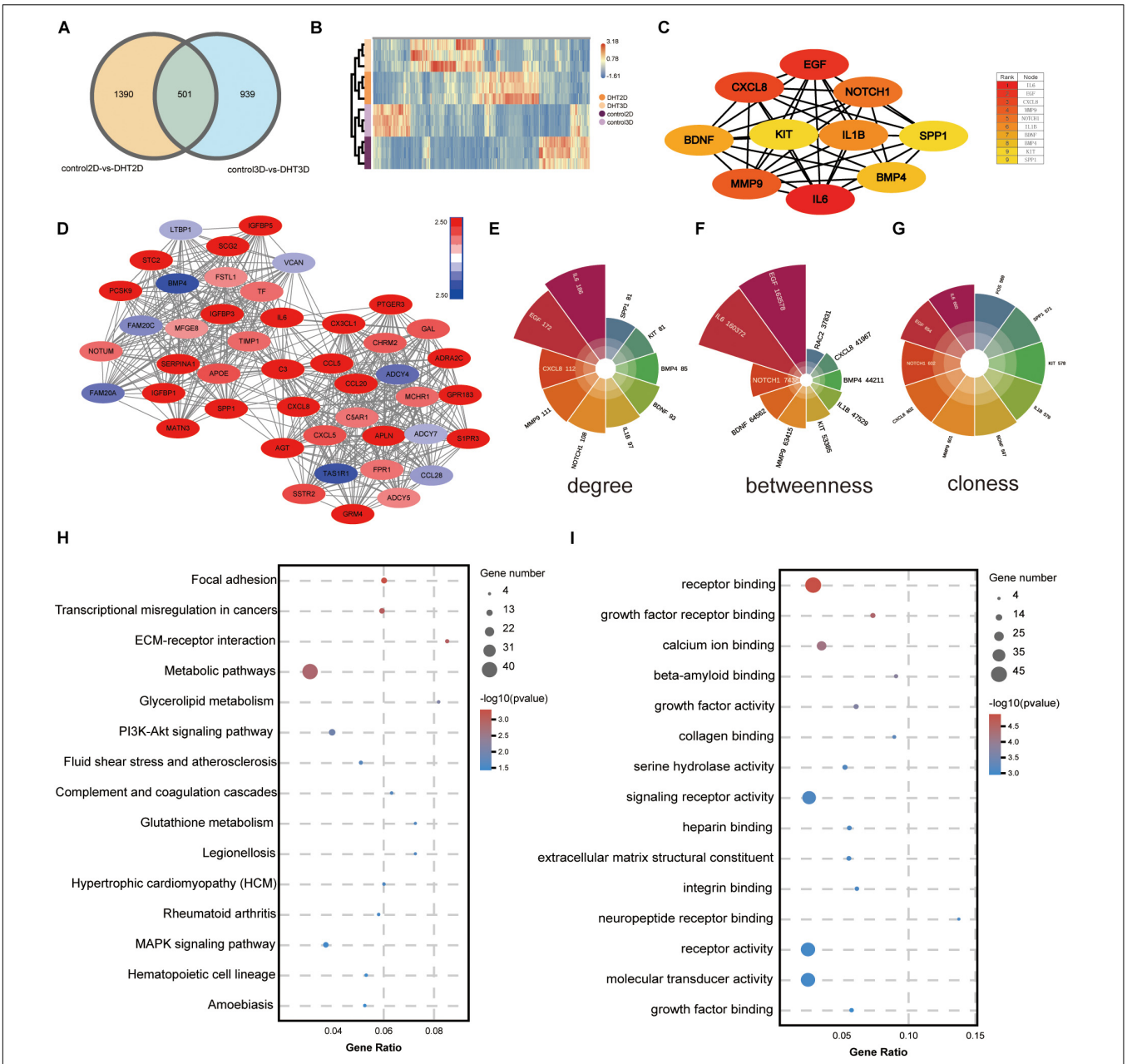

FIGURE 10 | Identification of the most significant module and hub genes of overlapping genes. **(A)** Venn diagram illustrating the number of overlapping DEGs between the two comparison groups (2D vs. 3D); 501 DEGs were common to both groups. **(B)** Unsupervised hierarchical clustering of the 501 overlapped genes, computed by Euclidean distance clustering and illustrated using a heatmap with normalized raw *z*-scores. **(C)** PPI network of hub genes, with 10 nodes and 39 edges. The color depth of the nodes represents the degree level; the deeper the color, the higher the degree. **(D)** The most significant module was obtained from the PPI network with 45 nodes and 540 edges. The more the genes were downregulated, the darker the blue; the more the genes were upregulated, the darker the red. Top 10 genes in the network were ranked based on degree **(E)**, betweenness **(F)**, and closeness **(G),** and depicted using Polar histograms. Different colors represent different genes, and the larger the area of the fan, the larger the data, and vice versa. **(H)** KEGG analysis of overlapping genes. The size of the bubble represents gene number, the color depth represents the *Q*-value, and the rich ratio represents the gene number/total gene number on the *y*-axis. **(I)** GO analysis of overlapping genes: the size of the bubble represents the gene number, the color depth represents the *p*-value, and the rich ratio indicates the gene number/total gene number on the *y*-axis. DEGs, differentially expressed genes; PPI, protein–protein interactions.

Selection and Analysis of Hub Genes

The top 10 genes with degrees ≥10 were identified as hub genes. The PPI network of the 10 hub genes (*IL-6*, *EGF*, *CXCL-8*, *MMP9*, *NOTCH1*, *IL-1*β, *BDNF*, *BMP4*, *KIT*, and *SPP1*) along with 10 nodes and 39 edges were identified using the Cytoscape CytoHubba application (**Figure 10C**). Moreover, we applied two algorithms ("betweenness" and "closeness") to further verify the importance of the 10 hub genes. The results showed that the node

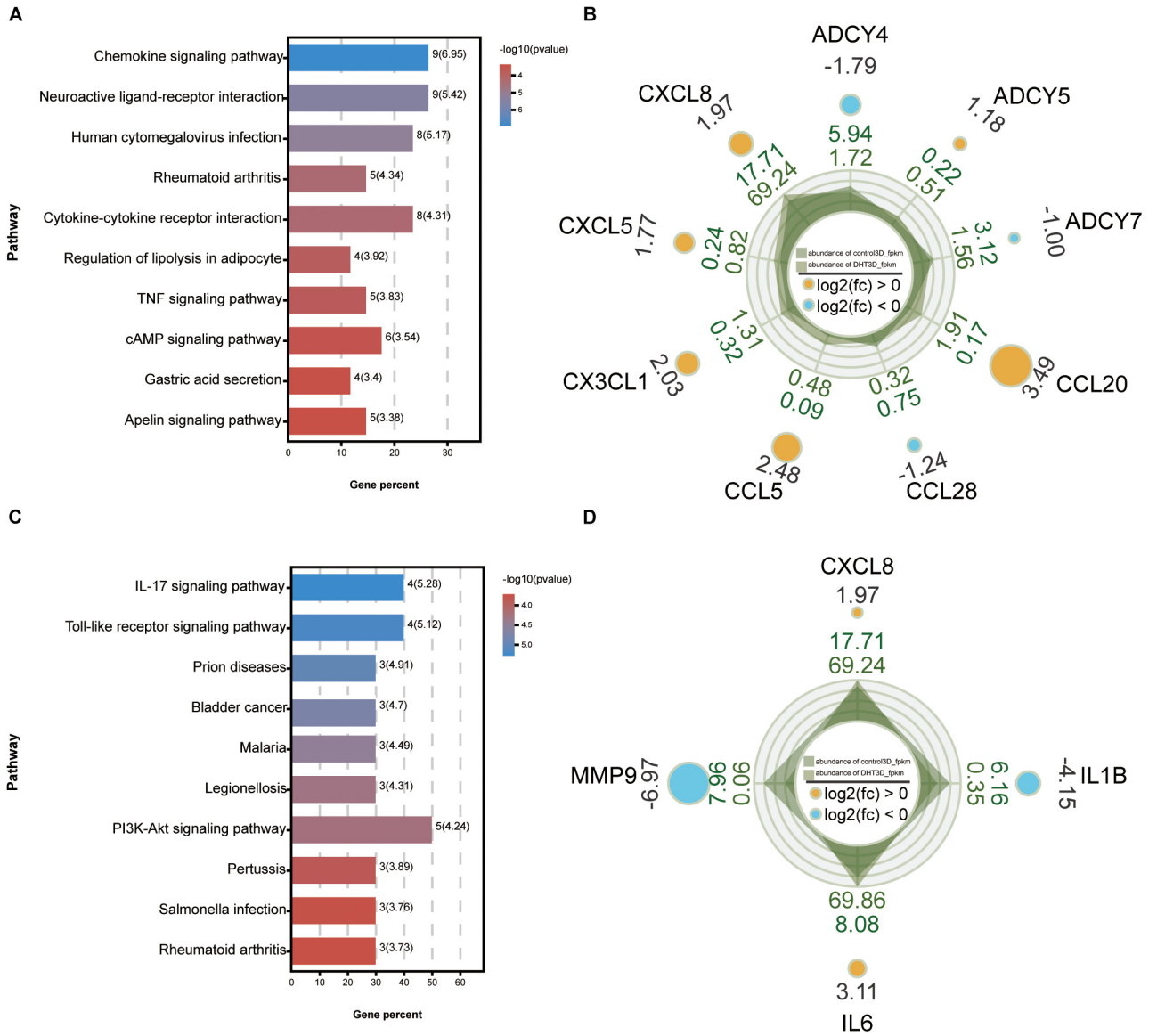

FIGURE 11 | Kyoto Encyclopedia of Genes and Genomes analysis of the maximum related module and 10 hub genes. KEGG analysis of genes from the most significant module **(A)** and 10 hub genes **(C)**. Each column represents a pathway, and the height of the column represents the number of genes that pathway contains. Legends indicate –log10(*p*-value). The higher the value, the bluer the color, and the smaller the value, the redder the color. Rader plot of enriched genes in the chemokine signaling pathway from the most significant module **(B)** and four hub genes of IL-17 signaling pathway **(D)** in control-3D vs. DHT-3D. The shadow part is the line chart of the expression abundance [log10(RPKM)] of each gene in the two groups (dark green is control-3D and light green is DHT-3D). The values outside the shadow are the expression abundance (RPKM) of each group. The outermost value represents log2(FC); the circle size represents the multiple of the difference of a single gene between the two groups, the bigger the circle, the greater the value. The color indicates upregulated and downregulated genes: orange indicates upregulation [log2(FC) > 0] and blue indicates downregulation [log2(FC) < 0], and the corresponding number is log2(FC). DHT, dihydrotestosterone; FC, fold change; RPKM, reads per kilo base per million mapped reads.

scores were basically consistent, and nine genes were identified by the three algorithms except *SPP1*, suggesting that the hub genes were indeed important (**Figures 10E–G**). KEGG analysis of these 10 hub genes revealed that four of them (*MMP9*, *CXCL-8*, *IL-1*β, and *IL-6*) were enriched in the IL-17 signaling pathway (**Figures 11C,D**). To analyze the function and interaction of these genes, GO_FULL analysis was used to calculate overrepresented GO terms in the network and displayed them as a network of significant GO terms using the Cytoscape BiNGO application. The biological process and molecular function analysis of the hub genes is shown in **Supplementary Figure 2**. According to BiNGO analysis, the top 10 GO terms the hub genes were involved in were primarily related to cell chemotaxis and regulation of chemokine biosynthetic, indicating that DHT may induce DPCs to secrete related chemokines and produce cell chemotaxis.

Expression Profiles of the Hub Genes and Quantitative Real-Time Reverse Transcription Polymerase Chain Reaction Verification

Control-2D, DHT-2D, control-3D, and DHT-3D fragments per kilobase million values of the hub genes are depicted in **Figures 12A–J**, revealing the changing trends of the hub genes among the four groups. The expression of *IL6* and *CXCL8* increased with an increase in DHT concentration in both the 2D and 3D groups, while the expression levels of *EGF*, *MMP9*, *IL1B*, *KIT*, *SPP1*, *BMP4*, and *NOTCH1* exhibited the opposite trend. The mRNA expression levels of the 10 hub genes were examined using qRT-PCR, and this confirmed the results of RNA-seq (**Figures 12K,L**).

Interactions of Transcription Factor-Gene and MicroRNA With Hub Genes

Transcription factor-gene interactions were collected using NetworkAnalyst. The TF-genes and miRNA for the hub genes were identified. The interaction of TF regulators and miRNAs with hub genes was visualized in **Figures 13A,B**.

Transcription Factor–MicroRNA Coregulatory Network

A TF–miRNA coregulatory network was generated using NetworkAnalyst. The analysis of the TF–miRNA coregulatory network delivered miRNAs and TFs interaction with the hub genes. This interaction may explain the regulation of expression of overlapping genes. The network created for the TF–miRNA coregulatory network comprises of 226 nodes and 364 edges; There were 148 miRNAs and 107 TF-genes that interacted with the hub genes. **Supplementary Figure 3** displays the TF–miRNA coregulatory network.

DISCUSSION

Some studies have reported that the full dermal papilla transcriptional signature can be partially restored by the growth of papilla cells in 3D spheroid cultures (Higgins et al., 2013; Lin G. et al., 2020). Thus, 3D DPC cultures represent useful models of dermal papillae. In the present study, we compared the effectiveness of 2D- and 3D-cultured DPCs in identifying new key genes and pathways associated with AGA under DHT treatment using high-throughput RNA-seq technology.

Androgen receptors are localized in the dermal papillae of hair follicles, making the dermal papillae the target of androgen action. Significantly more ARs exist in the DPCs of balding scalp hair follicles than in those derived from non-balding follicles (Hibberts et al., 1998). AR methylation, which results in decreased AR expression, may prevent the miniaturization of hair follicles and hair loss (Cobb et al., 2011). Therefore, DPCs in culture models should be rich in ARs to further simulate androgen-induced hair loss *in vivo*. Accordingly, we selected DPCs with the highest AR expression (P2) for the 2D and 3D co-culture experiment. The transport of ARs from the cytoplasm to the nucleus also indicated activation of the androgen metabolic pathway, which interacts with pathways related to hair follicle growth, such as the Wnt/β-catenin pathway (Chesire and Isaacs, 2002; Kitagawa et al., 2009).

Herein, we used cell models for the co-culture experiment instead of animal models and AGA hair follicles because human hair DPCs were the focus of the study. Over the past 30 years, DPCs have been clearly shown to play indispensable roles in the induction and maintenance of epithelial cell growth (Reynolds et al., 1991), as well as in the release of growth factors that act in a paracrine manner on other follicle cells (Paus and Cotsarelis, 1999). Another reason is that animal and human hair follicles consist of several types of cells, such as dermal fibroblasts, epidermal keratinocytes, hair matrix cells, inner root sheath cells, and ORS cells (Shimomura and Christiano, 2010), which may affect the cell of interest. Moreover, there are some limitations associated with animal models, such as species differences and poor ability to predict the actual human response. Additionally, once the organs or tissues of interest are isolated, it becomes impossible for them to be stimulated by androgen, making it difficult to explore the paracrine effect of a single cell type (DPC) on hair follicle epidermal cell growth under androgen treatment. In previous studies, researchers tended to choose a group of factors and a signal pathway, often leading to incomplete results. Therefore, we used specific cell models to identify genes related to AGA under DHT treatment.

In our models, DPCs from balding men were treated with different concentrations of DHT and ORS cell proliferation was used to represent hair follicle growth *in vivo*, with an increase in ORS number indicating hair follicle growth. A concentration of only 10 μM DHT significantly inhibited the proliferation of both 2D- and 3D-cultured DPCs. The ORS cell number in the control-3D group was significantly higher than that in the control-2D group; however, DHT treatment significantly decreased the ORS cell number in both models. Moreover, DHT treatment did not affect the proliferation of epidermal cells without DPCs. This confirmed that 3D-cultured DPCs induce the proliferation of epidermal cells and that the effect of DHT on the hair follicle epidermis is mediated by DPCs indirectly, which is consistent with the findings of previous *in vivo* studies (Pan et al., 1999; Kwack et al., 2008). Additionally, the significant decrease and increase in Ki67 and cleaved caspase-3 expression in ORS cells in both models indicates a decrease in ORS cell proliferation, which may be mediated by DPC-secreted proteins under DHT treatment. Overall, the data indicate that our co-culture system mimicked androgen-induced alopecia to some extent.

In this study, we pioneered the use of ultra-low attachment 96-well plates to convert scattered 2D structured DPCs into 3D structured multicellular spheres with a diameter of 200 μm, similar to the structure and size of dermal papillae of hair follicles *in vivo*. Generally, 2D cells do not have the same architecture as cells *in vivo* that are arranged in 3D structures unattached to planar surfaces (Haykal et al., 2020), and cells in monolayer culture proliferate at an unusually faster rate than cells *in vivo* (Langhans, 2018). Indeed, we confirmed a higher

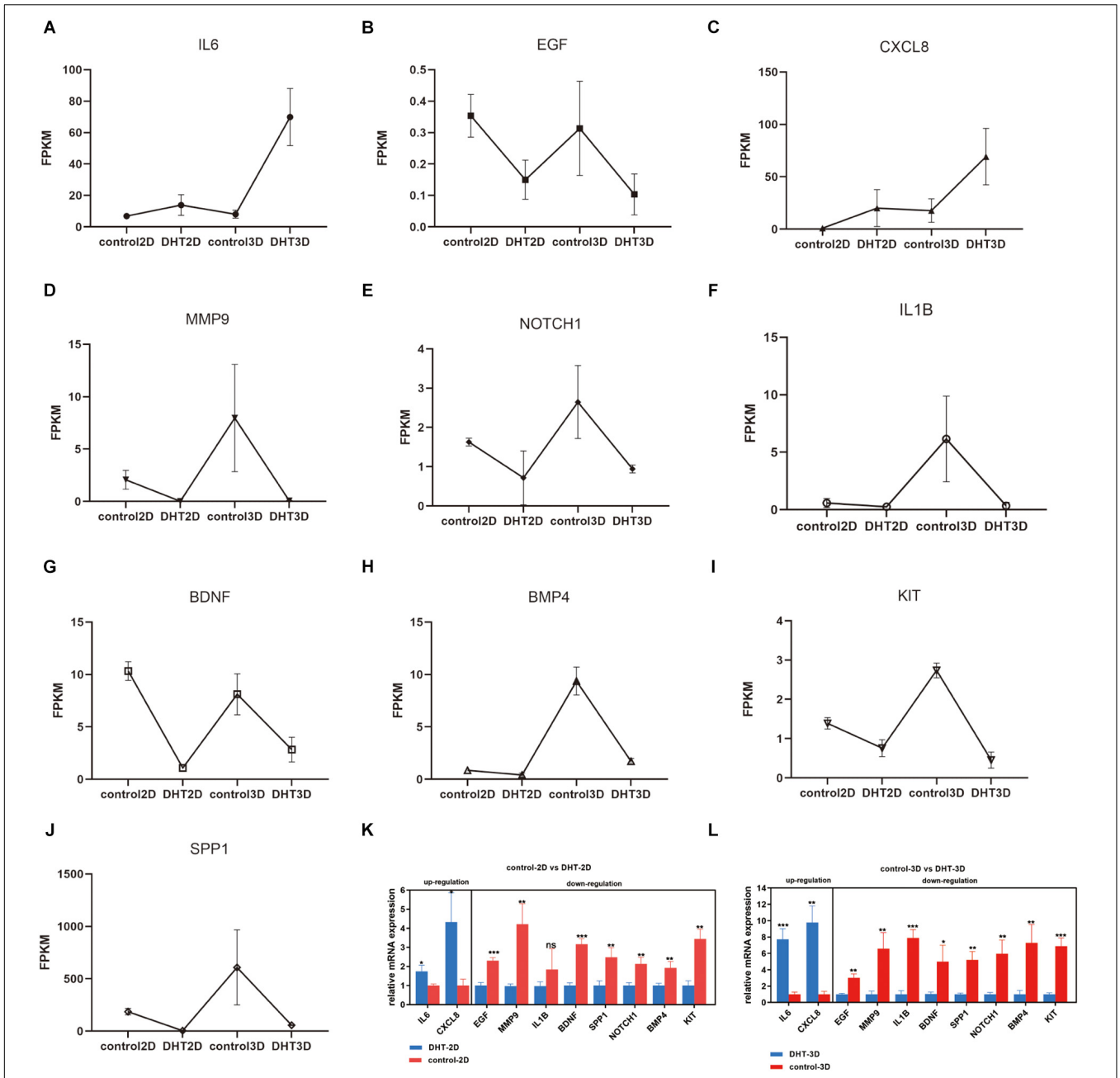

FIGURE 12 | Expression of hub genes and qRT-PCR verification. **(A–J)** Expression of 10 hub genes in four groups. *y*-axis item is FPKM. Relative mRNA expression levels of two upregulated and eight downregulated hub genes in the 2D **(K)** and 3D **(L)** groups. ns, not significant $^{*}p < 0.05$; $^{**}p < 0.01$; $^{***}p < 0.001$ when compared with the respective controls by one-way ANOVA and Student's *t*-test. FPKM, fragments per kilo base per million mapped reads.

proliferation rate of DPCs in the 2D model than in the 3D model. Moreover, 2D cells differ in gene and protein expression and dynamic processes, such as cell migration and division compared with that of vivo models (Ben-David et al., 2017); this is because the connection between cells and the ECM are not recapitulated in 2D culture models. Herein, RNA-seq of DPCs used to identify previously unknown transcripts (Mortazavi et al., 2008) demonstrated that DEGs between the models were mainly enriched in ECM–receptor interaction and that genes related to ECM–receptor interaction were upregulated due to cell aggregation. This indicates that compared to the ECM in the 2D model, the ECM in the 3D model was more similar to the dermal papillae of hair follicles. Additionally, 3D-cultured DPCs possessed high hair follicle regeneration ability (upregulated β−catenin and NCAM genes), similar to that of primary DPCs *in vivo* (Lin G. et al., 2020), indicating that the 3D model is more representative of the hair follicle microenvironment (Lin B. et al., 2020). β−Catenin and NCAM are dermal papillae biomarkers

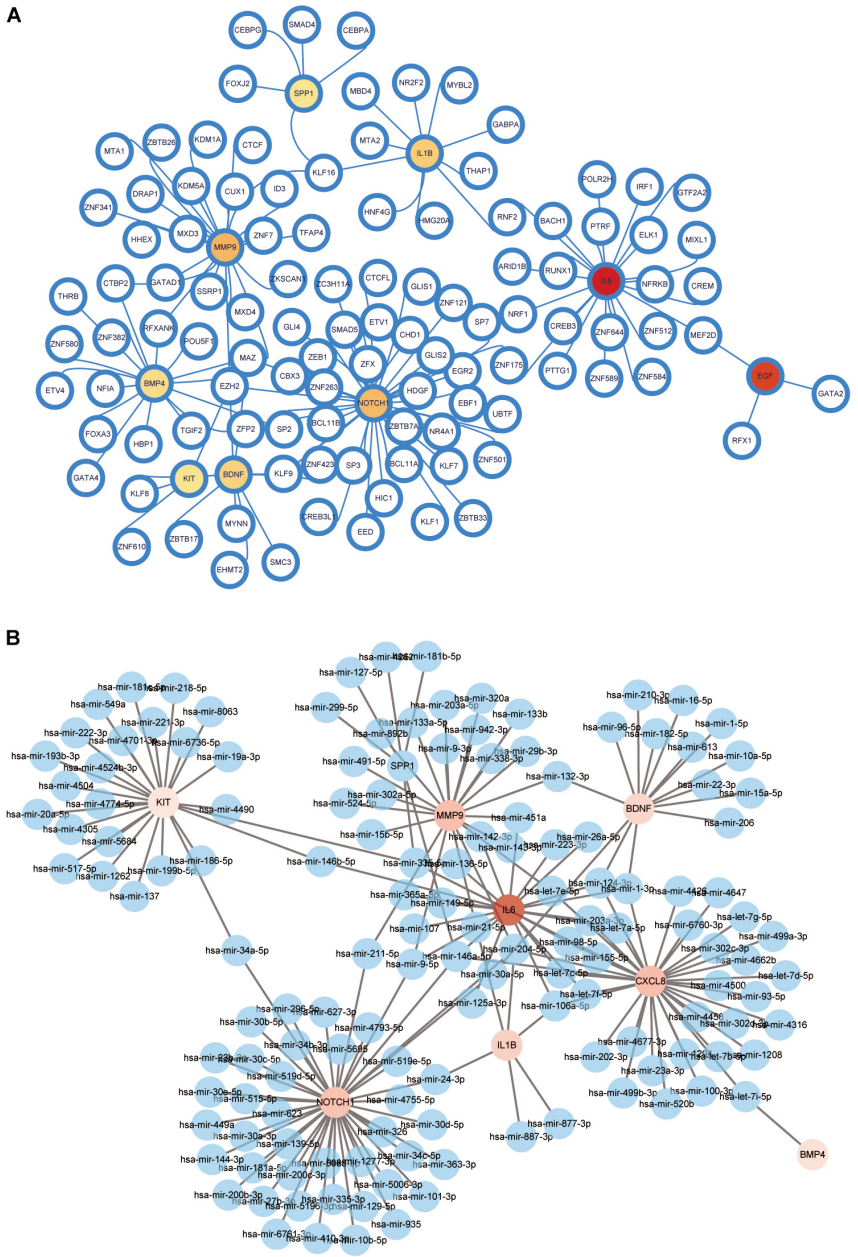

FIGURE 13 | Network for transcription factor-gene and miRNA interaction with hub genes. **(A)** Network for TF-gene interaction with hub genes. The white node represents the TF-genes and other nodes represent hub genes. The network consists of 116 nodes and 126 edges. **(B)** Network for miRNA interaction with hub genes. The blue nodes represent the miRNA genes, and other nodes represent hub genes. The network consists of 151 nodes and 176 edges. TF, transcription factor.

(Müller-Röver et al., 1998; Enshell-Seijffers et al., 2010), and β−catenin promotes hair follicle regeneration and the expression of dermal papillae-specific ECM *in vivo* (Maretto et al., 2003). Therefore, the advantages of the 3D model over the 2D model indicates that there may be differences in the DPC response to androgen. Most previous studies examined the pathogenesis of AGA using 2D co-culture models; however, as 2D models are not a proper representation of *in vivo* conditions, important key genes may not have been identified.

The KEGG network diagram demonstrated that the 3D model had more nodes (pathways), genes, and complex relationships than the 2D model, suggesting that the 3D model provides a more accurate representation of *in vivo* conditions. DEGs in 3D-cultured DPCs were primarily enriched in the MAPK signaling pathway, TNF signaling pathway, ECM–receptor interaction, cytokine–cytokine receptor interaction, Rap1 signaling pathway, PI3K–Akt, and extracellular matrix organization in our study. From these results, the most widely studied pathway related to

AGA is the Wnt signaling pathway, which involves functional crosstalk between AR and Wnt signaling pathways in target tissues (Van Mater et al., 2003; Lo Celso et al., 2004; Kitagawa et al., 2009). Hair follicle regeneration is reportedly related to upregulation of the Akt pathway, which is induced by HFSC proliferation (Kim et al., 2019) and downregulation of the p53 pathway (Qu et al., 2021). Activated platelet-rich plasma supernatant also increases the quantity of DPCs by activating the MAPK and Akt signaling pathways (Xiao et al., 2019). Meanwhile, a significant link exists between TNF-α antagonist exposure and the development of alopecia (Béné et al., 2014) and EGFR–RAS–RAF signaling in epidermal stem cells is inextricably linked to the beginning and end of the hair cycle (Doma et al., 2013). Moreover, DPC proliferation is promoted by VEGF through the VEGFR-2/ERK pathway (Qu et al., 2021). Therefore, the pathways observed to be enriched in the current study may be related to the effect of DPCs on epidermal composition under DHT treatment.

Gene Set Enrichment Analysis identified two gene sets in the 3D (mTORC1 signaling and inflammatory response) and 2D (E2F targets and G2M checkpoint) models. mTOR was previously reported to activate HFSCs (Castilho et al., 2009) and DHT to activate mTOR, which inhibits DPC proliferation (Kang et al., 2015). mTORC1 signaling also inhibits BMP signaling, which may be the main mechanism facilitating HFSC activation (Deng et al., 2015). Chai et al. (2019) discovered that autophagy through inhibition of mTOR signaling is sufficient for activating telogen, initiating a new anagen phase of hair growth. In the past, microinflammation of hair follicles has been recognized to play an active role in the progression of AGA (Mahé et al., 2000). Similarly, hair follicle microinflammation appeared necessary to AGA, and collagen gradually accumulated in the perifollicular sheath, leading to fibrosis or complete destruction of hair follicles (El-Domyati et al., 2009). E2F, a TF encoding cell cycle genes, is primarily involved in DNA replication and cell cycle progression (Bracken et al., 2004), whereas G2M represents genes involved in the G2/M checkpoint of the cell cycle. DHT reduces cyclin D1, CDK2, and $p27^{kip1}$ levels in immortalized DPCs, arresting the cell cycle from the G1 phase to the S phase (Kang et al., 2015). However, these previous findings showed that the above-mentioned pathways are mainly associated with hair growth and hair cycle regulation, with limited studies on their role in androgen-induced alopecia.

Protein–protein interaction analysis of the overlapping genes showed that the chemokine signaling pathway was significantly enriched under DHT treatment. However, few reports have suggested that chemokines are associated with DPCs under DHT treatment and can cause androgen-induced alopecia. A chemokine is a small chemotactic cytokine and is known for inducing leukocyte migration to target tissue in the inflammatory response. However, chemokines also play important roles in the development and homeostasis of hematopoietic and immune cells (Rossi and Zlotnik, 2000). Lefebvre et al. (2012) proposed an interaction between chemokines and skin appendage morphogenesis and reported that the number of primary hair follicles was reduced in *CXCR3*-deficient mice. Heath and Mueller (2012) reported that some chemokines that affect the recruitment of Langerhans cells to the epidermis are expressed in specific areas of hair follicles. Based on our results, we speculated that chemokine expression in DPCs is site-specific. The expression of chemokines under DHT treatment resulted in changes in cell migration, cell survival, and adhesion.

The identified top 10 hub genes showed a significant increase in *IL6* and *CXCL8* expression in the absence of DHT, and a significant decrease in *EGF*, *MMP9*, *NOTCH1*, *IL-1*β, *BDNF*, *BMP4*, *KIT*, and *SPP1* expression in the presence of DHT. However, the specific effect of chemokines needs to be further studied. Epidermal growth factor (EGF) has been identified in follicular differentiation (du Cros, 1993) and promotion of the transition of the hair cycle from telogen to anagen, as well as growth of the hair shaft (Zhao et al., 2020). Rendl et al. (2008) found that when DPCs are cultured in a medium containing BMP4 *in vitro*, there is a significant increase in hair follicle formation, hair growth, and alkaline phosphatase expression. Notch1 deletion inhibits the maturation of hair follicles from the late embryonic stage (Blanpain et al., 2006; Moriyama et al., 2008); one of the ways β-catenin regulates its effects on the hair follicle cycle and maintenance is through the Notch pathway (Vauclair et al., 2005; Estrach et al., 2006). A recent study showed that skin bacteria promote the complete regeneration of skin and hair follicles in wounds through the IL-1β pathway (Wang et al., 2021). However, most of these factors have not been revealed in the pathogenesis of AGA and the other five genes have not yet been studied.

A TF-gene and miRNA interaction network was obtained with the hub genes. TF-genes are involved in the regulation of gene expression through TF binding with targeted genes and miRNAs; they can also regulate gene expression through mRNA degradation (Wang et al., 2018). From the network, NOTCH1 showed a high interaction rate with other TF-genes and miRNAs. The degree value of NOTCH1 was 37 in the TF-gene interaction network and 44 in the miRNA interaction network. Among all TF-genes and miRNAs, NFKB1 had the highest degree value of 7. EZH2, MAZ, has-miR-204-5p, and has-miR-146a-5p exhibited significant interaction with degree values of 5, 4, 5, and 4, respectively, in the TF-gene and miRNA interactions network. EZH2 accelerates differentiation of HFSCs and hair growth by downregulating miR-22 (Cai et al., 2020). miR-200 family members play a vital role in the regulation of cell adhesion and proliferation in hair morphogenesis (Hoefert et al., 2018). Given that regulatory biomolecules are potential biomarkers in numerous complex diseases, further studies are needed to examine the roles of the hub genes and chemokines on morphological changes of DPCs and animal hair follicles *in vitro* and *in vivo*.

The two culture models employed in this study were sufficient to identify the effects of DHT-treated DPCs on hair follicle keratinocytes to a limited extent. We identified 501 overlapping DEGs, 10 hub genes, chemokines, and related signaling pathways in DPCs cultured using the 2D and 3D models. The identified DEGs were involved in AGA in DPCs and may be potential biomarkers for hair growth. The hub genes may also be potential biomarkers for the diagnosis and treatment of androgen-induced alopecia. Additionally, our findings suggest that chemokines

and the IL-17 pathway may be related to AGA; however, this requires further investigation. Moreover, upregulation of *EGF*, *MMP9*, *NOTCH1*, *IL-1*β, *BDNF*, *BMP4*, *KIT*, and *SPP1*, and downregulation of *IL6* and *CXCL8* may lead to the growth and maintenance of hair follicles. Overall, the findings provide the first global transcriptome of DPCs in 2D and 3D co-cultured models under DHT treatment and highlight the 3D model as a useful tool for elucidating hair follicle induction and hair growth.

DATA AVAILABILITY STATEMENT

The data presented in the study are deposited in the GEO repository, accession number GSE178374.

ETHICS STATEMENT

The studies involving human participants were reviewed and approved by the Medical Ethical Committee of the Southern Medical University. The patients/participants provided their written informed consent to participate in this study.

AUTHOR CONTRIBUTIONS

YZ, JH, DF, ZL, and HW performed all of the experiments and prepared the figures and schemes. JW, QQ, KL, and ZF provided statistical assistance. YZ wrote the first draft of this manuscript. JH and YM revised the manuscript for important intellectual content. ZH and JH contributed to the conception and design of the study. All authors contributed to manuscript revision, and read and approved the submitted version.

FUNDING

This study was funded by the National Natural Science Foundation of China (Grant Nos. 81701929, 81772104, and 81971889).

ACKNOWLEDGMENTS

We thank Guangdong Provincial Key Laboratory of Construction and Detection in Tissue Engineering, and the Translational Cell Biology Laboratory, Shenzhen Kurh-Life Technology Co., Ltd., for providing experimental instruments, and the Department of Plastic and Esthetic Surgery, Nanfang Hospital of Southern Medical University, Guangzhou, for providing the hair follicles. We would also like to thank Editage (www.editage.cn) for English language editing.

SUPPLEMENTARY MATERIAL

The Supplementary Material for this article can be found online at: https://www.frontiersin.org/articles/10.3389/fcell.2021.724310/full#supplementary-material

REFERENCES

Abaci, H. E., Coffman, A., Doucet, Y., Chen, J., Jacków, J., Wang, E., et al. (2018). Tissue engineering of human hair follicles using a biomimetic developmental approach. *Nat. Commun.* 9:5301. doi: 10.1038/s41467-018-07579-y

Andl, T., Reddy, S. T., Gaddapara, T., and Millar, S. E. (2002). WNT signals are required for the initiation of hair follicle development. *Dev. Cell* 2, 643–653. doi: 10.1016/s1534-5807(02)00167-3

Ben-David, U., Ha, G., Tseng, Y. Y., Greenwald, N. F., Oh, C., Shih, J., et al. (2017). Patient-derived xenografts undergo mouse-specific tumor evolution. *Nat. Genet.* 49, 1567–1575. doi: 10.1038/ng.3967

Béné, J., Moulis, G., Auffret, M., Lefevre, G., Coquerelle, P., Coupe, P., et al. (2014). Alopecia induced by tumour necrosis factor-alpha antagonists: description of 52 cases and disproportionality analysis in a nationwide pharmacovigilance database. *Rheumatology* 53, 1465–1469. doi: 10.1093/rheumatology/keu145

Blanpain, C., Lowry, W. E., Pasolli, H. A., and Fuchs, E. (2006). Canonical notch signaling functions as a commitment switch in the epidermal lineage. *Genes Dev.* 20, 3022–3035. doi: 10.1101/gad.1477606

Bracken, A. P., Ciro, M., Cocito, A., and Helin, K. (2004). E2F target genes: unraveling the biology. *Trends Biochem. Sci.* 29, 409–417. doi: 10.1016/j.tibs.2004.06.006

Cai, B., Li, M., Zheng, Y., Yin, Y., Jin, F., Li, X., et al. (2020). EZH2-mediated inhibition of microRNA-22 promotes differentiation of hair follicle stem cells by elevating STK40 expression. *Aging* 12, 12726–12739. doi: 10.18632/aging.103165

Castilho, R. M., Squarize, C. H., Chodosh, L. A., Williams, B. O., and Gutkind, J. S. (2009). mTOR mediates Wnt-induced epidermal stem cell exhaustion and aging. *Cell Stem Cell* 5, 279–289. doi: 10.1016/j.stem.2009.06.017

Chai, M., Jiang, M., Vergnes, L., Fu, X., de Barros, S. C., Doan, N. B., et al. (2019). Stimulation of hair growth by small molecules that activate autophagy. *Cell Rep.* 27, 3413–3421.e3. doi: 10.1016/j.celrep.2019.05.070

Chesire, D. R., and Isaacs, W. B. (2002). Ligand-dependent inhibition of beta-catenin/TCF signaling by androgen receptor. *Oncogene* 21, 8453–8469. doi: 10.1038/sj.onc.1206049

Cobb, J. E., Wong, N. C., Yip, L. W., Martinick, J., Bosnich, R., Sinclair, R. D., et al. (2011). Evidence of increased DNA methylation of the androgen receptor gene in occipital hair follicles from men with androgenetic alopecia. *Br. J. Dermatol.* 165, 210–213. doi: 10.1111/j.1365-2133.2011.10335.x

Dallob, A. L., Sadick, N. S., Unger, W., Lipert, S., Geissler, L. A., Gregoire, S. L., et al. (1994). The effect of finasteride, a 5 alpha-reductase inhibitor, on scalp skin testosterone and dihydrotestosterone concentrations in patients with male pattern baldness. *J. Clin. Endocrinol. Metab.* 79, 703–706. doi: 10.1210/jcem.79.3.8077349

Deng, Z., Lei, X., Zhang, X., Zhang, H., Liu, S., Chen, Q., et al. (2015). mTOR signaling promotes stem cell activation via counterbalancing BMP-mediated suppression during hair regeneration. *J. Mol. Cell Biol.* 7, 62–72. doi: 10.1093/jmcb/mjv005

Dhouailly, D. (1973). Dermo-epidermal interactions between birds and mammals: differentiation of cutaneous appendages. *J. Embryol. Exp. Morphol.* 30, 587–603.

Doma, E., Rupp, C., and Baccarini, M. (2013). EGFR-ras-raf signaling in epidermal stem cells: roles in hair follicle development, regeneration, tissue remodeling and epidermal cancers. *Int. J. Mol. Sci.* 14, 19361–19384. doi: 10.3390/ijms141019361

du Cros, D. L. (1993). Fibroblast growth factor and epidermal growth factor in hair development. *J. Invest. Dermatol.* 101(Suppl. 1), 106s–113s. doi: 10.1111/1523-1747.ep12363020

El-Domyati, M., Attia, S., Saleh, F., and Abdel-Wahab, H. (2009). Androgenetic alopecia in males: a histopathological and ultrastructural study. *J. Cosmet. Dermatol.* 8, 83–91. doi: 10.1111/j.1473-2165.2009.00439.x

Enshell-Seijffers, D., Lindon, C., Kashiwagi, M., and Morgan, B. A. (2010). beta-catenin activity in the dermal papilla regulates morphogenesis and regeneration of hair. *Dev. Cell* 18, 633–642. doi: 10.1016/j.devcel.2010.01.016

Estrach, S., Ambler, C. A., Lo Celso, C., Hozumi, K., and Watt, F. M. (2006). Jagged 1 is a beta-catenin target gene required for ectopic hair follicle formation in adult epidermis. *Development* 133, 4427–4438. doi: 10.1242/dev.02644

Haykal, M. M., Nahmias, C., Varon, C., and Martin, O. C. B. (2020). Organotypic modeling of the tumor landscape. *Front. Cell Dev. Biol.* 8:606039. doi: 10.3389/fcell.2020.606039

Heath, W. R., and Mueller, S. N. (2012). Hair follicles: gatekeepers to the epidermis. *Nat. Immunol.* 13, 715–717. doi: 10.1038/ni.2374

Hibberts, N. A., Howell, A. E., and Randall, V. A. (1998). Balding hair follicle dermal papilla cells contain higher levels of androgen receptors than those from non-balding scalp. *J. Endocrinol.* 156, 59–65. doi: 10.1677/joe.0.1560059

Higgins, C. A., Chen, J. C., Cerise, J. E., Jahoda, C. A., and Christiano, A. M. (2013). Microenvironmental reprogramming by three-dimensional culture enables dermal papilla cells to induce de novo human hair-follicle growth. *Proc. Natl. Acad. Sci. U.S.A.* 110, 19679–19688. doi: 10.1073/pnas.1309970110

Hoefert, J. E., Bjerke, G. A., Wang, D., and Yi, R. (2018). The microRNA-200 family coordinately regulates cell adhesion and proliferation in hair morphogenesis. *J. Cell Biol.* 217, 2185–2204. doi: 10.1083/jcb.201708173

Huang, D. W., Sherman, B. T., Tan, Q., Collins, J. R., Alvord, W. G., Roayaei, J., et al. (2007). The DAVID Gene Functional Classification Tool: a novel biological module-centric algorithm to functionally analyze large gene lists. *Genome Biol.* 8:R183. doi: 10.1186/gb-2007-8-9-r183

Inui, S., Fukuzato, Y., Nakajima, T., Yoshikawa, K., and Itami, S. (2002). Androgen-inducible TGF-beta1 from balding dermal papilla cells inhibits epithelial cell growth: a clue to understand paradoxical effects of androgen on human hair growth. *Faseb J.* 16, 1967–1969. doi: 10.1096/fj.02-0043fje

Itami, S., Kurata, S., Sonoda, T., and Takayasu, S. (1995). Interaction between dermal papilla cells and follicular epithelial cells in vitro: effect of androgen. *Br. J. Dermatol.* 132, 527–532.

Jahoda, C. A. (1998). Cellular and developmental aspects of androgenetic alopecia. *Exp. Dermatol.* 7, 235–248.

Kang, J. I., Kim, S. C., Kim, M. K., Boo, H. J., Kim, E. J., Im, G. J., et al. (2015). Effects of dihydrotestosterone on rat dermal papilla cells in vitro. *Eur. J. Pharmacol.* 757, 74–83. doi: 10.1016/j.ejphar.2015.03.055

Kim, J. Y., Ohn, J., Yoon, J. S., Kang, B. M., Park, M., Kim, S., et al. (2019). Priming mobilization of hair follicle stem cells triggers permanent loss of regeneration after alkylating chemotherapy. *Nat. Commun.* 10:3694. doi: 10.1038/s41467-019-11665-0

Kitagawa, T., Matsuda, K., Inui, S., Takenaka, H., Katoh, N., Itami, S., et al. (2009). Keratinocyte growth inhibition through the modification of Wnt signaling by androgen in balding dermal papilla cells. *J. Clin. Endocrinol. Metab.* 94, 1288–1294. doi: 10.1210/jc.2008-1053

Kwack, M. H., Ahn, J. S., Kim, M. K., Kim, J. C., and Sung, Y. K. (2012). Dihydrotestosterone-inducible IL-6 inhibits elongation of human hair shafts by suppressing matrix cell proliferation and promotes regression of hair follicles in mice. *J. Invest. Dermatol.* 132, 43–49. doi: 10.1038/jid.2011.274

Kwack, M. H., Sung, Y. K., Chung, E. J., Im, S. U., Ahn, J. S., Kim, M. K., et al. (2008). Dihydrotestosterone-inducible dickkopf 1 from balding dermal papilla cells causes apoptosis in follicular keratinocytes. *J. Invest. Dermatol.* 128, 262–269. doi: 10.1038/sj.jid.5700999

Langhans, S. A. (2018). Three-dimensional in vitro cell culture models in drug discovery and drug repositioning. *Front. Pharmacol.* 9:6. doi: 10.3389/fphar.2018.00006

Lefebvre, S., Fliniaux, I., Schneider, P., and Mikkola, M. L. (2012). Identification of ectodysplasin target genes reveals the involvement of chemokines in hair development. *J. Invest. Dermatol.* 132, 1094–1102. doi: 10.1038/jid.2011.453

Leirós, G. J., Ceruti, J. M., Castellanos, M. L., Kusinsky, A. G., and Balañá, M. E. (2017). Androgens modify Wnt agonists/antagonists expression balance in dermal papilla cells preventing hair follicle stem cell differentiation in androgenetic alopecia. *Mol. Cell. Endocrinol.* 439, 26–34. doi: 10.1016/j.mce.2016.10.018

Lin, B., Lin, G., Zhu, J., Yin, G., Huang, D., and Yan, Y. Y. (2020). LncRNA-PCAT1 maintains characteristics of dermal papilla cells and promotes hair follicle regeneration by regulating miR-329/Wnt10b axis. *Exp. Cell Res.* 394:112031. doi: 10.1016/j.yexcr.2020.112031

Lin, B., Miao, Y., Wang, J., Fan, Z., Du, L., Su, Y., et al. (2016). Surface Tension guided hanging-drop: producing controllable 3D spheroid of high-passaged human dermal papilla cells and forming inductive microtissues for hair-follicle regeneration. *ACS Appl. Mater. Interfaces* 8, 5906–5916. doi: 10.1021/acsami.6b00202

Lin, G., Yin, G., Ye, J., Pan, X., Zhu, J., and Lin, B. (2020). RNA sequence analysis of dermal papilla cells' regeneration in 3D culture. *J. Cell. Mol. Med.* 24, 13421–13430. doi: 10.1111/jcmm.15965

Lo Celso, C., Prowse, D. M., and Watt, F. M. (2004). Transient activation of beta-catenin signalling in adult mouse epidermis is sufficient to induce new hair follicles but continuous activation is required to maintain hair follicle tumours. *Development* 131, 1787–1799. doi: 10.1242/dev.01052

Love, M. I., Huber, W., and Anders, S. (2014). Moderated estimation of fold change and dispersion for RNA-seq data with DESeq2. *Genome Biol.* 15:550. doi: 10.1186/s13059-014-0550-8

Mahé, Y. F., Michelet, J. F., Billoni, N., Jarrousse, F., Buan, B., Commo, S., et al. (2000). Androgenetic alopecia and microinflammation. *Int. J. Dermatol.* 39, 576–584. doi: 10.1046/j.1365-4362.2000.00612.x

Maretto, S., Cordenonsi, M., Dupont, S., Braghetta, P., Broccoli, V., Hassan, A. B., et al. (2003). Mapping Wnt/beta-catenin signaling during mouse development and in colorectal tumors. *Proc. Natl. Acad. Sci. U.S.A.* 100, 3299–3304. doi: 10.1073/pnas.0434590100

McElwee, K. J., and Shapiro, J. S. (2012). Promising therapies for treating and/or preventing androgenic alopecia. *Skin Therapy Lett.* 17, 1–4.

Moriyama, M., Durham, A. D., Moriyama, H., Hasegawa, K., Nishikawa, S., Radtke, F., et al. (2008). Multiple roles of Notch signaling in the regulation of epidermal development. *Dev. Cell* 14, 594–604. doi: 10.1016/j.devcel.2008.01.017

Mortazavi, A., Williams, B. A., McCue, K., Schaeffer, L., and Wold, B. (2008). Mapping and quantifying mammalian transcriptomes by RNA-Seq. *Nat. Methods* 5, 621–628. doi: 10.1038/nmeth.1226

Müller-Röver, S., Peters, E. J., Botchkarev, V. A., Panteleyev, A., and Paus, R. (1998). Distinct patterns of NCAM expression are associated with defined stages of murine hair follicle morphogenesis and regression. *J. Histochem. Cytochem.* 46, 1401–1410. doi: 10.1177/002215549804601209

Nagalakshmi, U., Wang, Z., Waern, K., Shou, C., Raha, D., Gerstein, M., et al. (2008). The transcriptional landscape of the yeast genome defined by RNA sequencing. *Science* 320, 1344–1349. doi: 10.1126/science.1158441

Ohyama, M., Kobayashi, T., Sasaki, T., Shimizu, A., and Amagai, M. (2012). Restoration of the intrinsic properties of human dermal papilla in vitro. *J. Cell Sci.* 125(Pt 17), 4114–4125. doi: 10.1242/jcs.105700

Osada, A., Iwabuchi, T., Kishimoto, J., Hamazaki, T. S., and Okochi, H. (2007). Long-term culture of mouse vibrissal dermal papilla cells and de novo hair follicle induction. *Tissue Eng.* 13, 975–982. doi: 10.1089/ten.2006.0304

Pan, H. J., Uno, H., Inui, S., Fulmer, N. O., and Chang, C. (1999). Roles of testosterone in the growth of keratinocytes through bald frontal dermal papilla cells. *Endocrine* 11, 321–327. doi: 10.1385/endo:11:3:321

Paus, R., and Cotsarelis, G. (1999). The biology of hair follicles. *N. Engl. J. Med.* 341, 491–497. doi: 10.1056/nejm199908123410706

Qu, Q., Zhou, Y., Shi, P., Du, L., Fan, Z., Wang, J., et al. (2021). Platelet-rich plasma for androgenic alopecia: a randomized, placebo-controlled, double-blind study and combined mice model experiment. *J. Cosmet. Dermatol.* doi: 10.1111/jocd.14089 [Epub ahead of print].

Randall, V. A., Hibberts, N. A., Thornton, M. J., Merrick, A. E., Hamada, K., Kato, S., et al. (2001). Do androgens influence hair growth by altering the paracrine factors secreted by dermal papilla cells? *Eur. J. Dermatol.* 11, 315–320.

Rendl, M., Polak, L., and Fuchs, E. (2008). BMP signaling in dermal papilla cells is required for their hair follicle-inductive properties. *Genes Dev.* 22, 543–557. doi: 10.1101/gad.1614408

Reynolds, A. J., Oliver, R. F., and Jahoda, C. A. (1991). Dermal cell populations show variable competence in epidermal cell support: stimulatory effects of hair papilla cells. *J. Cell Sci.* 98(Pt 1), 75–83.

Rossi, D., and Zlotnik, A. (2000). The biology of chemokines and their receptors. *Annu. Rev. Immunol.* 18, 217–242. doi: 10.1146/annurev.immunol.18.1.217

Shimomura, Y., and Christiano, A. M. (2010). Biology and genetics of hair. *Annu. Rev. Genomics Hum. Genet.* 11, 109–132. doi: 10.1146/annurev-genom-021610-131501

Szklarczyk, D., Morris, J. H., Cook, H., Kuhn, M., Wyder, S., Simonovic, M., et al. (2017). The STRING database in 2017: quality-controlled protein-protein association networks, made broadly accessible. *Nucleic Acids Res.* 45, D362–D368. doi: 10.1093/nar/gkw937

Tan, J. J. Y., Common, J. E., Wu, C., Ho, P. C. L., and Kang, L. (2019). Keratinocytes maintain compartmentalization between dermal papilla and fibroblasts in 3D heterotypic tri-cultures. *Cell Prolif.* 52:e12668. doi: 10.1111/cpr.12668

Thippabhotla, S., Zhong, C., and He, M. (2019). 3D cell culture stimulates the secretion of in vivo like extracellular vesicles. *Sci. Rep.* 9:13012. doi: 10.1038/s41598-019-49671-3

Van Mater, D., Kolligs, F. T., Dlugosz, A. A., and Fearon, E. R. (2003). Transient activation of beta -catenin signaling in cutaneous keratinocytes is sufficient to trigger the active growth phase of the hair cycle in mice. *Genes Dev.* 17, 1219–1224. doi: 10.1101/gad.1076103

Vauclair, S., Nicolas, M., Barrandon, Y., and Radtke, F. (2005). Notch1 is essential for postnatal hair follicle development and homeostasis. *Dev. Biol.* 284, 184–193. doi: 10.1016/j.ydbio.2005.05.018

Wang, G., Sweren, E., Liu, H., Wier, E., Alphonse, M. P., Chen, R., et al. (2021). Bacteria induce skin regeneration via IL-1β signaling. *Cell Host Microbe* 29, 777–791. doi: 10.1016/j.chom.2021.03.003

Wang, L., Huang, W., Zhang, L., Chen, Q., and Zhao, H. (2018). Molecular pathogenesis involved in human idiopathic pulmonary fibrosis based on an integrated microRNA-mRNA interaction network. *Mol. Med. Rep.* 18, 4365–4373. doi: 10.3892/mmr.2018.9456

Xiao, S., Wang, J., Chen, Q., Miao, Y., and Hu, Z. (2019). The mechanism of activated platelet-rich plasma supernatant promotion of hair growth by cultured dermal papilla cells. *J. Cosmet. Dermatol.* 18, 1711–1716. doi: 10.1111/jocd.12919

Zhao, B., Li, J., Chen, Q., Yang, N., Bao, Z., Hu, S., et al. (2020). A treatment combination of IGF and EGF promotes hair growth in the Angora rabbit. *Genes* 12:24. doi: 10.3390/genes12010024

Conflict of Interest: The authors declare that the research was conducted in the absence of any commercial or financial relationships that could be construed as a potential conflict of interest.

Publisher's Note: All claims expressed in this article are solely those of the authors and do not necessarily represent those of their affiliated organizations, or those of the publisher, the editors and the reviewers. Any product that may be evaluated in this article, or claim that may be made by its manufacturer, is not guaranteed or endorsed by the publisher.

Copyright © 2021 Zhang, Huang, Fu, Liu, Wang, Wang, Qu, Li, Fan, Hu and Miao. This is an open-access article distributed under the terms of the Creative Commons Attribution License (CC BY). The use, distribution or reproduction in other forums is permitted, provided the original author(s) and the copyright owner(s) are credited and that the original publication in this journal is cited, in accordance with accepted academic practice. No use, distribution or reproduction is permitted which does not comply with these terms.

Advantages of publishing in Frontiers

OPEN ACCESS
Articles are free to read for greatest visibility and readership

FAST PUBLICATION
Around 90 days from submission to decision

HIGH QUALITY PEER-REVIEW
Rigorous, collaborative, and constructive peer-review

TRANSPARENT PEER-REVIEW
Editors and reviewers acknowledged by name on published articles

Frontiers
Avenue du Tribunal-Fédéral 34
1005 Lausanne | Switzerland

Visit us: www.frontiersin.org
Contact us: frontiersin.org/about/contact

REPRODUCIBILITY OF RESEARCH
Support open data and methods to enhance research reproducibility

DIGITAL PUBLISHING
Articles designed for optimal readership across devices

FOLLOW US
@frontiersin

IMPACT METRICS
Advanced article metrics track visibility across digital media

EXTENSIVE PROMOTION
Marketing and promotion of impactful research

LOOP RESEARCH NETWORK
Our network increases your article's readership